Characterising the Role of ICAM-3 and Apoptotic Cell-derived Extracellular Vesicles in the Clearance of Apoptotic Cells

by

Khaled W A Alghareeb
Doctor of Philosophy

Aston University
September 2017

Thesis Summary

Apoptotic cells (AC) are removed by macrophages (MØ) quickly to maintain healthy tissues. Apoptotic cell-derived extracellular vesicles (ACdEV) and ICAM-3 are shed during apoptosis and aid in AC removal by attracting macrophages (MØ). ICAM-3 on AC also mediates tethering to MØ. However the mechanism of ICAM-3 action is not known. This project aims to characterise the role of ICAM-3 and ACdEVs in the clearance of apoptotic cells.

In agreement with previous studies, human lymphocytes were induced to apoptosis by UV irradiation and ACdEV were isolated and characterised. Using qNano, this work reveals, for the first time, release of ACdEV (~200nm) from early (6h) to late (18h) stages of apoptosis. Furthermore, the ability of ICAM-3 on ACdEV to promote phagocyte recruitment was confirmed and extended by using both vertical and horizontal migration assays. Also, ICAM-3 is confirmed as an apoptotic cell ligand that promotes interaction of AC with MØ.

How ICAM-3 on ACdEV promotes MØ migration is not clear but novel data here suggests that it may be acting as an adhesion molecule to improve EV-MØ binding. Using *in vitro* assays of inflammation, AC and their EV were assessed for anti-inflammatory effects though any anti-inflammatory effect were unexpectedly small.

In novel *in vivo* studies using a xenograft model, data show that anti-ICAM-3 mAb is capable of causing a significant reduction in growth of a transplanted ICAM-3^{+} tumour. The mAb also reduced MØ number within the tumours suggesting ICAM-3 can function *in vivo* for MØ recruitment to sites of cell death.

Analyses of partner proteins for ICAM-3 was done in further novel studies. These were problematic as CO-IP approaches to the isolation of ICAM-3 were inefficient. However, mass spec analysis of crude membrane preparations revealed two proteins upregulated in apoptotic HeLa-ICAM-3 cells that may function to reorganize cytoskeleton. Future work is required to test if these observations are significant for the function of ICAM-3 in AC clearance.

Acknowledgements

I take this opportunity to thank and express my sincere gratitude to each and every one who made it possible for me to write this doctoral thesis.

I would like to start thanking my supervisor Prof. Andrew Devitt for his support encouragement, patience, guidance, inspiration and constructive criticism throughout this PhD. I would also like to thank my secondary supervisor Prof. Helen Griffiths.

I would like to thank Dr. Ivana Milic for her advice and help, in addition to support, and friendship throughout. I would like to thank Dr. James Brown and Dr. Alice Rothnie for their help. I would like to thank Prof. Chris Gregory and Lynsey Melville from Edinburgh Universtiy for their help. *I would like to thank my lab colleagues (Allan Cameron, Sowmya Castro, Parbata Chauhan, Roberta Liccardo, Ross Pallet and Laura Feather) for their endless help, support, friendship and fun times we had in the lab. I would like to thank David Hardy for his help in the lab. I would like to thank Charlie Bland for her help with the confocal microscope. I would also like to thank everyone in our office room.*

I would like to acknowledge the academic and technical support of Aston University.

I would like to thank my friends and family for their emotional support and continuous encouragement throughout my journey.

I would like to thank my beloved mother and father for their endless support, encouragement, advice and love, I also would like to thank my precious daughters Fajer and Amal for being with me throughout this journey.

Finally, I would like to thank my lovely wife Abrar for being at my side the whole time, thank you for your patience, endless support, advice and love, which helped me achieve this huge accomplishment.

Table of Contents

Abbreviations list

AC	Apoptotic cell(s)
ACAMP	Apoptotic cell-associated molecular pattern(s)
ACdEV	Apoptotic cell-derived extracellular vesicle(s)
APAF-1	Apoptotic protease activating factor
APC	Antigen presenting cell
AxV	Annexin V
ATP	Adenosine triphosphate
BAI1	Brain-specific angiogenesis inhibitor 1
BL	Burkitt's lymphoma cells
CAD	Caspase activated DNase
CRD	Carbohydrate recognition domains
cRPMI	Complete RPMI
DAMP	Damage-associated molecular pattern(s)
DAPI	4', 6-diamidion-2-phenylindole, dihydrochloride
DC-SIGN	Dendritic cell-specific ICAM-3-grabbing non-integrin
DD	Death domain
DFF40	DNA fragmentation factor
dH_2O	Distilled water
DISC	Death-inducing signaling complex
DMEM	Dulbecco's modified Eagle medium
DMSO	Dimethyl sulphoxide
DNA	Deoxyribonucleic acid
DS	Double-stimulated (with PMA and VD3)
EDTA	Ethylenediaminetetra-acetic acid disodium salt
ER	Endoplasmic reticulum
ELISA	Enzyme linked immunosorbent assay
EV	Extracellular vesicle(s)
FADD	Fas-associated death domain protein
FBS	Foetal bovine serum
GAS-6	Growth arrest-specific 6

GDP	Guanosine diphosphate
GTP	Guanosine triphosphate
HEK	Human embryonic kidney cells
HMGB1	High-mobility group box-1 protein
HRP	Horse radish peroxidase
IAP	Inhibitors of apoptosis
IL	Interlukin
ICAM-3	Intercellular adhesion molecule 3
LBP	Lipopolysaccharide-binding protein
LFA-1	Leukocyte-associated function antigen 1
LPC	Lysophosphatidylcholine
LPS	Lipopolysaccharide
mAb	Monoclonal antibody
MØ	Macrophage(s)
MFG-E8	Milk fat globule epidermal growth factor 8
MLC	Myosin light chain
MMP	Matrix metalloproteinase
MP	Microparticle
MPT	Mitochondrial permeability transition
NØ	Neutrophil(s)
OD	Optical density
OPD	*o*-phenylenediamine dihydrochloride
PAMP	Pathogen-associated molecular pattern
PBS	Phosphate-buffered saline
PGE2	Prostaglandin-E2
PI	Propidium Iodide
PKC	Protein kinase C
PMA	Phorbol 12-myristate 13-acetate
PRR	Pattern recognition receptor(s)
PS	Phosphatidylserine
RANTES	Regulated on Activation, Normal T cell Expressed and Secreted/CCL5
RNA	Ribonucleic acid
ROCK1	Rho-associated kinase 1
S1P	Sphingosine-1-phosphate

SLE	Systemic lupus erythematosus
TGF-β	Transforming growth factor beta
TIM-1/4	T cell immunoglobulin mucin-1/ 4
TRADD	TNF receptor-associated death domain
TRL	Toll-like receptor
TNF-α	Tumour-necrosis factor alpha
TSP-1	Thrombospondin-1
UTP	Uridine 5'-triphosphate
UV	Ultraviolet
VD3	Dihydroxyvitamin D3
WC	Whole cell culture
WT	Wild type

List of figures and tables

List of figures

List of tables

1. Introduction

1.1 Apoptosis

The process of programmed cell death also termed apoptosis is a key player in the development, maintenance and control of mammalian tissues. It was identified morphologically in the early 1970s and was proposed to be basic biological phenomenon that acted with mitosis to control cell numbers (Kerr *et al.*, 1972). Damaged, aged or excess cells are removed by this apoptosis programme in a neat and a very regulated manner without any harm to the surrounding tissues (Cohen, 1991). As a cell undergoes apoptosis, it goes through some characteristic morphological changes such as cell shrinkage, chromatin condensation, collapsing of the cytoskeleton, disassembly of the nuclear envelope, breaking of the nuclear DNA into fragments and apoptotic body formation through budding of the plasma membrane (Kerr et al., 1972, Wyllie *et al.*, 1980). The apoptotic bodies that are formed are composed of cytosol with tightly-packed organelles and may contain nuclear fragments (**Figure 1**). The apoptotic cells preserve their cytoplasmic membrane integrity, which prevents the leakage of contents into the surrounding interstitial tissue thereby preventing an inflammatory response (Elmore, 2007). Also extracellular vesicles (EV) derived from the plasma membrane (also known as micro-particles or micro-vesicles) are shed during apoptosis by loss of cell membrane, which aid in apoptotic cell removal (Segundo *et al.*, 1999).

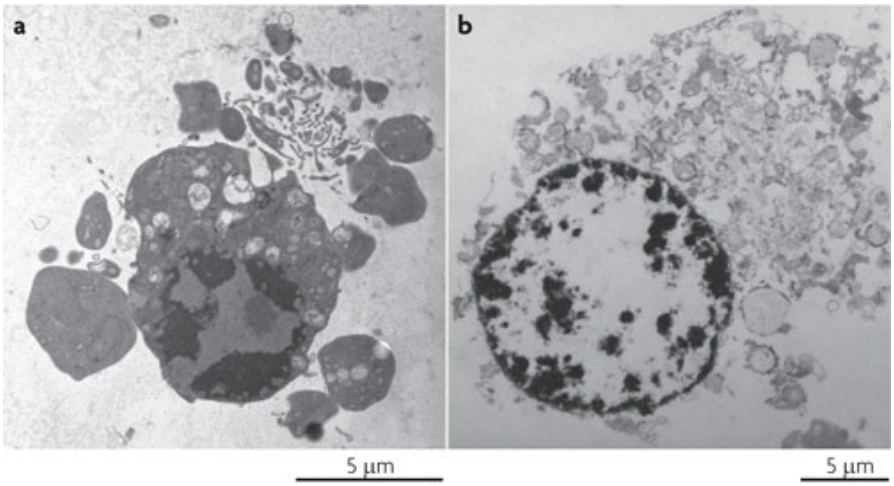

Figure 1. Morphology of apoptotic and necrotic cells. Electron micrographs (**a**) An apoptotic cell, showing condensed cytosol, marginalized chromatin and nuclear fragmentation, blebbing of the intact plasma membrane and apoptotic body formation; (**b**) A necrotic cell with ruptured plasma membrane and spillage of its contents in to the extracellular environment (Vandenabeele *et al.*, 2010).

1.1.1 Induction of Apoptosis

Apoptosis induction depends on an intracellular proteolytic cascade that is mediated by caspases (Thornberry and Lazebnik, 1998). Caspases are cysteine-dependent aspartate-specific proteases, where they have a proteolytic activity and are able to cleave proteins at aspartic acid residues. They are synthesized in an inactive state called procaspases and once activated they activate other procaspases and initiate the caspase cascade. Some procaspases can auto-activate each other due to aggregation and this initiates the signaling cascade. Once the caspase cascade is initiated it becomes an irreversible process towards cell death (Earnshaw *et al.*, 1999). Caspases have been broadly categorized into initiators (caspase-2, 8,9,10) which initiate the cascade and executioners (caspase-3, 6, 7) which mediate cell death (Cohen, 1997). Caspases are activated by two apoptotic pathways, which are the extrinsic pathway and intrinsic pathway (**Figure 2**).

The contribution of caspases to dismantling the dying cell and apoptosis can be seen in several aspects of the cell death process, such as in the destruction of the nuclear lamins proteins, where the caspases cleave the lamins, which causes nuclear shrinking and budding (Rao *et al.*, 1996, Buendia *et al.*, 1999). Another contribution of caspases in dismantling the cell is seen in their cleavage of cytoskeletal proteins such as gelsolin and fodrin, resulting in a loss of cell structure enabling the dying cell to become released from its position in a tissue and be free to be removed (Kothakota *et al.*, 1997). Another hallmark of apoptosis that is also caused by caspases is classical DNA fragmentation. The DNA fragmentation is caused by an active nuclease called CAD (Caspase activated DNase) also known as DFF40 (DNA fragmentation factor). As CAD is so potentially dangerous to cell, it is found in an inactive form within the cell by being bound to its inhibitor ICAD, also known as DFF45. The association of ICAD with CAD occurs as CAD is being translated and ICAD acts as a chaperone to help fold the CAD. During apoptosis, active caspase 3 cleaves ICAD to release CAD and, in this active form, CAD can promote DNA condensation and fragmentation (Enari *et al.*, 1998, Liu *et al.*). Membrane blebbing, where the plasma membrane bulges from the cells, is a common physical characteristic of apoptosis which relies on the contractile force generated by actin-myosin cytoskeleton. The actin-myosin effect is achieved by caspases cleaving their regulator, which is a serine/threonine kinase called ROCK1 (Rho-associated kinase 1). Caspase 3 cleaves the ROCK1 causing it to be constantly activated, which phosphorylates Myosin light chain (MLC) leading to contraction and membrane blebbing (Coleman *et al.*, 2001, Sebbagh *et al.*, 2001).

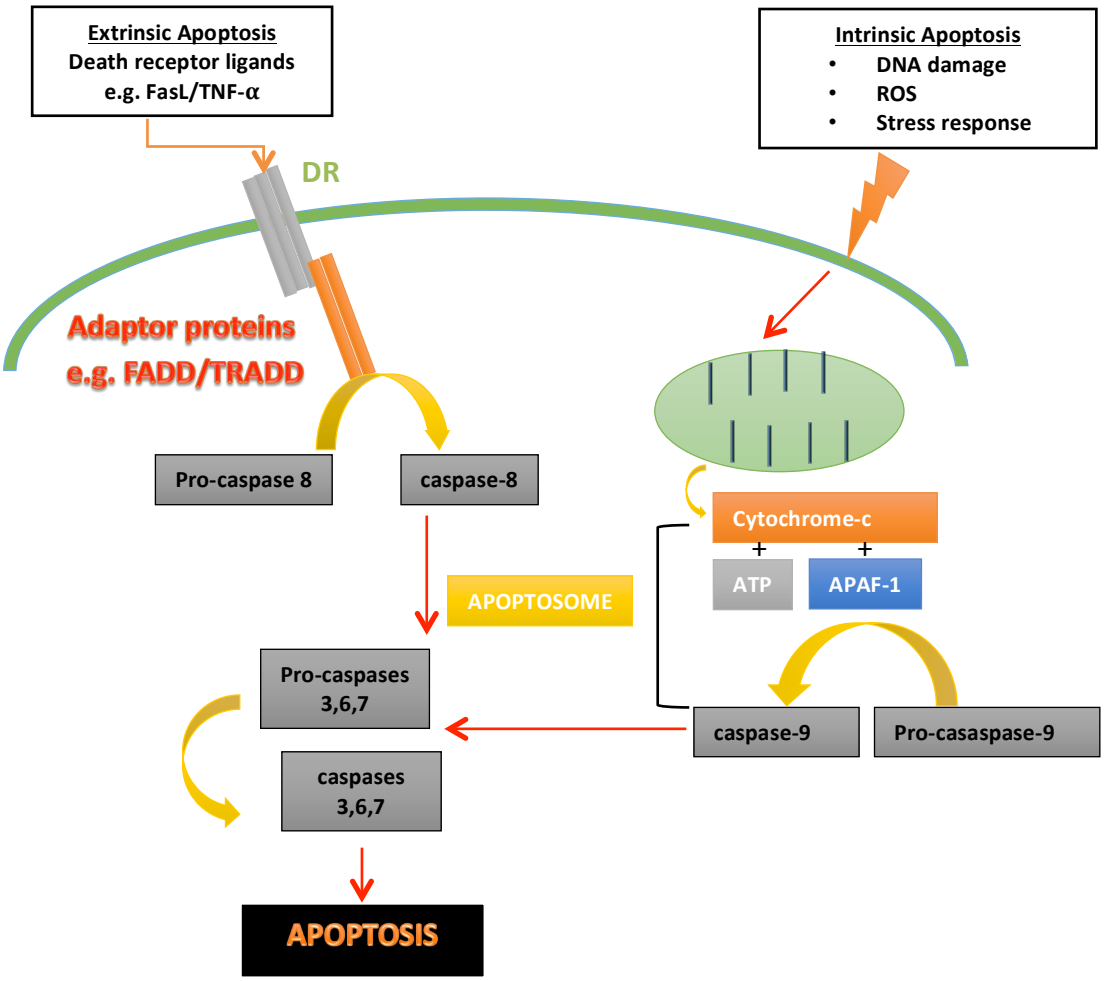

Figure 2. Extrinsic and intrinsic pathways of apoptosis induction. The extrinsic apoptosis pathway is activated through the binding of death receptor ligands (e.g. FasL/TNF-α) to death receptors (DR e.g. FasR/TNFR1), which causes receptor trimerisation. Consequent adaptor protein (e.g. FADD/TRADD) recruitment causes recruitment, oligomerisation and activation of caspase-8 (an initiator caspase). Activated caspase-8 initiates apoptosis via the cleavage and activation of executioner caspases (3, 6, 7). The intrinsic apoptosis pathway can be activated through various cellular stresses that lead to cytochrome c release from mitochondria and the subsequent formation of the apoptosome (APAF-1, cytochrome c, ATP, and pro-caspase-9), resulting in the activation of caspase-9. Activated caspase-9 then initiates apoptosis by cleaving and activating executioner caspases (3, 6, 7). Adapted from (Olsson and Zhivotovsky, 2011).

1.1.2 Extrinsic Pathway of Apoptosis Induction

The extrinsic pathway for the induction of apoptotic cell death involves extracellular ligands that bind to cell surface transmembrane receptors, which are termed 'death receptors' (**Figure 2**). Death receptors are members of the tumour necrosis factor (TNF) receptor family. The TNF receptor family members have a cytoplasmic domain called a 'death domain' (DD), which is about 80 amino acids (Ashkenazi and Dixit, 1998). The death domain has a vital role where, upon receptor ligation, the DD transmits death signals from the cell surface to the intracellular signaling pathway by enabling a signaling complex of proteins to assemble. There are several ligands (death factors) that bind to death receptors, such as Fas ligand (FasL) and TNF-α which bind to FasR and TNFR1 respectively. Once the FasL and TNF-α bind to their specific receptors (FasR/TNFR1) the receptors trimerise and in this format, their DD allow recruitment of cytoplasmic adaptor proteins FADD (Fas-associated death domain protein) and TRADD (TNF receptor-associated death domain*)*. After the recruitment and binding of FADD to the cytosolic tail of the Fas death domain, it causes recruitment of the initiator procaspase 8. The recruitment forms a 'Death Inducing-Signaling-Complex' (DISC), which results in an auto-catalytic activation of the procaspase 8 as a result of the close association of multiple pro-caspase molecules (Kischkel *et al.*, 1995). This activation of initiator caspases leads to the activation of downstream executioner caspases through the enzyme activity of the initiator caspases forming a cascade of activation. These caspases then collectively induce cell disassembly and apoptosis.

The extrinsic pathway has some 'security measures' or safeguards in place to prevent inappropriate activation of apoptosis (Scaffidi *et al.*, 1999). For example, cells have an intracellular blocking protein called FLIP, which is similar to the initiator procaspases as it has a DD but no proteolytic activity. FLIP competes with procaspases in binding with DISC thereby preventing the activation of the procaspases and eventually apoptosis. Inappropriate overexpression of these 'safeguards' can drive disease with cancers widely inhibiting apoptosis in order to drive tumour progression. This highlights the importance of a tightly controlled cell death programme to maintain healthy cell populations.

1.1.3 Intrinsic Pathway of Apoptosis Induction

The intrinsic pathway of apoptosis induces apoptosis in an intracellular manner (**Figure 2**) but the two different pathways share similarities in their activation. The pathway is initiated by various non-receptor mediated stimuli that relay intracellular signals acting on targets within the cell and are mitochondrial-initiated events (Liu *et al.,* Zhivotovsky *et al.*, 1998). Examples of stimuli that initiate the intrinsic pathway are cell damage due to toxins, free radicals or radiation. Also the stimuli could be viral infections, DNA damage or lack of oxygen, nutrients or extracellular survival signals (Elmore, 2007, Tait and Green, 2010). Crucially, these stimuli cause changes to the inner mitochondrial membrane that leads to the opening of a mitochondrial permeability transition (MPT) pore. The opening of the MPT pore results in loss of transmembrane potential causes the release of a protein called cytochrome c and pro-apoptotic proteins SMAC/Diablo and HtrA2/Omi (Saelens *et al.*, 2004). The pro-apoptotic proteins inhibit those endogenous cellular Inhibitors of Apoptosis (IAP) proteins (that act as safeguards to inappropriate activation of apoptosis). The cytochrome c binds to an adaptor protein called apoptotic protease activating factor (Apaf-1), which causes oligomerisation of Apaf-1 with cytochrome c and ATP into a complex known as the apoptosome. This apoptosome complex acts in a similar manner to the DISC from the extrinsic pathway as it acts as a focus to recruit initiator procaspase proteins (procaspase-9) through its caspase recruitment domain (CARD). As with the extrinsic pathway, the accumulation of initiator procaspases allows autoactivation and the activated caspase-9 activates additional, executioner procaspases downstream causing a caspase cascade leading to apoptosis induction (Chinnaiyan, 1999).

The apoptotic-mitochondrial events are controlled and regulated by members of the Bcl-2 family proteins. The Bcl-2 family has pro-apoptotic proteins such as Bax, Bak, Bad, Bim, Bid, Puma and Noxa. It also has anti-apoptotic proteins such as Bcl-2 and Bcl-X_L. These proteins determine whether the cell commits to apoptosis or aborts the process. Their primary function is regulating the release of cytochrome c from the mitochondria through changes on the membrane permeability of the mitochondria. The Bcl-2 family of proteins are regulated by the tumour suppressor protein *p53* (Schuler and Green, 2001).

1.1.4 Clearance of apoptotic cells

After induction of apoptosis (extrinsic/intrinsic) and execution of cells, the next step is the rapid recognition and clearance of the cell corpse. As apoptosis is a process committed to removal of unwanted cells, this step is arguably the most important step and is vital in the development, maintenance of tissue homeostasis, control of immune response and resolution of inflammation (Erwig and Henson, 2008).

Apoptotic cells are recognized, engulfed and digested by viable neighboring cells but it is thought that in cases where the level of cell death is very high and may overwhelm that ability of local 'amateur' phagocytes to remove dying cells (Monks *et al.*, 2005, Gregory and Devitt, 2004), professional phagocytes such as macrophages are recruited and act as the main phagocytes (Devitt & Marshall, 2011). These dying cell clearance events are thought to occur rapidly *in vivo* as free apoptotic cells are rarely seen, except under conditions of high cell death in disease (Kerr et al., 1972)The reason for the rapid and efficient clearance of apoptotic cells, is to prevent the apoptotic cells proceeding to necrotic and allowing leakage of potentially cytotoxic or antigenic contents that could provoke an autoimmune or inflammatory response (Gregory and Devitt, 2004). The clearance process appears complex with many phagocyte surface receptors and apoptotic cell surface ligands molecules and soluble adaptors identified as involved (**Figure 3**).

Figure 3. Schematic view of molecules associated with phagocyte-apoptotic cell interactions. The diagram depicts all phagocyte receptors, apoptotic cell-associated ligands and soluble bridging molecules that can promote recognition, binding and engulfment of AC by phagocytes. It is likely that all of these do not operate together as not all cells express all indicated molecules (Hawkins and Devitt, 2013).

Whilst a lot of work was done to identify the receptors, ligands and soluble factors, the assays were mostly based *in vitro* and so these studies did not take account of the *in vivo* need for professional phagocytes to be recruited to any site of cell death. So the process is made much more complex by recent studies of chemotactic molecules that are involved in recruiting phagocytes to sites of cell death (Hawkins & Devitt, 2013). Additionally, loss of *don't eat me* signals from viable cells is also important in allowing dying cells to be identified as different to viable cells and then specifically removed. The whole process of apoptotic cell clearance can be summarized in four main stages (**Figure 4**). The first one being phagocyte recruitment, followed by apoptotic cell recognition, tethering and, finally, signalling and engulfment.

Figure 4. Stages of apoptotic cell clearance. A schematic diagram showing the different stages of the apoptotic cell clearance process and molecules that have been suggested to function at each stage. (Hawkins and Devitt, 2013).

1.1.4.1 Phagocyte recruitment ('Find me' signals)

In the phagocyte recruitment stage, professional phagocytes (e.g. macrophages-MØ) are recruited via soluble molecules or apoptotic cell-derived extracellular vesicles (ACdEV) *find me* signals that are released by apoptotic cells. Examples of these signals are lysophosphatidylcholine (LPC) (Lauber *et al.*, 2003) sphingosine-1-phosphate (S1P) (Gude *et al.*, 2008), nucleotides (ATP/UTP) (Elliott *et al.*, 2009), chemokines such as CX3CL1 (fractalkine) (Truman *et al.*, 2008), and ACdEV and their components ICAM-3 (Torr *et al.*, 2011).

Lysophosphatidylcholine (LPC) is a lipid mediator that is released by apoptotic cells via caspase-3-dependent activation, where caspase-3 induces the cleavage and activation of calcium-independent phospholipase A2. The activated A2 processes the phosphatidylecholine into lysophosphatidylcholine (LPC) (Lauber *et al.*, 2003). The process of LPC release from apoptotic cells requires the ATP-binding cassette transporter (ABCA1) (Peter *et al.*, 2012). Once released from the apoptotic cells, LPC binds to the G-protein coupled receptor G2A on macrophages which subsequently assists the migration of the macrophages towards the apoptotic cells (Peter *et al.*, 2008). Sphingosine-1-phosphate (S1P) is another bioactive lipid mediator that is released by apoptotic cells to act as a *find me* signal which attracts phagocytes. The enzyme sphingosine kinase converts sphingosine to sphingosine-1-phosphate (S1P); the S1P is released from the apoptotic cells in a caspase-3 dependent manner. After the S1P release it binds to the S1P-R receptor on macrophages which facilitates cell migration towards the apoptotic cells (Gude et al., 2008). The third *find me* signals mentioned earlier are the nucleotides (ATP/UTP), which are released from apoptotic cells via a caspase-3 dependent manner which opens the annexin 1 channels on the dying cell plasma membrane releasing the nucleotides. Once the nucleotides are released they bind to the P2Y2 receptor on the macrophages leading to their chemotactic migration towards the apoptotic cells (Elliott et al., 2009).

Another *find me* signal released by apoptotic cells is the chemokine CX3CL1 (also known as fractalkine). Chemokines are well established as a broad family of attractive factors, used widely in the immune system for cell recruitment. In the case of apoptotic cell removal, fractalkine was the first identified chemokine to be involved. The fractalkine is produced as a membrane-associated protein where it is capable of acting as an adhesion molecule but it is released by apoptotic cells in association with ACdEV. The CX3CL1, once released, binds the CX3CR1 receptor on phagocytes (e.g. microglia and macrophages), which leads to phagocyte chemotactic migration towards

the apoptotic cells (Truman et al., 2008). The validation of CX3CL1 being a *find me* signal was shown *in vivo* where CX3CL1 deficient mice have shown a decrease in monocyte migration towards apoptotic cells (Truman et al., 2008).

More recently, ICAM-3 has been shown to promote macrophage migration to dying cells as a result of ICAM-3 release on ACdEV (Torr et al., 2011). However, relatively little is known about how ICAM-3 functions and this will be a major focus of this thesis.

In addition to the fact that apoptotic cells release chemotactic signals (*find me* signals), they also have been shown to release 'keep out' signals such as Lactoferrin that compete with *find me* signals, to prevent inflammatory cell migration. Lactoferrin is a glycoprotein that is known to inhibit neutrophil and granulocyte migration (Bournazou *et al.*, 2009, Bournazou *et al.*, 2010).

1.1.4.2 Recognition and Tethering ('Eat me' and 'don't eat me' signals)

Once phagocytes are recruited, they must identify ACs as phagocytic targets. This is achieved by the recognition of *eat me* signals on the ACs. These markers allow recognition and tethering of AC to phagocytes.

Several molecules on the ACs act as *eat me* markers. The most studied example is phosphatidylserine (PS), which gets exposed on the outer leaflet of the apoptotic cell plasma membrane (Fadok *et al.*, 1992, Fadok *et al.*, 2001b). PS is a well-established *eat me* signal, and it is hidden in the inner leaflet of the plasma membrane on viable cells, but once a cell undergoes apoptosis, PS flips out and acts as an *eat me* signal (Fadok et al., 2001b). When exposed, PS is recognized via specific PS recognition receptors such as brain-specific angiogenesis inhibitor-1 (BAI1) (Park *et al.*, 2007a), T cell immunoglobulin mucin-1 (TIM-1) and (TIM-4) (Kobayashi *et al.*, 2007) and Stabilin-2 (Park *et al.*, 2007b) or the scavenger receptors such as CD36 (Greenberg *et al.*, 2006).

In addition to these direct PS receptors, the PS may also bind indirectly to phagocyte receptors through the activity of soluble bridging molecules (e.g. milk fat globule; MFG-E8; protein S, Gas 6). These bridging molecules bridge PS to surface receptors on phagocytes. MFG-E8 bridges to the integrin $\alpha_V\beta_3$ whilst Gas6 and protein S bridge PS to the MerTK receptors on phagocytes (Bratton and Henson). In addition to the PS being an *eat me* signal, another molecule is exposed on the surface of apoptotic cells which serves also as an *eat me* signal and it is calreticulin (CRT). The CRT is

recognized and is bound to the phagocyte receptor CD91 which is a low density lipoprotein (LDL) (Gardai *et al.*, 2005).

Complement components also participate in AC clearance by opsonizing apoptotic cells e.g. C1q bridges AC to its receptor complex CD91/calreticulin on the phagocyte (Ogden *et al.*, 2001). Intercellular adhesion molecules (ICAM)-3 on apoptotic cells also participates in facilitating apoptotic leaukocyte binding to phagocytes (Moffatt *et al.*, 1999, Torr et al., 2011). Soluble CD14 has also been shown to bind PS and apoptotic cells, but its role in apoptotic cell clearance has been shown to be unclear (Devitt *et al.*, 2004).

There is a fine balance within the clearance process in terms of *eat me* versus *don't eat me* signals, and this balance holds the whole process intact. PS exposure has been shown to occur in viable cells but they are not engulfed by phagocytes. This suggests that the exposure of an *eat me* signal (PS) is not sufficient for cell clearance (van den Eijnde *et al.*, 2001, Segawa *et al.*, 2011) and this supports the idea that there are additional signals that prevent inappropriate cell engulfment. These *don't eat me* signals that are displayed on the cells, prevent the cell from being tethered and subsequently phagocytosed by a phagocyte. Examples of these *don't eat me* signals are CD31 and CD47. These signals are expressed on viable cells. CD31 (platelet and endothelial cell adhesion molecule) prevents viable cell ingestion, but as a cell undergoes apoptosis, CD31 becomes altered so that it cannot prevent the tethering and it changes its function to be an *eat me* signal (Brown *et al.*, 2002). CD47 (integrin-associated protein) has also been shown to exert its inhibitory effect on tethering viable cells via the receptor SIRPα (Jaiswal *et al.*, 2009).

1.1.4.3 Signaling and Engulfment

After the recognition/tethering stages, signalling events are initiated to reorganize the phagocyte cytoskeleton leading to engulfment and internalization of the apoptotic cells. So once tethering occurs, such as the binding of α_V integrins (Albert *et al.*, 2000), (TAM) family receptor Mer (Wu *et al.*, 2005), and (BA1) (Park et al., 2007a) to exposed PS on the apoptotic cells, they activate the CrkII-Dock180-ELMO complex, which in turn initiates Rac activation through GDP-GTP exchange (Brugnera *et al.*, 2002). The Rac activations leads to Scar/WAVE mediated cytoskeletal rearrangements (Miki *et al.*, 1998, Machesky and Insall). The phagocytes subsequently engulf the apoptotic cells following the cytoskeletal rearrangements, and the generated phagosome containing

the cell corpse fuses with lysosomes (McNeil *et al.*, 1983), which result in apoptotic cell digestion.

Whilst the clearance of apoptotic cells occurs throughout the body, the specific molecular pathways used may vary depending on the tissue and individual cells involved (Erwig and Henson, 2008). For example, ICAM-3 is only present on leukocytes (Fawcett *et al.*, 1992) and thus its activity as an *eat me* signal is limited to those cells.

1.1.5 Importance of apoptotic cell clearance

Apoptotic cell clearance is not entirely for the sake of cell corpse removal; it has a pivotal function in the control and resolution of inflammation (Gilroy and Lawrence, 2008). Inflammation is a firmly regulated process that is evoked by tissue injury from exogenous or endogenous stimuli. The main function of inflammation is the removal of the causative agent (e.g. microbes or toxins), removal of damaged or dead tissue and replacement with normal tissue to restore its function. The microbes and toxins (e.g. LPS) carry pathogen-associated molecular patterns (PAMPs) whilst damaged tissue carries damage-associated molecular patters (DAMPs). These patterns (PAMPs and DAMPs) are recognised by pattern recognition receptors (PRR) (e.g. Toll-Like receptors TLR) that are present on a range of immune cells including antigen-presenting cells (APC) such as macrophages and dendrtitic cells (DC) (Medzhitov, 2007). These ligand-receptor interactions help to initiate inflammation which can be classified into acute inflammation, which occurs over hours and resolves within a few days, and chronic inflammation, which occurs over longer times and persists (Serhan and Savill, 2005).

Acute inflammation (**Figure 5**) is typically characterized by the rapid influx of fluid and recruitment of blood granulocytes, normally neutrophils. This is followed by a wave of monocytes to the site of injury or infection. Neutrophils are guided and recruited to the site of injury by a range of factors and chemoattractants that promote cell recruitment. As PAMPs (e.g. LPS) or DAMPs are recognised and bound by PRR on the resident macrophages, the resident macrophages are activated and start to produce and secrete pro-inflammatory cytokines (e.g. TNF-α, IL-6), chemokines (e.g IL-8) lipid mediators (e.g. prostaglandins and leukotrienes) (Funk, 2001). These secreted cytokines, chemokines and lipid mediators activate local blood vessels and act as chemotactic signals that attract and recruit neutrophils from the blood, across the endothelium and through the tissue to the site of injury (Gilroy and Lawrence, 2008).

Once recruited, neutrophils start to eliminate pathogens by phagocytosis. The next phase is the resolution of the inflammatory reaction. This prevents inflammation from spreading, becoming chronic and eventually causing disease and thus the resolution phase helps to restore the tissue to its normal state. This phase is summarized by the reduction of recruitment of new leukocytes and removal of leukocytes that have been recruited. As part of the resolution phase, recruited neutrophils undergo apoptosis and release chemotactic signals (*find me* signals) to attract monocytes and macrophages (Serhan and Savill, 2005). Recruited monocytes mature locally into macrophages and thereby support the functions of the resident tissue macrophages to remove pathogens and also apoptotic cells. Collectively these events return the tissue to its pre-inflamed state and tissue function is restored.

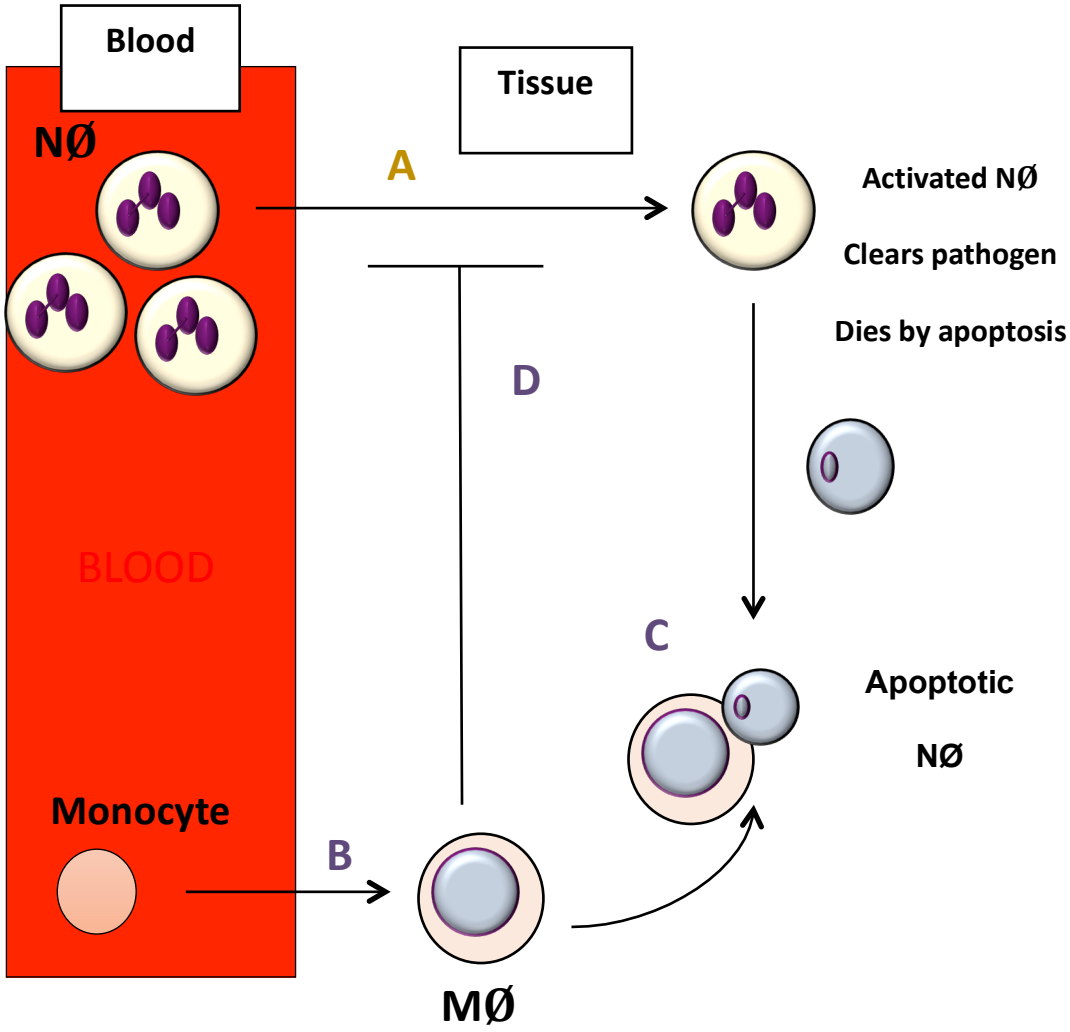

Figure 5. **Initiation and resolution of inflammation.** A schematic diagram showing the process of acute inflammation and its resolution. Inflammation is invoked by tissue injury (e.g. infection), which results in a rapid influx and recruitment of neutrophils (NØ) from the blood stream to the injured tissue site (A). NØ are guided by chemoatrractants to the site of injury, and then eliminate pathogens by phagocytosis and oxygen-dependent and independent mechanisms. After eliminating pathogens, NØ undergo apoptosis. Monocytes are recruited from the blood stream (B) and differentiate into MØ when moving from the blood into the tissue. Resolution of inflammation is mediated by MØ removing apoptotic NØ (C) and inhibiting further influx of viable inflammatory NØ through the use of 'keep out' signals (e.g. lactoferrin) (D). By preventing recruitment of new inflammatory cells and removal of dying NØ, resolution of inflammation can occur. Adapted from (Soehnlein and Lindbom, 2010).

Fadok *et al*. (1998b) demonstrated that the clearance process of apoptotic neutrophils was more than simple dead cell removal as it also caused immune modulation with an inhibition of proinflammatory mediators (e.g. GM-CSF, IL-1β, IL-8 and TNF-α) production by macrophages. It also showed an increase in the production of anti-inflammatory mediator TGF-β1. This work illustrates an important function of apoptotic

cell clearance in the resolution of inflammation, where it removes leukocytes, produces anti-inflammatory mediators and suppresses pro-inflammatory mediators. It also has been reported that another anti-inflammatory mediator, IL-10, is produced during the clearance of apoptotic cells (Fadok *et al.*, 1998, Voll *et al.*, 1997). The anti-inflammatory effects of apoptotic cells have also been more widely reported, with PS recognition as a main event in the induction of TGF-β1 secretion (Huynh *et al.*, 2002, Freire-de-Lima *et al.*, 2006).

The importance of apoptotic cell clearance is seen dramatically when the process fails or is poorly controlled as it causes the progression of acute inflammation to chronic inflammation and autoimmunity. If apoptotic cells are not efficiently cleared, their membrane integrity is lost and the apoptotic cells progress to secondary necrosis. The progression to secondary necrosis is accompanied by the release of intracellular contents from necrotic cells and these can provoke inflammatory responses. Necrotic cells also have the ability to switch macrophage responses from anti-inflammatory to pro-inflammatory (Gilroy and Lawrence, 2008). The dysfunctional clearance of apoptotic cells has been linked to the development of autoimmune diseases, such as systemic lupus erythematosus (SLE) and rheumatoid arthritis (Elliott and Ravichandran, 2010). SLE development can be caused by C1q deficiency. C1q is vital in AC clearance: C1q deficient mice were shown to have detectable free (i.e. non-macrophage associated) apoptotic cells not cleared properly, the apoptotic cells became necrotic leading to loss of membrane integrity and release of intracellular contents such as high mobility group 1 (HMGB1) which led to the autoimmune disease SLE (Botto and Walport, 2002, Scaffidi *et al.*, 2002). The C1q deficient mouse is the most clearly defined causal link between a failure in apoptotic cell clearance and chronic inflammation.

Atherosclerosis, a cardiovascular condition, is also driven, at least in part, by dysfunctional AC clearance. Within the atherosclerotic plaque macrophages gorge upon lipid present in the wall of an affected artery and they become foam cells and die in response to the toxic environment. The plaque develops as monocytes/macrophages are recruited to remove dying foam cells but become trapped and they too die. The result is a failure of AC clearance and persistent recruitment of phagocytes, thus the pathology of the disease is driven without any resolution of the inflammation (Björkerud and Björkerud, 1996). It is therefore desirable to understand how MØ are recruited to AC as this may allow the design of new therapies to interfere with recruitment, as a potential treatment for atherosclerosis.

1.2 Origin of Extracellular Vesicles (EVs) and their Generation/Release

Extracellular vesicles (EVs) are membrane vesicles that are released in to the extracellular environment from most cell types ranging from prokaryotes to higher eukaryotes both in physiological and pathological conditions (Yanez-Mo *et al.*, 2015).

The EVs are spherically shaped and encapsulated by lipid bilayers and contain cargo of lipids, proteins and nucleic acids such as mRNA and miRNA (Valadi *et al.*, 2007). An important challenge in the field of EV research is to define the function of the many different cargo molecules carried by EV.

EVs are found in human body fluids such as semen (Park *et al.*, 2011), saliva (Ogawa *et al.*, 2011), urine and breast milk (Admyre *et al.*, 2007). They are heterogeneous in phenotype but they have been classified broadly into three main categories: apoptotic bodies, microparticles/microvesicles and exosomes (Thery *et al.*, 2009). These categories are classified according to their size, the arbitrary size of them ranges from 500-5000 nm for apoptotic bodies, 100-500 nm for microvesicles and exosomes are from 40-100 nm (Thery et al., 2009, El Andaloussi *et al.*, 2013, Raposo and Stoorvogel, 2013). In Kerr *et al.,* (1972) which first described the apoptotic bodies, have not characterized their size specifically, but have said they “vary greatly”. The sizes of the three different categories of EVs are entirely arbitrary and it is not clear that size of EV defines function. It seems most likely that the function of any EV will depend on its molecular composition though size may affect the ability of EV to diffuse away from where they were produced.

Apoptotic bodies and microparticles/microvesicles are released from the plasma membrane when the cells are undergoing apoptosis. However, microparticles/microvesicles are also shed from viable cells whilst exosomes come from the intracellular compartment rather than the plasma membrane. The release of microvesicles is by budding from the plasma membrane, whilst the exosomes are formed intracellulary via the endocytic invagination, which are released into a structure called multivesicular body (MVB) that fuses the with plasma membrane to release its cargo of small exosomes to the extracellular space.(Harding *et al.*, 1983, Raposo *et al.*, 1996). An ongoing challenge within the field is to establish a standard method that allows the proper characterization of the different types of EVs in terms of their size, protein content, morphology and buoyant density (Bobrie *et al.*, 2011).

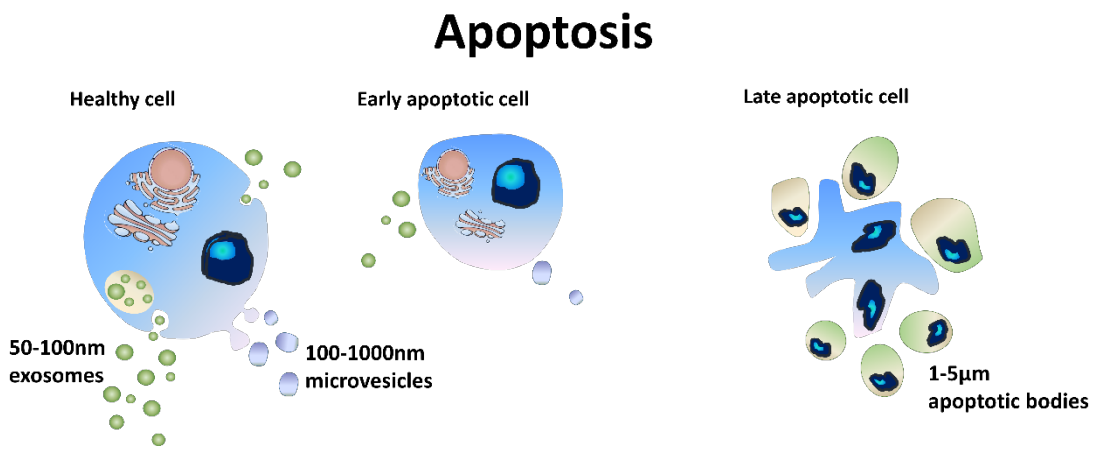

Figure 6. **A schematic diagram of the generation of extracellular vesicles.** Exosomes are small and derived from the intracellular compartment of viable cells. Apoptotic cells release small vesicles (microparticles/microvesicles) from the plasma membrane and larger plasma membrane-derived vesicles (apoptotic bodies).

1.2.1 Molecular markers of EVs

EVs have certain molecular markers that help to identify them and the cell that they came from. The first example is the well-established marker tetraspanins. Tetraspanins (CD63, CD9, CD81) are cell surface membrane protein markers that are very abundant on EVs. Initially they were considered specific to exosomes but were also observed in apoptotic bodies and microvesicles (Yanez-Mo et al., 2015). As CD antigens gain their designation (i.e. their 'number') from being expressed as cell surface markers and identified through the Human Leukocyte Differentiation Antigen Workshops, it does not seem likely that these CD antigens alone can be specific markers of exosomes. Phosphatidylserine (PS) is another marker and is found on both apoptotic bodies and microvesicles (Schwende *et al.*, 1996). There are many studies looking at EV from different cellular sources, purified by different methods and it is clear that there is no single diagnostic marker for any one particular EV. So a key challenge within the field is a standard method for isolating EV and a robust method to identify them.

Cytosolic proteins such as heat shock proteins (HSPs), Tsg101 and the Endosomal Sorting Complex Required for Transport (ESCRT-3) are also molecular markers but they are found on exosomes (Raposo and Stoorvogel, 2013).The ESCRT proteins are involved in the formation of exosomes and their release. ESCRT consists of four complexes, where ESCRT-0 is responsible for cargo clustering, ESCRT-I and ESCRT-II are involved in inducing bud formation, whereas ESCRT-III is involved with vesicle

formation. Tsg101 is a member of the ESCRT protein family, specifically an ESCRT-I component; it was shown in (Baietti *et al.*, 2012) when Tsg101 was depleted it caused reduced secretion of exosomes in the tumour cells.

1.2.2 EV interaction with recipient cells

EVs have been shown to have a vital role in cellular communication, where they can transfer their contents (nuclear material, lipids and protein; **Figure 7**) to neighboring (recipient) cells, which can elicit reactions. EVs have been shown to be involved in inducing responses in many cells and in affecting many processes. Inflammation, immune disorders, neurological diseases, and cancer. The involvement of EVs in cellular communication gives it an enormous potential in diagnostic and therapeutic applications.

If communication is a main function of EV, then the way they interact with other cells is important for delivering their 'message' and perhaps delivering it specifically to some cells over others. Multiple methods of EV uptake have been studied. These can be broadly divided into endocytosis (where the EV as a whole is taken up into a cell by one of a variety of mechanisms) or membrane fusion (where the EV lipid bilayer fuses with the recipient cell membrane to deliver the intracellular contents into the cytosol of the recipient cell. However there are likely to be many uptake mechanisms that depend on a range of specific ligands (on EV) and receptors (on recipient cells). This complexity is similar to that seen with the removal of AC by MØ. Endocytosis can be sub-divided in to a range of processes that can vary a lot, including: phagocytosis, micropinocytosis, clathrin-mediated endocytosis and non-clathrin mediated endocytosis (e.g. through caveolae) reviewed by (Mulcahy *et al.*, 2014).

The ligand-receptor interactions that govern the EV-recipient cell interactions are widely studied. Several EV proteins have been suggested to interact with membrane receptors of the target cells. For example, antibodies to CD9 and CD81 expressed on exosomes have been shown to reduce EV uptake by dendritic cells (Morelli *et al.*, 2004). This study also showed that antibodies to LFA-1 and ICAM-1reduced EV uptake, and MFG-E8 promoted EV uptake. Heparin sulphate proteoglycans (HSPGs) on the recipient cell have also been suggested to be involved in EV uptake. It is interesting that some of the factors involved in the uptake of EV are also those involved in the uptake of apoptotic cells. For example, MFG-E8 opsonises EV (Théry *et al.*, 1999) and apoptotic cells. HSPGs on recipients cells mediate uptake of EV (Morelli et al., 2004) and apoptotic cells (Hanayama *et al.*, 2002, Nadella *et al.*, 2015).

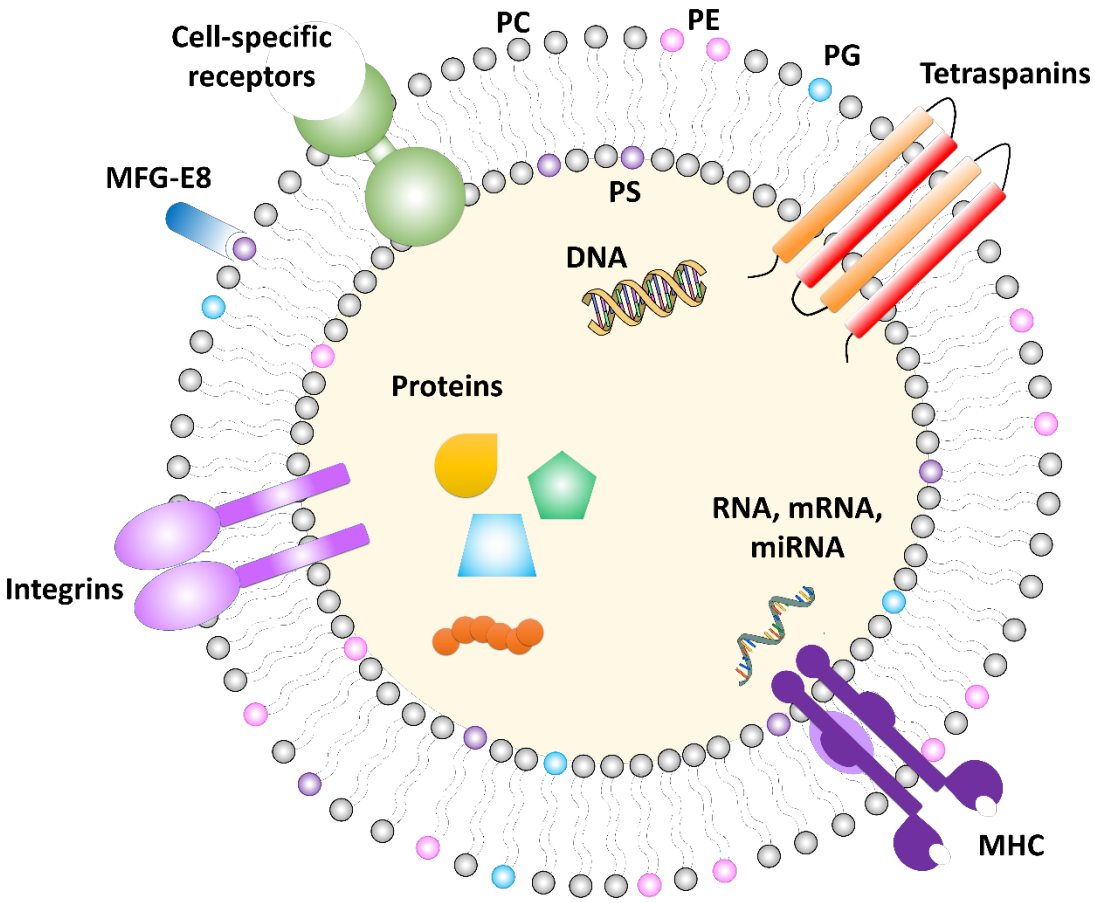

Figure 7. A schematic representation of the structure of an extracellular vesicle. EV carry a range of cargo molecules within their lipid bilayer. At the surface, a range of proteins and lipids may act as ligands to interact specifically with recipient cells directly or via bridging molecules (e.g. MFG-E8).

1.2.2 Apoptotic cell-derived extracellular vesicles (ACdEV) and their involvement in cell migration.

It has been known for nearly 50 years that cells undergoing apoptosis release EV and that these are of greatly varying size with large EV being eaten by phagocytes and smaller EV diffusing away (Kerr et al., 1972). However, the function of these EV has not been shown clearly until more recently. Recent research has shown that EVs are released from dying leukocytes and that these contain surface molecules lost from the surface of the dying cell (Segundo et al., 1999, Truman et al., 2008, Torr et al., 2011). To avoid any confusion over the source (plasma membrane or multivesicular body) or size of the EV, these have recently been termed 'apoptotic cell-derived extracellular vesicles' (ACdEV) (Hawkins and Devitt, 2013). These ACdEV have been shown to have chemoattractive abilities, where they attract the macrophages (Segundo et al., 1999, Truman et al., 2008, Torr et al., 2011). Truman *et al*. demonstrated that the

chemoattractive abilities were specifically due to the presence of the chemokine CX3CL1 (fractalkine). Torr *et al*. revealed that ICAM-3 on ACdEV also played a role in the chemoattractive abilities (Torr et al., 2011). These findings were the first in attempting to explain how ACdEV and its contents (lipids, proteins) are involved in cell migration. So it seems clear that ACdEV are more functional than simply being smaller dying cell fragments that are easier for a phagocyte to eat. However there is much more that needs to be understood about the ACdEV content and function.

1.3 Macrophages; the cell death janitors

Macrophages are essential cells of the innate immune system that are remarkably plastic, having their phenotype change in response to the local microenvironment. Their phenotypes can be classified into two broad categories: (M1) the classically-activated macrophages, which are pro-inflammatory, cytotoxic macrophages that respond to pathogenic stimuli, and (M2) the alternatively-activated macrophages that are reparative as they clear apoptotic cells and help to resolve inflammation (Martinez *et al.*, 2008, Mosser and Edwards, 2008). In both phenotypes the method of response is engulfment and phagocytosis i.e. removal of waste, hence the nickname 'janitors'. However the anti-inflammatory effects of apoptotic cell clearance suggests that their role is more than simple waste disposal (Savill *et al.*, 2002).

Practically all tissues have macrophage-related cells residing in them, such as Kuppfer cells in the liver, microglia in the central nervous system and osteoblasts in bone. In addition, macrophages may differentiate from monocytes circulating in the blood. The circulating monocytes can migrate into tissues in response to tissue damage, infection or the presence of dead and dying cells (Martinez et al., 2008). Together the resident and recruited cells promote tissue homeostasis.

Monocytes originate in the bone marrow from hematopoietic stem cells. Their differentiation starts from myeloid progenitor cells (granulocyte/macrophage colony forming- units) that proceed to monoblast, pro-monocytes and become monocytes. The formed monocytes leave the bone marrow and enter the blood stream. Monocytes have at least two subpopulations that are characterized by their surface receptor expressions, the classical monocytes ($CD14^{hi}CD16^{-}$) and the non-classical monocytes ($CD14^{low}CD16^{+}$) (Geissmann *et al.*, 2003).

1.4 Intercellular adhesion molecule 3 (ICAM-3)

ICAM-3 (CD50) is a highly glycosylated adhesion molecule that belongs to the immunoglobulin superfamily (IgSF). It is the third member of the ICAM family. It is exclusively expressed on leukocytes and has five extracellular Ig-like domains, which are highly similar to the equivalent domains of ICAM-1 and 2 (Fawcett et al., 1992, de Fougerolles *et al.*, 1994). The similarity is observed at the amino acid level, where 52% of the amino acids on ICAM-3 are identical to ICAM-1, whereas 37% of the amino acids on the first two domains are identical to the two domains of ICAM-2 (de Fougerolles et al., 1994). Purified ICAM-3 from T-lymphocytic cell lines showed molecular size bands between 110-130kD, while purified ICAM-3 from neutrophils showed between 120-160kD, but all were reduced to 62kD after N-glycanase treatment (de Fougerolles *et al.*, 1995). ICAM-3 is heavily glycosylated and is exclusively N- linked, which has fifteen potential N-linked glycosylation sites, and it is comprised of approximately six carbohydrate chains per ICAM-3 molecule (Funatsu *et al.*, 2001). The three ICAMs also share the function of being a ligand for the β_2 integrin LFA-1 (CD11a/CD18, α_L/β_2). Regardless of the homology between these ICAMs, they have specific specialized roles. ICAM-3 also binds to another β_2 integrin ($\alpha_d\beta_2$) (Bell *et al.*, 1998). ICAM-3 is considered to be an adhesion molecule with some involvement in signal transduction and initiation of immune responses by promoting interactions between T cells and antigen-presenting cells. The signal transducing abilities are observed when ICAM-3 is activated; it changes the Ca^{2+} flux and phosphorylation in the T cell (Bell et al., 1998). Importantly, the function of ICAM-3 appears different between viable cells and apoptotic cells though the reason for this is not fully understood.

1.4.1 Functions of ICAM-3 on viable leukocytes

It has been shown that ICAM-3 is expressed constitutively on resting T lymphocytes, where it has a function in mediating the interaction between the T lymphocytes and antigen presenting cells (APC) through LFA-1/ICAM-3 binding (Montoya *et al.*, 2002). ICAM-3 has another receptor other than the integrins, where it also facilitates the binding of T lymphocytes to APC and eventual T cell activation. This receptor is the dendritic cell-specific ICAM-3 grabbing non-integrin (DC-SIGN). DC-SIGN is a C type lectin expressed by dendritic cells, a professional APC and considered the strongest APC, capable of activating naïve T cells (Banchereau and Steinman, 1998). Being a C type lectin, Ca^{2+} governs the binding of ICAM-3 to DC-SIGN through Ca^{2+}dependent

extracellular carbohydrate recognition domains (CRDS). In summary, ICAM-3 functions on viable cells to mediate intercellular interactions to initiate an immune response.

1.4.2 Functions of ICAM-3 on apoptotic leukocytes

As leukocytes die by apoptosis, the function of ICAM-3 shifts from being part of immune response initiation to aiding the clearance of apoptotic cells (Moffatt et al., 1999) but the mechanism responsible for this change of function remain unknown. ICAM-3 becomes an important apoptotic cell-associated ligand, where it acts as both a *find me* signal and *eat me* signal. ICAM-3 acts as a *find me* signal when released on extracellular vesicles (EV) from the apoptotic cells. These EV diffuse away from the dying cell to attract phagocytes in a directed manner, chemotaxis (Segundo et al., 1999, Torr et al., 2011). The '*eat me'* function of ICAM-3 occurs when ICAM-3 on the dying cell corpse (rather than the EV) acts as a ligand for macrophage receptors. This ICAM-3 was shown to promote interaction between the macrophages and the apoptotic cell (Moffatt *et al.*, 1999). More recent work has more precisely shown that ICAM-3 acts to promote tethering of apoptotic cells to phagocytes, a role that supports ICAM-3 as an important adhesion molecule (Torr et al., 2011).

1.4.3 Experimental measures on ICAM-3 function on apoptotic cells

Moffatt *et al*. identified ICAM-3 function in apoptotic cell clearance through the use of anti-ICAM-3 mAbs (Moffatt et al., 1999). They induced B lymphocyte cells into apoptosis by three different mechanisms, 1) Ca^{2+} ionophore ionomycin, 2) the protein kinase C-inhibitor staurosporine and 3) low temperature pretreatment (cold shock), then pretreated cells with anti-ICAM-3 mAbs (3A9 & BU68) before a co-incubation with macrophages. These mAbs are ICAM-3 domain 1 region specific (the domain most distant to the cell membrane). These studies revealed that these mAbs (but not other mAbs that bound elsewhere to ICAM-3) prevented the interaction between the apoptotic B-lymphocytes with the macrophages. The results confirmed that the method of apoptosis induction did not affect the involvement of ICAM-3 and suggested ICAM-3 as an important ligand for apoptotic leukocyte clearance.

Within this study Moffatt *et al.* (1999) tested if ICAM-3 on viable phagocyte cells was active in removing AC. ICAM-3 is leukocyte-restricted and present on both the viable macrophage and the apoptotic B cells but preincubation of macrophages with the ICAM-3 mAb, resulted in no inhibition of the interaction between macrophages/apoptotic B-lymphocytes. Pretreatment of apoptotic B-lymphocytes on

the other hand, showed an inhibition in the interaction between macrophages/apoptotic B-lymphocytes suggesting that apoptotic cell-associated ICAM-3, rather than MØ-associated ICAM-3, is functional in allowing the dying cell to be recognized by macrophages, whereas in viable cells (macrophages) ICAM-3 is nonfunctional for this phagocytosis. However, the alterations that must occur during apoptosis to allow this new function of ICAM-3 were not identified and are still not known.

Moffat *et al.* (1999) also tested the functionality of ICAM-3 on non-leukocyte cells by overexpression of ICAM-3 on HEK 293 human embryonic kidney derived cells. Apoptotic HEK 293 cells were recognized by macrophages but this recognition improved if ICAM-3 was present. ICAM-3 mAbs showed inhibition of this interaction. This work clearly showed that ICAM-3 on apoptotic cells promoted clearance of apoptotic cells. However the nature of the receptor to which ICAM-3 bound remains unclear.

In order to address this, this work also tested the known ICAM-3 receptors LFA-1 and $\alpha_d\beta_2$ integrins to assess their role in the interaction between the macrophages and the apoptotic leukocytes. Six mAb (three to CD11a, three CD18) that were known to block binding of LFA-1 to ICAM 1, ICAM-2, and ICAM-3 were tested and they all failed to inhibit the binding of macrophages to ICAM-3 on apoptotic leukocytes. Also, α_d specific mAb were tested and no effect was shown on the interaction. These data suggest that the receptor for ICAM-3 on apoptotic cells is likely to be different to the receptor for ICAM-3 on viable cells. To support this further, another mAb (KIM 127) was used to activate LFA-1 receptor on the macrophages and this promoted binding to viable cells but not apoptotic cells. These data strongly suggest that the known ICAM-3 receptors LFA-1, $\alpha_d\beta_2$ and $\alpha_v\beta_3$ are not involved in the binding of apoptotic cell ICAM-3 for the promotion of apoptotic leukocyte with macrophages. These results suggest that during apoptosis, the ability of interaction between ICAM-3 and LFA-1 is lost and that ICAM-3 is recognized by a different receptor.

Another approach on ICAM-3 function has been published that claims LFA-1 as the receptor for both viable and apoptotic cell ICAM-3 (Kristóf *et al.*, 2013). In their work they used apoptotic neuotrophils as their leukocyte cell source, whilst Moffatt *et al* (1999) used apoptotic B lymphocytes as the leukocyte cell source. Both papers blocked the LFA-1 integrins (with mAb). Kristóf *et al.* (2013) also silenced the α (CD11a) and β (CD18) integrins, while the Moffatt *et al.* (1999) activated LFA-1 receptors using the mAb (KIM 127) which promotes binding between LFA-1 and ICAM-3. It is not clear why both papers suggest different results. However, the mechanism

that allows ICAM-3 to be a ligand for phagocytosis (with apoptotic cells) or simply cell binding (viable cells) remains to be addressed and is an aim of current research project.

In addition, CD14 has been suggested as a possible receptor for ICAM-3 (Moffatt *et al.*, 1999). However, this claim was based on the observation that mAbs to ICAM-3 and CD14 do not provide any additive effect on blocking apoptotic cell clearance. There has been no formal proof that CD14 and ICAM-3 interact directly. It is noteworthy, that many papers have suggested that CD14 and ICAM-3 interact directly, despite the lack of proof.

Recently, a more defined and broad role for ICAM-3's function has been demonstrated. Torr *et al*. (2011) also tested the ICAM-3 abilities in aiding apoptotic cell clearance and to understand why during apoptosis, the level of surface ICAM-3 reduced despite it becoming important in removal of dying leukocytes (Torr et al., 2011). They demonstrated that apoptotic cell-associated ICAM-3 acts to tether the apoptotic cell to phagocytes. This was revealed by co-incubating apoptotic leukocytes with phagocytes at 21°C, a temperature which allows tethering but not phagocytosis. They compared the results with the incubation in 37°C. Also, apoptotic cells expressing low levels of ICAM-3 (ICAM-3^{LOW} Burkitt's lymphoma (BL) cells) showed decreased tethering, implying that ICAM-3 is a tethering ligand for apoptotic cells. They have also shown that ICAM-3 levels reduce as a result of it being released into EV during apoptosis.

1.4.4 What underlies the difference in ICAM-3 function on viable and apoptotic cells?

Three studies have focused on ICAM-3 in apoptotic cell clearance and have addressed different aspects of the ICAM-3 function on apoptotic leukocytes (Moffatt et al., 1999, Torr et al., 2011, Kristóf et al., 2013). The primary outcome from these studies is that ICAM-3 on viable cells functions differently to ICAM-3 on apoptotic cells and suggests that ICAM-3 goes through qualitative changes when cells undergo apoptosis. That in turn causes an alteration to the receptor binding properties and allows direct or indirect interaction with a macrophage-borne molecule or molecular complex that leads to apoptotic cell engulfment. However, the molecular and cellular changes that cause this change in ICAM-3 function remain poorly defined and the receptor to which apoptotic cell ICAM-3 binds remains contentious.

1.5 Aims and Objectives

Whilst there is existing knowledge of the role of ICAM-3 as a molecule on AC that tethers AC to MØ (Moffatt *et al*., 1999; Torr *et al*., 2011) and an important molecule on EV that recruits MØ (Torr *et al*., 2011), there is little detail on ICAM-3's mechanism of action. This PhD project will address the gaps in our current understanding by addressing the following research questions:

1. What is the precise role of ICAM-3 on EV?

Whilst ICAM-3 is active in recruiting MØ, it is not clear if (a) ICAM-3 on EVs released from AC acts to tether EV efficiently to MØ so that they can be activated to migrate (through other molecules providing an activating signal); or (b) EV bind to MØ independently of ICAM-3 but the presence of ICAM-3 can provide an activating signal to the MØ? As ICAM-3 is an established adhesion molecule and is known to tether AC to MØ, this project will test the hypothesis that ICAM-3 on EV acts to bind EV efficiently to MØ and thus promote MØ activation to migrate.

2. Do EV have functions other than promoting MØ attraction?

It is established that AC exert anti-inflammatory effects on phagocytes (Fadok et al., 1998) but activity of EV in this regard has not been addressed. This project will therefore address the research questions: Are EV anti-inflammatory and, if so, is ICAM-3 involved in this function? As AC are known to be anti-inflammatory and EV are derived from the surface of AC, this project will test the hypothesis that EV are anti-inflammatory particles like AC, and that ICAM-3 is essential for this anti-inflammatory function.

3. Does ICAM-3 function *in vivo* for the clearance of apoptotic cells?

To date all research addressing ICAM-3 has been *in vitro*. *In vivo* studies to assess ICAM-3 function are absent because ICAM-3 is not expressed in rodents (usual models for *in vivo* research). This PhD project will assess whether ICAM-3 functions *in vivo* for the attraction of MØ and removal of AC by introducing human BL cells into immune-compromised mice. An immune-compromised mouse is required so the BL tumour cells are not rejected. *In situ* spontaneous death of these human BL cells will release ICAM-3 on EV and macrophage migration to these sites can then be assessed in the presence or absence of blocking mAbs.

4. What changes happen to ICAM-3 in the viable to apoptotic cell transition that allows ICAM-3 can take on its new function to mediate apoptotic cell engulfment?

Previous work has shown that ICAM-3 on viable and apoptotic cells appears unchanged in size by western blot analyses suggesting no large difference in structure between ICAM-3 on viable and apoptotic cells (Moffatt et al., 1999, Torr et al., 2011). Thus the hypothesis to be tested here is that ICAM-3, on the surface of apoptotic and viable cells, is associated with different partner proteins and that this alteration permits it to function differently in each cell context.

2. Materials and Methods

2.1 Equipment and software

- Automated Cell Tracking system and accompanying software (Cell-IQ, CM technologies, Tampere, Finland)
- Chemotaxis Dunn chamber, DCC100 (Hawksley and sons Ltd, West Sussex, UK)
- Chromato-Vue C-71 light box and UVX radiometer. (UV-P Inc., Upland, CA, USA)
- Confocal microscope (TCS SP5 II by Leica Microsystems, Frankfurt am Mein, Germany)
- Cryo-freezing container NALGENE (Fisher, Loughborough, UK)
- Electrophoresis apparatus and Western Blot wet transfer system (BIO-RAD, Watford, UK)
- Electrospray emitter tips (TaperTip, New Objective, Berlin, Germany)
- Flow cytometer (FC500, Beckman Coulter, High Wycombe, UK)
- Flow cytometric analysis software (FlowJo, Oregon, USA)
- Haemocytometer (Camlab Ltd, Cambridge, UK)
- Inverted fluorescence microscope (Zeiss Axiovert 200M, Hertfordshire, UK)
- Mascot deamon (MatrixScience, Ltd, London, UK)
- Mass spectrometer (5600 Triple Tof, ABSciex, Warrington, UK)
- Multiplex (MAGPIX, Powered by Luminex XMAP technology, Austin, Texas, USA)
- Nano drop (1000 spectrophotomer, Thermo Fisher Scientific, Warrington, UK)
- Nano high performance liquid chromatoghraphy analytical column (Acclaim™ PepMap™ C18, 3 µm, 100 Å, 75 µm x 150 mm, Thermo Fisher Scientific, Warrington, UK)
- Nano high performance liquid chromatography trap column (PepMap™ C18, 5 µm, 100 Å, 300 µm x 1 mm, Thermo Scientific, UK)
- Nano high performance liquid chromatotography with automated autosampler (nLC, 3000 Dionex, Therm Scientific, UK)
- Plate reader (BioTek EL800, BioTek Instruments, UK)
- Plate reader (MULTISKAN GO spectrophotometer, Thermo Scientific, UK)
- Progenesis QI for Proteomics, Nonlinear Dynamics, Waters, Manchester, UK

- qNano Particle analyser (Izon Science Ltd, Oxford, UK)
- qPCR Machine (STRATAGENE-Mx3000P-Agilent Technologies, USA)
- Tabletop centrifuges (Centrifuge 5418, Eppendorf, Germany)
- Thermal cycler (TECHNE TC-312, GENEFLOW, UK)
- Thermoshaker (Thermo Scientific, UK)
- Ultracentrifuges (Optima MAX-UP, Optima XP, Beckman-Coulter, USA)
- Ultracentrifuge rotors (TLA-110, 45Ti, 70Ti, Beckman-Coulter, USA)
- Vacuum concentrator (Concentrator plus with rotor F-45-48-11, Eppendorf, Hamburg, Germany)

2.2 Reagents and chemicals

- Annexin V-FITC / Propidium iodide staining kit (Bender MedSystems, Vienna, Austria)
- Anisomycin (Abcam, UK)
- Bio-Rad protein assay kit **(**Bio-Rad, Hemel Hempstead, UK)
- BODIPY stain: N-(2-aminoethyl)maleimade (molecular probes by life technologies, UK)
- Dihydroxyvitamin D3 (vitamin D3) (Enzo Life Sciences, Exeter, UK)
- ECL Chemiluminescence Reagents (Thermo Scientific, UK)
- Geneticin G418 (Sigma-Aldrich)
- Lipopolysaccharide from Escherichia coli 0111:B4 (Sigma-Aldrich, UK)
- Pierce Co-Immunoprecipitation kit (Thermo Scientific, UK)
- PKH26 Red Fluorescent Cell Linker Kit for General Cell Membrane Labeling (Sigma-Aldrich, UK)
- Precision nanoScript 2 Reverse transcription kit (Primerdesign Ltd, UK)
- Restriction enzymes: *Not* I-HF, *Sca* I-HF & *Hind* III-HF (New England Biolabs, UK)
- TNF-α ELISA kit (R&D, UK)
- Trypsin-EDTA solution (Sigma-Aldrich, UK)

2.3 Antibodies

- Goat Anti-mouse IgG FITC conjugated (Sigma-Aldrich, UK)
- Mouse IgG isotype control (MOPC21, Sigma-Aldrich, UK)
- mAb mouse IgG isotype control-PE (MOPC21, Biolegend, UK)
- mAb anti-human CD14-PE (Biolegend, UK)

- Horse Anti-mouse IgG HRP-linked (Cell Signaling TECHNOLOGY, UK)
- Mouse anti-human ICAM-3 Monoclonal Antibody (MA4, MEDIMABS, Quebec, Canada)
- Anti-mouse β-Actin (Sigma-Aldrich, UK)
- mAb mouse IgG His Tag Antibody (R&D systems, UK)
- Anti-mouse IgG, HRP conjugated antibody (New England Biolabs, UK)
- Mouse anti-human ICAM-3 Monoclonal Antibody (Abcam, UK)
- Anti-rabbit IgG HRP conjugated antibody (Abcam, UK)
- mAb anti-human CD50-PE (ICAM-3) (Biolegend, UK)
- Anti-CD204 Ab (50129-RP02-SI Sino Biologicals); Anti-rabbit-biotin (Vector BA-1000)
- Anti-F4/80 mAb (Invitrogen MF48000).

2.4 Cell Culture

2.4.1 Cell lines

- **Mutu I BL cells**: EBV-positive Burkitt's lymphoma cell lines provided kindly by Prof Gregory (Edinburgh University). Mutu cells expressing normal amounts of ICAM-3 were termed wild-type (WT) (Gregory *et al.*, 1990). A Mutu variant that expresses low levels of ICAM-3 (ICAM-3^{LOW}) were isolated by sequential flow cytometry and characterized previously (Torr et al., 2011).
- **THP-1**: Human monocytic leukaemia cell lines, they are capable of differentiating into macrophages when stimulated with VD3 (Dihydroxyvitamin D3) or PMA. ATCC Cell ine TIB-202
- **Jurkat**: Human T cell leukemia cell line. ATCC Cell line CRL-1573.
- **HeLa**: An adherent human cervical cancer cell line. ATCC Cell line CCL-2.
- **HEK-293**: An adherent adenovirus transformed human embryonic kidney cell lines (Graham *et al.*, 1977)

2.4.2 Cell culture solutions and media

- **Growth medium for suspension cells complete RPMI (cRPMI):** RPMI 1640 supplemented with 100 µg/ml streptomycin, 2 mM L-glutamine & 10% (v/v) foetal bovine serum.
- **Growth medium for adherent cell complete DMEM (cDMEM):** DMEM, 100µg/ml streptomycin, 2 mM L-glutamine & 10% (v/v) foetal bovine serum.

- **Medium for Macrophage-Apoptotic cell interactions:** serum-free RPMI, 100 µg/ml streptomycin, 2 mM L-glutamine & 0.2% (w/v) Bovine serum albumin (BSA).
- **Cell freezing medium:** 5% (v/v) Dimethyl sulphoxide (DMSO) in FBS.
- **Flow cytometry wash buffer:** 0.1% (w/v) BSA in PBS.
- **Binding buffer (BB):** 150 mM $NaCl_2$, 10 mM HEPES pH 7.4, 2.5 mM $CaCl_2$ in dH_2O.
- **Jenner-Giemsa (JG) Buffer:** 200 mM Na_2HPO_4 +190 ml of 200 mM NaH_2PO_4 until pH is 5.6, dH_2O is added until 1 l.

2.4.2 Tissue culture

All cell lines were cultured routinely every 2-3 days in pre-warmed complete RPMI (for suspension cultures) or complete DMEM (for adherent cells) medium and maintained in a humidified incubator (37 °C, 5% CO_2). For suspension cells, the culturing process was performed under aseptic conditions by re-suspending the cells, replacing 70-80% of the culture medium with fresh prewarmed cRPMI medium. For adherent cell lines, cultures were rinsed with 1× PBS, then treated with 0.05% Trypsin/EDTA in PBS for 5-10 min. Following incubation, the flask was tapped to detach adherent cells; cells were resuspended in cDMEM, 80-90% of cells removed and stored for further use as appropriate, and the flask refilled with fresh prewarmed medium (cDMEM).

2.4.3 Freezing the cells

Healthy cells were pelleted (300x*g*) centrifugation and resuspended in 1 ml of 5% (v/v) Dimethyl sulphoxide (DMSO) in FBS. The resuspended pellets are placed in cryovials and placed in -80 °C in the cryovial containers for 1-2 days. Afterwards the cryovials are transferred to the liquid vapour cylinders for long duration storage.

2.4.4 Thawing the cells

Frozen cells were kept in cryovials in nitrogen vapour. They were thawed rapidly by being placed in a 37 °C water bath. After the cells were defrosted they were transferred under under aseptic conditions to a 25 ml universal tube, and 10 ml prewarmed complete RPMI medium added dropwise with mixing. Then the cells were centrifuged at 300x*g* for 5 min, the supernatant discarded and cells resuspended in complete RMI media before being kept in the incubator at 37 °C to grow.

Cells were routinely incubated for 48-72 h at 37 °C to grow and then passed to yield

the cultured cells. Cells were split with a ratio of 1/3 (3.5 ml of cells are kept in the culture flask and 7 ml of complete RPMI medium is added). The spare cells were either used in experiments, frozen down or discarded.

2.5 Differentiation of THP-1 into macrophage-like cells

THP-1 cells were differentiated into macrophage-like cells by stimulating them with 100 nM dihydroxyvitamin D3 (vitamin D3, VD3) (Enzo Life Sciences, Exeter, UK), 250 nM phorbol 13-myristate 12-acetate (PMA, Sigma-Aldrich, Dorset, UK) or both (double stimulated) for 48-72 h at 37 °C in 5% CO_2 humidified incubator.

2.6 Assessment of cell viability

Cells were routinely checked using light microscopy to observe their viability, to asses for any morphological features of apoptosis, such as cell shrinkage, nuclear condensation and blebbing. Flow cytometric analysis was also used to check the viability of the cells by forward and side scatter analysis.

2.6.1 Annexin V / Propidium Iodide (PI) staining

Binding Buffer (BB): 150 mM NaCl, 10 mM HEPES (pH7-7.5), 2.5 mM $CaCl_2$ in dH_2O. Annexin V-FITC (Bender MedSystems, Vienna, Austria). This staining method allows the cells to be analyzed by flow cytometry to show the population proportion of live and dead cells. AxV dye binds to the phosphatidylserine (PS) of the cell membrane and PI binds to the DNA. The AxV stain will identify those cells that have started to progress into apoptosis where the PS of the cell membrane flips from the inner to the outer leaflet, while the PI stain shows proportion of cells with leaky cell membrane, which is a sign of necrosis. Routinely, 50 µl of cell culture is added to 500 µl of BB + 1 µl of stock AxV-FITC dye (1µl per $2x10^5$ cells), and then directly before running the sample in the flow, 5 µl of stock PI dye (20 µg/ml) is added. As a negative control, unstained cells were used.

2.7 Apoptosis induction

Cells were irradiated with UV light using the UVP UXV Chromato-Vue C-71 light box. The dose of the UV differed with each cell type to induce apoptosis yet achieve minimal secondary necrosis; The Mutu B cell line was irradiated with (50 mJ/cm^2), whilst the Jurkat T cell line was with (100 mJ/cm^2). The cells were resuspended in

serum-free RPMI + 0.2% (w/v) BSA at a cell density of (3-5×10^6 cell/ml) before being irradiated.

After exposing cells to UV, they were incubated in a humidified incubator (37 °C, 5% CO_2) for 18-24 h to allow apoptosis to proceed. In confirming the level of apoptosis within a culture, light microscopy and flow cytometry were used. Levels of apoptosis of cells in each individual assay was confirmed by taking a sample of the apoptotic cells, fixing them with 1% (w/v) formaldehyde in PBS and running it in the flow for a forward and a side scatter analysis.

The adherent cell lines (HEK293 & HeLa) were induced into apoptosis by treating them with anisomycin (5 µg/ml) as used previously (Torr et al., 2011), the treated cells were kept in the humidified incubator (37 °C, 5% CO_2) for 6 h. The confirmation steps of apoptosis were the same as for the cells irradiated with UV dose.

2.8 Isolation of extracellular vesicles from apoptotic cells

Extracellular vesicles (EV) are generated during cell death (Torr *et al*., 2011). As required, EV were harvested for use in further experiments (e.g. anti-inflammatory and chemotaxis assays). To harvest EV, Mutu B cells and Jurkat T cells were resuspended in serum-free RPMI at cell density of (3-5×10^6 cells/ml). Then they were irradiated with 50 mJ/cm^2 & 100 mJ/cm^2, of UV dose respectively and incubated at 37 °C for 18-24 h to allow apoptosis to proceed. After incubation cultures were centrifuged to pellet apoptotic cells (2000×*g*, 20 min). The pellet was re-suspended in fresh cRPMI and used as a source of 'apoptotic cells' in further assays. The supernatant was then ultracentrifuged (120,000×*g*, 70 min). The pellet of EV was re-suspended in fresh serum-free RPMI and used in further experiments where EV were required.

2.8.1 Measurement of the size and concentration of extracellular vesicles using iZON qNano (tunable resistive pulse sensing TRPS)

The qNano characterizes nanoparticles, where it was used here to characterize the apoptotic cell derived-extracellular vesicles. A 150 nm flexible polyurethane membrane tunable nanopore was used to characterize the apoptotic cell derived extracellular vesicles (ACdEV). The pore was placed on the device firmly, stretched out to the desired distance (47 mm, affecting pore size), washed with PBS, pressure was set on

0.7 kPa and the electrical connections made to the device to run the current. 35 μl of sample was placed in the device and the current was recorded to give out detailed information about the size and distribution number of ACdEV, as each particle causes a current blockade that can be measured for information on particle size and the density of the particles. The device was calibrated using the calibration particles of 100 nm mean diameter under the same experimental conditions..

2.9 Assay of Interaction of Macrophages (MØ) with apoptotic cells

THP-1 cells were seeded at 5×10^4 cells/well on a 4 well glass slide in cRPMI with double stimulants (250 nM PMA, 100 nM VD3) for 48-72 h at 37 °C incubator. Differentiation to MØ was confirmed by microscopy. After differentiation, culture medium was removed from the wells and MØ washed in PBS. AC were added to each well (1MØ: 10AC ratio) with and without anti-ICAM-3 mAb (MA4) as required by the experiment. A control isotype antibody MOPC21 (Sigma-Aldrich, UK) was also included as appropriate. MØ and AC were co-cultured for 1 h at 37 °C to allow interactions to occur. Slides were washed with ice-cold PBS three times by dipping to remove unbound AC and fixed in 1% (w/v) formaldehyde in PBS or methanol and stored at 4°C until staining. Slides were subsequently stained with Jenner-Giemsa stains and the percentage of MØ interacting with (both tethering and engulfing) apoptotic cells scored under light microscopy. At least 200 MØ per well were scored per well.

2.9.1 Jenner/Giemsa staining method

- Jenner-Giemsa (JG) Buffer: 200 mM Na_2HPO_4 +190 ml of 200 mM NaH_2PO_4 until pH is 5.6, dH_2O is added until 1 l.

Slides were stained with Jenner-Giemsa stains prior to light microscopy for analysis of MØ-AC interaction. Stains (Raymond Lamb Ltd) were diluted prior to use in Jenner-Giemsa Buffer. Jenner and Giemsa stains were used at dilutions of 1/3 and 1/10 in JG (Jenner/Giemsa) buffer respectively.

Slides were immersed in diluted Jenner stain for 4.5 min and washed by dipping in Jenner/Giemsa buffer three times. Slides were then immersed in diluted Giemsa stain for 9.5 min followed by washing by dipping in JG buffer three times. The slides were

then dipped once in distilled water and allowed to air dry completely, before mounting them with DePeX (Fisher, UK) and covering them with glass coverslips. Stained and mounted slides were then analysed by light microscopy.

2.10 Flow cytometry staining

2.10.1 Direct Immunofluorescence staining

The density of cells that were used in staining was 5×10^5 cells/tube. The cells were washed with wash buffer (PBS + 0.1% (w/v) BSA) and centrifugation (300×*g*, 5 min). The supernatant was discarded and the cell pellet disturbed by tapping the tube. Primary mAb conjugated with PE (concentration as appropriate) was added to the added to the pellet and incubated in the dark on ice (4 °C) for 15-30 minutes. After the incubation cells were washed twice and resuspended in ice-cold fixative (1% w/v formaldehyde in PBS) and stored at 4 °C prior to flow cytometry analysis. Flow cytometry was undertaken using a Beckman-Coulter FC500 flow cytometer and at least 5000 events were analysed per sample. Data was analysed using FlowJo cytometry software.

2.10.2 Indirect Immunofluorescence staining

The density of cells that were used in staining was 5×10^5 cells/tube. The cells were washed with wash buffer (PBS + 0.1% (w/v) BSA) and centrifugation (300×*g*, 5 min). The supernatant was discarded and the cell pellet disturbed by tapping the tube. Primary mAb (concentration as appropriate) was added to the added to the pellet and incubated in the dark on ice for 15-30 min. After the incubation, cells were washed twice followed by staining the cells with fluorochrome-conjugated goat anti-mouse secondary mAb (concentration as appropriate) and incubated in the dark on ice for 15-30 min. After the incubation, the cells were washed twice and resuspended in ice-cold fixative (1% (w/v) formaldehyde in PBS) and stored at 4 °C prior to flow cytometry for analysis. Flow cytometry was undertaken using a Beckman-Coulter FC500 flow cytometer and at least 5000 events were analysed per sample. Data was analysed using FlowJo cytometry software.

2.11 Vertical chemotaxis assay

EV from AC (Mutu WT/ Jurkat WT or ICAM-3^{LOW}) were added to a 24-well plate (700 µl/well), followed by the addition of 8 µm micro-porous transwells (Corning, Life Sciences, NY, USA). MØ ($5x10^5$ cell/ml) derived from THP-1 stimulated with VD3 (100 nM, 48-72h, 37°C) were added to the transwells (300 µl/transwell at a density of $5×10^5$ cells/ml) and the plate covered with the Cell IQ cell tracking cover. The plate was placed in the Cell IQ tracking system device (CM Technologies) and the appearance of MØ in the lower chamber recorded for 12 h. The data was analysed via the software of the Cell IQ system.

2.12 Investigating ICAM-3 and ACdEV anti-inflammatory effects

THP-1 cells were simulated with VD3 (100nM) to generate differentiated cells (MØ). After the differentiation period, the MØ were resuspended at $8×10^5$ cells/ml and 750 µl ($6×10^5$ cells/ml) seeded per well of a 24-well plate in fresh cRPMI media. AC or ACdEV (Mutu WT/ ICAM-3^{LOW}) were added to each well (100 µl/well) and co-incubated with the MØ for 18-24h. After this time 100 µl of 160 ng/ml LPS (from *E. coli* O111:B4, Sigma- Aldrich, Uk) and 100 µl of human serum (LBP) diluted in sfRPMI were added and the cells: LPS/LBP incubated for 4 h. Supernatants were then harvested and stored at -20 °C until ELISA analysis.

2.12.1 Measurement of TNF-α (pro-inflammatory cytokine) production via Enzyme-Linked Immuno-Sorbent assay (ELISA)

Production of TNF-α was assayed using a capture ELISA as per the manufacturer's instructions (Peprotech; New Jersy, USA). An ELISA plate (Maxisorp, Nunc) was coated with 2 µg/ml capture Ab in PBS overnight at 4 °C. The plate was washed three times with wash buffer (0.9 (w/v) sodium chloride, 0.05% (v/v) Tween 20) and 200 µl of block buffer (1% (w/v) BSA, 5%(w/v) sucrose in PBS) added to each well for 1 h at 37 °C. Wells were then washed and recombinant TNF-α serial dilutions (diluted in PBS (T): PBS + 0.05% v/v Tween 20) or experimental culture supernatants added (100 µl/well). The recombinant TNF-α serial dilutions used were (0.0, 0.03, 0.06, 0.125, 0.250, 0.500, 1.0, 2.0, 4.0 ng/ml). The plate was incubated (2 h, 37 °C), washed three times before addition of TNF-α detection antibody (200 ng/ml, 100µl/well). Following incubation (2h, 37°C) and washing three times, 100µl/well streptavidin-HRP (1:2000 in

PBS-T) and incubated for 1 h at 37 °C. Plates were emptied and washed four times, 100 µl of substrate OPD added per well and the colour, allowed to develop. The reaction was stopped with the addition of (50 µl/well) 1M HCL and the ELISA plate read at 490 nm.

2.13 MØ interaction with stained EV from AC

MØ ($5x10^5$ cells) differentiated from THP-1/VD3 were incubated with Bodipy stained ACdEV for different time lapse in the 37 °C incubator. Afterwards the cells were washed with PBS+0.1% BSA and fixed in ice-cold fixative (1% (w/v) formaldehyde in PBS) and stored at 4°C prior to flow cytometry for analysis.

2.13.1 Bodipy staining of EV

The ACdEV (supernatant) from the 2000x*g* centrifugation were incubated with (0.5 µM) Bodipy (molecular probes by life technologies) for 1-2 h in 4 °C fully covered by aluminum foil. The bodipy was diluted with the ACdEV supernatant. After the incubation, the stained ACdEV were run in qEV column to remove unbound dye, where 4ml was run through at a time. The first 3.5 ml was discarded and the next 4ml collected as PBS was used to run the sample through the column.

2.14 Molecular Biology

2.14.1 Molecular Biology Reagents

- Agarose, Broad Separation Range for DNA/RNA/Genetic Analysis Grade (Fisher, UK)
- Bis-Acrylamide 37.5:1 (Fisher, UK)
- DNA Ladder 1kb (Thermo Scientific, UK)
- Ethidium bromide (Invitrogen, UK)
- EZNA ISOLATION KIT TOTAL RNA I (Omega Bio-tek, GA, USA)
- Pierce Prestained Protein Molecular Weight Marker (Thermo Scientific, UK)
- Pierce Co-Immunoprecepitation kit (Thermo Scientific, UK)
- Plasmid miniprep and maxiprep kits (Thermo Scientific, UK)
- TEMED (Fisher BioReagents, UK)
- TransIT-LT1 Transfection Reagent (Geneflow, UK)

2.14.2 Molecular Biology Solutions

- Lysis Buffer: 50 mM Tris pH 7.4, 150 mM NaCl, 1% (v/v) Triton X-100, 1 mM EDTA and 1% (v/v) protease inhibitors.
- Protease inhibitor cocktail: 1 µM pepstatin, 1.3 µM benzamidine, and 1.8 µM leupeptin, diluted in dH_2O.
- Lysis Buffer: 50 mM Tris pH 7.4, 2% (w/v) CHAPS, 2 M Thiourea and 7 M Urea.
- Resolving buffer: 1.5 M Tris-HCl pH 8.8
- Separating buffer: 0.5 M Tris-HCl pH 6.5
- SDS-Page Buffer (10x): 30 g Tris, 144 g Glycine and 10 g SDS in 1 l of dH_2O.
- TBS (10x): 24.2 g Tris, 88 g NaCl in 1 l of dH_2O pH 7.5
- Wash Buffer TBS-T: 1x TBS, 0.1% Tween-20
- Transfer Buffer (10x): 30 g Tris, 144 g Glycine in 1l of dH_2O. 1x is used in the assay with the addition of 20% methanol.
- Blocking buffer: 5% (w/w) Powdered skimmed milk in 1 x TBS-T.
- Homogenisation buffer: 50 mM Tris (4 g per 500 ml of dH_2O),
- 250mM Sucrose (43 g per 500 ml of dH_2O pH 7.4), 0.25 mM $CaCl_2$.

Table 1. Materials used for casting of SDS polyacrylamide gels

Resolving gel (10%)	**3 gels**	**4 gels**
H_2O	11.63ml	18ml
Acrylamide/Bisacrylamide	6.38ml	10.2ml
1.5M Tris pH 8.8	6.5ml	10.4ml
10% SDS	0.25ml	0.4ml
10% APS	0.25ml	0.4ml
TEMED	25µl	40µl
Stacking gel (3.7%)	**3 gels**	**4 gels**
H_2O	7.86ml	12.58ml
Acrylamide/Bisacrylamide	1.25ml	2.0ml
0.5M Tris pH 8.8	3.125ml	5ml
10% SDS	0.125ml	0.2ml
10% APS	0.125ml	0.2ml
TEMED	12.5µl	20µl

2.14.3 RNA extraction from MØ, AC & ACdEV incubations

900µl (5×10^5 cells) of THP-1/VD3 derived MØ were seeded per well of a 24-well plate in fresh cRPMI media. AC or ACdEV (Jurkat WT/ ICAM-3^{LOW}) were added to each well (100µl/well) and co-incubated with the MØ for 6 h at 37 °C. RNA from MØ, AC, ACdEV and their incubated ones were extracted by using TOTAL RNA I kit (OMEGA-biotek). After incubation, the samples were centrifuged at 500x*g* for 5 min and the pellet was kept, whereas the ACdEV alone pellet was collected after the two centrifugation steps (2000x*g* 20 min and 120,000x*g* 70 min) as mentioned in the EV extraction section. 350 µl of TRK lysis buffer was added to the pellets and were homogenized by pipetting. 350 µl of 70% ethanol was added and the samples vortexed. The 700 µl total volume was transferred to the HiBind RNA Mini column in a 2 ml collection tube followed by centrifugation at 10,000x*g* for 1 min. The flow through was discarded followed by the addition of 500 µl of RNA Wash Buffer and centrifuged at 10,000x*g* for 1 min. The RNA Wash buffer step was repeated again with discarding of the flow through in both steps. The HiBind RNA Mini column was completely dried by centrifugation at 14,000x*g* for 2 min, and the flow through discarded. The column was transferred to a new centrifuge 1.5 ml tube where the RNA was eluted by addition of 70 µl of DEPC-water to the column followed by centrifugation at 14,000x*g* for min. The eluted RNA concentration was measured in the Nanodrop. The RNA was stored at -80 °C.

2.14.4 Agarose gel electrophoresis (DNA & RNA sample runs)

Agarose gels were prepared by using 1% (w/v) agarose in 1x TAE buffer and the addition of ethidium bromide (0.5 µg/ml). The DNA samples were mixed with the gel-loading buffer (6x) before being loaded into the gel and 5 µl of DNA ladder 1 kb was also added to each gel. The gel electrophoresis was run on 100 V for 1h and viewed afterwards in a UV transilluminator.

2.15 RT-PCR

After RNA extraction, the RNA was reverse transcribed to cDNA, where 100 ng/ml of RNA was mixed with reverse transcription primers and heat shocked at 65 °C for 5 min and left on ice immediately. The next step was extension, where the master mix was added to the RNA+ reverse transcription primers and placed in the thermocycler.

Reverse transcription primers (Primerdesign Ltd), UK used as following:

Component	1 Reaction
RNA template (100ng/ µl) (sample)	X µl -depending on the RNA conc. available and diluted to 100ng/ µl
Reverse transcription primer (YELLOW)	1.0 µl
RNAse/DNAse free water (WHITE)	X µl -volume added to make final volume 10µl
Final volume	10 µl

Extension step reaction mixture

Component	1 Reaction
Nanoscript2 4X buffer	5.0 µl
dNTP mix 10mM	1.0 µl
RNAse/DNAse free water	3.0 µl
Nanoscript2 enzyme	1.0 µl
Final volume	10 µl

The thermocycler program used was: 42 °C for 20 min, 75 °C for 10 min. The generated cDNA was stored at -20°C until further use.

2.15.1 Reverse Transcription Polymerase chain reaction (RT-PCR)

A master mix of house-keeping gene and the gene of interest were prepared. 5 µl of the cDNA (diluted in 1:10) was added to the PCR plate with 15 µl of master mix (housekeeping gene or gene of interest). Each 96-well plate had triplicates of housekeeping gene, the gene of interest and controls. The PCR plate was sealed and spun briefly to allow the SYBR green to mix with the samples. The plate was then placed in the PCR machine and the following program initiated. SYBR green thermal cycle: 10 minutes at 95 ºC, 15 sec at 95 ºC and 1 minute at 60 ºC for 40 cycles, 30 sec at 95 ºC, 30 sec at 55 ºC and 30 sec at 95 ºC.

Housekeeping gene (β-actin, Invitrogen by Thermo Fisher Scientific, UK) was used as following:

Component	1 Reaction
SYBR (Syber green)	10.0 µl
Water (Molecular biology RNAse/DNAse free water)	3.0 µl
Actin Forward	1.0 µl
Actin Reverse	1.0 µl

β-actin forward primer: 5' CTGGAACGGTGAAGGTGACA 3'

β-actin reverse primer: 5' AAGGGACTTCCTGTAACAATGCA 3'

Gene of interest expression: IL-10 and TGF-β (Primerdesign Ltd, UK):

Component	1 Reaction
SYBR (Syber green)	10.0 µl
Water (Molecular biology RNAse/DNAse free water)	4.0 µl
IL-10/TGF-β	1.0 µl

IL-10 forward primer: 5' GCTGGAGGACTTTAAGGGTTAC 3'

IL-10 reverse primer: 5' TGATGTCTGGGTCTTGGTTCT 3'

TGF-β1 forward primer: 5' CACTCCCACTCCCTCTCTC 3'

TGF-β1 reverse primer: 5' GTCCCCTGTGCCTTGATG 3'

2.16 Small-scale plasmid isolation and purification (Mini-prep)

DH5-α competent cells transformed with pcDNA3 plasmid were spread on LB agar plates containing ampicillin (100 µg/ml) to grow overnight at 37 °C. A colony was picked from the plate of grown colonies and inoculated to a tube containing 5 ml LB broth supplemented with ampicillin (100 µg/ml). This culture was grown overnight at 37 °C with shaking to saturation of the culture. Small scale plasmid preparations were made using the (Thermo Scientific GeneJET Plasmid Miniprep Kit) following the manufacturer's instructions. 1-4 ml of the liquid culture was harvested to micro centrifuge tubes and the bacterial cells isolated by centrifugation (6800x*g* for 2 min) and discarded the supernatant. 250 µl of the resuspention solution was added to the pellets and the cells were resuspended well (vortex/pippeting). 250 µl of the lysis solution was added to the mix and inverted gently until the solution became viscous and slightly clear. This was followed by the addition of 350 µl of Neutralization solution

and mixed thoroughly and immediately by inverting 4-6 times which became cloudy. The mix was centrifuged for 5 min at 6800x*g* to remove genomic DNA. The supernatant carrying soluble plasmid DNA was transferred to the GeneJET spin column and centrifuged for 1min at 14,000 rpm, the flow through was discarded. 500 µl of Wash solution was added to the column and centrifuged for 1min at 14,000 rpm and the flow through discarded. The wash was repeated a second time. Afterwards the GeneJET spin column was transferred to a new 1.5 microcentrifuge tube followed by the addition of 50 µl of elution buffer and incubated for 2min at room temperature. After the incubation, the column was centrifuged for 2 min at 14,000 rpm to elute the plasmid DNA. The eluted purified plasmid DNA concentration was measured by Nanodrop and the DNA was stored at -20 °C.

2.16.1 Linearisation of plasmid DNA by restriction enzymes

A digestion mix was generated for the digestion of plasmids: 1 µg of DNA was mixed with 1 µl (10 units) of appropriate restriction enzyme (time saver-qualified enzyme; New England Bioscience), 5 µl of 10x restriction enzyme buffer and dH_2O to reach a 50 µl reaction volume. The mix was left for 5-15 min on ice to digest followed by running the sample on agarose gel to confirm the digestion.

2.16.2 Nanodrop

Depending on whether RNA/DNA or protein was to be measured, the appropriate option was chosen from the software. 100% ethanol was initially used to clean the sample loading position on the Nanodrop device, followed by adding 1 µl of dH_2O on the sample loading position to calibrate and blank the device. 1 µl of sample (DNA, RNA or protein) was added to the loading position and measured The 260/280 readings were noted and the curve result analysed to assess quantity and purity of the sample under study.

2.16.3 Large-scale plasmid isolation and purification (Maxiprep)

Following appropriate confirmation of the plasmid DNA prepared from small scale culture and miniprep, large scale preparations were undertaken. 1 ml of the 5 ml miniprep culture was used to inoculate a conical flask containing 200 ml of LB broth supplemented with ampicillin. This culture was left to grow overnight at 37°C with shaking. The large-scale plasmid DNA preparation was undertaken as per the manufacturer's instructions (Thermo Scientifc-GeneJET plasmid Maxiprep Kit).

2.17 Transient transfection using (Mirus TransIT-LT1)

18-24 h prior to transfection, cells were passaged and plated in 2.5 ml in (35 mm) 6-well plates. The procedure followed the recommendations manufacturer's recommended protocol. The cell density used was between 0.8-3.0x10^5 cells/ml, 2.5x10^5 cells/ml was used in the protocol. Cells were left overnight to stick and spread in the incubator at 37 °C. The cell confluence was around 80% after this overnight incubation, in line with the recommended confluence for transfection. The *Trans*IT-LT1 transfection reagent was prepared by warming room temperature and vortexing gently. For each well to be transfected, 250 µl of serum-free DMEM was added to a polypropylene tube followed by the addition of 2.5 µg of stock plasmid DNA and were mixed gently by pipetting. 7.5 µl of *Trans*IT-LT1 was added to the diluted plasmid DNA, mixed gently by pipetting and incubated at room temperature for 15-30 min. As appropriate to the experiment, the amounts of DNA or transfection reagent were altered in an attempt to optimize the transfection efficiency. The prepared transfection mixture was added to each well of cells, seeded in complete DMEM medium, in a drop-wise fashion across different regions of the well. The 6 well plate was then rocked, side to side and back and forth, to distribute the transfection mixture. The cells were incubated with the transfection mixture for 24-72 h in the incubator at 37 °C and then they were harvested by using ice-cold 5 mM EDTA in PBS. Harvested cells were assessed for transfection efficiency by flow cytometry, fluorescent microscopy and western blot.

2.17.1 Calcium phosphate-mediated Transient transfection of HEK293 cells

The HEK293 cells were passaged, counted and resuspended in complete DMEM to the appropriate density (2.5x10^5 cells/ml), which are required per well in a 6-well plate. To prepare the precipitates for transfection, two tubes were set up (per 35 mm well to be transfected): tube 1 contained 125 µl of 2x HBS; tube 2 contained 125 µl of $CaCl_2$ and 0.5 µg of plasmid DNA. Then tube2 contents were added in a drop-wise fashion to tube1 and mixed gently by bubbling air through a sterile glass pipette. After mixing, the tubes were incubated at room temperature for 5 min to let the precipitate form. Afterwards, the precipitate was added with the suspension cells directly in the wells and incubated at 37 °C to allow the transfection to proceed and the cells to adhere. Harvested cells were assessed for transfection efficiency by flow cytometry, fluorescent microscopy and western blot.

2.17.2 Stable cell transfection production using geneticin (G418)

The first step in producing stable cells was generating a kill curve, where non-transfected cells were seeded in 6-well plates and incubated with doubling diluted concentrations (4 mg/ml to 62.5 µg/ml) of the antibiotic geneticin (G418) to determine the lowest concentration that kills the cells after a week. The geneticin was diluted in complete DMEM prior to incubation. Every 2-3 days, the medium with the selective antibiotic was changed. A control of cells without antibiotic treatment was included in the assay. The cells were observed by microscopy to assess cell viability in order to determine the optimal dose. After identifying the optimal dose (1mg/ml), the transfected cells, which carry the ampicillin resistance gene in the transfected plasmid, were incubated with the 1 mg/ml G418. Every 2-3 days this selective medium was changed**.** The transfected cells that resisted antibiotic killing were expanded to new flasks for further study or frozen for storage.

2.18 Whole cell lysis & Protein quantification

Protein concentrations of required samples were quantified using the Bradford assay. The protein standard used was BSA (1.35 mg/ml stock conc.) diluted with dH_2O into different concentrations from 30 µg/ml – 1 µg/ml. 200 µl of Bradford Dye reagent (1/5 dilution in dH_2O) was added to the protein standards and assay samples in a 96-well plate, before incubation at room temperature for 5 min and reading in the micro-plate spectrophotometer at a wavelength of 595 nm. The protein standard absorbance results were plotted against the concentration, to allow the estimation of the protein concentration in the assay samples by interpolation of a linear fitted line.

2.19 Styrene Maleic Acid Lipid ParticleS (SMALPS) extractions

Initially, cells were pelleted by centrifugation (300x*g*) and washed with 1x PBS, followed by homogenization to extract the membranes. The pellets were suspended in 10-20 ml of homogenization buffer with 10-20 µl of protease inhibitors and vortexed. This was followed by transferring the suspended pellet into the nitrogen chamber and locked firmly. The nitrogen cylinder hose was connected to the locked chamber and opened until the pressured reached 500 PSI. The hose was released from the chamber and the chamber placed on ice for 15 min. Afterwards, the chamber nozzle was opened slowly and the released sample was collected and centrifuged at 1800

rpm for 10 min. The supernatant was collected and centrifuged at 100,000x*g* for 20 min.

The pellet was resuspended in SMA buffer at 60 mg/ml wet pellet weight. The resuspended pellet was mixed vigorously by vortexing, pipetting and by a small needle with syringe pipetting. After achieving homogenization, 30 mg/ml concentration was prepared by mixing (1:1 ratio) of 5% w/v SMA solution and homogenised sample. This 30mg/ml sample was incubated at room temperature for 1 h on a shaker before centrifugation (20 min at 100,000x*g*). The supernatant was collected and labelled as 'soluble', whereas the pellet was resuspended in SMA buffer with 10% w/v SDS in an equivalent volume to the supernatant.

2.20 Western blot

2.20.1 Sodium Dodecyl- Sulphate Polyacrylamide Gel Electrophoresis (SDS-PAGE)

After quantifying protein concentrations, SDS-PAGE was used to separate proteins according to their size. A polyacrylamide gel consisting of 10% stacking and 3.7% resolving gels was prepared (as per **Table 1**). The resolving gel was first prepared and allowed to polymerise (30min) under isopropanol to exclude oxygen, even the surface and remove air bubbles. The isopropanol was removed by washing with water and dried with filter paper. The stacking gel was prepared and polymerised on the resolving gel taking care to remove any air bubbles when placing the well comb. The polymerized gel and plates were placed in the gel tank under 1x SDS buffer (running buffer).

2.20.2 Sample preparation and running of SDS-PAGE

Protein samples were mixed with 2x Laemmli buffer and denatured by heating at 65 °C for 10 min prior to being loaded into the gels. The well combs were removed, the wells filled with running buffer and the prestained protein marker and the denatured protein samples loaded. Initially, the gels were run on 120 V for 5 min to allow the samples pass through the stacking gel, and afterwards 180-200 V for 45-55 min until the dye front reached the bottom of the resolving gel.

2.20.3 Protein Transfer

After separating protein samples by SDS-PAGE, the proteins were transferred from the gel to a nitrocellulose membrane by electroblotting. The gel was carefully packed in western blot sandwich cassettes in the following sequence: sponge, filter paper, gel, nitrocellulose membrane, filter paper and sponge again. The contents were soaked in blotting buffer whilst being assembled. Following assembly, the sandwich cassettes were placed in the Bio-Rad blotting tank and covered with blotting buffer and an ice pack added. The transfer was done with constant electric voltage of 100 V for 1 h. The nitrocellulose was removed carefully and blocked overnight at 4 °C. As appropriate, the primary mAb (1°mAb) was incubated with the nitrocellulose membrane for 2h at room temperature on a shaker. The 1°mAb step was followed by 3 washes, 5 min each and then the 2° detection Ab added and incubated with the nitrocellulose for 1 h at room temperature on a shaker. The nitrocellulose membrane was then washed 5 times, 5 min each on a shaker. The ECL Chemiluminescent substrate was added to the nitrocellulose membrane for 2 min and viewed in the G box to look for the luminescence of the 2° reagent, when bound to the primary mAb which is bound to the protein of interest.

2.21 Co-Immunoprecipitation (Pierce Co-immunoprecipitation kit)

2.21.1 Antibody Immobilization

This step's preparation undertaken at room temperature, in line with the manufacturer's instruction. Briefly, 50 µl of the resin slurry was added to the Pierce spin column and centrifuged for 1 min at 1000x*g* and flow through was discarded. Two washes were applied to the resin (200 µl 1x coupling buffer with centrifugation 1000x*g* for 1 min) and the flow through discarded. 75 µg of antibody was prepared in a 200 µl volume of 1x coupling buffer and it was added to the resin in the column and left on the mixer for 10min followed by the addition of 3 µl of sodium cyanoborohydride. The column was closed and left on the mixer at room temperature for 120 min, and overnight at 4 °C. After incubation, the column was centrifuged (1000x*g* for 1 min) and the flow through was saved for verification of antibody-resin coupling. 200 µl of 1x coupling buffer was added to the column and centrifuged (1000x*g* for 1min) and the flow through discarded. This step wash step was repeated once. This was followed by addition of 200 µl of Quenching buffer to the column and centrifugation (1000x*g* for 1min) and the

flow through discarded. The bottom plug was attached to the column, and 200 µl of Quenching buffer and 3 µl of sodium cyanoborohydride added before mixing for 15 min at room temperature. The column was then emptied by centrifugation and washed eight times with 1x coupling buffer and centrifugation, and the flow through discarded. This final coupled column was used for the Co-IP. To store the resin coupled to the antibody column, the column was washed with 200 µl of 1x coupling buffers twice and incubated with 200 µl of 1x coupling buffer at 4 °C.

2.21.2 Co-IP

All of the Co-IP steps were performed at 4°C unless otherwise indicated.

The bait:prey protein mixtures (SMALP sample) were diluted 1:1 with 1x PBS in 500 µl total volume (250 µl SMALP+250 µL 1X PBS). The column containing resin coupled to the antibody was washed twice with 200 µl of 1x PBS, where each wash step was centrifuged at 1000x*g* for 1min and discarded the flow through. Afterwards the bait:prey protein mixture was added to the column and incubated with gentle shaking at room temperature for 120 min or at 4 °C overnight. Following incubation, the column was centrifuged at 1000x*g* for 1 min and the flow through was saved for future analysis. Three wash steps were performed to the column using 200 µl of 1x PBS, where each wash step was centrifuged at 1000x*g* for 1 min and the flow through was kept to be tested to make sure there was no presence of protein. Nanodrop and Bradford protein assay were used to test for the presence of protein. The final step invovled eluting the Co-IP, by the addition of 10 µl of elution buffer and centrifugation (1000xg) and the flow through (anticipated to the ICAM-3 and partner proteins precitpiated) saved. An additional 50 µl of elution buffer was added to the column and incubated for 10 min at room temperature followed by centrifugation at 1000x*g* for 1 min. The flow through from the two-elution steps was tested in the Nanodrop A_{280}, Bradford protein assay and SDS-PAGE.

2.22 Mass spectrometry

2.22.1 Lysis of samples and SDS-PAGE

Samples for Western blotting and mass spectrometry (membrane preparations and extracellular vesicles pellets) were lysed in 1.5 mM Tris-HCl pH 7.4 with 2% CHAPS, 8 M urea and 2 mM thiourea. Samples were sonicated in polypropylene tube on ice following two 30 sec long sonication and resting

cycles using a sonicator probe working at 67 % of full power. Samples were centrifuged at 14,000x*g* for 10 min. supernatants were collected and transferred into a new tube. Protein concentration was estimated against BSA calibration curve in Bradford assay.

Samples (30 µg) were mixed with reducing Laemmli buffer (Sigma Aldrich, UK) and heated at 65 °C for 15 min. Proteins were resolved on 10 cm long 10 % SDS polyacrylamide gel casted in house. Proteins were visualised using Coomassie blue stain (G 250, VWR, UK) in aqueous 40 % methanol (VWR, UK) with 10 % glacial acetic acid (Fisher, UK). After 1h, gels were destined in aqueous 10 % ethanol with 7.5 % glacial acetic acid. Gels were kept in distaining solution at 4 °C prior in-gel digestion.

2.22.2 In-gel digestion

In-gel digestion was performed following the protocol of Schevchenko *et al*. (Shevchenko *et al.*, 2007) with smaller modifications. Gels were layered over the clean glass slide, and each sample lane was cut into five pieces of approximately the same size, diced and transferred into polypropylene tube (1.5 ml, Eppendorf, Germany). Gels were further distained with 50 % acetonitrile (Fisher, UK) in 50 mM aqueous ammonium bicarbonate (Sigma Aldrich, UK) on a thermoshaker (37 °C 550 rpm) until all due was removed. Gels pieces were further fully dehydrated with 100 % acetonitrile, and dried under vacuum for 30 min. The dried gel pieces were used immediately for the in-gel digestion or stored at -20 °C prior analysis. Solution of 250 ng of trypsin (Trypsin gold, sequencing grade, Promega, UK) in 40 µl of aqueous 3 mM ammonium bicarbonate was used to hydrate gel pieces. Once gel pieces were fully hydrated with trypsin solution, 200 µl of 3 mM ammonium bicarbonate was used to cover the gel pieces in solution. In-gel digestion was carried overnight (approximately 15 h) on a thermoshaker (37 °C, 550 rpm).

2.22.3 Extraction of peptides

Samples were treated with 150 µl of 100% acetonitrile and sonicated in the ultrasonic bath for 15 min. Solution containing a portion of peptides was collected and transferred into a new polypropylene tube. This process was

repeated two times more with 200 µl of 50% acetonitrile in aqueous 50 mM ammonium bicarbonate. Each time the solution containing fraction of peptides was collected and transferred into a corresponding tube. In the last step, gel pieces were fully dehydrated with 350 µl of 100 % acetonitrile, solution was collected and transferred into a corresponding tube. Peptide extracts were fully dried under vacuum. Samples were stored at -20 °C prior analysis.

2.22.4 Mass spectrometry

Dried peptide extracts were dissolved in 30 µl of aqueous 3 % acetonitrile with 0.1 % formic acid (Fisher, UK) and transferred into a clean borosilicate vial and placed at 10 °C into the automated autosampler (Dionex 3000, ThermoScientific, UK). Half of the sample content was injected onto a trap column (PepMap^{TM}, C18, 5 µm, 100 Å, 300 µm x 1 mm, ThermoScientific, UK). Peptides were trapped and washed for 3 min with 2% B (eluent A: 2% acetonitrile in aqueous 0.1 % formic acid; eluent B: 98% acetonitrile in aqueous 0.1 % formic acid) at a flow rate of 30 µl/min. Peptides were separated on the analytical column (Acclaim^{TM}, PepMap^{TM} C18, 3 µm, 100 Å, 75 µm x 150 mm, ThermoScientific, UK) with a following gradient: 0-3 min 2% B, 3-48 min 2-45% B, 48-52 min 45-90% B, 52-55 min 90% B, 55-70 min 2% B). Electrospray was formed by spraying the nLC eluate at 2500 V using the PicoTip^{TM} emitter (New Objective, Germany). Data was acquired on the 5600 TripleTof (AB Sciex, UK) mass spectrometer operating in information dependent mode (IDA) where one IDA cycle consisted of a MS survey scan (*m*/*z* range from 300 to 2000) followed by consecutive CID fragmentations (rolling collision energy) of the six most abundant ions in MS survey scan. Acquired ions were temporarily excluded from MS/MS acquisition for 300 sec. Mass spectrometer was calibrated prior acquisition to ensure the highest mass accuracy (<10 ppm) on the both MS and tandem mass spectrometry (MS/MS) levels.

2.22.5 Data analysis

Acquired data were analysed using Progenesis for proteomics software (version 4, Nonlinear dynamics – Waters, UK). Merged files were analysed using relative quantitation using top 3 peptides. Anova (significance higher than

95%) test was applied as a measure of statistical significance. Created files in .mgf mode were submitted for a search using Mascot Deamon (version 2.5) search engine against SwissProt database restricting the search to following parameters: mass tolerance of 0.1 Da for MS and 0.6 Da for MS/MS spectra, maximum of 2 trypsin misscleavages, human taxonomy, variable modifications of methionine oxidation and cysteine carbamidomethylation.

2.23 *In Vivo* work (injecting SCID mice with MA4)

Mutu I BL cells (ICAM3 expressing: ICAM-3^{+}) were provided to Ms Lynsey Melville in Professor Gregory's team at Edinburgh University, to undertake the Home Office licensed *in vivo* work. Twenty 20 female SCID (severe combined immunodeficient) mice (Harlan) were injected with viable Mutu cells. The mice were 7-9 weeks old and were injected subcutaneously in the right flank with 1x10^{7} Mutu (BL) cells per animal. Rodents do not express ICAM3, making them a useful model in which to study this Mutu (ICAM3 +ve) xenograft as all ICAM-3 effects would be as a result of the injected cell ICAM-3. Following injection of Mutu cells, the animals were monitored for appearance of tumours at the site of infection. Mutu cells have high spontaneous rate of cell death, which promotes development of the tumour (Ford *et al.*, 2015). After the tumour had developed to ~5 mm × 5 mm in size when examined, the mice were injected intra-tumourly every other day with 50 µl of anti-ICAM3 monoclonal antibody MA4 (10 mice) or 50 µl of sterile PBS for the control mice (10 mice). The maximum number of injections allowable under the licence were four or until the tumour size reached its maximum (12 mm×12 mm), at which point the animals was sacrificed. Over time the tumour sizes in each mouse was monitored in two dimensions with calipers. This was undertaken as part of daily husbandry of the animals. Following sacrifice, the tumours were excised from the mice and formalin fixed prior to further analysis.

2.23.1 Immunohistochemistry

Harvested tissues were formalin-fixed and paraffin-embedded by Ms Lynsey Melville (University of Edinburgh). Tissue sections of xenograft tumour tissue from different regions of the mouse (subcutaneous (SC), ovarian, kidney) were taken. All tumour tissue was formed following SC injection of 1x10^{7} viable Mutu (BL) into SCID mice.

2.23.2 CD204 immunohistochemistry of paraffin tissue sections of tumours

The prepared tumour sections were dewaxed in Histoclear (National Diagnostics) twice for 5 min each. This was followed by rehydrating through alcohol (100% IMS, 90% IMS, & 70% IMS) 5 min each. The tissue slides were washed twice in dH_2O for 5 min and the slides were transferred to a plastic slide rack. Antigens were revealed in the sections by immersion in Antigen Unmasking solution (Citric acid-based; Vector Labs) diluted 1/100 in dH_2O followed by four 5 min cycles of microwave. After each cycle, the slide rack was rotated 90 °C. Following heating, the slides were left to cool for 30 min and placed under running water for 10 min. A freshly prepared hydrogen peroxide (2%(v/v) H_2O_2 in dH_2O) was incubated with the slides on a rocker for 15 min before washing the slides in (TBS+0.05% Tween-20) twice for 5 min. This was followed by loading the slides in the SEQUENZA chambers. 125 µl of 5% normal goat serum in PBS (per-slide) was added to the SEQUENZA chambers containing the slides for 20 min before the primary rabbit anti-CD204 antibody (2 µg/ml; 125 µl per slide) was added and incubated for 1.5-2 h or overnight at room temperature. After incubation, the slides were washed twice in TBS+0.05% Tween-20 and secondary anti-rabbit-biotin antibody added (125 µl per-slide; 1/250 diluted in 5% NGS; Vector Labs) for 30-40 min incubation at room temperature. The slides were washed twice in TBS+0.05% Tween-20. Three drops per slide of ready to use Vectastain Elite ABC-HRP reagent (Vector Labs) was added and incubated at room temperature for 30 min prior to two washes (TBS+0.05% Tween-20; 5 min each). The slides were then incubated with DAB peroxidase substrate kit (125 µl per slide; 5-10 min; Vector Labs) before two washes (TBS+0.05% Tween-20; 5 min each). The slides were removed from the SEQUENZA chambers and transferred to the staining rack containing dH_2O. The slides were counterstained in haematoxylin for 20 sec, followed by several washes in tap water. The slides were added to Blue stain in 0.1% sodium bicarbonate for 1 min, rinsed in tap water and dehydrated in industrial methylated spirits (3 min each of two 95% and 100%). It was followed by soaking the slides in clearing Histoclear (5 min) and then mounting Histoclear (5 min). The slides were mounted in Histomount.

2.23.3 F4/80 immunohistochemistry on paraffin tissue sections of tumours

The prepared tissue tumour was dewaxed in Histoclear (National Diagnostics) twice for 5 min each. This was followed by rehydrating through alcohol (100% IMS, 90% IMS, & 70% IMS) 5 min each. The tissue slides were washed in dH_2O for 5 min twice. A freshly prepared hydrogen peroxide (2% (v/v) H_2O_2 in dH_2O) was incubated with the slides on a rocker for 15 min. Next step was washing the slides in PBS twice for 5 min. This was followed by loading the slides in the SEQUENZA chambers. 125 µl of 2.5% normal rabbit blocking serum in PBS (per-slide) was added to the SEQUENZA chambers containing the slides for 20 min before the primary antibody anti-F4/80 (4 µg/ml; 125 µl per-slide; Invitrogen MF48000) was added and incubated overnight at 4 °C. After incubation, the slides were washed in PBS twice for 5 min each and secondary anti-rat-biotin anti-body was added (125 µl per-slide; 1/125 diluted in 2.5% rabbit serum; Vector Labs BA-4001) for 30 min incubation at room temperature. The slides were washed in PBS twice for 5 min afterwards. Three drops per slide of ready to use Vectastain Elite ABC-HRP reagent (Vector Labs) was added and incubated at room temperature for 30 min prior to two washes (PBS; 5 min each). The slides were then incubated with DAB peroxidase substrate kit (125 µl per slide; 5-10 min; Vector Labs) before two washes (dH_2O; 5 min each). The slides were removed from the SEQUENZA chambers and transferred to the staining rack containing dH_2O. The slides were counterstained in haematoxylin for 30 sec, followed by several washes in tap water. The slides were added to Blue stain in 0.1% sodium bicarbonate for 1 min, rinsed in tap water and dehydrated in industrial methylated spirits (3 min each of two 95% and 100%). It was followed by soaking the slides in clearing Histoclear (5 min) and then mounting Histoclear (5 min). The slides were mounted in Histomount.

2.23.4 CD68 Immunohistochemistry on frozen tissue sections of tumours.

The tissue sections were warmed at room temperature for 1 h prior staining. The tissue section slides were washed in PBS for 5 min. Then the slides were incubated in a freshly prepared hydrogen peroxide 0.1% (v/v) H_2O_2 in methanol for 3 min. Followed by two washes in PBS for 5 min each. This was followed by loading the slides in the SEQUENZA chambers. Three drops per slide of ready to use Vector Avidin Block (SP-2001) was added and incubated for 10 min at room temperature prior to one wash in PBS for 5 min. 10x casein solution (125 µl per-slide; 1/10 diluted in dH_2O; Vector Labs SP-5020) was added and incubated for 10min at room temperature before the primary

antibody anti-CD68 (10 µg/ml; 125 µl per-slide (Serotec Lab MCA1957); diluted in 1x casein solution Invitrogen Vector Lab SP-5020) was added and incubated 1.5-2 h at room temperature or overnight at 4 °C. After incubation, the slides were washed in PBS twice for 5 min each and secondary antibody anti-rat-biotin was added (125 µl per-slide; 1/200 diluted in 1x casein solution; Vector Labs BA-4001) for 30 min incubation at room temperature. The slides were washed in PBS twice for 5 min afterwards. Three drops per slide of ready to use Vectastain Elite ABC-HRP reagent (Vector Labs) was added and incubated at room temperature for 30 min prior to two washes (PBS; 5 min each). The slides were then incubated with DAB peroxidase substrate kit (125 µl per slide; 10 min; Vector Labs) before two washes (dH_2O; 5 min each). The slides were removed from the SEQUENZA chambers and transferred to the staining rack containing dH_2O. The slides were counterstained in haematoxylin for 20 sec, followed by several washes in tap water. The slides were added to Blue stain in 0.1% sodium bicarbonate for 1 min, rinsed in tap water and dehydrated in industrial methylated spirits (3 min each of two 95% and 100%). It was followed by soaking the slides in clearing Histoclear (5 min) and then mounting Histoclear (5 min). The slides were mounted in Histomount.

2.24 Statistical analysis

Data are expressed as the mean ± S.E.M for at least three independent experiments (n ≥3) each undertaken in triplicate unless otherwise mentioned differently in figure legends and were undertaken using Prism software (GraphPad, USA). Statistical analyses of the results were undertaken using one-way analysis of variance (ANOVA) using a post-test depending on the requirement.

3. Results

3.1 Chapter 1 - ICAM-3 & ACdEV in chemotaxis

ICAM-3 is an intercellular adhesion molecule that has several functions depending on the status of the cell (viable/apoptotic). On viable cells it functions by mediating the interaction between T lymphocytes and antigen presenting cells (APC) through LFA-1/ICAM-3 binding (Montoya et al., 2002). Whilst on apoptotic cells, ICAM-3 has been shown to be involved in promoting the clearance of the apoptotic cells. The precise details of the functional shift and the molecular basis for this change in function are not fully understood, but the integrin receptors of ICAM-3 in viable cells (LFA-1) do not appear to interact with ICAM-3 when in the apoptotic status (Moffatt et al., 1999). In apoptotic cells, ICAM-3 mediates the binding and tethering of apoptotic cells to macrophages (Torr et al., 2011, Moffatt et al., 1999). It has also been shown that ICAM-3 released from apoptotic cells on ACdEV promotes the chemoattraction of macrophages (Torr et al., 2011).

Whilst ICAM-3 is active in recruiting MØ, it is not clear if ICAM-3 on ACdEV acts (a) to tether EV efficiently to MØ so that the MØ can be activated to migrate (through other EV cargo molecules, e.g. classical chemokines such as CX3CL1, providing an activating signal); (b) EV binds to MØ independently of ICAM-3 where the presence of ICAM-3 can provide an activating signal to the MØ; or (c) ICAM-3 acts both as a tethering and activating signal. As ICAM-3 is an established adhesion molecule and is known to tether AC to MØ, this chapter will test the hypothesis that ICAM-3 on ACdEV acts to bind EV efficiently to MØ and thus promote MØ activation to enable migrate.

3.1.1 Titrating the UV radiation dose required for apoptosis induction

In order to investigate the role of ICAM-3 and EVs in AC clearance, it was necessary to establish a method of generating ACs that was robust, rapid and synchronous. Some cell death-inducing agents (e.g. DNA damaging agents) tend to induce apoptosis in a manner that is dependent on the phase of cell cycle, resulting in a slower death of the cell population (Cregan *et al.*, 1999). UV radiation was the chosen method as it has been reported to induce synchronous apoptosis that proceeds rapidly (Devitt *et al.*, 2003). Initially, titrating the optimum dose of UV in order to achieve high apoptosis levels with minimal necrosis in B cells was undertaken using well established methods

of annexin V staining (for available PS) and propidium iodide (for membrane integrity). In **Figure 8** six doses of UV were tested (25, 50, 75, 100,150, 200 mJ/cm^2) to fit with those doses of UV widely used in previous studies with leukocytes (Devitt et al., 2003, Torr et al., 2011). After irradiation of viable B cells with the indicated dose of UV, the cells were allowed to progress through apoptosis by incubating the cells for 18-24 h at 37°C. After the incubation period, samples of the treated cell cultures were stained with AxV/PI and analysed by flow cytometry to assess the viability and apoptosis levels. The flow cytometer (Beckman Coulter FC500) uses a 488nm blue laser to excite AxV-FITC or PI if bound to the cells resulting in green or red emitted light that the cytometer measures and records. FITC stained cells emit green light and PI emits back red/orange light, proportional to the amount of FITC or PI present. PI binds to the DNA (only accessible to the dye when a cell is necrotic) whilst AxV binds to phosphatidylserine (PS) of the cell membrane if accessible. When a cell undergoes apoptosis, the PS flips from the inner leaflet to the outer leaflet of the plasma membrane where it can be stained by AxV but the membrane remains intact so the cells are not stained by PI. During necrosis, the cell membrane becomes leaky in necrosis (primary) and secondary necrosis (i.e late apoptosis), which allows the PI to enter the cell and bind to the DNA. In addition, necrotic cells also stain positive for AxV as the PS is accessible either by flipping to the outer leaflet of the plasma membrane and/or by AxV gaining access to the leaky cell to stain the inner leaflet of the plasma membrane. Unstained samples were run to assess baseline fluorescence (negative control for staining) and also to assess cell size and granularity as this provides important information on cell viability through an alternative method. Using forward scatter (FS) and side scatter (SS) analyses of laser light in the flow cytometer it is possible to distinguish viable cells and apoptotic cells (Dive *et al.*, 1992). Viable cells are large (i.e. high FS) but not granular (i.e. low SS). On the other hand, apoptotic cells shrink (i.e. lower FS) during apoptosis and become more granular (higher SS) due to condensation of DNA. These analyses generate large amounts of data from over 5000 events per assay and so representative data is shown here to confirm that UV treatment of Mutu cells (WT or ICAM-3^{LOW}) generates cell death via apoptosis, not necrosis.

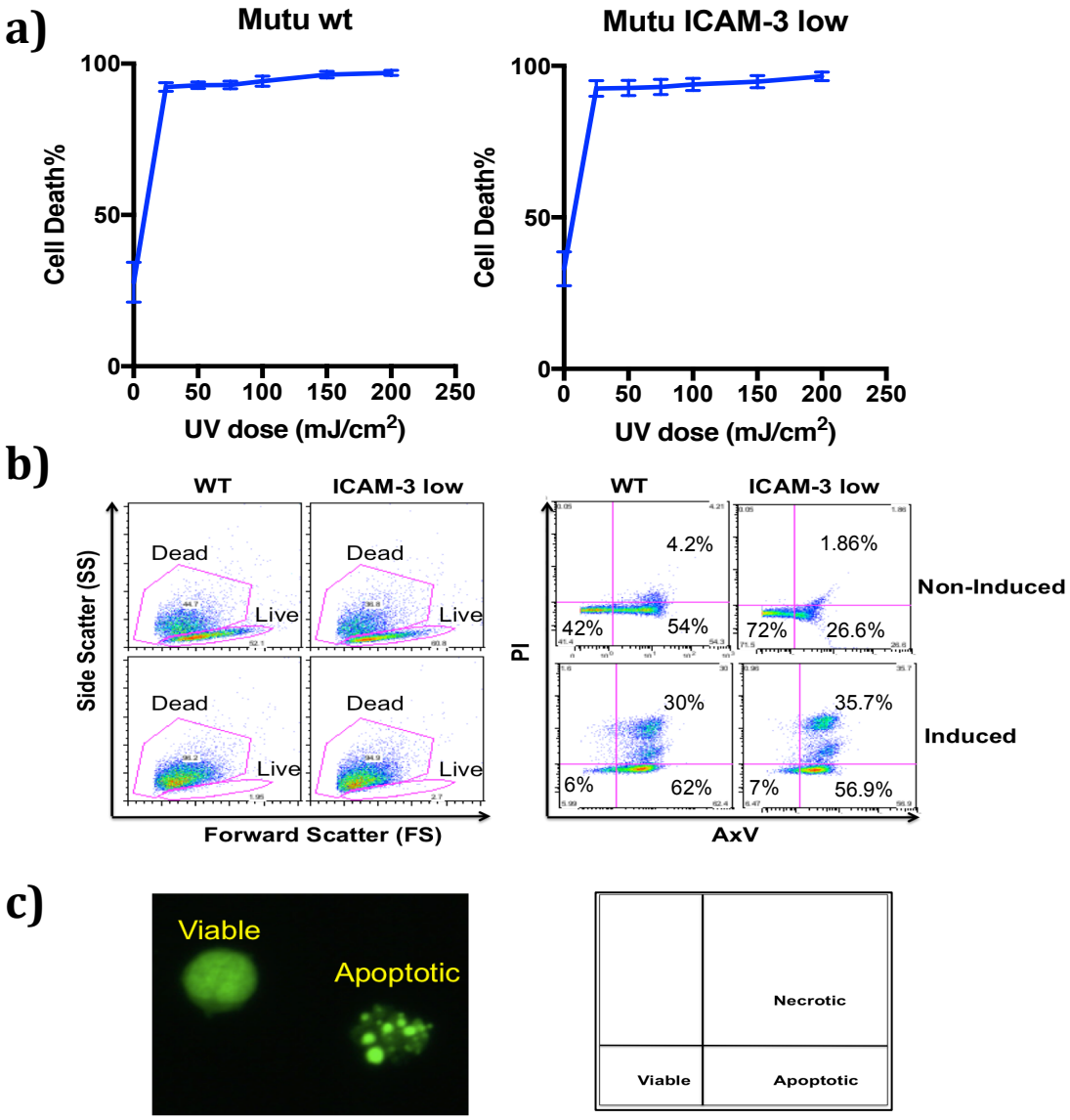

Figure 8. Titration of appropriate UV radiation dose to induce maximum apoptosis. Mutu B cells that express normal (WT) or reduced ICAM-3 (ICAM-3^{LOW}) were irradiated with the indicated doses of UV in order to induce apoptosis. After irradiation, cells were incubated for 18-24 h at 37°C to allow apoptosis to progress before analysis of cell death by AxV/PI staining and flow cytometry. (**a**) Data showing cell death (%) based on FS/SS light scatter analysis for the different doses of UV. (**b**) Representative FS/SS and AxV/PI staining results from flow cytometry detection of non-induced and 50 mJ/cm^2 UV-induced cells (WT/ICAM-3 low). The FS/SS plots show the 'dead' and 'live' cell regions (pink regions). (**c**) A representative fluorescent microscopy image showing acridine orange (DNA) stained viable and apoptotic cells (50 mJ/cm^2), where the apoptotic cell shows the characteristic morphological features of apoptosis: DNA condensation and nuclear disassembly in apoptotic bodies formed. Results shown are Mean ± SEM of 3 independent experiments (n=3).

Figure 8 shows the cell death analysis results for the titration of UV dose. All doses of UV tested (25, 25, 50, 75, 100, 150, 200 mJ/cm^2) induced high levels of apoptosis

assessed by FS/SS and AxV/PI staining (**Figure 8a**). The dose of 50 mJ/cm^2 was the chosen dose, as it caused high apoptosis levels in a reproducible manner without proceeding directly into necrosis (**Figure 8b**). It is clear that following irradiation, cells no longer appeared in the 'viable zone' of the FS/SS plots indicating loss of viability. These FS v SS analyses in **Figure 8b** show characteristic changes following UV suggesting strong apoptosis induction. This can also be seen by loss of cells from the AxV$^-$/PI$^-$ zone of the AxV/PI stained plots. Whilst it may be necessary to titrate to lower doses of UV to see a dose effect of UV, it is important to note that the UV doses used here produced apoptosis as detected by analysis of nuclear structure (acridine orange stained cells to reveal nuclear morphology; (**Figure 8c)**. Given that apoptosis was a biological phenomenon discovered through morphological analyses, morphology can be considered the gold standard for the detection of apoptosis. 50 mJ/cm^2 is a dose in similar with that used by other workers in the field (Caricchio *et al.*, 2003, Torr et al., 2011). Additionally, Mutu cells appeared to die to the same degree whether they expressed ICAM-3 at normal or low levels. Mutu cells also have a high level of spontaneous apoptosis (Dive et al., 1992). The Mutu ICAM-3^{LOW} were generated by (Torr et al., 2011), where they used sequential fluorescence-activated cell sorting of a WT Mutu population to generate the ICAM-3^{LOW} Mutu expressing cells.

This is important for future studies that will compare the effect of these two different cells on macrophage functions.

3.1.2 Monitoring apoptosis progression of (Mutu) B lymphocytic cells after apoptosis induction.

As the chosen UV dose (50 mJ/cm^2) produced clear apoptosis following 18-24 hours incubation without inducing primary necrosis and this dose was similar to that used in other work (Torr et al., 2011), the next step was monitoring the speed of apoptosis progression following this dose of UV. This would allow us to assess how synchronously the cells died. Mutu B cells, WT and ICAM-3^{LOW}, were irradiated with UV (50 mJ/cm^2) and incubated at 37 °C. After various intervals (1, 2, 3, 4, 24 h) cell cultures were sampled, stained with AxV/PI and analysed by flow cytometry to observe the status of apoptosis. The control sample was where the cell culture samples were analyzed without UV exposure. The results are shown in **Figure 9** WT and **Figure 10** ICAM-3^{LOW}, where they show the progression of apoptosis post-UV radiation over time in the WT and ICAM-3^{LOW} cells respectively. During the first 2-3 hours post-UV irradiation the progression to apoptosis begins as assessed by FS/SS, AxV or AxV/PI. At 3h and 4h post-UV there is a significant induction of apoptosis (AxV+/PI-) seen in

ICAM-3^{LOW} and Mutu WT compared to their controls, which are non-irradiated cells. When compared directly, this induction of apoptosis was similar and not significantly different in both Mutu cells with high and low ICAM-3 (**Figures 11**). After 24 hours, apoptosis reached higher levels but this was associated with some secondary necrosis (as seen in **Figure 8b**). Apoptotic cells are clearly evident from 3-4 hours post-UV as seen in AxV/PI staining (**Figures 9b and 10b**). Changes in cell size and granularity (FS and SS) occur much later, with differences in FS v SS only visible in this time course after 24 hours suggesting AxV/PI staining may provide a more sensitive analysis of early apoptosis. For this reason, the appearance of AxV staining within cells in the FS/SS 'viable' zone (**Figure 8b**) was studied**.** These AxV/PI data are showing the early viability changes towards apoptosis that clearly precede changes in the FS v SS where the 'viable' region becomes empty as all cells have undergone later changes of apoptosis (cell shrinkage and increased granularity). Movement of cells to the 'dead' zone appears to correlate with the onset of PI staining and thus no sign of emitted fluorescence of PI is noted in the 24h timepoint, within the 'live' zone. The histograms of AxV staining, (AxV stained only: **Figures 9c and 10c**) show how the number of dying cells increases with time with large numbers of AxV+ cells at 3-4h post-UV. These results are shown for independent experiments in figure 2d and 3d, where the appearance of apoptosis and loss of viability are shown. The control (non-induced cells) is showing cell death only over longer times and this is due to spontaneous cell death as the Mutu cell lines are fragile and tend to die easily following handling (Devitt *et al.*, 2003). Both WT and ICAM-3^{LOW} cells' rate of apoptosis were compared as shown (**Figure 11**). This comparison shows that they have similar death rates and there was no significant difference in their death rate.

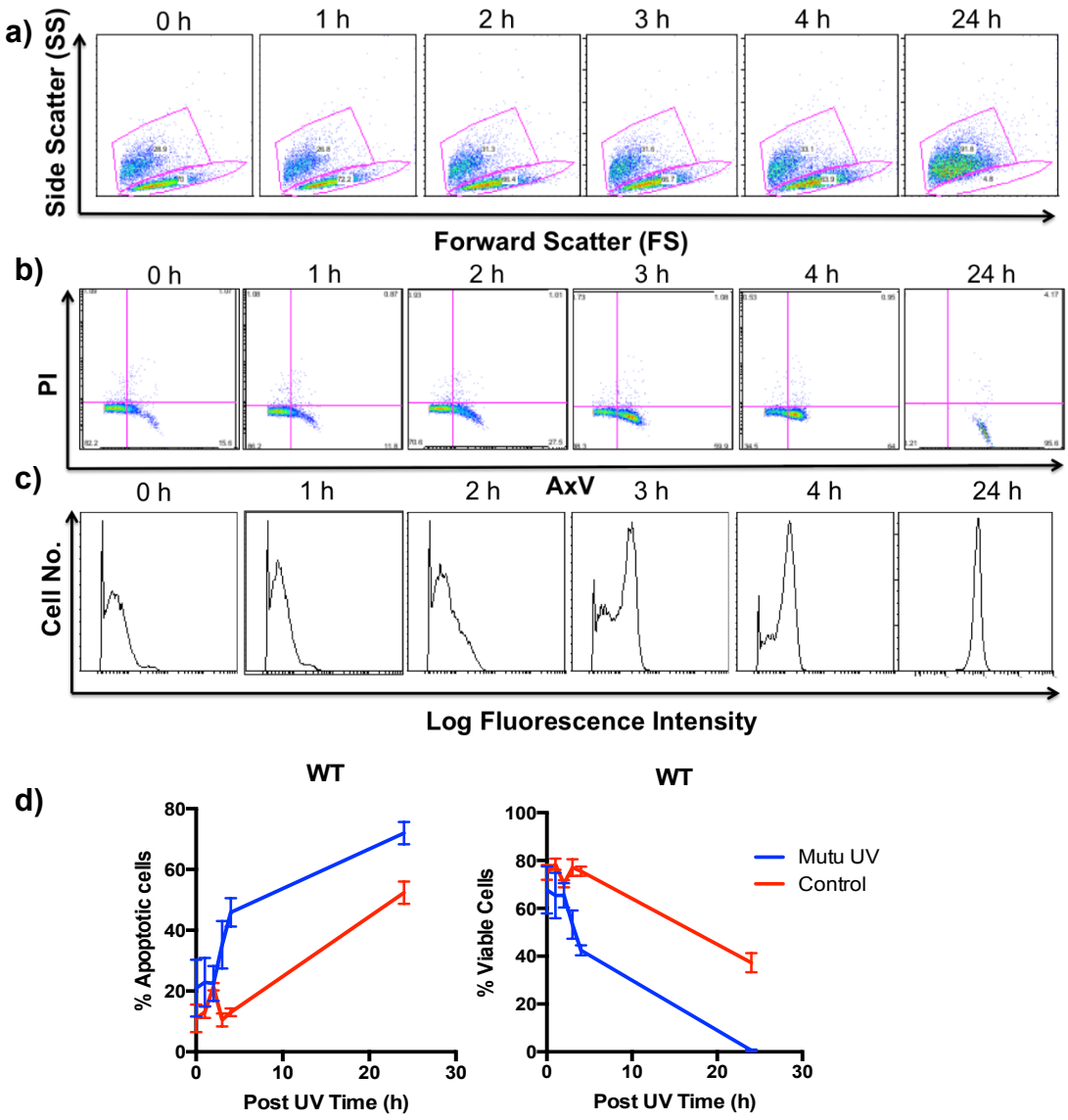

Figure 9. Analysis of the rate of apoptosis in Mutu WT B lymphocytes after UV radiation. Mutu WT B lymphocytes, were irradiated with UV (50 mJ/cm^2) and incubated at 37°C. At the indicated times, cell culture samples were stained with AxV/PI and analysed by flow cytometry to analyze the status of apoptosis and the viability of the cell population. From a representative experiment: (**a**) showing FS versus SS light scatter changes over time with profound loss of cells in the viable zone over time; (**b**) showing AxV/PI staining changes over time with the appearance of apoptotic cells (AxV$^+$/PI$^-$) visible in the lower right quadrant of each plot, and (**c**) showing AxV staining alone showing increased AxV staining over time. 0 h is the control and 1, 2, 3, 4, 24 hours were the time points tested post UV exposure. The 24 h post UV showed maximum cell death and zero cell viability. From three independent experiments (**d**) the percentage apoptosis (AxV$^+$/PI$^-$; left) or viability (AxV$^-$/PI$^-$; right) are shown from AxV/PI analyses. Results shown are Mean ± SEM of independent experiments (n=3). Clear differences in induction of apoptosis are evident at early time points (<4h) with a significant increase in apoptosis first detectable at 4h post-UV (ANOVA with Dunnett's post-test) (*P< 0.05).

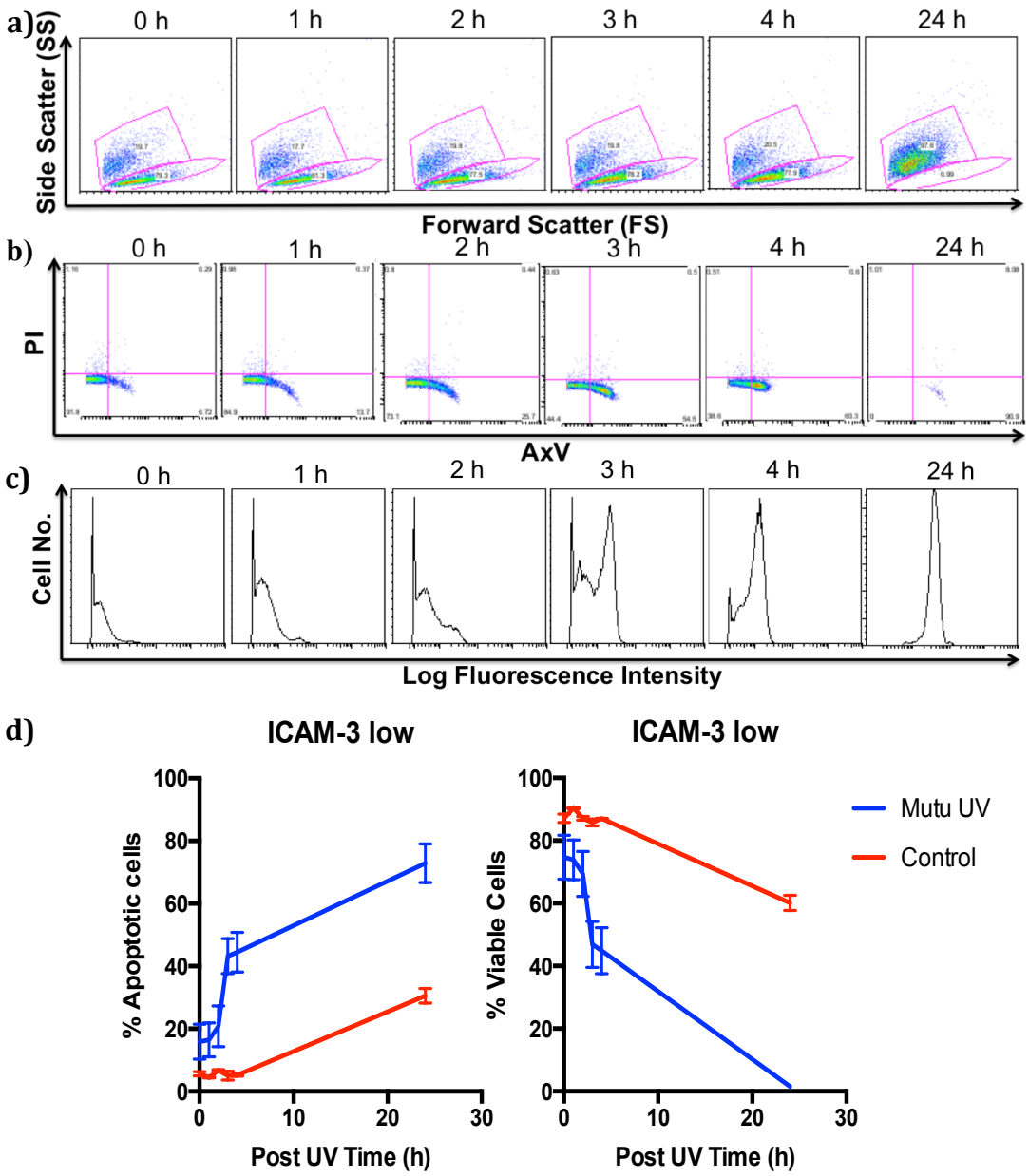

Figure 10. Analysis of the rate of apoptosis in Mutu ICAM-3^{LOW} B lymphocytes after UV radiation. Mutu ICAM-3^{LOW} B lymphocytes, were irradiated with UV (50 mJ/cm^2) and incubated at 37°C. At the indicated times cell culture samples were stained with AxV/PI and analysed by flow cytometry to analyze the status of apoptosis and the viability of the cells. From a single representative experiments, (**a**) showing FS versus SS changes over time, (**b**) showing AxV/PI staining changes over time with the appearance of apoptotic cells visible in the lower right quadrant of each plot and (**c**) showing AxV staining alone over time, showing increased AxV staining over time. 0 h is the control and 1, 2, 3, 4, 24 hours were the tested post UV exposure times. The 24 h post UV showed maximum cell death and zero cell viability. From three independent experiments (**d**) the percentage apoptosis (AxV$^+$/PI$^-$; left) or viability (AxV$^-$/PI$^-$; right) are shown from AxV/PI analyses. Results shown are Mean ± SEM of independent experiments (n=3). Clear differences in induction of apoptosis are evident at early time points (<4h) with a significant increase in apoptosis first detectable at 3 h post-UV (ANOVA with Dunnett's post-test) (***P< 0.001).

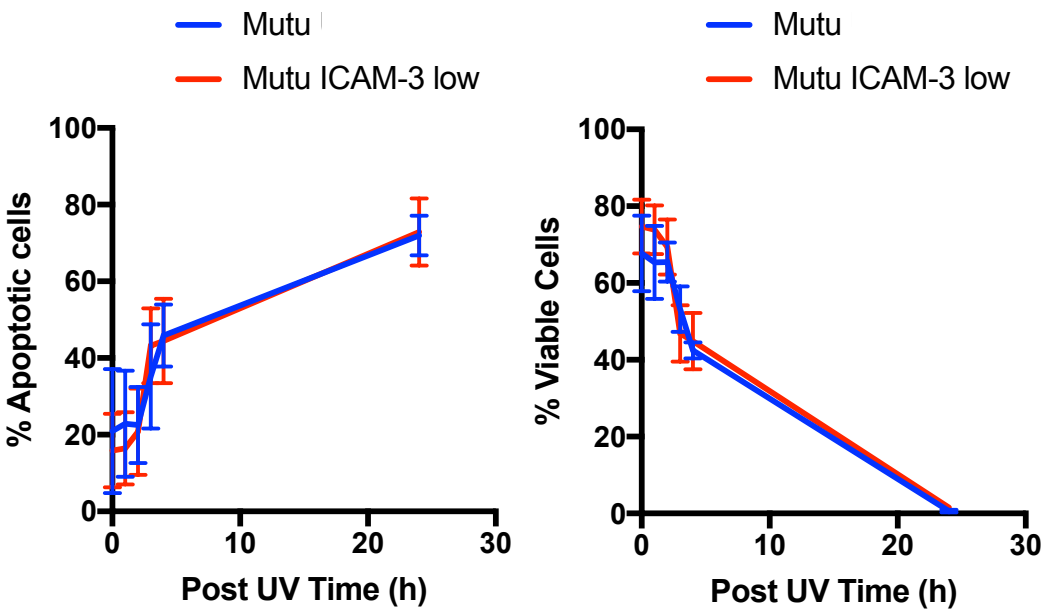

Figure 11. Comparison between Mutu WT and ICAM-3^{LOW} B lymphocytes rate of apoptosis after UV radiation. Data shown are the % of apoptosis and viability after UV radiation in Mutu WT & ICAM-3^{LOW} showing a similar rate of cell death, as the percentage of apoptosis and viability changes in a similar manner for each cell type. Results shown are Mean ± SEM of independent experiments (n=3). No significant difference between WT and ICAM-3^{LOW} in terms of increase of percentage of apoptotic cells and decrease of viable cells at all time points. Statistical analysis used (One Way ANOVA with Tukey's post-test).

3.1.3 Assessing the apoptotic cell derived extracellular vesicles (ACdEV) release from T (Jurkat) and B (Mutu) lymphocytes

Apoptotic cells that express reduced levels of ICAM-3 have been shown to be less able to recruit macrophages by an EV-dependent mechanism (Torr et al., 2011). In order to assess if this is linked to the release of EV from the different cell types, different types of lymphocytes were tested for EV release after induction of apoptosis, B cells (Mutu) and T cells (Jurkat) that were WT (normal ICAM-3 expression) or ICAM3 low were irradiated with UV to induce apoptosis. They were monitored for apoptosis and EV release after 6 h and 18 h post UV exposure. The time points were chosen as they corresponded to high levels of apoptosis (6 h) and post-apoptosis changes (18 h). AxV/PI staining was used to stain induced cells and address PS exposure and membrane integrity. These analyses were done using a flow cytometer to confirm cell staining status (i.e. live (AxV^-/PI^-); early apoptotic (AxV^+/PI^-) & late apoptotic/necrotic (AxV^+/PI^+). Induced cell cultures were centrifuged (2000x*g*) to remove cells and debris and supernatants assessed for EV. The EV were analysed using Tunable Resistive

Pulse Sensing (TRPS) technology with the iZON qNano instrument to give an estimate of EV concentration and size. The results shown in **Figure 12** suggest that there is EV release by 6 h as the medium alone control had a particle count below the level of detection for the instrument. These data also show an increase in EV concentration from 6 h to 18 h post-induction, which correlates with the phase of apoptosis where dying cells progress through apoptosis resulting in more apoptotic body formation and shedding of the plasma membrane. Whilst there is a trend to higher EV numbers at later times, the presence or absence of ICAM-3 had no effect on this. The mean EV diameter at 6h for Mutu WT/ICAM3^{LOW} was 221.3 nm & 241 nm respectively whereas; at 18h the mean diameters were 248.6 nm and 280.6 nm respectively. As for the Jurkat WT/ICAM3 low the mean EV diameter size for 6 h was 239.3 nm and 241.6 nm; the size at 18 h was 228.6 nm and 229.3 nm. Therefore, it appears that the size of released EV from Mutu and Jurkat EV over time (6 h and 18 h) does not show significant differences. Also, size of EV appears not to change on these in these cells with differing ICAM-3 expression (WT/ICAM3^{LOW}). The EV at 18h were viewed in transmission electron microscope in (**Figure 13).**

Importantly, there was no significant difference in concentration in EV release from WT or ICAM-3^{LOW} cells. Also there was no significant difference in terms of EV sizes in WT/ICAM-3^{LOW} cells.

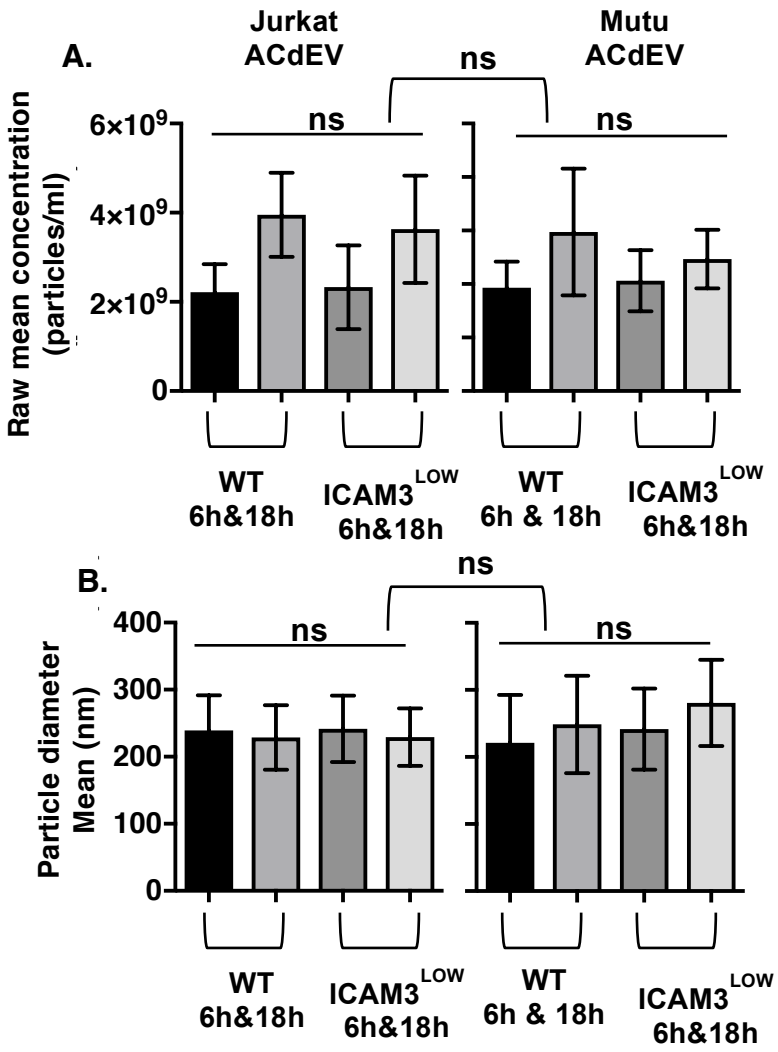

Figure 12. Time course of release of ACdEV from T (Jurkat) and B (Mutu) lymphocytes. T cells (Jurkat cells at 3×10^6 cells/ml) and B cells (Mutu at 3×10^6 cells/ml) were induced into apoptosis with UV doses (100 & 50 mJ/cm^2 respectively) and incubated up to 18 h to allow apoptosis to proceed. For each cell type, WT and another counterpart with a low expression of ICAM3 were analysed. After 6 h and 18 h post UV exposure, the cells culture were centrifuged at 2000*xg* for 20 min, the supernatant was run in the iZON qNano to characterize the ACdEV. Serum free RPMI medium was run alone in the qNano as a control and it was below level of detection. (**a**) Jurkat & Mutu WT/ICAM3-low EV released after 6 h & 18 h post UV exposure. The data shows that there is an increase in ACdEV released from 6 h to 18 h but not significantly different, also there is no significant difference in terms of concentration between Jurkat and Mutu cells. (**b**) Particle diameter mean of the released ACdEV (Jurkat & Mutu WT/ICAM-3^{LOW}) post 6h & 18h apoptosis induction. The data shows no significant difference between 6h and 18h in Jurkat and Mutu and between the cell types in terms of size. Data shown are Mean ± SEM for independent experiments (n=3). Statistical analysis used (One Way ANOVA with Tukey's post-test).

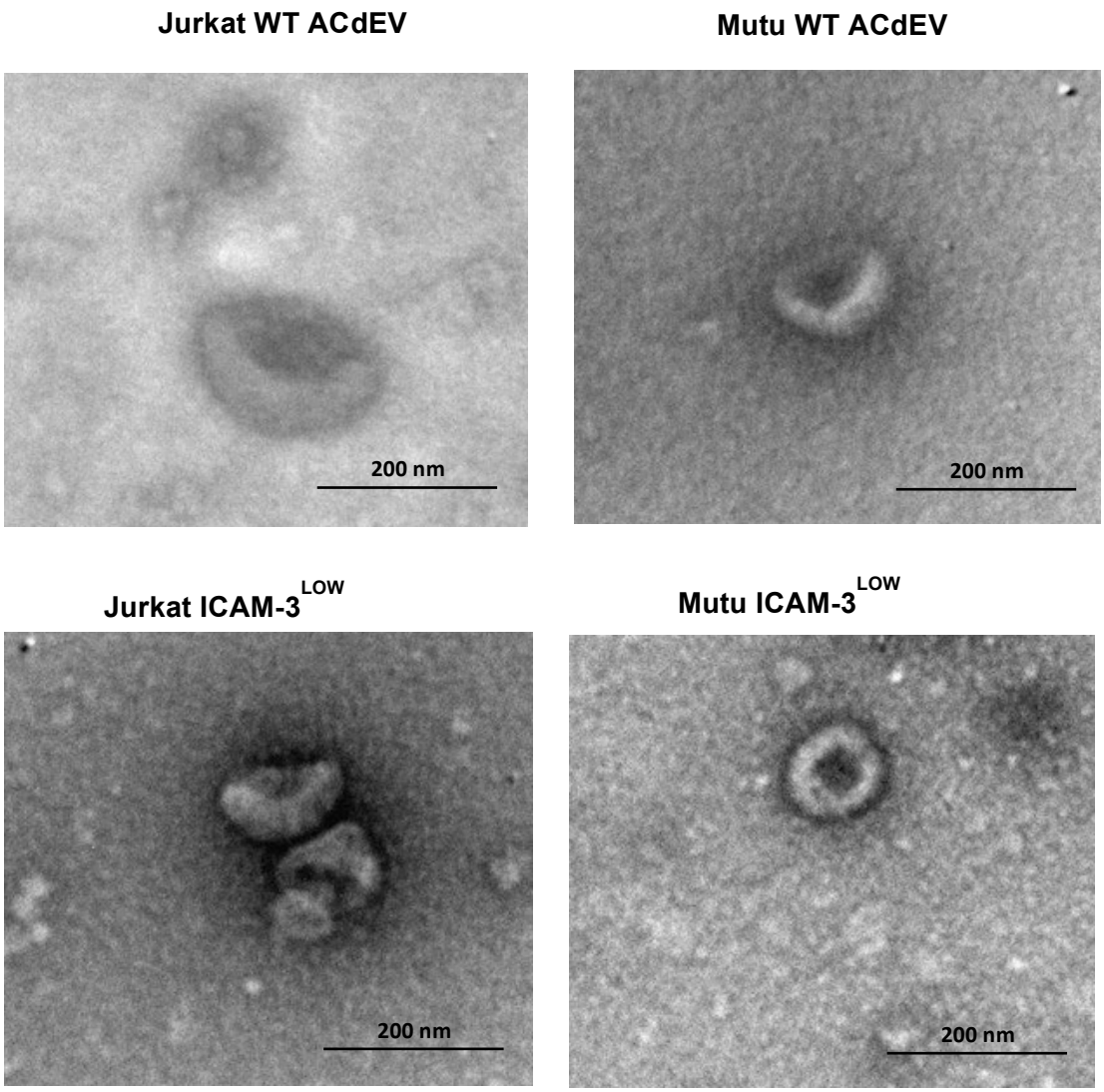

Figure 13. Transmission electron microscopy of ACdEV from T (Jurkat) and B (Mutu) lymphocytes. Samples provided by this project to Aberystwyth University for the TEM.

3.1.4 Establishing a MØ model: using THP-1 cells stimulated with different stimulants

In order to study the clearance of apoptotic cells and the response of macrophages to apoptotic cells, it was necessary to have an established model of macrophages to use as phagocytes. This would allow investigation of the role of ICAM-3 and EV in AC clearance. The THP-1 human monocytic leukaemic cell line was chosen as a monocyte line and was differentiated into MØs by VD3, PMA or double stimulation (VD3/PMA) as has been used previously (Thomas *et al.*, 2013, Torr *et al.*, 2011). After adding stimulants to the THP-1 cells, they were incubated for 48 h at 37°C to allow

differentiation into MØs. The cell phenotype (morphology, adherence and CD14 expression) of the resultant MØ was characterized. The morphology was assessed by observation under the light microscope (**Figure 14**). Photomicrograph images of the THP-1 cells and the range of resultant differentiated MØs reveal clear differences in MØ phenotype generated by the different methods, in agreement with earlier work (Thomas *et al.*, 2013) PMA and DS cause the cells to be elongated and larger in size. They also they become strongly adherent compared to non-stimulated THP-1 cells and are not easily detached from the plastic. However, VD3 stimulated THP-1 cells appear rather similar to the non-stimulated THP-1 cells in shape and morphology though they are slightly more adherent as seen by their sticking to plastic. However, VD3 stimulated THP-1 could be detached by pipetting unlike the PMA and DS cells which remained firmly attached. Previous work has shown that there are large differences between parent THP-1 cells and THP/VD3 (Thomas et al., 2013) and this can lead to differences in cell function. These different features of cells are of use in the range of assays used later in the thesis.

The next cell characterisation was examining the surface protein expression of the cells, specifically CD14 expression. The CD14 expression is an established differentiation marker in the THP-1/MØ assessment studies and is a key receptor for apoptotic cells (Devitt *et al.*, 1998). The cells were stained using indirect immunofluorescence with anti-CD14 mAb 61D3 to assess the CD14 expression (**Figure 15**). The results in F**igure 15a** are showing the cells positive for CD14, in the differently stimulated cells (VD3, PMA and DS) all showing significant differences compared to the non-stimulated THP-1 cells. The three methods of stimulation resulting in MØs are not significantly different in their ability to induce CD14 expression though differences in the level of CD14 expression are clear (**Figure 15b, c**). The DS results in MØs with a significantly higher mean fluorescence intensity compared to VD3, PMA and the non-stimulated THP-1 cells, showing higher levels of CD14 expression. The different stimulants all produced differentiated MØs, though the extent of differentiation may differ in each case (morphology, adherence and CD14 expression).

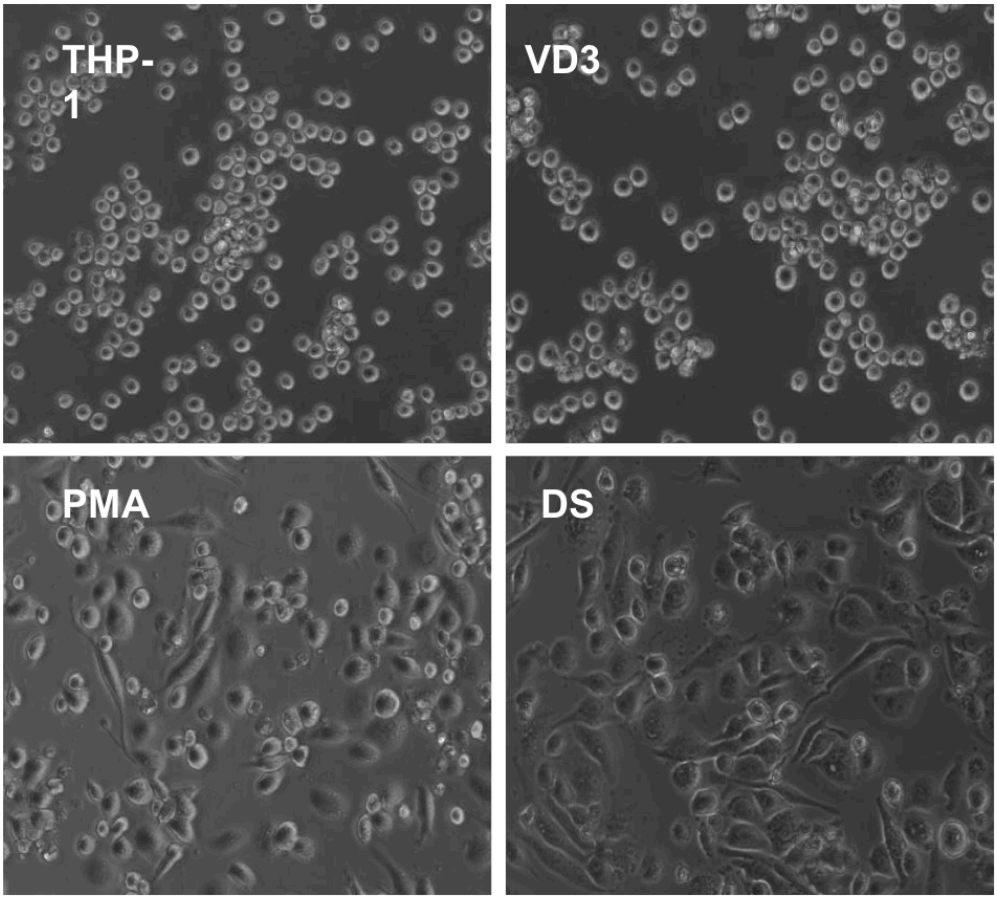

Figure 14. Microscopic analysis of the phenotype of THP-1 cells stimulated to differentiate. THP-1 cells were seeded to 6 well plates at a density of 4×10^5 cells per well with VD3 (100nM), PMA (250nM) or both (VD3/PMA) and incubated for 48-72 h at 37°C to allow them to differentiate to MØs. After the incubation period the cell phenotypes were viewed under a Zeiss Axiovert light microscope and pictures were taken using phase contrast. Representative images are shown of at least three independent experiments. VD3-stimulated cells' phenotype differs from unstimulated THP-1 cells in only being slightly more adherent to plastic whereas the PMA and DS produce larger, elongated cells that are very much more adherent than unstimulated cells.

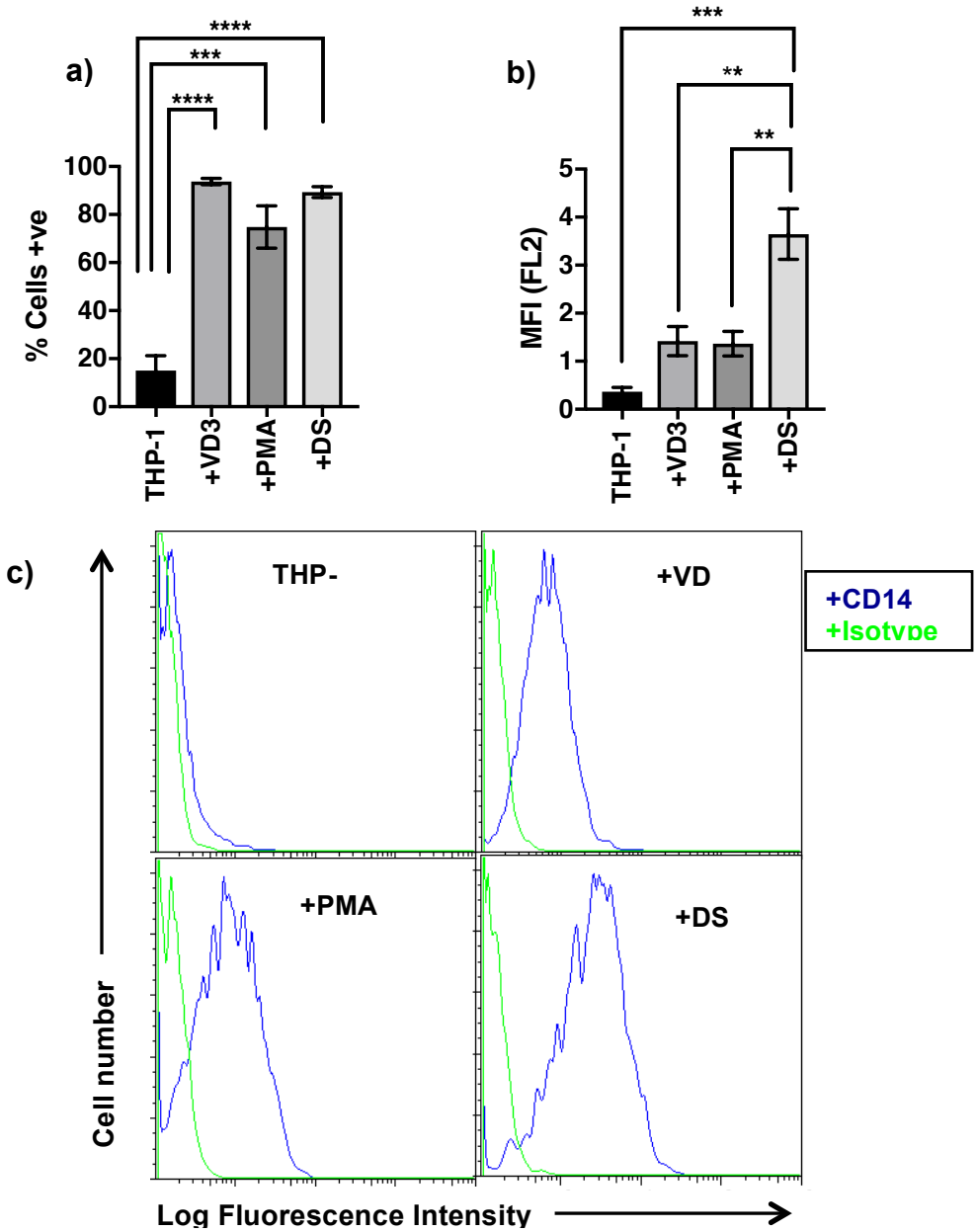

Figure 15. Assessment of CD14 differentiation antigen expression on THP-1 cells stimulated to differentiate. THP-1 cells were seeded to 6 well plates at a density of 4×10^5 cells/well with VD3 (100 nM), PMA (250 nM) or both **(**VD3/PMA) and incubated for 48-72 h at 37 °C to allow them to differentiate to MØs. After the incubation period, the cells were stained using indirect immunofluorescence with anti-CD14 mAb 61D3 followed by goat anti-mouse pAb conjugated with PE. Cells were analysed by flow cytometry to detect surface expressed CD14. A minimum of 5000 events were analysed per sample. (**a**) Showing the positive stained cells with the mAb (61D3-PE) for the different stimulants (**b**) Mean fluorescence intensity (MFI) data comparison between the various stimulants. (**c**) Log fluorescence graphs showing the expressed CD14 on the differentiated THP-1 (MØ) from the different stimulants stained with anti-CD14 mAb 61D3 and isotypes for control. Data shown are Mean ± SEM of independent experiments (n=3). Statistical analysis used was ONE-WAY ANOVA with Tukey's post-test. (**P<0.01)(*** P<0.001)(**** P<0.0001).

3.1.5 Establishing MØ-AC interaction assay

After having acquired the apoptosis induction method through optimizing the dose of UV and establishing the MØ model, the next step was to use both of these cell systems to establish assays of AC clearance. This would allow confirmation and extension of earlier published work regarding ICAM-3. In this section, a MØ-AC interaction assay was established, where the THP-1-derived MØs were seeded to four well glass slides with stimulant at a density of 5×10^4 per ml and incubated for 48 h at 37°C to allow MØ differentiation *in situ* on the glass slides. This generated a sub-confluent density of MØ suitable for microscopy of individual phagocyte cells. PMA-stimulated THP-1 cells were used as they are highly adherent (**Figure 14**) and this enables unbound apoptotic cells to be removed with washing without risk of loss of phagocytes. Also, they have previously been reported to interact with apoptotic cells (Torr et al., 2011, Thomas et al., 2013). The ACs used in these assays were Mutu B cell WT and ICAM-3^{LOW} that were induced to apoptosis by 50 mJ/cm^2 of UV radiation dose and incubated for 18-24 h at 37°C. After the MØ differentiation period, slides were washed with PBS and ACs (WT or ICAM-3 low) were seeded to the four well slides at a ratio of 10 AC:1 MØ with and without the established anti-ICAM-3 mAb MA4 that is capable of blocking ICAM-3 mediated clearance of AC (Torr *et al.*, 2011). The control mAb used in this assay was an isotype-matched control of MA4, MOPC21 of the same structure (mouse IgG1/kappa) but not function (MA4 binds ICAM-3, MOPC21 does not). MA4 and MOPC21 were used at the same concentration. MØ and AC were co-cultured on slides (1 h at 37°C) to allow the interactions between the MØ and the ACs to occur. After this incubation, slides were washed with cold PBS to remove unbound AC, fixed in methanol and stained with Jenner-Giemsa stains. The percentage of MØ interacting with AC (where interaction is the combination of tethering and engulfment) were calculated by scoring them under light microscopy. The data are shown in **Figure 16** and indicate that WT Mutu B cells interact to a greater level than ICAM-3^{LOW} B cells, suggesting ICAM-3 is mediating the interaction between MØ and ACs. That is also suggested by the MA4 mAb which, when added to the assay, significantly reduces the interaction between MØ and WT AC alone. ICAM-3^{LOW} ACs with MØ is not inhibited by MA4, showing specificity for ICAM-3. Interaction is never reduced to zero, most likely because other clearance mechanisms will also be functional. MOPC21 showed no reduction in the percentage of interaction. These experiments show a clear role for ICAM-3 in the interaction of ACs and MØs in agreement with previous work (Torr et al., 2011) and also demonstrate that apoptotic cell associated ICAM-3 is the active ICAM-3.

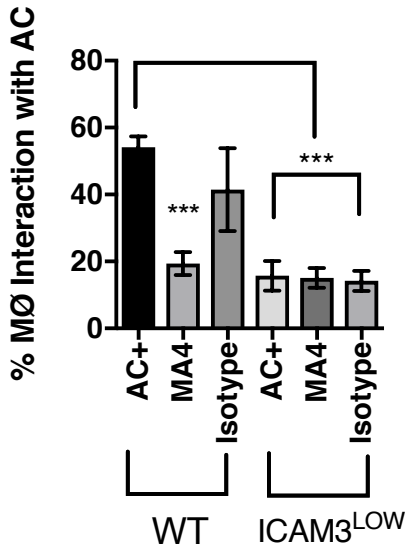

Figure 16. ICAM-3 mediates interaction of apoptotic B (Mutu) lymphocytes with MØ. THP-1 cell were stimulated with PMA for 48 h on four well glass slides to generate macrophages. UV-induced (50 mJ/cm^2 UV & 18-24 h incubation) apoptotic Mutu B lymphocytes that were wild type for ICAM-3 (WT) or reduced for ICAM-3 (ICAM-3low) were co-cultured on macrophages at 37°C. Where indicated, a blocking anti-ICAM-3 mAb (MA4) or an isotype control mAb (MOPC21) was added to the co-culture. After 1 h co-culture, unbound apoptotic cells were removed by washing three times in ice-cold PBS before slide fixation in methanol (10 min). Slides were subsequently stained with Jenner-Giemsa and the percentage of MØ interacting (both tethering and engulfing) with apoptotic cells was scored under light microscopy. At least 200 MØ per well were scored with at least 4 technical replicates per treatment. Data shown are Mean ± SEM for independent experiments (n=3). One Way ANOVA with Dunnett's post-test. ***P<0.001

3.1.6 Establishing and assessing ACdEV interaction with MØ

After assessing the release of the apoptotic cell-derived extracellular vesicles and establishing a MØ-AC interaction, the next step was to investigate the ACdEV interaction with MØ. Of course the main molecule of interest is ICAM-3, where in the previous assay (MØ-AC interaction) it revealed that the interaction of AC with MØ is ICAM-3-dependant, which confirms previous published work (Torr et al., 2011). It has also been shown that ICAM-3 when released on ACdEV promotes MØ migration (Torr et al., 2011). This next series of experiments aims to assess whether ICAM-3 acts as a simple adhesion molecule for EV to enable other cargo to promote MØ migration, or whether ICAM-3 itself is an active attractant. This second situation is as seen for the adhesion molecule fractalkine (CX3CL1) which can act as both as adhesion molecule or classical chemokine (Truman et al., 2008).

In order to observe whether ACdEV interact with MØ, the ACdEV were stained with a fluorescent dye (bodipy).

3.1.6.1 Staining the ACdEV with fluorescent dye bodipy and characterising their physical feature

ACdEV were generated by inducing Jurkat T cells (WT/ICAM-3^{LOW}) into apoptosis by UV radiation, followed by centrifuging the formed AC cultures at 2000x*g* for 20 min to remove apoptotic cell, debris and large apoptotic bodies. The supernatant from that centrugation which contains the ACdEV, where stained with 0.5 µM bodipy. The fluorescent dye bodipy was incubated with the supernatant for 1-2h at 4°C in the dark. After the incubation period, the stained supernatants (containing stained ACdEV and free dye) were run in qEV size exclusion column to remove unbound dye and other soluble factors from the EV fraction. After the qEV size exclusion column, samples were analysed via the iZON qNano to characterise the physical features of the stained ACdEV (WT/ICAM-3^{LOW}). The results (**Figure 17a**) show that the ACdEV mean concentration for WT is $8.9x10^8$ cells/ml, while for ICAM-3^{LOW} it was $1.2x10^9$ cells/ml but they are not signifcantly different, implying that the ACdEV are released at the same rate in the WT and ICAM-3^{LOW} cells as they undergo apoptosis. The ACdEV in the WT and ICAM-3^{LOW} were also shown to have similar mean diameter sizes, where in the WT the mean size was 233.3 nm while in the ICAM-3^{LOW} it was 230.6 nm. Again this indicates that there was no significant difference in sizes of WT and ICAM-3^{LOW} ACdEV (**Figure 17b**).

The next step was to test the fluorescence of the ACdEV from WT/ICAM-3^{LOW} cells to assess equivalent staining. ACdEV stained preparations were run in a fluorescence plate reader and the results show that for the volume of EV tested, they have similar fluorescence and any difference is not significantly different (**Figure 17c**). The fluorescence results correlate with the physical features characterisation, where the concentration and size of ACdEV WT/ICAM-3^{LOW} are similar.

The outcome of this physical features characterisation of WT/ICAM-3^{LOW} ACdEV suggests that both showed similar concentrations and similar sizes. In an attempt to see the effect of staining and qEV exclusion column on the ACdEV concentration and size, the characterised bodipy stained ACdEV WT/ICAM-3^{LOW} were compared to the characterised non-stained ACdEV WT/ICAM-3 which was not run in the qEV exclusion column. In **Figure 18a**, the results are showing that the concentration of the ACdEV that were not run in the qEV column are slightly higher compared to the qEV coumn

run ACdEV, but the they were not significantly different. The ACdEV size was also compared as shown in **Figure 18b**, the results show similar sizes and no significant differences between them. The slight decrease in concentration of ACdEV run in the qEV compared to the non-run ACdEV, may be due to the qEV column removing some EV by non-specific binding.

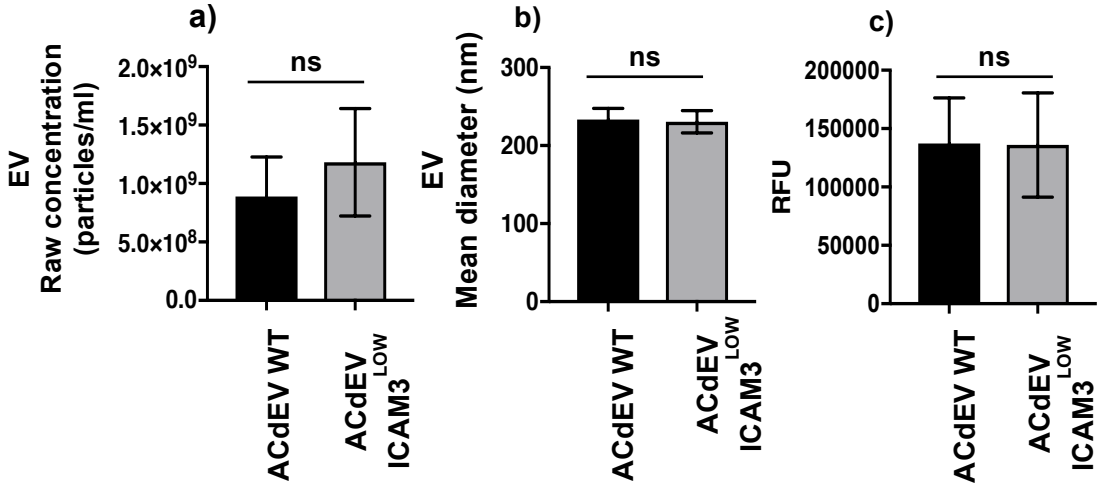

Figure 17. Characterisation of bodipy-stained ACdEV preparations. Jurkat (T) cells (3×10^6 cells/ml) were induced to apoptosis by 100 mJ/cm^2 of UV dose. At 18 h post apoptosis induction, cell cultures were centrifuged at 2000×*g* for 20 min and the supernatant (containing ACdEV) were stained with bodipy, the stained ACdEV were isolated using a qEV size exclusion column to remove unbound dye and other soluble factors. The output from the qEV column was analysed by qNano for characterisation of physical features. (**a**) Concentration of ACdEV WT and ICAM-3^{LOW}, their concentrations showed no significant difference. (**b**) Showing the mean diameter size of the ACdEV WT & ICAM-3^{LOW}, the data shows they have similar mean diameter and no significant difference. (**c**) Fluorescence plate reader data of the bodipy stained ACdEV WT & ICAM-3^{LOW}, the relative fluorescence unit from both samples were shown to be similar and no significant difference. Data shown are Mean ± SEM for independent experiments (n=3).

Overall, this work suggests that the EV can be effectively stained and from the different cell types, the features of the EV were the same. Thus the stained EVs are a useful tool for assessing association of EV with MØ to enable comparison between EV types.

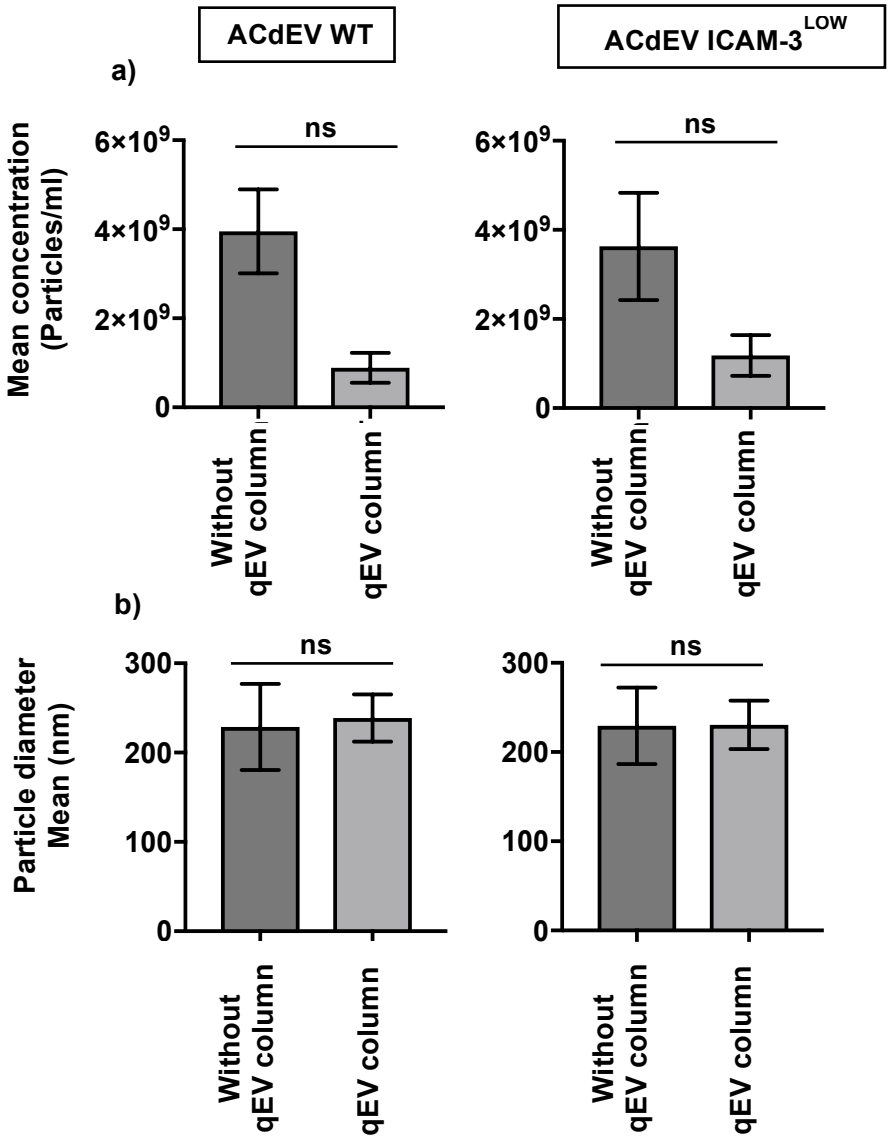

Figure 18. Comparison of the ACdEV characteristics between with and without the use qEV exclusion column. Jurkat (T) cells (3×10^6 cells/ml) were induced to apoptosis by 100 mJ/cm^2 of UV dose. At 18h post apoptosis induction, cell cultures were centrifuged at 2000×*g* for 20 min and the supernatant (containing ACdEV) were stained with bodipy, the stained ACdEV were isolated using a qEV size exclusion column to remove unbound dye and other soluble factors. The output from the qEV column was analysed by qNano for characterisation of physical features. Some of the supernatant (containing ACdEV) was not stained, where it was directly analysed by qNano to be compared with the bodipy stained ACdEV that was run in the qEV exclusion column. (**a**) Concentration of ACdEV WT and ICAM-3^{LOW} with and without qEV column, their concentrations showed no significant difference. (**b**) Showing the mean diameter size of the ACdEV WT & ICAM-3^{LOW} with and without qEV column, the data shows they have similar mean diameter and no significant difference. Data shown are Mean ± SEM for independent experiments (n=3).

3.1.6.2 Bodipy stained ACdEV interaction with MØ

Following the staining of ACdEV WT/ICAM-3^{LOW} with bodipy and characterising them, and concluding that WT/ICAM-3^{LOW} have similar concentration, size and fluorescence, the next step was to incubate them with MØs to test the hypothesis that ICAM-3 promotes MØ recruitment by acting as an adhesion molecule to promote ACdEV association with MØ. In this case, reduced interaction of ICAM-3^{LOW} EV with MØ would be expected.

The bodipy stained ACdEV WT/ICAM-3^{LOW} were incubated with MØ for different time points (0, 10, 30, 60, 120 min) at 37 °C. At each time point, a sample of each of the cells were run in flow cytometer to assess the extent of fluorescence associated with MØ as a measure of EV interaction between the ACdEV and MØs. The data was interpreted by running MØ alone in the flow cytometer for 5000 events and gating the region of the MØ cells in the forward scatter (FS) and side scatter (SS) plot. Then the stained ACdEV were run alone in the flow cytometer for 5000 events to see where they fell. Given their predicted size from the qNano data **(Figure 17**) they were expected to fall outside of this cell zone. Their presence in the forward scatter/side scatter is not significantly in the MØ gated region as shown in **Figure 19a**. After defining the 'MØ cell region' in the flow cytometer FS/SS plot (**Figure 19a**). The co-incubated samples (stained ACdEV+ MØ) were run in the flow cytometer to quantify the percentage of MØ now carrying fluorescence (i.e. associated with EV). In **Figure 19b** the results reveal are showing that after co-incubation, there is significant fluorescence associated with MØ, implying that there is interaction between ACdEV and MØs. After incubation with ACdEV WT the fluorescence intensity histograms reveal higher MØ-associated fluorescence with peaks significantly shifted positively than following incubation with ACdEV ICAM-3^{LOW}. Further detailed analysis of the flow cytometry results from independent replicates reveal that the MØ mean fluorescence intensity (MFI) following incubation with either ACdEV (WT or ICAM-3^{LOW}) was not significantly different (**Figure 20**). Similarly, the percentage of MØ positive for fluorescence was not significantly different. However, in all cases the ACdEV WT showed a trend towards more positive results. Interestingly, the ratio of MFI (ICAM-3^{LOW}: WT) was plotted and the results suggest that there is a difference between ICAM-3^{LOW} and WT, where the ratio figures are below 0.5 suggesting greater association of WT ACdEV and reduced association of ACdEV in the absence of ICAM-3.

To further investigate the interaction and address the involvement of ICAM-3 in the ACdEV interaction, confocal microscopy images were taken of the ACdEV (WT/ICAM-

3^{LOW}) incubated with the MØs. In **Figure 21** the photomicrograph shows a MØ associating with fluorescent ACdEV. The ACdEV WT image suggests a higher number of fluorescent ACdEV bound to the MØ compared to the ACdEV ICAM-3^{LOW}.

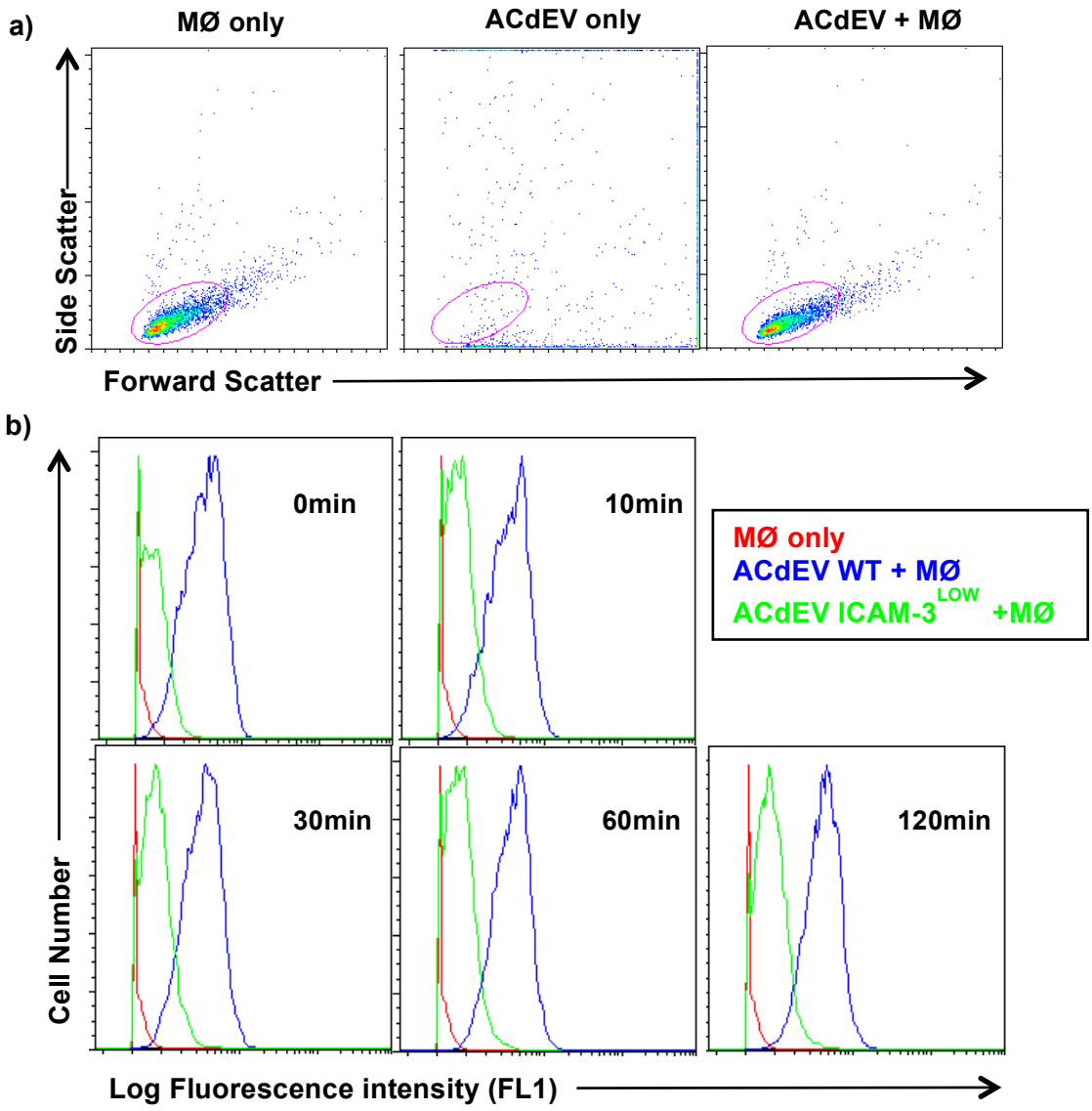

Figure 19. Flow cytometer data of bodipy stained ACdEV incubated with MØ. Bodipy stained ACdEV WT & ICAM-3^{LOW} (1 ml) were incubated with MØ (1 ml 5×10^5 cells/ml) for the indicated times. After each incubation period, the sample mix (ACdEV+MØ) was run directly in the flow cytometer. (**a**) Assay setup plots; MØ only cells were run in flow and gated in the FS/SS, followed by running the stained ACdEV only in the flow, which were shown to be not within the gated region. (**b**) Data shown are representative fluorescence histograms of MØ incubated with the indicated ACdEV or alone during different incubation time points.

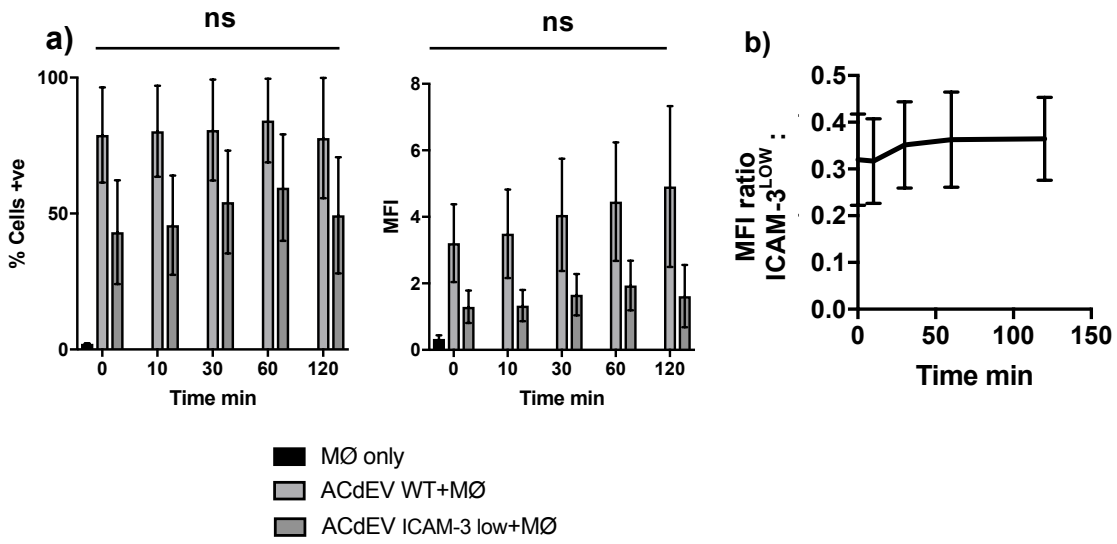

Figure 20. Flow cytometer assessment of bodipy stained ACdEV interaction with MØ. Bodipy stained ACdEV WT & ICAM3^{LOW} (1 ml) were incubated with MØ (1 ml 5×10^5 cells/ml) for the indicated times. After each incubation period, the sample mix (ACdEV+MØ) was run directly in the flow cytometer. (**a**) Flow cytometry data of MØ positive for bodipy stain revealing MØ interaction with stained ACdEV. No significant difference between WT and ICAM-3^{LOW} in terms of % of cells positive and mean fluorescence intensity (**b**) Mean fluorescence intensity ratio of ACdEV ICAM-3^{LOW}. WT, the data reveals relative interaction differences. Data shown are Mean ± SEM for independent experiments (n=3).

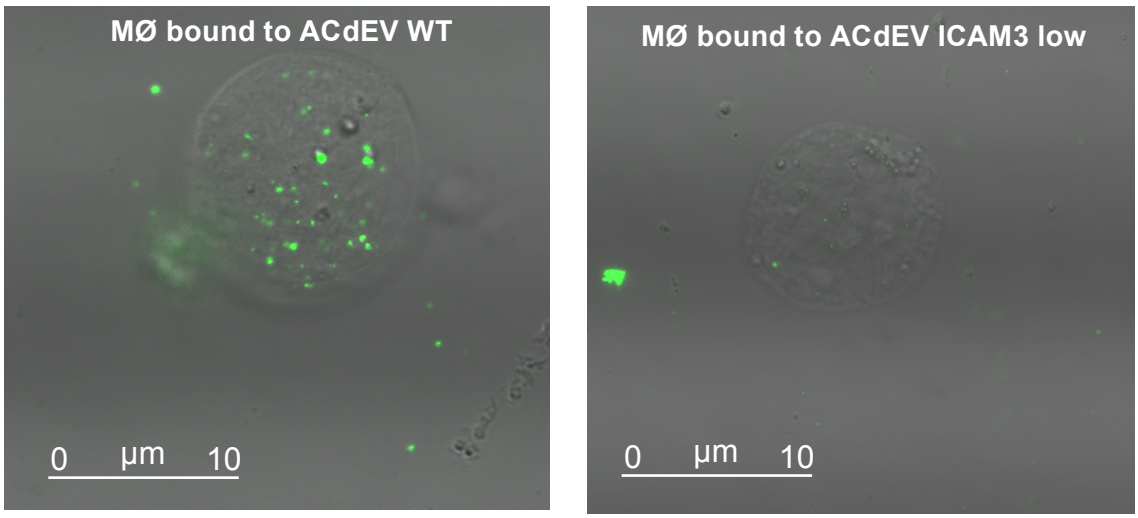

Figure 21. Confocal microscopy images of bodipy stained ACdEV bound to MØ. Bodipy stained ACdEV WT & ICAM3 low (1 ml) were incubated with MØ (1 ml of 5×10^5 cells/ml) for 1 h. After the incubation period, cells were fixed with 1% w/v formaldehyde in PBS and mounted on a glass slide to be viewed by confocal microscopy. Images shown are representative of MØ appearance.

3.1.7 Chemotaxis

After addressing the involvement of ICAM-3 in mediating the interaction between MØ and ACs, the next phase was assessing the chemoattractive abilities of ICAM-3 released from AC. A vertical migration assay was used to assess the chemoattractive abilities of ICAM-3 on ACdEV. In the assay, apoptotic cell-derived extracellular vesicles (ACdEV) from Jurkat T cells & Mutu B cells (WT or ICAM-3^{LOW}) were tested to see if they have chemoattractive abilities in line with previous studies that had previously addressed ACdEV only from B cells (Torr et al., 2011).

3.1.7.1 Vertical Chemotaxis

This method enables investigation of the chemoattraction potential of ACdEV and of ICAM-3 carried on those EVs by using ACdEV from WT or ICAM-3^{LOW} cells. Early work used a different vertical chamber and only apoptotic B cell EV (Torr et al., 2011). Here a new automated system was established that has the potential advantage that many replicates can be run at one time in an automated fashion allowing repeated measures of the same wells throughout the assay. This novel assay enables the kinetics of migration to be assessed and this has not been done before with the ACdEV used here. In this method, apoptotic cell derived EV (WT and ICAM-3^{LOW}), were generated as follows: cultures of UV induced ACs (Jurkat & Mutu) were spun in two stages: the first was 2000×*g* for 20 min to pellet cells and large cell debris and then the supernatant was spun at 120000×*g* for 70 min to pellet the EV. The EVs were resuspended in fresh serum-free RPMI and added to 24-well plates, followed by the placement of 8.0 µm pore transwell which had THP-1-derived MØ added to their upper well (**Figure 22**). The THP-1 derived MØ were seeded at a density of 5×10^5 cells/well with the stimulant VD3. The Cell IQ tracking system scored the migration by assessing the appearance of MØ in the lower well and the activity was recorded for 12 h.

The data were analysed via the Cell IQ software. The results shown in **Figure 22** reveal the number of MØ migrated towards the Jurkat & Mutu ACdEV (WT/ICAM-3^{LOW}) over a 12 h period. The Jurkat T cell ACdEV results show significant MØ migration towards ACdEV over time but that the number of MØ migrated towards ACdEV WT (with ICAM-3) is statistically significant compared to ACdEV ICAM-3^{LOW} (**Figures 22 and 23**). The data do show that ACdEV, regardless of ICAM-3 levels, are chemoattractive, as there was significant difference between migrations to ACdEV (ICAM-3 WT or ICAM-3^{LOW}) compared to the negative control (serum-free RPMI).

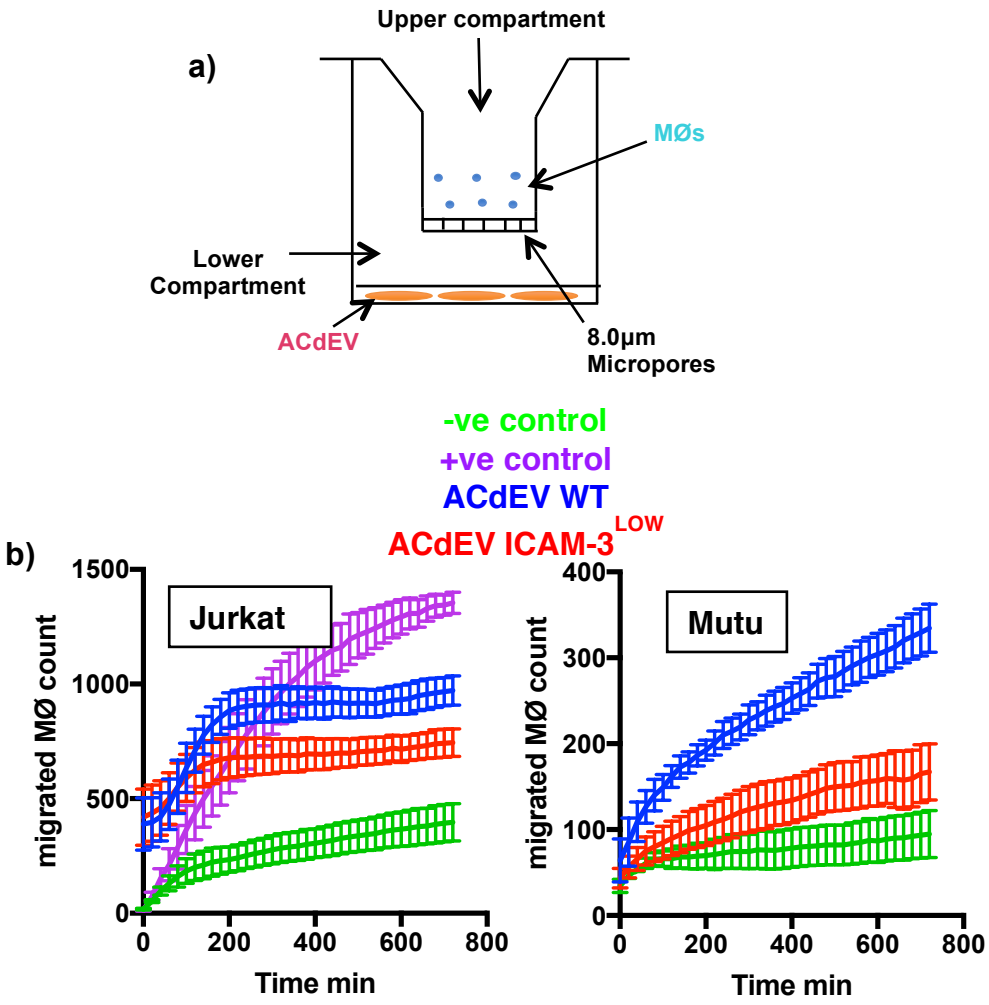

Figure 22. Assessing the chemoattractive potential of ACdEV and ICAM3 for MØ in a vertical chemotaxis assay. Jurkat (T) & Mutu (B) cells (3×10^6 cells/ml) were induced to apoptosis via UV (100 & 50 mJ/cm^2 respectively) and incubated for 18-24h to allow apoptosis to proceed. After the incubation period, the cells were centrifuged at 2000×*g* for 20 min to remove cells and large debris; the supernatant was collected and centrifuged at 120000×*g* for 70 min. The ACdEV pellet was resuspended in serum-free RPMI and used as a putative chemoattractant for the assay. The MØ density used in the assay used was (5×10^5 cells/ml). (**a**) Diagram of assay set up showing the lower compartment where the ACdEV are loaded (700 µl) and the upper transwell compartment where MØ were placed (300µl). (**b**) Migration of MØ to ACdEV from two cell types (Jurkat & Mutu). ACdEV harvested from UV-induced apoptotic Jurkat & Mutu cells (WT & ICAM-3 low) were placed in the lower well of 24-well plates and transwells with MØ (derived from THP-1 stimulated with VD3) were placed on top of them in the wells. Wells were monitored for 12 h in the Cell IQ tracking system to score MØ appearance in the lower compartment as a result of MØ migration from the upper compartment. Migration of MØ towards ACdEV from Jurkat & Mutu WT (blue) ICAM-3low (red) are shown. Data shown are mean SEM ± of independent experiments (n=3) with 5 technical replicates from each independent experiment.

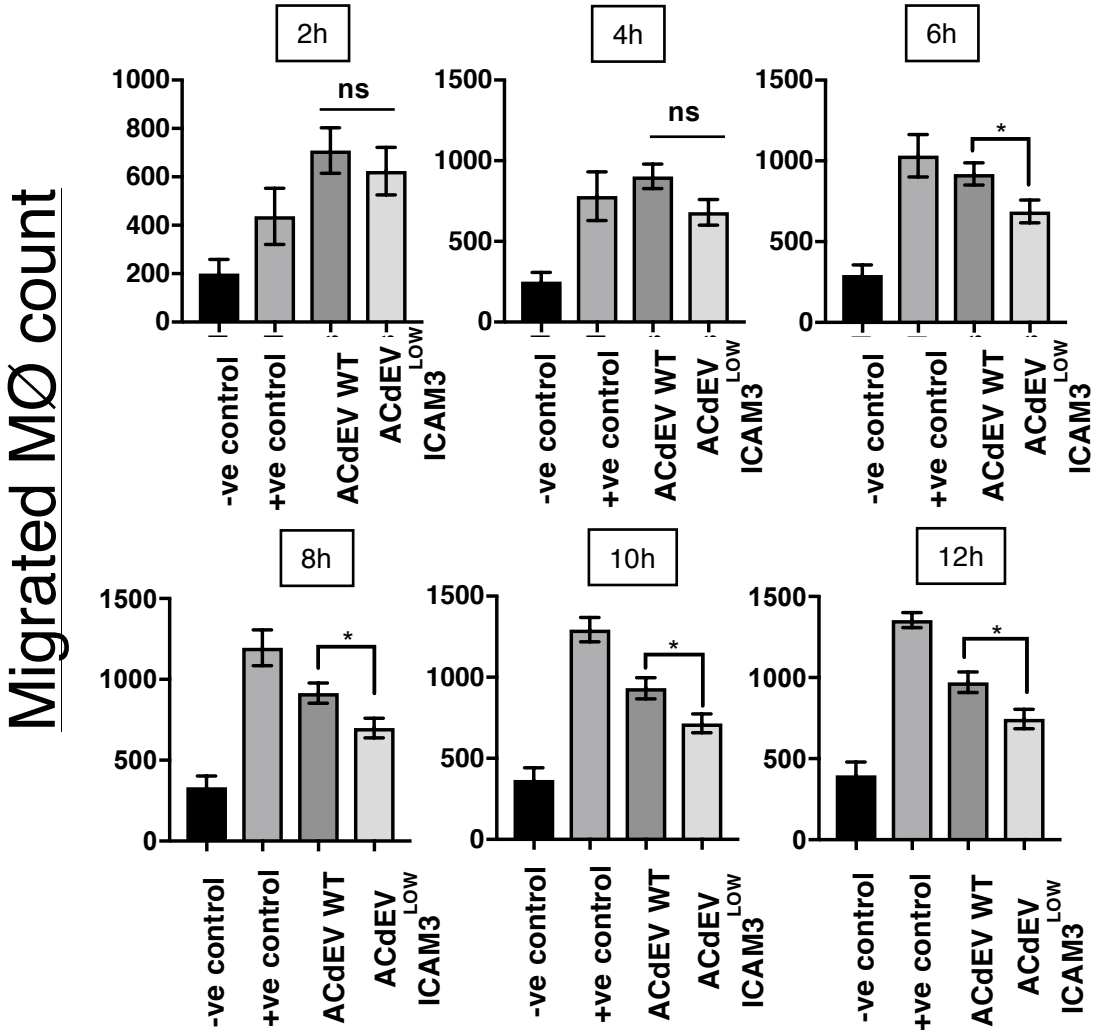

Figure 23. Analysis of the chemoattractive potential of T cell-derived ACdEV and ICAM3 for MØ. The data from **Figure14C**, which were accumulated up to 12 h, were dissected into 2 h each for further analysis. The data shows the number of migrated MØ towards ACdEV WT & ICAM3^{LOW} are significantly different from 6 h to 12 h, the difference insignificance is observed from 2 h to 4 h. Data shown are mean SEM ± of independent experiments (n=3) with 5 technical replicates from each independent experiment. Statistical analysis used was (One-Way Anova with LSD Fisher post-test) (*P<0.1).

On the other hand, MØ migration to Mutu B cell ACdEV reveal a significant difference between ACdEV ICAM-3 WT and ICAM-3^{LOW} in terms of number of MØ migrated from early time points (**Figures 22b and 24**). Interestingly, in this experimental set up, the ACdEV ICAM-3^{LOW} are not significantly chemoattractive when compared to the negative control (serum-free RPMI), but the ACdEV WT has shown significantly higher recruitment compared to the negative control. This may suggest that the basic level of EV chemoattractive potential differs between different cells.

In summary, the results in **Figures 22, 23 and 24** reveal that ACdEV from Jurkat T cells and Mutu B cells are chemoattractive when carrying ICAM-3, and that ICAM-3 on EV can promote the migration.

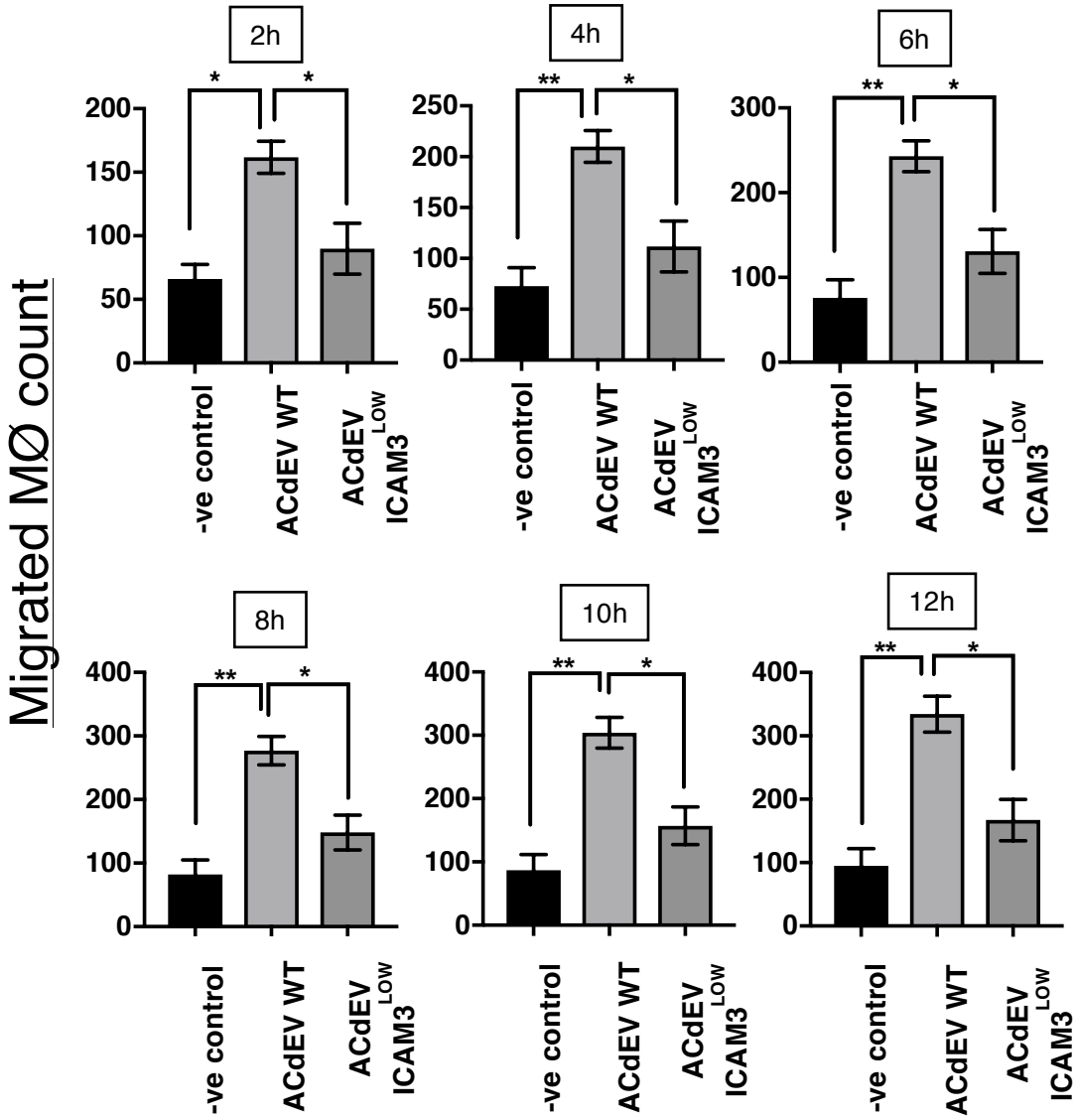

Figure 24. Analysis of the vertical chemotaxis assay of MØ migrating towards the ACdEV from Mutu (B) cells. The data from the previous figure, which were accumulated up to 12 h, were dissected into 2 h each for further analysis. The data shows the number of migrated MØ towards ACdEV WT & ICAM3^{LOW} are significantly different. The difference significance is observed in all of the times from 2 h to 12 h. Data shown are mean SEM ± of independent experiments (n=3) with 5 technical replicates from each independent experiment. **(**One-way ANOVA with Tukey's post-test) (**P*<0.05) (***P*<0.01).

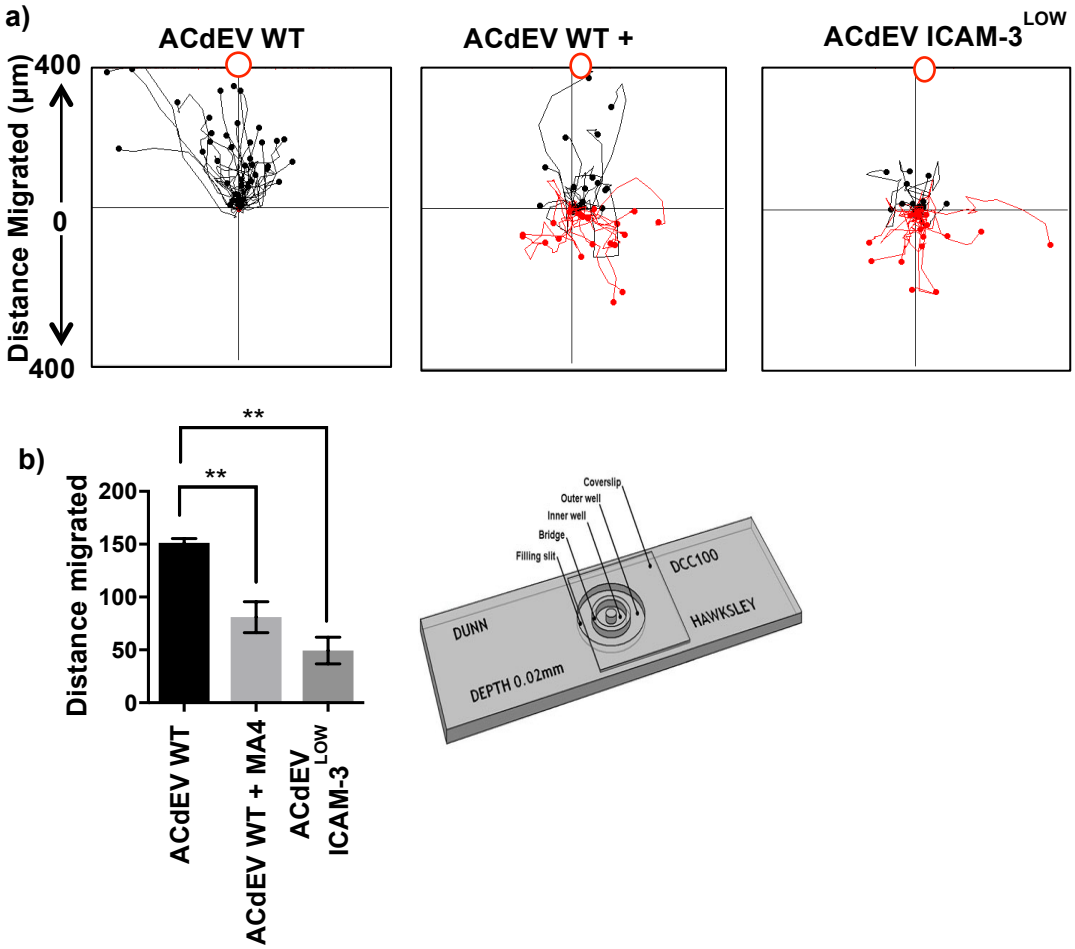

Figure 25. Assessing the chemoattractive potential of ACdEV and ICAM-3 for MØ in a horizontal chemotaxis assay. THP-1 cells were stimulated with VD3 (100 nM) and seeded to glass coverslips (4×10^5 cells/coverslip) to generate MØ (following 48-72h stimulation). After differentiation, coverslips were inverted on Dunn chamber slides to observe and record their migration towards ACdEV (WT and ICAM-3^{LOW}). Mutu (B) cells (3×10^6 cells/ml) were induced to apoptosis via UV (50 mJ/cm^2) and incubated for 18-24h to allow apoptosis to proceed. After the incubation period, the cells were centrifuged at 300x*g* and the supernatant (containing ACdEV) was collected, the ACdEVs were added to the outer chamber of the slide, and the bridge between the two chambers was where migration was observed. The observation and recording was done by time lapse imaging phase contrast microscopy (Zeiss Axiovert motorised microscope) with images taken every 10 min for 2 h. (**a**) Horizontal chemotaxis plot data showing migration of MØ towards the ACdEV WT/ICAM-3^{LOW}, the red circle is the chemoattractant source. MØs were tracked and plotted following analysis with Image J & Chemotaxis migration tool. 40 cells were tracked in line with manufacturer's guidance. (**b**) Plotted distance of migrated MØs towards the ACdEV WT/ICAM-3^{LOW}, there was significant difference in distance migrated between the AcdEV WT and ICAM-3^{LOW} and between AcdEV WT and the AcdEV WT treated with anti-ICAM-3 mAb MA4. Dunn chamber slide is shown in the right. Data shown are mean SEM ± of independent experiments (n=3). Statistical analysis used (One-Way Anova with Dunnett's post-test) (**P<0.01) Work done by colleague (Parbata Chauhan).

There are several potential downsides for this automated technique of chemotaxis. Firstly MØ migration could be aided by gravity and mask real chemotaxis and inappropriately assess chemokinesis as directional recruitment. Secondly, the analysis software is labour intensive, where the protocol must be set up manually and the software instructed which particles in an image are MØ and this has been very time consuming. However, this vertical system allows multiple replicates and treatments to be undertaken at a single time. Updating the intelligence of the software is constant to produce a robust analysis protocol.

There is another form of chemotaxis assay that assesses chemoattraction and it is a horizontal chemotaxis assay. The horizontal assay removes the aspect of gravity, where it will test the chemoattraction more thoroughly with the gravity effect out of the equation. Due to microscopic failure it was not possible to apply this assay, however a student colleague (Parbata Chauhan) effectively used it before the microscopic failure. This assay had tested the chemoattraction abilities of ICAM-3 on ACdEV, she acquired the ACdEV from 300x*g* centrifugation of UV induced apoptotic Mutu B cells. The results of this work showed that ACdEV WT showed chemoattraction abilities and that there was significant difference between ACdEV WT and ICAM-3^{LOW} in terms of distance migrated by MØs (**Figure 25a and 25b**). Also the ICAM-3 chemoattraction abilities was tested by adding anti-ICAM-3 mAb MA4 to ACdEV WT and it showed significant difference compared to the untreated ACdEV WT (**Figure 25a and 25b**). Together, these data suggest that ICAM-3 and ACdEV can promote directional migration of macrophages rather than just stimulating random movement.

3.1.8 Assessing purified ICAM-3 protein in vertical chemotaxis assay

The results above suggest that ICAM-3 may function as an adhesion molecule in ACdEV and it can, in at least some cases, promote chemoattraction of MØ. In these cases, ICAM-3 chemoattraction functions were tested within the context of ACdEV. It was therefore considered sensible to test the chemoattractive potential of purified ICAM-3, to assess whether the chemoattraction abilities are solely due to ICAM-3 without the help of other proteins within the ACdEV. Previous work has shown that CX3CL1 can act as both an adhesion molecule and a chemoattractant when released from cell surfaces (Truman et al., 2008). To test this, purified recombinant ICAM-3-Fc fusion protein was tested as a potential chemoattractant in the vertical chemotaxis assay as used in (**Figure 22)**. The results in **Figure 26** show the number of MØ migrated towards purified ICAM-3-Fc fusion protein in comparison to human IgG

as a control Fc-containing protein or serum-free RPMI as a negative control. The ICAM-3-Fc shows a non-significant trend towards increased MØ migration compared to serum-free RPMI. However, ICAM-3-Fc did not show chemoattractive potential above IgG alone suggesting that purified ICAM-3 protein has no chemattraction abilities.

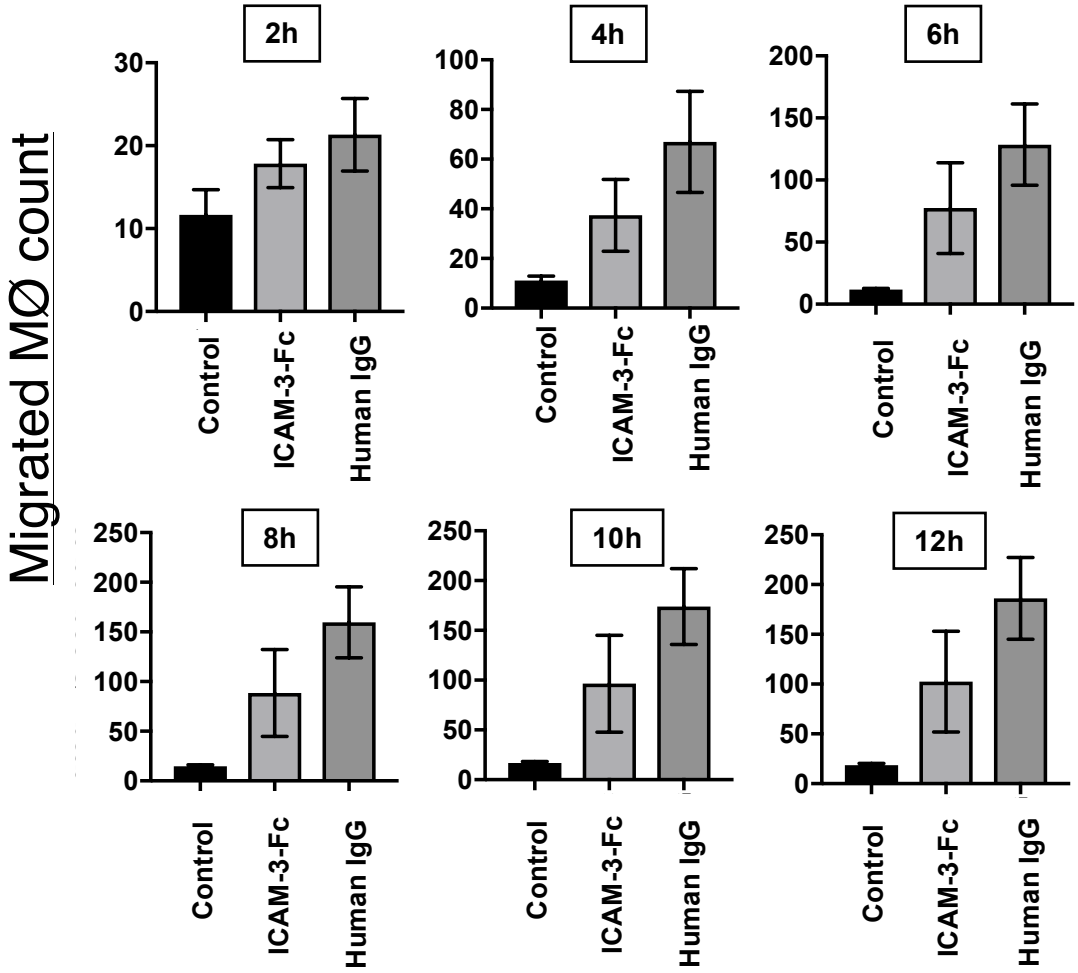

Figure 26. Assessing the chemoattractive abilities of purified ICAM-3 protein conjugated with Fc in attracting MØ in a vertical chemotaxis assay. Purified ICAM-3 conjugated with Fc region was tested in a vertical chemotaxis assay, by adding (10 μg/ml) in the bottom well of the 24-well plate, and the transwells with MØ (derived from THP-1 stimulated with VD3) were placed on top of them in the wells. Wells were monitored for 12 h in the Cell IQ tracking system to score MØ appearance in the lower compartment as a result of MØ migration from the upper compartment. The data accumulated from the 12 h were dissected into 2 h and their data plotted at each 2 h period. Data shown are mean SEM ± of independent experiments (n=3) with 5 technical replicates from each independent experiment.

3.2 Discussion - Chapter 1 - ICAM-3 & ACdEV in chemotaxis

A role for ICAM-3 in the clearance of apoptotic cells has been known for nearly 20 years (Moffatt et al., 1999) though there is a significant lack of knowledge surrounding exactly how ICAM-3 functions as an *eat me* signal. More recent work has shown that ICAM-3 lost from the surface of dying leukocytes and that this ICAM-3 can be found in vesicles released during cell death (Torr et al., 2011). This work showed that ICAM-3 on EV promoted the chemoattraction of MØ. However, the mechanism of action of ICAM-3 is not known. As ICAM-3 is an established adhesion molecule (Fawcett et al., 1992, Bleijs *et al.*, 2000), it seems reasonable that ICAM-3 on EV may act to bind the EV to the recipient MØ cells and other EV-associated molecules may activate the migration. However, it is possible that ICAM-3 itself is the activating factor (i.e. chemoattractant), or it may work in both facilitating tethering and acting as an activating signal. This chapter attempted to test the hypothesis that ICAM-3 functions on apoptotic leukocyte-derived EV to promote efficient binding of the EV to the MØ.

In the present study, in order to test the hypothesis that ICAM-3 on ACdEV acts to bind EV efficiently to MØ and thus promote MØ activation to enable migration, the initial step required was to establish a robust model of apoptosis. This was central to the generation of apoptotic cells and vesicles. The method chosen was UV irradiation as this has been widely used as it induces rapid and synchronous apoptosis (Devitt et al., 2003, Devitt et al., 2004, Salucci *et al.*, 2013). Previous work from the Devitt group has also used many other inducers of apoptosis (e.g. staurosporine, calcium ionophores, cold shock, serum starvation, etoposide), these other methods often induced apoptosis slowly, asynchronously and generated high levels of necrotic cells (Devitt et al., 1998, Moffatt et al., 1999, Devitt et al., 2003, Turner *et al.*, 2003, Devitt et al., 2004). So the ability of UV to induce rapid and synchronous apoptosis would be valuable. This would be also important for generation of EV as cells at different phases of apoptosis may induce different responses.

UV radiation induces apoptosis mainly via the intrinsic mitochondrial pathway (Dunkern *et al.*, 2001). Initially, the UV irradiation dose was titrated to assess the effect on promoting cell death. The results revealed that all doses of UV tested (25-200 mJ/cm^2) induced high levels of apoptosis with an overnight incubation to allow apoptosis to proceed. Previous studies (Devitt et al., 2003, Turner et al., 2003, Devitt et al., 2004)

have used 100 mJ/cm^2 but data shown here indicate such high levels of UV are not needed. Importantly, induction of primary apoptosis without primary necrosis (where cells become leaky without first becoming apoptotic) was the aim. Data shown here demonstrates that 50 mJ/cm^2 was efficient in inducing apoptosis in Mutu B cells, where it produced a high rate of apoptotic cells without promoting necrosis. A lower dose of UV may be possible and future work could identify the lowest dose needed. However, UV can induce cell death by a range of mechanisms: direct DNA damage and oxidative stress (Chan and Yu, 2000, Lee *et al.*, 2013). Lower doses of UV may reduce oxidative stress and possibly slow down the cell death induction as DNA damage would be cell cycle dependent. A slower, less synchronous cell death would not have been useful for these studies.

The chosen 50 mJ/cm^2 dose of UV was consistent in inducing apoptosis in both types of B cells used (WT and ICAM-3^{LOW}; **Figure 11**). This was confirmed using nuclear morphological staining and AxV/PI, where AxV/PI staining via flow cytometric analysis showed a high rate of apoptotic cell death. The AxV positivity (in the absence of PI staining) reveals that the cells have flipped their PS to the outer leaflet of the cell membrane, which is a characteristic sign of apoptosis (Fadok et al., 1992). Whereas PI positivity shows that the cell are losing their membrane integrity allowing the PI to go inside the cell and bind to the DNA, indicating the cells have started to proceed to necrosis. In the experiments reported here, necrosis was only seen after overnight incubation and this necrosis is secondary necrosis where the loss of membrane integrity follows apoptosis, which was demonstrated using nuclear morphology assessment to reveal classic apoptotic morphology (condensed chromatin). This compares to primary necrosis where cells directly become leaky after a stimulus. Thus the method of apoptosis induction used here agrees with previous work conducted (Devitt *et al*., 2003) and although the measured dose used differed (50 versus 100 mJ/cm^2), the induction of cell death was equivalent. This apparent difference could be due to the method of measuring the wavelengths of UV as different detectors may be detecting different ranges of UV and the original work did not attempt to find the lowest useable dose of UV. Importantly, the overall results are that both doses of UV induced strong apoptosis in B cell lines and 50 mJ/cm^2 was chosen for future studies. The Mutu B cell line was chosen because it expresses ICAM-3 (as this is a human leukocyte specific antigen) and they have been widely used in studies of ICAM-3 and apoptotic cell clearance.

Studies of the rate of apoptosis progression in UV-induced B cells (WT/ICAM-3^{LOW}) also support the chosen UV dose. Apoptosis in Mutu cells was monitored post-UV exposure and results demonstrate rapid apoptosis with early phases of apoptosis clearly detectable in a large proportion of cells at 3-4h post UV exposure. At this time point, the cells were considered in early phases of apoptosis because they showed AxV positivity and PI negativity (i.e. the cells have exposed their PS and yet maintain their plasma membrane integrity). Also this change in PS exposure occurred before changes in cell size and granularity (assessed by FS v SS). Late apoptotic/secondary necrotic cells are smaller in size and more granular than live/early apoptotic cells which are larger in size and less granular. The later time points show the progression into secondary necrosis. Interestingly, this late stage of apoptotic cells has been widely used in AC clearance studies (Devitt et al., 2003, Devitt et al., 1998). Non UV-treated cells also showed some death over the time course of the experiment. This is because Mutu cells have a high tendency to die spontaneously (Dive et al., 1992). This feature of high spontaneous apoptosis will be used later in this thesis as it is a benefit to the *in vivo* studies shown later.

The data showing the progression of apoptosis following UV was compared for cells expressing wild type and low levels of ICAM-3 (Mutu-WT & Mutu-ICAM-3^{LOW}). The appearance of apoptosis and the simultaneous loss of viability, was equivalent in the two cell types. This is an important result as different kinetics of death in the two cell lines may have resulted in the generation of different EV preparations that could have functioned differently in later experiments.

3.2.1 Establishing a MØ model and a MØ-AC interaction assay.

Acquiring a robust MØ model was vital in this project, as it would pave the way for further investigation into the AC clearance, as MØ are key players in that process. THP-1 human monocytic cells were differentiated into MØ with different stimulants which are commonly used to model macrophage functions (Schwende et al., 1996, Daigneault *et al.*, 2010). THP-1 were treated with 1,25-dihydroxyvitamin D3 (VD3), phorbol -1,3-acetate (PMA) or both stimulants i.e. double-stimulated: DS (VD3/PMA) for 48-72h. The VD3 stimulant alone produced MØ phenotypes similar to unstimulated THP-1 cells when viewed by microscopy though they were slightly more adherent than non-stimulated cells. However, THP cells stimulated with PMA or double stimulated (DS) produced very different phenotypes with respect to morphology (size, shape and spreading). VD3 and PMA are known to up regulate protein kinase C (PKC) isoenzyme expression, but the PMA treatment differs by causing the translocation of the PKC

isoenzymes to the membrane. PKC isoenzymes are involved in various cellular processes such as regulation of cell proliferation, and differentiation (Monick *et al.*, 1998, Lin *et al.*, 2007).

The VD3 treated THP cells were shown to be loosely adherent, which makes them excellent for migration assays as they can detach and migrate easily. However they would not be practical in MØ-AC interaction assays. These assays are undertaken on glass slides and unbound apoptotic cells are removed by extensive washing. In this assay, weakly adherent MØ (e.g. THP/VD3) would get washed off slides and this would significantly impact on the results that could be obtained.

The PMA and DS treated THP-1 cells were shown to be strongly adherent and had lamellipodia-like structures, and they were not detachable by shaking nor by PBS washing. THP/PMA and THP/DS cells required EDTA for prolonged periods to allow them to round up (i.e. to detach partially) and they then required extensive pipetting to detach them fully. Their extremely strong adherence is excellent in MØ-AC interaction assays (as they are not easily washed away). However, it is not a desirable feature for using them in MØ migration assays as they adhere too strongly to release from the slides and migrate.

All of the different stimulation approaches used upregulated CD14 (a highly characterised MØ marker) expression on the MØ, but the DS showed the highest expression of CD14 compared to the other stimulants. The common result from the different stimulants is that they produce MØ that eat AC well (Thomas *et al*., 2013). It is possible that each of the different models generates a slightly different stage of differentiated cell. Monocytes are suspension cells found in the blood but during activation they increase their differentiation markers (e.g. CD14) and become more adherent so that they can emigrate the blood and migrate towards inflammatory stimuli in the tissues. So it seems possible that THP/VD3 cells may be less differentiated than the other cells. The results shown here correlate with previous work conducted (Schwende et al., 1996, Thomas et al., 2013). This previous work showed that VD3 treated THP-1 cells have high CD14 expression, even though the phenotype by microscopy did not differ from the THP-1 alone. Thomas *et al*. (2013) compared in detail the phenotypes of MØ from the three stimulants and suggested that they could be M1 and M2 categories of the MØs. M1 being pro-inflammatory and M2 are types of repair MØ, but this has never been confirmed due to the fact that there are no simple diagnostic markers of M1 and M2 MØ for human cells (Mosser and Edwards, 2008).

The establishing of the MØ and apoptosis models allowed previous work to be confirmed and extended. The apoptotic B cells (WT/ICAM-3^{LOW}) were tested in a MØ-AC interaction assay to confirm the function of ICAM-3 in apoptotic cell clearance by macrophages, as done by previous work (Moffatt et al., 1999, Torr et al., 2011). The results demonstrate that apoptotic leukocytes were efficiently cleared by MØ (THP-1/PMA) and that this clearance was less efficient if the apoptotic cells were reduced in their expression of ICAM-3. This significant decrease in the percentage of MØ interacting with AC suggests that ICAM-3 is involved in the clearance of apoptotic leukocytes by MØ. This conclusion was further confirmed by the use of the ICAM-3 blocking mAb MA4. When MA4 was co-cultured with ICAM-3-expressing AC (WT) and MØ, it resulted in a significant decrease in the percentage of MØ-AC interaction too. In both cases, the low expression of ICAM-3 or blocking of ICAM-3 showed similar results. This emphasizes the vital role of ICAM-3 in mediating the interaction of apoptotic lymphocytes with MØ. Importantly, these data also showed that the Ab MA4 was acting on ICAM-3 on the apoptotic cell as it only inhibited apoptotic cell clearance when the AC expressed ICAM-3. These results correlate with previous work (Moffatt et al., 1999, Torr et al., 2011). Moffat *et al*. (1999) used a different anti-ICAM-3 mAb to show the same effect, and also they showed overexpression of ICAM-3 in HEK293 transfected with ICAM-3 enhanced the AC clearance. Given these results and those from previous work and the current work, it clearly highlights the importance of ICAM-3 in AC clearance. This work also establishes the necessary experimental approaches for the analysis of ICAM-3 within this thesis.

3.2.2 Assessing ACdEV release and assessing their interaction with MØ

Having confirmed the role of ICAM-3 in AC clearance in aiding the tethering between the apoptotic cells and the phagocytes, in agreement with previous work ((Moffatt et al., 1999, Torr et al., 2011), the loss of ICAM-3 to ACdEV and the function of ICAM-3 was addressed. Given that it was shown previously that ICAM-3 in ACdEV was functional in attracting phagocytes ((Moffatt et al., 1999, Torr et al., 2011), the role of EV and ICAM-3 in this process was assessed. Initially, release of EV from apoptotic Jurkat T and Mutu B cells (WT/ICAM-3^{LOW}) was assessed. The T and B cell lines were induced into apoptosis by UV irradiation. Two time points were chosen to look for the ACdEV release, (6h) and (18h) post apoptosis induction. 6h corresponds to high levels of apoptosis and 18h corresponds to post-apoptosis changes. The released EV concentrations from the Jurkat T and Mutu B cells (WT or ICAM-3^{LOW}) at 6h and 18h were not significantly different. As expected, the 18h EV concentration was higher

than the 6h, though this was a non-significant trend, because the 18h preparation also contained particles from the 6h sample. These data suggest that EV are released rapidly from AC and are at significant levels when primary apoptosis is present. They also suggest that EV release may continue past the appearance of early apoptosis, as EV counts continue to increase slightly. Further work is required to count EV numbers over a range of times in relation to the progression of apoptosis and this work is currently being undertaken by other members of the Devitt group.

As EV number appears equivalent between Jurkat and Mutu cells irrespective of their ICAM-3 expression, the EV sizes were also unchanged within the Jurkat T and Mutu B cells (WT/ICAM-3^{LOW}) and between them. This observation is perhaps expected given that the method of preparing the EV for counting by the qNano TRPS device relied upon a similar preparation method (2000xg spin). It is therefore possible that there are difference in EV released from different cell types at different stages of apoptosis. However, in order to count the particles by the qNano, without blocking the tunable pore, this preparation method was necessary. To assess the full size range of EV released is a challenge with the qNano as no one pore size will allow detection of all EV sizes. It may be possible in future work to assess EV count and size by alternative methods such as Nanoparticle tracking devices.

The size of EV detected within these studies has a modal size range of just over 200nm. This size is typical of the microparticle/microvesicle size range (Cocucci *et al.*, 2009, Raposo and Stoorvogel, 2013). This size range would often be considered as typical of EV released from the plasma membrane. However, in this work there is no attempt to discriminate between EV from different cellular sources. Instead of this, the combined EV released from AC are being assessed together for function and characterisation. Future work could look to sub-divide the released EV to assess the relative functions of the different EV.

After characterizing ACdEV release and confirming that this was equivalent in cells expressing WT or low levels of ICAM-3, the next step was to assess a staining method that would allow their detection. A range of methods have been used for staining EV but these are mostly based on lipophilic dyes such as the PKH dyes. Previous work has used PKH dyes to stain apoptotic cells and these have been shown to be stable and not leak out of the AC. This made them useful for undertaking a fluorescence-based interaction assay (Jersmann *et al.*, 2003). However, PKH dyes are prone to precipitation and when analyzing small particles, precipitates could easily be misidentified as EV. Additionally, the PKH dyes were used here but did not show

strong staining (data not shown). To address these issues, an alternative dye was used. This was identified because results were presented in an oral presentation at an EV conference. The fluorescence molecule was Bodipy in the form of Bodipy-maleimide which meant that the dye was reactive with thiol (SH groups) groups, so it would conjugate to the amino acid cysteine in proteins of the EV.

Prior to testing the interactions between stained ACdEV and MØ, the bodipy stained ACdEV were characterized, firstly by running them into qEV size exclusion column to remove isolate EV independent of unconjugated or precipitated dye or other soluble factors from the EV fraction. A key concern with EV studies, is that the staining protocol may alter the appearance of the EV and therefore their function (Mulcahy et al., 2014). To assess any effects of staining on EV physical characteristics, EV were stained and analysed in the qNano. After qEV size-exclusion chromatography, there was a trend to a reduced number of EV though this was not a significant reduction. Importantly, the size of EV appeared unchanged by the staining and qEV protocol. These studies were undertaken with ACdEV from Jurkat T cells (WT/ICAM-3^{LOW}) at 18 h.

Following bodipy staining of the ACdEV, the fluorescence associated with the EV was also tested. These results showed that the EV preparations had similar fluorescence in the WT/ICAM-3^{LOW} ACdEV. Further qNano analyses showed that the stained ACdEV following qEV isolation were slightly reduced in number, as expected. However, the size of the EV was the same irrespective of the ICAM-3 expression. This equivalent EV preparation and staining enabled additional studies to be effectively undertaken without any concern over variation in EV preparation or staining from different cells.

Having established a protocol for robust EV staining, it was not possible to test the hypothesis that ICAM-3 presence enabled improved binding of EV to MØ, and that his may explain the higher chemoattractive ability of EV that contained ICAM-3. The stained ACdEV were incubated with MØ for different times (0min to 120min) and the association of fluorescence (stained EV) with MØ was assessed by flow cytometry. The results show binding between the ACdEV and the MØ. This binding was seen even at the first time point. Clearly EV-MØ binding could happen even in the short amout of time it took at add EV to MØ and then run immediately on the flow cytometer. The binding appeared stable from 0 min to 120min. This rapid binding may be the result of extremely high affinity interactions. However, it is clear that the ICAM-3^{LOW} EV bind quickly but not to the same extent as the WT EV. The difference between the WT and the ICAM-3^{LOW} ACdEV in terms of binding was noted by looking at both the

mean fluorescence intensity (how fluorescent individual MØ are) and the percentage of cells positive (what proportion of MØ are positive). Importantly, the shifts seen could not be explained by free EV falling within the 'cell zone' set using FS/SS. These data suggest that ICAM-3 may promote a higher level of binding of EV to MØ. However, the comparison of WT to ICAM-3^{LOW} were not significant even though the WT (ICAM-3 +ve) ACdEV showed a trend of higher MFI and percentage of cells positive. The effect appeared robust but future work is essential to confirm these preliminary observations.

In following the idiom (seeing is believing) the bodipy stained ACdEV (WT/ICAM-3^{LOW}) interacting with the MØ were examined using confocal microscopy, and the intial results showed that fluorescent WT ACdEV appeared to bind more to MØ than the ICAM-3^{LOW} ACdEV. The challenge of microscopy is that it is a low-throughout analysis. Also, in the images shown, there was an unfocused fluorescent blob in the WT image, which would affect the fluorescence in the flow results but it could be excluded from the microscopy counting. Taken together, it seems that ICAM-3 may promote EV binding to MØ but this requires further study to achieve the necessary statistical power.

3.2.3 Chemotaxis: Assessing the chemoattractive abilities of ICAM-3

Given that the role of ICAM-3 in mediating AC-MØ interaction is well established, the ability of ICAM-3 in chemoattracting MØ was also tested. Two methods of chemotaxis were conducted that each test the chemoattraction capacity of ICAM-3 on EV. These were based on a vertical and a horizontal chemotaxis method.

The vertical chemotaxis method conducted in this project was different to the one conducted by Torr *et al*. (2011). The current vertical chemotaxis is performed and analysed by a system called CELL IQ tracking system. This system monitors and captures images of MØ that have migrated to the lower compartment (containing the attractant) from the upper compartment of the transwell and this analysis is done in real time allowing, for the first time, an analysis of the speed to effect of ICAM-3 on MØ migration. The system however needs a lot of optimization, where its ability to accurately identify and count MØ needs to be 'educated' to ensure the automated system counts MØ effectively and does not confuse it with EV or AC. Also the focusing of the system when capturing images requires much optimization, as it lost focus in many experiments reducing the quality of the captured images and, therefore, the ability of the Cell IQ image analysis system to identify MØ based on phenotype.

The ACdEV under test were collected from Jurkat T and Mutu B lymphocytes (WT and

ICAM-3^{LOW}). ACdEV from both cell types showed that they had chemoattractive potential and that ICAM-3 improved MØ migration compared to ACdEV from ICAM-3^{LOW} cells. In Jurkat T cells, this ICAM-3 compared to ACdEV ICAM-3^{LOW} starting from the 6^{th} hour of the migration assay, whereas in Mutu B cells, ICAM-3 appears to promote a significant improvement in MØ attraction from as early 2^{nd} hour of the migration. However, it is noticeable that apoptotic Jurkat T cells seem more potent as a source of attractants than the apoptotic B cells. This may be an interesting observation that would be worth studying in detail in future work to identify important attractive factors released from apoptotic cells.

These results clearly show that ICAM-3 has chemoattraction abilities and they correlate with previous results (Torr et al., 2011). However, there are differences between the work presented here and that done by Torr *et al.,* (2011). Here, ACdEV were collected by a two centrifugation process (2000x*g* 20min and 120000x*g* 70min) so that centrifuged EV were resuspended in fresh medium. Torr *et al.,* collected the ACdEV by a single 350x*g* 7min centrifugation resulting in soluble factors also being present in the EV preparation. Therefore the work presented here, for the first time, shows that particles (i.e. EV) released from the apoptotic cells are capable of recruiting MØ in a mechanism that is promoted by ICAM-3 on EV. This is also confirmed by the EM observations that show EV particles present in the EV preparations. The approaches used here provide increased confidence that EV are the active factor released from apoptotic cells, in line with concerns in the field over pinpointing EV as active biological factors (Lötvall *et al.*, 2014).

An alternative method of migration analysis was also used. The horizontal chemotaxis assay monitors MØ migration along a true gradient of attractant. The vertical assay has a 'step gradient' i.e. the upper well has no attractant and the lower well has attractant. The results shown here suggest that EV carrying ICAM-3 (WT) induce the MØ to migrate towards them, whereas the EV ICAM-3^{LOW} showed very much less migration distance compared to the WT. Also, the anti-ICAM-3 mAb MA4 also confirmed the chemoattraction abilities of ICAM-3, as it reduced the migration of MØ towards ACdEV from apoptotic WT cells (i.e. ICAM-3 positive EV). These results also demonstrate the chemoattraction abilities of ICAM-3 and these results correlate with the vertical chemotaxis assays and with (Torr *et al.*, 2011).

Whlist there is a clear advantage to the horizontal assay (as it has a true gradient and can show directional movement clearly), is only suitable for undertaking one assay at a time and this limits it usefulness. However, it has the advantage of not having the

'gravity effect' that is in the vertical chemotaxis assay. Due to the breakdown and unavailability of the microscope that was used for horizontal chemotaxis, it was not possible to perform this assay in the required replicates. Given that all this work has shown that ICAM-3 can promote MØ migration, it was sensible to test whether ICAM-3 on its own can promote migration. There is previous work that has shown that an adhesion molecule can also act as a chemoattractant: CX3CL1 is released from apoptotic B cells. Whilst it can act as a classic adhesion molecule, it can also be released and act as a chemoattractant (Truman et al., 2008). Therefore to address the ability of purified ICAM-3 to act as a chemoattractant, purified ICAM-3-Fc protein was used in a vertical chemotaxis assay. In this assay, pure ICAM-3 showed no chemoattraction abilities. This may suggest that ICAM-3 is not functional as an attractant. But it is also possible the ICAM-3 needs other molecules to aid in the chemoattraction or maybe it needs structural changes (e.g. changes in glycosylation) when the cell is undergoing into apoptosis so that it can take on a new role as an attractant. Future work will need to address if ICAM-3 on EV is an attractant. The work presented here suggests that ICAM-3 may promote binding of EV to MØ but additional work is required to confirm this observation.

3.3 Chapter 2 - Assessing immunomodulatory effects of ICAM-3 and EV

3.3.1 Introduction

Previous research has established the clearance of apoptotic cells as more than a simple waste disposal. Apoptotic cells are known to induce an immunomodulatory effect on phagocytes (Voll et al., 1997, Fadok et al., 1998). This 'alternative activation' of MØ has also been called 'M'2 and involves the production of TGF-β1 and IL10 in response to apoptotic cells. This response is in contrast to the 'classical activation' of MØ leading to an 'M1' phenotype which is characterized by the production of TNF-α and pro-inflammatory cytokines. The different sorts of M2 and M1 MØ generated are considered 'repair' or 'defence' MØ (Gordon, 2003). It has been suggested that exposed PS is a key ligand on AC that induces this alternative activation but the role of ICAM-3 in this activation process has never been assessed. Similarly, whilst it is known that ACdEV promote MØ recruitment, it is not known if ACdEV are capable of modulating the inflammatory responses of MØ. It is also not known if ICAM-3 on EV plays a role. This chapter will address these issues.

3.3.2 Establishing an LPS response

Having established a robust macrophage model, the next phase of experimental development was establishing a macrophage response to different LPS concentrations as an *in vitro* model of inflammation. LPS is known to induce 'classical' M1 type MØ (Mosser and Edwards, 2008). In order to set up this model, THP-1/VD3 MØ were used as they have previously been shown to be LPS responsive, to express the pattern-recognition receptor CD14, to migrate towards apoptotic cells and to bind and clear apoptotic cells (Torr et al., 2011, Thomas et al., 2013).

THP-1/VD3-derived macrophages were seeded to 24-well plates at a density of 6×10^5 cells/ml at 750 µl per well. This was followed by the addition of different concentrations of LPS (0, 0.16, 0.8, 4, 20, 100 or 500 µg/ml) and normal human serum as a source of lipopolysaccharide-binding protein (LBP). The macrophages were incubated with the LPS for 4h at 37 °C to allow cytokine release, in line with previous studies (Devitt et al., 1998). Post incubation, the responsiveness was assessed by measuring TNF-α (pro-inflammatory cytokine) in cell culture supernatants. A TNF-α capture ELISA was used for measuring the TNF-α produced in response to the different LPS concentrations.

The results in **Figure 27** show the different concentrations of TNF-α produced in response to the different concentrations of LPS. All of the LPS concentrations effectively induced significant concentrations of TNF-α, in a dose-dependent manner, when compared to the control (MØs alone). The concentration of LPS chosen for future experiments was 0.16 µg/ml, because it successfully induced TNF-α with a significant difference compared to the control. It also did not induce maximal TNF-α concentration (saturated production) compared to the effects of the higher LPS concentrations. This is important so future experiments could reveal the effects of ICAM-3 and EV in either a pro- or anti-inflammatory manner as this intermediate TNF-α concentration produced allows the assessment of the different effects in the further investigations planned.

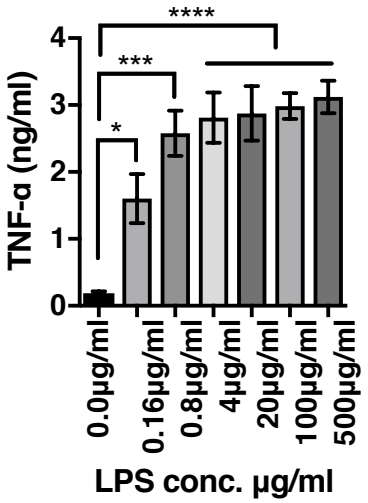

Figure 27. Titration of LPS to induce MØ production of TNF-α. THP-1 cells were stimulated with VD3 for 48 h to differentiate into MØ, the MØ were seeded in 24 well plates at a density of 6×10^5 cells/ml at 750 µl per well. LPS was added to the indicated final concentrations in the presence of 10% v/v normal human serum as a source of LBP. After an incubation of 4 h at 37 °C the supernatant was tested for produced TNF-α using a capture ELISA. TNF-α produced is shown from MØ alone (0 LPS) or stimulated with the indicated LPS concentrations. Data shown are Mean ± SEM for independent experiments (n=4). Statistical analysis was conducted using ANOVA with Dunnett's post-test. (****P< 0.0001) ((***P< 0.001) (*P< 0.05).

3.3.3 Assessing the anti-inflammatory effects of AC, ICAM-3 and ACdEV

After establishing a macrophage model and an *in vitro* model of inflammation using an LPS concentration that induces an intermediate TNF-α response, the next step was to investigate the potential immune-modulatory (pro- or anti-inflammatory) effects of apoptotic cells (AC), ICAM-3 and ACdEV. THP1-/VD3 derived MØ were incubated with UV-induced apoptotic Mutu B cells (WT/ICAM-3^{Low}) and ACdEV (resuspended pellets of 120000x*g* centrifugation) harvested from Mutu B cells (WT/ICAM-3^{LOW}) for 18 h at 37 °C in 24-well plates. This pre-incubation step was chosen to allow time for responses to AC to be initiated (e.g. TGF-β1 production) and is in line with those times chosen in previous work (Fadok et al., 1998). Following the 18 h incubation, 0.16 µg/ml of LPS was added to the mix and incubated for 4 h at 37 °C. Cell culture supernatants were tested for TNF-α production using a capture ELISA. Results in **Figure 28** show TNF-α concentrations that were produced in this investigation. LPS induced TNF-α as expected whilst apoptotic cells alone did not. The results also show that AC (WT or ICAM-3^{LOW}) did not significantly reduce the TNF-α production compared to the control (MØ+LPS) though there was a trend to reduced TNF-α production. In addition, it is important to note that there was no difference in response between AC that were ICAM-3 WT or ICAM-3^{LOW} were used.

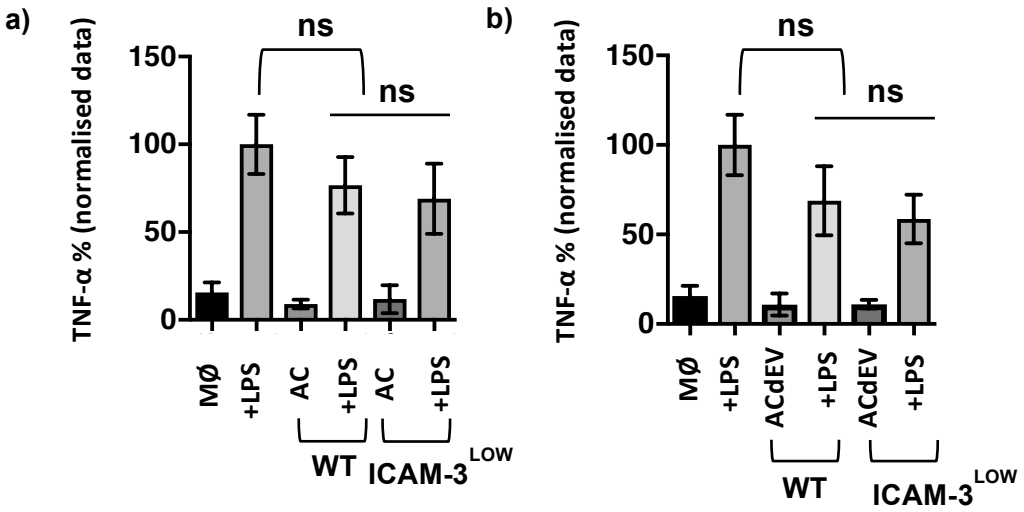

Figure 28. Assessing the anti-inflammatory potential of AC, ICAM-3 and ACdEV. MØ derived from THP-1 stimulated with VD3, were incubated with apoptotic Mutu cells (AC WT or ICAM-3^{LOW}) or ACdEV harvested from apoptotic Mutu (WT or ICAM-3^{LOW}) for 18 h at 37 °C in a 24-well plate. Following this, LPS at 0.16 µg/ml was added and after 4 h at 37 °C culture supernatants were harvested and tested using a capture ELISA to measure the TNF-α (pro-inflammatory cytokine) production. (**a**) Production of TNF-α from MØ treated as indicated with LPS in the presence or absence of AC. (**b**) Production of TNF-α from MØ treated as indicated with LPS in the presence or absence of ACdEV. Data shown are mean ± SEM of independent experiments (n=5) and normalized to MØ + LPS. Experiment had 3 technical replicates. Statistical analysis was conducted using ANOVA with Dunnett's post-test.

Additional experiments carried out in parallel studied the potential for ACdEV from these same apoptotic cell cultures to change inflammatory responses and the results are shown in figure **28b**. In these experiments, EV did not induce TNF-α and the ACdEV WT or ICAM-3^{LOW} did not show significant anti-inflammatory effects. However, there was a trend to reduced TNF-α in the presence of EV. Again, the carriage of ICAM-3 on these EV had no effect on the responses induced by these EV.

These results suggest no strong anti-inflammatory effects in AC, ICAM-3 or ACdEV, even though previous work (Fadok *et al* 1998) has shown that AC have anti-inflammatory effects. These differences may be the result of different cellular systems (macrophage and apoptotic cell) used.

Given the lack of responses noted in TNF-α production, an alternative method of investigation was applied. This was using the Luminex cytokine panel which allowed a greater range of cytokines to be analysed.

ACdEV harvested from Mutu WT/ICAM-3^{LOW} were incubated with MØ for 18 h followed by LPS addition for 4 h. Their cell culture supernatants were then tested in the Luminex cytokine panel to assess inflammatory modulation effects (e.g. an increase in anti-inflammatory cytokine/decrease in pro-inflammatory cytokines). A panel of cytokines detected is shown in **Figure 29.** The results show that in the presence of ACdEV, there is no significant difference in terms of the majority of cytokines compared to the control (MØ+LPS). Only two cytokines showed some significance changes. TNF-α cytokine production following treatment with LPS and ACdEV ICAM-3^{LOW} was significantly lower than the control (MØ+LPS) but this was not the case for ACdEV WT where the trend to reduced TNF-α was not significant. Also, the IL-17 cytokine production in macrophages treated with LPS and ACdEV WT was significantly higher compared to the control (MØ+LPS) though ACdEV that were ICAM-3^{LOW} did not show this increase. In the anti-inflammatory cytokine (IL-13) there was an increase in its concentration by the effects of ACdEV WT+LPS, but it was not significant compared to the control. There were other cytokines in the panel (IL-10, RANTES, Eotaxin, MIP-1α, GM-CSF, MIP-1β, IL-5, IFN-α, IL-1RA, IL-2, IP-10, IL-2R, MIG, IL-8.) that were below the levels of detection.

This investigative approach also suggests that ACdEV WT have no anti-inflammatory effects. However, ACdEV ICAM-3^{LOW} are shown, in one case, to be anti-inflammatory where it significantly reduced TNF-α production compared to the control. This is perhaps in partial agreement with **Figure 28**, where both ACdEV WT/ICAM-3^{LOW} showed a trend towards reduced TNF-α though this was not significant.

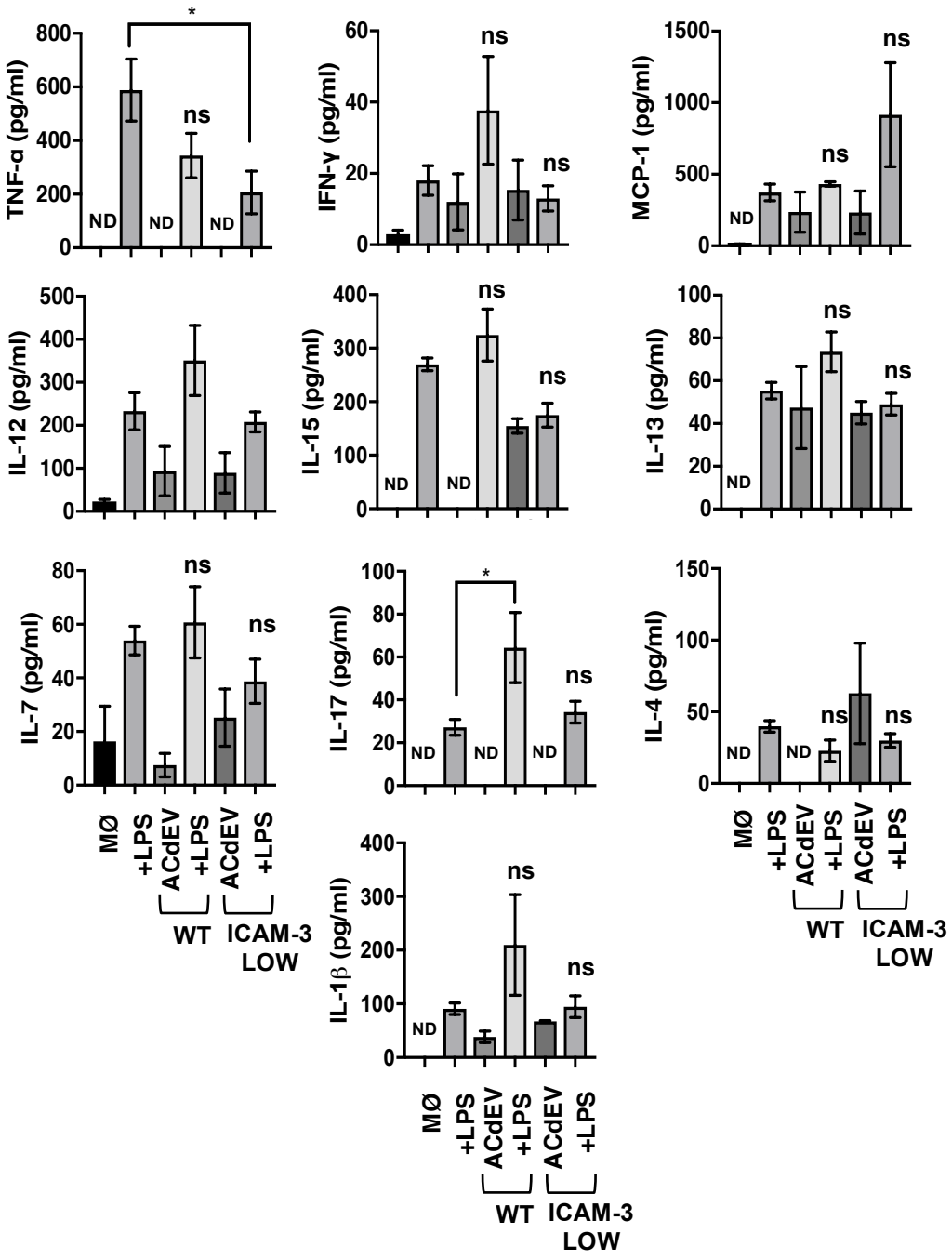

Figure 29. Assessing the anti-inflammatory potential of ICAM-3 and ACdEV via Luminex cytokine panel. MØ derived from THP-1 stimulated with VD3, were incubated with ACdEV harvested from Mutu (WT or ICAM-3^{LOW}) for 18 h at 37 °C in a 24-well plate. Afterwards they were stimulated with LPS for 4 h 37 °C. Culture supernatants were tested using Luminex assay (magnetic beads specific for various cytokine). The kit tests for a panel of pro & anti-inflammatory cytokines, as indicated. The cytokines assayed were: IL-1β, IL-10, IL-13, IL-6, IL-12, RANTES, Eotaxin, IL-17, MIP-1α, GM-CSF, MIP-1β, MCP-1, IL-15, IL-5, IFN-γ, IFN-α, IL-1RA, TNF-α, IL-2, IL-7, IP-10, IL-2R, MIG, IL-4, IL-8. In some cases, the cytokines were below the level of detection and so not detected (ND). Data shown are from independent experiments (n=4). Each experiment had two technical replicates. Statistical analysis Anova with Dunnett's post-test (*P<0.05).

3.3.3.1 Assessing the anti-inflammatory effects of AC, ICAM-3 & ACdEV by measuring the produced mRNA of cytokines

These previous methods to detect immune modulation effects relied upon the detection of protein and it is possible that the low sensitivity of these assays may be failing to detect low levels of cytokine changes. In these cases the level of protein produced must be of sufficient amount to detect within the range of the standard curve. In a more sensitive approach of detecting cytokine gene expression, produced messenger RNA of cytokines was tested using reverse transcription real time PCR (qRT-PCR). The amplification cycles of the PCR enable extremely low numbers of template to be amplified. Additionally, this approach allowed the detection directly of expression of the anti-inflammatory cytokines TGF-β1 and IL10 that have been shown previously to mediate the anti-inflammatory effects of AC (Voll et al., 1997, Fadok et al., 1998). This removed the need for LPS induced inflammation to be included.

In order to undertake the RT-PCR procedure, THP-1/VD3 derived MØ were incubated with apoptotic Jurkat T cells WT/ICAM-3^{LOW} or ACdEV harvested from Jurkat T cells WT/ICAM-3^{LOW}. The incubation period was 6h at 37°C. The 6h duration was selected as appropriate for a high expression of RNA production similar to previous TGF-β1 and IL10 work in the literature (Hartel *et al.*, 1999, Fitzpatrick *et al.*, 2009). After the incubation period, RNA was extracted from cell cultures and transcribed to cDNA to be analysed in qRT-PCR. The results in **Figure 30a** show the relative fold change of IL-10 mRNA (anti-inflammatory cytokine) production in the presence or absence of the AC WT/ICAM-3^{LOW}. In each case, the AC incubation resulted in no significant difference compared to the control (MØ alone). As with the protein detection, there was a trend towards a change. Additionally there was no difference in IL10 response between treatments with AC WT ICAM-3 or ICAM-3^{LOW}. Similar results were seen with MØ incubation with ACdEV WT/ICAM-3 low where they also showed no significant difference in terms of IL-10 relative fold change compared to control (MØ alone) and between them (WT versus ICAM-3^{LOW}).

A similar experimental approach was taken for the analysis of TGF-β1 mRNA. **Figure 30b** results show the relative fold TGF-β1 mRNA (anti-inflammatory cytokine) production. In this case, the AC WT appear to induce a significant increase in TGF-β1 compared to control (MØ alone), but not significantly different compared to AC ICAM-3^{LOW}. However, whilst the AC ICAM-3^{LOW} showed a trend towards increased TGF-β1 mRNA, there was no significant difference compared to the control. As for the ACdEV

WT/ICAM-3^{LOW}, they both showed no significant difference compared to the control (MØ alone) and between them (WT versus ICAM-3^{LOW}).

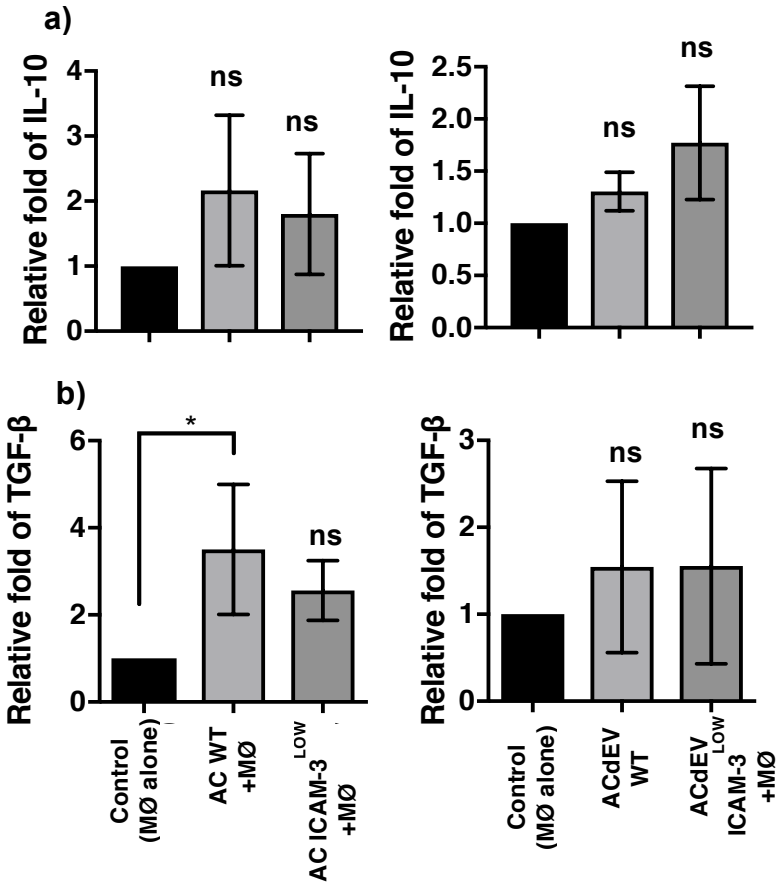

Figure 30. Assessing potential of AC, ICAM-3 and ACdEV to induce expression of anti-inflammatory TGF-β and IL-10 mRNA. MØ derived from THP-1 stimulated with VD3, were incubated with AC (Mutu WT or ICAM-3^{LOW}) or ACdEV harvested from Jurkat (WT or ICAM-3 low), for 6 h at 37 °C in a 24-well plate. RNA was extracted from MØ following the different treatments of MØ with AC and ACdEV WT/ ICAM-3 low. The extracted RNAs were reverse transcribed to cDNA and were used in real time-PCR. (**a**) An IL-10 (anti-inflammatory) gene transcription results ratio from AC & ACdEV incubated with MØ. (**b**) TGF-β (anti-inflammatory) gene expression results ratio from AC & ACdEV incubated with MØ. Data shown are mean ± SEM of independent experiments (n=3). Statistical analysis was conducted using ANOVA with Dunnett's post-test (*P< 0.05).

In summary, one aspect of these results correlates with previous studies that have shown AC to induce TGF-β production (Fadok et al., 1998). These results also suggest that ICAM-3 and ACdEV have no significant anti-inflammatory effects though it is possible that the experimental set up was not sufficiently optimized to the reveal any AC or ACdEV changes in a sensitive manner.

3.4 Discussion – Chapter 2 – Assessing immunomodulatory effects of ICAM-3 and EV

For many years, the disposal of apoptotic cells by phagocytes was thought to be a simple removal process. This is seen in early literature where phagocytes were considered to be 'undertakers' that simply bury the dead and dying cells, often named as 'corpses'. CD36, one of the first apoptotic cell receptors (Savill *et al.*, 1992) when discovered in *Drosophila*, was named '*croquemort'*, the French word for undertaker (Franc *et al.*, 1996). These early studies looked at the apoptotic cell clearance process simply. However, years later it has been seen that apoptotic cells induce responses in macrophages that can help to control inflammation (Savill and Fadok, 2000, Savill et al., 2002, Serhan and Savill, 2005).

The anti-inflammatory effects of AC on phagocytes have been established for 20 yrs (Voll et al., 1997, Fadok et al., 1998, Huynh et al., 2002). This work, looked closely at the role of PS exposure in mediating the anti-inflammatory effects as PS and its receptor was a major focus in the field at the time (Huynh et al., 2002). The work also focused on the ability of apoptotic cells to inhibit the inflammation induced by LPS treatment of mononuclear cells (Voll et al., 1997, Fadok et al., 1998). To date there has been no assessment of the role of ICAM-3 in possibly promoting any anti-inflammatory effects of apoptotic cells. Also, whilst AC are established as having anti-inflammatory potential, there has been no assessment of ACdEV function to turn off inflammatory responses. So the hypothesis in this project is that EV are anti-inflammatory particles like AC, and that ICAM-3 is essential for this anti-inflammatory function.

In order to test this hypothesis, a macrophage response to different LPS concentrations as an *in vitro* model of inflammation was established. LPS induced inflammation has been widely used in the field and this seemed an appropriate model to establish here. THP-1/VD3 derived MØ were used as they have previously been shown to be LPS responsive, to express the pattern-recognition receptor CD14, to migrate towards apoptotic cells and to bind and clear apoptotic cells (Torr et al., 2011, Thomas et al., 2013) in the same way as primary monocytes/macrophages (Devitt et al., 1998). All of these features support the use of this MØ model for the *in vitro* assessment of inflammation and its control.

All of the different LPS concentrations used in the assay induced MØ to produce the proinflammatory cytokine TNF-α, which was quantified by ELISA. Again, this measurement of inflammation is one that has been widely used in the field (Voll et al., 1997, Fadok et al., 1998, Huynh et al., 2002). The chosen LPS concentration to be used in the later experiments was 0.16 μg/ml. This concentration was chosen because it produced an intermediate TNF-α concentration that was significantly above that produced by unstimulated control MØ. It was also not a saturating effect as seen in the higher LPS concentrations (0.8, 4, 20, 100, 500 μg/ml). The reason for the intermediate TNF-α concentration production was because it allowed for the detection of increased or decreased TNF production. This was thought to be important as Lucas *et al*. have previously shown that at early time points, AC and LPS resulted in an increase in TNF-α compared to the effect of LPS alone on MØ (Lucas *et al.*, 2003). This result was unexpected but the experimental design used here would allow for such unexpected responses. However, they did see that at later times (4-24 h) the presence of apoptotic cells induced a significant decrease in TNF-α produced compared to the LPS only. So it is clear that balancing the combination of AC with LPS in controlling inflammation is very complicated.

Having established the *in vitro* model of inflammation using the LPS concentration that induced an intermediate TNF-α response, the work presented here moved on to testing the pro- or anti-inflammatory (immune modulatory) effects of ACdEV and ICAM-3. AC or ACdEV from Mutu B cells (WT/ICAM-3^{LOW}) collected after 18 h post apoptosis induction were incubated with THP-1/VD3-derived MØ for 18 h followed by 4 h with LPS. The pre-incubation of AC or ACdEV with MØ prior to the addition of LPS was chosen to attempt to increase the chance of detecting anti-inflammatory effects, as previous published work was shown that this can benefit. For example, Voll *et al.* showed a bigger anti-inflammatory effect as the AC-MØ pre-incubation period increased (up to 4h) (Voll et al., 1997). Also, Fadok *et al*. showed that apoptotic human neutrophils induced strong IL10 and TGFβ1 expression after 18 h of co-culture (Fadok et al., 1998). Here, TNF-α secreted concentration quantification by ELISA was the method for the assessing their inflammatory effect. The results show that AC and ACdEV have no anti-inflammatory effects as there was no change in the production of LPS-induced TNF-α production from MØ. It was therefore not surprising that ICAM-3 had no effect either on the TNF-α secretion. There was a trend to slightly reduced TNF-α production though this was not significant.

These results assessing the anti-inflammatory effects of apoptotic Mutu cells (WT or ICAM-3^{LOW}) are different to those previously reported (Voll et al., 1997, Fadok et al., 1998, Huynh et al., 2002), which showed anti-inflammatory effects. The reasons for these differences are not clear but these contradicting results may be due to the nature of the different cell types or stimulants used in the different studies. Here, the human THP cells were used as a phagocyte, human B cells as the source of apoptotic cell and LPS as the inducer. Lucas *et al*. used mouse bone-marrow derived MØ with apoptotic human neutrophils and LPS (Lucas et al., 2003). This shows that their system was a combination of mouse and human systems that may have affected their results. Voll *et al.* used primary human blood as a source of phagocytes, as isolated peripheral blood mononuclear cells (a mix of lymphocytes and monocytes) and UV-irradiated mononuclear cells as the source of apoptotic cells with LPS as stimulant (Voll et al., 1997). Fadok *et al.* used human monocyte-derived MØ as their source of phagocytes with either neutrophils or Jurkat as a source of apoptotic cells (Fadok et al., 1998). It is also not always clear whether the apoptotic cell preparations in earlier studies, were used in a crude fashion (i.e. apoptotic cell cultures with EV and soluble factors). So it is clear that while these studies are all trying to study the same effect, there are potentially big differences between the work and this might affect the results.

There were also other experimental differences between these studies. The timing of supernatant harvesting and incubations used in Fadok *et al.,* (1998) were different to those used here. Fadok *et al.* prepared AC after only 3-4h post-apoptosis induction and incubated AC with MØ for 18 h. This was very different to the approach used here. It could be that the current work using harvesting of AC and ACdEV (at 18 h post-UV) followed by 18 h incubation with MØ could cause the AC/ACdEV to become leaky (necrotic) as the AC used here were in a late apoptotic phase. The possibility of the cells becoming necrotic could cause the release of HGMB1 protein which is pro-inflammatory and that leads to pro-inflammatory cytokine secretion (Scaffidi et al., 2002). Additional work by Fadok *et al*. may also help explain these effects (Fadok *et al.*, 2001a). This work revealed that early apoptotic (neutrophil) cells induce the strongest TGFβ1 production and this is reduced to little detectable TGFβ1 if those cells were lysed (i.e. necrotic). It is possible that it is more important that neutrophils undergoing apoptosis are most anti-inflammatory as they have the biggest potential to induce damage if they lyse because of their anti-microbial granules. This work by Fadok also showed that the the inflammatory effects of apoptotic neutrophils are largely mediated by proteases contained within the released granules. It is thought still possible that apoptotic B cells do have anti-inflammatory effects but additional work is

required to optimize the assays. It may be that the precise stage of cells death or the ratio of AC-MØ is important to reveal any effects. Future work could optimize the experiments required. However, the work shown here does show that AC do not induce inflammation.

The work presented here also showed that ACdEV were not able to inhibit LPS-induced TNF-a production. Again, the reasons for this may be related to the cells used or possibly the dose of EV added to the MØ and any pre-incubation required. Whilst there has been no significant work on ACdEV, much work has looked at the ability of EV to modify immune responses. There is a lot of work on EV in studies that are very varied in terms of the assays used, the EV preparations and the results they show. For example, EV from platelets have been shown to induce pro-inflammatory phenotypes in vascular smooth muscle cells in a manner that is dependent on CX3Cl1 (Vajen *et al.*, 2017). Conversely, EV from tumour cells have been shown to suppress immune responses by reducing dendritic cell presentation of antigen (Iero *et al.*, 2007). There is also a lot of interest in stem cells and the mechanisms by which they may help repair. Recent work has suggested that EV from mesenchymal stem cells are the main mediators of the anti-inflammatory effects of stem cells and that this is done by modifying MØ polarisation (M1 v M2) (Lo Sicco *et al.*, 2017). This would be possibly similar to the effects expected from ACdEV as AC are known to modify MØ phenotype (Sica and Mantovani, 2012).

Due to the poor response seen in TNF-α production, an alternative method of investigation was applied. A wider range of cytokines was tested using the Luminex cytokine array in the hope that other cytokines may show a greater difference in production in the presence or absence of ACdEV. The Luminex results for the ACdEV (WT/ICAM-3^{LOW}) have shown no anti-inflammatory effects, which was similar to the TNF-α ELISA assay. The pro-inflammatory cytokines in the Luminex panel were not decreased in the presence of AC compared to the LPS stimulated control, and in agreement, the anti-inflammatory cytokine (IL-13) was not increased. As with the discussion above, the timing of the ACdEV harvest could have had an effect on the assay. Interestingly, ACdEV from ICAM-3^{LOW} cells appeared to reduce TNF-α. This result may suggest that the trends towards reduced TNF-α in the presence of AC and ACdEV may be important though additional replicates are required before any definite claims can be made.

The work assessing cytokine protein production did not yield any clear result in terms of effect of AC or ACdEV. So, an alternative approach was also tried: to assess the produced messenger RNA of anti-inflammatory cytokines. This was done in RNA that was extracted from AC-MØ that were incubated together for 6h and the mRNA was quantified by qRT-PCR.

The mRNA for the anti-inflammatory cytokines TGF-β1 and IL10 were quantified by qRT-PCR to see if they were more highly expressed following treatment of MØ with AC or ACdEV. The results showed AC and ACdEV (WT/ICAM-3^{LOW}) did not cause a significant increase of IL-10 mRNA compared to the control, though again there was a possible trend to increased mRNA. However, with the TGF-β1 cytokine it was significantly increased in MØ treated with AC (WT) only but it was not significantly increased with treatment of MØ with AC ICAM-3^{LOW}. In addition, the ACdEV (WT/ICAM-3^{LOW}) did not show any significant increase in TGF-β1 cytokine compared to the control MØ or to each other.

In summary, the work presented here suggests that there may be small reductions in the production of pro-inflammatory cytokines or small increases in the production of anti-inflammatory TGF-β1 in responses to AC or ACdEV. However, future work is needed to undertake more optimisation experiments. These experiments could assess the dose of AC or ACdEV required for the experimental conditions required to reveal any immune modulating effects of ICAM-3 on AC or ACdEV.

3.5 Chapter 3 - *In vivo* Role of Apoptotic Cell-derived ICAM-3

3.5.1 Introduction

Many receptors and ligands involved in apoptotic cell clearance have been studied *in vivo* through the use of a range of model systems including *C. elegans*, *Drosophila* and mice. To date however the role of ICAM-3 *in vivo* has not been studied with its role in apoptotic cell clearance being studied entirely *in vitro* through the use of human cells in culture (Moffatt et al., 1999) Rodents do not express ICAM-3 and this has made the study of ICAM-3 challenging. However, it has been shown that ICAM-3 on apoptotic human cells is recognised by mouse MØ to promote clearance of apoptotic cells, suggesting that whilst mice lack ICAM-3, they retain the ability to utilize ICAM-3 (Torr et al., 2011).

Work to this point has studied the release of ICAM-3 on ACdEV, the activity of these ACdEV to promote macrophage migration and to modify inflammatory responses *in vitro*. The aim of this chapter is to specifically address for the first time, the ability of apoptosis and ICAM-3 to promote macrophage migration *in vivo*. So this chapter will test the hypothesis that ICAM-3 released from dying leukocytes will promote MØ migration that can be inhibited by the blocking mAb MA4.

3.5.2 *In vivo* investigative approach on ICAM-3 chemoattraction functions

In order to study ICAM-3 chemoattraction function *in vivo*, rodents were chosen as a model subject. To overcome the issue that mice are naturally deficient in ICAM-3, Mutu WT (ICAM-3 +ve) cells were grafted into immunodeficient rodents (SCID mice). This model is an established model to xenograft a tumour to mice (Ford et al., 2015). The result is a mouse (lacking ICAM-3) that is carrying a human tumour (that expresses ICAM-3). Mutu cells have a characteristic, high spontaneous cell death within the tumour. This cell death has been shown to be critical in promoting development of the tumour through (a) macrophage recruitment to dying cells, and (b) phenotypic changes to the MØ so that they provide growth support to the viable tumour cells (Ford et al., 2015). Overall, this xenograft model provides a highly specific system for the analysis

of ICAM-3 on tumour cells and enables MØ recruitment to apoptotic human tumour cells to be assessed *in vivo* for the first time.

After injection, tumour development was assessed daily until development of the tumours had reached a large enough size (~5mm x 5mm) to be palpated. At this point, mice were injected intra-tumourally every other day with either PBS or the anti-ICAM-3 mAb MA4. Ten animals received 50µl PBS every other day for a maximum of four injections or until the tumour mass reached maximum size (12mm x 12mm) at which point the mice were sacrificed in accordance with Home Office regulations. The other ten animals received 50 µl of anti-ICAM-3 mAb MA4 every other day for a maximum of four injections or until the tumour mass reached maximum size (12mm x 12mm). The size of tumours was assessed over time by palpating the tumour and using calipers to measure the tumour size in two dimensions. This work was undertaken at the University of Edinburgh animal facility by Ms Lynsey Melville, an expert in the use of Burkitt's lymphoma xenografts. The illustration of the *in vivo* investigation is shown in (**Figure 31**).

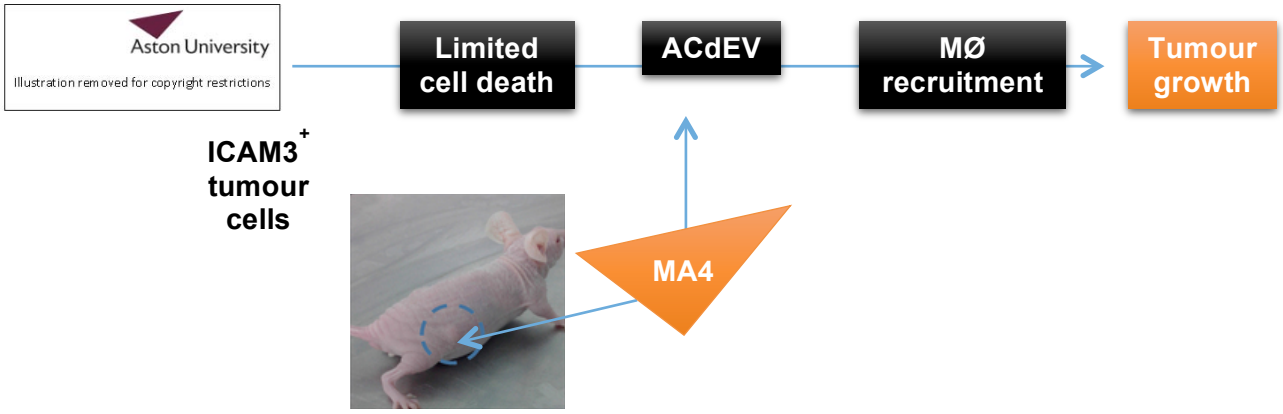

Figure 31. Schematic diagram of the *in vivo* experimental approach for testing ICAM-3 function in attracting MØ. Mutu I BL cells (ICAM-3 WT) $1x10^7$ were injected (subcutaneously in the right flank) into 20 female SCID mice (Harlan). After injection, the tumours were allowed to develop. After the tumour has developed to a size that can be held (~5mm×5mm) in size, the mice were injected intra-tumourly every other day with 50µl of anti-ICAM3 monoclonal antibody MA4 (10 mice) or 50µl of PBS for the control mice (10 mice). The maximum injections were up to four or until the tumour size reached its maximum (12mm×12mm) at which point the animals were sacrificed in line with Home Office approvals. The tumor size was recorded for each animal until the endpoint. Size was measured in two dimensions using calipers to give an area as a measure of size. Following sacrifice, tumours were prepared for histology and immunohistochemistry.

The analysis of this study was conducted by two methods. First, was the analysis of tumour sizes post MA4/mock injections to score the development of the tumour over time. Second, was preparation of immunohistological stained tissues to quantify MØ count, to assess whether there is an increased or decreased number of MØ infiltrating the tumour as a result of the anti-ICAM-3 mAb treatment. Previous work has shown that tumour size provides an indirect measure of MØ recruitment, as the MØ recruitment to cell death is essential for tumour development (Ford et al., 2015). Histology provides a more direct and specific assessment of MØ recruitment to the tumours with the use of Ab-staining for MØ-specific markers.

3.5.2.1 Analysis of tumour growth in SCID mice post anti-ICAM-3 mAb injection

Following grafting of Mutu cells to the mice, the appearance of tumours was monitored and post-injection with either anti-ICAM-3 mAb or mock (PBS) injection to the tumours, tumour sizes were measured and compared (treated: MA4 mAb & control: PBS). The results in **Figure 32a** show the timescale of the tumour growth in the MA4 mAb treated and the control, from day 0 when the BL cells were injected to the mice. The data indicate that the tumours started to appear on the 23rd day post-Mutu B cell injection. The growth of the tumours in each treatment group are also shown and these raw data suggest that tumours injected with anti-ICAM-3 mAb (shown in red) do not grow so quickly. Expanding the axis to reveal the relevant time period where tumour growth was occurring, **r**esults in **Figure 32b** more clearly show the timescale of tumour growth from when they first began to appear (day 23 day post Mutu B cells injection). The MA4 mAb and the control (PBS) were injected after the tumours reached a safe size for injection (~5mm x 5mm) every two days for 4 injections maximum. These data suggest that MA4 injection reduces average tumour size (red versus blue: **Figures 32a and 32b**). In an attempt to compare the effect of MA4 mAb and PBS on tumour size, at day 33 post-Mutu B cell injection, the tumuor sizes were compared and there was significant difference between MA4 mAb and the control, where the control injected mice carried larger tumours compared to the MA4 mAb-treated tumours (**Figure 32c**).

These raw data (**Figure 32 a-c**) suggest anti-ICAM-3 reduces tumour growth. However, as tumours did not all arise on the same day and therefore injections to tumours in each individual animals were initiated at different days, the data were analysed more closely. To further analyse the data and look for mAb-induced effects on tumour size, the data from **Figure 32a** was re-plotted. In this case, day 1 was considered to be the first appearance of the tumour, one day before the rapid growth of

the tumour in each individual animal to remove the influence of different timings of tumour appearance in each individual animal. The results are shown in **Figure 32d**. Day 2 corresponded to the date of the first injection in each animal. These data reveal a clear difference in terms of tumour size development between MA4 mAb-treated mice and the controls. The results in F**igure 32d** were plotted in histograms to compare and analyse for differences in tumour sizes at each day post tumour development. The plotted data are shown in **Figure 33** and the data show that from day 4 and onwards there is a significant reduction in tumour size in MA4-treated mice when compared to the control.

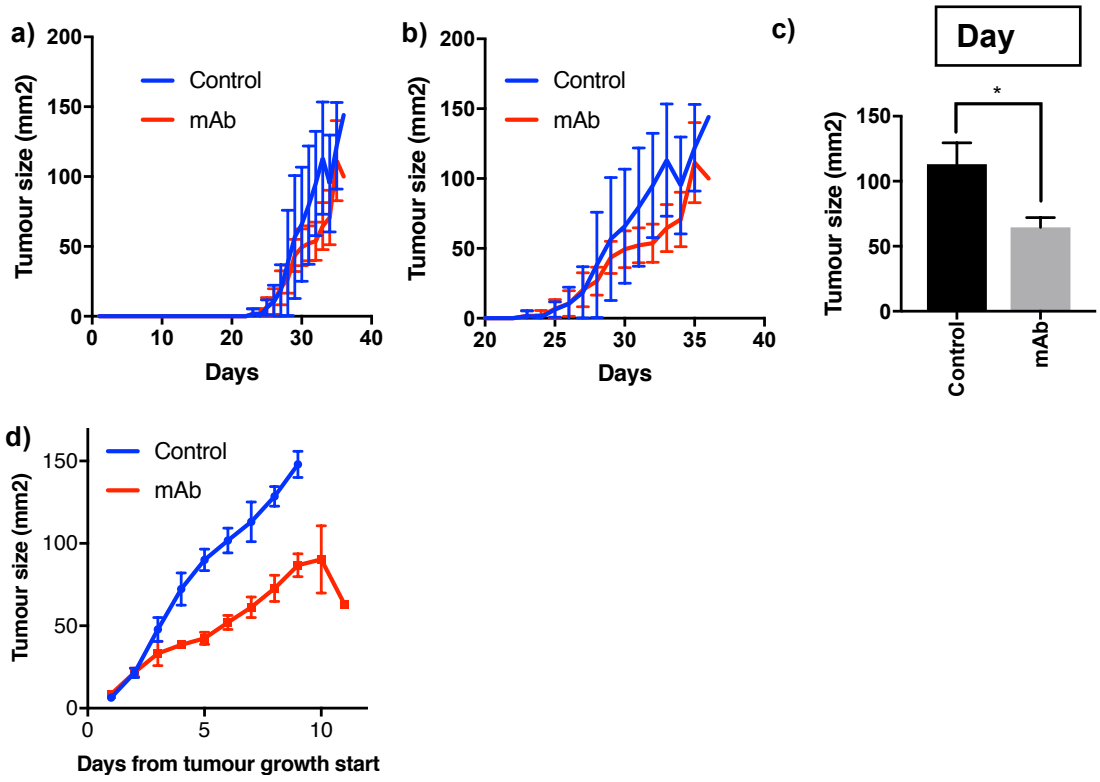

Figure 32. Tumour growth development in SCID mice treated with anti-ICAM-3 MA4 mAb over time post Mutu cells injection. Mutu I BL cells (ICAM-3 WT) $1x10^7$ were injected into (subcutaneously in the right flank) 20 female SCID mice (Harlan), and allowed for tumours to develop to ~5mm × 5mm in size. The mice were injected intra-tumourly every other day with 50 µl of anti-ICAM3 monoclonal antibody MA4 (10 mice) or 50 µl of PBS for the control mice (10 mice). The maximum injections were up to four or until the tumour size reached its maximum (12mm×12mm) at which point the animals were sacrificed in line with Home Office approvals. The tumour size was recorded for each animal until the endpoint. Size was measured in two dimensions using calipers to give an area as a measure of size. Following sacrifice, tumours were prepared for histology and immunohistochemistry. (**a**) Tumour growth over time for treated and untreated animals from day 0 (cell injection day). (**b**) The same data as from part **a**, but the x axis data start from day 20. (**c**) Day 33 data taken from part **a**, the control mice tumour size have shown to be significantly larger than the tumours of the MA4 mAb treated mice. (**d**) Adjusted data from part **a**, where the tumour sizes of the mice were plotted 1 day before the large tumour size spike. Data shown are from one independent experiment, 5 mice each per data bar. (*P< 0.05) Statistics: Unpaired t-test (two-tailed).

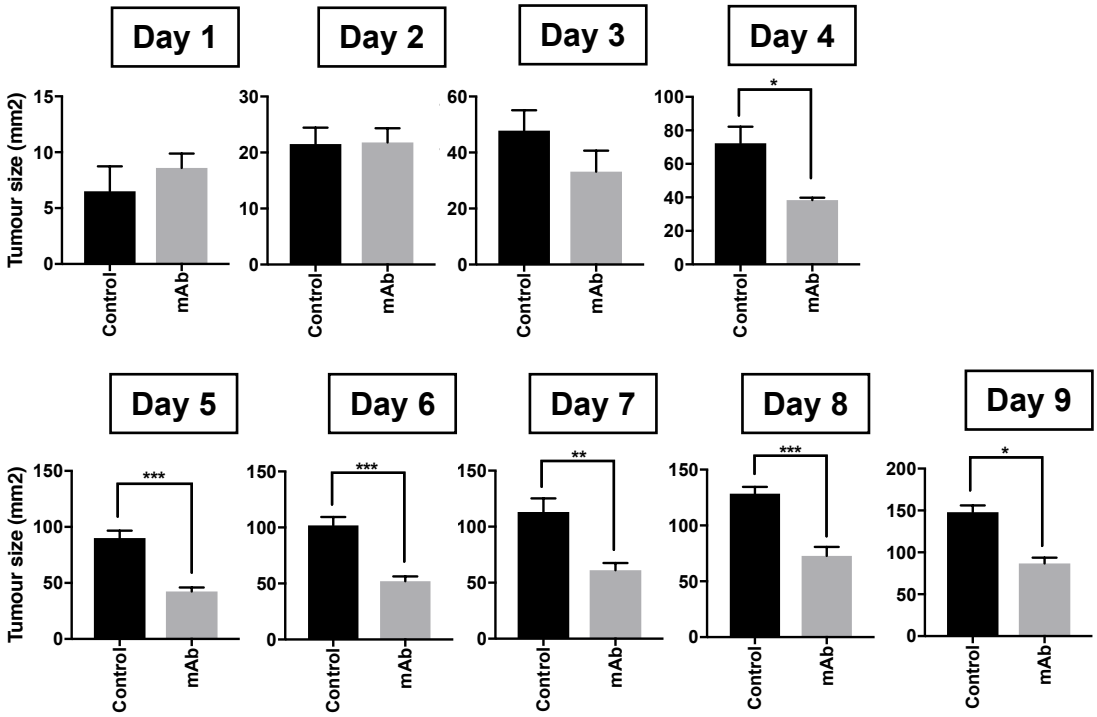

Figure 33. Tumour size differences between control and Anti-ICAM-3 MA4 mAb treated SCID mice. These data were taken from the previous figure part **d**, the individual days data were plotted and compared to each other. From day 4 till day 9, the tumour size of the control mice have shown to be significantly larger than the MA4 mAb treated mice. Data shown are from one independent experiment, 5 mice each per data bar. (**P*< 0.05) (***P*< 0.01) (****P*<0.001) Statistics: Unpaired t-test (two-tailed).

3.5.2.2 MØ count assessment in tissues of MA4 mAb treated SCID mice

The growth of the tumours is an indirect assessment of MØ recruitment to the tumour as this is essential for tumour growth (Ford et al., 2015). These data suggest that mAb treatment reduces MØ recruitment to the tumour, resulting in reduced tumour growth. However, to directly assess MØ numbers and to assess tissue morphology, histological analysis of tissues from the tumours of the SCID mice were undertaken (MA4 mAb treated and the PBS control). The histology slides were stained in multiple different ways. Firstly, sections were stained with non-MØ specific tissue stain (hematoxylin and eosin). MØ were identified by morphology which is characteristic of BL tumours. The tumours have a 'starry sky at night' appearance where the stars (unstained regions) are the MØ and the dark sky (highly stained) are the cancer cells. This characteristic appearance is shown in **Figure 34a**. The MØ were counted in the H&E stained slides and a comparison was conducted between the MA4 mAb-treated and the control-treated tumours. In **Figure 34,** the MØ count comparison in the H&E stained slides is shown. Whilst there is a trend to reduced MØ numbers when the

tumours were injected with MA4, there is no significant difference between the MA4 mAb-treated mice tumours and the control.

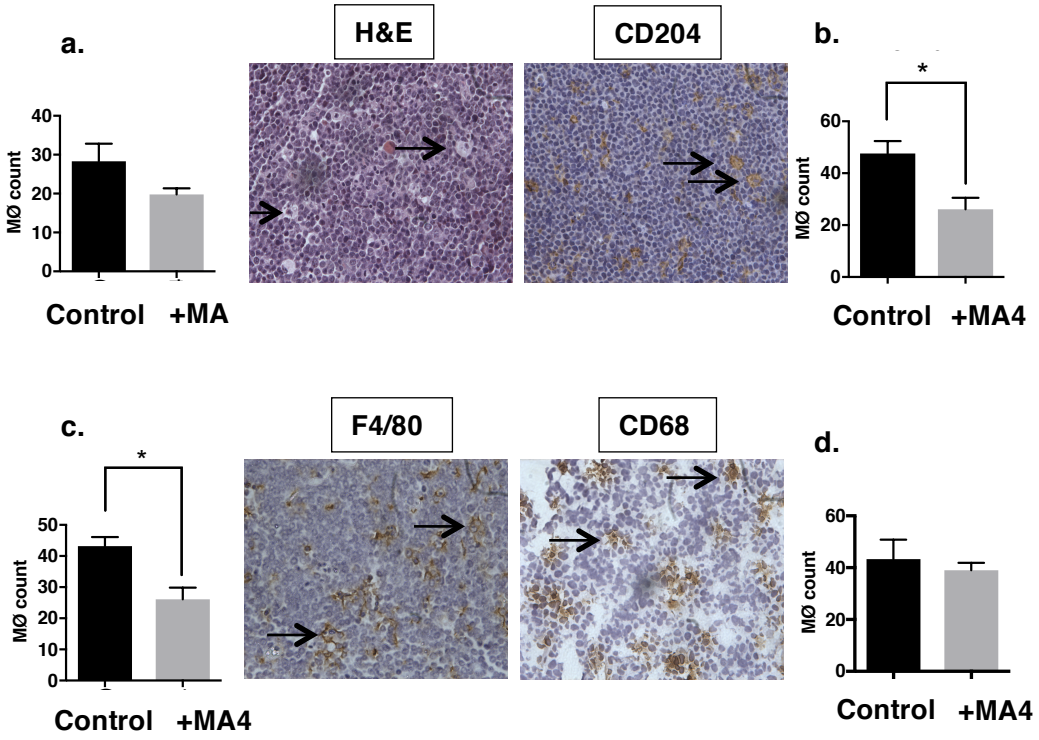

Figure 34. Assessment of the effect of anti-ICAM3 mAb (MA4) on tumour development. Xenografted tumours in SCID mice were injected intratumouraly with anti-ICAM-3 or PBS. Tumours were harvested when their size reached its maximum (12mm × 12mm) at which point the animals were sacrificed in line with Home Office approvals, it differed for each animal but the range was between day 33-36 post Mutu I BL cells (ICAM3 WT) injection, and sections were stained with H&E or stained by immunohistochemistry; (**a**) H&E stained tissue section from treated SCID mice; the data shows no significant difference in terms of number of MØ between control and MA4 treated mice; (**b & c**) MØ specific stains CD204 & F4/80 images of the treated mice, the data shows significant difference between the control and MA4 treated mice in terms of MØ number, where the MA4 treated showed lower number of MØ compared to control; (**d**) MØ specific stain CD68 images of the treated mice, the data shows no significant difference between the control and MA4 treated mice in terms of MØ number.

Subsequent staining looked directly for MØ, using MØ specific immunohistochemical staining. In this more specific and thorough approach to identify and score MØ, the MØ specific stains used were CD204, F4/80 and CD68. The results of the specific stains are shown in **Figure 34 b, c & d.** It is interesting to note that the scored MØ numbers appear higher than for H&E staining. This may be because H&E staining relies on the main cell body being visible (as a large white 'star') whilst the specific stains are more sensitive to detect cells. The IHC data reveal a significant reduction in MØ in CD204 & F4/80 stained sections after MA4 mAb treatment of mice tumours compared to control. This shows a direct reduction in MØ numbers. In the case of CD68, the stained slides suggest that there is not a significant difference in the presence of CD68 positive cells when compared between MA4 mAb-treated mice tumours and controls. The difference in MØ count with each Ab stain may be the result of different efficiency of staining or may be detecting different sub-sets of MØ.

In summary, these results suggest for the first time that ICAM-3 has chemoattraction functions *in vivo*, where the anti-ICAM-3 mAb MA4 has inhibited the migration of MØ towards the spontaneous death with the BL tumours that had developed in the SCID mice. The effect of the MA4 mAb was seen to significantly reduce the tumour size development. These results correlate with the *in vitro* findings that ICAM-3 has chemoattraction abilities.

3.6 Discussion – Chapter 3 - *In vivo* Role of Apoptotic Cell-derived ICAM3

Apoptotic cell clearance and the receptors and ligands involved with it have been studied *in vivo* through the use of a range of model systems such as C.*elegans, Drosophila* and mice. These *in vivo* studies were necessary as most molecules identified in AC clearance, were identified *in vitro* through the use of inhibitory Abs. The *in vivo* results can help to highlight how important a molecule may be in the clearance process and therefore can show the biological significance of individual molecules. For example, mice defective in CD14, a MØ receptor that binds AC, showed apoptotic cells *in vivo* that persisted and were not cleared efficiently by MØ but this was without any inflammatory consequences (Devitt et al., 2004). This work would suggest that it is possible to separate AC clearance functions of some molecules from the anti-inflammatory functions mediated by other molecules. In contrast, the C1q defective mouse model has a strong phenotype where apoptotic cell persist but that these drive chronic inflammatory disease (glomerulonephritis) autoimmune disease (SLE) (Botto *et al.*, 1998, Walport *et al.*, 1998, Taylor *et al.*, 2000). This disease will be driven by persistent apoptotic cells becoming necrotic and stimulating the immune system suggesting that C1q is involved in both the clearance and immune modulating functions of AC. Interestingly, some molecules that are known to have a function *in vitro* for the clearance of apoptotic cells, do not seem to show a phenotype when that molecule is knocked out *in vivo*. This is true for the scavenger receptor A which has a clear role *in vitro* (Platt *et al.*, 1996) but no phenotype *in vivo* (Platt *et al.*, 2000)with no detectable increase in AC within these animals, suggesting that there is redundancy in the system i.e. another molecule can stand in for the SRA when it is absent. However the role of ICAM-3 in apoptotic cell clearance has never been studied *in vivo* despite the fact that it has been studied *in vitro* (Moffatt et al., 1999, Torr et al., 2011). This chapter shows the first ever analyses of ICAM-3 function *in vivo* and tests the hypothesis that **ICAM-3, when released from dying leukocytes, will promote MØ migration that can be inhibited by the blocking mAb MA4**.

A major challenge for the *in vivo* study of ICAM-3 is that rodents do not naturally express ICAM-3 and so ICAM-$3^{-/-}$ animals and ICAM-3^{WT} expressing animals are not available. Putative ICAM-3 homologues, according to the NCBI HomoloGene database, have only been identified in humans, chimpanzee, Rhesus macaque, dog and cattle and none of these species are easily used for *in vivo* studies. This therefore

presented a problem for the *in vivo* study of ICAM-3. However, recent work by the collaborating laboratory of Prof C. D. Gregory (Edinburgh University) had established a xenograft system for transplanting human (ICAM-3 expressing) lymphocyte cells in immunocompromised mice and allowing them to form a tumour (Ford et al., 2015). Importantly, this work showed that some of the transferred tumour cells died by spontaneous apoptosis and this promoted tumour growth by modulating the phenotype of murine MØ in the tumour. So this model was used here as a potential way in which the *in vivo* effects of ICAM-3 and apoptotic cells could be assessed. It provided a very clean model system as the only ICAM-3 present would be on the tumour cells. Additionally, previous work from the Devitt group had shown that ICAM-3 on human apoptotic cells could be recognised by mouse macrophages (Torr et al., 2011).

So to assess the role of ICAM-3 *in vivo*, Mutu WT (ICAM-3 +ve) cells were grafted into immunodeficient rodents (SCID mice) that are naturally deficient in ICAM-3. The SCID mice have a severe combined immunodefiency, where the adaptive immunity is dysfunctional as they are impaired in their ability to make functional T or B lymphocytes (Fulop and Phillips, 1990). However the innate immune system including MØ is functional and so this was considered a good system to test the recruitment of MØ to ICAM-3 on apoptotic cells *in vivo*. The data shown here demonstrates a successful xenograft of the ICAM-3 positive tumour cells in this established model (Ford et al., 2015). Due to the high spontaneous cell death rate that is characteristic of Mutu cells (Ogden *et al.*, 2005), this would promote MØ recruitment and subversion of the MØ to support tumour growth as it has been shown that this cell death is vital in the tumour development by recruiting tumour associated-macrophages (Ford et al., 2015). The recruited tumour associated macrophages (TAM) appear to support the tumour growth as they get polarized into as alternative activation phenotype, M2, which promotes angiogenesis and provides growth support to the viable tumour cells (Mantovani and Sica, 2010, Colegio *et al.*, 2014, Franklin *et al.*, 2014).

This experimental approach to testing the ability of ICAM-3 to recruit MØ to apoptotic tumour cells *in vivo* is completely novel. After waiting for the tumours to grow to suitable size for detection and handling in the mice and treating with anti-ICAM-3 mAb (MA4) from their first appearance, the growth of the tumours was assessed until the mice were euthanised after the tumour sizes reached the maximal allowable size (12mmx12mm). The analysis of the tumours was performed by two methods. The first method was measuring the tumour sizes in control and MA4-treated mice. The results of the first analysis have shown significant tumour sizes difference between the MA4

treated mice and the control. A challenge in the interpretation of the data came from the fact that the tumours appeared on different days after injection of the tumour cells. This lack of synchronous growth tended to hide the difference between the treatment groups (control versus MA4) when they were presented as an average tumour size. So it was decided that the data should be realigned so that time 0 was the day before the appearance of the tumour. This allowed the analysis of tumours over the same time period. This then showed a very significant difference in the two groups. Overall, the MA4-treated tumours were smaller compared to the control. These data suggest that the anti-ICAM-3 treatment prevented the increase in the tumour size. Since the Tumour-associated macrophages (TAM) are necessary for tumour growth (Mantovani and Sica, 2010, Colegio et al., 2014, Franklin et al., 2014, Ford et al., 2015), it seemed likely that the anti-ICAM-3 had inhibited tumour growth by preventing MØ recruitment. This would then mean that the tumour cells lacked the necessary microenvironment with alternatively-activated MØ to allow strong tumour growth. These data, along with the previous work showing shedding of ICAM-3 on ACdEV promoting MØ migration, would suggest that ICAM-3 associated with ACdEV is capable of recruiting MØ *in vivo* which is highly novel.

To address directly if the treatment of MØ which reduced tumour size had resulted in reduced MØ presence in the tumour, as would be expected from the hypothesis under test, a second set of tumour analyses were done. This second analysis method involved counting MØ numbers within the harvested tumour tissues prepared from the MA4 treated and control mice. This approach used different stains to try to identify MØ. A general histology stain was used first – the Haematoxylin and eosin (H&E) stain to reveal the tumour morphology. This stain is a gold standard in pathology studies for assessing tumour morphology. MØ specific immunohistochemistry stains were also used to identify cells positive for: CD204 (the macrophage scavenger receptor 1); CD68 (another scavenger receptor); and F4/80 (a murine specific MØ marker). Together these stains were planned to detect MØ in a comprehensive manner.

The results showed MØ numbers were slightly reduced but not significantly changed with MA4 treatment though this stain relied upon identification of the MØ cell body as a relatively unstained ‘star’ in the dark ‘ tumour cell ‘sky’. The MØ specific CD68 stained tissues also showed no significance in MØ numbers between the MA4 treated and the control. However, the use of Abs for CD204 and F4/80 for MØ detection (by immunohistochemistry) revealed more dramatic differences. The significance in MØ

numbers was clearly seen in the CD204 and F4/80 MØ specific stained tissues, where there was a significant reduction in the number of MØ compared to the control.

CD204 is scavenger receptor class A (SR-A), which are specifically expressed on macrophages and have been found to be highly expressed on M2 macrophages (Komohara *et al.*, 2008, Kurahara *et al.*, 2011, Komohara *et al.*, 2014). So the increased presence of $CD204^+$ cells in the control tumours would support the hypothesis that MØ recruited to the tumour, as a result of ICAM-3 on ACdEV, promote production of M2 TAM that support the tumour to grow.

CD68 in mice is macrosialin which is the homologue of of human CD68, it is a highly glycosylated transmembrane protein that is almost found expressed exclusively on macrophages (Kurushima *et al.*, 2000). It also used as a macrophage specific marker in cancer studies, being expressed on M2 tumour associated macrophages (Chistiakov *et al.*, 2017). It is perhaps surprising that CD68 positive cells are not at higher levels in the control tumours as these are predicted to contain higher numbers of M2 TAM. It is possible that the lack of different is the result of poor staining and this may be most likely as the results for CD68 and CD204 differ, even though they both are highly expressed in M2 MØ.

F4/80 is a membrane protein that expressed on macrophages that is widely used as a mature mouse macrophage marker. Its level of expression on macrophages depends on several factors such as the maturation and the type of the macrophage (Austyn and Gordon, 1981). The results from F4/80 suggest fewer $F4/80^+$ MØ are present in tumours and this result would also support the hypothesis that MØ are recruited to the tumour as a result of the presence of ICAM-3 on ACdEV.

These different results seen with the specific MØ stains, could be due to not all antigens are expressed on the MØ within the tumours and the antibodies may detect different sub-populations of MØ. This may be due to the status of the activation of the MØ that are tumour-associated.

The hypothesis under test in this chapter was focused on ICAM-3 released from dying cells. However, it must be considered that ICAM-3 was also present on the viable tumour cells and it is possible that the mAb had its effect by acting on viable cell associated ICAM-3. MA4 is a mouse antibody (IgG1/kappa) and it is possible that any mouse antibody binding to the tumour cells may cause a similar effect to that seen with MA4. The control used here was PBS injection. This was necessary as the cost

associated with the commercial production of LPS-free mAb was very high. However, the injection of a control, isotype-matched Ab is future work. Ideally this could also include an isotype-matched Ab that binds to ICAM-3 but doesn't inhibit apoptotic cell clearance or MØ recruitment *in vitro*. This control would be ideal as it would rule out the possibility that binding of any mAb to the tumour cells would cause the effect.

However, it might be expected that if the MA4 was having its effect by stimulating innate immune responses to tumour cells, you might expect that there would be more MØ present in the smaller tumours. Altogether these results would suggest that the effect is ICAM-3 specific.

It also isn't certain that the effects are ACdEV specific. Ford *et al* have shown that tumour cells expressing Bcl-2 do not promote tumour growth (Ford et al., 2015). This was very surprising as Bcl2 or $BclX_L$, anti-apoptotic oncogenes, but they suggest it is the lack of apoptosis that prevents strong tumour growth. So, to test a role for ACdEV and ICAM-3 on ACdEV as the active factors in recruiting MØ to the tumour, Mutu/bcl2 cells could be grafted into SCID mice, with and without ACdEV to see if they promote strong tumour growth. By including ICAM-3^{WT} or ICAM-3^{LOW} ACdEV, the role of ICAM-3 could also be tested.

These results are exciting and suggest that it might be possible to block MØ recruitment to sites of cell death. This may have potential therapeutic benefit in some pathological conditions. For example, this may be useful in human Burkitt's lymphoma. This might first be used in those children with BL whose treatment options are very limited. Another site where MØ recruitment to dying cells drives disease, is in atherosclerosis. In this case, monocytes are recruited to a developing plaque and once recruited, they become trapped and die (van Gils *et al.*, 2012). It seems possible that this high level of monocyte death could drive further monocyte recruitment and that this would help the plaque grow. To inhibit this monocyte recruitment might help to break the vicious cycle of death-recruitment-death.

In summary, this novel approach has shown *in vivo* that ICAM-3 promotes MØ numbers in the tumour suggesting that ICAM-3 on ACdEV has chemoattractive abilities to promote recruitment of MØ *in vivo*. This might form a first step in novel therapeutics for diseases caused by unwanted MØ recruitment towards apoptotic leukocytes.

3.7 Chapter 4 - Molecular analysis of ICAM-3 partner molecules (viable VS apoptotic)

3.7.1 Introduction

ICAM-3 appears to function differently when present on viable or apoptotic cells. When leukocytes are in the viable state, ICAM-3 interacts with the leukointegrin LFA-1 (CD11a(α_L)/CD18(β_2)) and this helps to promote adaptive immune responses (Bell et al., 1998). But when a leukocyte becomes apoptotic, ICAM-3 was shown not to interact with the LFA-1 (Moffatt et al., 1999). The mechanism that allows this change of function isn't clear. This chapter's aims are to investigate the molecular partners of ICAM-3 that might assist ICAM-3 in doing its function in the apoptotic phase of leukocyte. This work will help to address the hypothesis that ICAM-3 functions differently on viable and apoptotic cells as a result of the presence or absence of partner proteins. This chapter explains the approaches taken to identify those ICAM-3 partner proteins on viable and apoptotic human leukocytes.

3.7.2 Assessing ICAM-3 abundance in Jurkat T cells and Mutu B cells

In order to conduct molecular analyses on ICAM-3, a high expression cell source of ICAM-3 needed to be identified and analysed. ICAM-3 is leukocyte expressed and so as a starting point Jurkat T cells and Mutu B cells were stained for ICAM-3 using indirect immunofluorescence with the anti-ICAM-3 mAb JA4. **Figure 35** is showing the flow cytometry frequency histograms of ICAM-3 stained Jurkat T cells and Mutu B cells. Mutu WT showed slightly higher mean fluorescence intensity compared to Jurkat WT, meaning slightly higher ICAM-3 expression. Overall, the level of ICAM-3 expression was relatively low and this would make analyses difficult. So transfection of ICAM-3 into HeLa and HEK293 cells was undertaken in an attempt to obtain higher levels of expression.

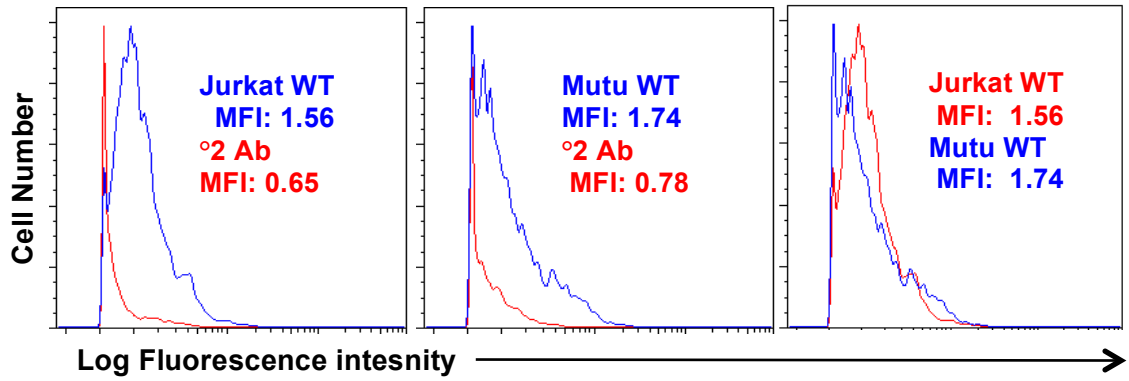

Figure 35. Flow cytometric analysis of ICAM-3 expression in T (Jurkat) & B (Mutu) cells. Viable Jurkat and Mutu cells were stained for ICAM-3 using indirect immunofluorescence with the anti-ICAM-3 mAb JA4 and a secondary anti-mouse-FITC detection reagent. Following staining, cells were analysed by flow cytometry. Frequency histograms are shown for Jurkat cells (left panel), Mutu cells (centre panel) and an overlay of Jurkat and Mutu (right panel). In each case, at least 5000 events were analysed and the data are representative of three independent experiments.

3.7.3 Establishing a robust transfection of ICAM-3 into HeLa and HEK293 cells

To generate a cell line expressing high levels of ICAM-3, ICAM-3 cDNA was required. As a source of ICAM-3 cDNA for transfection, plasmid constructs encoding ICAM-3-emGFP or ICAM-3-His were expanded in bacteria on agar plates (containing ampicillin), where the pcDNA3 plasmid conferred resistance to ampicillin allowing selection of the bacterial clones containing the desired cDNA constructs. The plasmid construct containing ICAM-3-His is shown in **Figure 36.** The TOPO cloning was undertaken previously within the lab by [redacted] and bacterial glycerol samples stored.

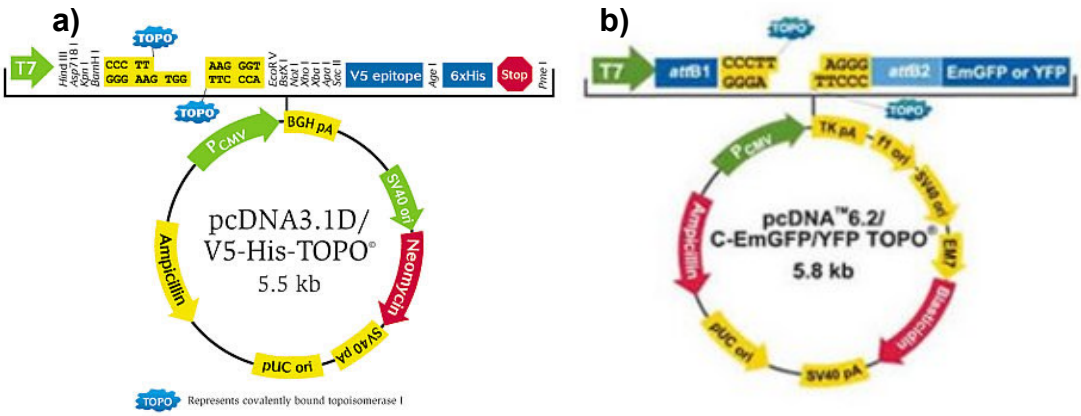

Figure 36. Schematic diagram of the plasmids into which the ICAM-3 was sub-cloned to express (A) ICAM3-His and (B) ICAM-3-EmGFP. The TOPO cloning was undertaken by [redacted]

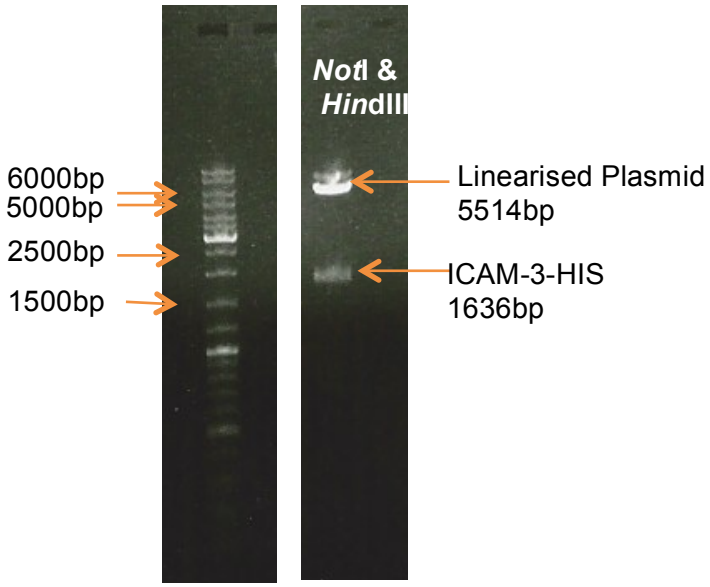

Figure 37. Confirmation plasmid construct pcDNA3-ICAM3-HIS. 1 µg of Plasmid DNA containing ICAM-3-His that was isolated by mini-prep and maxi-prep was digested with two restriction enzymes, *Not*I and *Hind*III and fragments separated by 1% agarose gel electrophoresis to confirm digestion and ICAM-3 insert presence. The ICAM-3-HIS was present after the digestion and its size was 1636bp and the plasmid size was 5514 bp.

After growth of the clones containing the constructs, a sample was taken from grown colonies and grown in 50 ml cultures followed by conducting a plasmid DNA miniprep. Isolated DNA was digested with restriction enzymes *Not*I and *Hind*III to linearise the plasmid and excise the cDNA. It was run on agarose gel electrophoresis to confirm insert size. A large scale cDNA 'maxiprep' was done after the confirmation of the miniprep, where larger volumes of growth was done followed by the maxiprep step.

The eluted DNA was also digested and run in agarose gel electrophoresis for confirmation; the gel electrophoresis results are shown in **Figure 37.**

3.7.3.1 Transient LT1-kit transfection titration

After acquiring sufficient ICAM-3-His & ICAM-3-emGFP DNA, several titration attempts were done using the Transient LT1 transfection kit. Initially the ICAM-3-emGFP DNA was transfected into HeLa cells as the level of transfection was easily monitored through the use of GFP and fluorescence microscopy and flow cytometry. A standard 1 µg of DNA was transfected to HeLa cells with different volumes (5.5, 6.5, and 7.5 µl) of LT1 reagent, in line with the manufacturer's instructions. The results are shown in **Figure 38**. The use of ICAM-3-emGFP was to confirm that the transfection was working well. **Figure 38a,** shows microscopy images of HeLa cells transfected with the ICAM-3-emGFP plasmid. For each volume of LT1 reagent used, representative fluorescence and phase contrast images are shown. The 5.5 µl volume of LT1 resulted in the best efficiency of transfection compared to the rest of the volumes tested. The fluorescence was assessed using flow cytometry (**Figure 38b**). The flow cytometric data confirm that the 5.5 µl volume of LT1 produced the best transfection efficiency, as it produced the highest mean fluorescence intensity and the greatest percentage of cells positive for GFP.

These results show that transfection has been successful and that high levels of ICAM-3 could be expressed in HeLa cells. This result led to the next step: titrating the volume of LT1 reagent and the concentration of DNA (ICAM-3-His) to be used in the transfection of the HIS-tagged ICAM-3. This transfection would enable efficient isolation of ICAM-3, using the HIS-tag, in subsequent experiments. The titration started with a constant volume of LT1 reagent with different concentrations of ICAM-3-His DNA (0.6, 1.2, 2.4, and 4.8 µg) in HeLa cells. The transfected HeLa cells were stained indirectly with the anti-ICAM-3 mAb JA4 and analysed by flow cytometry. The resultant mean fluorescence intensity of the different DNA concentrations were compared to each other (**Figure 39a**). The results indicate no significant difference in transfection, in terms of mean fluorescence intensity, between the different DNA concentrations used in the test titration. Another approach taken in the titration was to use different volumes of LT1 reagents with different concentration of DNA (0.6, 1.2 and 2.4 µg) and the results of indirect immunofluorescence staining and flow cytometry are shown (**Figure 39b**). The results indicate that transfection levels are low with the greatest mean fluorescence intensity seen in the use of 0.6 µg of DNA with 2.5 µl of LT1 against the control (mock transfection). All of the other results have shown no significant

difference. Due to poor transfection efficiency of ICAM-3-HIS with the LT-1 transfection method, and limited time, the titration was abandoned and maneuvered to a new transfection method.

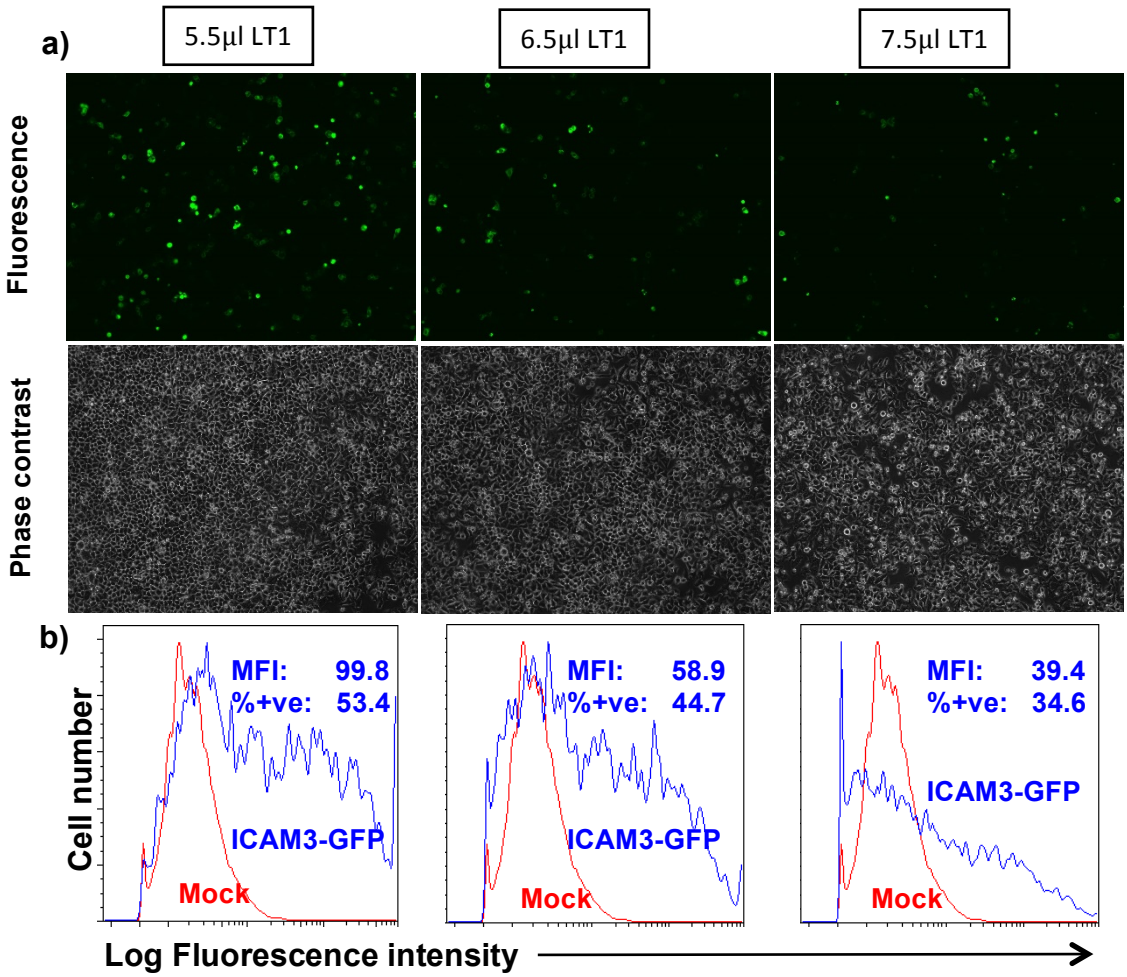

Figure 38. Microscopic and flow cytometric analysis of HeLa transfected with ICAM3-emGFP. HeLa cells were transfected with ICAM3-emGFP (1 µg) using the indicated amounts of LT-1 transfection reagent. After 48h, cells were analysed. (**a**) Fluorescence and phase contrast microscopy images of HeLa cells transfected with ICAM3-emGFP. (**b**) Flow cytometric frequency histogram data of HeLa cells transfected with ICAM3-emGFP compared to mock transfected cells. Data presented are from a single experiment.

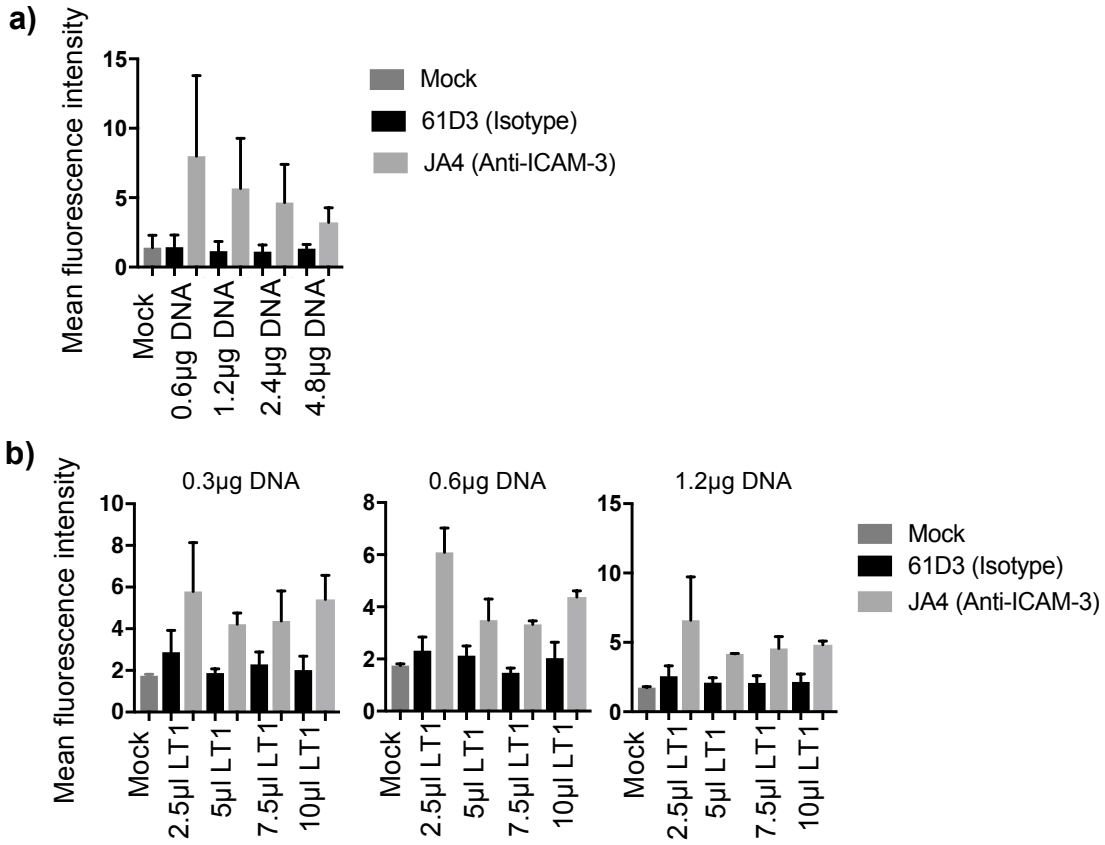

Figure 39. Transient-LT1 transfection optimisation. HeLa cells were transfected with the indicated different amounts of ICAM3-His DNA and LT1 reagent volumes. At 48 h post-transfection incubation, transfected cells were harvested using 5 mM cold EDTA in PBS and were stained using indirect immunofluorescence using the anti-ICAM-3 mAb JA4 and a secondary anti-mouse-FITC detection reagent. Following staining, cells were analysed by flow cytometry for analysis. (**a**) A constant volume of LT1 reagent (7.5 µl) was used with different amounts of the ICAM3-His DNA in the transfection of HeLa cells. (**b**) Different amounts of ICAM3-His and different volumes of LT1 were used in the transfection of the HeLa cells. Data shown are mean ± SEM of two independent experiments (n=2).

3.7.3.2 Comparison of transient calcium phosphate transfection (HEK293-ICAM-3) to stable transfected HeLa-ICAM-3 in pcDNA3

A new approach of transfection was chosen - the transient calcium phosphate transfection. This method has been used to great success in the lab and was used in the original ICAM-3 work where ICAM-3 was overexpressed in HEK293 cells and was shown to be active for the clearance of those cells when apoptotic (Moffatt et al., 1999). ICAM-3-His DNA was transfected into HEK293 cells, and to save some time in downstream analyses, stable transfected HeLa cells with ICAM-3 in pcDNA3 vector **(made by Liz Torr)** were thawed to be compared with in terms of ICAM-3 expression abundance. In **Figure 40a,** the results are showing flow cytometric fluorescence

frequency histograms of HEK293 cells transfected with ICAM-3-His or HeLa cells stably transfected with ICAM-3 in pcDNA3, stained with anti-ICAM-3 mAb JA4 using indirect immunofluorescence. The stable HeLa-ICAM-3 showed a higher mean fluorescence intensity and percentage of cells positive for ICAM-3 staining compared to the transient HEK293-ICAM-3-His. Flow cytometry using viable cell staining, reveals ICAM-3 expression at the cell surface, where the mAb is able to access. In another approach, total ICAM-3 expression was assessed in both transfected cells via anti-ICAM-3 western blotting of whole cell lysates. In this case, an alternative Ab (abcam anti-ICAM-3 mAb) was used to probe the blots as it was most suitable for western blotting. The results of the western blot are shown in **Figure 40b**. The blot shows the ICAM-3 bands in HeLa-ICAM3 are stronger than in HEK293-ICAM-3, which correlates with the mean fluorescence intensity in the flow cytometer data.

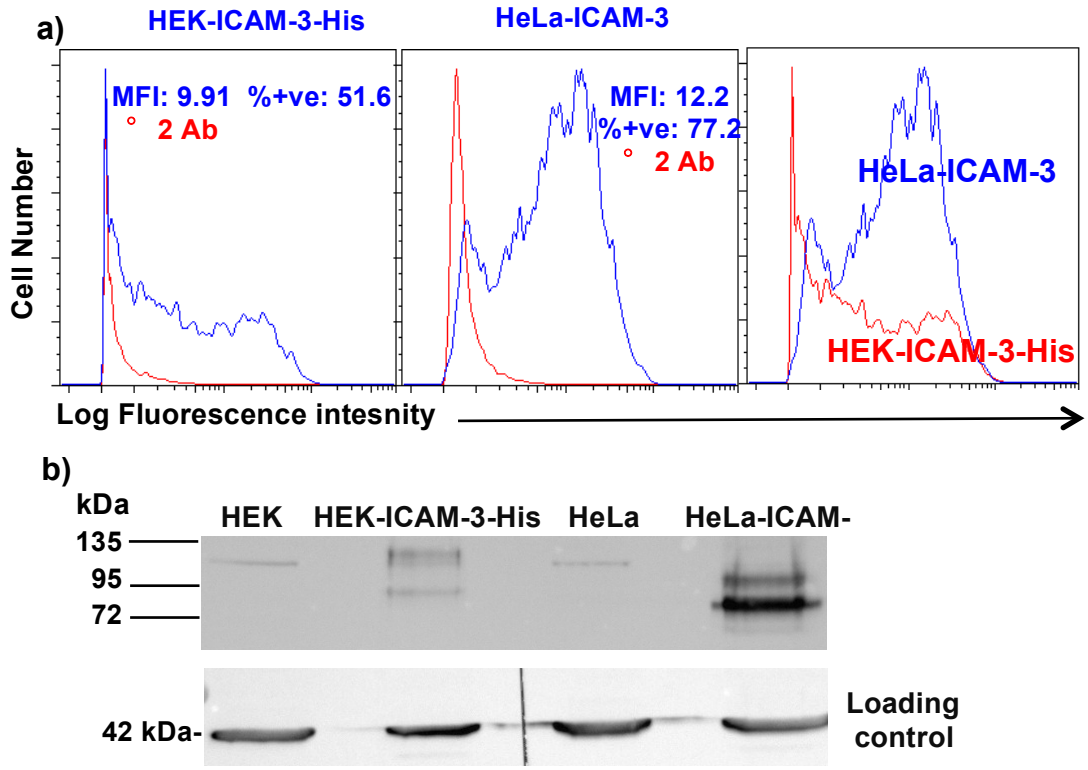

Figure 40. ICAM-3 expression comparison between transient transfected HEK-ICAM3-His and stable transfected HeLa-ICAM-3 in pcDNA3. ICAM-3-His DNA (1 µg) was transiently transfected into HEK293 cells using the calcium phosphate transfection method, whilst the HeLa-ICAM-3 in pcDNA3 vector were stable transfectants. (**a**) Flow cytometric data of HEK-ICAM-3-His & HeLa-ICAM-3 stained with anti-ICAM-3 (JA4) mAb by indirect immunofluorescence staining. (**b**) 37 µg of protein from HEK293, HEK-ICAM-3-His, HeLa & HeLa-ICAM-3 (whole cell lysates) were loaded into the lanes and subjected to SDS-PAGE; the membranes after western blotting were probed with abcam rabbit monoclonal anti-ICAM-3 (1 µg/ml). Equal loading was verified by anti-β actin antibody.

As a result of these studies, and with the challenges of consistent high level transient transfections, stable HeLa-ICAM-3 in pcDNA3 vector was chosen for molecular analyses of ICAM-3 due to the abundance of high ICAM-3 expression.

3.7.4 Apoptosis induction of stable transfected HeLa-ICAM-3 and assessing the rate of the ICAM-3 decrease post apoptosis induction

The molecular analysis of ICAM-3 plan was to identify and compare, in the viable state and apoptotic state, the molecules ICAM-3 associates with. Any change in association may help to explain the change in function of ICAM-3 seen in viable and apoptotic cells. A key part of this is the successful induction of apoptosis so that ICAM-3 is functional in apoptotic cell clearance. HeLa cells do not usually express ICAM-3 as they are non-leukocyte but previous work has shown that HeLa cells expressing ICAM-3, when apoptotic, use ICAM-3 to be removed. Consequently, the high expressing stable transfectants are a useful system for studying ICAM-3 at a higher level of expression than in lymphocytes (**Figure 35**). In order to induce apoptosis in the HeLa cells, a method of apoptosis induction was chosen, cells were treated and viewed microscopically to assess cell death. The stable transfected HeLa-ICAM-3 in pcDNA3 were induced to apoptosis using anisomycin at 5µg/ml as used previously (Torr *et al* 2011). After treatment, the HeLa-ICAM-3 cells were monitored using the CELL-IQ automated cell tracking microscope to assess morphology changes typical of cell death. The images shown in **Figure 41** show how the cells become apoptotic with time, showing cell rounding, detachment and shrinkage - morphology typical of apoptosis, when compared to the untreated cells. In previous work from the Devitt group, the 6h post apoptosis induction was recommended for induction of apoptotic cells with minimal amounts of necrosis (Torr *et al.,* 2011). To confirm this for this thesis study, AxV/PI staining was used to stain the cells every two hours up to 6 h post induction and the stained cells were analysed by flow cytometry. The results can be seen in **Figure 42**. The AxV/PI staining reveals apoptosis proceeds and is detectable at 4h post-induction though at this time point there are still many viable cells. At 6 h post-induction, it is clear that the viable cells are no longer present and necrotic cells are beginning to appear (**Figure 42a**). When viewing cells stained with AxV alone, the results are confirmed with maximal AxV staining seen at 6 h with some AxV negative (viable) cells remaining at 4 h (**Figure 42b**).

In summary, these results confirm that apoptosis induction via anisomycin treatment is efficient and in line with previous work, in terms of dose and time point post induction to be used later in the research.

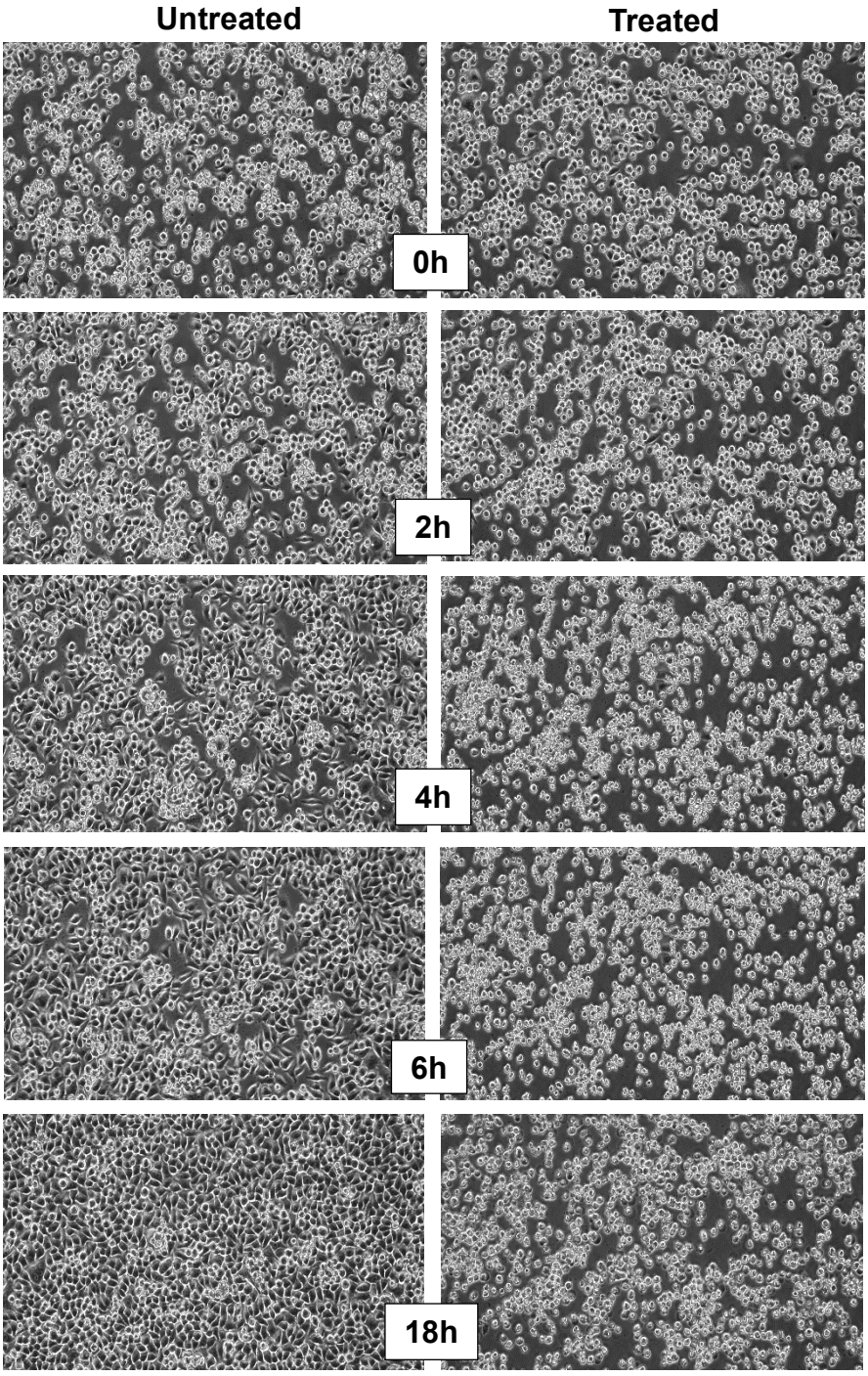

Figure 41. Microscopy images of stable HeLa-ICAM-3 cells induced into apoptosis by anisomycin. HeLa cells were treated with 5 µg/ml of anisomycin and were observed under CELL-IQ microscope technology for 18 h. Every two hours an image was taken to observe the change in morphology of the cells.

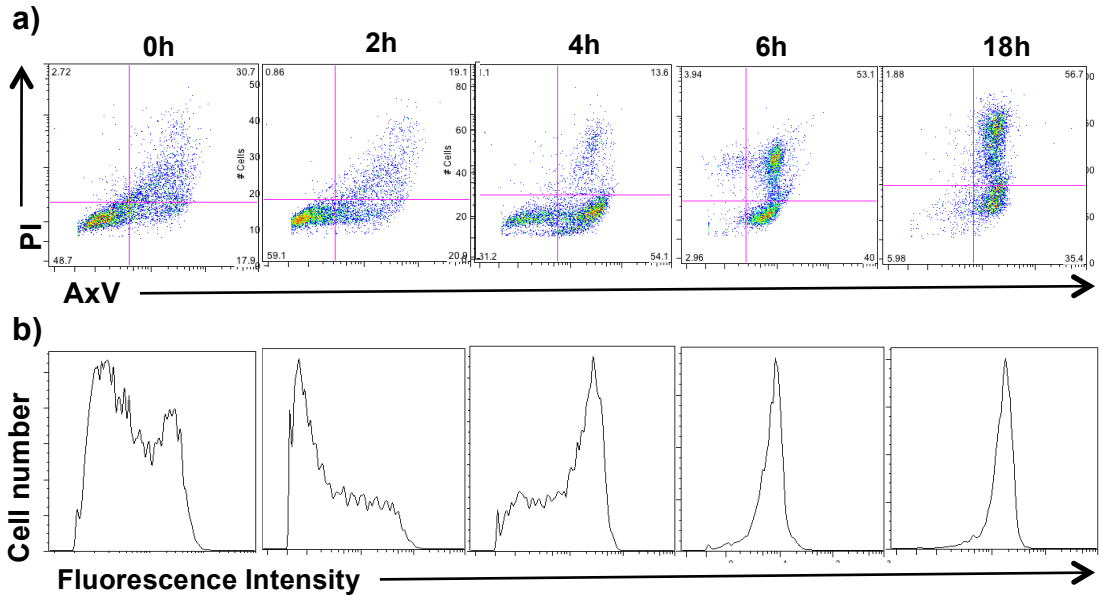

Figure 42. Induction of apoptosis in stable HeLa-ICAM-3 after anisomycin treatment. HeLa-ICAM-3 cells were treated with 5 µg/ml anisomycin and incubated at 37 °C to enable apoptosis to proceed. At the indicated times cell culture samples were stained with AxV/PI and analysed by flow cytometry to analyse the status of apoptosis and the viability of the cells. Data shown are from a single representative experiment, (**a**) showing AxV/PI staining changes over time, apoptotic cells appear in the lower right quadrant of each plot. (**b**) Showing AxV staining alone over time, showing increased AxV staining over time. 0h is the control, whilst 2, 4, 6,18 h were time points post-anisomycin treatment.

Previous work has shown that as apoptosis proceeds, ICAM-3 levels reduce at the cell surface. So, the next assessment within this work using HeLa cells was to investigate any reduction in ICAM-3, and the rate of ICAM-3 decrease post-induction of apoptosis induction. To do this, the HeLa-ICAM-3 cells were stained with anti-ICAM-3 mAb conjugated with PE before and as apoptosis proceeded. After apoptosis induction, the cells were analysed by flow cytometer at specific time points (2, 4, 6 and 18 h) to assess the presence and level of ICAM-3 (**Figure 43**). The results reveal how the mean fluorescence intensity and the percentage of cells positive for ICAM-3 decreases with time post apoptosis induction. The decrease in the ICAM-3 staining was significant compared to cells at 0h (non-induced). This can be seen with the amount of ICAM-3 on cells (i.e. MFI measure) across all of the time points (18, 6, 4 and 2h), while the percentage of cells positive for ICAM-3 was significantly different at 18 h and 6 h post-induction when compared to 0 h.

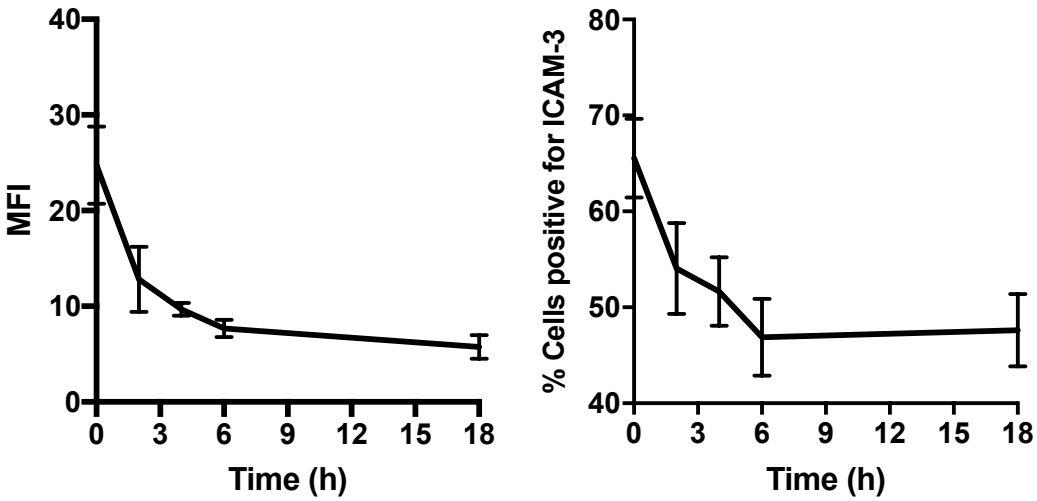

Figure 43. Rate of decrease of ICAM-3 expression in stable HeLa-ICAM-3 after apoptosis induction by anisomycin. HeLa-ICAM-3 cells were treated with 5µg/ml anisomycin and incubated at 37 °C. Post anisomycin treatment, every two hours, cell cultures of treated cells were stained with ICAM-3-PE stain (anti-ICAM-3 mAb conjugated to PE) and analysed by flow cytometry. Data shown are mean fluorescence intensity and percent of cells positive for ICAM-3. The decrease of ICAM-3 post-apoptosis induction is shown as a decrease in the mean fluorescence intensity and the +ve staining percentages, where there was significant decrease in MFI in all time points compared to 0h. The +ve staining percentages also showed significant difference from 18 h and 6 h compared to 0 h. Results shown are Mean ± SEM of independent experiments (n=3). Statistical analysis used (One-Way ANOVA with Dunnett's post-test). (*P<0.01) (**P<0.001).

3.7.5 Construction of SMALPs

Due to the fact that ICAM-3 is a transmembrane protein, an isolation technique called styrene maleic acid lipid particles (SMALPs) was used to isolate ICAM-3. It is a technique that preserves the native lipid bilayer of a membrane protein during its purification. Consequently, it was felt that this technique might help to preserve the interaction of ICAM-3 with partner proteins most effectively (**Figure 44)**. Large amounts of viable & apoptotic stable transfected HeLa-ICAM-3 pelleted cells were used to make membrane preparations via nitrogen chambers followed by applying the SMALPs technique for the membrane protein isolation.

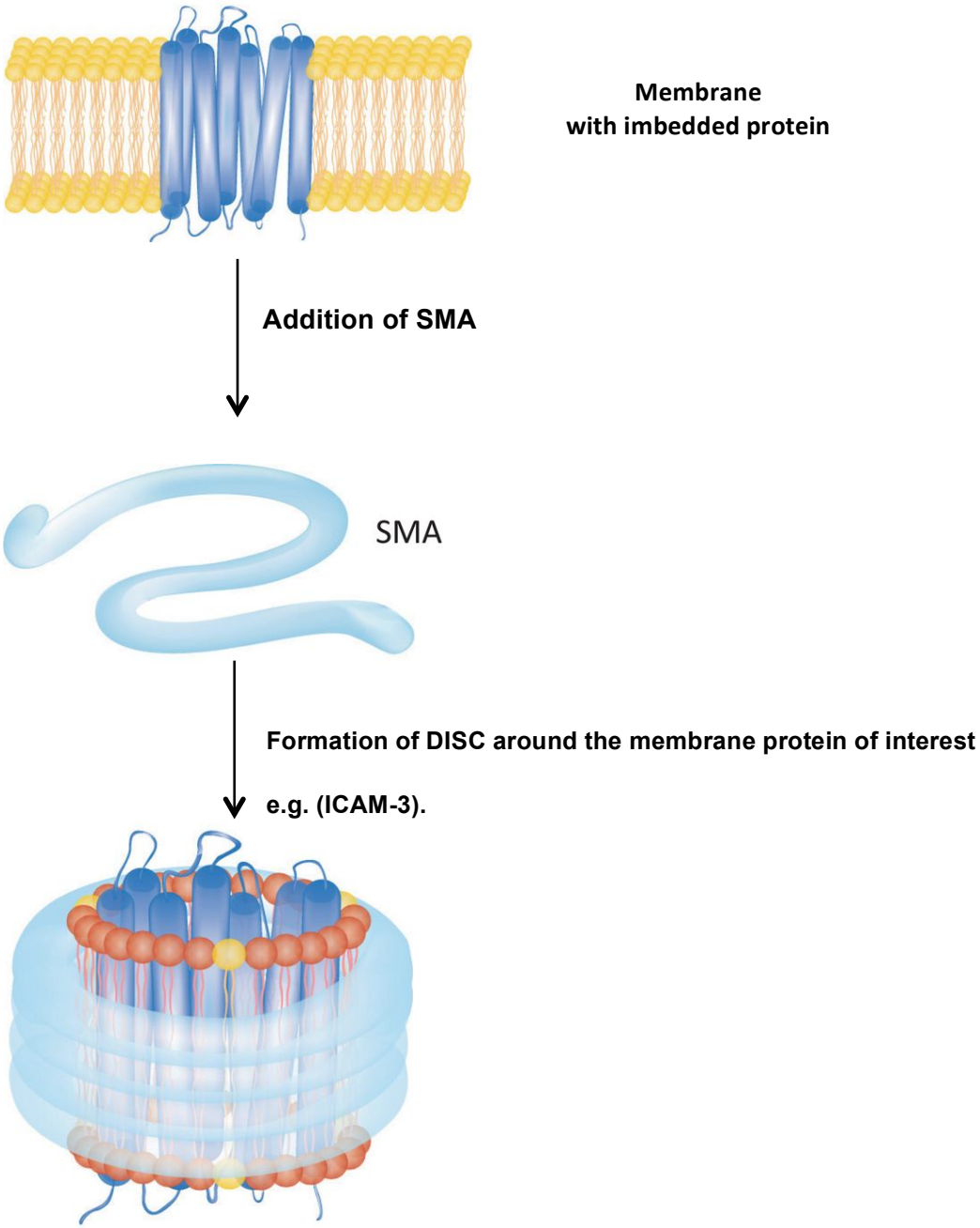

Figure 44. Schematic diagram of SMALP technique. . A diagram showing how SMALPs are formed, where once the SMA co-poymer is added to the membrane containing the protein that is embedded in it, the SMA co-polymer forms a DISC shape around the protein e.g. (ICAM-3) therbey encapsulates the protein, the DISC formed is in state that allows protein purification methods possible to perform. Figure is adjusted from **(Jamshad *et al.*, 2011).**

The SMALPs extractions were analysed for ICAM-3 presence to assess if the preparation was successful. To do this SMALP extractions were subjected to SDS-PAGE under reducing conditions to separate the constituents, followed by probing with abcam ant-ICAM-3 mAb (**Figure 45**). The blot shows clear bands that can be confirmed as ICAM-3 bands because the non-transfected HeLa cell extracts were clear. Four bands were shown, band A (288 kDa), band B (180 kDa), band C (115 kDa) and band D (87 kDa), the band A could be ICAM-3 that were not fully reduced ICAM-3 dimer or heavily glycosylated ICAM-3. Bands C and D of the ICAM-3 are what were seen in Moffat *et al.,* which were 124 kDa and 96 kDa. Analysis of the extracts from viable and apoptotic cells suggests some differences in the appearance of ICAM-3. The difference in the ICAM-3 bands between the viable and apoptotic HeLa-ICAM-3 is that the band D (87 kDa), the band is significantly reduced in apoptotic cells. The control cell (HeLa only) is showing no ICAM-3 bands.

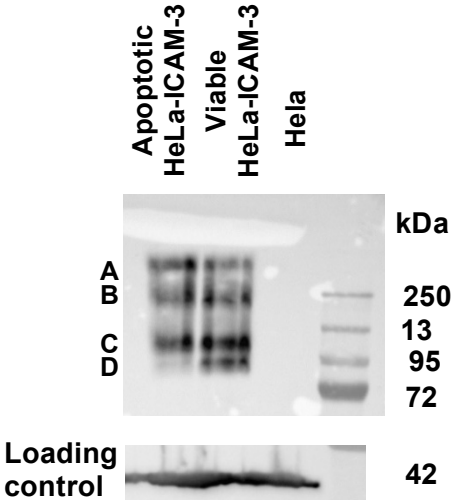

Figure 45. Western blot of SMALP extractions from viable & apoptotic HeLa cells expressing ICAM-3. Stable HeLa-ICAM-3 cell pellets (viable & apoptotic) were used to prepare membrane preps by using the nitrogen cavitation chamber, SMALP extracted samples were prepared afterwards using the isolated membrane preps. Per sample, 37 µg of protein were loaded into the lanes and subjected to SDS-PAGE. The membranes after western blotting were probed with abcam rabbit monoclonal anti-ICAM-3 (1 µg/ml) and anti-rabbit-HRP. Equal loading was verified by anti-β actin antibody. This result is a representative of two experiments.

The apparent loss of the band D of ICAM-3 in apoptotic cells led to the hypothesis that, during apoptosis, ICAM-3 is actively loaded into extracellular vesicles and released from the parent cell resulting in loss of the low molecular weight ICAM-3. If this were true, then it may be expected that this low molecular weight band would be seen at

relatively high levels in EV. This new hypothesis was tested here with apoptotic cell derived extracellular vesicles (ACdEV) from stable transfected HeLa-ICAM-3 separated by SDS-PAGE alongside membrane preps of viable and apoptotic HeLa cells as controls, and probed with abcam ant-ICAM-3 mAb. The results of this study are shown in **Figure 46**. The ICAM-3 blot once again shows the relative loss of the low ICAM-3 band D from apoptotic cells relative to viable cells. In the lane for ACdEV from HeLa-ICAM-3, a single ICAM-3 band C is visible but this does not correspond to the lower molecular weight band in question that is lost from the cells. Thus, the decrease in the low molecular weight ICAM-3 band D is likely not due to the preferential loading of ICAM-3 of this given MW to the ACdEVs. Nevertheless, ACdEVs from HeLa-ICAM-3 are showing the presence of ICAM-3. These data show good correlation with previously published work from Torr *et al.* where the authors, for the first time, described that as the ICAM-3 positive leukocytes undergo apoptosis, their overall ICAM-3 load reduced. Here the presented results show that this is due to the increased secretion of EVs from apoptotic cells.

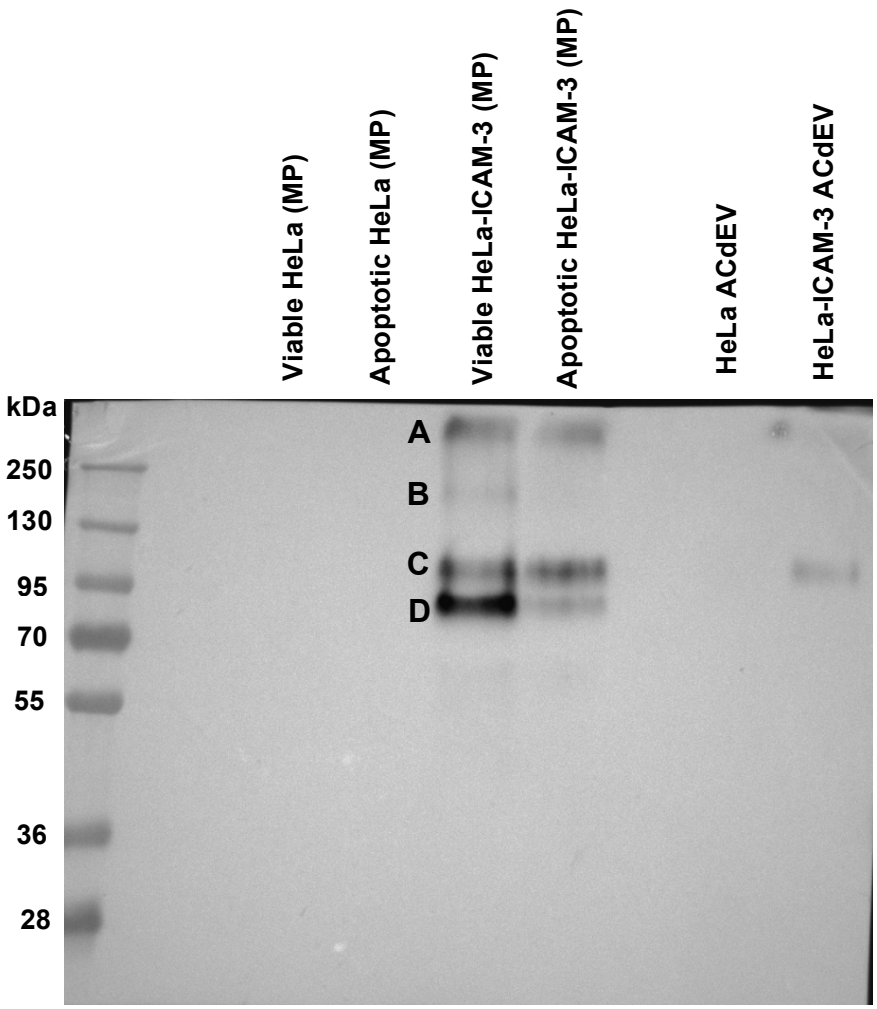

Figure 46. ICAM-3 western blot of membrane preps from viable cells, apoptotic cells and ACdEV from HeLa-ICAM-3. Membrane preps (MP) from viable & apoptotic HeLa & HeLa-ICAM-3 were prepared to be compared to the extracted ACdEV from apoptotic HeLa & HeLa-ICAM-3. Their proteins were quantified using the Bradford assay. 37 µg of protein from the indicated samples was loaded in each lane and subjected to SDS-PAGE. The membranes after western blotting were probed with abcam rabbit monoclonal anti-ICAM-3 (1 µg/ml) and anti-rabbit-HRP. Four ICAM-3 bands were detected. Their calculated MW are as follows: **A** – 288 kDa, **B** – 180 kDa, **C** – 115 kDa and **D** – 87 kDa.

In summary, using the SMALPs technology it was possible to prepare membrane preps from both viable and apoptotic HeLa-ICAM-3 stable cells. Blotting against ICAM-3 showed that ICAM-3 is present in viable and apoptotic HeLa-ICAM-3 as well as in the corresponding ACdEVs. That being the case, the next research objective was to immunoprecipitate ICAM-3-containing SMALPs to look for the ICAM-3 interacting partners.

3.7.6 Co-immunoprecipitation of ICAM-3

After having successfully acquired the SMALP extracts from viable and apoptotic stable transfected HeLa-ICAM-3, the next step was to perform the co-immunoprecipitation of ICAM-3-containing membrane discs. Firstly, the Ab of interest had to be immobilized on the resin within the column. This approach was taken to make a reusable mAb coated column that would not release the mAb into the preparations for downstream mass-spectrometry analysis. Previous results showed that MA4 is the mAb of choice when the native form of ICAM-3 is being targeted for detection. Earlier flow cytometry staining showed that MA4 was effective at staining native ICAM-3 within membranes, while the abcam anti-ICAM-3 mAb worked more effectively for the detection of ICAM-3 in its reduced, denatured linear form. Thus, MA4 mAb was chosen for the Co-IP of the ICAM-3-containing membrane discs.

The role of MA4 was to capture the ICAM-3 on the surface of membrane disc while the SMALP extracted sample passed through the column, and thereby immobilize it. The antibody immobilization required some optimization, and a few of immobilization attempts were undertaken with limited success (**Figure 47**). To immobilize MA4 mAb on the resin, the resin was incubated with the Ab in the presence of coupling buffer in a Co-IP column for two hours as suggested by the manufacturer's instructions. After this the column was centrifuged to remove the excess liquid/unbound mAb as a 'flow through'. If the immobilization was successful, the flow through fraction should not contain Ab, as the amount of Ab incubated was not sufficient to saturate the column. Initially the flow through of the resin co-incubated with MA4 mAb and blotted against MA4 showed the presence of heavy and light chains of MA4 mAb (approximately 50 kDa and 25 kDa respectively; data not shown) indicating that immobilization was not successful. Thus, in the second attempt MA4 mAb was co-incubated with resin and coupling buffer for an extended period (overnight) at 4 °C, thereby allowing more time for the immobilization. However, this resulted in the multimerisation of the mAb chains, since the very strong band corresponding to the 130 kDa was detected in a WB (**Figure 47a**).

The Pierce Co-IP kit used allows for the Ab to covalently and irreversibly bind to the amine-reactive resin, as advertised by the manufacturer. For that to take place, it was assumed that resin is rich in the surface exposed carbonyl-like groups (e.g. -C=O), which will as strong electrophiles readily react with nucleophilic amine of the Ab N-terminus (-NH_2). Thus, the sole purpose of 'coupling buffer' would be to stabilize Schiff

base (-N=C<) by reducing it (-NH-CH< + H_2O). In the following optimization attempt, resin and MA4 mAb were firstly co-incubated for 30 min after which the coupling buffer was added to the mix and incubated for another 90 min at the RT. The flow through was blotted against MA4 (**Figure 47b**) and it showed complete absence of MA4 bands indicating that the MA4 mAb was successfully fully coupled to the Co-IP resin.

Once MA4 mAb was successfully coupled to the resin, it was possible to proceed with the Co-IP of ICAM-3-containing membrane discs. Thus, SMALP preparations of viable and apoptotic HeLa-ICAM-3 cells were added to the column packed with resin-immobilized MA4 mAb, and co-incubated overnight to maximize the capture of ICAM-3 containing membrane discs. As a negative control wild type HeLa cell extracts were also used. **Figure 48** shows the ICAM-3 western blot of flow-through fractions (i.e. unbound proteins) of extracts of viable HeLa-ICAM-3 (lane 1), apoptotic HeLa-ICAM-3 (lane 2) and WT HeLa cells (lane 3). The corresponding SMALP preparations prior to Co-IP are shown in lanes 4, 5 and 6 respectively, serving as positive controls for ICAM-3. It is clear that ICAM-3 bands are present in all lanes. The presence of ICAM-3 bands for both viable and apoptotic HeLa-ICAM-3 in flow through fractions, coupled with no detectable protein within eluted fractions (data not shown) showed that Co-IP was not successful. This may be due to several factors e.g. there may be the interference of SMALP with ICAM-3-MA4 coupling. More, coupling of the N-terminus of MA4 mAb (with the N terminus being the antigen binding site) to the resin might shield the antigen-binding site to the exposed ICAM-3 and prevent from successful immobilization of ICAM-3 to the column resin. Due to the limited time available, Co-IP was not further optimized. To look for ICAM-3 binding partners, mass spectrometry-based approach was further tested.

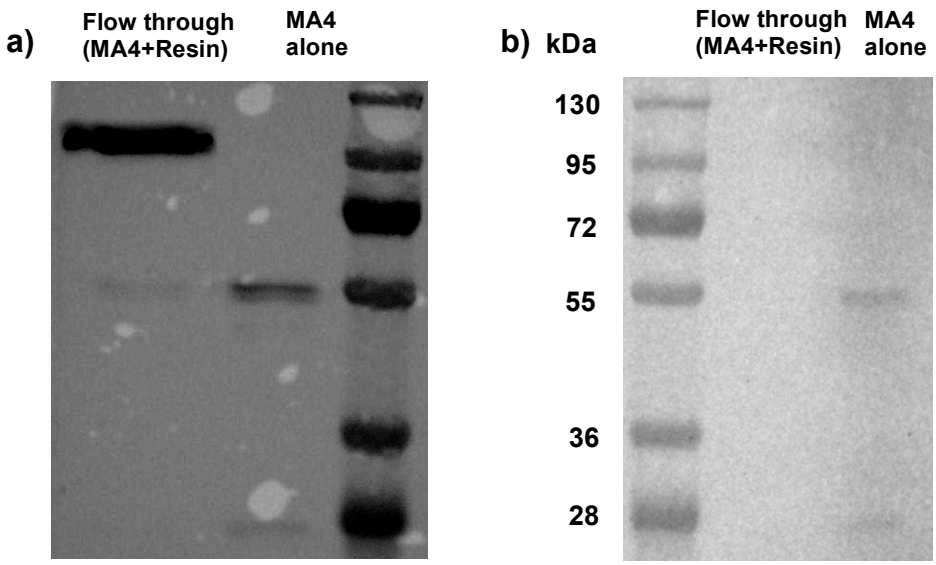

Figure 47. Optimisation of Antibody Immobilization for co-immunoprecipitation studies. 75 µg of purified anti-ICAM-3 mAb MA4 was added to the mixture of Co-IP antibody immobilization buffer, to be bound to the resin in the column. (**a**) Western blot of MA4 mix (control) which is MA4+dH_2O+coupling buffer and the MA4+resin flow though. The blots were probed with anti-mouse secondary antibody HRP conjugate. The flow though showed a dimerised heavy chain of MA4 mAb, which meant the immobilization, did not work. (**b**) A second trial of the antibody immobilization, showing that the flow though sample has shown no sign of ICAM-3 mAb, meaning the immobilisation has worked.

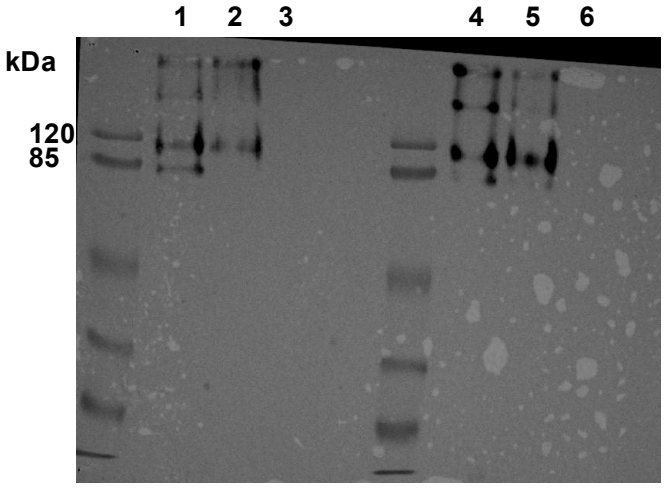

1.FL (incubated HeLa-ICAM-3 viable SMALP+MA4)
2.FL (incubated HeLa-ICAM-3 apoptotic SMALP+MA4)
3.FL (incubated HeLa viable SMALP+MA4)
4. HeLa-ICAM-3-viable SMALP
5. HeLa-ICAM-3-apoptotic SMALP
6. HeLa viable SMALP

Figure 48. Co-Immunoprecipitation optimization. Viable and apoptotic SMALP extracted samples from HeLa & HeLa-ICAM-3 were run in the Co-IP kit. The flow through of the Co-IP kit (FL: samples incubated with mAb MA4) were compared to the SMALPs extracted samples. The compared samples were subjected to SDS-PAGE. The membranes after western blotting were probed with abcam rabbit monoclonal anti-ICAM-3 (1 µg/ml) and anti-rabbit-HRP. The flow through samples have shown that ICAM-3 did not bind to MA4 in the column, suggesting that the capture has not worked effectively. If capture was complete, the flow through samples would show nothing on the blot.

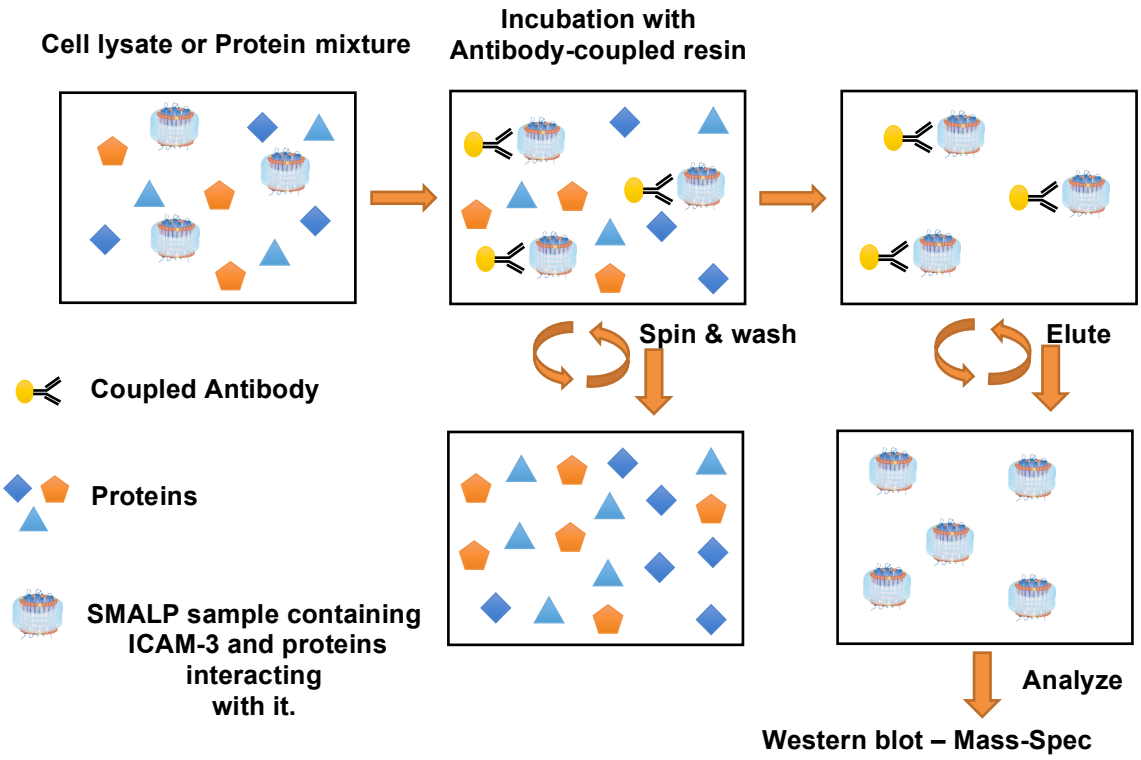

Figure 49. Schematic representation of CO-IP experiment. A diagram is showing how the CO-IP works, where the cell lysate containing the SMALP sample is incubated with the Antibody e.g. (anti-ICAM-3) coupled to the resin, the coupled antibody binds to the SMALP sample containing ICAM-3 and the proteins that are interacting with it, afterwards it gets eluted and analyzed.

3.7.7 Mass spectrometry as a tool to study protein-protein interactions in cells

A direct approach to address whether the expression of ICAM-3 and the induction of apoptosis affected expression of additional proteins, mass spectrometry (MS) analyses of viable and apoptotic HeLa and HeLa-ICAM-3 cells was undertaken. This approach could identify if, in any of these conditions, a new protein was expressed or turned off, upregulated or downregulated. Such proteins may be potential partners of ICAM-3 and could be studied in the future work. Additionally, bioinformatics tools can be applied to the large proteomics datasets to look for a protein known to interact with ICAM-3 or that together, with ICAM-3, contribute to relevant biological effects. This approach to look for protein-protein interactions is significantly less targeted than the co-IP approach followed by MS since it relies upon a large, clear difference in partner

molecule expression being induced by the presence of ICAM-3 and the induction of apoptosis, and the ability of MS to detect low expression of proteins.

Following the initial hypothesis that any ICAM-3 partner protein that enables its change of function in apoptosis is also a membrane protein, membrane preparations from each cell type, rather than the full cell lysates, were analyzed by MS. This first step helped to reduce the sample complexity and to support detection of low abundant proteins by MS. In the second step, complexity of membrane lysates was reduced further by SDS-PAGE where each lane of separated proteins was cut into five pieces of the same size (piece 1= <~25 kDa; piece 2= ~25-41 kDa; piece 3= ~41-73 kDa; piece 4= ~73-131 kDa; piece 5= >~131 kDa) and, following in-gel trypsin digestion, the resultant peptides from each gel piece were analysed by liquid chromatography (LC) online coupled to tandem mass spectrometry (MS/MS). This work was undertaken with expert MS support from [redacted]

In total, analysis of viable HeLa WT and viable HeLa-ICAM-3 membrane preparations identified 1203 proteins (**Table S1**). The same analysis of apoptotic HeLa WT and HeLa/ICAM-3 cells identified 1175 proteins in membrane fractions (**Table S3**). These large datasets were analysed using a bioinformatics approach. Firstly, they were analysed by String software to identify proteins from different cellular sources (**Table 2**). Results indicate that from approximately 1200 proteins detected in each dataset, roughly half were known to be membrane associated, including organelle (e.g. mitochondria) membranes. Additionally, large protein counts (>390) were related to cytosol, cytoskeleton (>160) and nucleoplasm (>300). These counts indicate that many of the proteins identified by MS are not highlighted by as membrane proteins. This may be due to the contaminating association of these proteins with membranes which is true for many cytosolic and cytoskeletal proteins as they are present in high levels, and/or due to a lack of sufficient washes of membrane-isolated fractions during the membrane preparation procedure.

Using mass spectrometry of membrane isolates, it was possible to identify ICAM-3 in the viable Hela-ICAM-3 cells (**Table S1**). Moreover, ICAM-3 is identified only in piece 4 of the resolving gel corresponding to the size range ~73-131 kDa where ICAM-3 band C (115 kDa) and D (87 kDa) were identified (**Figure 46**). However, MS failed to positively identify ICAM-3 peptides in membrane isolates of apoptotic Hela-ICAM-3 cells (**Table S2**). Since ICAM-3 is observed in the corresponding WB (**Figure 46**), it is likely that MS failed to identify ICAM-3 because of the large sample complexity and relatively low ICAM-3 levels.

Table 2. Summary table of major cellular sources of identified proteins. HeLa WT and HeLa-ICAM-3 cell (viable and apoptotic) membrane preparations were analysed and the identified proteins classified into Cellular components using the gene ontology tool String. False discovery rate is a measure of probability for a given group of proteins to be a random one within the whole identified proteome. This table is a summary of **Table S1 and S3**.

Cellular component	Counts in the gene set (viable/apoptotic)	False discovery rate (viable/apoptotic)
Membrane	642 / 640	8.23×10^{-30} / 2.90×10^{-26}
Cytosol	448 / 395	1.88×10^{-91} / 1.28×10^{-64}
Focal adhesion	107 / 105	1.43×10^{-46} / 1.41×10^{-45}
Cytoskeleton	187 / 166	1.31×10^{-15} / 4.54×10^{-50}
Nucleus	593 / 591	9.88×10^{-47} / 2.49×10^{-49}
Nucleoplasm	316 / 306	1.76×10^{-37} / 1.21×10^{-32}
Mitochondrial membrane	120 / 124	5.17×10^{-32} / 2.05×10^{-35}
Ribosome	89 / 80	2.32×10^{-55} / 4.93×10^{-46}
Endoplasmic reticulum	131 / 139	3.15×10^{-6} / 1.33×10^{-8}

Protein changes in viable HeLa WT versus HeLa/ICAM-3 cells: From 1203 proteins identified in membrane preparations from viable Hela WT and viable Hela-ICAM-3 cells, 94 proteins were significantly upregulated in Hela-ICAM-3 cells, while 149 were significantly downregulated (**Table S1**). These proteins may represent potential ICAM-3 interacting partners. Importantly, only ICAM-3 is detected as a newly expressed protein in Hela-ICAM-3 cells, as a result of the stable transfection. This number of identified proteins is too large for each to be tested as a potential partner of ICAM-3 in apoptotic cell clearance as this would require each of these to be over-expressed (to assess its function in promoting AC clearance) or each to be silenced either by a blocking mAb or siRNA to reduce expression (to reduce AC clearance).

To reduce the number of proteins to be taken forward for future analyses, it was considered necessary to rely on existing data of protein-protein interactions to identify, from existing bioinformatics information, potential partner molecules known to interact with ICAM-3. String is a free gene ontology tool that searches for the known protein-protein interactions in any given protein dataset. These interactions may not necessarily be covalent, since String searches also for those protein pairs that jointly contribute to any given function, and assigns an interaction score (0.15-0.4 low interaction, 0.4-0.7 medium interaction, 0.7-0.9 high interactions, >0.9 highest interaction). Thus, to proceed with this approach for analysis, it is further hypothesized

that any ICAM-3 partner is a protein that is already been identified to interact with or has a joint mode of action with ICAM-3. This limits the potential for new partner discovery but it would allow an existing ICAM-3 partner to be linked with the process of AC clearance for the first time. Altogether, 33 proteins were identified as known to interact with ICAM-3. A full list can be found in **Table S2**, while a summary list of ICAM-3-interacting proteins with statistically significant differences between the different conditions (Viable HeLa WT versus viable HeLa/ICAM-3 and apoptotic HeLa WT versus apoptotic HeLa/ICAM-3) is in **Table 3, left hand column**.

Changes in the expression of ICAM-3 interacting partners in viable HeLa WT versus HeLa/ICAM-3 cells: Moesin (GN=MSN) is known to interact strongly with ICAM-3. However, moesin levels were significantly decreased in viable HeLa-ICAM-3 cells. Furthermore, ezrin (GN=EZR), junctional adhesion molecule A (GN=F11R), CD44 antigen (GN=CD44), albumin (GN=ALB), spectrin alpha light chain (non-cardiac 1, GN=SPTAN1) and integrin beta 1 (GN=ITGB1) were identified and are known to have a medium interaction with ICAM-3, although none of these proteins underwent a significant change in the levels in HeLa-ICAM-3 cells compared to HeLa WT. Out of 26 proteins with low interaction scores with ICAM-3, complement decay-accelerating factor (GN=CD55) and calreticulin (GN=CALR) were significantly reduced in viable ICAM-3 transfected HeLa cells, while levels of von Willebrand factor (GN=VWF) and 78 kDa glucose-regulated protein (GN=HSPA5) are found to be upregulated.

Table 3. Summary table of ICAM-3 interacting proteins identified in membrane preparations of viable and apoptotic HeLa WT and HeLa-ICAM-3 cells based on the String search. Confidence scores: 0.15-0.4 low interaction, 0.4-0.7 medium interaction, 0.7-0.9 high interactions, >0.9 highest interaction. Proteins are represented by their gene names. This table is a summary of **Table S2**.

		Viable cells		Apoptotic cells	
Protein (gene)	**Combined score**	**Protein identification**	**Significantly increased**	**Protein identification**	**Significantly increased**
MSN	0.799	+	WT, 1.81x, *p* 0.02	+	no
ITGB1	0.415	+	no	+	WT, 1.48x, *p* 0.04
CD81	0.349	-	N/A	+	WT, 44.1x, *p* 0.04
CD63	0.304	-	N/A	+	WT, 5.84x, *p* 0.02
LMNA	0.265	+	-	+	WT, 1.46x, *p* 0.01
VWF	0.232	+	ICAM3, 11.7x, *p* 0.02	-	N/A
CD22	0.232	+	WT, ∞	-	N/A
VTN	0.2	+	-	+	WT, 3.03x, *p* 0.004
CD55	0.188	+	WT, 2.78x, *p* 0.005	+	-
CALR	0.183	+	WT, 5.57x, *p* 0.01	+	-
CDC42	0.168	-	N/A	+	ICAM3, 5.87x, *p* 0.02
DECR1	0.152	+	-	+	WT, 3x, *p* 0.02
DNM2	0.151	+	-	+	ICAM3, 9.4x, *p* 0.02
HSPA5	0.15	+	ICAM3, 2.63x, *p* 0.000001	+	-

Protein changes in apoptotic HeLa WT versus HeLa/ICAM-3 cells: Different results are observed from the analysis of apoptotic HeLa cells. From 1175 proteins in membranes from apoptotic HeLa WT and apoptotic HeLa-ICAM-3 cells, 77 proteins were significantly upregulated in HeLa-ICAM-3 cells, while 150 were significantly downregulated (**Table S3**).

Changes in the expression of ICAM-3 interacting partners in apoptotic HeLa WT versus HeLa/ICAM-3 cells: Although ICAM-3 was not identified by MS, its presence in apoptotic HeLa-ICAM-3 cells was confirmed by WB (**Figure 45**). Thus ICAM-3 was included in the String search together with 1175 proteins identified by MS, and 25 proteins were identified to interact with ICAM-3. With the exception of junctional adhesion molecule A, the same set of proteins with strong and medium interaction levels was detected in apoptotic cells (**Table S2, Table 3, right hand column**). Levels of integrin beta 1, CD63 antigen (GN=CD63), CD81 antigen (GN=CD81), prelamin-A/C (GN=LMNA), vitronectin (GN=VTN), 2,4-dienoyl-CoA reductase, mitochondrial (GN=DECR1) were shown to be significantly decreased in the membrane fractions of HeLa-ICAM-3 compared to Hela WT cells. In contrast, cell division control protein 42 homolog (GN=CDC42) and dynamin-2 (GN=DNM2) were expressed more in ICAM-3 transfected HeLa cells than WT.

Protein changes in viable versus apoptotic HeLa/ICAM-3 cells: It is of interest to monitor how apoptosis influences proteome and expression of proteins that interact with ICAM-3 as this is most relevant to the function under study (i.e. apoptosis-associated changes in ICAM-3 and its partners). Thus, proteomes of viable and apoptotic HeLa-ICAM-3 membranes were compared. Altogether 1119 proteins were identified (**Table S4**) indicating that apoptosis did not induce synthesis of a new protein, nor a disappearance of an existing protein. The levels of 874 proteins remained unchanged. However, apoptosis in HeLa-ICAM-3 cells significantly decreased levels of 124 proteins, while 121 proteins got upregulated. The proteins that showed the greatest increase in apoptotic HeLa/ICAM-3 are RL7L (530 fold increase); KAD1 (285 fold increase); THOC2 (74 fold increase); CSPG4 (67 fold increase); MCTS1 (27 fold increase); TET2 (15 fold increase); RFIP4 (13 fold increase); SPN1 (10 fold increase); MUC18 (2 fold increase). Whilst these appear to be large changes, none of these are known ICAM-3 interactors.

In summary, these studies have shown that there are a variety of known ICAM-3 interacting partners that are present and altered in their expression under the variety of experimental conditions studied. However, there is no large, clear difference in partner molecule expression being induced by the presence of ICAM-3, as was hoped at the start of this approach.

3.7.8 Mass spectrometry as a tool to study protein-protein interactions in ACdEV

Macrophage migration assays have previously shown that apoptotic cells and ACdEVs induce relatively similar chemotaxis of macrophages in the both vertical and horizontal migration assays in a manner that is ICAM-3 dependent (Results – Chapter1 - **Figures 22-25**). However, purified ICAM-3-Fc showed no ability to induce chemoattraction of macrophages suggesting that ICAM-3 alone is not sufficient to induce MØ migration. These results suggest that a protein partner might interact with ICAM-3 to support the clearance of dying cells. Thus, mapping of the proteome of ACdEV from ICAM-3 positive cells to look for potential ICAM-3 protein partners is of great interest.

Following the bottom-up proteomics approach, 631 proteins were identified in ACdEVs from Hela WT and Hela-ICAM-3 cells (**Table S5**), of which 331 were recognized as extracellular exosome-related according to the String analysis (**Table 4**). Indeed, many EV-specific proteins (**Figure 50**) were identified, such as CD63, CD81, CD109, heat shock proteins (HSP70, HSP90 etc.), annexins (ANX11, ANXA1, ANXA2, ANXA4, ANXA5, ANXA6), enolase (ENOA, ENOG) and a number of cytoskeletal proteins (ACTN, TUB, MOES, EZRI, 14-3-3 family). This information, together with qNano measurements and TEM characterization, serves as an additional level of confirmation that ACdEVs were successfully isolated by differential centrifugation. Additionally, 220 proteins were associated with the cell membrane, 269 with the cytosol, 107 with the cytoskeleton, 92 with focal adhesions and 42 with the cell surface. Due to time limitations, ACdEVs were isolated in a single biological replicate and measured as a single technical replicate. Thus, statistical information on protein expression is not available.

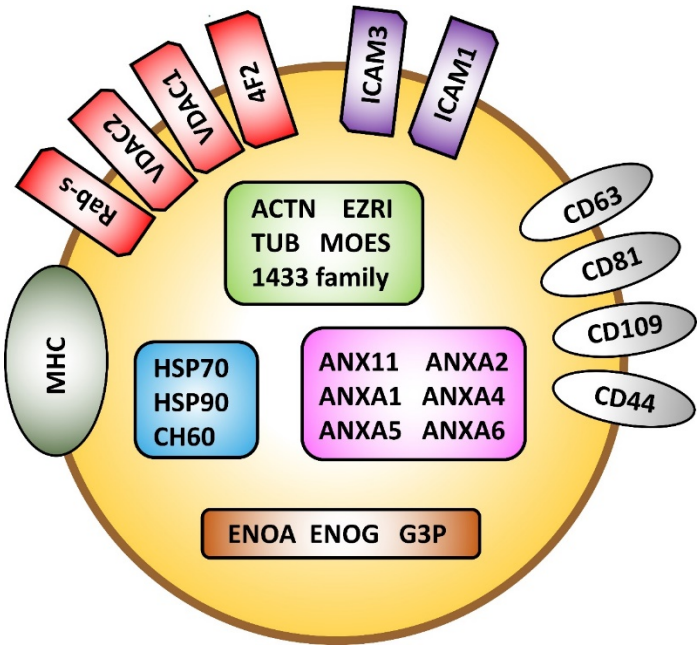

Figure 50. Proteins identified in this study correspond to the most common protein families identified in extracellular vesicles.

Table 4. Summary table of major cellular sources of identified proteins found in ACdEV. ACdEV were collected from apoptotic HeLa WT and apoptotic HeLa-ICAM-3 cells, measured by MS and analysed by String software. Identified proteins are classified into Cellular components using the gene ontology tool String. False discovery rate is a measure of probability for a given group of proteins to be a random one within the whole identified proteome. This table is a summary of **Table S5**.

Cellular component	Counts in the gene set	False discovery rate
Extracellular vesicle	331	2.95×10^{-149}
Cytosol	269	3.53×10^{-75}
Focal adhesion	92	1.49×10^{-61}
Membrane	220	2.11×10^{-18}
Cytoskeleton	107	7.55×10^{-14}
Cell surface	42	8.26×10^{-6}

Table 5. Summary table of ICAM-3 interacting proteins identified in ACdEV from HeLa WT and HeLa-ICAM-3 cells based on the String search. *Proteins not found in other datasets to interact with ICAM-3. Confidence scores: 0.15-0.4 low interaction, 0.4-0.7 medium interaction, 0.7-0.9 high interactions, >0.9 highest interaction. Proteins are represented by their gene names.

Protein (gene)	Combined score	Protein (gene)	Combined score	Protein (gene)	Combined score
ICAM1*	0.808	CD81	0.349	LAMP1	0.21
MSN	0.799	LCK*	0.322	VTN	0.2
EZR	0.583	CD63	0.304	FYN	0.199
CD44	0.476	CORO1A*	0.299	ACADM	0.193
PTPRC*	0.456	FCGR2A*	0.284	CD55	0.188
ALB	0.44	ITGAV	0.265	CALR	0.183
SPTAN1	0.435	ANXA5	0.26	RHOA	0.176
MRC1*	0.424	GAPDH	0.254	CDC42	0.168
ITGB1	0.415	TFRC*	0.241	TCOF1	0.167
ITGA4*	0.353	C3*	0.214	HSPA5	0.15

ICAM-3 was not identified by mass spectrometry of ACdEV, although WB of Hela-ICAM-3 membrane preparation clearly showed ICAM-3 C band (**Figure 46**) with a molecular weight of approximately 115 kDa. Thus, with an aim to search for the interacting proteins ICAM-3 was included in the String search together with 631 previously identified ACdEVs proteins. Under the same search parameters as previously described, String analysis identified 30 interacting partners of ICAM-3 (**Table 5**). Out of these, 9 proteins such as intercellular adhesion molecule 1 (GN=ICAM1), receptor-type tyrosine-protein phosphatase C (GN=PTPRC), macrophage mannose receptor 1 (GN=MRC1), integrin alpha-1 (GN=ITGA4), tyrosine-protein kinase Lck (GN=LCK), coronin-1A (GN=CORO1A), Low affinity immunoglobulin gamma Fc region receptor II-a (GN= FCGR2A) and complement C3 (GN=C3) were found to interact with ICAM-3, or to have a joint mode of action with ICAM-3, only in the proteome of ACdEVs.

In summary, a range of interacting ICAM-3 proteins were identified on ACdEV but the significance of these in the biological function of ACdEV requires additional future work.

3.8 Discussion – Chapter 4 - Molecular analysis of ICAM3 partner molecules (viable VS apoptotic)

It was previously shown that ICAM-3 on viable leukocytes interacts with leukocyte function antigen 1 (LFA-1), where it is involved in signal transduction and initiation of immune responses by promoting interactions between T cells and antigen-presenting cells (Moffatt et al., 1999, Montoya et al., 2002). But when the leukocytes become apoptotic, the ICAM-3 does not interact with LFA-1 and it gets involved in apoptotic cell clearance (Moffatt et al., 1999). From this intriguing change in function, a range of possible explanations are possible:

- ICAM-3 may become changed during apoptosis so that it binds a new receptor;
- ICAM-3 may become changed and associate with a soluble factor(s) to bridge the apoptotic cell to the MØ;
- ICAM-3 may be changed or unchanged but associates with a new partner molecule so that a new receptor may bind;
- ICAM-3 may be changed or unchanged but dissociates from an existing partner so that a new receptor may bind.

Previous work has suggested that there appear to be no big changes in molecular mass associated with ICAM-3 on western blots (Moffat *et al.,* 1999, Shingler, 2003, Torr *et al.,* 2011). This work might suggest that option 1 is less likely. However, ICAM-3 is very glycosylated (Funatsu et al., 2001) and this results in diffuse bands on western blots which might hide changes that could be occurring. The association of new partners or dissociation of partners could happen because of the big changes in membrane structure that happen as a cell undergoes apoptosis. For example, large scale exposure of PS occurs (Martin *et al.*, 1995) and this changes the 'packing' of the lipids in a membrane (Reid *et al.*, 1996, Hammill *et al.*, 1999, Mcevoy *et al.*, 1988). These changes might mean that membrane components may move around more easily in apoptotic cells.

These possibilities were addressed within this chapter but the main hypothesis to be tested here is that ICAM-3, on the surface of apoptotic and viable cells, is associated

with different partner proteins and that this alteration permits it to function differently in each cell context (viable or apoptotic).

To test this hypothesis, different leukocytes (T and B cells) were assessed for their ICAM-3 abundance, which showed relatively low level of expression. The lymphocyte system has the advantage that the level of ICAM-3 is 'natural' and we know ICAM-3 functions fully for the recruitment of MØ and AC clearance. However, the low level of ICAM-3 may present problems in the isolation of sufficient ICAM-3 and therefore any partner molecules for MS analyses.

So to address this potential interest, another approach was taken, where the natural expression state of ICAM-3 was disregarded and moved to higher expression of ICAM-3 by transfecting ICAM-3 into HEK293 and HeLa cells. It was expected that this could result in much higher levels of ICAM-3 expression. This would help in ICAM-3 isolation but there are risks associated with this approach. It is possible that overexpression of ICAM-3 may result in alternative partner molecules being associated with ICAM-3 as the 'normal' partner molecules would not be overexpressed. However, it is known that ICAM-3 transfection into HEK cells (Moffatt et al., 1999) and HeLa cells (Torr et al., 2011) does result in a cell that uses ICAM-3 for clearance of apoptotic cells so an overexpression system seemed appropriate to use with these studies.

Different transfection methods were performed with optimizations. The initial aim was to use cells transiently transfected with ICAM-3-HIS as this would help in the ICAM-3 purification suggested by our collaborators. The initial studies suggested that the transfections were successful with ICAM-3 being expressed. However, the level of transfection (percent of cells positive) was low. This low level of transfection would not be a useful step forward from the lymphocytes. Simlar results were seen with transient transfection with ICAM-3-GFP.

Due to limited time, stable transfectants of HeLa-ICAM-3 in pcDNA3 vector was used, which was made previously by a member of Devitt group (Liz Torr). These cells showed high level of expression of ICAM-3 in nearly 80% opf cells and so were selected as the preferred model for studying ICAM-3. The drawback to these cells was that the ICAM-3 was not tagged and so needed a mAb-based purification method to be used.

The stable HeLa-ICAM-3 transfectants were induced into apoptosis and assessed for cell death and ICAM-3 levels. Cell death was induced strongly with the addition of

anisomycin. Anisomycin is an antibiotic that inhibits eukaryotic protein synthesis (Grollman and Walsh, 1967). Apoptosis happened quickly with high levels of apoptosis detected by 6h. An important observation here was also the level of ICAM-3 expression. Previous work has shown that as leukocytes die, ICAM-3 is lost [(Moffatt et al., 1999) and this has been shown to be loss of ICAM-3 into EV (Torr et al., 2011). In a similar manner, the results here show for the first time that transfected HeLa cells also lost ICAM-3 during cell death, in a manner similar to lymphocytes. This ICAM-3 reduction was seen in the MFI and percent cells positive measure across the time points (2, 4, 6 and 18 h) when compared to the control (0 h). This indicates that ICAM-3 is lost from early time points. These data also show that most of the changes have occurred by 6h (early apoptotic phase) post-anisomycin with not much further change by 18 h post-anisomycin (late apoptotic phase). At this point, the model system for analyzing ICAM-3 partner changes during apoptosis was fully established.

The next step in this experimental approach to identify partner molecules of ICAM-3 was how to isolate and purify ICAM-3. The approach to be used was designed to allow ICAM-3 to be isolated in its most natural state with minimal interference to it. To do this, the SMALP (styrene-maleic acid co-polymer) technique was used to isolate ICAM-3 from the stable transfected HeLa-ICAM-3. SMALP is a technique that uses a polymer to insert into membranes and extract a disc/core of membrane bilayer and proteins. This approach removes the need for detergents and so it preserves the native lipid bilayer environment of a membrane protein during its purification to cut out a disc of membrane complete with contained proteins (Lee *et al.*, 2016). This technique is used for looking at protein structure in membranes rather than detergent isolated. For this work, it appeared a gentle method that would allow a small piece of membrane to be extracted that would hopefully contain ICAM-3 and its partner molecules.

After conducting SMALP extractions from membrane preparations for the ICAM-3 samples in the viable and apoptotic phase, they were assessed by western blotting to look for the presence of ICAM-3 as a conformation that the extraction had worked. It was clear that the extracted membrane samples contained ICAM-3 confirming that the SMALP extraction was able to extract ICAM-3 from cells.

These results were interesting as they showed a difference in the western blot pattern of ICAM-3 on viable and apoptotic cells. These bands were labelled A-D (**Figure 45 and 46**). There were clear differences in the ICAM-3 bands between the viable and apoptotic. In these experiments, it appeared that ICAM-3 band D (87 kDa) **(Figure 45**) was very faint in apoptotic cells whilst it was very strong in the viable cells. This is an

interesting observation that might suggest that ICAM-3 can undergo structural changes during apoptosis that might explain its change of function. This has never been seen before but my work is the first time that ICAM-3 has been analysed in isolated membrane preparations from viable and apoptotic cells. Previous work has looked at whole cell lysates and this may have hidden the change (Moffat *et al.,* 1999, Shingler, 2003, Torr *et al.,* 2011). This reduction in ICAM-3 band D could be due to the ICAM-3 reduction seen in the flow cytometer data (**Figure 43**).

This difference in presence of band D between viable and apoptotic state of the cell is interesting. It seemed likely that the loss of ICAM-3 band D could be due to this form of ICAM-3 being released to the ACdEV. This might mean that band D is the chemoattraction promoting form of ICAM-3 on ACdEV. To see if this were true, ACdEV were extracted from apoptotic HeLa-ICAM-3 and membrane preps were prepared and blotted to see the ICAM-3 bands in order to see if band D was found mostly in ACdEV. Surprisingly, ACdEV did not have any band D present. Instead they seemed to have band C. This suggests that it isn't that band D is simply shed from viable cells into ACdEV.

Another possibility for future study, is that band D (high on viable cells) associates with a partner molecule (to increase its size to band C) when cells undergo apoptosis. This band C may then act as a *find me* signal on ACdEV and as an *eat me* signal on apoptotic cells. However, if this was true, the partner molecule would have to bind to ICAM-3 in such a way that it didn't dissociate in the preparation for SDS-PAGE which was done under denaturing and reducing conditions. Glycosylation changes could explain this. To address this idea, future work could isolate bands C and bands D directly from gels or blots to identify the molecules present.

Continuing with the investigation of ICAM-3 molecule partners, the ICAM-3 SMALP samples were used within co-immunoprecipitation studies. Initially the antibody (MA4) was optimized to be immobilized to the resin column in the CO-IP kit. The work showed successful removal of the MA4 from the immobilisation buffer. This suggests successful conjugation of mAb to the resin in the IP column. This column was then used to attempt to purify the SMALP extracts containing ICAM-3. This work suggested that it binding of ICAM-3 to the column was not efficient. There was no loss of ICAM-3 from the samples after passing through the column. Also, when the column was eluted, there was no detectable protein released. These experiments suggest that the capture step of this CO-IP procedure was not working effectively. There are a number of possible reasons for this. It could be due to the interference of the SMALP with

ICAM-3-MA4 antigen-antibody binding. This could be checked in future work by doing an ELISA based assay to see if SMALPs interfered with the result. The affinity of the Ab for ICAM-3 may also be a problem. This could be addressed easily in future work by using a mix of monoclonal antibodies or a polyclonal antibody. This would increase the overall strength of binding of ICAM-3 to the column. If more time had been available, this CO-IP could have been optimized as it would have allowed me to look at the partner molecules and to test the hypothesis.

As the CO-IP approach was not successful, an alternative approach was used. This new approach looked at ICAM-3 and possible partner presence in membrane preparations of cells. This method would not allow us to see the proteins present with isolated ICAM-3. Instead this approach could only look at the total proteins present in the presence or absence of ICAM-3 on viable or apoptotic cells. This work is less focused than the CO-IP approach. It tried to address how expression of ICAM-3 and the induction of apoptosis affected the expression of additional proteins that could have changed the ICAM-3 function, mass spectrometry (MS) (done by Dr. Ivana Milic) was used to analyse the viable and apoptotic HeLa-ICAM-3 cells. Membrane preparations were prepared from the viable and apoptotic HeLa and HeLa-ICAM-3, full cell lysates were not used to reduce the complexity of the sample and to allow detection of low proteins.

A range of comparisons were done within the data sets of identified proteins. It was interesting that around 1200 proteins were detected in the MS results. Half of them were known to be membrane-associated proteins. The rest were grouped as distributed between cytosolic origin, cytoskeleton-related and nucleoplasm-related. These counts indicate that many of the proteins identified by MS are not highlighted as membrane proteins. This may be due to the contaminating association of these proteins with membranes, which is true for many cytosolic and cytoskeletal proteins as they are present in high levels, and/or due to a lack of sufficient washes of membrane-isolated fractions during the membrane preparation procedure.

ICAM-3 was detected in the viable HeLa-ICAM-3 cells, however it was not detected in the apoptotic HeLa-ICAM-3 even though it was shown in the WB in (**Figure 46**). It is likely that MS failed to identify ICAM-3 because of the large sample complexity and relatively low ICAM-3 levels.

When comparing the membrane prep proteins from viable HeLa-WT versus HeLa-ICAM-3 cells, 94 proteins were upregulated in the presence of ICAM-3 (**Table S1**).

When doing the same comparison on apoptotic HeLa-WT versus HeLa-ICAM-3, 77 proteins were upregulated in the presence of ICAM-3 (**Table S2**). These identified proteins could be potential ICAM-3 partners.

This is too many proteins to take on to further studies. So, these 94 proteins and 77 proteins were analysed further using bioinformatics to identify those that are already known in the literature to be associated with ICAM-3. These results suggested 14 proteins with changed expression with ICAM-3 and cell viability (**Table 3**). Of these, only two were significantly upregulated in apoptotic ICAM-3 membrane preparations. These proteins were cdc42 and dynamin-2. Cdc42 is a GTP-ase of the Rho family and so acts as a signaling molecule to drive a range of cell functions including cell cycle, endocytosis and cell structure. Dynamin 2 is also a GTP-ase associated with the cytoskeleton. As both of these proteins are involved in cytoskeletal changes, it is possible that they are involved in membrane reorganisation associated with apoptosis and release of ACdEV with ICAM-3. Dynamin has been suggested to promote generation of cytoplasmic vesicles (as they bud into the cytoplasm during endocytosis) (Henley *et al.*, 1999). It is not clear that it can promote release of EV. However, dynamin is involved in the uptake of EV by recipient cells (Barrès *et al.*, 2010, Tian *et al.*, 2010, Morelli, 2006).

When comparing the membrane prep proteins from viable HeLa-ICAM-3 versus apoptotic HeLa-ICAM-3 cells, these results indicated that there were no new proteins appearing as a result of apoptosis. 124 proteins decreased and 121 proteins increased their expression during apoptosis but none of these were known ICAM-3 interacting proteins. For this reason, these datasets were not analysed further.

When comparing the membrane prep proteins from ACdEV of HeLa-WT versus HeLa-ICAM-3 cells, many proteins were identified that were known to be EV associated. Of these, a number were known to be associated with ICAM-3 by the bioinformatics approach (**Table 5, Figure 51**). These include a range of receptors (e.g. ICAM-1; integrin αV, α4, β1; calreticulin). Calreticulin is interesting as this has been shown to be upregulated and redistributed during apoptosis to mediate uptake of apoptotic cells (Ogden et al., 2001, Gardai et al., 2005). However, there is no formal experimental link between calreticulin and ICAM-3. Importantly, these ACdEV studies were based on a single technical replicate and require additional work.

In summary, a number of proteins have been identified that change their expression with a change in viability or on expression of ICAM-3. However, in order to assess the true interacting ICAM-3 partners that might mediate ICAM-3's change of function, an optimized co-IP approach is required. This is significant future work and this wasn't possible due to the time available.

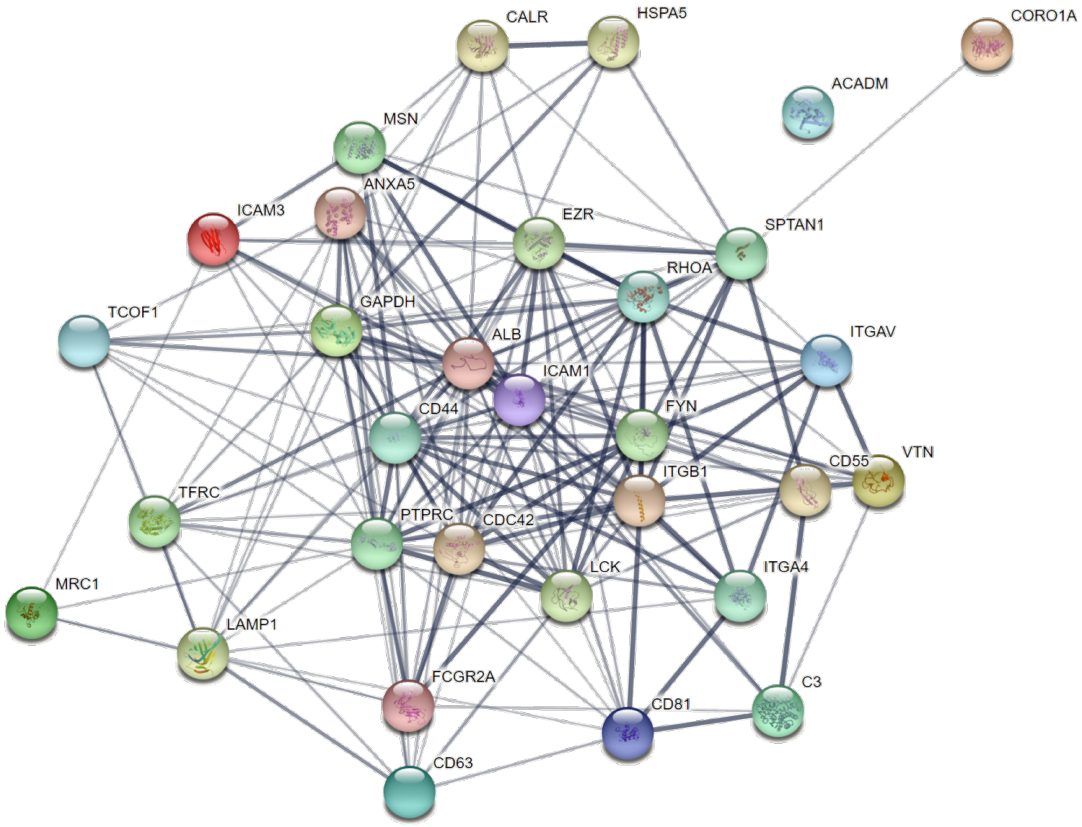

Figure 51. Protein-protein interaction designed using ICAM-3 and 30 ICAM-3-interacting proteins from Table 5. For the simpler graphical representations, only the proteins with the confidence score higher than 0.4 are connected on the graph. Proteins are coded for their corresponding gene names.

4.1 Summary Discussion for all chapters and Future work.

Although ICAM-3's role in apoptotic clearance has been known for nearly 20 years (Moffatt et al., 1999), there is still a lack of detailed knowledge of how ICAM-3 functions as an *eat me* signal. This detail would help to explain the proposed change of receptor for ICAM-3. More recent work has shown that ICAM-3 is lost from the surface of apoptotic leukocytes and is found in EV that are released during cell death (Torr et al., 2011). Whilst ICAM-3 on EV was shown to promote the chemoattraction of MØ to leukocyte death, the mechanism of action of ICAM-3 in this function was not known. Due to the established role of ICAM-3 as an adhesion molecule (Fawcett et al., 1992, Bleijs et al., 2000), it seemed sensible to assume that ICAM-3 may help the interaction between the EV and the recipient MØ. The hypothesis tested in this work was that ICAM-3 functions on apoptotic leukocyte-derived EV to promote efficient binding of the EV to the MØ. The outcomes of the experimental procedures to test this hypothesis have suggested ICAM-3 may promote binding of EV to MØ. However, future work, additional work is needed to confirm this suggestion.

For many years, the process of apoptotic cell clearance by phagocytes was considered to be a simple removal process for binding and phagocytosis of dying cells. It was also thought that dying cells were found as MØ encountered them by chance as they were on patrol in the tissues. However, this simple consideration changed over time, and it has been shown that apoptotic cells induce a range of functions other than just simply clearing the dead and dying cells. Apoptotic cells are known to induce MØ migration as they actively recruit MØ to sites of cell death. The work presented here confirms previous observations and extends them with the use of both horizontal and vertical migration systems. ACdEV were shown to be released from early time points in apoptosis and these EV recruit MØ in an ICAM-3-dependent way.

Apoptotic cells are also now reported to induce responses in the MØ that help in controlling inflammation (Savill and Fadok, 2000, Savill et al., 2002, Serhan and Savill, 2005). The precise function of AC is anti-inflammatory to MØ, (Voll et al., 1997, Fadok et al., 1998, Huynh et al., 2002). Taken this early work in to account that AC potentially induce anti-inflammatory responses in MØ, it is not known if ICAM-3 has any role in this process. It is also not known if ACdEV have anti-inflammatory effects. It is possible that as ACdEV and ICAM-3 attract MØ and, at the same time, induce those

MØ to become alternatively activated (i.e. M2) and to be anti-inflammatory. This project tested the hypothesis that EV are anti-inflammatory particles like AC, and that ICAM-3 is essential for this anti-inflammatory function. The results from testing this hypothesis suggested that EV are not strongly anti-inflammatory and ICAM-3 has no strong role in the anti-inflammatory effects. Whilst some limited experiments suggested a significant anti-inflammatory effect of ACdEV carrying ICAM-3 (inhibition of LPS-induced TNF detected by Luminex multiplex) and an anti-inflammatory effect of AC carrying ICAM-3 (induction of TGF-b1 assessed by qPCR), the effect of AC, ACdEV or ICAM-3 was not strong. Future work, will require additional optimisation in the experimental setups, perhaps to refine the AC-MØ or ACdEV-MØ ratios, or to test the anti-inflammatory effects of AC from a different (earlier) stage of apoptosis.

ICAM-3 has never been studied *in vivo*; it was always addressed *in vitro*. There is a primary obstacle that prevents the *in vivo* studies of ICAM-3, which is that ICAM-3 is not expressed by rodents (Sugino, 2005). The only species that naturally express ICAM-3 are higher mammals (human, pig, primate, cattle) rather than rodents that are usually used for *in vivo* research models. This problem was avoided by using a mouse xenograft model, injecting human BL (Mutu) cells (ICAM-3^{+}) into recipient SCID mice. Mutu cells have a characteristic, high spontaneous cell death within the developing tumour and this cell death promotes development of the tumour through (**a**) macrophage recruitment to dying cells, and (**b**) phenotypic changes to the MØ so that they provide growth support to the viable tumour cells (Ford et al., 2015). Overall, this xenograft model provided a highly specific system for the analysis of ICAM-3 on tumour cells and enabled MØ recruitment to apoptotic human tumour cells to be assessed *in vivo* for the first time. This novel approach revealed *in vivo* that ICAM-3 promotes MØ numbers within the tumour suggesting that ICAM-3 on ACdEV has chemoattractive abilities to promote recruitment of MØ *in vivo*. This might form a first step in novel therapeutics for diseases caused by unwanted MØ recruitment towards apoptotic leukocytes. Future work will need to address this through the use of the mAb MA4.

It was previously shown that ICAM-3 on viable leukocytes interacts with leukocyte function antigen 1 (LFA-1), where it is involved in signal transduction and initiation of immune responses by promoting interactions between T cells and antigen-presenting cells (Moffatt et al., 1999, Montoya et al., 2002). However, when leukocytes become apoptotic, the ICAM-3 does not interact with LFA-1 and it becomes involved in apoptotic cell clearance (Moffatt et al., 1999). The reason for this change of receptor is

not clear. Previous work has shown that ICAM-3 on viable and apoptotic cells appears unchanged in size by western blot analyses suggesting no large difference in structure between ICAM-3 on viable and apoptotic cells (Moffat *et al.,* 1999, Shingler, 2003, Torr *et al.,* 2011). Thus the hypothesis to be tested here was that ICAM-3, on the surface of apoptotic and viable cells, is associated with different partner proteins and that this alteration permits it to function differently in each cell context (viable or apoptotic). Mass spectrometry was the primary method analyzing the partner molecules involved with ICAM-3. Unfortunately, immunoprecipitation of ICAM-3 and partners was not successful and this limited the ability to detect novel partners. The outcome of the alternative experimental procedures used to test the hypothesis, revealed two proteins significantly upregulated in apoptotic HeLa/ICAM-3 cells. These proteins were cdc42 and dynamin-2. Cdc42 is a GTP-ase of the Rho family and so acts as a signaling molecule to drive a range of cell functions including cell cycle, endocytosis and cell structure. Dynamin 2 is also a GTP-ase associated with the cytoskeleton. As both of these proteins are involved in cytoskeletal changes, it is possible that they are involved in membrane reorganisation associated with apoptosis and release of ACdEV with ICAM-3. Dynamin has been suggested to promote generation of cytoplasmic vesicles (as they bud into the cytoplasm during endocytosis) (Henley et al., 1999). It is not clear that it can promote release of EV. However, dynamin is involved in the uptake of EV by recipient cells (Barrès et al., 2010, Tian et al., 2010, Morelli, 2006). When comparing the membrane preparation proteins from viable HeLa-ICAM-3 versus apoptotic HeLa-ICAM-3 cells, these results indicated that there were no new proteins appearing as a result of apoptosis.

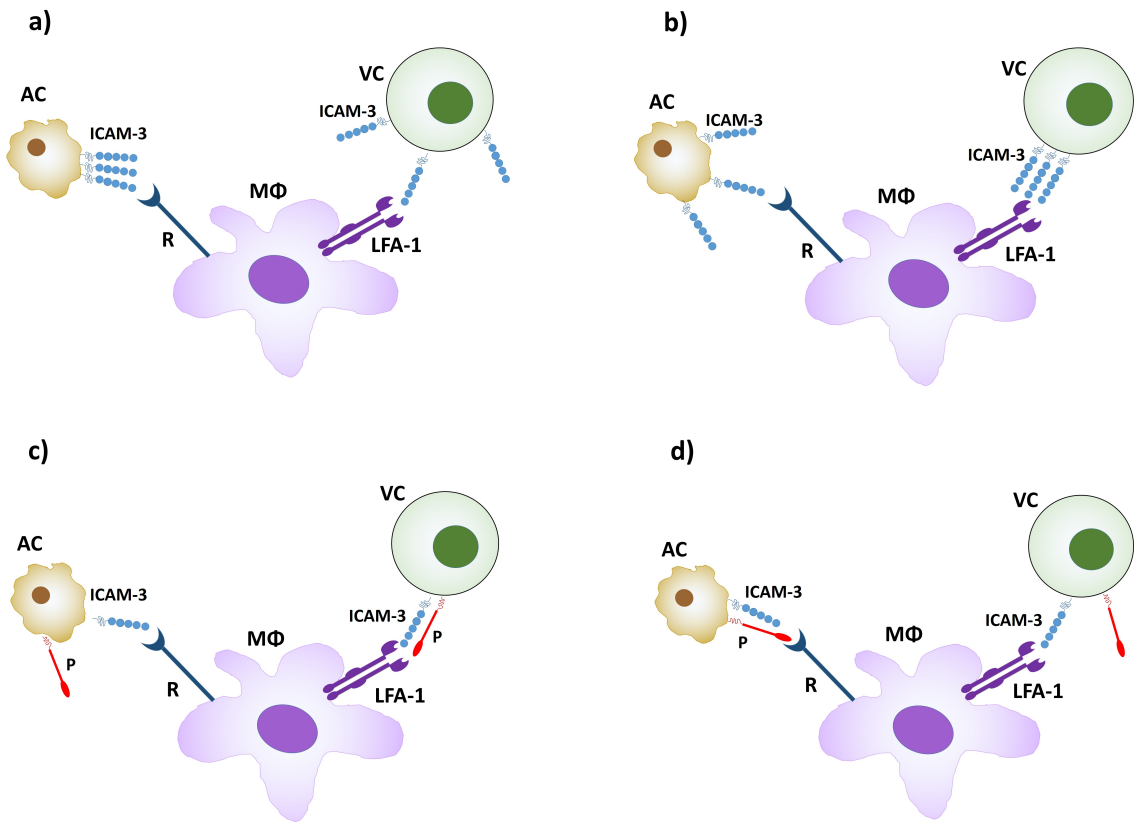

Figure 52. Possible scenarios for interaction of viable cell and apoptotic cell interactions with MØ. In order to stop binding to LFA-1 and to begin binding to a new MØ receptor, ICAM-3 on apoptotic cells: (**a**) may undergo redistribution (e.g. self-association) to stop binding to LFA-1 and to gain binding to a new MØ receptor; (**b**) may undergo redistribution to dissociate from itself; (**c**) may dissociate from an existing partner protein (**d**) may associate with a new partner molecule (possibly a protein).
In each of these possible cases, soluble molecules may also become involved to bridge apoptotic cells to MØ. AC – apoptotic cell; VC – viable cell; R – receptor; P – ICAM-3 partner protein.

In summary, a number of proteins were identified that changed their expression with a change in viability or on expression of ICAM-3. However, in order to assess the true interacting ICAM-3 partners that might mediate ICAM-3's change of function, an optimized co-IP approach is required. This is significant future work and this wasn't possible due to the time available. Possible scenarios of the changes in ICAM-3 between viable and apoptotic leukocytes that might cause the change in receptor are shown (**Figure 52**). This will require further work to address the apoptotic cell associated changes.

4.2 Future work.

Since the Co-IP with the SMALP (ICAM-3) extraction was not effective, the Co-IP is in need of further optimization. This could include optimisation of co-incubation timings between the SMALP sample (containing ICAM-3) and the Co-IP column. Another approach would be the use of an alternative solid phase e.g. Dynabeads Co-IP that is another form of Co-IP technique using magnetic beads for isolation. There is a possibility that SMALPs may interfere with the Co-IP (i.e. mAb activity), so it is worth attempting alternative mAbs to ICAM-3 (which may not be sensitive to SMALP interference) or to try immunoprecipitating directly from membrane preparations containing the ICAM-3. The SMALPs technique was used because it preserves the native lipid bilayer of a membrane protein during its purification.

An additional and potentially important direction for future work may be to assess the role of ICAM-3 in translational studies. Since ICAM-3 released from apoptotic cells has been shown to be an attractant for MØ, this information could be used to investigate if blocking ICAM-3 can have a therapeutic benefit in atherosclerosis. In atherosclerosis, MØ migrate towards the inflamed tissue containing apoptotic leukocytes, engulf the oxidised lipoproteins and become foam cells, before progressing to becoming apoptotic cells. These apoptotic foam cells attract more MØ and the cycle continues, promoting the plaque formation. To block MØ recruitment here would be of potential benefit in stopping plaque progression. Thus, testing the ability of mAb MA4 in models of atherosclerosis would be valuable.

References

ADMYRE, C., JOHANSSON, S. M., QAZI, K. R., FILEN, J. J., LAHESMAA, R., NORMAN, M., NEVE, E. P., SCHEYNIUS, A. & GABRIELSSON, S. 2007. Exosomes with immune modulatory features are present in human breast milk. *J Immunol,* 179**,** 1969-78.

ALBERT, M. L., KIM, J.-I. & BIRGE, R. B. 2000. [alpha]v[beta]5 integrin recruits the CrkII-Dock180-Rac1 complex for phagocytosis of apoptotic cells. *Nat Cell Biol,* 2**,** 899-905.

ASHKENAZI, A. & DIXIT, V. M. 1998. Death receptors: signaling and modulation. *Science,* 281**,** 1305-8.

AUSTYN, J. M. & GORDON, S. 1981. F4/80, a monoclonal antibody directed specifically against the mouse macrophage. *European Journal of Immunology,* 11**,** 805-815.

BAIETTI, M. F., ZHANG, Z., MORTIER, E., MELCHIOR, A., DEGEEST, G., GEERAERTS, A., IVARSSON, Y., DEPOORTERE, F., COOMANS, C., VERMEIREN, E., ZIMMERMANN, P. & DAVID, G. 2012. Syndecan-syntenin-ALIX regulates the biogenesis of exosomes. *Nat Cell Biol,* 14**,** 677-85.

BANCHEREAU, J. & STEINMAN, R. M. 1998. Dendritic cells and the control of immunity. *Nature,* 392**,** 245-52.

BARRÈS, C., BLANC, L., BETTE-BOBILLO, P., ANDRÉ, S., MAMOUN, R., GABIUS, H.-J. & VIDAL, M. 2010. Galectin-5 is bound onto the surface of rat reticulocyte exosomes and modulates vesicle uptake by macrophages. *Blood,* 115**,** 696-705.

BELL, E. D., MAY, A. P. & SIMMONS, D. L. 1998. The Leukocyte Function-Associated Antigen-1 (LFA-1)-Binding Site on ICAM-3 Comprises Residues on Both Faces of the First Immunoglobulin Domain. *The Journal of Immunology,* 161**,** 1363-1370.

BJÖRKERUD, S. & BJÖRKERUD, B. 1996. Apoptosis is abundant in human atherosclerotic lesions, especially in inflammatory cells (macrophages and T cells), and may contribute to the accumulation of gruel and plaque instability. *The American Journal of Pathology,* 149**,** 367-380.

BLEIJS, D. A., BINNERTS, M. E., VAN VLIET, S. J., FIGDOR, C. G. & VAN KOOYK, Y. 2000. Low-affinity LFA-1/ICAM-3 interactions augment LFA-1/ICAM-1-mediated T cell adhesion and signaling by redistribution of LFA-1. *Journal of Cell Science,* 113**,** 391-400.

BOBRIE, A., COLOMBO, M., RAPOSO, G. & THERY, C. 2011. Exosome Secretion: Molecular Mechanisms and Roles in Immune Responses. *Traffic,* 12**,** 1659-1668.

BOTTO, M., DELL'AGNOLA, C., BYGRAVE, A. E., THOMPSON, E. M., COOK, H. T., PETRY, F., LOOS, M., PANDOLFI, P. P. & WALPORT, M. J. 1998. Homozygous C1q deficiency causes glomerulonephritis associated with multiple apoptotic bodies. *Nat Genet,* 19**,** 56-9.

BOTTO, M. & WALPORT, M. J. 2002. C1q, autoimmunity and apoptosis. *Immunobiology,* 205**,** 395-406.

BOURNAZOU, I., MACKENZIE, K. J., DUFFIN, R., ROSSI, A. G. & GREGORY, C. D. 2010. Inhibition of eosinophil migration by lactoferrin. *Immunol Cell Biol,* 88**,** 220-3.

BOURNAZOU, I., POUND, J. D., DUFFIN, R., BOURNAZOS, S., MELVILLE, L. A., BROWN, S. B., ROSSI, A. G. & GREGORY, C. D. 2009. Apoptotic human cells inhibit migration of granulocytes via release of lactoferrin. *J Clin Invest,* 119**,** 20-32.

BRATTON, D. L. & HENSON, PETER M. Apoptotic Cell Recognition: Will the Real Phosphatidylserine Receptor(s) Please Stand up? *Current Biology,* 18**,** R76-R79.

BROWN, S., HEINISCH, I., ROSS, E., SHAW, K., BUCKLEY, C. D. & SAVILL, J. 2002. Apoptosis disables CD31-mediated cell detachment from phagocytes promoting binding and engulfment. *Nature,* 418**,** 200-3.

BRUGNERA, E., HANEY, L., GRIMSLEY, C., LU, M., WALK, S. F., TOSELLO-TRAMPONT, A.-C., MACARA, I. G., MADHANI, H., FINK, G. R. & RAVICHANDRAN, K. S. 2002. Unconventional Rac-GEF activity is mediated through the Dock180-ELMO complex. *Nat Cell Biol,* 4**,** 574-582.

BUENDIA, B., SANTA-MARIA, A. & COURVALIN, J. C. 1999. Caspase-dependent proteolysis of integral and peripheral proteins of nuclear membranes and nuclear pore complex proteins during apoptosis. *Journal of Cell Science,* 112**,** 1743-1753.

CARICCHIO, R., MCPHIE, L. & COHEN, P. L. 2003. Ultraviolet B radiation-induced cell death: critical role of ultraviolet dose in inflammation and lupus autoantigen redistribution. *J Immunol,* 171**,** 5778-86.

CHAN, W.-H. & YU, J.-S. 2000. Inhibition of UV irradiation–induced oxidative stress and apoptotic biochemical changes in human epidermal carcinoma A431 cells by genistein. *Journal of Cellular Biochemistry,* 78**,** 73-84.

CHINNAIYAN, A. M. 1999. The apoptosome: heart and soul of the cell death machine. *Neoplasia,* 1**,** 5-15.

CHISTIAKOV, D. A., KILLINGSWORTH, M. C., MYASOEDOVA, V. A., OREKHOV, A. N. & BOBRYSHEV, Y. V. 2017. CD68/macrosialin: not just a histochemical marker. *Lab Invest,* 97**,** 4-13.

COCUCCI, E., RACCHETTI, G. & MELDOLESI, J. 2009. Shedding microvesicles: artefacts no more. *Trends in cell biology,* 19**,** 43-51.

COHEN, G. M. 1997. Caspases: the executioners of apoptosis. *Biochem J,* 326 (Pt 1)**,** 1-16.

COHEN, J. J. 1991. Programmed cell death in the immune system. *Adv Immunol,* 50**,** 55-85.

COLEGIO, O. R., CHU, N.-Q., SZABO, A. L., CHU, T., RHEBERGEN, A. M., JAIRAM, V., CYRUS, N., BROKOWSKI, C. E., EISENBARTH, S. C., PHILLIPS, G. M., CLINE, G. W., PHILLIPS, A. J. & MEDZHITOV, R. 2014. Functional polarization of tumour-associated macrophages by tumour-derived lactic acid. *Nature,* 513**,** 559-563.

COLEMAN, M. L., SAHAI, E. A., YEO, M., BOSCH, M., DEWAR, A. & OLSON, M. F. 2001. Membrane blebbing during apoptosis results from caspase-mediated activation of ROCK I. *Nat Cell Biol,* 3**,** 339-345.

CREGAN, S. P., SMITH, B. P., BROWN, D. L. & MITCHEL, R. E. 1999. Two pathways for the induction of apoptosis in human lymphocytes. *Int J Radiat Biol,* 75**,** 1069-86.

DAIGNEAULT, M., PRESTON, J. A., MARRIOTT, H. M., WHYTE, M. K. B. & DOCKRELL, D. H. 2010. The Identification of Markers of Macrophage Differentiation in PMA-Stimulated THP-1 Cells and Monocyte-Derived Macrophages. *PLOS ONE,* 5**,** e8668.

DE FOUGEROLLES, A. R., DIAMOND, M. S. & SPRINGER, T. A. 1995. Heterogenous glycosylation of ICAM-3 and lack of interaction with Mac-1 and p150,95. *Eur J Immunol,* 25**,** 1008-12.

DE FOUGEROLLES, A. R., QIN, X. & SPRINGER, T. A. 1994. Characterization of the function of intercellular adhesion molecule (ICAM)-3 and comparison with ICAM-1 and ICAM-2 in immune responses. *The Journal of Experimental Medicine,* 179**,** 619-629.

DEVITT, A., MOFFATT, O. D., RAYKUNDALIA, C., CAPRA, J. D., SIMMONS, D. L. & GREGORY, C. D. 1998. Human CD14 mediates recognition and phagocytosis of apoptotic cells. *Nature,* 392**,** 505-509.

DEVITT, A., PARKER, K. G., OGDEN, C. A., OLDREIVE, C., CLAY, M. F., MELVILLE, L. A., BELLAMY, C. O., LACY-HULBERT, A., GANGLOFF, S. C., GOYERT, S. M. & GREGORY, C. D. 2004. Persistence of apoptotic cells without autoimmune disease or inflammation in CD14-/- mice. *The Journal of cell biology,* 167**,** 1161-70.

DEVITT, A., PIERCE, S., OLDREIVE, C., SHINGLER, W. H. & GREGORY, C. D. 2003. CD14-dependent clearance of apoptotic cells by human macrophages: the role of phosphatidylserine. *Cell Death Differ,* 10**,** 371-82.

DIVE, C., GREGORY, C. D., PHIPPS, D. J., EVANS, D. L., MILNER, A. E. & WYLLIE, A. H. 1992. Analysis and discrimination of necrosis and apoptosis (programmed cell death) by multiparameter flow cytometry. *Biochim Biophys Acta,* 1133**,** 275-85.

DUNKERN, T. R., FRITZ, G. & KAINA, B. 2001. Ultraviolet light-induced DNA damage triggers apoptosis in nucleotide excision repair-deficient cells via Bcl-2 decline and caspase-3/-8 activation. *Oncogene,* 20**,** 6026-38.

EARNSHAW, W. C., MARTINS, L. M. & KAUFMANN, S. H. 1999. Mammalian caspases: Structure, activation, substrates, and functions during apoptosis. *Annual Review of Biochemistry,* 68**,** 383-424.

EL ANDALOUSSI, S., MAGER, I., BREAKEFIELD, X. O. & WOOD, M. J. A. 2013. Extracellular vesicles: biology and emerging therapeutic opportunities. *Nat Rev Drug Discov,* 12**,** 347-357.

ELLIOTT, M. R., CHEKENI, F. B., TRAMPONT, P. C., LAZAROWSKI, E. R., KADL, A., WALK, S. F., PARK, D., WOODSON, R. I., OSTANKOVICH, M., SHARMA, P., LYSIAK, J. J., HARDEN, T. K., LEITINGER, N. & RAVICHANDRAN, K. S. 2009. Nucleotides released by apoptotic cells act as a find-me signal for phagocytic clearance. *Nature,* 461**,** 282-286.

ELLIOTT, M. R. & RAVICHANDRAN, K. S. 2010. Clearance of apoptotic cells: implications in health and disease. *The Journal of cell biology,* 189**,** 1059-70.

ELMORE, S. 2007. Apoptosis: a review of programmed cell death. *Toxicol Pathol,* 35**,** 495-516.

ENARI, M., SAKAHIRA, H., YOKOYAMA, H., OKAWA, K., IWAMATSU, A. & NAGATA, S. 1998. A caspase-activated DNase that degrades DNA during apoptosis, and its inhibitor ICAD. *Nature,* 391**,** 43-50.

ERWIG, L. P. & HENSON, P. M. 2008. Clearance of apoptotic cells by phagocytes. *Cell death and differentiation,* 15**,** 243-50.

FADOK, V. A., BRATTON, D. L., GUTHRIE, L. & HENSON, P. M. 2001a. Differential Effects of Apoptotic Versus Lysed Cells on Macrophage Production of Cytokines: Role of Proteases. *The Journal of Immunology,* 166**,** 6847-6854.

FADOK, V. A., BRATTON, D. L., KONOWAL, A., FREED, P. W., WESTCOTT, J. Y. & HENSON, P. M. 1998. Macrophages that have ingested apoptotic cells in vitro inhibit proinflammatory cytokine production through autocrine/paracrine mechanisms involving TGF-beta, PGE2, and PAF. *The Journal of clinical investigation,* 101**,** 890-8.

FADOK, V. A., DE CATHELINEAU, A., DALEKE, D. L., HENSON, P. M. & BRATTON, D. L. 2001b. Loss of Phospholipid Asymmetry and Surface Exposure of Phosphatidylserine Is Required for Phagocytosis of Apoptotic Cells by Macrophages and Fibroblasts. *Journal of Biological Chemistry,* 276**,** 1071-1077.

FADOK, V. A., VOELKER, D. R., CAMPBELL, P. A., COHEN, J. J., BRATTON, D. L. & HENSON, P. M. 1992. Exposure of phosphatidylserine on the surface of apoptotic lymphocytes triggers specific recognition and removal by macrophages. *J Immunol,* 148**,** 2207-16.

FAWCETT, J., HOLNESS, C. L., NEEDHAM, L. A., TURLEY, H., GATTER, K. C., MASON, D. Y. & SIMMONS, D. L. 1992. Molecular cloning of ICAM-3, a third ligand for LFA-1, constitutively expressed on resting leukocytes. *Nature,* 360**,** 481-4.

FITZPATRICK, R. E., APRICO, A., WIJEYEWICKREMA, L. C., PAGEL, C. N., WONG, D. M., POTEMPA, J., MACKIE, E. J. & PIKE, R. N. 2009. High molecular weight gingipains from Porphyromonas gingivalis induce cytokine responses from human macrophage-like cells via a non-proteolytic mechanism. *Journal of innate immunity,* 1**,** 109-117.

FORD, CATRIONA A., PETROVA, S., POUND, JOHN D., VOSS, JORINE J., MELVILLE, L., PATERSON, M., FARNWORTH, SARAH L., GALLIMORE, AWEN M., CUFF, S., WHEADON, H., DOBBIN, E., OGDEN, CAROL A., DUMITRIU, INGRID E., DUNBAR, DONALD R., MURRAY, PAUL G., RUCKERL, D., ALLEN, JUDITH E., HUME, DAVID A., VAN ROOIJEN, N., GOODLAD, JOHN R., FREEMAN, TOM C. & GREGORY, CHRISTOPHER D. 2015. Oncogenic Properties of Apoptotic Tumor Cells in Aggressive B Cell Lymphoma. *Current Biology,* 25**,** 577-588.

FRANC, N. C., DIMARCQ, J.-L., LAGUEUX, M., HOFFMANN, J. & EZEKOWITZ, R. A. B. 1996. Croquemort, A Novel Drosophila Hemocyte/Macrophage Receptor that Recognizes Apoptotic Cells. *Immunity,* 4**,** 431-443.

FRANKLIN, R. A., LIAO, W., SARKAR, A., KIM, M. V., BIVONA, M. R., LIU, K., PAMER, E. G. & LI, M. O. 2014. The Cellular and Molecular Origin of Tumor-associated Macrophages. *Science (New York, N.Y.),* 344**,** 921-925.

FREIRE-DE-LIMA, C. G., XIAO, Y. Q., GARDAI, S. J., BRATTON, D. L., SCHIEMANN, W. P. & HENSON, P. M. 2006. Apoptotic Cells, through Transforming Growth Factor-β, Coordinately Induce Anti-inflammatory and Suppress Pro-inflammatory Eicosanoid and NO Synthesis in Murine Macrophages. *Journal of Biological Chemistry,* 281**,** 38376-38384.

FULOP, G. M. & PHILLIPS, R. A. 1990. The scid mutation in mice causes a general defect in DNA repair. *Nature,* 347**,** 479-482.

FUNATSU, O., SATO, T., KOTOVUORI, P., GAHMBERG, C. G., IKEKITA, M. & FURUKAWA, K. 2001. Structural study of N-linked oligosaccharides of human intercellular adhesion molecule-3 (CD50). *European Journal of Biochemistry,* 268**,** 1020-1029.

FUNK, C. D. 2001. Prostaglandins and Leukotrienes: Advances in Eicosanoid Biology. *Science,* 294**,** 1871-1875.

GARDAI, S. J., MCPHILLIPS, K. A., FRASCH, S. C., JANSSEN, W. J., STAREFELDT, A., MURPHY-ULLRICH, J. E., BRATTON, D. L., OLDENBORG, P.-A., MICHALAK, M. & HENSON, P. M. 2005. Cell-Surface Calreticulin Initiates Clearance of Viable or Apoptotic Cells through trans-Activation of LRP on the Phagocyte. *Cell,* 123**,** 321-334.

GEISSMANN, F., JUNG, S. & LITTMAN, D. R. 2003. Blood Monocytes Consist of Two Principal Subsets with Distinct Migratory Properties. *Immunity,* 19**,** 71-82.

GILROY, D. & LAWRENCE, T. 2008. *The resolution of acute inflammation: A 'tipping point' in the development of chronic inflammatory diseases*.

GORDON, S. 2003. Alternative activation of macrophages. *Nat Rev Immunol,* 3**,** 23-35.

GRAHAM, F. L., SMILEY, J., RUSSELL, W. C. & NAIRN, R. 1977. Characteristics of a Human Cell Line Transformed by DNA from Human Adenovirus Type 5. *Journal of General Virology,* 36**,** 59-72.

GREENBERG, M. E., SUN, M., ZHANG, R., FEBBRAIO, M., SILVERSTEIN, R. & HAZEN, S. L. 2006. Oxidized phosphatidylserine–CD36 interactions play an essential role in macrophage-dependent phagocytosis of apoptotic cells. *The Journal of Experimental Medicine,* 203**,** 2613-2625.

GREGORY, C. D. & DEVITT, A. 2004. The macrophage and the apoptotic cell: an innate immune interaction viewed simplistically? *Immunology,* 113**,** 1-14.

GREGORY, C. D., ROWE, M. & RICKINSON, A. B. 1990. Different Epstein—Barr virus—B cell interactions in phenotypically distinct clones of a Burkitt's lymphoma cell line. *Journal of General Virology,* 71**,** 1481-1495.

GROLLMAN, A. P. & WALSH, W. T. T. A. O. M. 1967. Inhibitors of Protein Biosynthesis: II. MODE OF ACTION OF ANISOMYCIN. *Journal of Biological Chemistry,* 242**,** 3226-3233.

GUDE, D. R., ALVAREZ, S. E., PAUGH, S. W., MITRA, P., YU, J., GRIFFITHS, R., BARBOUR, S. E., MILSTIEN, S. & SPIEGEL, S. 2008. Apoptosis induces expression of sphingosine kinase 1 to release sphingosine-1-phosphate as a "come-and-get-me" signal. *The FASEB Journal,* 22**,** 2629-2638.

HAMMILL, A. K., UHR, J. W. & SCHEUERMANN, R. H. 1999. Annexin V Staining Due to Loss of Membrane Asymmetry Can Be Reversible and Precede Commitment to Apoptotic Death. *Experimental Cell Research,* 251**,** 16-21.

HANAYAMA, R., TANAKA, M., MIWA, K., SHINOHARA, A., IWAMATSU, A. & NAGATA, S. 2002. Identification of a factor that links apoptotic cells to phagocytes. *Nature,* 417**,** 182-187.

HARDING, C., HEUSER, J. & STAHL, P. 1983. Receptor-Mediated Endocytosis of Transferrin and Recycling of the Transferrin Receptor in Rat Reticulocytes. *Journal of Cell Biology,* 97**,** 329-339.

HARTEL, C., BEIN, G., KIRCHNER, H. & KLUTER, H. 1999. A human whole-blood assay for analysis of T-cell function by quantification of cytokine mRNA. *Scand J Immunol,* 49**,** 649-54.

HAWKINS, L. A. & DEVITT, A. 2013. Current Understanding of the Mechanisms for Clearance of Apoptotic Cells—A Fine Balance. *Journal of Cell Death,* 6**,** 57-68.

HENLEY, J. R., CAO, H. & MCNIVEN, M. A. 1999. Participation of dynamin in the biogenesis of cytoplasmic vesicles. *FASEB J,* 13 Suppl 2**,** S243-7.

HUYNH, M.-L. N., FADOK, V. A. & HENSON, P. M. 2002. Phosphatidylserine-dependent ingestion of apoptotic cells promotes TGF-β1 secretion and the resolution of inflammation. *The Journal of Clinical Investigation,* 109**,** 41-50.

IERO, M., VALENTI, R., HUBER, V., FILIPAZZI, P., PARMIANI, G., FAIS, S. & RIVOLTINI, L. 2007. Tumour-released exosomes and their implications in cancer immunity. *Cell Death Differ,* 15**,** 80-88.

JAISWAL, S., JAMIESON, C. H. M., PANG, W. W., PARK, C. Y., CHAO, M. P., MAJETI, R., TRAVER, D., VAN ROOIJEN, N. & WEISSMAN, I. L. 2009. CD47 is up-regulated on circulating hematopoietic stem cells and leukemia cells to avoid phagocytosis. *Cell,* 138**,** 271-285.

JAMSHAD, M., LIN, Y.-P., KNOWLES, TIMOTHY J., PARSLOW, ROSEMARY A., HARRIS, C., WHEATLEY, M., POYNER, DAVID R., BILL, ROSLYN M., THOMAS, OWEN R. T., OVERDUIN, M. & DAFFORN, TIM R. 2011. Surfactant-free purification of membrane proteins with intact native membrane environment. *Biochemical Society Transactions,* 39**,** 813-818.

JERSMANN, H. P. A., ROSS, K. A., VIVERS, S., BROWN, S. B., HASLETT, C. & DRANSFIELD, I. 2003. Phagocytosis of apoptotic cells by human macrophages: Analysis by multiparameter flow cytometry. *Cytometry Part A,* 51A**,** 7-15.

KERR, J. F. R., WYLLIE, A. H. & CURRIE, A. R. 1972. Apoptosis: A Basic Biological Phenomenon with Wide-ranging Implications in Tissue Kinetics. *British Journal of Cancer,* 26**,** 239-257.

KISCHKEL, F. C., HELLBARDT, S., BEHRMANN, I., GERMER, M., PAWLITA, M., KRAMMER, P. H. & PETER, M. E. 1995. Cytotoxicity-dependent APO-1 (Fas/CD95)-associated proteins form a death-inducing signaling complex (DISC) with the receptor. *EMBO J,* 14**,** 5579-88.

KOBAYASHI, N., KARISOLA, P., PEÑA-CRUZ, V., DORFMAN, D. M., JINUSHI, M., UMETSU, S. E., BUTTE, M. J., NAGUMO, H., CHERNOVA, I., ZHU, B., SHARPE, A. H., ITO, S., DRANOFF, G., KAPLAN, G. G., CASASNOVAS, J. M., UMETSU, D. T., DEKRUYFF, R. H. & FREEMAN, G. J. 2007. T cell Immunoglobulin Mucin Protein (TIM)-4 binds phosphatidylserine and mediates uptake of apoptotic cells. *Immunity,* 27**,** 927-940.

KOMOHARA, Y., JINUSHI, M. & TAKEYA, M. 2014. Clinical significance of macrophage heterogeneity in human malignant tumors. *Cancer Science,* 105**,** 1-8.

KOMOHARA, Y., OHNISHI, K., KURATSU, J. & TAKEYA, M. 2008. Possible involvement of the M2 anti-inflammatory macrophage phenotype in growth of human gliomas. *The Journal of Pathology,* 216**,** 15-24.

KOTHAKOTA, S., AZUMA, T., REINHARD, C., KLIPPEL, A., TANG, J., CHU, K. T., MCGARRY, T. J., KIRSCHNER, M. W., KOTHS, K., KWIATKOWSKI, D. J. & WILLIAMS, L. T. 1997. Caspase-3-generated fragment of gelsolin: Effector of morphological change in apoptosis. *Science,* 278**,** 294-298.

KRISTÓF, E., ZAHUCZKY, G., KATONA, K., DORÓ, Z., NAGY, É. & FÉSÜS, L. 2013. Novel role of ICAM3 and LFA-1 in the clearance of apoptotic neutrophils by human macrophages. *Apoptosis,* 18**,** 1235-1251.

KURAHARA, H., SHINCHI, H., MATAKI, Y., MAEMURA, K., NOMA, H., KUBO, F., SAKODA, M., UENO, S., NATSUGOE, S. & TAKAO, S. 2011. Significance of M2-

polarized tumor-associated macrophage in pancreatic cancer. *J Surg Res,* 167**,** e211-9.

KURUSHIMA, H., RAMPRASAD, M., KONDRATENKO, N., FOSTER, D. M., QUEHENBERGER, O. & STEINBERG, D. 2000. Surface expression and rapid internalization of macrosialin (mouse CD68) on elicited mouse peritoneal macrophages. *Journal of Leukocyte Biology,* 67**,** 104-8.

LEE, C.-H., WU, S.-B., HONG, C.-H., YU, H.-S. & WEI, Y.-H. 2013. Molecular Mechanisms of UV-Induced Apoptosis and Its Effects on Skin Residential Cells: The Implication in UV-Based Phototherapy. *International Journal of Molecular Sciences,* 14**,** 6414.

LEE, S. C., KNOWLES, T. J., POSTIS, V. L. G., JAMSHAD, M., PARSLOW, R. A., LIN, Y. P., GOLDMAN, A., SRIDHAR, P., OVERDUIN, M., MUENCH, S. P. & DAFFORN, T. R. 2016. A method for detergent-free isolation of membrane proteins in their local lipid environment. *Nature Protocols,* 11**,** 1149-1162.

LIN, Y.-F., LEE, H.-M., LEU, S.-J. & TSAI, Y.-H. 2007. The essentiality of PKCα and PKCβI translocation for CD14+monocyte differentiation towards macrophages and dendritic cells, respectively. *Journal of Cellular Biochemistry,* 102**,** 429-441.

LIU, X., KIM, C. N., YANG, J., JEMMERSON, R. & WANG, X. Induction of Apoptotic Program in Cell-Free Extracts: Requirement for dATP and Cytochrome c. *Cell,* 86**,** 147-157.

LIU, X., ZOU, H., SLAUGHTER, C. & WANG, X. DFF, a Heterodimeric Protein That Functions Downstream of Caspase-3 to Trigger DNA Fragmentation during Apoptosis. *Cell,* 89**,** 175-184.

LO SICCO, C., REVERBERI, D., BALBI, C., ULIVI, V., PRINCIPI, E., PASCUCCI, L., BECHERINI, P., BOSCO, M. C., VARESIO, L., FRANZIN, C., POZZOBON, M., CANCEDDA, R. & TASSO, R. 2017. Mesenchymal Stem Cell-Derived Extracellular Vesicles as Mediators of Anti-Inflammatory Effects: Endorsement of Macrophage Polarization. *STEM CELLS Translational Medicine,* 6**,** 1018-1028.

LÖTVALL, J., HILL, A. F., HOCHBERG, F., BUZÁS, E. I., DI VIZIO, D., GARDINER, C., GHO, Y. S., KUROCHKIN, I. V., MATHIVANAN, S., QUESENBERRY, P., SAHOO, S., TAHARA, H., WAUBEN, M. H., WITWER, K. W. & THÉRY, C. 2014. Minimal experimental requirements for definition of extracellular vesicles and their functions: a position statement from the International Society for Extracellular Vesicles. *Journal of Extracellular Vesicles,* 3**,** 10.3402/jev.v3.26913.

LUCAS, M., STUART, L. M., SAVILL, J. & LACY-HULBERT, A. 2003. Apoptotic Cells and Innate Immune Stimuli Combine to Regulate Macrophage Cytokine Secretion. *The Journal of Immunology,* 171**,** 2610-2615.

MACHESKY, L. M. & INSALL, R. H. Scar1 and the related Wiskott–Aldrich syndrome protein, WASP, regulate the actin cytoskeleton through the Arp2/3 complex. *Current Biology,* 8**,** 1347-1356.

MANTOVANI, A. & SICA, A. 2010. Macrophages, innate immunity and cancer: balance, tolerance, and diversity. *Curr Opin Immunol,* 22**,** 231-7.

MARTIN, S. J., REUTELINGSPERGER, C. P., MCGAHON, A. J., RADER, J. A., VAN SCHIE, R. C., LAFACE, D. M. & GREEN, D. R. 1995. Early redistribution of plasma membrane phosphatidylserine is a general feature of apoptosis

regardless of the initiating stimulus: inhibition by overexpression of Bcl-2 and Abl. *The Journal of Experimental Medicine,* 182**,** 1545-1556.

MARTINEZ, F. O., SICA, A., MANTOVANI, A. & LOCATI, M. 2008. Macrophage activation and polarization. *Front Biosci,* 13**,** 453-61.

MCEVOY, L., SCHLEGEL, R. A., WILLIAMSON, P. & DELBUONO, B. J. 1988. Merocyanine 540 as a Flow Cytometric Probe of Membrane Lipid Organization in Leukocytes. *Journal of Leukocyte Biology,* 44**,** 337-344.

MCNEIL, P. L., TANASUGARN, L., MEIGS, J. B. & TAYLOR, D. L. 1983. Acidification of phagosomes is initiated before lysosomal enzyme activity is detected. *The Journal of Cell Biology,* 97**,** 692-702.

MEDZHITOV, R. 2007. Recognition of microorganisms and activation of the immune response. *Nature,* 449**,** 819-826.

MIKI, H., SUETSUGU, S. & TAKENAWA, T. 1998. WAVE, a novel WASP-family protein involved in actin reorganization induced by Rac. *The EMBO Journal,* 17**,** 6932-6941.

MOFFATT, O. D., DEVITT, A., BELL, E. D., SIMMONS, D. L. & GREGORY, C. D. 1999. Macrophage recognition of ICAM-3 on apoptotic leukocytes. *J Immunol,* 162**,** 6800-10.

MONICK, M. M., CARTER, A. B., GUDMUNDSSON, G., GEIST, L. J. & HUNNINGHAKE, G. W. 1998. Changes in PKC isoforms in human alveolar macrophages compared with blood monocytes. *American Journal of Physiology - Lung Cellular and Molecular Physiology,* 275**,** L389-L397.

MONKS, J., ROSNER, D., JON GESKE, F., LEHMAN, L., HANSON, L., NEVILLE, M. C. & FADOK, V. A. 2005. Epithelial cells as phagocytes: apoptotic epithelial cells are engulfed by mammary alveolar epithelial cells and repress inflammatory mediator release. *Cell Death Differ,* 12**,** 107-114.

MONTOYA, M. C., SANCHO, D., BONELLO, G., COLLETTE, Y., LANGLET, C., HE, H. T., APARICIO, P., ALCOVER, A., OLIVE, D. & SANCHEZ-MADRID, F. 2002. Role of ICAM-3 in the initial interaction of T lymphocytes and APCs. *Nat Immunol,* 3**,** 159-168.

MORELLI, A. E. 2006. The Immune Regulatory Effect of Apoptotic Cells and Exosomes on Dendritic Cells: Its Impact on Transplantation. *American Journal of Transplantation,* 6**,** 254-261.

MORELLI, A. E., LARREGINA, A. T., SHUFESKY, W. J., SULLIVAN, M. L. G., STOLZ, D. B., PAPWORTH, G. D., ZAHORCHAK, A. F., LOGAR, A. J., WANG, Z., WATKINS, S. C., FALO, L. D. & THOMSON, A. W. 2004. Endocytosis, intracellular sorting, and processing of exosomes by dendritic cells. *Blood,* 104**,** 3257-3266.

MOSSER, D. M. & EDWARDS, J. P. 2008. Exploring the full spectrum of macrophage activation. *Nat Rev Immunol,* 8**,** 958-69.

MULCAHY, L. A., PINK, R. C. & CARTER, D. R. 2014. Routes and mechanisms of extracellular vesicle uptake. *J Extracell Vesicles,* 3.

NADELLA, V., WANG, Z., JOHNSON, T. S., GRIFFIN, M. & DEVITT, A. 2015. Transglutaminase 2 interacts with syndecan-4 and CD44 at the surface of human macrophages to promote removal of apoptotic cells. *Biochimica et Biophysica Acta (BBA) - Molecular Cell Research,* 1853**,** 201-212.

OGAWA, Y., MIURA, Y., HARAZONO, A., KANAI-AZUMA, M., AKIMOTO, Y., KAWAKAMI, H., YAMAGUCHI, T., TODA, T., ENDO, T., TSUBUKI, M. & YANOSHITA, R. 2011. Proteomic analysis of two types of exosomes in human whole saliva. *Biol Pharm Bull,* 34**,** 13-23.

OGDEN, C. A., DECATHELINEAU, A., HOFFMANN, P. R., BRATTON, D., GHEBREHIWET, B., FADOK, V. A. & HENSON, P. M. 2001. C1q and Mannose Binding Lectin Engagement of Cell Surface Calreticulin and Cd91 Initiates Macropinocytosis and Uptake of Apoptotic Cells. *The Journal of Experimental Medicine,* 194**,** 781-796.

OGDEN, C. A., POUND, J. D., BATTH, B. K., OWENS, S., JOHANNESSEN, I., WOOD, K. & GREGORY, C. D. 2005. Enhanced Apoptotic Cell Clearance Capacity and B Cell Survival Factor Production by IL-10-Activated Macrophages: Implications for Burkitt's Lymphoma. *The Journal of Immunology,* 174**,** 3015-3023.

OLSSON, M. & ZHIVOTOVSKY, B. 2011. Caspases and cancer. *Cell Death Differ,* 18**,** 1441-1449.

PARK, D., TOSELLO-TRAMPONT, A.-C., ELLIOTT, M. R., LU, M., HANEY, L. B., MA, Z., KLIBANOV, A. L., MANDELL, J. W. & RAVICHANDRAN, K. S. 2007a. BAI1 is an engulfment receptor for apoptotic cells upstream of the ELMO/Dock180/Rac module. *Nature,* 450**,** 430-434.

PARK, K. H., KIM, B. J., KANG, J., NAM, T. S., LIM, J. M., KIM, H. T., PARK, J. K., KIM, Y. G., CHAE, S. W. & KIM, U. H. 2011. Ca2+ signaling tools acquired from prostasomes are required for progesterone-induced sperm motility. *Sci Signal,* 4**,** ra31.

PARK, S. Y., JUNG, M. Y., KIM, H. J., LEE, S. J., KIM, S. Y., LEE, B. H., KWON, T. H., PARK, R. W. & KIM, I. S. 2007b. Rapid cell corpse clearance by stabilin-2, a membrane phosphatidylserine receptor. *Cell Death Differ,* 15**,** 192-201.

PETER, C., WAIBEL, M., KEPPELER, H., LEHMANN, R., XU, G., HALAMA, A., ADAMSKI, J., SCHULZE-OSTHOFF, K., WESSELBORG, S. & LAUBER, K. 2012. Release of lysophospholipid 'find-me' signals during apoptosis requires the ATP-binding cassette transporter A1. *Autoimmunity,* 45**,** 568-573.

PETER, C., WAIBEL, M., RADU, C. G., YANG, L. V., WITTE, O. N., SCHULZE-OSTHOFF, K., WESSELBORG, S. & LAUBER, K. 2008. Migration to Apoptotic "Find-me" Signals Is Mediated via the Phagocyte Receptor G2A. *Journal of Biological Chemistry,* 283**,** 5296-5305.

PLATT, N., SUZUKI, H., KODAMA, T. & GORDON, S. 2000. Apoptotic Thymocyte Clearance in Scavenger Receptor Class A-Deficient Mice Is Apparently Normal. *The Journal of Immunology,* 164**,** 4861-4867.

PLATT, N., SUZUKI, H., KURIHARA, Y., KODAMA, T. & GORDON, S. 1996. Role for the class A macrophage scavenger receptor in the phagocytosis of apoptotic thymocytes in vitro. *Proc Natl Acad Sci U S A,* 93**,** 12456-60.

RAO, L., PEREZ, D. & WHITE, E. 1996. Lamin proteolysis facilitates nuclear events during apoptosis. *Journal of Cell Biology,* 135**,** 1441-1455.

RAPOSO, G., NIJMAN, H. W., STOORVOGEL, W., LEIJENDEKKER, R., HARDING, C. V., MELIEF, C. J. M. & GEUZE, H. J. 1996. B lymphocytes secrete antigen-presenting vesicles. *Journal of Experimental Medicine,* 183**,** 1161-1172.

RAPOSO, G. & STOORVOGEL, W. 2013. Extracellular vesicles: exosomes, microvesicles, and friends. *J Cell Biol,* 200**,** 373-83.

REID, S., CROSS, R. & SNOW, E. C. 1996. Combined Hoechst 33342 and merocyanine 540 staining to examine murine B cell cycle stage, viability and apoptosis. *J Immunol Methods,* 192**,** 43-54.

SAELENS, X., FESTJENS, N., VANDE WALLE, L., VAN GURP, M., VAN LOO, G. & VANDENABEELE, P. 2004. Toxic proteins released from mitochondria in cell death. *Oncogene,* 23**,** 2861-74.

SALUCCI, S., BURATTINI, S., BATTISTELLI, M., BALDASSARRI, V., MALTARELLO, M. C. & FALCIERI, E. 2013. Ultraviolet B (UVB) Irradiation-Induced Apoptosis in Various Cell Lineages in Vitro. *International Journal of Molecular Sciences,* 14**,** 532-546.

SAVILL, J., DRANSFIELD, I., GREGORY, C. & HASLETT, C. 2002. A blast from the past: clearance of apoptotic cells regulates immune responses. *Nature reviews. Immunology,* 2**,** 965-75.

SAVILL, J. & FADOK, V. 2000. Corpse clearance defines the meaning of cell death. *Nature,* 407**,** 784-788.

SAVILL, J., HOGG, N., REN, Y. & HASLETT, C. 1992. Thrombospondin cooperates with CD36 and the vitronectin receptor in macrophage recognition of neutrophils undergoing apoptosis. *Journal of Clinical Investigation,* 90**,** 1513-1522.

SCAFFIDI, C., SCHMITZ, I., KRAMMER, P. H. & PETER, M. E. 1999. The role of c-FLIP in modulation of CD95-induced apoptosis. *J Biol Chem,* 274**,** 1541-8.

SCAFFIDI, P., MISTELI, T. & BIANCHI, M. E. 2002. Release of chromatin protein HMGB1 by necrotic cells triggers inflammation. *Nature,* 418**,** 191-195.

SCHULER, M. & GREEN, D. R. 2001. Mechanisms of p53-dependent apoptosis. *Biochem Soc Trans,* 29**,** 684-8.

SCHWENDE, H., FITZKE, E., AMBS, P. & DIETER, P. 1996. Differences in the state of differentiation of THP-1 cells induced by phorbol ester and 1,25-dihydroxyvitamin D3. *J Leukoc Biol,* 59**,** 555-61.

SEBBAGH, M., RENVOIZE, C., HAMELIN, J., RICHE, N., BERTOGLIO, J. & BREARD, J. 2001. Caspase-3-mediated cleavage of ROCK I induces MLC phosphorylation and apoptotic membrane blebbing. *Nat Cell Biol,* 3**,** 346-352.

SEGAWA, K., SUZUKI, J. & NAGATA, S. 2011. Constitutive exposure of phosphatidylserine on viable cells. *Proceedings of the National Academy of Sciences of the United States of America,* 108**,** 19246-19251.

SEGUNDO, C., MEDINA, F., RODRIGUEZ, C., MARTINEZ-PALENCIA, R., LEYVA-COBIAN, F. & BRIEVA, J. A. 1999. Surface molecule loss and bleb formation by human germinal center B cells undergoing apoptosis: role of apoptotic blebs in monocyte chemotaxis. *Blood,* 94**,** 1012-20.

SERHAN, C. N. & SAVILL, J. 2005. Resolution of inflammation: the beginning programs the end. *Nature immunology,* 6**,** 1191-7.

SHEVCHENKO, A., TOMAS, H., HAVLIS, J., OLSEN, J. V. & MANN, M. 2007. In-gel digestion for mass spectrometric characterization of proteins and proteomes. *Nat. Protocols,* 1**,** 2856-2860.

SICA, A. & MANTOVANI, A. 2012. Macrophage plasticity and polarization: in vivo veritas. *The Journal of Clinical Investigation,* 122**,** 787-795.

SOEHNLEIN, O. & LINDBOM, L. 2010. Phagocyte partnership during the onset and resolution of inflammation. *Nat Rev Immunol,* 10**,** 427-439.

SUGINO, H. 2005. ICAM-3, a ligand for DC-SIGN, was duplicated from ICAM-1 in mammalian evolution, but was lost in the rodent genome. *FEBS Letters,* 579**,** 2901-2906.

TAIT, S. W. & GREEN, D. R. 2010. Mitochondria and cell death: outer membrane permeabilization and beyond. *Nat Rev Mol Cell Biol,* 11**,** 621-32.

TAYLOR, P. R., CARUGATI, A., FADOK, V. A., COOK, H. T., ANDREWS, M., CARROLL, M. C., SAVILL, J. S., HENSON, P. M., BOTTO, M. & WALPORT, M. J. 2000. A hierarchical role for classical pathway complement proteins in the clearance of apoptotic cells in vivo. *J Exp Med,* 192**,** 359-66.

THERY, C., OSTROWSKI, M. & SEGURA, E. 2009. Membrane vesicles as conveyors of immune responses. *Nat Rev Immunol,* 9**,** 581-593.

THÉRY, C., REGNAULT, A., GARIN, J., WOLFERS, J., ZITVOGEL, L., RICCIARDI-CASTAGNOLI, P., RAPOSO, G. & AMIGORENA, S. 1999. Molecular Characterization of Dendritic Cell-Derived Exosomes: Selective Accumulation of the Heat Shock Protein Hsc73. *The Journal of Cell Biology,* 147**,** 599-610.

THOMAS, L., BIELEMEIER, A., LAMBERT, P. A., DARVEAU, R. P., MARSHALL, L. J. & DEVITT, A. 2013. The N-Terminus of CD14 Acts to Bind Apoptotic Cells and Confers Rapid-Tethering Capabilities on Non-Myeloid Cells. *PLoS ONE,* 8**,** e70691.

THORNBERRY, N. A. & LAZEBNIK, Y. 1998. Caspases: Enemies Within. *Science,* 281**,** 1312-1316.

TIAN, T., WANG, Y., WANG, H., ZHU, Z. & XIAO, Z. 2010. Visualizing of the cellular uptake and intracellular trafficking of exosomes by live-cell microscopy. *Journal of Cellular Biochemistry,* 111**,** 488-496.

TORR, E. E., GARDNER, D. H., THOMAS, L., GOODALL, D. M., BIELEMEIER, A., WILLETTS, R., GRIFFITHS, H. R., MARSHALL, L. J. & DEVITT, A. 2011. Apoptotic cell-derived ICAM-3 promotes both macrophage chemoattraction to and tethering of apoptotic cells. *Cell Death and Differentiation,* 19**,** 671-679.

TRUMAN, L. A., FORD, C. A., PASIKOWSKA, M., POUND, J. D., WILKINSON, S. J., DUMITRIU, I. E., MELVILLE, L., MELROSE, L. A., OGDEN, C. A., NIBBS, R., GRAHAM, G., COMBADIERE, C. & GREGORY, C. D. 2008. CX₃CL1/fractalkine is released from apoptotic lymphocytes to stimulate macrophage chemotaxis. *Blood*.

TURNER, C., DEVITT, A., PARKER, K., MACFARLANE, M., GIULIANO, M., COHEN, G. M. & GREGORY, C. D. 2003. Macrophage-mediated clearance of cells undergoing caspase-3-independent death. *Cell Death Differ,* 10**,** 302-12.

VAJEN, T., BENEDIKTER, B. J., HEINZMANN, A. C. A., VASINA, E. M., HENSKENS, Y., PARSONS, M., MAGUIRE, P. B., STASSEN, F. R., HEEMSKERK, J. W. M., SCHURGERS, L. J. & KOENEN, R. R. 2017. Platelet extracellular vesicles induce a pro-inflammatory smooth muscle cell phenotype. *Journal of Extracellular Vesicles,* 6**,** 1322454.

VALADI, H., EKSTROM, K., BOSSIOS, A., SJOSTRAND, M., LEE, J. J. & LOTVALL, J. O. 2007. Exosome-mediated transfer of mRNAs and microRNAs is a novel mechanism of genetic exchange between cells. *Nat Cell Biol,* 9**,** 654-659.

VAN DEN EIJNDE, S. M., VAN DEN HOFF, M. J. B., REUTELINGSPERGER, C. P. M., VAN HEERDE, W. L., HENFLING, M. E. R., VERMEIJ-KEERS, C., SCHUTTE, B., BORGERS, M. & RAMAEKERS, F. C. S. 2001. Transient expression of phosphatidylserine at cell-cell contact areas is required for myotube formation. *Journal of Cell Science,* 114**,** 3631-3642.

VAN GILS, J. M., DERBY, M. C., FERNANDES, L. R., RAMKHELAWON, B., RAY, T. D., RAYNER, K. J., PARATHATH, S., DISTEL, E., FEIG, J. L., ALVAREZ-LEITE, J. I., RAYNER, A. J., MCDONALD, T. O., O'BRIEN, K. D., STUART, L. M., FISHER, E. A., LACY-HULBERT, A. & MOORE, K. J. 2012. The neuroimmune guidance cue netrin-1 promotes atherosclerosis by inhibiting the emigration of macrophages from plaques. *Nat Immunol,* 13**,** 136-143.

VANDENABEELE, P., GALLUZZI, L., VANDEN BERGHE, T. & KROEMER, G. 2010. Molecular mechanisms of necroptosis: an ordered cellular explosion. *Nat Rev Mol Cell Biol,* 11**,** 700-14.

VOLL, R. E., HERRMANN, M., ROTH, E. A., STACH, C., KALDEN, J. R. & GIRKONTAITE, I. 1997. Immunosuppressive effects of apoptotic cells. *Nature,* 390**,** 350-1.

WALPORT, M. J., DAVIES, K. A. & BOTTO, M. 1998. C1q and systemic lupus erythematosus. *Immunobiology,* 199**,** 265-85.

WU, Y., SINGH, S., GEORGESCU, M.-M. & BIRGE, R. B. 2005. A role for Mer tyrosine kinase in αvβ5 integrin-mediated phagocytosis of apoptotic cells. *Journal of Cell Science,* 118**,** 539-553.

WYLLIE, A. H., KERR, J. F. & CURRIE, A. R. 1980. Cell death: the significance of apoptosis. *Int Rev Cytol,* 68**,** 251-306.

YANEZ-MO, M., SILJANDER, P. R. M., ANDREU, Z., ZAVEC, A. B., BORRAS, F. E., BUZAS, E. I., BUZAS, K., CASAL, E., CAPPELLO, F., CARVALHO, J., COLAS, E., CORDEIRO-DA SILVA, A., FAIS, S., FALCON-PEREZ, J. M., GHOBRIAL, I. M., GIEBEL, B., GIMONA, M., GRANER, M., GURSEL, I., GURSEL, M., HEEGAARD, N. H. H., HENDRIX, A., KIERULF, P., KOKUBUN, K., KOSANOVIC, M., KRALJ-IGLIC, V., KRAMER-ALBERS, E. M., LAITINEN, S., LASSER, C., LENER, T., LIGETI, E., LINE, A., LIPPS, G., LLORENTE, A., LOTVALL, J., MANCEK-KEBER, M., MARCILLA, A., MITTELBRUNN, M., NAZARENKO, I., NOLTE-T' HOEN, E. N. M., NYMAN, T. A., O'DRISCOLL, L., OLIVAN, M., OLIVEIRA, C., PALLINGER, E., DEL PORTILLO, H. A., REVENTOS, J., RIGAU, M., ROHDE, E., SAMMAR, M., SANCHEZ-MADRID, F., SANTAREM, N., SCHALLMOSER, K., OSTENFELD, M. S., STOORVOGEL, W., STUKELJ, R., VAN DER GREIN, S. G., VASCONCELOS, M. H., WAUBEN, M. H. M. & DE WEVER, O. 2015. Biological properties of extracellular vesicles and their physiological functions. *Journal of Extracellular Vesicles,* 4.

ZHIVOTOVSKY, B., ORRENIUS, S., BRUSTUGUN, O. T. & DOSKELAND, S. O. 1998. Injected cytochrome c induces apoptosis. *Nature,* 391**,** 449-50.

Supplementary Material

Table S1. Proteins (1203 in total) identified by bottom-up proteomics approach in membrane preparations of Hela WT (WT) and Hela-ICAM3 (ICAM3) viable cells. Proteins were considered identified if at least one unique peptide was confidently identified by searching against SwissProt data base. Relative quantification was performed using Progenesis QI for proteomics software. Three most intense peptides per protein were used for quantification. Data in the table are normalised to the lower protein content (1.00). Values higher that 1.00 are 'fold increase' compared to the value 1.00. Measurements of three biological replicates allowed for Anova test to be performed on quantified results.

Uniprot ID	Identified peptides (unique)	Score	Anova, *p*	Protein name	WT	ICAM-3
AHNK_HUMAN	208 (65)	7094.05	0.27	Neuroblast differentiation-associated protein AHNAK	1.21	1
PLEC_HUMAN	134 (49)	6287.14	0.36	Plectin	1.24	1
CPSM_HUMAN	90 (34)	6150.13	0.4	Carbamoyl-phosphate synthase [ammonia], mitochondrial	1.23	1
GRP78_HUMAN	58 (22)	5767.27	1.36E-06	78 kDa glucose-regulated protein	1	2.63
SPTN1_HUMAN	80 (30)	4961.31	0.02	Spectrin alpha chain, non-erythrocytic 1	1.89	1
CH60_HUMAN	59 (32)	4545.68	0.03	60 kDa heat shock protein, mitochondrial	2.04	1
ATPB_HUMAN	42 (22)	3875.72	0.48	ATP synthase subunit beta, mitochondrial	1.14	1
ACTG_HUMAN	38 (2)	3746.38	0.11	Actin, cytoplasmic 2	8.32	1
ACTB_HUMAN	38 (3)	3713.83	0.65	Actin, cytoplasmic 1	1.13	1
VIME_HUMAN	38 (23)	3612.26	0.43	Vimentin	1	1.25
ANXA2_HUMAN	45 (22)	3586.27	0.54	Annexin A2	1	1.14
HS90B_HUMAN	54 (9)	3478.6	0.05	Heat shock protein HSP 90-beta	4.13	1
MYH9_HUMAN	56 (27)	3356.06	0.54	Myosin-9	1.11	1
ENPL_HUMAN	44 (21)	3340.09	0.15	Endoplasmin	1	1.46
HSP7C_HUMAN	40 (19)	3232.62	0.91	Heat shock cognate 71 kDa protein	1.03	1
EF2_HUMAN	51 (19)	3215.47	0.58	Elongation factor 2	1.15	1
ATPA_HUMAN	39 (20)	3203.1	0.1	ATP synthase subunit alpha, mitochondrial	1.27	1
FLNA_HUMAN	54 (23)	3184.3	0.5	Filamin-A	1	1.37
LMNA_HUMAN	49 (22)	3136.51	0.97	Prelamin-A/C	1	1.03
PRKDC_HUMAN	74 (28)	3096.4	0.03	DNA-dependent protein kinase catalytic subunit	1.48	1
GRP75_HUMAN	37 (16)	2967.39	0.29	Stress-70 protein, mitochondrial	1	1.49
LPPRC_HUMAN	55 (26)	2933.43	0.06	Leucine-rich PPR motif-containing protein, mitochondrial	1.19	1
SPTB2_HUMAN	55 (23)	2761.27	0.55	Spectrin beta chain, non-erythrocytic 1	1.1	1
HS71A_HUMAN	35 (9)	2544.31	0.04	Heat shock 70 kDa protein 1A	1	1.77
TBB5_HUMAN	33 (6)	2428.21	0.66	Tubulin beta chain	1	1.13
ANXA5_HUMAN	29 (19)	2418.65	0.45	Annexin A5	1	1.25
HS90A_HUMAN	35 (6)	2401.55	0.07	Heat shock protein HSP 90-alpha	1.79	1
KPYM_HUMAN	41 (19)	2370.18	0.31	Pyruvate kinase PKM	1.39	1
HNRPU_HUMAN	56 (26)	2364.44	0.14	Heterogeneous nuclear ribonucleoprotein U	1	1.56
NUCL_HUMAN	44 (15)	2295.39	0.74	Nucleolin	1.09	1
DESP_HUMAN	58 (24)	2293.03	0.13	Desmoplakin	1.29	1
G3P_HUMAN	30 (17)	2258.33	0.35	Glyceraldehyde-3-phosphate dehydrogenase	1	1.45
IQGA1_HUMAN	53 (18)	2254.97	0.15	Ras GTPase-activating-like protein IQGAP1	1.48	1
ACTA_HUMAN	30 (1)	2243.03	0.71	Actin, aortic smooth muscle	2.36	1
XRCC5_HUMAN	37 (21)	2208.78	0.14	X-ray repair cross-complementing protein 5	1.29	1
CLH1_HUMAN	34 (13)	2193.6	0.34	Clathrin heavy chain 1	1.26	1
NPM_HUMAN	18 (14)	2054.23	0.55	Nucleophosmin	1	1.19
SND1_HUMAN	39 (20)	2040.38	0.89	Staphylococcal nuclease domain-containing protein 1	1	1.1
FAS_HUMAN	39 (25)	2038.42	3.01E-04	Fatty acid synthase	1.67	1
IF4A1_HUMAN	33 (13)	2036.95	0.11	Eukaryotic initiation factor 4A-I	2.23	1

TBB4B_HUMAN	29 (1)	2033.52	3.59E-03	Tubulin beta-4B chain	2.58	1
C1TC_HUMAN	38 (19)	2029.99	0.84	C-1-tetrahydrofolate synthase, cytoplasmic	1.03	1
ENOA_HUMAN	32 (15)	2011.91	0.12	Alpha-enolase	1.35	1
PARP1_HUMAN	60 (22)	1988.36	0.13	Poly [ADP-ribose] polymerase 1	1.32	1
4F2_HUMAN	24 (15)	1969.82	0.34	4F2 cell-surface antigen heavy chain	1.19	1
EF1A1_HUMAN	28 (9)	1920.01	0.42	Elongation factor 1-alpha 1	1	1.16
CALX_HUMAN	23 (14)	1913.04	8.54E-03	Calnexin	1.99	1
ROA2_HUMAN	26 (14)	1845.33	0.49	Heterogeneous nuclear ribonucleoproteins A2/B1	1	1.2
PPIB_HUMAN	24 (14)	1811.33	0.39	Peptidyl-prolyl cis-trans isomerase B	1.34	1
PDIA1_HUMAN	34 (17)	1779.89	0.02	Protein disulfide-isomerase	2.32	1
ANXA1_HUMAN	18 (13)	1744.42	0.44	Annexin A1	1	1.32
PDIA3_HUMAN	24 (16)	1737.73	0.82	Protein disulfide-isomerase A3	1.03	1
ANXA6_HUMAN	43 (19)	1660.99	0.51	Annexin A6	1.22	1
BASP1_HUMAN	24 (15)	1641.24	0.12	Brain acid soluble protein 1	1.33	1
XRCC6_HUMAN	32 (16)	1619.45	0.88	X-ray repair cross-complementing protein 6	1	1.03
TBA1C_HUMAN	27 (1)	1598.42	0.02	Tubulin alpha-1C chain	1	4.98
LONM_HUMAN	25 (13)	1559.87	0.2	Lon protease homolog, mitochondrial	1	1.24
ALDOA_HUMAN	21 (9)	1544.76	0.29	Fructose-bisphosphate aldolase A	1	1.97
DHX9_HUMAN	38 (15)	1518.26	0.37	ATP-dependent RNA helicase A	1	2.52
PGK1_HUMAN	27 (10)	1508.75	0.01	Phosphoglycerate kinase 1	1	1.97
ECH1_HUMAN	20 (13)	1495.52	0.32	Delta(3,5)-Delta(2,4)-dienoyl-CoA isomerase, mitochondrial	1	1.34
PHB2_HUMAN	20 (4)	1455.71	0.83	Prohibitin-2	1.66	1
CKAP4_HUMAN	26 (13)	1440.51	0.06	Cytoskeleton-associated protein 4	1.29	1
TFR1_HUMAN	34 (14)	1432.62	0.16	Transferrin receptor protein 1	1.29	1
EZRI_HUMAN	35 (12)	1429.35	0.43	Ezrin	1	1.28
ILF3_HUMAN	33 (10)	1427.14	0.82	Interleukin enhancer-binding factor 3	1.11	1
NONO_HUMAN	31 (13)	1424.15	0.63	Non-POU domain-containing octamer-binding protein	1.07	1
PTBP1_HUMAN	19 (12)	1415.93	0.06	Polypyrimidine tract-binding protein 1	1	1.33
SYEP_HUMAN	35 (17)	1415.39	0.8	Bifunctional glutamate/proline--tRNA ligase	1.02	1
RS3_HUMAN	25 (15)	1401.14	0.6	40S ribosomal protein S3	1	1.09
PDIA6_HUMAN	16 (9)	1400.36	0.02	Protein disulfide-isomerase A6	1	1.5
PHB_HUMAN	15 (11)	1394.63	0.28	Prohibitin	1.52	1
PAIRB_HUMAN	24 (17)	1317.49	0.02	Plasminogen activator inhibitor 1 RNA-binding protein	2.62	1
TCPE_HUMAN	25 (13)	1312.98	0.61	T-complex protein 1 subunit epsilon	1.3	1
RS7_HUMAN	17 (13)	1304.46	0.02	40S ribosomal protein S7	3	1
EIF3A_HUMAN	40 (16)	1300.41	0.42	Eukaryotic translation initiation factor 3 subunit A	1	1.31
HNRPK_HUMAN	24 (14)	1299.98	0.75	Heterogeneous nuclear ribonucleoprotein K	1	1.05
TRAP1_HUMAN	21 (10)	1283.37	0.7	Heat shock protein 75 kDa, mitochondrial	1.21	1
RL7_HUMAN	23 (17)	1271.58	0.05	60S ribosomal protein L7	3.15	1
PA2G4_HUMAN	24 (17)	1268.32	0.64	Proliferation-associated protein 2G4	1	1.09
VIGLN_HUMAN	29 (9)	1263.61	0.1	Vigilin	1	1.54
EPIPL_HUMAN	33 (12)	1263.48	0.18	Epiplakin	1.57	1
TCPB_HUMAN	25 (10)	1225.56	0.12	T-complex protein 1 subunit beta	1	2.17
HCD2_HUMAN	13 (10)	1223.54	0.31	3-hydroxyacyl-CoA dehydrogenase type-2	1.55	1
TCPQ_HUMAN	25 (15)	1219.28	0.19	T-complex protein 1 subunit theta	1.31	1
EFTU_HUMAN	21 (12)	1214.71	0.79	Elongation factor Tu, mitochondrial	1	1.05
RS4X_HUMAN	21 (11)	1207.93	0.56	40S ribosomal protein S4, X isoform	1.58	1
RL4_HUMAN	24 (13)	1194.49	0.19	60S ribosomal protein L4	1.51	1
HYOU1_HUMAN	27 (15)	1176.33	0.12	Hypoxia up-regulated protein 1	1	1.51
TCPA_HUMAN	25 (13)	1167.8	0.3	T-complex protein 1 subunit alpha	1.44	1
VDAC1_HUMAN	17 (9)	1156.33	0.91	Voltage-dependent anion-selective channel protein 1	1.13	1
RS3A_HUMAN	26 (12)	1141.26	0.32	40S ribosomal protein S3a	1	1.43
RS15_HUMAN	16 (11)	1126.83	0.02	40S ribosomal protein S15	20.46	1
MAP4_HUMAN	19 (6)	1120.56	0.61	Microtubule-associated protein 4	1.08	1
MATR3_HUMAN	22 (13)	1117.04	0.04	Matrin-3	1.4	1
RL7A_HUMAN	20 (11)	1115.86	0.28	60S ribosomal protein L7a	1.65	1
GCN1_HUMAN	30 (13)	1112.05	0.11	eIF-2-alpha kinase activator GCN1	1	4.15
HSP72_HUMAN	16 (1)	1106.24	4.92E-03	Heat shock-related 70 kDa protein 2	22.14	1

MDHM_HUMAN	12 (4)	1100.65	0.25	Malate dehydrogenase, mitochondrial	1	2.33
RL5_HUMAN	24 (11)	1099.53	0.2	60S ribosomal protein L5	1	1.76
SFPQ_HUMAN	23 (9)	1096.41	0.38	Splicing factor, proline- and glutamine-rich	1	1.12
TLN1_HUMAN	43 (18)	1089.31	0.74	Talin-1	1.04	1
GANAB_HUMAN	22 (12)	1082.05	0.84	Neutral alpha-glucosidase AB	1.06	1
TAGL2_HUMAN	13 (10)	1080.71	0.21	Transgelin-2	1.75	1
NACAM_HUMAN	26 (12)	1070.85	0.96	Nascent polypeptide-associated complex subunit alpha, muscle-specific form	1.33	1
NCPR_HUMAN	20 (7)	1068.77	0.6	NADPH--cytochrome P450 reductase	1	1.15
RL13_HUMAN	16 (8)	1058.37	0.05	60S ribosomal protein L13	2.22	1
HNRPM_HUMAN	36 (14)	1056.43	0.21	Heterogeneous nuclear ribonucleoprotein M	1	1.34
RL6_HUMAN	17 (6)	1054.32	0.39	60S ribosomal protein L6	1.38	1
GLYM_HUMAN	18 (9)	1032.6	0.21	Serine hydroxymethyltransferase, mitochondrial	1.08	1
ILF2_HUMAN	12 (9)	1031.39	0.86	Interleukin enhancer-binding factor 2	1	1.01
RLA0_HUMAN	17 (7)	1026.79	0.55	60S acidic ribosomal protein P0	1.3	1
CALR_HUMAN	12 (6)	1020.61	0.01	Calreticulin	5.57	1
H14_HUMAN	15 (1)	1019.53	0.06	Histone H1.4	1	3.83
RSSA_HUMAN	13 (8)	1018.87	0.71	40S ribosomal protein SA	1.09	1
TERA_HUMAN	25 (14)	1003.61	0.2	Transitional endoplasmic reticulum ATPase	1	1.35
PABP1_HUMAN	29 (5)	998.75	0.06	Polyadenylate-binding protein 1	1	2.18
LDHA_HUMAN	15 (6)	996.76	0.68	L-lactate dehydrogenase A chain	1	1.09
EF1G_HUMAN	16 (8)	993.29	0.03	Elongation factor 1-gamma	1.67	1
AT1A1_HUMAN	19 (5)	991.57	0.29	Sodium/potassium-transporting ATPase subunit alpha-1	1.23	1
G3BP1_HUMAN	19 (11)	969.76	0.01	Ras GTPase-activating protein-binding protein 1	2.68	1
PRDX1_HUMAN	14 (5)	966.28	0.12	Peroxiredoxin-1	1.47	1
TCPH_HUMAN	17 (13)	957.65	0.11	T-complex protein 1 subunit eta	1.77	1
ANXA4_HUMAN	13 (8)	952.21	0.67	Annexin A4	1	1.08
RL9_HUMAN	12 (8)	952	0.19	60S ribosomal protein L9	2.12	1
KTN1_HUMAN	37 (7)	940.39	0.44	Kinectin	1.23	1
FLNB_HUMAN	26 (8)	932.08	0.65	Filamin-B	1.06	1
FUMH_HUMAN	12 (8)	928.97	6.00E-04	Fumarate hydratase, mitochondrial	1.5	1
HNRPC_HUMAN	16 (5)	927.78	0.06	Heterogeneous nuclear ribonucleoproteins C1/C2	1	2.66
GDE_HUMAN	22 (7)	927.04	0.89	Glycogen debranching enzyme	1	1.06
CAPR1_HUMAN	17 (9)	918.04	0.18	Caprin-1	1.65	1
MOES_HUMAN	22 (6)	917.08	0.03	Moesin	1.81	1
TPIS_HUMAN	13 (9)	915.87	0.04	Triosephosphate isomerase	1.81	1
PABP4_HUMAN	23 (8)	914.24	0.87	Polyadenylate-binding protein 4	1.01	1
KAD2_HUMAN	15 (12)	913.05	0.79	Adenylate kinase 2, mitochondrial	1.04	1
H12_HUMAN	14 (2)	912.45	0.3	Histone H1.2	1	10.5
RACK1_HUMAN	15 (10)	904.18	0.75	Receptor of activated protein C kinase 1	1.03	1
1433Z_HUMAN	14 (6)	895.76	0.03	14-3-3 protein zeta/delta	3.22	1
EF1A2_HUMAN	21 (2)	883.55	0.07	Elongation factor 1-alpha 2	1	16.39
HMGB1_HUMAN	15 (7)	865.28	0.69	High mobility group protein B1	1	1.12
THIL_HUMAN	14 (6)	860.33	0.52	Acetyl-CoA acetyltransferase, mitochondrial	1	1.11
ACON_HUMAN	13 (7)	859.41	0.81	Aconitate hydratase, mitochondrial	1.12	1
RS8_HUMAN	13 (7)	855.95	0.01	40S ribosomal protein S8	2.03	1
RAB1B_HUMAN	11 (1)	854.04	0.11	Ras-related protein Rab-1B	3.41	1
RAB5C_HUMAN	11 (4)	852.59	0.28	Ras-related protein Rab-5C	1.2	1
TCPG_HUMAN	23 (11)	850.62	0.26	T-complex protein 1 subunit gamma	1.52	1
TCPZ_HUMAN	19 (9)	848.83	0.33	T-complex protein 1 subunit zeta	1.42	1
H15_HUMAN	16 (7)	843.97	0.26	Histone H1.5	1	1.65
ROA1_HUMAN	14 (1)	837.07	0.12	Heterogeneous nuclear ribonucleoprotein A1	1	3.64
TBB6_HUMAN	19 (1)	836.35	0.05	Tubulin beta-6 chain	1.83	1
SERPH_HUMAN	18 (11)	832.9	0.28	Serpin H1	1.14	1
RS9_HUMAN	17 (14)	832.5	0.02	40S ribosomal protein S9	5.57	1
G6PI_HUMAN	15 (10)	827.25	0.56	Glucose-6-phosphate isomerase	1.12	1
EIF3B_HUMAN	20 (12)	823.13	0.2	Eukaryotic translation initiation factor 3 subunit B	1	1.28
POTEE_HUMAN	20 (1)	820.12	0.35	POTE ankyrin domain family member E	6.43	1
H2B1B_HUMAN	8 (1)	818.58	0.88	Histone H2B type 1-B	2.1	1

ETFA_HUMAN	12 (7)	816.05	0.37	Electron transfer flavoprotein subunit alpha, mitochondrial	1	1.42
DHE3_HUMAN	16 (3)	815.27	0.08	Glutamate dehydrogenase 1, mitochondrial	1.06	1
ATPO_HUMAN	13 (7)	806.54	0.06	ATP synthase subunit O, mitochondrial	1.77	1
LMNB1_HUMAN	23 (7)	803.82	0.25	Lamin-B1	1.43	1
P5CR1_HUMAN	16 (11)	801.13	0.08	Pyrroline-5-carboxylate reductase 1, mitochondrial	1	2.47
AIFM1_HUMAN	21 (15)	794.66	0.29	Apoptosis-inducing factor 1, mitochondrial	1.37	1
RL10_HUMAN	17 (8)	794.13	0.07	60S ribosomal protein L10	3.33	1
QCR1_HUMAN	14 (8)	788.1	0.02	Cytochrome b-c1 complex subunit 1, mitochondrial	2.44	1
RRBP1_HUMAN	36 (7)	783.02	0.26	Ribosome-binding protein 1	1.23	1
UBA1_HUMAN	17 (9)	782.37	0.11	Ubiquitin-like modifier-activating enzyme 1	1	3
ECHA_HUMAN	12 (7)	779.46	0.17	Trifunctional enzyme subunit alpha, mitochondrial	1	2.18
SYIC_HUMAN	21 (8)	773.01	0.83	Isoleucine--tRNA ligase, cytoplasmic	1	1.02
SERA_HUMAN	17 (7)	769.63	0.91	D-3-phosphoglycerate dehydrogenase	1	1.14
L1CAM_HUMAN	21 (6)	768.66	0.41	Neural cell adhesion molecule L1	1.28	1
H13_HUMAN	16 (2)	757.02	0.94	Histone H1.3	1.06	1
SYLC_HUMAN	28 (6)	756.85	0.94	Leucine--tRNA ligase, cytoplasmic	1	1.06
SCOT1_HUMAN	18 (8)	746.12	0.06	Succinyl-CoA:3-ketoacid coenzyme A transferase 1, mitochondrial	1.64	1
TCPD_HUMAN	11 (6)	745.62	0.05	T-complex protein 1 subunit delta	1.86	1
1433E_HUMAN	19 (6)	741.14	0.56	14-3-3 protein epsilon	3.55	1
PYC_HUMAN	25 (15)	736.32	0.03	Pyruvate carboxylase, mitochondrial	1	3.26
PDCD6_HUMAN	11 (10)	735.73	0.05	Programmed cell death protein 6	2.11	1
ACADM_HUMAN	15 (9)	728.13	0.09	Medium-chain specific acyl-CoA dehydrogenase, mitochondrial	1.69	1
TKT_HUMAN	17 (9)	723.78	0.83	Transketolase	1.04	1
BASI_HUMAN	10 (5)	722.96	0.06	Basigin	1.5	1
EF1D_HUMAN	12 (8)	719.16	0.37	Elongation factor 1-delta	1	1.4
NB5R3_HUMAN	9 (6)	717.74	0.93	NADH-cytochrome b5 reductase 3	1.04	1
RAB1A_HUMAN	8 (1)	708.21	0.08	Ras-related protein Rab-1A	1	2.99
MIC60_HUMAN	14 (7)	704.96	0.06	MICOS complex subunit MIC60	1.66	1
ATP5H_HUMAN	13 (8)	703.87	0.21	ATP synthase subunit d, mitochondrial	3.49	1
QCR2_HUMAN	11 (9)	702.32	0.1	Cytochrome b-c1 complex subunit 2, mitochondrial	1.92	1
HSP76_HUMAN	11 (1)	681.77	0.02	Heat shock 70 kDa protein 6	1	7.3
ACLY_HUMAN	23 (10)	680.43	0.14	ATP-citrate synthase	2.42	1
H2B1C_HUMAN	8 (1)	678.34	0.48	Histone H2B type 1-C/E/F/G/I	1	1.06
DDX17_HUMAN	23 (7)	676.39	0.46	Probable ATP-dependent RNA helicase DDX17	1	1.22
SEPT2_HUMAN	12 (8)	676.32	0.38	Septin-2	1	1.32
EIF3F_HUMAN	7 (5)	673.8	0.1	Eukaryotic translation initiation factor 3 subunit F	1	1.56
DDX3X_HUMAN	14 (7)	673.75	0.1	ATP-dependent RNA helicase DDX3X	1.41	1
IF4A3_HUMAN	20 (8)	672.81	0.16	Eukaryotic initiation factor 4A-III	1.88	1
RL3_HUMAN	21 (7)	668.67	0.13	60S ribosomal protein L3	1.95	1
RAB7A_HUMAN	11 (6)	664.79	0.12	Ras-related protein Rab-7a	1.64	1
ACTN4_HUMAN	13 (5)	662.99	0.47	Alpha-actinin-4	1.2	1
RS6_HUMAN	8 (6)	656.18	0.54	40S ribosomal protein S6	1.22	1
RPN1_HUMAN	17 (6)	649.33	0.03	Dolichyl-diphosphooligosaccharide--protein glycosyltransferase subunit 1	1.46	1
RL26_HUMAN	14 (1)	646.9	0.04	60S ribosomal protein L26	166.55	1
RL17_HUMAN	12 (8)	641.52	5.75E-03	60S ribosomal protein L17	5.5	1
STML2_HUMAN	13 (6)	639.63	0.63	Stomatin-like protein 2, mitochondrial	1.03	1
POTEI_HUMAN	17 (1)	639.36	0.21	POTE ankyrin domain family member I	2.66	1
MYO1C_HUMAN	22 (9)	639.22	0.26	Unconventional myosin-Ic	1	1.27
HNRPL_HUMAN	16 (7)	638.94	0.43	Heterogeneous nuclear ribonucleoprotein L	3.05	1
RL18_HUMAN	9 (2)	635.69	0.03	60S ribosomal protein L18	2.65	1
HNRH1_HUMAN	13 (1)	632.15	0.02	Heterogeneous nuclear ribonucleoprotein H	1	1.35
RL21_HUMAN	13 (4)	631.85	0.71	60S ribosomal protein L21	3.93	1
RL8_HUMAN	10 (6)	628.39	0.83	60S ribosomal protein L8	1.26	1
SYAC_HUMAN	29 (7)	627.44	0.81	Alanine--tRNA ligase, cytoplasmic	1.02	1
LDHB_HUMAN	10 (4)	625.26	0.99	L-lactate dehydrogenase B chain	1.07	1
PDC6I_HUMAN	14 (6)	623.44	0.03	Programmed cell death 6-interacting protein	2.6	1
NDUS3_HUMAN	9 (8)	621.03	0.09	NADH dehydrogenase [ubiquinone] iron-sulfur protein 3, mitochondrial	1.57	1
RL10A_HUMAN	12 (8)	620.46	0.27	60S ribosomal protein L10a	1.93	1

ADT2_HUMAN	21 (6)	618.06	0.32	ADP/ATP translocase 2	1.5	1
MYOF_HUMAN	27 (6)	615.33	0.45	Myoferlin	1.11	1
H90B2_HUMAN	12 (1)	612.49	0.46	Putative heat shock protein HSP 90-beta 2	4.83	1
NSUN2_HUMAN	14 (7)	611.13	0.81	tRNA (cytosine(34)-C(5))-methyltransferase	1	1.3
ODPB_HUMAN	12 (5)	610.94	0.2	Pyruvate dehydrogenase E1 component subunit beta, mitochondrial	1	1.95
HNRPF_HUMAN	14 (4)	608.56	0.81	Heterogeneous nuclear ribonucleoprotein F	1.16	1
VDAC2_HUMAN	10 (7)	607.33	0.84	Voltage-dependent anion-selective channel protein 2	1.17	1
HNRPR_HUMAN	12 (3)	605.75	0.47	Heterogeneous nuclear ribonucleoprotein R	1	1.15
DDX21_HUMAN	19 (3)	605.13	0.38	Nucleolar RNA helicase 2	1	1.86
ACADV_HUMAN	23 (6)	602.13	0.29	Very long-chain specific acyl-CoA dehydrogenase, mitochondrial	1	1.31
RS17_HUMAN	10 (5)	601.46	5.46E-03	40S ribosomal protein S17	7.69	1
1433G_HUMAN	11 (3)	599.44	0.72	14-3-3 protein gamma	1.15	1
FEN1_HUMAN	12 (7)	597.91	0.32	Flap endonuclease 1	1	1.21
ASSY_HUMAN	13 (8)	596.95	0.62	Argininosuccinate synthase	1.17	1
NOMO1_HUMAN	14 (7)	595.49	0.24	Nodal modulator 1	1.46	1
RL24_HUMAN	12 (5)	592.77	0.21	60S ribosomal protein L24	2.64	1
HNRPQ_HUMAN	13 (4)	592.35	0.41	Heterogeneous nuclear ribonucleoprotein Q	1.28	1
ROA3_HUMAN	10 (4)	591.92	0.32	Heterogeneous nuclear ribonucleoprotein A3	1	1.89
BTF3_HUMAN	8 (7)	587.11	3.18E-03	Transcription factor BTF3	8.46	1
FUBP2_HUMAN	14 (5)	584.19	0.79	Far upstream element-binding protein 2	1.03	1
PRDX3_HUMAN	10 (6)	579.36	0.11	Thioredoxin-dependent peroxide reductase, mitochondrial	1.34	1
DDX1_HUMAN	16 (8)	578.92	0.73	ATP-dependent RNA helicase DDX1	1	1.04
RAB1C_HUMAN	9 (1)	578.78	0.59	Putative Ras-related protein Rab-1C	1	1.1
PRDX2_HUMAN	8 (6)	575.64	0.13	Peroxiredoxin-2	1.74	1
RADI_HUMAN	13 (1)	572.37	0.24	Radixin	1	1.66
H4_HUMAN	11 (7)	570.55	0.74	Histone H4	1.03	1
IF4B_HUMAN	22 (8)	570.07	0.1	Eukaryotic translation initiation factor 4B	1	1.89
NDUS1_HUMAN	12 (4)	563.56	0.15	NADH-ubiquinone oxidoreductase 75 kDa subunit, mitochondrial	1	1.46
ITB1_HUMAN	13 (8)	562.87	0.36	Integrin beta-1	1	1.24
RA1L2_HUMAN	14 (1)	558.93	0.55	Heterogeneous nuclear ribonucleoprotein A1-like 2	1.71	1
SYTC_HUMAN	18 (5)	555.18	0.14	Threonine--tRNA ligase, cytoplasmic	1.54	1
1433B_HUMAN	13 (7)	553.62	0.13	14-3-3 protein beta/alpha	1	1.95
VINC_HUMAN	32 (12)	553.12	3.02E-03	Vinculin	1	2.45
IMB1_HUMAN	10 (6)	552.87	0.29	Importin subunit beta-1	1.19	1
CN166_HUMAN	8 (8)	552.35	0.46	UPF0568 protein C14orf166	2.04	1
ACTBM_HUMAN	12 (1)	551.66	0.14	Putative beta-actin-like protein 3	288.14	1
PGM1_HUMAN	14 (5)	549.65	5.93E-03	Phosphoglucomutase-1	1	6.38
U5S1_HUMAN	18 (6)	546.4	0.61	116 kDa U5 small nuclear ribonucleoprotein component	1.08	1
RL23A_HUMAN	10 (5)	546.09	6.81E-03	60S ribosomal protein L23a	3.08	1
UBP2L_HUMAN	12 (9)	541.99	0.02	Ubiquitin-associated protein 2-like	1.24	1
FUBP1_HUMAN	10 (4)	541.25	0.94	Far upstream element-binding protein 1	1	1.02
C1QBP_HUMAN	8 (5)	539.08	0.7	Complement component 1 Q subcomponent-binding protein, mitochondrial	1.02	1
HSPB1_HUMAN	7 (4)	538	0.47	Heat shock protein beta-1	1.54	1
DLDH_HUMAN	11 (4)	537.7	0.04	Dihydrolipoyl dehydrogenase, mitochondrial	1.42	1
SMC3_HUMAN	39 (7)	536.96	0.67	Structural maintenance of chromosomes protein 3	1.06	1
SYFA_HUMAN	9 (7)	536.04	0.04	Phenylalanine--tRNA ligase alpha subunit	1	6.42
FUS_HUMAN	10 (6)	533.47	0.09	RNA-binding protein FUS	1.12	1
SFXN1_HUMAN	8 (6)	531.58	0.65	Sideroflexin-1	1.48	1
AT5F1_HUMAN	11 (7)	528.44	0.04	ATP synthase F(0) complex subunit B1, mitochondrial	3.43	1
NEBU_HUMAN	125 (24)	523.96	0.09	Nebulin	1	2.54
TMEDA_HUMAN	11 (9)	523.95	0.13	Transmembrane emp24 domain-containing protein 10	2.3	1
NMT1_HUMAN	16 (3)	517.8	0.36	Glycylpeptide N-tetradecanoyltransferase 1	3.21	1
ATPG_HUMAN	12 (8)	517.39	0.06	ATP synthase subunit gamma, mitochondrial	1	2.94
RS2_HUMAN	13 (4)	515.86	0.88	40S ribosomal protein S2	1.18	1
CISY_HUMAN	11 (7)	514.52	0.36	Citrate synthase, mitochondrial	1.46	1
DYN2_HUMAN	20 (5)	510.84	0.54	Dynamin-2	1.43	1
AATM_HUMAN	9 (4)	508.92	0.15	Aspartate aminotransferase, mitochondrial	1	3.55
HCDH_HUMAN	10 (7)	506.92	0.55	Hydroxyacyl-coenzyme A dehydrogenase, mitochondrial	1	1.03

POTEJ_HUMAN	16 (3)	505.03	0.75	POTE ankyrin domain family member J	1	2.97
RTCB_HUMAN	12 (4)	504.02	6.39E-03	tRNA-splicing ligase RtcB homolog	1	6.64
MOT1_HUMAN	11 (4)	501.28	0.34	Monocarboxylate transporter 1	1	1.29
EIFCL_HUMAN	19 (6)	497.92	0.71	Eukaryotic translation initiation factor 3 subunit C-like protein	1	1.06
ANXA7_HUMAN	11 (6)	496.82	0.78	Annexin A7	1.01	1
SMC1A_HUMAN	21 (5)	495.38	0.17	Structural maintenance of chromosomes protein 1A	1.49	1
SDHA_HUMAN	12 (5)	495.37	0.05	Succinate dehydrogenase [ubiquinone] flavoprotein subunit, mitochondrial	2.77	1
2AAA_HUMAN	18 (4)	494.51	0.72	Serine/threonine-protein phosphatase 2A 65 kDa regulatory subunit A alpha isoform	1.21	1
YBOX1_HUMAN	8 (2)	492.13	0.59	Nuclease-sensitive element-binding protein 1	1	1.12
RPN2_HUMAN	10 (5)	490.8	0.06	Dolichyl-diphosphooligosaccharide--protein glycosyltransferase subunit 2	2.95	1
ECHM_HUMAN	9 (4)	489.69	0.27	Enoyl-CoA hydratase, mitochondrial	1	2.8
RL13A_HUMAN	21 (7)	488.67	0.09	60S ribosomal protein L13a	2.63	1
RAB2A_HUMAN	6 (5)	488.36	0.09	Ras-related protein Rab-2A	1.61	1
RS13_HUMAN	11 (6)	484.62	9.58E-03	40S ribosomal protein S13	9.16	1
RS5_HUMAN	9 (4)	482.22	0.2	40S ribosomal protein S5	3.88	1
GDIB_HUMAN	9 (3)	481.69	0.33	Rab GDP dissociation inhibitor beta	1.36	1
ADT3_HUMAN	12 (1)	481.44	0.43	ADP/ATP translocase 3	1	1.23
PDIA4_HUMAN	16 (7)	481.04	7.05E-03	Protein disulfide-isomerase A4	1	1.99
TOM40_HUMAN	9 (7)	480.71	0.91	Mitochondrial import receptor subunit TOM40 homolog	1.26	1
ESYT1_HUMAN	14 (5)	478.93	0.09	Extended synaptotagmin-1	1	1.41
LRC59_HUMAN	13 (5)	476.66	0.28	Leucine-rich repeat-containing protein 59	1	1.64
RENT1_HUMAN	14 (5)	475.69	0.6	Regulator of nonsense transcripts 1	1	1.08
HNRH2_HUMAN	9 (2)	474.39	0.57	Heterogeneous nuclear ribonucleoprotein H2	1	1.24
CPSF5_HUMAN	10 (8)	472.87	0.07	Cleavage and polyadenylation specificity factor subunit 5	1	1.37
ERP29_HUMAN	8 (7)	466.67	0.58	Endoplasmic reticulum resident protein 29	1.13	1
DYHC1_HUMAN	33 (8)	465.23	0.08	Cytoplasmic dynein 1 heavy chain 1	2.18	1
LAT1_HUMAN	7 (2)	463.73	0.12	Large neutral amino acids transporter small subunit 1	4.54	1
IF2A_HUMAN	13 (7)	458.62	0.36	Eukaryotic translation initiation factor 2 subunit 1	1	1.43
LAMP1_HUMAN	9 (5)	458.46	0.07	Lysosome-associated membrane glycoprotein 1	1.33	1
CYBP_HUMAN	10 (6)	457.9	0.64	Calcyclin-binding protein	1	1.03
COX2_HUMAN	8 (6)	457.12	0.3	Cytochrome c oxidase subunit 2	1.96	1
HMGB2_HUMAN	13 (3)	451.53	0.78	High mobility group protein B2	1	1.03
RL15_HUMAN	7 (5)	450.52	0.05	60S ribosomal protein L15	5.43	1
SYVC_HUMAN	22 (4)	447.33	0.12	Valine--tRNA ligase	1.82	1
U520_HUMAN	22 (7)	445.11	0.55	U5 small nuclear ribonucleoprotein 200 kDa helicase	1	1.19
PRDX4_HUMAN	6 (3)	445.1	0.3	Peroxiredoxin-4	1.53	1
COF1_HUMAN	8 (2)	444.76	0.01	Cofilin-1	5.15	1
MYH10_HUMAN	21 (1)	444.42	0.6	Myosin-10	1	1.11
SF3B2_HUMAN	21 (10)	444.19	0.51	Splicing factor 3B subunit 2	1	1.16
RBMX_HUMAN	11 (4)	443.14	0.25	RNA-binding motif protein, X chromosome	1	1.56
SF3A1_HUMAN	15 (5)	442.31	0.16	Splicing factor 3A subunit 1	1.64	1
DHX15_HUMAN	18 (6)	440.59	0.06	Pre-mRNA-splicing factor ATP-dependent RNA helicase DHX15	1	1.62
COPA_HUMAN	19 (7)	440.14	0.68	Coatomer subunit alpha	1.04	1
SRP14_HUMAN	6 (6)	438.37	0.07	Signal recognition particle 14 kDa protein	2.7	1
PLAK_HUMAN	9 (3)	437.42	7.34E-03	Junction plakoglobin	2.85	1
SYMC_HUMAN	16 (6)	436.12	0.04	Methionine--tRNA ligase, cytoplasmic	1.6	1
GNAS2_HUMAN	11 (5)	435.82	0.29	Guanine nucleotide-binding protein G(s) subunit alpha isoforms short	2.3	1
GLU2B_HUMAN	9 (3)	435.72	0.15	Glucosidase 2 subunit beta	1.85	1
MSH2_HUMAN	6 (2)	434.7	0.61	DNA mismatch repair protein Msh2	1.09	1
ETFB_HUMAN	10 (6)	429.64	0.18	Electron transfer flavoprotein subunit beta	1.51	1
ALDOC_HUMAN	11 (3)	429.09	0.05	Fructose-bisphosphate aldolase C	1	3.86
MOT4_HUMAN	8 (5)	427.03	0.02	Monocarboxylate transporter 4	1.88	1
APEX1_HUMAN	6 (4)	426.75	0.35	DNA-(apurinic or apyrimidinic site) lyase	1	1.45
STIP1_HUMAN	15 (7)	425.91	0.7	Stress-induced-phosphoprotein 1	1.1	1
SEPT9_HUMAN	8 (2)	425.78	0.91	Septin-9	1.21	1
RHOA_HUMAN	6 (3)	423.22	0.12	Transforming protein RhoA	2.34	1
RAP1B_HUMAN	6 (4)	421.7	0.03	Ras-related protein Rap-1b	4.05	1
THOC4_HUMAN	11 (8)	417.09	0.71	THO complex subunit 4	1	1.38

FBRL_HUMAN	10 (3)	416.38	0.07	rRNA 2'-O-methyltransferase fibrillarin	1	2.59
RS18_HUMAN	10 (3)	416.04	2.87E-04	40S ribosomal protein S18	4.97	1
SMC2_HUMAN	33 (6)	413.13	4.75E-03	Structural maintenance of chromosomes protein 2	1	5.97
IPO5_HUMAN	13 (4)	412.99	0.2	Importin-5	2.03	1
NDKA_HUMAN	7 (1)	408.93	0.48	Nucleoside diphosphate kinase A	70.64	1
SYYC_HUMAN	14 (6)	406.59	0.61	Tyrosine--tRNA ligase, cytoplasmic	1.79	1
PGK2_HUMAN	13 (2)	406.26	0.76	Phosphoglycerate kinase 2	4.97	1
SC31A_HUMAN	12 (5)	405.48	0.29	Protein transport protein Sec31A	1	1.14
SNAA_HUMAN	5 (3)	399.03	0.84	Alpha-soluble NSF attachment protein	1.11	1
THIM_HUMAN	5 (4)	398.24	0.05	3-ketoacyl-CoA thiolase, mitochondrial	2.37	1
EIF2A_HUMAN	11 (6)	394.57	0.24	Eukaryotic translation initiation factor 2A	1.6	1
DDX5_HUMAN	15 (5)	394.28	0.66	Probable ATP-dependent RNA helicase DDX5	1	1.14
RAB5A_HUMAN	8 (1)	391.71	0.75	Ras-related protein Rab-5A	1.3	1
GSTK1_HUMAN	7 (5)	391.33	0.9	Glutathione S-transferase kappa 1	2.08	1
PPIA_HUMAN	11 (6)	386.26	0.04	Peptidyl-prolyl cis-trans isomerase A	3.27	1
HNRPD_HUMAN	6 (2)	385.46	0.15	Heterogeneous nuclear ribonucleoprotein D0	7.38	1
SMHD1_HUMAN	29 (6)	385.04	0.55	Structural maintenance of chromosomes flexible hinge domain-containing protein 1	1	1.88
PABP3_HUMAN	16 (1)	382.49	0.35	Polyadenylate-binding protein 3	1	4.92
TP4A1_HUMAN	6 (5)	380.47	0.06	Protein tyrosine phosphatase type IVA 1	2.4	1
RL12_HUMAN	4 (3)	380.23	0.19	60S ribosomal protein L12	4.47	1
SSRD_HUMAN	6 (6)	377.53	0.01	Translocon-associated protein subunit delta	4.3	1
G3BP2_HUMAN	8 (2)	376.22	0.08	Ras GTPase-activating protein-binding protein 2	6.51	1
AP2B1_HUMAN	10 (2)	375.55	0.04	AP-2 complex subunit beta	1.99	1
1433T_HUMAN	8 (3)	373.75	0.15	14-3-3 protein theta	8.86	1
RS11_HUMAN	9 (4)	369.3	0.09	40S ribosomal protein S11	6.99	1
LIMA1_HUMAN	7 (3)	366.23	0.02	LIM domain and actin-binding protein 1	2.79	1
SSRA_HUMAN	4 (1)	361.45	0.6	Translocon-associated protein subunit alpha	1	1.08
SP16H_HUMAN	14 (5)	360.61	0.89	FACT complex subunit SPT16	1.13	1
CAND1_HUMAN	18 (2)	360.31	0.64	Cullin-associated NEDD8-dissociated protein 1	1	1.48
SC22B_HUMAN	7 (4)	359.88	0.14	Vesicle-trafficking protein SEC22b	1	1.51
RS24_HUMAN	6 (4)	359.76	0.03	40S ribosomal protein S24	5.04	1
IF2G_HUMAN	9 (4)	359.21	0.92	Eukaryotic translation initiation factor 2 subunit 3	1	1.19
SRRT_HUMAN	11 (4)	359.18	0.02	Serrate RNA effector molecule homolog	3.86	1
FKBP3_HUMAN	11 (7)	358.69	0.54	Peptidyl-prolyl cis-trans isomerase FKBP3	1	1.22
IF4G1_HUMAN	15 (4)	356.41	0.54	Eukaryotic translation initiation factor 4 gamma 1	1.06	1
IDH3A_HUMAN	14 (7)	355.61	0.67	Isocitrate dehydrogenase [NAD] subunit alpha, mitochondrial	1.38	1
MCM3_HUMAN	7 (2)	355.57	0.61	DNA replication licensing factor MCM3	1	1.57
DHB4_HUMAN	12 (6)	354.73	0.41	Peroxisomal multifunctional enzyme type 2	1	1.15
UCRI_HUMAN	7 (2)	351.03	0.04	Cytochrome b-c1 complex subunit Rieske, mitochondrial	46.07	1
PRDX6_HUMAN	7 (3)	350.49	0.02	Peroxiredoxin-6	2.49	1
ODPA_HUMAN	11 (1)	350.15	0.07	Pyruvate dehydrogenase E1 component subunit alpha, somatic form, mitochondrial	1	26.45
MYH11_HUMAN	16 (2)	349.69	0.83	Myosin-11	1.01	1
KCRU_HUMAN	8 (1)	345.46	0.56	Creatine kinase U-type, mitochondrial	1.42	1
SPTN2_HUMAN	42 (4)	342	0.81	Spectrin beta chain, non-erythrocytic 2	1	1.03
CCD47_HUMAN	8 (5)	340.9	0.35	Coiled-coil domain-containing protein 47	1.24	1
ALBU_HUMAN	18 (4)	340.31	0.97	Serum albumin	1.51	1
EIF3E_HUMAN	11 (5)	336.91	0.03	Eukaryotic translation initiation factor 3 subunit E	1	7.49
RLA2_HUMAN	4 (1)	336.19	0.06	60S acidic ribosomal protein P2	3.9	1
ECI2_HUMAN	10 (4)	334.98	0.52	Enoyl-CoA delta isomerase 2, mitochondrial	1.23	1
RAN_HUMAN	9 (2)	333.51	0.11	GTP-binding nuclear protein Ran	1.61	1
TIF1B_HUMAN	12 (5)	332.31	0.03	Transcription intermediary factor 1-beta	1	2.75
COPE_HUMAN	7 (2)	330.78	0.24	Coatomer subunit epsilon	4	1
ELAV1_HUMAN	6 (3)	330.44	0.32	ELAV-like protein 1	1	1.25
PGAM1_HUMAN	7 (2)	329.78	0.02	Phosphoglycerate mutase 1	1	4.44
KI67_HUMAN	35 (12)	328.31	0.13	Proliferation marker protein Ki-67	1	4.29
CPNS1_HUMAN	5 (3)	328	0.02	Calpain small subunit 1	2.82	1
H31T_HUMAN	7 (1)	327.11	0.9	Histone H3.1t	1.68	1
RL11_HUMAN	7 (4)	325.98	0.75	60S ribosomal protein L11	3.06	1

RL29_HUMAN	5 (2)	324.44	0.1	60S ribosomal protein L29	4.21	1
GOGA2_HUMAN	13 (4)	324.41	8.31E-03	Golgin subfamily A member 2	1	1.44
NDK8_HUMAN	6 (1)	324.37	0.26	Putative nucleoside diphosphate kinase	1	2.5
PSA7_HUMAN	6 (3)	324.32	0.5	Proteasome subunit alpha type-7	1	1.16
RB11B_HUMAN	6 (3)	321.27	0.88	Ras-related protein Rab-11B	1.19	1
ECI1_HUMAN	9 (3)	321.04	0.65	Enoyl-CoA delta isomerase 1, mitochondrial	1	1.02
VDAC3_HUMAN	4 (2)	319.96	1.40E-03	Voltage-dependent anion-selective channel protein 3	1	5.59
SYQ_HUMAN	9 (5)	318.75	0.57	Glutamine--tRNA ligase	1.1	1
SDHB_HUMAN	8 (4)	318.23	0.04	Succinate dehydrogenase [ubiquinone] iron-sulfur subunit, mitochondrial	1.91	1
FRIH_HUMAN	7 (3)	317.3	0.46	Ferritin heavy chain	1.57	1
TPD52_HUMAN	8 (2)	314.18	0.92	Tumor protein D52	1.72	1
IF2B_HUMAN	11 (6)	313.46	9.42E-03	Eukaryotic translation initiation factor 2 subunit 2	2.3	1
MYH14_HUMAN	20 (3)	310.97	0.78	Myosin-14	1	1.14
RAB6A_HUMAN	9 (4)	309.26	0.27	Ras-related protein Rab-6	1.52	1
SYSC_HUMAN	11 (4)	308.34	0.27	Serine--tRNA ligase, cytoplasmic	1	1.48
RS25_HUMAN	4 (2)	308.32	0.02	40S ribosomal protein S25	3.39	1
RHOC_HUMAN	6 (1)	304.95	0.31	Rho-related GTP-binding protein RhoC	9.38	1
TPD54_HUMAN	7 (5)	303.38	7.28E-03	Tumor protein D54	1	3.16
GTF2I_HUMAN	20 (7)	303.01	0.23	General transcription factor II-I	1.32	1
ABCF1_HUMAN	11 (5)	300.11	0.96	ATP-binding cassette sub-family F member 1	1	1.01
CPNE1_HUMAN	10 (3)	299.52	0.23	Copine-1	1.5	1
TMED9_HUMAN	5 (3)	295.54	0.28	Transmembrane emp24 domain-containing protein 9	1	1.57
PSA2_HUMAN	6 (5)	295.13	0.97	Proteasome subunit alpha type-2	1.38	1
EF1B_HUMAN	4 (1)	294.52	0.03	Elongation factor 1-beta	1	22.3
RS4Y2_HUMAN	10 (1)	294.07	0.41	40S ribosomal protein S4, Y isoform 2	1	1.57
NICA_HUMAN	11 (4)	294.01	0.11	Nicastrin	1.7	1
CD44_HUMAN	8 (4)	293.6	0.35	CD44 antigen	1	1.84
RL19_HUMAN	3 (3)	292.87	0.32	60S ribosomal protein L19	2.45	1
AIMP1_HUMAN	11 (4)	292.6	0.06	Aminoacyl tRNA synthase complex-interacting multifunctional protein 1	1	3.61
AT1B3_HUMAN	7 (3)	291.89	0.45	Sodium/potassium-transporting ATPase subunit beta-3	1.33	1
SRSF7_HUMAN	7 (1)	291.21	0.54	Serine/arginine-rich splicing factor 7	1	1.19
ANX11_HUMAN	12 (5)	289.82	0.57	Annexin A11	1.16	1
NIPS1_HUMAN	6 (3)	289.8	0.43	Protein NipSnap homolog 1	1	1.16
RUVB1_HUMAN	8 (4)	288.9	0.66	RuvB-like 1	1.09	1
API5_HUMAN	10 (6)	288.84	0.53	Apoptosis inhibitor 5	1.61	1
P5CS_HUMAN	10 (1)	288.05	0.15	Delta-1-pyrroline-5-carboxylate synthase	1	2.42
RS16_HUMAN	9 (3)	287.12	0.33	40S ribosomal protein S16	8.87	1
RAB5B_HUMAN	7 (1)	284.6	0.2	Ras-related protein Rab-5B	1	1.91
RCC2_HUMAN	6 (3)	283.83	1.09E-03	Protein RCC2	2.09	1
HSDL2_HUMAN	6 (1)	283.21	0.56	Hydroxysteroid dehydrogenase-like protein 2	1.56	1
AP1B1_HUMAN	14 (2)	283	0.08	AP-1 complex subunit beta-1	1.43	1
PCBP1_HUMAN	6 (4)	282.17	0.77	Poly(rC)-binding protein 1	2.34	1
FXR1_HUMAN	14 (5)	281.05	0.08	Fragile X mental retardation syndrome-related protein 1	1	2.58
RS14_HUMAN	7 (3)	280.82	0.37	40S ribosomal protein S14	4.44	1
LETM1_HUMAN	9 (3)	279.99	0.51	Mitochondrial proton/calcium exchanger protein	1.05	1
SRSF3_HUMAN	7 (3)	279.58	0.32	Serine/arginine-rich splicing factor 3	1.21	1
GPDM_HUMAN	8 (3)	279.32	0.56	Glycerol-3-phosphate dehydrogenase, mitochondrial	1.97	1
SARNP_HUMAN	5 (3)	277.33	0.35	SAP domain-containing ribonucleoprotein	1	1.38
ARF1_HUMAN	6 (2)	277.2	0.04	ADP-ribosylation factor 1	2.79	1
RIR1_HUMAN	8 (4)	276.95	0.32	Ribonucleoside-diphosphate reductase large subunit	1.38	1
ARF4_HUMAN	7 (1)	275.93	0.93	ADP-ribosylation factor 4	1.8	1
SRSF1_HUMAN	9 (5)	275.89	0.22	Serine/arginine-rich splicing factor 1	1	1.57
HSP74_HUMAN	16 (5)	275.21	0.09	Heat shock 70 kDa protein 4	1	1.43
NOLC1_HUMAN	11 (2)	273.99	0.02	Nucleolar and coiled-body phosphoprotein 1	1	4.6
CBX3_HUMAN	3 (1)	271.72	0.26	Chromobox protein homolog 3	1	1.48
TOM22_HUMAN	4 (4)	270.9	0.02	Mitochondrial import receptor subunit TOM22 homolog	13.54	1
LARP1_HUMAN	15 (3)	269.06	0.11	La-related protein 1	1.88	1
RL14_HUMAN	8 (4)	268.77	0.02	60S ribosomal protein L14	10.34	1

ERF1_HUMAN	8 (4)	268.59	0.38	Eukaryotic peptide chain release factor subunit 1	1.09	1
HNRL2_HUMAN	13 (4)	268.06	0.24	Heterogeneous nuclear ribonucleoprotein U-like protein 2	1	1.9
RAB10_HUMAN	8 (3)	267.72	0.81	Ras-related protein Rab-10	1	1.01
DNJA1_HUMAN	6 (2)	267.58	0.69	DnaJ homolog subfamily A member 1	1.02	1
DDX6_HUMAN	10 (3)	265.89	0.02	Probable ATP-dependent RNA helicase DDX6	3.21	1
IF5A1_HUMAN	6 (2)	265.45	0.24	Eukaryotic translation initiation factor 5A-1	4.84	1
TIM50_HUMAN	5 (4)	265.24	0.05	Mitochondrial import inner membrane translocase subunit TIM50	2.64	1
RUVB2_HUMAN	9 (2)	264.76	0.29	RuvB-like 2	1.35	1
DPM1_HUMAN	7 (3)	264.76	0.02	Dolichol-phosphate mannosyltransferase subunit 1	5.43	1
H2A1B_HUMAN	4 (2)	262.47	0.06	Histone H2A type 1-B/E	2.85	1
3HIDH_HUMAN	6 (3)	262.03	0.13	3-hydroxyisobutyrate dehydrogenase, mitochondrial	3.44	1
CAP1_HUMAN	4 (2)	260.99	0.21	Adenylyl cyclase-associated protein 1	1.92	1
DHX30_HUMAN	17 (5)	260.97	0.63	Putative ATP-dependent RNA helicase DHX30	1	1.98
NU155_HUMAN	5 (4)	259.93	0.77	Nuclear pore complex protein Nup155	1	1.05
NP1L1_HUMAN	9 (4)	259.58	0.03	Nucleosome assembly protein 1-like 1	1.22	1
LAP2B_HUMAN	12 (4)	259	0.04	Lamina-associated polypeptide 2, isoforms beta/gamma	3.86	1
NUMA1_HUMAN	22 (3)	258.74	0.86	Nuclear mitotic apparatus protein 1	1	1.02
SPRE_HUMAN	7 (4)	258.45	0.97	Sepiapterin reductase	1.89	1
RL1D1_HUMAN	8 (4)	257.74	0.35	Ribosomal L1 domain-containing protein 1	1	1.34
GNAS1_HUMAN	9 (1)	256.28	0.2	Guanine nucleotide-binding protein G(s) subunit alpha isoforms Xlas	1	3.33
MUC19_HUMAN	43 (10)	255.82	0.02	Mucin-19	1	2.44
PRC2C_HUMAN	26 (1)	255.7	0.32	Protein PRRC2C	6.86	1
TXND5_HUMAN	6 (1)	252.69	0.14	Thioredoxin domain-containing protein 5	2.08	1
RS19_HUMAN	8 (4)	251.63	0.25	40S ribosomal protein S19	3.08	1
NDUA9_HUMAN	6 (3)	251.3	0.97	NADH dehydrogenase [ubiquinone] 1 alpha subcomplex subunit 9, mitochondrial	1.52	1
EFTS_HUMAN	5 (3)	249.49	1	Elongation factor Ts, mitochondrial	1.31	1
MAP2_HUMAN	4 (2)	247.96	0.08	Methionine aminopeptidase 2	15.68	1
IFRD1_HUMAN	5 (5)	247.19	0.55	Interferon-related developmental regulator 1	1	1.08
UCRIL_HUMAN	5 (1)	247.18	0.35	Putative cytochrome b-c1 complex subunit Rieske-like protein 1	3.23	1
RL27_HUMAN	11 (7)	245.58	6.29E-03	60S ribosomal protein L27	2.68	1
TPR_HUMAN	20 (5)	243.62	0.45	Nucleoprotein TPR	1	3.07
MUC16_HUMAN	39 (6)	243.47	0.34	Mucin-16	2.16	1
RBBP7_HUMAN	6 (2)	242.41	0.72	Histone-binding protein RBBP7	1.11	1
PYR1_HUMAN	13 (2)	242.19	0.14	CAD protei	1	2.63
FSCN1_HUMAN	4 (3)	241.36	8.29E-03	Fascin	1.59	1
DYH17_HUMAN	33 (1)	241.2	0.68	Dynein heavy chain 17, axonemal	1	1.86
UTRO_HUMAN	36 (5)	239.69	0.36	Utrophin	2.91	1
ROA0_HUMAN	3 (2)	239.55	0.2	Heterogeneous nuclear ribonucleoprotein A0	1	2.37
LMAN2_HUMAN	6 (3)	238.62	0.2	Vesicular integral-membrane protein VIP36	1	1.87
SMRC2_HUMAN	15 (6)	236.64	0.95	SWI/SNF complex subunit SMARCC2	1	1.02
HNRH3_HUMAN	5 (1)	236.18	0.64	Heterogeneous nuclear ribonucleoprotein H3	1	1.21
RL35_HUMAN	4 (3)	235.9	0.03	60S ribosomal protein L35	10.82	1
SORCN_HUMAN	6 (1)	235.8	0.11	Sorcin	1	5.65
RASN_HUMAN	5 (2)	233.91	0.07	GTPase Nras	8.35	1
BZW2_HUMAN	8 (2)	232.47	0.33	Basic leucine zipper and W2 domain-containing protein 2	1.65	1
RAB14_HUMAN	3 (2)	230.37	0.88	Ras-related protein Rab-14	1.15	1
NOP58_HUMAN	5 (2)	230.31	0.26	Nucleolar protein 58	1	1.42
SYFB_HUMAN	13 (1)	229.88	0.08	Phenylalanine--tRNA ligase beta subunit	1	1.59
PLIN3_HUMAN	4 (2)	227.96	0.06	Perilipin-3	1	5.77
PSDE_HUMAN	7 (2)	227.51	0.57	26S proteasome non-ATPase regulatory subunit 14	1.48	1
PLOD3_HUMAN	6 (2)	227.41	0.09	Procollagen-lysine,2-oxoglutarate 5-dioxygenase 3	1	2.51
1433F_HUMAN	6 (1)	227.3	0.06	14-3-3 protein eta	1	21.12
TCRG1_HUMAN	13 (2)	226.79	0.75	Transcription elongation regulator 1	1.06	1
SYDC_HUMAN	5 (2)	226.09	0.99	Aspartate--tRNA ligase, cytoplasmic	1.2	1
RS20_HUMAN	8 (3)	225.91	0.01	40S ribosomal protein S20	6.24	1
PSA5_HUMAN	4 (3)	225.87	0.8	Proteasome subunit alpha type-5	1.64	1
AAAT_HUMAN	4 (2)	224.63	0.31	Neutral amino acid transporter B(0)	1.29	1
OST48_HUMAN	6 (4)	223.74	0.53	Dolichyl-diphosphooligosaccharide--protein glycosyltransferase 48 kDa subunit	1.44	1

RS26_HUMAN	4 (1)	223.28	0.25	40S ribosomal protein S26	2.06	1
RL31_HUMAN	8 (2)	222.51	0.93	60S ribosomal protein L31	3.33	1
CY1_HUMAN	5 (5)	221.88	0.37	Cytochrome c1, heme protein, mitochondrial	2.76	1
TBA4B_HUMAN	4 (1)	221.7	0.04	Putative tubulin-like protein alpha-4B	9.02	1
AT1A4_HUMAN	13 (2)	220.55	0.01	Sodium/potassium-transporting ATPase subunit alpha-4	1	13.59
PODXL_HUMAN	5 (2)	219.95	8.16E-04	Podocalyxin	5.88	1
BUB3_HUMAN	8 (4)	219.85	0.26	Mitotic checkpoint protein BUB3	1	1.44
PACN3_HUMAN	6 (1)	218.71	0.03	Protein kinase C and casein kinase substrate in neurons protein 3	2.65	1
RL22_HUMAN	3 (1)	218.26	0.12	60S ribosomal protein L22	2.11	1
MDHC_HUMAN	9 (2)	217.33	0.06	Malate dehydrogenase, cytoplasmic	1	6.45
TPM3_HUMAN	11 (3)	216.46	0.11	Tropomyosin alpha-3 chain	2.84	1
FXR2_HUMAN	5 (2)	214.81	0.12	Fragile X mental retardation syndrome-related protein 2	2.99	1
DNJC9_HUMAN	6 (4)	214.8	0.11	DnaJ homolog subfamily C member 9	1	4.08
DDB1_HUMAN	6 (3)	214	0.03	DNA damage-binding protein 1	1	3.38
RAB8A_HUMAN	4 (1)	213.04	0.36	Ras-related protein Rab-8A	2.83	1
SCAM3_HUMAN	3 (1)	212.47	0.02	Secretory carrier-associated membrane protein 3	1	8.76
DYN3_HUMAN	11 (1)	211.62	0.01	Dynamin-3	2	1
PGES2_HUMAN	5 (2)	211.59	0.36	Prostaglandin E synthase 2	7.53	1
DYN1_HUMAN	15 (3)	209.66	0.03	Dynamin-1	1	5.95
ADT4_HUMAN	11 (3)	208.43	0.77	ADP/ATP translocase 4	1.73	1
DYH5_HUMAN	30 (3)	208.33	0.19	Dynein heavy chain 5, axonemal	1.37	1
RBCC1_HUMAN	27 (1)	208.17	0.87	RB1-inducible coiled-coil protein 1	1	3.24
PCBP2_HUMAN	4 (1)	208.09	0.4	Poly(rC)-binding protein 2	4.55	1
BAG2_HUMAN	4 (2)	206.96	0.06	BAG family molecular chaperone regulator 2	1	2
CTNA1_HUMAN	10 (4)	206.35	0.22	Catenin alpha-1	1.65	1
TM14C_HUMAN	3 (1)	206.16	0.04	Transmembrane protein 14C	4.81	1
PARK7_HUMAN	5 (4)	205.85	0.07	Protein DJ-1	1	4.53
KAP2_HUMAN	4 (3)	205.51	0.03	cAMP-dependent protein kinase type II-alpha regulatory subunit	5.41	1
PSA1_HUMAN	5 (4)	205.44	0.71	Proteasome subunit alpha type-1	1.07	1
DYH9_HUMAN	41 (7)	204.54	0.1	Dynein heavy chain 9, axonemal	1	2.29
RU2A_HUMAN	7 (4)	204.16	0.78	U2 small nuclear ribonucleoprotein A'	1.08	1
RM12_HUMAN	5 (4)	203.19	0.75	39S ribosomal protein L12, mitochondrial	1.87	1
PSIP1_HUMAN	8 (3)	202.89	2.03E-04	PC4 and SFRS1-interacting protein	2.12	1
GNL3_HUMAN	6 (3)	202.77	0.43	Guanine nucleotide-binding protein-like 3	1	1.33
GNAI3_HUMAN	9 (1)	202.75	0.73	Guanine nucleotide-binding protein G(k) subunit alpha	1.4	1
NP1L4_HUMAN	4 (2)	202.36	0.07	Nucleosome assembly protein 1-like 4	2.73	1
PRS6A_HUMAN	6 (3)	202.26	0.86	26S proteasome regulatory subunit 6A	1.14	1
RS10_HUMAN	7 (4)	201.53	1.22E-03	40S ribosomal protein S10	9.84	1
TCTP_HUMAN	6 (1)	201.32	0.41	Translationally-controlled tumor protein	3.72	1
SF3B3_HUMAN	11 (3)	200.72	0.65	Splicing factor 3B subunit 3	1	1.09
DEK_HUMAN	8 (3)	200.68	0.09	Protein DEK	1	1.88
1433S_HUMAN	5 (2)	200.21	0.01	14-3-3 protein sigma	1	6.18
IMDH2_HUMAN	5 (1)	199.02	0.02	Inosine-5'-monophosphate dehydrogenase 2	40.21	1
PRS6B_HUMAN	5 (3)	198.88	0.03	26S proteasome regulatory subunit 6B	4.48	1
PGAM4_HUMAN	5 (1)	196.94	0.73	Probable phosphoglycerate mutase 4	1.3	1
SSRG_HUMAN	6 (2)	196.6	0.72	Translocon-associated protein subunit gamma	1	1.03
ROAA_HUMAN	6 (4)	195.19	0.51	Heterogeneous nuclear ribonucleoprotein A/B	1.47	1
CAPG_HUMAN	3 (1)	194.91	0.13	Macrophage-capping protein	1	4.22
SEPT7_HUMAN	6 (1)	194.87	0.68	Septin-7	1.73	1
PDCD4_HUMAN	9 (4)	193.37	0.24	Programmed cell death protein 4	1	1.69
KHDR1_HUMAN	10 (2)	192.87	0.31	KH domain-containing, RNA-binding, signal transduction-associated protein 1	4.79	1
PSB1_HUMAN	5 (2)	192.51	0.38	Proteasome subunit beta type-1	2.04	1
BAP31_HUMAN	6 (3)	192.34	0.96	B-cell receptor-associated protein 31	1	2.99
NMT2_HUMAN	15 (1)	190.82	0.05	Glycylpeptide N-tetradecanoyltransferase 2	1	4.34
SRSF2_HUMAN	3 (1)	188.75	0.24	Serine/arginine-rich splicing factor 2	2.13	1
KCRB_HUMAN	1 (1)	188.11	0.29	Creatine kinase B-type	2.03	1
SMC4_HUMAN	12 (1)	187.95	0.25	Structural maintenance of chromosomes protein 4	1.76	1
TMED4_HUMAN	5 (1)	187.78	0.04	Transmembrane emp24 domain-containing protein 4	1.29	1

DNJA3_HUMAN	11 (2)	186.9	0.1	DnaJ homolog subfamily A member 3, mitochondrial	1	1.72
RAB13_HUMAN	6 (1)	185.98	0.17	Ras-related protein Rab-13	2.04	1
PRP8_HUMAN	15 (3)	185.74	0.02	Pre-mRNA-processing-splicing factor 8	3.62	1
RL27A_HUMAN	4 (3)	185.2	0.02	60S ribosomal protein L27a	6.15	1
ACINU_HUMAN	12 (3)	185.1	0.85	Apoptotic chromatin condensation inducer in the nucleus	1	1.94
IF4H_HUMAN	6 (4)	184.04	0.57	Eukaryotic translation initiation factor 4H	1.69	1
CNPY2_HUMAN	2 (1)	183.98	0.91	Protein canopy homolog 2	7.28	1
LEG3_HUMAN	5 (2)	183.7	0.99	Galectin-3	1.32	1
RBM8A_HUMAN	4 (2)	183.13	0.32	RNA-binding protein 8A	1	2.1
CMC2_HUMAN	8 (3)	181.86	0.16	Calcium-binding mitochondrial carrier protein Aralar2	4.26	1
PRS4_HUMAN	8 (3)	181.74	0.38	26S proteasome regulatory subunit 4	1	2.19
TCEA1_HUMAN	5 (1)	180.72	0.34	Transcription elongation factor A protein 1	1.34	1
CC124_HUMAN	7 (4)	178.96	0.27	Coiled-coil domain-containing protein 124	1	1.69
HMOX2_HUMAN	8 (3)	178.72	0.82	Heme oxygenase 2	1	1.07
DECR_HUMAN	4 (2)	178.33	0.83	2,4-dienoyl-CoA reductase, mitochondrial	1.6	1
MYO1B_HUMAN	9 (1)	177.31	0.34	Unconventional myosin-Ib	1.79	1
PCNT_HUMAN	24 (5)	177.06	0.12	Pericentrin	1	3.24
DSRAD_HUMAN	23 (2)	176.98	0.14	Double-stranded RNA-specific adenosine deaminase	1	1.56
RS15A_HUMAN	11 (4)	176.29	0.95	40S ribosomal protein S15a	1	1.01
IDH3B_HUMAN	3 (1)	176.09	0.17	Isocitrate dehydrogenase [NAD] subunit beta, mitochondrial	1	1.95
EWS_HUMAN	6 (1)	176.03	0.87	RNA-binding protein EWS	1.06	1
TSR1_HUMAN	12 (4)	175.91	0.64	Pre-rRNA-processing protein TSR1 homolog	1	1.06
IF2B3_HUMAN	8 (2)	175.78	1.94E-03	Insulin-like growth factor 2 mRNA-binding protein 3	1	3.33
PRP19_HUMAN	5 (3)	175.51	0.34	Pre-mRNA-processing factor 19	1	1.14
NDUV2_HUMAN	3 (3)	174.52	0.39	NADH dehydrogenase [ubiquinone] flavoprotein 2, mitochondrial	1.1	1
RL32_HUMAN	5 (4)	174.45	1.02E-04	60S ribosomal protein L32	7.02	1
GBF1_HUMAN	22 (3)	173.89	0.84	Golgi-specific brefeldin A-resistance guanine nucleotide exchange factor 1	1	1.12
GARS_HUMAN	7 (2)	173.25	0.79	Glycine--tRNA ligase	1.38	1
PUF60_HUMAN	8 (4)	173.03	0.2	Poly(U)-binding-splicing factor PUF60	1	2.9
BZW1_HUMAN	11 (3)	172.85	0.3	Basic leucine zipper and W2 domain-containing protein 1	1	1.31
COPG1_HUMAN	14 (3)	172.57	0.32	Coatomer subunit gamma-1	1	3.7
DJB11_HUMAN	5 (4)	171.9	0.96	DnaJ homolog subfamily B member 11	1.17	1
RL40_HUMAN	5 (3)	171.76	0.87	Ubiquitin-60S ribosomal protein L40	1	1.08
TBAL3_HUMAN	9 (1)	171.76	0.13	Tubulin alpha chain-like 3	2.56	1
RMXL1_HUMAN	6 (1)	171.29	0.99	RNA binding motif protein, X-linked-like-1	1	8.36
PCYOX_HUMAN	4 (2)	170.19	0.8	Prenylcysteine oxidase 1	1	1.42
GDIA_HUMAN	7 (1)	169.7	0.91	Rab GDP dissociation inhibitor alpha	1	2.11
WBP11_HUMAN	9 (1)	169.5	6.58E-03	WW domain-binding protein 11	1	2.75
H2BFS_HUMAN	9 (1)	169.33	0.34	Histone H2B type F-S	1.9	1
PCKGM_HUMAN	8 (4)	168.33	0.02	Phosphoenolpyruvate carboxykinase [GTP], mitochondrial	1	11.58
EIF3K_HUMAN	9 (2)	168.24	0.43	Eukaryotic translation initiation factor 3 subunit K	3.19	1
ARPC3_HUMAN	3 (2)	168.24	0.08	Actin-related protein 2/3 complex subunit 3	4.38	1
RBP56_HUMAN	3 (2)	168.06	0.46	TATA-binding protein-associated factor 2N	1	1.21
HNRDL_HUMAN	5 (1)	168.06	0.37	Heterogeneous nuclear ribonucleoprotein D-like	1.91	1
CLIC1_HUMAN	5 (2)	167.62	9.70E-03	Chloride intracellular channel protein 1	1	3.46
MCM4_HUMAN	8 (1)	167.48	0.65	DNA replication licensing factor MCM4	1.17	1
TOM70_HUMAN	5 (2)	166.94	0.54	Mitochondrial import receptor subunit TOM70	1.59	1
SCMC1_HUMAN	7 (5)	166.84	0.78	Calcium-binding mitochondrial carrier protein SCaMC-1	1	1.12
PUR2_HUMAN	7 (2)	166.82	0.5	Trifunctional purine biosynthetic protein adenosine-3	1	1.61
CPNE3_HUMAN	7 (1)	166.36	0.04	Copine-3	1	16.72
PININ_HUMAN	12 (4)	165.88	0.1	Pinin	2.03	1
TADBP_HUMAN	7 (3)	165.54	0.17	TAR DNA-binding protein 43	2.57	1
EIF3I_HUMAN	3 (2)	165.46	0.66	Eukaryotic translation initiation factor 3 subunit I	1	1.29
PLOD1_HUMAN	6 (1)	165.22	0.38	Procollagen-lysine,2-oxoglutarate 5-dioxygenase 1	1	1.1
DX39B_HUMAN	6 (1)	164.44	0.18	Spliceosome RNA helicase DDX39B	1	2.61
S10AB_HUMAN	1 (1)	164.15	0.53	Protein S100-A11	2.86	1
IF2P_HUMAN	7 (2)	163.99	0.88	Eukaryotic translation initiation factor 5B	1	1.03
F120A_HUMAN	7 (1)	163.92	0.49	Constitutive coactivator of PPAR-gamma-like protein 1	1	1.44

HP1B3_HUMAN	7 (2)	162.92	0.31	Heterochromatin protein 1-binding protein 3	1	1.28
ODB2_HUMAN	7 (3)	162.61	0.1	Lipoamide acyltransferase component of branched-chain alpha-keto acid dehydrogenase complex, mitochondrial	2	1
U2AF2_HUMAN	6 (2)	162.47	0.77	Splicing factor U2AF 65 kDa subunit	1.21	1
MYO6_HUMAN	20 (2)	162.34	0.58	Unconventional myosin-VI	1	1.94
ACTN3_HUMAN	7 (2)	161.47	0.88	Alpha-actinin-3	1.48	1
ECHB_HUMAN	3 (2)	160.18	0.3	Trifunctional enzyme subunit beta, mitochondrial	2.73	1
PDS5A_HUMAN	14 (5)	160.02	0.1	Sister chromatid cohesion protein PDS5 homolog A	1	3.71
MCA3_HUMAN	4 (2)	159.86	0.05	Eukaryotic translation elongation factor 1 epsilon-1=1	2.91	1
UGGG1_HUMAN	13 (2)	159.28	0.87	UDP-glucose:glycoprotein glucosyltransferase 1	1	1.32
DNMT1_HUMAN	18 (2)	159.22	0.93	DNA (cytosine-5)-methyltransferase 1	1	1.54
CROCC_HUMAN	19 (3)	158.83	0.27	Rootletin	1.07	1
GTR1_HUMAN	4 (3)	158.63	0.81	Solute carrier family 2, facilitated glucose transporter member 1	1	1.12
LC7L2_HUMAN	3 (2)	158.46	0.48	Putative RNA-binding protein Luc7-like 2	1.2	1
ODO1_HUMAN	8 (1)	158.45	4.23E-03	2-oxoglutarate dehydrogenase, mitochondrial	1	13.01
LRRK2_HUMAN	17 (3)	158.42	0.97	Leucine-rich repeat serine/threonine-protein kinase 2	1.18	1
CIP4_HUMAN	7 (3)	157.65	0.32	Cdc42-interacting protein 4	2.1	1
TCP4_HUMAN	3 (1)	157.57	0.33	Activated RNA polymerase II transcriptional coactivator p15	56.05	1
TOP2A_HUMAN	11 (3)	157.37	0.59	DNA topoisomerase 2-alpha	1.04	1
GYS1_HUMAN	10 (3)	156.98	0.33	Glycogen [starch] synthase, muscle	1.35	1
PRPS2_HUMAN	6 (1)	156.44	0.96	Ribose-phosphate pyrophosphokinase 2	1.02	1
LAP2A_HUMAN	5 (2)	156.1	0.92	Lamina-associated polypeptide 2, isoform alpha	1	1.01
ZC3HD_HUMAN	26 (5)	156.02	0.33	Zinc finger CCCH domain-containing protein 13	1	1.48
RAD50_HUMAN	21 (1)	155.84	5.52E-03	DNA repair protein RAD50	17.04	1
NOP2_HUMAN	6 (3)	155.27	0.31	Probable 28S rRNA (cytosine(4447)-C(5))-methyltransferase	1.64	1
CHIP_HUMAN	5 (1)	155.15	0.22	E3 ubiquitin-protein ligase CHIP	1.68	1
IF2B1_HUMAN	9 (2)	154.95	0.92	Insulin-like growth factor 2 mRNA-binding protein 1	1.5	1
RL18A_HUMAN	7 (4)	153.84	4.99E-03	60S ribosomal protein L18a	10.24	1
QOR_HUMAN	7 (1)	153.6	0.79	Quinone oxidoreductase	1.69	1
RFC2_HUMAN	2 (2)	153.15	2.97E-04	Replication factor C subunit 2	1	6.58
SMCA5_HUMAN	13 (2)	152.63	0.58	SWI/SNF-related matrix-associated actin-dependent regulator of chromatin subfamily A member 5	1	1.07
SSRP1_HUMAN	4 (2)	152.58	0.14	FACT complex subunit SSRP1	2.4	1
RCN1_HUMAN	6 (3)	152.57	0.12	Reticulocalbin-1	5.8	1
RD23B_HUMAN	3 (2)	151.81	0.88	UV excision repair protein RAD23 homolog B	1.28	1
MBB1A_HUMAN	14 (4)	151.7	0.32	Myb-binding protein 1A	1	1.91
ML12A_HUMAN	4 (1)	151.09	0.02	Myosin regulatory light chain 12A	12.07	1
H1X_HUMAN	5 (1)	149.21	1	Histone H1x	1.18	1
PURA_HUMAN	4 (2)	148.97	0.46	Transcriptional activator protein Pur-alpha	1	1.89
GNA11_HUMAN	7 (1)	148.6	7.25E-03	Guanine nucleotide-binding protein subunit alpha-11	2.48	1
ITAV_HUMAN	9 (4)	148.57	0.07	Integrin alpha-V	1	2.84
ABCA4_HUMAN	25 (5)	148.12	0.18	Retinal-specific ATP-binding cassette transporter	1	3.73
PSB5_HUMAN	4 (2)	147.49	0.87	Proteasome subunit beta type-5	1.27	1
RPAC1_HUMAN	4 (2)	146.92	0.05	DNA-directed RNA polymerases I and III subunit RPAC1	1	4.53
PP1B_HUMAN	5 (1)	146.79	0.22	Serine/threonine-protein phosphatase PP1-beta catalytic subunit	1	1.43
DHRS4_HUMAN	9 (3)	146.48	0.75	Dehydrogenase/reductase SDR family member 4	1.24	1
CKAP5_HUMAN	17 (1)	145.7	0.06	Cytoskeleton-associated protein 5	4.95	1
DC1I2_HUMAN	4 (1)	145.68	0.9	Cytoplasmic dynein 1 intermediate chain 2	1.09	1
PGRC2_HUMAN	4 (1)	145.16	0.16	Membrane-associated progesterone receptor component 2	1	1.31
IF6_HUMAN	2 (2)	144.95	0.41	Eukaryotic translation initiation factor 6	1	1.15
ACOX1_HUMAN	9 (1)	143.53	0.31	Peroxisomal acyl-coenzyme A oxidase 1	1.37	1
ICAL_HUMAN	7 (3)	143.34	0.22	Calpastatin	1.33	1
FUBP3_HUMAN	6 (1)	142.67	0.05	Far upstream element-binding protein 3	1	13.78
ATPK_HUMAN	2 (1)	142.62	0.64	ATP synthase subunit f, mitochondrial	1.17	1
RS23_HUMAN	3 (1)	142.53	0.04	40S ribosomal protein S23	3.27	1
GFAP_HUMAN	11 (2)	142.45	6.63E-03	Glial fibrillary acidic protein	1	2.8
SYK_HUMAN	8 (4)	142.15	0.02	Lysine--tRNA ligase	1	1.78
GTR14_HUMAN	5 (1)	141.92	0.07	Solute carrier family 2, facilitated glucose transporter member 14	1	10.52
IF5_HUMAN	4 (2)	141.46	0.46	Eukaryotic translation initiation factor 5	1.26	1
SRP72_HUMAN	4 (1)	141.35	0.68	Signal recognition particle subunit SRP72	1.02	1

ICAM3_HUMAN	3 (1)	141.01	7.91E-03	Intercellular adhesion molecule 3	0	∞
ACTN2_HUMAN	6 (1)	140.52	5.61E-03	Alpha-actinin-2	6.11	1
MCM7_HUMAN	11 (2)	140.34	0.63	DNA replication licensing factor MCM7	1.08	1
RSU1_HUMAN	7 (2)	140.13	0.35	Ras suppressor protein 1	1	1.38
EIF3M_HUMAN	3 (2)	139.95	0.08	Eukaryotic translation initiation factor 3 subunit M	1	23.84
CYB5B_HUMAN	3 (2)	139.28	0.97	Cytochrome b5 type B	12.06	1
MIC19_HUMAN	7 (1)	138.94	0.06	MICOS complex subunit MIC19	5.65	1
OLA1_HUMAN	3 (1)	138.45	0.47	Obg-like ATPase 1	1	1.2
KTNB1_HUMAN	10 (2)	137.31	0.03	Katanin p80 WD40 repeat-containing subunit B1	1	4.7
SF3B1_HUMAN	10 (2)	137.28	0.36	Splicing factor 3B subunit 1	1	2.16
KPYR_HUMAN	7 (2)	136.37	0.01	Pyruvate kinase PKLR	1	2.17
RL28_HUMAN	8 (3)	136.24	6.81E-03	60S ribosomal protein L28	6.61	1
ARPC4_HUMAN	5 (4)	135.37	0.71	Actin-related protein 2/3 complex subunit 4	1.15	1
RU1C_HUMAN	2 (2)	135.34	0.53	U1 small nuclear ribonucleoprotein C	1	1.1
AT1B1_HUMAN	3 (2)	135.2	0.56	Sodium/potassium-transporting ATPase subunit beta-1	1.18	1
MICA3_HUMAN	17 (1)	133.66	0.5	[F-actin]-methionine sulfoxide oxidase MICAL3	2.63	1
SC24C_HUMAN	14 (1)	133.66	0.39	Protein transport protein Sec24C	5.56	1
MFAP1_HUMAN	10 (3)	133.3	0.13	Microfibrillar-associated protein 1	1	1.66
IF4G3_HUMAN	10 (2)	133.18	0.38	Eukaryotic translation initiation factor 4 gamma 3	1	1.33
IF1AY_HUMAN	5 (3)	132.54	0.05	Eukaryotic translation initiation factor 1A, Y-chromosomal	6.63	1
RBM25_HUMAN	8 (1)	131.76	0.4	RNA-binding protein 25	1	2.26
MAST4_HUMAN	23 (3)	131.75	0.28	Microtubule-associated serine/threonine-protein kinase 4	1	1.7
H2AY_HUMAN	6 (1)	131.68	0.17	Core histone macro-H2A.1	1	2.69
DNJB1_HUMAN	5 (2)	131.66	0.11	DnaJ homolog subfamily B member 1	2.37	1
CDK1_HUMAN	6 (1)	131.4	0.37	Cyclin-dependent kinase 1	20.73	1
DDX46_HUMAN	16 (3)	131.16	0.51	Probable ATP-dependent RNA helicase DDX46	1	1.41
PGAM5_HUMAN	5 (1)	131.08	0.96	Serine/threonine-protein phosphatase PGAM5, mitochondrial	1.07	1
IPYR_HUMAN	2 (1)	130.77	0.84	Inorganic pyrophosphatase	1.44	1
NIPS2_HUMAN	6 (2)	130.73	0.03	Protein NipSnap homolog 2	1	3.01
PSB3_HUMAN	5 (5)	130.16	2.26E-04	Proteasome subunit beta type-3	1	2.57
ATX2L_HUMAN	14 (3)	130.11	0.09	Ataxin-2-like protein	1	2.8
RB11A_HUMAN	3 (2)	129.67	0.63	Ras-related protein Rab-11A	2.55	1
NHRF1_HUMAN	5 (2)	129.17	0.04	Na(+)/H(+) exchange regulatory cofactor NHE-RF1	1.5	1
SRRM2_HUMAN	22 (3)	128.98	0.06	Serine/arginine repetitive matrix protein 2	1	5.14
PSB6_HUMAN	3 (3)	128.88	0.03	Proteasome subunit beta type-6	2.17	1
S38A2_HUMAN	3 (2)	128.37	0.05	Sodium-coupled neutral amino acid transporter 2	2.24	1
IF2B2_HUMAN	3 (1)	128.3	0.44	Insulin-like growth factor 2 mRNA-binding protein 2	1	6.23
MARC1_HUMAN	5 (1)	128.26	0.21	Mitochondrial amidoxime-reducing component 1	3.46	1
TOM34_HUMAN	6 (1)	127.24	0.83	Mitochondrial import receptor subunit TOM34	1.11	1
ODO2_HUMAN	7 (2)	127.21	0.27	Dihydrolipoyllysine-residue succinyltransferase component of 2-oxoglutarate dehydrogenase complex, mitochondrial	1	1.64
RBM28_HUMAN	13 (3)	127.16	0.04	RNA-binding protein 28	1	6.32
VAT1_HUMAN	6 (3)	126.98	0.54	Synaptic vesicle membrane protein VAT-1 homolog	1.31	1
IF4G2_HUMAN	15 (4)	126.31	7.60E-03	Eukaryotic translation initiation factor 4 gamma 2	1	1.5
PYM1_HUMAN	3 (3)	126.2	0.4	Partner of Y14 and mago	1	1.19
CO7A1_HUMAN	18 (2)	125.96	0.28	Collagen alpha-1(VII) chain	1.72	1
PSA3_HUMAN	8 (5)	125.62	0.49	Proteasome subunit alpha type-3	1	1.21
RYR3_HUMAN	27 (1)	125.21	0.52	Ryanodine receptor 3	4.04	1
ARF5_HUMAN	4 (1)	124.92	0.38	ADP-ribosylation factor 5	21.59	1
CCD51_HUMAN	7 (3)	124.29	0.17	Coiled-coil domain-containing protein 51	1	3.21
CLPP_HUMAN	7 (1)	124.15	0.06	ATP-dependent Clp protease proteolytic subunit, mitochondrial	1	3.86
GOGA4_HUMAN	15 (1)	124.09	0.97	Golgin subfamily A member 4	1	1.08
STRAP_HUMAN	3 (2)	124.04	0.38	Serine-threonine kinase receptor-associated protein	1	1.42
MYO7A_HUMAN	17 (2)	123.88	0.75	Unconventional myosin-VIIa	1.48	1
TOP2B_HUMAN	13 (1)	123.76	0.82	DNA topoisomerase 2-beta	1	4.11
CAZA1_HUMAN	2 (1)	123.51	0.51	F-actin-capping protein subunit alpha-1	1	1.15
TFAM_HUMAN	6 (1)	123.45	0.44	Transcription factor A, mitochondrial	1.86	1
HEXB_HUMAN	4 (2)	123.19	0.4	Beta-hexosaminidase subunit bet	1	1.33
ODP2_HUMAN	10 (2)	122.69	6.46E-04	Dihydrolipoyllysine-residue acetyltransferase component of pyruvate dehydrogenase complex, mitochondrial	1	7.46

DDRGK_HUMAN	4 (2)	121.99	0.43	DDRGK domain-containing protein 1	2.23	1
GOGB1_HUMAN	14 (1)	121.56	0.44	Golgin subfamily B member 1	1.13	1
ACACB_HUMAN	14 (1)	120.45	0.25	Acetyl-CoA carboxylase 2	1	3.08
H2AW_HUMAN	7 (1)	120.32	0.05	Core histone macro-H2A.2	1	2.49
NEP1_HUMAN	5 (1)	120.27	0.98	Ribosomal RNA small subunit methyltransferase NEP1	1.42	1
IMA1_HUMAN	5 (3)	119.95	0.11	Importin subunit alpha-1	1	3.7
STOM_HUMAN	5 (2)	119.77	0.15	Erythrocyte band 7 integral membrane protein	1	18.22
RT07_HUMAN	2 (1)	119.63	0.48	28S ribosomal protein S7, mitochondrial	1	1
TIAR_HUMAN	4 (1)	119.36	0.97	Nucleolysin TIAR	1	2.05
PSB2_HUMAN	6 (3)	119.35	0.2	Proteasome subunit beta type-2	1.61	1
RALY_HUMAN	6 (1)	118.97	0.02	RNA-binding protein Raly	1	5.1
FLII_HUMAN	10 (2)	118.93	0.02	Protein flightless-1 homolog	2.18	1
MSH6_HUMAN	11 (5)	118.2	0.16	DNA mismatch repair protein Msh6	1	8.22
PCH2_HUMAN	2 (1)	118.15	0.25	Pachytene checkpoint protein 2 homolog	7.58	1
MARCS_HUMAN	2 (1)	117.55	6.36E-04	Myristoylated alanine-rich C-kinase substrate	270.53	1
SYWC_HUMAN	3 (1)	117.04	0.42	Tryptophan--tRNA ligase, cytoplasmic	1.29	1
PCNA_HUMAN	8 (2)	116.82	0.5	Proliferating cell nuclear antigen	1.03	1
RMD3_HUMAN	9 (2)	116.64	6.80E-03	Regulator of microtubule dynamics protein 3	5.7	1
OTOG_HUMAN	6 (3)	116.57	0.64	Otogelin	1.5	1
DRG1_HUMAN	6 (1)	116.5	0.02	Developmentally-regulated GTP-binding protein 1	1	50.95
BLK_HUMAN	9 (2)	116.46	0.04	Tyrosine-protein kinase Blk	1	3.13
HAP28_HUMAN	4 (3)	116.44	0.06	28 kDa heat- and acid-stable phosphoprotein	1	1.93
PRS56_HUMAN	4 (2)	116.16	0.2	Serine protease 56	6.15	1
RAP2A_HUMAN	2 (1)	115.55	0.03	Ras-related protein Rap-2a	58.29	1
RFC4_HUMAN	6 (2)	115.11	0.06	Replication factor C subunit 4	1	2.16
RL36_HUMAN	7 (1)	114.38	0.08	60S ribosomal protein L36	2.19	1
RS27_HUMAN	4 (2)	113.54	0.77	40S ribosomal protein S27	1	1.4
NUDC_HUMAN	4 (2)	113.04	0.02	Nuclear migration protein nudC	11.31	1
CHMP5_HUMAN	3 (1)	113.02	0.36	Charged multivesicular body protein 5	2.88	1
1B35_HUMAN	2 (1)	112.88	0.81	HLA class I histocompatibility antigen, B-35 alpha chain	13.98	1
DIC_HUMAN	4 (1)	112.39	0.31	Mitochondrial dicarboxylate carrier	58.45	1
RSMB_HUMAN	6 (2)	112.31	0.08	Small nuclear ribonucleoprotein-associated proteins B and B'	1	3.99
MAP1A_HUMAN	16 (1)	112.29	0.99	Microtubule-associated protein 1A 6	1.17	1
AP3B1_HUMAN	10 (3)	112.27	2.03E-03	AP-3 complex subunit beta-1	1	4
AP180_HUMAN	7 (3)	112.18	0.15	Clathrin coat assembly protein AP180	1	3.5
RAB6B_HUMAN	4 (1)	111.88	0.58	Ras-related protein Rab-6B	1	1.31
RL23_HUMAN	2 (2)	111.78	0.25	60S ribosomal protein L23	10.97	1
TIM23_HUMAN	2 (1)	111.04	0.77	Mitochondrial import inner membrane translocase subunit Tim23	1.99	1
DTD1_HUMAN	4 (1)	110.71	0.17	D-tyrosyl-tRNA(Tyr) deacylase 1	1	23.95
TLN2_HUMAN	13 (2)	110.49	0.41	Talin-2	1.17	1
ATP9B_HUMAN	11 (2)	110.01	0.53	Probable phospholipid-transporting ATPase IIB	1	1.76
RU17_HUMAN	7 (2)	109.97	0.42	U1 small nuclear ribonucleoprotein 70 kDa	1.18	1
CAPZB_HUMAN	4 (2)	109.72	0.69	F-actin-capping protein subunit beta	1	1.09
ZCH18_HUMAN	10 (2)	109.62	0.07	Zinc finger CCCH domain-containing protein 18	5.95	1
RM28_HUMAN	5 (1)	109.59	0.19	39S ribosomal protein L28, mitochondrial	1	4.23
FRIL_HUMAN	3 (1)	109.29	9.20E-03	Ferritin light chain	1.34	1
DNLI3_HUMAN	9 (3)	108.96	0.24	DNA ligase 3	5.62	1
RGPD1_HUMAN	18 (2)	108.86	0.47	RANBP2-like and GRIP domain-containing protein 1	1.16	1
NAT10_HUMAN	5 (1)	108.83	0.3	RNA cytidine acetyltransferase	3.02	1
MOV10_HUMAN	8 (1)	108.66	0.69	Putative helicase MOV-10	1	1.23
RM11_HUMAN	5 (2)	108.5	0.34	39S ribosomal protein L11, mitochondrial	1	1.4
RNBP6_HUMAN	11 (1)	108.21	0.11	Ran-binding protein 6	1	4.6
E2AK2_HUMAN	9 (1)	108	0.16	Interferon-induced, double-stranded RNA-activated protein kinase	1	1.8
TECR_HUMAN	6 (3)	107.71	0.2	Very-long-chain enoyl-CoA reductase	3.05	1
AKAP1_HUMAN	4 (1)	107.7	0.72	A-kinase anchor protein 1, mitochondrial	2.95	1
PLCA_HUMAN	11 (5)	107.62	3.40E-03	1-acyl-sn-glycerol-3-phosphate acyltransferase alpha	1	3.33
AP3D1_HUMAN	8 (2)	107.6	0.01	AP-3 complex subunit delta-1	3.13	1
TRPM7_HUMAN	19 (4)	107.51	5.84E-03	Transient receptor potential cation channel subfamily M member 7	3.18	1

PIWL4_HUMAN	12 (2)	107.11	0.52	Piwi-like protein 4	1	1.06
UBP10_HUMAN	4 (1)	106.59	0.29	Ubiquitin carboxyl-terminal hydrolase 10	2.33	1
AL3A2_HUMAN	4 (1)	105.87	6.13E-03	Fatty aldehyde dehydrogenase	4.38	1
OCAD1_HUMAN	3 (1)	105.63	0.81	OCIA domain-containing protein 1	1.13	1
VTNC_HUMAN	2 (2)	105.39	0.8	Vitronectin	1.08	1
KAD4_HUMAN	4 (2)	105.04	0.49	Adenylate kinase 4, mitochondrial	1	1.25
ACAD9_HUMAN	5 (1)	104.58	0.44	Acyl-CoA dehydrogenase family member 9, mitochondrial	8.51	1
ACSL3_HUMAN	3 (2)	104.53	1.36E-04	Long-chain-fatty-acid--CoA ligase 3	4.81	1
U2AF1_HUMAN	7 (1)	104.52	0.14	Splicing factor U2AF 35 kDa subunit	1	2.61
DDX50_HUMAN	7 (1)	104.33	0.18	ATP-dependent RNA helicase DDX50	1	5.91
SMD1_HUMAN	5 (1)	103.74	0.81	Small nuclear ribonucleoprotein Sm D1	16.02	1
NUCB2_HUMAN	3 (3)	103.49	0.9	Nucleobindin-2	1	1.29
SRPRB_HUMAN	6 (1)	103.32	0.19	Signal recognition particle receptor subunit beta	1	2.8
IMA3_HUMAN	4 (3)	103.02	0.35	Importin subunit alpha-3	1.29	1
LARP4_HUMAN	4 (1)	102.96	0.13	La-related protein 4	1	1.52
RM39_HUMAN	5 (1)	102.93	0.11	39S ribosomal protein L39, mitochondrial	141.41	1
NDUA8_HUMAN	3 (1)	102.67	0.37	NADH dehydrogenase [ubiquinone] 1 alpha subcomplex subunit 8	2.84	1
PADI1_HUMAN	8 (2)	101.94	0.44	Protein-arginine deiminase type-1	3.72	1
IDHP_HUMAN	6 (2)	101.37	0.48	Isocitrate dehydrogenase [NADP], mitochondrial	1	11.95
TCOF_HUMAN	11 (2)	101.3	0.77	Treacle protein	1	2.1
SNRPA_HUMAN	2 (2)	101.07	2.28E-04	U1 small nuclear ribonucleoprotein A	1	10.58
SYRC_HUMAN	10 (3)	100.72	0.05	Arginine--tRNA ligase, cytoplasmic	1	8.12
NDUBA_HUMAN	3 (2)	100.71	0.81	NADH dehydrogenase [ubiquinone] 1 beta subcomplex subunit 10	1.09	1
GRSF1_HUMAN	6 (3)	100.51	5.52E-03	G-rich sequence factor 1	1	5.48
EIF3H_HUMAN	6 (2)	100.36	0.08	Eukaryotic translation initiation factor 3 subunit H	1	6.54
CATZ_HUMAN	2 (1)	100.27	0.38	Cathepsin Z	1.15	1
PSD12_HUMAN	6 (3)	100.15	0.02	26S proteasome non-ATPase regulatory subunit 12	5.72	1
FYN_HUMAN	7 (1)	100.04	0.94	Tyrosine-protein kinase Fyn	1.02	1
TIA1_HUMAN	2 (2)	99.96	3.14E-03	Nucleolysin TIA-1 isoform p40	2.07	1
PSME1_HUMAN	8 (2)	99.66	0.05	Proteasome activator complex subunit 1	5.33	1
PEBP1_HUMAN	1 (1)	99.54	0.77	Phosphatidylethanolamine-binding protein 1	1.66	1
PEF1_HUMAN	2 (1)	99.26	0.62	Peflin	1	1.02
PAP1M_HUMAN	7 (1)	99.13	0.38	Polyadenylate-binding protein 1-like 2	10.71	1
ATD3A_HUMAN	6 (1)	99.08	0.2	ATPase family AAA domain-containing protein 3A	292.84	1
NOMO2_HUMAN	3 (1)	98.87	0.31	Nodal modulator 2	5.47	1
ABCCB_HUMAN	9 (3)	98.07	0.6	ATP-binding cassette sub-family C member 11	1.04	1
IPO7_HUMAN	6 (4)	97.89	0.13	Importin-7	1.57	1
DHX29_HUMAN	7 (2)	97.82	0.93	ATP-dependent RNA helicase DHX29	1	4.09
RALB_HUMAN	3 (2)	97.74	0.31	Ras-related protein Ral-B	1.9	1
ACTL8_HUMAN	4 (1)	97.69	0.2	Actin-like protein 8	1	7.44
CDC37_HUMAN	3 (1)	97.24	0.34	Hsp90 co-chaperone Cdc37	3.16	1
APT_HUMAN	5 (3)	97.08	0.54	Adenine phosphoribosyltransferase	1.98	1
NDUAA_HUMAN	3 (1)	96.75	0.65	NADH dehydrogenase [ubiquinone] 1 alpha subcomplex subunit 10, mitochondrial	1	1.05
DAF_HUMAN	2 (1)	96.66	4.65E-03	Complement decay-accelerating factor	2.7	1
RM13_HUMAN	2 (2)	96.19	0.55	39S ribosomal protein L13, mitochondrial	1	1.1
COR1C_HUMAN	5 (2)	95.09	0.01	Coronin-1C	3.65	1
NDUV1_HUMAN	6 (3)	94.76	0.99	NADH dehydrogenase [ubiquinone] flavoprotein 1, mitochondrial	1.1	1
DCTN1_HUMAN	11 (2)	94.66	0.37	Dynactin subunit 1	1	1.27
NAA50_HUMAN	3 (2)	94.15	0.17	N-alpha-acetyltransferase 50	11.53	1
G6PD_HUMAN	5 (3)	94.08	0.68	Glucose-6-phosphate 1-dehydrogenase	1	2.03
ERBB2_HUMAN	6 (1)	93.98	0.16	Receptor tyrosine-protein kinase erbB-2	1.57	1
LAMB1_HUMAN	15 (1)	93.92	0.63	Laminin subunit beta-1	1	7.01
ATX10_HUMAN	5 (2)	93.55	0.83	Ataxin-10 OS=Homo sapiens	1	2.66
JAM1_HUMAN	5 (2)	93.24	0.13	Junctional adhesion molecule A	3.87	1
PON2_HUMAN	2 (1)	93.23	0.29	Serum paraoxonase/arylesterase 2	1.81	1
VPS35_HUMAN	6 (1)	93.08	0.24	Vacuolar protein sorting-associated protein 35	2.16	1
PSB7_HUMAN	5 (4)	92.85	0.55	Proteasome subunit beta type-7	1	4.35
AP2A1_HUMAN	4 (1)	92.83	0.13	AP-2 complex subunit alpha-1	2.09	1

STML1_HUMAN	12 (2)	92.7	0.75	Stomatin-like protein 1	1	1.49
PLCB3_HUMAN	10 (1)	92.47	0.13	1-phosphatidylinositol 4,5-bisphosphate phosphodiesterase beta-3	2.22	1
AT11B_HUMAN	7 (2)	92.28	0.31	Probable phospholipid-transporting ATPase IF	1	1.61
NFH_HUMAN	7 (1)	91.57	0.09	Neurofilament heavy polypeptide	1	7.38
SDCB1_HUMAN	2 (1)	91.39	0.01	Syntenin-1	1.66	1
TAGL3_HUMAN	5 (1)	91.3	0.4	Transgelin-3	1	1.19
GGYF2_HUMAN	6 (1)	91.25	0.77	GRB10-interacting GYF protein 2	1.26	1
METK2_HUMAN	2 (1)	91.25	0.81	S-adenosylmethionine synthase isoform type-2	2.13	1
ARP3_HUMAN	2 (1)	91.18	0.67	Actin-related protein 3	1.36	1
LMNB2_HUMAN	6 (1)	90.91	0.26	Lamin-B2	1	3.91
RAC1_HUMAN	3 (2)	90.76	0.39	Ras-related C3 botulinum toxin substrate 1	1	1.29
CHTOP_HUMAN	5 (1)	90.44	0.28	Chromatin target of PRMT1 protein	1	2.42
SGO2_HUMAN	16 (3)	90.27	0.88	Shugoshin 2	1.21	1
TPP1_HUMAN	1 (1)	90	0.08	Tripeptidyl-peptidase 1	6.96	1
TF2B_HUMAN	6 (2)	89.83	0.82	Transcription initiation factor IIB	1.47	1
CCAR2_HUMAN	4 (3)	89.62	0.19	Cell cycle and apoptosis regulator protein 2	1	1.43
CDK3_HUMAN	5 (1)	89.54	0.36	Cyclin-dependent kinase 3	1.65	1
NDRG1_HUMAN	4 (2)	89.27	0.06	Protein NDRG1	1	1.96
RT28_HUMAN	3 (2)	89.23	0.09	28S ribosomal protein S28, mitochondrial	16.97	1
PSME2_HUMAN	5 (1)	89.14	0.04	Proteasome activator complex subunit 2	1	144.94
STX4_HUMAN	2 (1)	88.98	0.24	Syntaxin-4	1	2.9
PA1B3_HUMAN	4 (2)	88.51	0.25	Platelet-activating factor acetylhydrolase IB subunit gamma	1	1.43
DDX18_HUMAN	6 (1)	88.47	0.36	ATP-dependent RNA helicase DDX18	1	1.09
RT26_HUMAN	4 (1)	88.31	0.48	28S ribosomal protein S26, mitochondrial	5.69	1
MARE1_HUMAN	4 (3)	88.05	0.11	Microtubule-associated protein RP/EB family member 1	1	1.61
STXB3_HUMAN	10 (1)	88.04	0.05	Syntaxin-binding protein 3	20.94	1
HPPD_HUMAN	3 (3)	87.81	0.4	4-hydroxyphenylpyruvate dioxygenase	1	3.37
PRP6_HUMAN	7 (2)	87.66	0.17	Pre-mRNA-processing factor 6	1	2.25
TMED2_HUMAN	2 (1)	87.02	0.06	Transmembrane emp24 domain-containing protein 2	11.15	1
RANG_HUMAN	6 (1)	86.79	0.33	Ran-specific GTPase-activating protein	3.89	1
LG3BP_HUMAN	5 (2)	86.56	0.22	Galectin-3-binding protein	1	1.53
MCM5_HUMAN	6 (1)	86.26	0.3	DNA replication licensing factor MCM5	1	1.2
CPSF7_HUMAN	3 (2)	86.21	0.38	Cleavage and polyadenylation specificity factor subunit 7	1.38	1
AHRR_HUMAN	8 (1)	86.02	0.05	Aryl hydrocarbon receptor repressor	1	7.89
UFD1_HUMAN	2 (2)	85.33	0.56	Ubiquitin recognition factor in ER-associated degradation protein 1	7.2	1
SPB6_HUMAN	3 (2)	85.33	0.33	Serpin B6	12.34	1
KCY_HUMAN	3 (1)	85.25	0.03	UMP-CMP kinase	11.08	1
MCM2_HUMAN	6 (1)	85.17	0.02	DNA replication licensing factor MCM2	1	121.02
MPRI_HUMAN	9 (1)	85.1	0.43	Cation-independent mannose-6-phosphate receptor	1.24	1
AIMP2_HUMAN	3 (1)	84.94	0.44	Aminoacyl tRNA synthase complex-interacting multifunctional protein 2	1	1.68
SRSF5_HUMAN	5 (3)	84.11	0.05	Serine/arginine-rich splicing factor 5	4.51	1
EI2BB_HUMAN	6 (1)	83.92	0.37	Translation initiation factor eIF-2B subunit beta	1	17.46
RM44_HUMAN	2 (1)	83.7	0.09	39S ribosomal protein L44, mitochondrial	1	2.99
RT35_HUMAN	9 (3)	83.67	0.03	28S ribosomal protein S35, mitochondrial	2.13	1
ELOA1_HUMAN	8 (1)	83.67	0.16	Elongin-A	5.79	1
PLP2_HUMAN	2 (1)	83.3	0.01	Proteolipid protein 2	4.44	1
IF4E2_HUMAN	3 (1)	82.76	0.24	Eukaryotic translation initiation factor 4E type 2	11.89	1
G3PT_HUMAN	7 (2)	82.71	0.12	Glyceraldehyde-3-phosphate dehydrogenase, testis-specific	1	1.2
TPT1L_HUMAN	2 (1)	82.35	0.01	TPT1-like protein	1	61.75
SPD2A_HUMAN	12 (3)	82.16	0.85	SH3 and PX domain-containing protein 2A	1	2.2
NTPCR_HUMAN	2 (2)	82.13	0.24	Cancer-related nucleoside-triphosphatase	1	1.36
CAV1_HUMAN	4 (2)	81.93	0.09	Caveolin-1	2.23	1
ARP3B_HUMAN	5 (1)	81.76	0.16	Actin-related protein 3B	1	1.89
KAD1_HUMAN	3 (1)	81.34	0.08	Adenylate kinase isoenzyme 1	426.51	1
PO210_HUMAN	6 (2)	81.17	0.03	Nuclear pore membrane glycoprotein 210	10.56	1
FA98B_HUMAN	5 (1)	80.76	0.61	Protein FAM98B	1.26	1
SRSF8_HUMAN	5 (2)	80.72	0.65	Serine/arginine-rich splicing factor 8	2.27	1
VATA_HUMAN	3 (1)	80.63	0.69	V-type proton ATPase catalytic subunit A	1	1.33

IF4E_HUMAN	2 (2)	80.62	0.85	Eukaryotic translation initiation factor 4E	1.05	1
RAI3_HUMAN	2 (1)	80.44	0.04	Retinoic acid-induced protein 3	2.22	1
RT34_HUMAN	2 (1)	80.11	0.93	28S ribosomal protein S34, mitochondrial	1.65	1
PA24A_HUMAN	6 (1)	79.83	0.07	Cytosolic phospholipase A2	2.43	1
SF3A3_HUMAN	2 (1)	79.49	0.09	Splicing factor 3A subunit 3	1	1.8
GDIR1_HUMAN	1 (1)	79.49	0.83	Rho GDP-dissociation inhibitor 1	1.17	1
RSMN_HUMAN	6 (3)	79.31	0.18	Small nuclear ribonucleoprotein-associated protein N	1	1.98
CAPS2_HUMAN	10 (1)	79.09	0.21	Calcium-dependent secretion activator 2	2.59	1
ASPH_HUMAN	9 (2)	78.85	0.04	Aspartyl/asparaginyl beta-hydroxylase	1	6.98
GSTM3_HUMAN	3 (1)	78.85	0.47	Glutathione S-transferase Mu 3	2.21	1
P3H1_HUMAN	4 (1)	78.79	9.44E-03	Prolyl 3-hydroxylase 1	17.63	1
RM40_HUMAN	5 (1)	78.73	0.96	39S ribosomal protein L40, mitochondrial	1.19	1
DDX27_HUMAN	7 (3)	78.67	0.36	Probable ATP-dependent RNA helicase DDX27	1	1.21
UN45A_HUMAN	9 (4)	78.65	0.03	Protein unc-45 homolog A	5.38	1
TKFC_HUMAN	5 (2)	78.54	0.71	Triokinase/FMN cyclase	1	1.71
PDXK_HUMAN	4 (2)	78.46	0.17	Pyridoxal kinase	1	5.59
CIRBP_HUMAN	2 (1)	78.28	3.51E-03	Cold-inducible RNA-binding protein	10.7	1
TBG1_HUMAN	4 (1)	78.24	0.74	Tubulin gamma-1 chain	1.66	1
PUR6_HUMAN	5 (3)	78.15	0.42	Multifunctional protein ADE2	1	1.22
TRPM3_HUMAN	14 (4)	78.15	0.77	Transient receptor potential cation channel subfamily M member 3	1.1	1
THOC6_HUMAN	3 (1)	77.78	0.04	THO complex subunit 6 homolog	1	12.29
TMOD3_HUMAN	4 (1)	77.42	0.03	Tropomodulin-3	1	5.01
MTCH2_HUMAN	3 (2)	77.27	0.16	Mitochondrial carrier homolog 2	5.88	1
FKB10_HUMAN	5 (1)	77.22	0.52	Peptidyl-prolyl cis-trans isomerase FKBP10	1	1.21
ZN516_HUMAN	9 (2)	76.89	0.02	Zinc finger protein 516	1	3.66
NDUS7_HUMAN	3 (2)	76.67	0.78	NADH dehydrogenase [ubiquinone] iron-sulfur protein 7, mitochondrial	1.21	1
SEP11_HUMAN	7 (1)	76.45	0.03	Septin-11	7.32	1
RAP2C_HUMAN	2 (1)	76.32	0.46	Ras-related protein Rap-2c	5.4	1
SCO1_HUMAN	4 (2)	76.19	3.70E-03	Protein SCO1 homolog, mitochondrial	1	18.37
BYST_HUMAN	4 (1)	75.76	4.96E-04	Bystin	3.31	1
CTNA2_HUMAN	10 (1)	75.54	0.99	Catenin alpha-2	1	1.28
COPB2_HUMAN	6 (1)	75.44	0.07	Coatomer subunit beta'	7.53	1
SYNC_HUMAN	4 (2)	75.27	0.59	Asparagine--tRNA ligase, cytoplasmic	1.3	1
NSDHL_HUMAN	4 (1)	75.06	0.33	Sterol-4-alpha-carboxylate 3-dehydrogenase, decarboxylating	1	1.29
NMD3A_HUMAN	14 (2)	75.01	0.51	Glutamate receptor ionotropic, NMDA 3A	1.29	1
EPHB4_HUMAN	14 (4)	74.97	0.15	Ephrin type-B receptor 4	3.01	1
NAA15_HUMAN	4 (1)	74.95	1.35E-03	N-alpha-acetyltransferase 15, NatA auxiliary subunit	1	17.56
SP100_HUMAN	7 (3)	74.95	0.24	Nuclear autoantigen Sp-100 =3	2.27	1
MMAB_HUMAN	6 (2)	74.64	0.04	Cob(I)yrinic acid a,c-diamide adenosyltransferase, mitochondrial	2.15	1
FA50A_HUMAN	7 (1)	74.57	0.07	Protein FAM50A	14.59	1
AL7A1_HUMAN	4 (1)	74.2	0.72	Alpha-aminoadipic semialdehyde dehydrogenase	1	1.19
DUT_HUMAN	4 (2)	73.6	0.49	Deoxyuridine 5'-triphosphate nucleotidohydrolase, mitochondrial	1	1.36
SYIM_HUMAN	8 (2)	73.57	0.01	Isoleucine--tRNA ligase, mitochondrial	1	2.62
TIM44_HUMAN	3 (1)	73.52	0.02	Mitochondrial import inner membrane translocase subunit TIM44	1	3.84
DDX23_HUMAN	8 (1)	73.45	0.48	Probable ATP-dependent RNA helicase DDX23	1.17	1
SAM50_HUMAN	6 (1)	73.09	9.86E-04	Sorting and assembly machinery component 50 homolog	1	13.06
CSRP1_HUMAN	1 (1)	73.06	0.21	Cysteine and glycine-rich protein 1	6.37	1
OPA1_HUMAN	9 (1)	72.91	0.53	Dynamin-like 120 kDa protein, mitochondrial	1.35	1
S10A4_HUMAN	3 (2)	72.67	0.9	Protein S100-A4	1.64	1
ERLN2_HUMAN	3 (1)	72.52	0.22	Erlin-2	1	3.02
DREB_HUMAN	3 (2)	72.46	0.11	Drebrin	2.8	1
ACSL4_HUMAN	7 (1)	72.2	0.58	Long-chain-fatty-acid--CoA ligase 4	1	1.04
CALU_HUMAN	6 (2)	72.11	0.01	Calumenin	4.25	1
PP1G_HUMAN	6 (2)	72.09	0.14	Serine/threonine-protein phosphatase PP1-gamma catalytic subunit	1	5.4
NVL_HUMAN	7 (3)	72.08	0.07	Nuclear valosin-containing protein-like	2.32	1
RS30_HUMAN	2 (1)	72	0.04	40S ribosomal protein S30	1.58	1
OSTF1_HUMAN	3 (2)	71.76	0.13	Osteoclast-stimulating factor 1	1	8.26
DHTK1_HUMAN	4 (1)	71.68	0.34	Probable 2-oxoglutarate dehydrogenase E1 component DHKTD1, mitochondrial	12.95	1

WDR61_HUMAN	2 (1)	71.67	0.12	WD repeat-containing protein 61	∞	0
SCOT2_HUMAN	6 (1)	71.62	0.89	Succinyl-CoA:3-ketoacid coenzyme A transferase 2, mitochondrial	1.06	1
PTPM1_HUMAN	2 (1)	71.43	0.23	Phosphatidylglycerophosphatase and protein-tyrosine phosphatase 1	1	1.13
ZNT1_HUMAN	4 (2)	70.74	0.06	Zinc transporter 1	8.38	1
RT27_HUMAN	5 (2)	70.61	0.38	28S ribosomal protein S27, mitochondrial	1	1.37
RT22_HUMAN	3 (1)	70.47	0.03	28S ribosomal protein S22, mitochondrial	14.78	1
TM109_HUMAN	2 (1)	70.21	0.24	Transmembrane protein 109	2.85	1
LSM4_HUMAN	4 (1)	70.16	7.35E-03	U6 snRNA-associated Sm-like protein LSm4	1	35.46
CH033_HUMAN	3 (1)	69.93	0.16	UPF0488 protein C8orf33	1	13.29
MYO1E_HUMAN	4 (2)	69.79	0.14	Unconventional myosin-Ie	1.43	1
RS12_HUMAN	4 (1)	69.78	0.89	40S ribosomal protein S12	4.29	1
PSA4_HUMAN	3 (1)	69.6	0.78	Proteasome subunit alpha type-4	8.04	1
GOLP3_HUMAN	4 (2)	69.48	0.1	Golgi phosphoprotein 3	1	2.43
CSN4_HUMAN	5 (1)	68.94	0.17	COP9 signalosome complex subunit 4	1	228.7
TPM2_HUMAN	3 (1)	68.94	0.02	Tropomyosin beta chain	19.39	1
DCXR_HUMAN	5 (1)	68.69	0.24	L-xylulose reductase	58.69	1
MAGBA_HUMAN	5 (1)	68.34	0.31	Melanoma-associated antigen B10	1	2.14
PLK1_HUMAN	8 (4)	68.24	0.05	Serine/threonine-protein kinase PLK1	1	4.53
TR150_HUMAN	6 (2)	68.02	0.07	Thyroid hormone receptor-associated protein 3	1	37.48
SUMF2_HUMAN	3 (2)	67.84	0.12	Sulfatase-modifying factor 2	1	1.99
RAB6C_HUMAN	4 (1)	67.77	0.17	Ras-related protein Rab-6C	1	3.44
NNRE_HUMAN	3 (1)	67.57	0.31	NAD(P)H-hydrate epimerase	1	1.07
RAPH1_HUMAN	5 (2)	67.47	0.26	Ras-associated and pleckstrin homology domains-containing protein 1	1	1.99
TAU_HUMAN	4 (1)	67.43	0.07	Microtubule-associated protein tau	1.85	1
PDC10_HUMAN	2 (1)	67.36	0.01	Programmed cell death protein 10	3.36	1
BCAT2_HUMAN	2 (1)	67.25	0.08	Branched-chain-amino-acid aminotransferase, mitochondrial	5.43	1
PLRG1_HUMAN	3 (1)	67.13	0.21	Pleiotropic regulator 1	5.34	1
GTPB1_HUMAN	6 (1)	67.09	0.05	GTP-binding protein 1	1	2.96
1B44_HUMAN	4 (1)	66.67	0.04	HLA class I histocompatibility antigen, B-44 alpha chain	1	22.29
SMD3_HUMAN	4 (1)	66.64	0.05	Small nuclear ribonucleoprotein Sm D3	11.8	1
NDUS2_HUMAN	4 (1)	66.38	0.58	NADH dehydrogenase [ubiquinone] iron-sulfur protein 2, mitochondrial	1	4.05
TMED7_HUMAN	1 (1)	66.37	0.64	Transmembrane emp24 domain-containing protein 7	1	1.38
SRS10_HUMAN	2 (1)	66.25	0.14	Serine/arginine-rich splicing factor 10	1	32.51
UBR5_HUMAN	7 (2)	66.23	0.21	E3 ubiquitin-protein ligase UBR5	2.93	1
EAA1_HUMAN	2 (1)	65.64	0.63	Excitatory amino acid transporter 1	1.19	1
MOGS_HUMAN	4 (1)	65.57	4.85E-03	Mannosyl-oligosaccharide glucosidase	129.19	1
C1TM_HUMAN	6 (2)	65.48	0.82	Monofunctional C1-tetrahydrofolate synthase, mitochondrial	1	1.04
PGRC1_HUMAN	1 (1)	65.39	0.12	Membrane-associated progesterone receptor component 1	1	∞
IQGA2_HUMAN	8 (1)	65.31	0.21	Ras GTPase-activating-like protein IQGAP2	1	18.77
APMAP_HUMAN	2 (1)	64.86	0.04	Adipocyte plasma membrane-associated protein	3.49	1
EXOS6_HUMAN	3 (1)	64.85	0.05	Exosome complex component MTR3	1	8.2
EXOS8_HUMAN	3 (2)	64.85	0.6	Exosome complex component RRP43	1.42	1
RBGPR_HUMAN	3 (1)	64.22	0.32	Rab3 GTPase-activating protein non-catalytic subunit	1	2.81
CATA_HUMAN	4 (1)	63.97	0.32	Catalase OS	5.85	1
BLVRB_HUMAN	3 (1)	63.75	0.66	Flavin reductase (NADPH)	1	4.5
AN32A_HUMAN	1 (1)	63.35	0.39	Acidic leucine-rich nuclear phosphoprotein 32 family member A	3.18	1
TTC37_HUMAN	11 (2)	63.25	0.13	Tetratricopeptide repeat protein 37	1	3.3
NU214_HUMAN	8 (1)	62.71	0.18	Nuclear pore complex protein Nup214	1	35.39
SEPT6_HUMAN	9 (1)	62.47	0.46	Septin-6	2.08	1
IFRD2_HUMAN	1 (1)	62.38	0.48	Interferon-related developmental regulator 2	17.23	1
RALYL_HUMAN	4 (1)	61.99	0.37	RNA-binding Raly-like protein	10.49	1
LYPA1_HUMAN	3 (1)	61.98	0.21	Acyl-protein thioesterase 1	1.79	1
HELQ_HUMAN	7 (1)	61.82	0.12	Helicase POLQ-like	1	11.32
NHP2_HUMAN	2 (1)	61.74	0.49	H/ACA ribonucleoprotein complex subunit 2	1	1.67
PEX1_HUMAN	9 (4)	61.48	0.99	Peroxisome biogenesis factor 1	1.78	1
MYPT1_HUMAN	6 (1)	61.47	0.06	Protein phosphatase 1 regulatory subunit 12A	6.91	1
SYYM_HUMAN	3 (1)	61.31	0.79	Tyrosine--tRNA ligase, mitochondrial	2.31	1
CALM1_HUMAN	3 (3)	61.28	0.41	Calmodulin-1	1	1.27

SYDM_HUMAN	2 (1)	61.25	0.71	Aspartate--tRNA ligase, mitochondrial	1.74	1
RO60_HUMAN	7 (1)	61.22	0.95	60 kDa SS-A/Ro ribonucleoprotein	2.55	1
MCM6_HUMAN	4 (2)	61.17	1.47E-03	DNA replication licensing factor MCM6	1	3.03
MIMIT_HUMAN	3 (1)	61.11	0.24	Mimitin, mitochondrial	8.05	1
THOC1_HUMAN	4 (1)	60.74	0.17	THO complex subunit 1	1	3.88
NIP7_HUMAN	2 (1)	60.45	0.17	60S ribosome subunit biogenesis protein NIP7 homolog	1	223.4
DNJC7_HUMAN	7 (1)	60.45	0.17	DnaJ homolog subfamily C member 7	1	1.75
ARL2_HUMAN	4 (1)	59.88	0.02	ADP-ribosylation factor-like protein 2	6	1
CC146_HUMAN	8 (1)	59.71	0.02	Coiled-coil domain-containing protein 146	39.53	1
VWF_HUMAN	10 (3)	59.53	0.02	von Willebrand factor	1	11.71
EFHD2_HUMAN	3 (2)	59.49	0.79	EF-hand domain-containing protein D2	2.03	1
FAF2_HUMAN	2 (1)	59.34	7.64E-04	FAS-associated factor 2	2.03	1
SRPRA_HUMAN	6 (2)	58.89	3.49E-03	Signal recognition particle receptor subunit alpha	8.58	1
EMC1_HUMAN	4 (1)	58.85	0.1	ER membrane protein complex subunit 1	1	18.36
M2OM_HUMAN	5 (1)	58.77	0.57	Mitochondrial 2-oxoglutarate/malate carrier protein	2.66	1
LGUL_HUMAN	1 (1)	58.65	0.29	Lactoylglutathione lyase	37.16	1
IPYR2_HUMAN	1 (1)	58.42	0.94	Inorganic pyrophosphatase 2, mitochondrial	1	1.55
ZCCHL_HUMAN	3 (1)	58.4	0.94	Zinc finger CCCH-type antiviral protein 1-like	1.01	1
FAM74_HUMAN	3 (1)	58.08	0.76	Protein FAM74A4/A6	22.66	1
VAPA_HUMAN	3 (1)	58	0.88	Vesicle-associated membrane protein-associated protein A	1.09	1
VAPB_HUMAN	2 (1)	57.78	0.01	Vesicle-associated membrane protein-associated protein B/C	1	8.52
EMAL4_HUMAN	8 (1)	57.68	0.45	Echinoderm microtubule-associated protein-like 4	1	1.27
MYL6_HUMAN	4 (1)	57.04	0.07	Myosin light polypeptide 6	61.91	1
MIC25_HUMAN	2 (1)	56.9	0.77	MICOS complex subunit MIC25	3.72	1
K1671_HUMAN	7 (1)	56.81	0.55	Uncharacterized protein KIAA1671	16.95	1
PSMD8_HUMAN	5 (1)	56.78	0.06	26S proteasome non-ATPase regulatory subunit 8	1	46.31
NSF_HUMAN	5 (1)	56.67	0.3	Vesicle-fusing ATPase	1	1.2
SQOR_HUMAN	6 (2)	56.34	1.48E-03	Sulfide:quinone oxidoreductase, mitochondrial	8.98	1
TTC33_HUMAN	4 (1)	56.16	0.05	Tetratricopeptide repeat protein 33	1	8.55
ERP44_HUMAN	4 (1)	55.99	0.57	Endoplasmic reticulum resident protein 44	1	2.78
CUL5_HUMAN	7 (1)	55.77	0.02	Cullin-5	1.7	1
NNTM_HUMAN	5 (2)	55.75	0.1	NAD(P) transhydrogenase, mitochondrial	1	1.64
T126A_HUMAN	2 (1)	55.31	0.81	Transmembrane protein 126A	3.14	1
RT29_HUMAN	4 (3)	55.19	0.81	28S ribosomal protein S29, mitochondrial	1.09	1
RS26L_HUMAN	3 (1)	54.97	0.1	Putative 40S ribosomal protein S26-like 1	6.07	1
SDF2L_HUMAN	1 (1)	54.66	0.14	Stromal cell-derived factor 2-like protein 1	1	3.17
SNP29_HUMAN	1 (1)	54.38	0.01	Synaptosomal-associated protein 29	1	50.45
TBCK_HUMAN	7 (1)	54.08	0.18	TBC domain-containing protein kinase-like protein	1	55
SNP23_HUMAN	4 (1)	54.06	0.41	Synaptosomal-associated protein 23	1	1.18
AATC_HUMAN	2 (1)	53.49	0.19	Aspartate aminotransferase, cytoplasmic	1	4.06
IDH3G_HUMAN	4 (1)	53.31	0.27	Isocitrate dehydrogenase [NAD] subunit gamma, mitochondrial	1	4.77
HYEP_HUMAN	5 (3)	53.28	0.02	Epoxide hydrolase 1	1	5.65
ITPA_HUMAN	2 (1)	53	0.18	Inosine triphosphate pyrophosphatase	11.84	1
RTN3_HUMAN	6 (1)	52.94	0.51	Reticulon-3	1	1.19
GPX8_HUMAN	3 (1)	52.88	0.05	Probable glutathione peroxidase 8	1.78	1
RRP12_HUMAN	5 (2)	52.6	0.17	RRP12-like protein	1	2.09
RL30_HUMAN	4 (1)	52.59	0.27	60S ribosomal protein L30	1.57	1
HVCN1_HUMAN	5 (3)	52.55	0.92	Voltage-gated hydrogen channel 1	1	2.19
AT2B1_HUMAN	8 (2)	52.51	0.14	Plasma membrane calcium-transporting ATPase 1	1	3.69
EIF3G_HUMAN	3 (1)	52.44	0.08	Eukaryotic translation initiation factor 3 subunit G	2.99	1
FAHD1_HUMAN	2 (2)	52.39	0.04	Acylpyruvase FAHD1, mitochondrial	4.51	1
CN37_HUMAN	4 (3)	52.3	0.88	2',3'-cyclic-nucleotide 3'-phosphodiesterase	1	1.15
CRTAP_HUMAN	3 (1)	52.09	0.59	Cartilage-associated protein	1.77	1
PWP2_HUMAN	6 (1)	52.07	0.19	Periodic tryptophan protein 2 homolog	1	2914.25
COASY_HUMAN	4 (1)	51.96	0.53	Bifunctional coenzyme A synthase	1	1.18
VA0D1_HUMAN	3 (3)	51.95	0.19	V-type proton ATPase subunit d 1	1	1.71
RAB31_HUMAN	2 (1)	51.72	0.6	Ras-related protein Rab-31	1.42	1
CCHL_HUMAN	2 (2)	51.37	0.45	Cytochrome c-type heme lyase	1	3.01

FCHO1_HUMAN	6 (2)	51.17	0.47	F-BAR domain only protein 1	1.8	1
ATP6_HUMAN	1 (1)	51.16	0.08	ATP synthase subunit a	17.48	1
ILVBL_HUMAN	1 (1)	50.79	0.33	Acetolactate synthase-like protein	1.71	1
NAA20_HUMAN	3 (1)	50.51	0.16	N-alpha-acetyltransferase 20	1	1.53
REEP6_HUMAN	1 (1)	50.51	0.02	Receptor expression-enhancing protein 6	1	76.75
MTA2_HUMAN	2 (1)	50.2	0.9	Metastasis-associated protein MTA2	1	1.15
UTP20_HUMAN	9 (1)	49.98	0.09	Small subunit processome component 20 homolog	1	204.62
ZC3H4_HUMAN	5 (2)	49.84	0.45	Zinc finger CCCH domain-containing protein 4	1	1.13
LEG12_HUMAN	3 (1)	49.82	0.43	Galectin-12	2.5	1
RTCA_HUMAN	3 (2)	49.09	0.05	RNA 3'-terminal phosphate cyclase	1	49.6
AGRF4_HUMAN	7 (2)	48.99	0.04	Adhesion G protein-coupled receptor F4	14.19	1
SGMR1_HUMAN	2 (1)	48.99	0.29	Sigma non-opioid intracellular receptor 1	88.25	1
PSD13_HUMAN	3 (1)	48.93	0.35	26S proteasome non-ATPase regulatory subunit 13	1	1.41
RM01_HUMAN	3 (1)	48.86	0.19	39S ribosomal protein L1, mitochondrial	3.13	1
CCHCR_HUMAN	7 (1)	48.66	0.74	Coiled-coil alpha-helical rod protein 1	3.82	1
RFIP4_HUMAN	5 (1)	48.64	0.56	Rab11 family-interacting protein 4	1.58	1
RT23_HUMAN	3 (1)	48.36	0.19	28S ribosomal protein S23, mitochondrial	3.16	1
DENR_HUMAN	3 (1)	48.23	4.71E-03	Density-regulated protein	1	242.05
NAA10_HUMAN	3 (1)	47.97	0.23	N-alpha-acetyltransferase 10	1.88	1
RNPS1_HUMAN	5 (2)	47.6	0.62	RNA-binding protein with serine-rich domain 1	2.02	1
RAD21_HUMAN	2 (1)	47.53	0.34	Double-strand-break repair protein rad21 homolog	1.78	1
BAX_HUMAN	2 (2)	47.1	0.04	Apoptosis regulator BAX	1	13.54
DNM1L_HUMAN	4 (1)	46.83	0.11	Dynamin-1-like protein	1	3.81
DDX47_HUMAN	2 (1)	46.34	0.2	Probable ATP-dependent RNA helicase DDX47	1	10.67
NQO1_HUMAN	2 (1)	46.08	0.1	NAD(P)H dehydrogenase [quinone] 1	9.92	1
MPRD_HUMAN	2 (1)	45.91	0.2	Cation-dependent mannose-6-phosphate receptor	91.77	1
RM45_HUMAN	5 (2)	45.87	0.74	39S ribosomal protein L45, mitochondrial	1	1
RASF1_HUMAN	3 (1)	45.56	0.98	Ras association domain-containing protein 1	4.82	1
BRX1_HUMAN	2 (1)	45.45	0.06	Ribosome biogenesis protein BRX1 homolog	1	7.55
MD13L_HUMAN	7 (1)	45.42	0.16	Mediator of RNA polymerase II transcription subunit 13-like	2.2	1
MINY4_HUMAN	9 (1)	45.35	0.06	Probable ubiquitin carboxyl-terminal hydrolase MINDY-4	14.1	1
PPE2_HUMAN	4 (1)	45.14	0.66	Serine/threonine-protein phosphatase with EF-hands 2	1.13	1
TOP1_HUMAN	3 (2)	45.08	0.93	DNA topoisomerase 1	1.09	1
KLH34_HUMAN	3 (3)	44.95	0.24	Kelch-like protein 34	1	2.31
STIM1_HUMAN	6 (1)	44.91	0.12	Stromal interaction molecule 1	∞	0
CK040_HUMAN	2 (1)	44.86	0.13	Putative uncharacterized protein C11orf40	9.3	1
NLTP_HUMAN	5 (3)	44.48	0.68	Non-specific lipid-transfer protein	1.38	1
FOXO6_HUMAN	4 (2)	44.39	9.26E-03	Forkhead box protein O6	1	3.4
CATD_HUMAN	3 (2)	44.38	0.83	Cathepsin D	1.22	1
MLEC_HUMAN	1 (1)	44.25	0.83	Malectin	1.56	1
DOCK6_HUMAN	7 (3)	43.73	0.29	Dedicator of cytokinesis protein 6	1	1.44
EYA2_HUMAN	2 (1)	43.69	0.1	Eyes absent homolog 2	1	4.8
PCNP_HUMAN	2 (1)	43.69	0.43	PEST proteolytic signal-containing nuclear protein	1.12	1
CD22_HUMAN	5 (1)	43.48	0.08	B-cell receptor CD22	∞	0
CG050_HUMAN	1 (1)	43.42	0.77	Uncharacterized protein C7orf50	1	5.8
NIBL1_HUMAN	3 (1)	43.01	0.15	Niban-like protein 1	3.12	1
DC1L2_HUMAN	3 (2)	42.71	0.25	Cytoplasmic dynein 1 light intermediate chain 2	4.37	1
PCCA_HUMAN	4 (1)	42.44	0.03	Propionyl-CoA carboxylase alpha chain, mitochondrial	1	27.85
CBPC4_HUMAN	4 (3)	42.29	0.03	Cytosolic carboxypeptidase 4	2.61	1
AASS_HUMAN	6 (2)	41.73	0.06	Alpha-aminoadipic semialdehyde synthase, mitochondrial	1	5.8
HPRT_HUMAN	2 (1)	41.51	0.08	Hypoxanthine-guanine phosphoribosyltransferase	1	1.3
SRPK2_HUMAN	6 (3)	41.46	8.99E-03	SRSF protein kinase 2	1	3.29
PSB4_HUMAN	1 (1)	40.56	0.65	Proteasome subunit beta type-4	4.52	1
SF01_HUMAN	4 (1)	40.12	0.79	Splicing factor 1	1	1
AVEN_HUMAN	5 (2)	39.69	0.08	Cell death regulator Aven	1.85	1
ZN622_HUMAN	2 (2)	39.66	0.06	Zinc finger protein 622	1	4.32
STAB1_HUMAN	7 (5)	39.33	0.23	Stabilin-1	2.65	1
WNT7A_HUMAN	6 (2)	39.31	0.03	Protein Wnt-7a	1	10.71

ARPC2_HUMAN	2 (1)	39.12	0.82	Actin-related protein 2/3 complex subunit 2	1.36	1
RL35A_HUMAN	2 (1)	38.92	0.52	60S ribosomal protein L35a	2.04	1
CHID1_HUMAN	3 (2)	38.74	0.5	Chitinase domain-containing protein 1	1	1.05
KRR1_HUMAN	2 (1)	38.36	0.05	KRR1 small subunit processome component homolog	1	4.42
MRT4_HUMAN	2 (1)	38.11	0.11	mRNA turnover protein 4 homolog	66.07	1
DPYL5_HUMAN	4 (2)	38.02	0.32	Dihydropyrimidinase-related protein 5	2.3	1
RAB9A_HUMAN	2 (1)	37.83	0.36	Ras-related protein Rab-9A	1.33	1
RT33_HUMAN	5 (1)	37.79	0.5	28S ribosomal protein S33, mitochondrial	3.49	1
PSMD3_HUMAN	2 (1)	37.65	0.14	26S proteasome non-ATPase regulatory subunit 3	1.43	1
ARP5L_HUMAN	1 (1)	37.54	0.92	Actin-related protein 2/3 complex subunit 5-like protein	2.6	1
NJMU_HUMAN	2 (1)	37.47	0.08	Protein Njmu-R1	9.24	1
DKC1_HUMAN	3 (1)	36.35	0.12	H/ACA ribonucleoprotein complex subunit 4	16.32	1
RISC_HUMAN	1 (1)	36.28	2.73E-03	Retinoid-inducible serine carboxypeptidase	1	15.83
ZN207_HUMAN	1 (1)	36.08	0.08	BUB3-interacting and GLEBS motif-containing protein ZNF207	1	3.08
6PGL_HUMAN	2 (2)	35.55	0.03	6-phosphogluconolactonase	3.35	1
HBA_HUMAN	2 (1)	35.14	0.67	Hemoglobin subunit alpha	1	1.5
MRGBP_HUMAN	2 (2)	34.99	0.06	MRG/MORF4L-binding protein	2.16	1
NPS3A_HUMAN	2 (1)	34.88	0.25	Protein NipSnap homolog 3A	5.76	1
HTRA2_HUMAN	3 (1)	34.84	0.13	Serine protease HTRA2, mitochondrial	1	2.08
GIPC3_HUMAN	3 (1)	34.82	0.82	PDZ domain-containing protein GIPC3	6.31	1
ABCD3_HUMAN	2 (1)	34.75	0.1	ATP-binding cassette sub-family D member 3	2.75	1
NDUB9_HUMAN	2 (1)	34.55	0.87	NADH dehydrogenase [ubiquinone] 1 beta subcomplex subunit 9	1.1	1
ADAP2_HUMAN	3 (1)	34.33	0.11	Arf-GAP with dual PH domain-containing protein 2	1	12.7
AXDN1_HUMAN	6 (1)	33.95	0.18	Axonemal dynein light chain domain-containing protein 1	2.28	1
VATL_HUMAN	1 (1)	33.69	0.34	V-type proton ATPase 16 kDa proteolipid subunit	2.11	1
SC23B_HUMAN	3 (1)	33.63	0.99	Protein transport protein Sec23B	1.1	1
H2B3B_HUMAN	3 (1)	31.97	0.01	Histone H2B type 3-B3	1	22.93
SODC_HUMAN	1 (1)	31.86	0.74	Superoxide dismutase [Cu-Zn]	2.48	1
LST2_HUMAN	3 (2)	31.15	0.87	Lateral signaling target protein 2 homolog	1	2.94
ERGI1_HUMAN	2 (1)	30.19	0.3	Endoplasmic reticulum-Golgi intermediate compartment protein 1	1	1.36
SPRY7_HUMAN	1 (1)	29.62	0.12	SPRY domain-containing protein 7	1	2.44
ORNT2_HUMAN	3 (1)	29.24	0.16	Mitochondrial ornithine transporter 2	1	3.88
DGKZ_HUMAN	3 (2)	28.26	0.71	Diacylglycerol kinase zeta	1.15	1
CLC4F_HUMAN	6 (1)	27.93	0.42	C-type lectin domain family 4 member F	1	1.44
SMG8_HUMAN	3 (1)	27.65	0.21	Protein SMG8	3.32	1
ABCAB_HUMAN	3 (1)	27.43	0.27	Putative ATP-binding cassette sub-family A member 11	1	1.28
CACO2_HUMAN	2 (2)	27.26	0.18	Calcium-binding and coiled-coil domain-containing protein 2	6.2	1
SPN1_HUMAN	3 (1)	26.91	0.93	Snurportin-1	2.94	1
FBX5_HUMAN	6 (2)	26.66	0.99	F-box only protein 5	1.58	1
CND2_HUMAN	2 (1)	26.41	0.36	Condensin complex subunit 2	2.32	1
MKLN1_HUMAN	6 (1)	26.19	0.08	Muskelin	1	2.76
PRDX5_HUMAN	1 (1)	25.89	0.6	Peroxiredoxin-5, mitochondrial	1.65	1
SAFB1_HUMAN	5 (2)	25.45	0.06	Scaffold attachment factor B1	1	5.9
HDGF_HUMAN	2 (1)	25.09	0.01	Hepatoma-derived growth factor	1	2.78
SRPK1_HUMAN	1 (1)	24.66	0.01	SRSF protein kinase 1	5.16	1
GTPB8_HUMAN	2 (1)	23.98	0.07	GTP-binding protein 8	1	39.16
VTM2B_HUMAN	2 (1)	22.68	0.06	V-set and transmembrane domain-containing protein 2B	1	3.89
RPP25_HUMAN	4 (2)	22.41	0.35	Ribonuclease P protein subunit p25	1.31	1
KBP_HUMAN	4 (1)	21.88	0.82	KIF1-binding protein	4.35	1
NEU1_HUMAN	3 (1)	21.51	0.14	Oxytocin-neurophysin 1	∞	0
MORC3_HUMAN	2 (1)	21.47	0.02	MORC family CW-type zinc finger protein 3	1	76.03
CD109_HUMAN	6 (1)	20.94	0.53	CD109 antigen	1.15	1
TM175_HUMAN	1 (1)	20.82	0.54	Endosomal/lysomomal potassium channel TMEM175	1.35	1
VATB2_HUMAN	1 (1)	20.12	0.36	V-type proton ATPase subunit B, brain isoform	1.5	1
DAZP1_HUMAN	2 (1)	19.49	0.69	DAZ-associated protein 1	2.71	1
DMBT1_HUMAN	4 (2)	19.29	0.81	Deleted in malignant brain tumors 1 protein	1	3.93
FST_HUMAN	2 (1)	18.01	0.1	Follistatin	1	38.03
VSXL2_HUMAN	3 (1)	17.87	0.45	V-set and immunoglobulin domain-containing protein 10-like 2	1	1.36

CAH12_HUMAN	3 (2)	16.65	0.56	Carbonic anhydrase 12	2.05	1
TPPC4_HUMAN	1 (1)	15.86	0.68	Trafficking protein particle complex subunit 4	1	3.28
ST1A3_HUMAN	1 (1)	13.25	0.12	Sulfotransferase 1A3	1	14.11

Table S2. ICAM-3 interacting proteins for proteins identified in membrane preparations of apoptotic and viable Hela WT and Hela-ICAM3 cells based on the String search. Confidence scores: 0.15-0.4 low interaction, 0.4-0.7 medium interaction, 0.7-0.9 high interactions, >0.9 highest interaction. Proteins are represents as their gene names.

		Viable cells		Apoptotic cells	
Protein (gene)	**Combined score**	**Protein identification**	**Significantly increased**	**Protein identification**	**Significantly increased**
MSN	0.799	+	WT, 1.81x, *p* 0.02	+	no
EZR	0.583	+	no	+	no
F11R	0.483	+	no	-	N/A
CD44	0.476	+	no	+	no
ALB	0.44	+	no	+	no
SPTAN1	0.435	+	no	+	no
ITGB1	0.415	+	no	+	WT, 1.48x, *p* 0.04
CD81	0.349	-	N/A	+	WT, 44.1x, *p* 0.04
RDX	0.343	+	no	-	N/A
CD63	0.304	-	N/A	+	WT, 5.84x, *p* 0.02
ITGAV	0.265	+	-	+	-
LMNA	0.265	+	-	+	WT, 1.46x, *p* 0.01
ANXA5	0.26	+	-	+	-
GAPDH	0.254	+	-	+	-
TFRC	0.241	+	-	+	-
VWF	0.232	+	ICAM3, 11.7x, *p* 0.02	-	N/A
CD22	0.232	+	WT, ∞	-	N/A
GOLPH3	0.215	+	-	-	N/A
DYNC1I2	0.212	+	-	-	N/A
LAMP1	0.21	+	-	+	-
RRM1	0.204	+	-	+	-
STAB1	0.204	+	-	-	N/A
VTN	0.2	+	-	+	WT, 3.03x, *p* 0.004
FYN	0.199	+	-	-	N/A
ACADM	0.193	+	-	+	-
CD55	0.188	+	WT, 2.78x, *p* 0.005	+	-
CALR	0.183	+	WT, 5.57x, *p* 0.01	+	-
RHOA	0.176	+	-	+	-
LGALS3	0.17	+	-	+	-
CDC42	0.168	-	N/A	+	ICAM3, 5.87x, *p* 0.02
TCOF1	0.167	+	-	-	N/A
MYH14	0.159	+	-	-	N/A
GTPBP1	0.154	+	-	-	N/A
DECR1	0.152	+	-	+	WT, 3x, *p* 0.02
DNM2	0.151	+	-	+	ICAM3, 9.4x, *p* 0.02
HSPA5	0.15	+	ICAM3, 2.63x, *p* 0.000001	+	-

Table S3. Proteins (1175 in total) identified by bottom-up proteomics approach in membrane preparations of apoptotic Hela WT and Hela-ICAM3 cells. Proteins were considered identified if at least one unique peptide was confidently identified by searching against SwissProt data base. Relative quantification was performed using Progenesis QI for proteomics software. Three most intense peptides per protein were used for quantification. Data in the table are normalised to the lower protein content (1.00). Values higher that 1.00 are 'fold increase' compared to the value 1.00. Measurements of three biological replicates allowed for Anova test to be performed on quantified results.

Uniprot ID	Identified peptides (unique)	Score	Anova, *p*	Protein name	WT	ICAM3
CPSM_HUMAN	114 (52)	8327.23	5.84E-03	Carbamoyl-phosphate synthase [ammonia], mitochondrial	1.68	1
GRP78_HUMAN	62 (34)	5714.72	0.45	78 kDa glucose-regulated protein	1.13	1
PLEC_HUMAN	113 (40)	5101.15	0.38	Plectin	1	1.18
CH60_HUMAN	66 (44)	4697.52	0.22	60 kDa heat shock protein, mitochondrial	1.69	1
ATPB_HUMAN	52 (25)	4519.24	0.39	ATP synthase subunit beta, mitochondrial	1.47	1
ACTB_HUMAN	36 (3)	3787.85	0.25	Actin, cytoplasmic 1	1	1.29
ENPL_HUMAN	56 (18)	3704.81	0.46	Endoplasmin	1	1.28
GRP75_HUMAN	47 (24)	3704.43	0.13	Stress-70 protein, mitochondrial O	2.94	1
ACTG_HUMAN	32 (1)	3670.28	0.09	Actin, cytoplasmic 2	1	2.43
CLH1_HUMAN	53 (19)	3545.9	2.44E-03	Clathrin heavy chain 1	2.6	1
ANXA2_HUMAN	44 (21)	3473.18	0.41	Annexin A2	1.13	1
ATPA_HUMAN	40 (19)	3382.56	0.53	ATP synthase subunit alpha, mitochondrial	1	1.01
HS90B_HUMAN	52 (9)	3245.81	0.42	Heat shock protein HSP 90-beta	1.64	1
HSP7C_HUMAN	41 (17)	3135.54	0.08	Heat shock cognate 71 kDa protein	1.46	1
LPPRC_HUMAN	57 (24)	3082.5	0.31	Leucine-rich PPR motif-containing protein, mitochondrial	1	1.46
MYH9_HUMAN	79 (31)	3068.16	9.29E-03	Myosin-9	2.86	1
G3P_HUMAN	37 (24)	2710.78	0.05	Glyceraldehyde-3-phosphate dehydrogenase	1.64	1
PRKDC_HUMAN	74 (30)	2686.23	0.48	DNA-dependent protein kinase catalytic subunit	1	1.07
NUCL_HUMAN	43 (17)	2509.41	0.29	Nucleolin	1.53	1
NPM_HUMAN	27 (17)	2480.85	0.07	Nucleophosmin	1	1.26
TBB5_HUMAN	35 (5)	2479.78	0.07	Tubulin beta chain	2.16	1
LONM_HUMAN	35 (13)	2443.01	0.03	Lon protease homolog, mitochondrial	1.47	1
LMNA_HUMAN	53 (25)	2419.96	9.64E-03	Prelamin-A/C	1.46	1
EF2_HUMAN	42 (19)	2389.22	0.19	Elongation factor 2	1	1.72
IQGA1_HUMAN	50 (19)	2348.41	0.14	Ras GTPase-activating-like protein IQGAP1	2.1	1
FLNA_HUMAN	55 (19)	2343.63	0.93	Filamin-A	1.3	1
ANXA5_HUMAN	26 (17)	2329.43	0.39	Annexin A5	1	1.18
HNRPU_HUMAN	43 (17)	2292.58	0.1	Heterogeneous nuclear ribonucleoprotein U	2.54	1
ACTA_HUMAN	29 (1)	2284.54	0.15	Actin, aortic smooth muscle	4.49	1
4F2_HUMAN	26 (16)	2223.45	0.7	4F2 cell-surface antigen heavy chain	1	1.11
ROA2_HUMAN	22 (8)	2163.32	0.78	Heterogeneous nuclear ribonucleoproteins A2/B1	1.22	1
HS90A_HUMAN	31 (3)	2089.88	0.96	Heat shock protein HSP 90-alpha	1.05	1
HNRPM_HUMAN	63 (31)	2085.44	0.89	Heterogeneous nuclear ribonucleoprotein M	1	1.08
ANXA1_HUMAN	23 (13)	1999.66	0.15	Annexin A1	1.22	1
C1TC_HUMAN	32 (20)	1986.44	0.31	C-1-tetrahydrofolate synthase, cytoplasmic	1.38	1
CALX_HUMAN	25 (14)	1977.33	3.11E-04	Calnexin	3.58	1
PDIA1_HUMAN	31 (14)	1969.99	0.05	Protein disulfide-isomerase	4.1	1
TBB4B_HUMAN	28 (1)	1935.99	0.3	Tubulin beta-4B chain	1.64	1
TRAP1_HUMAN	30 (15)	1851.92	0.78	Heat shock protein 75 kDa, mitochondrial	1	1.03
HS71A_HUMAN	28 (7)	1808.52	0.29	Heat shock 70 kDa protein 1A	1.74	1
SYEP_HUMAN	35 (22)	1747.72	0.51	Bifunctional glutamate/proline--tRNA ligase	1.28	1
TBA1A_HUMAN	22 (2)	1744.05	0.27	Tubulin alpha-1A chain	1.71	1
AHNK_HUMAN	149 (38)	1736.85	0.43	Neuroblast differentiation-associated protein AHNAK	1	1.46

PPIB_HUMAN	21 (8)	1685.31	0.82	Peptidyl-prolyl cis-trans isomerase B	1	1
VDAC1_HUMAN	22 (15)	1671.34	0.04	Voltage-dependent anion-selective channel protein 1	1.49	1
TBB2A_HUMAN	27 (1)	1668.08	0.22	Tubulin beta-2A chain	1.95	1
TFR1_HUMAN	29 (8)	1664.29	0.31	Transferrin receptor protein 1 2	1.39	1
BASP1_HUMAN	19 (15)	1638.29	0.1	Brain acid soluble protein 1	3.89	1
EFTU_HUMAN	23 (17)	1624.94	0.13	Elongation factor Tu, mitochondrial	1	2.58
CKAP4_HUMAN	27 (15)	1616.97	0.22	Cytoskeleton-associated protein 4	1.84	1
VIME_HUMAN	27 (19)	1547.8	0.66	Vimentin	1	1.13
TERA_HUMAN	28 (14)	1540.62	0.16	Transitional endoplasmic reticulum ATPase	1.93	1
PARP1_HUMAN	47 (19)	1538.94	0.39	Poly [ADP-ribose] polymerase 1	1.36	1
MDHM_HUMAN	15 (5)	1531.23	0.13	Malate dehydrogenase, mitochondrial	1	3.75
ILF3_HUMAN	31 (11)	1516.86	0.11	Interleukin enhancer-binding factor 3	1	1.79
AT1A1_HUMAN	32 (7)	1514.52	0.12	Sodium/potassium-transporting ATPase subunit alpha-1	1.59	1
PHB2_HUMAN	25 (10)	1510.95	0.25	Prohibitin-2	1.46	1
PHB_HUMAN	15 (11)	1497.73	0.08	Prohibitin	5.24	1
ACON_HUMAN	18 (10)	1496.03	0.16	Aconitate hydratase, mitochondrial	1.45	1
ECHA_HUMAN	29 (12)	1480	0.15	Trifunctional enzyme subunit alpha, mitochondrial	1	1.59
SFPQ_HUMAN	31 (14)	1478.47	0.26	Splicing factor, proline- and glutamine-rich	1.51	1
PDIA3_HUMAN	22 (12)	1476.31	0.34	Protein disulfide-isomerase A3	1.37	1
HCD2_HUMAN	15 (10)	1471.98	1.26E-03	3-hydroxyacyl-CoA dehydrogenase type-2	1.94	1
HYOU1_HUMAN	32 (14)	1471.55	0.45	Hypoxia up-regulated protein 1	1.84	1
HNRPC_HUMAN	23 (6)	1454.85	0.52	Heterogeneous nuclear ribonucleoproteins C1/C2	1	1.12
KPYM_HUMAN	31 (15)	1392.77	0.08	Pyruvate kinase PKM	1.6	1
ECH1_HUMAN	20 (12)	1392.3	0.16	Delta(3,5)-Delta(2,4)-dienoyl-CoA isomerase, mitochondrial	1	1.7
TBB3_HUMAN	26 (1)	1370.83	0.41	Tubulin beta-3 chain	1.34	1
ANXA6_HUMAN	39 (17)	1352.94	0.77	Annexin A6	1.32	1
ACADM_HUMAN	19 (12)	1349.32	0.85	Medium-chain specific acyl-CoA dehydrogenase, mitochondrial	1	1.02
SND1_HUMAN	32 (18)	1346.51	0.41	Staphylococcal nuclease domain-containing protein 1	1.33	1
ROA1_HUMAN	18 (2)	1346.07	0.83	Heterogeneous nuclear ribonucleoprotein A1	1.1	1
GANAB_HUMAN	21 (9)	1345.26	0.11	Neutral alpha-glucosidase AB	1.22	1
GLYM_HUMAN	23 (12)	1344.64	0.22	Serine hydroxymethyltransferase, mitochondrial	1.3	1
DHX9_HUMAN	22 (10)	1343.5	0.03	ATP-dependent RNA helicase A	1.68	1
TBB4A_HUMAN	24 (1)	1337.08	0.71	Tubulin beta-4A chain	1	1.22
ENOA_HUMAN	19 (14)	1336.56	0.76	Alpha-enolase	1	1.27
TBA4A_HUMAN	20 (2)	1320.77	0.24	Tubulin alpha-4A chain	1.93	1
IF4A1_HUMAN	27 (11)	1299.73	0.17	Eukaryotic initiation factor 4A-I	1.52	1
EF1A1_HUMAN	20 (6)	1289.08	0.45	Elongation factor 1-alpha 1	1	1.1
CALR_HUMAN	15 (10)	1286.49	0.38	Calreticulin	1.42	1
PDIA6_HUMAN	17 (11)	1280.16	0.92	Protein disulfide-isomerase A6	1	1.41
ODPB_HUMAN	17 (11)	1268.97	0.94	Pyruvate dehydrogenase E1 component subunit beta, mitochondrial	1	1.03
TCPB_HUMAN	27 (15)	1262.45	0.13	T-complex protein 1 subunit beta	1	10.26
EIF3A_HUMAN	38 (16)	1255.73	0.23	Eukaryotic translation initiation factor 3 subunit A	1	1.31
ACADV_HUMAN	27 (13)	1232.5	0.01	Very long-chain specific acyl-CoA dehydrogenase, mitochondrial	1	2.23
RL7_HUMAN	26 (11)	1231.43	0.76	60S ribosomal protein L7	1.12	1
PYC_HUMAN	30 (16)	1226.77	5.60E-03	Pyruvate carboxylase, mitochondrial O	1.69	1
MIC60_HUMAN	26 (9)	1201.49	0.72	MICOS complex subunit MIC60	1	1.06
QCR2_HUMAN	16 (8)	1199.43	6.81E-03	Cytochrome b-c1 complex subunit 2, mitochondrial	1.16	1
H14_HUMAN	17 (2)	1180.19	0.51	Histone H1.4	1.52	1
RLA0_HUMAN	19 (7)	1163.96	0.02	60S acidic ribosomal protein P0	1	2.05
PTBP1_HUMAN	12 (8)	1160.23	0.54	Polypyrimidine tract-binding protein 1	1	1.12
XRCC6_HUMAN	23 (10)	1134.6	0.18	X-ray repair cross-complementing protein 6	1.61	1
PGK1_HUMAN	24 (7)	1124.63	0.32	Phosphoglycerate kinase 1	1	1.44
ACTBL_HUMAN	27 (1)	1123.01	0.69	Beta-actin-like protein 2	1.12	1
NCPR_HUMAN	24 (10)	1118.07	0.61	NADPH--cytochrome P450 reductase	1	1.09
H4_HUMAN	19 (11)	1091.08	0.14	Histone H4	2.62	1
NONO_HUMAN	31 (13)	1073.31	0.01	Non-POU domain-containing octamer-binding protein	2.3	1
RL6_HUMAN	19 (7)	1071.64	0.04	60S ribosomal protein L6	1	1.97
H12_HUMAN	17 (1)	1071.21	0.03	Histone H1.2	2.3	1

DDX21_HUMAN	30 (12)	1066.1	0.06	Nucleolar RNA helicase 2	1	1.41
H90B3_HUMAN	23 (1)	1065.12	0.97	Putative heat shock protein HSP 90-beta-3	1.06	1
PRDX1_HUMAN	18 (6)	1052.44	0.95	Peroxiredoxin-1	1.07	1
RS3A_HUMAN	22 (12)	1037.22	0.18	40S ribosomal protein S3a	1	1.8
P5CR1_HUMAN	17 (12)	1033.09	0.37	Pyrroline-5-carboxylate reductase 1, mitochondrial	2.1	1
H2B1B_HUMAN	10 (1)	1029.23	0.08	Histone H2B type 1-B	2.58	1
THIL_HUMAN	16 (11)	1024.97	0.89	Acetyl-CoA acetyltransferase, mitochondrial	1	1.01
ACTN4_HUMAN	18 (5)	1022.62	0.07	Alpha-actinin-4	2.05	1
HNRPK_HUMAN	23 (13)	1011.56	0.71	Heterogeneous nuclear ribonucleoprotein K	1.06	1
RSSA_HUMAN	16 (11)	997.58	0.64	40S ribosomal protein SA	1	1.07
ANXA4_HUMAN	15 (9)	993.64	0.12	Annexin A4	1	1.92
CLH2_HUMAN	16 (2)	992.35	0.57	Clathrin heavy chain 2	1	1.18
RL7A_HUMAN	19 (10)	989.85	0.07	60S ribosomal protein L7a	1	1.45
FUMH_HUMAN	15 (14)	989.48	0.2	Fumarate hydratase, mitochondrial	2.19	1
HNRC1_HUMAN	16 (1)	973.05	0.18	Heterogeneous nuclear ribonucleoprotein C-like 1	1.71	1
RL5_HUMAN	18 (10)	962.04	0.73	60S ribosomal protein L5	1.39	1
ATP5H_HUMAN	15 (7)	956.07	0.12	ATP synthase subunit d, mitochondrial	1.82	1
AATM_HUMAN	19 (8)	947	0.33	Aspartate aminotransferase, mitochondrial	1	1.3
RS3_HUMAN	20 (12)	937.54	0.56	40S ribosomal protein S3	1	1.11
SPTN1_HUMAN	48 (9)	936.42	0.43	Spectrin alpha chain, non-erythrocytic 1	1.41	1
RL13_HUMAN	14 (8)	934.37	0.06	60S ribosomal protein L13	1	1.49
XRCC5_HUMAN	18 (9)	927.48	0.04	X-ray repair cross-complementing protein 5	1.7	1
TITIN_HUMAN	169 (32)	925.56	0.07	Titin	1	2.66
PA2G4_HUMAN	20 (11)	924.46	0.69	Proliferation-associated protein 2G4	1	1.25
ALDOA_HUMAN	16 (6)	923.29	0.72	Fructose-bisphosphate aldolase A	1.56	1
LDHA_HUMAN	15 (8)	919.33	1	L-lactate dehydrogenase A chain	1.1	1
AIFM1_HUMAN	18 (11)	919.12	0.3	Apoptosis-inducing factor 1, mitochondrial	1.54	1
SCOT1_HUMAN	17 (7)	917.93	0.02	Succinyl-CoA:3-ketoacid coenzyme A transferase 1, mitochondrial	2.89	1
RAB1B_HUMAN	14 (3)	914.38	0.06	Ras-related protein Rab-1B	5.1	1
RACK1_HUMAN	11 (7)	910.99	0.1	Receptor of activated protein C kinase 1	1.3	1
RA1L2_HUMAN	17 (1)	904.33	0.86	Heterogeneous nuclear ribonucleoprotein A1-like 2	1	1.04
ETFA_HUMAN	12 (9)	903.42	0.27	Electron transfer flavoprotein subunit alpha, mitochondrial	1.94	1
PDCD6_HUMAN	12 (8)	894.45	0.18	Programmed cell death protein 6	1.67	1
VDAC2_HUMAN	11 (6)	890.69	0.33	Voltage-dependent anion-selective channel protein 2	1.2	1
POTEE_HUMAN	23 (1)	886.03	0.63	POTE ankyrin domain family member E	9.52	1
TPIS_HUMAN	11 (2)	883.77	0.22	Triosephosphate isomerase	2.59	1
ATPO_HUMAN	12 (3)	882.18	0.04	ATP synthase subunit O, mitochondrial	3.22	1
ILF2_HUMAN	10 (7)	880.47	0.03	Interleukin enhancer-binding factor 2	1	1.29
L1CAM_HUMAN	16 (7)	879.91	0.12	Neural cell adhesion molecule L1	1.72	1
SPTB2_HUMAN	40 (9)	878.14	0.04	Spectrin beta chain, non-erythrocytic 1	2.03	1
ROA3_HUMAN	13 (6)	877.02	0.05	Heterogeneous nuclear ribonucleoprotein A3	1	1.37
HSPB1_HUMAN	13 (8)	874.19	0.33	Heat shock protein beta-1	1.29	1
PDIA4_HUMAN	18 (8)	861.29	0.45	Protein disulfide-isomerase A4	1	1.18
PAIRB_HUMAN	17 (10)	852.08	0.68	Plasminogen activator inhibitor 1 RNA-binding protein	1	1.41
H13_HUMAN	12 (1)	850	0.55	Histone H1.3	1.47	1
EZRI_HUMAN	24 (8)	845.28	0.35	Ezrin	1	1.32
RAB5C_HUMAN	13 (4)	835.71	0.09	Ras-related protein Rab-5C	1	2.09
TBB6_HUMAN	21 (2)	824.19	0.28	Tubulin beta-6 chain	1.53	1
HMGB1_HUMAN	13 (4)	819.95	0.03	High mobility group protein B1	1	2.06
MAP4_HUMAN	26 (9)	817.37	0.96	Microtubule-associated protein 4	1.15	1
SERA_HUMAN	20 (9)	814.96	0.21	D-3-phosphoglycerate dehydrogenase	1.73	1
DDX17_HUMAN	24 (10)	814.93	0.56	Probable ATP-dependent RNA helicase DDX17	1	1.11
RL4_HUMAN	19 (10)	810.67	0.9	60S ribosomal protein L4	1	1.11
RS4X_HUMAN	14 (7)	810.14	0.46	40S ribosomal protein S4, X isoform	1	1.19
TCPA_HUMAN	22 (8)	808.97	0.45	T-complex protein 1 subunit alpha	1	1.4
MYOF_HUMAN	22 (11)	802.73	0.16	Myoferlin	2.49	1
DHE3_HUMAN	17 (4)	799.55	0.46	Glutamate dehydrogenase 1, mitochondrial	1.19	1
EF1G_HUMAN	16 (7)	796.34	0.2	Elongation factor 1-gamma	1.92	1

SYIC_HUMAN	23 (6)	788.24	0.02	Isoleucine--tRNA ligase, cytoplasmic	2.17	1
RL9_HUMAN	9 (5)	781.3	0.55	60S ribosomal protein L9	1.32	1
EF1D_HUMAN	12 (6)	778.15	0.06	Elongation factor 1-delta	1.91	1
MATR3_HUMAN	15 (6)	775.45	0.83	Matrin-3	1.1	1
DDX3X_HUMAN	24 (10)	768.92	0.08	ATP-dependent RNA helicase DDX3X	1.52	1
STML2_HUMAN	12 (8)	768.32	0.29	Stomatin-like protein 2, mitochondrial	1	2.16
ADT2_HUMAN	22 (4)	763.2	0.41	ADP/ATP translocase 2	1.94	1
TCPQ_HUMAN	25 (13)	751.84	0.1	T-complex protein 1 subunit theta	2.43	1
CISY_HUMAN	16 (9)	737.63	0.91	Citrate synthase, mitochondrial	1.39	1
DESP_HUMAN	45 (8)	730.26	0.09	Desmoplakin	1.83	1
HCDH_HUMAN	11 (5)	728.26	0.74	Hydroxyacyl-coenzyme A dehydrogenase, mitochondrial	1	1.03
TCPZ_HUMAN	15 (5)	726.66	8.30E-03	T-complex protein 1 subunit zeta	2.24	1
RPN1_HUMAN	15 (11)	724.8	0.03	Dolichyl-diphosphooligosaccharide--protein glycosyltransferase subunit 1	1.59	1
H15_HUMAN	16 (7)	715.46	0.23	Histone H1.5	1	1.44
NACAM_HUMAN	17 (9)	710.01	0.14	Nascent polypeptide-associated complex subunit alpha, muscle-specific form	1.26	1
TCPE_HUMAN	22 (9)	709.18	0.29	T-complex protein 1 subunit epsilon	1.63	1
IDH3A_HUMAN	17 (8)	704.1	0.93	Isocitrate dehydrogenase [NAD] subunit alpha, mitochondrial	1.03	1
TMEDA_HUMAN	11 (6)	703.53	0.09	Transmembrane emp24 domain-containing protein 10	2.02	1
NB5R3_HUMAN	10 (9)	703.1	0.81	NADH-cytochrome b5 reductase 3	1.01	1
MOES_HUMAN	23 (3)	696.81	0.95	Moesin	1	1
SMC1A_HUMAN	34 (10)	694.88	0.03	Structural maintenance of chromosomes protein 1A	1	2.75
DLDH_HUMAN	17 (6)	694.68	0.73	Dihydrolipoyl dehydrogenase, mitochondrial	1	1.51
TCPG_HUMAN	28 (11)	693.25	0.48	T-complex protein 1 subunit gamma	1.23	1
1433E_HUMAN	14 (10)	692.77	0.77	14-3-3 protein epsilon	1	1
TCPD_HUMAN	12 (4)	691.26	0.38	T-complex protein 1 subunit delta	1.47	1
BASI_HUMAN	10 (7)	688.17	4.09E-03	Basigin	1.74	1
ADT3_HUMAN	18 (1)	684.11	0.12	ADP/ATP translocase 3	3.3	1
EPIPL_HUMAN	50 (14)	683.34	0.37	Epiplakin	1.5	1
HNRPD_HUMAN	13 (7)	668.56	0.83	Heterogeneous nuclear ribonucleoprotein D0	1	1.02
GCN1_HUMAN	26 (8)	668.42	0.42	eIF-2-alpha kinase activator GCN1	1.36	1
SERPH_HUMAN	14 (7)	661.58	0.09	Serpin H1	2.13	1
RS8_HUMAN	8 (4)	661.16	0.14	40S ribosomal protein S8	1	1.35
HNRPF_HUMAN	15 (4)	660.52	0.09	Heterogeneous nuclear ribonucleoprotein F	2.52	1
FEN1_HUMAN	14 (9)	660.31	0.22	Flap endonuclease 1	1	1.18
NDUS1_HUMAN	15 (6)	648.59	0.08	NADH-ubiquinone oxidoreductase 75 kDa subunit, mitochondrial	2.39	1
GDE_HUMAN	16 (4)	643.88	0.38	Glycogen debranching enzyme	1.12	1
U520_HUMAN	29 (7)	642.8	0.7	U5 small nuclear ribonucleoprotein 200 kDa helicase	1.01	1
RL24_HUMAN	8 (2)	642.77	0.02	60S ribosomal protein L24	1	1.39
HNRH1_HUMAN	10 (2)	642.12	0.15	Heterogeneous nuclear ribonucleoprotein H	1.62	1
SFXN1_HUMAN	11 (7)	638.41	0.12	Sideroflexin-1	2.25	1
RL10_HUMAN	10 (5)	638.21	0.86	60S ribosomal protein L10	1.1	1
RAB1A_HUMAN	9 (1)	635.5	0.38	Ras-related protein Rab-1A	1.53	1
RBMX_HUMAN	16 (2)	633.68	1	RNA-binding motif protein, X chromosome	1.01	1
TKT_HUMAN	14 (9)	632.81	0.88	Transketolase	1	1.18
IMB1_HUMAN	15 (5)	632.66	0.33	Importin subunit beta-1	3.39	1
RRBP1_HUMAN	28 (5)	632.55	0.03	Ribosome-binding protein 1	3.07	1
LDHB_HUMAN	11 (5)	631.18	3.91E-03	L-lactate dehydrogenase B chain	1.86	1
ECHM_HUMAN	13 (6)	628.42	0.09	Enoyl-CoA hydratase, mitochondrial	1.46	1
AT5F1_HUMAN	9 (9)	623.92	0.19	ATP synthase F(0) complex subunit B1, mitochondrial	2.05	1
NDUS3_HUMAN	8 (5)	623.6	0.42	NADH dehydrogenase [ubiquinone] iron-sulfur protein 3, mitochondrial	1.15	1
COX2_HUMAN	9 (7)	618.31	0.81	Cytochrome c oxidase subunit 2	1.14	1
FRIH_HUMAN	10 (5)	610.59	0.08	Ferritin heavy chain	1.82	1
QCR1_HUMAN	12 (7)	609.34	0.31	Cytochrome b-c1 complex subunit 1, mitochondrial	2.27	1
ATPG_HUMAN	9 (5)	605.89	0.95	ATP synthase subunit gamma, mitochondrial	1.01	1
LAT1_HUMAN	12 (4)	603.5	0.03	Large neutral amino acids transporter small subunit 1	21.94	1
RAB7A_HUMAN	10 (6)	603.23	4.97E-03	Ras-related protein Rab-7a	1.67	1
FLNB_HUMAN	23 (10)	602.63	0.2	Filamin-B	1.44	1
TOM40_HUMAN	7 (3)	600.52	0.43	Mitochondrial import receptor subunit TOM40 homolog	2.2	1

PABP1_HUMAN	15 (2)	597.03	0.83	Polyadenylate-binding protein 1	1.04	1
RL40_HUMAN	10 (5)	596.17	0.02	Ubiquitin-60S ribosomal protein L40	1.91	1
P5CS_HUMAN	15 (4)	593.75	0.04	Delta-1-pyrroline-5-carboxylate synthase	1	5.84
ITB1_HUMAN	13 (9)	588.76	0.04	Integrin beta-1	1.48	1
RS7_HUMAN	11 (8)	582.24	0.07	40S ribosomal protein S7	1	1.69
ASSY_HUMAN	11 (9)	578.93	0.22	Argininosuccinate synthase	1	2.08
RS6_HUMAN	11 (5)	575.88	0.4	40S ribosomal protein S6	1	1.24
U5S1_HUMAN	12 (5)	574.62	0.02	116 kDa U5 small nuclear ribonucleoprotein component	2.47	1
PRDX2_HUMAN	10 (6)	573.06	0.48	Peroxiredoxin-2	1.1	1
RL17_HUMAN	12 (6)	571.85	0.48	60S ribosomal protein L17	1.16	1
TAGL2_HUMAN	6 (4)	567.03	0.79	Transgelin-2	1	1.07
UBA1_HUMAN	14 (7)	565.99	0.9	Ubiquitin-like modifier-activating enzyme 1	1.21	1
RL21_HUMAN	11 (6)	563.46	0.02	60S ribosomal protein L21	2.77	1
ERP29_HUMAN	12 (8)	562.05	0.02	Endoplasmic reticulum resident protein 29	1.19	1
TCPH_HUMAN	12 (6)	559.79	0.86	T-complex protein 1 subunit eta	1	1.08
IF4A2_HUMAN	14 (1)	557.06	0.13	Eukaryotic initiation factor 4A-II	2.46	1
THIM_HUMAN	8 (5)	551.78	0.27	3-ketoacyl-CoA thiolase, mitochondrial	1	1.84
SDHA_HUMAN	13 (7)	548.9	0.83	Succinate dehydrogenase [ubiquinone] flavoprotein subunit, mitochondrial	1.1	1
RL10A_HUMAN	10 (9)	548.09	0.71	60S ribosomal protein L10a	1	1.05
NSUN2_HUMAN	19 (4)	547.59	0.07	tRNA (cytosine(34)-C(5))-methyltransferase	1.87	1
ODPA_HUMAN	13 (5)	547.44	0.54	Pyruvate dehydrogenase E1 component subunit alpha, somatic form, mitochondrial	1	1.26
TPR_HUMAN	28 (7)	546.84	0.39	Nucleoprotein TPR	1	1.91
TLN1_HUMAN	27 (11)	546.76	0.52	Talin-1	1.31	1
PRDX4_HUMAN	9 (3)	546.18	0.05	Peroxiredoxin-4	1.31	1
CD109_HUMAN	11 (4)	544.16	0.28	CD109 antigen	1.76	1
APEX1_HUMAN	7 (6)	543.76	0.32	DNA-(apurinic or apyrimidinic site) lyase	1.48	1
PRDX3_HUMAN	7 (6)	543.67	0.16	Thioredoxin-dependent peroxide reductase, mitochondrial	1.39	1
CAPR1_HUMAN	11 (4)	542.17	0.74	Caprin-1	1.07	1
VIGLN_HUMAN	20 (5)	539.99	2.09E-03	Vigilin	1	4.93
IF2A_HUMAN	12 (5)	536.41	0.19	Eukaryotic translation initiation factor 2 subunit 1	1.35	1
ELAV1_HUMAN	9 (4)	533.93	0.51	ELAV-like protein 1	1.08	1
IF4A3_HUMAN	13 (5)	532.29	0.85	Eukaryotic initiation factor 4A-III	1.22	1
PRDX6_HUMAN	10 (7)	532.2	0.15	Peroxiredoxin-6	1.35	1
1433Z_HUMAN	9 (6)	531.99	0.07	14-3-3 protein zeta/delta	1.61	1
H11_HUMAN	14 (4)	519.5	0.02	Histone H1.1	1	3.16
AT2A2_HUMAN	16 (4)	517.07	0.5	Sarcoplasmic/endoplasmic reticulum calcium ATPase 2	1.97	1
SYLC_HUMAN	27 (7)	516.94	0.16	Leucine--tRNA ligase, cytoplasmic	1	1.09
TBB8_HUMAN	10 (1)	516.28	0.03	Tubulin beta-8 chain	1465.84	1
ETFB_HUMAN	11 (5)	511.12	0.27	Electron transfer flavoprotein subunit beta	1	1.29
FBRL_HUMAN	13 (3)	511.09	0.94	rRNA 2'-O-methyltransferase fibrillarin	1.08	1
SCMC1_HUMAN	13 (5)	510.04	0.18	Calcium-binding mitochondrial carrier protein SCaMC-1	1	2.38
C1QBP_HUMAN	5 (4)	505.77	0.58	Complement component 1 Q subcomponent-binding protein, mitochondrial	1.19	1
LMNB1_HUMAN	17 (7)	503.44	0.7	Lamin-B1	1	1.9
YBOX1_HUMAN	9 (7)	503.41	0.36	Nuclease-sensitive element-binding protein 1	1.65	1
SPRE_HUMAN	8 (7)	502.07	0.08	Sepiapterin reductase	1	2.4
RL23A_HUMAN	9 (1)	501.85	0.06	60S ribosomal protein L23a	7.48	1
SUCB2_HUMAN	16 (10)	494.5	0.62	Succinate--CoA ligase [GDP-forming] subunit beta, mitochondrial	1.07	1
RAB2A_HUMAN	6 (3)	494.22	9.63E-03	Ras-related protein Rab-2A	2.38	1
RLA2_HUMAN	4 (1)	493.99	0.09	60S acidic ribosomal protein P2	2.71	1
KI67_HUMAN	57 (8)	488.35	0.39	Proliferation marker protein Ki-67	1	1.12
RL18_HUMAN	10 (2)	487.56	0.97	60S ribosomal protein L18	1.1	1
PYR1_HUMAN	22 (6)	487.02	0.26	CAD protein	2.55	1
DHE4_HUMAN	9 (1)	482.17	0.47	Glutamate dehydrogenase 2, mitochondrial	1.21	1
ECI1_HUMAN	11 (5)	481.25	0.12	Enoyl-CoA delta isomerase 1, mitochondrial	1.78	1
SYTC_HUMAN	18 (5)	479.64	0.5	Threonine--tRNA ligase, cytoplasmic	1.72	1
H2A2A_HUMAN	6 (1)	477.85	0.05	Histone H2A type 2-A	1.9	1
HNRH2_HUMAN	11 (3)	474.78	0.33	Heterogeneous nuclear ribonucleoprotein H2	1.79	1
PABP4_HUMAN	15 (5)	471.82	0.12	Polyadenylate-binding protein	1.58	1

G3BP1_HUMAN	14 (8)	471.05	0.47	Ras GTPase-activating protein-binding protein 1	1	1.99
HNRPL_HUMAN	11 (8)	466.45	0.58	Heterogeneous nuclear ribonucleoprotein L	1.32	1
SEPT2_HUMAN	10 (9)	465.43	0.1	Septin-2	1.76	1
ALBU_HUMAN	24 (8)	464.45	0.07	Serum albumin	1	2.29
RS27A_HUMAN	9 (3)	464.05	5.17E-03	Ubiquitin-40S ribosomal protein S27a	3.16	1
DHB4_HUMAN	15 (6)	463.14	0.46	Peroxisomal multifunctional enzyme type 2	1.21	1
HNRPR_HUMAN	12 (2)	461.42	9.59E-03	Heterogeneous nuclear ribonucleoprotein R	1.78	1
SRSF1_HUMAN	10 (6)	460.94	0.06	Serine/arginine-rich splicing factor 1	2.55	1
UCRI_HUMAN	8 (4)	460.35	0.44	Cytochrome b-c1 complex subunit Rieske, mitochondrial	1	1.31
VINC_HUMAN	31 (8)	460.05	0.86	Vinculin	1.26	1
GARS_HUMAN	11 (3)	458.33	0.69	Glycine--tRNA ligase	2.1	1
RS2_HUMAN	11 (6)	458.31	0.22	40S ribosomal protein S2	1.26	1
SC31A_HUMAN	14 (3)	455.37	0.57	Protein transport protein Sec31A	1	1.15
DYHC1_HUMAN	24 (9)	453.82	6.25E-03	Cytoplasmic dynein 1 heavy chain 1	1.61	1
H2AY_HUMAN	11 (6)	452.84	0.88	Core histone macro-H2A.1	1	1.06
ROAA_HUMAN	12 (6)	450.42	0.22	Heterogeneous nuclear ribonucleoprotein A/B	3.18	1
RL26_HUMAN	9 (3)	450.26	0.37	60S ribosomal protein L26	1.51	1
RS15_HUMAN	7 (5)	449.02	0.85	40S ribosomal protein S15	2.18	1
EF1B_HUMAN	7 (5)	446.85	0.53	Elongation factor 1-beta	1.35	1
SYMC_HUMAN	11 (6)	445.1	7.81E-06	Methionine--tRNA ligase, cytoplasmic	1.69	1
RS9_HUMAN	10 (7)	444.42	0.31	40S ribosomal protein S9	1	1.22
EIF3B_HUMAN	15 (8)	444.39	0.06	Eukaryotic translation initiation factor 3 subunit B	1.76	1
HNRPQ_HUMAN	10 (1)	443.65	0.2	Heterogeneous nuclear ribonucleoprotein Q	1.63	1
SYIM_HUMAN	15 (4)	442.11	0.53	Isoleucine--tRNA ligase, mitochondrial	1	1.12
PDC6I_HUMAN	14 (6)	435.65	0.09	Programmed cell death 6-interacting protein	2.06	1
DHX15_HUMAN	17 (4)	435.44	0.03	Pre-mRNA-splicing factor ATP-dependent RNA helicase DHX15	1	1.96
NEBU_HUMAN	83 (13)	433.91	3.63E-03	Nebulin	1	5.64
LAMP1_HUMAN	8 (1)	431.24	0.66	Lysosome-associated membrane glycoprotein 1	1.24	1
MYH10_HUMAN	24 (3)	429.4	0.2	Myosin-10	1.93	1
RL8_HUMAN	10 (4)	428.83	0.14	60S ribosomal protein L8	3.78	1
FAS_HUMAN	15 (5)	427.4	0.01	Fatty acid synthase	2.73	1
DDX5_HUMAN	18 (5)	427.12	0.09	Probable ATP-dependent RNA helicase DDX5 1	1	1.51
RADI_HUMAN	15 (1)	425.96	0.74	Radixin	1.07	1
RAB14_HUMAN	6 (2)	425.38	2.96E-03	Ras-related protein Rab-14	1.92	1
GPDM_HUMAN	15 (3)	424.96	0.58	Glycerol-3-phosphate dehydrogenase, mitochondrial	1.84	1
FUS_HUMAN	16 (6)	424.5	0.85	RNA-binding protein FUS	1	1.13
RU2A_HUMAN	12 (5)	423.04	0.6	U2 small nuclear ribonucleoprotein A'	1	1.24
PCBP1_HUMAN	10 (4)	418.11	8.00E-03	Poly(rC)-binding protein 1	1	5.5
RL1D1_HUMAN	10 (5)	416.97	0.67	Ribosomal L1 domain-containing protein 1	1	6.08
CYBP_HUMAN	11 (5)	415.17	0.23	Calcyclin-binding protein	1	2.14
THOC4_HUMAN	12 (5)	414.98	0.64	THO complex subunit 4	1	1.26
CBX3_HUMAN	7 (3)	410.54	6.84E-03	Chromobox protein homolog 3	1.61	1
SMC3_HUMAN	27 (6)	406.79	0.1	Structural maintenance of chromosomes protein 3	2.02	1
PNPT1_HUMAN	13 (5)	403.83	0.74	Polyribonucleotide nucleotidyltransferase 1, mitochondrial	1.24	1
PCKGM_HUMAN	10 (4)	403.09	0.1	Phosphoenolpyruvate carboxykinase [GTP], mitochondrial	3.76	1
TOP2A_HUMAN	16 (4)	402.47	0.05	DNA topoisomerase 2-alpha	1	1.3
LRC59_HUMAN	10 (3)	400.78	0.32	Leucine-rich repeat-containing protein 59	1	1.26
MOT4_HUMAN	7 (3)	399.9	0.21	Monocarboxylate transporter 4	1	7.54
HNRL2_HUMAN	9 (3)	399.22	0.37	Heterogeneous nuclear ribonucleoprotein U-like protein 2	1.58	1
TOM22_HUMAN	4 (4)	395.47	0.18	Mitochondrial import receptor subunit TOM22 homolog	2.52	1
SMC2_HUMAN	29 (6)	393.41	0.83	Structural maintenance of chromosomes protein 2	1.2	1
PLIN3_HUMAN	6 (4)	390.01	0.95	Perilipin-3	1.01	1
EFTS_HUMAN	5 (4)	389.11	0.14	Elongation factor Ts, mitochondrial	2.2	1
RM12_HUMAN	9 (4)	388.11	1.55E-03	39S ribosomal protein L12, mitochondrial	1.89	1
DYH9_HUMAN	67 (12)	387.39	0.11	Dynein heavy chain 9, axonemal	1	4.57
RL15_HUMAN	7 (5)	387.16	0.23	60S ribosomal protein L15	1.56	1
SYNE1_HUMAN	48 (6)	386.81	0.1	Nesprin-1	1	1.33
SSRD_HUMAN	8 (6)	386.59	0.07	Translocon-associated protein subunit delta	2.26	1

TPD52_HUMAN	6 (1)	384.67	0.03	Tumor protein D52	2.69	1
GLU2B_HUMAN	9 (2)	383.78	0.81	Glucosidase 2 subunit beta	1.53	1
MYO1C_HUMAN	19 (8)	377.96	0.61	Unconventional myosin-Ic	1	1.28
DNJA3_HUMAN	10 (4)	375.83	0.08	DnaJ homolog subfamily A member 3, mitochondrial	1	1.3
ECI2_HUMAN	11 (6)	374.63	0.08	Enoyl-CoA delta isomerase 2, mitochondrial	1	1.45
ECHB_HUMAN	12 (5)	373.81	0.39	Trifunctional enzyme subunit beta, mitochondrial	2.55	1
ANXA7_HUMAN	12 (3)	371.57	5.67E-04	Annexin A7	1.57	1
RMXL1_HUMAN	12 (1)	370.83	1	RNA binding motif protein, X-linked-like-1	1.01	1
GNAS1_HUMAN	13 (4)	370.37	0.02	Guanine nucleotide-binding protein G(s) subunit alpha isoforms XLas	1	2.6
HSP74_HUMAN	14 (5)	369.41	0.63	Heat shock 70 kDa protein 4	1.72	1
SMRC2_HUMAN	13 (3)	367.78	5.51E-05	SWI/SNF complex subunit SMARCC2	1	2.56
SC22B_HUMAN	8 (6)	367.17	0.1	Vesicle-trafficking protein SEC22b	1	1.6
AT1A4_HUMAN	14 (3)	365.5	0.74	Sodium/potassium-transporting ATPase subunit alpha-4	1	1.06
RIR1_HUMAN	13 (4)	365.17	0.18	Ribonucleoside-diphosphate reductase large subunit	1	1.74
DDB1_HUMAN	10 (3)	364.5	0.38	DNA damage-binding protein 1	1.22	1
PGM1_HUMAN	11 (4)	361.03	0.17	Phosphoglucomutase-1	1	7.44
CD44_HUMAN	7 (3)	359.49	0.92	CD44 antigen	1.63	1
GSTK1_HUMAN	6 (3)	358.6	0.79	Glutathione S-transferase kappa 1	1.05	1
RAP1B_HUMAN	6 (1)	358.33	6.10E-03	Ras-related protein Rap-1b	3.43	1
SF3A1_HUMAN	12 (4)	358.32	0.86	Splicing factor 3A subunit 1	1.01	1
SRSF7_HUMAN	10 (1)	356.84	0.45	Serine/arginine-rich splicing factor 7	1.41	1
MOT1_HUMAN	7 (3)	355.97	0.39	Monocarboxylate transporter 1	2.51	1
SSRA_HUMAN	4 (1)	352.8	1	Translocon-associated protein subunit alpha	1.31	1
EIF3F_HUMAN	5 (4)	351.9	0.87	Eukaryotic translation initiation factor 3 subunit F	1	1.05
KCRU_HUMAN	10 (3)	350.93	0.03	Creatine kinase U-type, mitochondrial	1	1.42
FUBP2_HUMAN	9 (2)	350.49	0.64	Far upstream element-binding protein 2	1.17	1
COPA_HUMAN	17 (1)	349.77	0.42	Coatomer subunit alpha	3.89	1
SP16H_HUMAN	11 (5)	348.84	0.03	FACT complex subunit SPT16	3.45	1
MIC19_HUMAN	7 (5)	347.5	0.82	MICOS complex subunit MIC19	1.06	1
TR150_HUMAN	19 (3)	347.41	0.1	Thyroid hormone receptor-associated protein 3	5.67	1
SYVC_HUMAN	13 (4)	346.46	0.26	Valine--tRNA ligase	1.24	1
UGGG1_HUMAN	15 (6)	342.85	0.72	UDP-glucose:glycoprotein glucosyltransferase 1	1	1.32
KAD2_HUMAN	12 (5)	341.8	9.19E-04	Adenylate kinase 2, mitochondrial	1	12.37
TIM50_HUMAN	5 (3)	341.25	0.29	Mitochondrial import inner membrane translocase subunit TIM50	1.51	1
RHOA_HUMAN	6 (2)	339.51	0.76	Transforming protein RhoA	1.4	1
CY1_HUMAN	6 (5)	338.35	0.21	Cytochrome c1, heme protein, mitochondrial	1.49	1
IDH3B_HUMAN	6 (4)	337.73	0.93	Isocitrate dehydrogenase [NAD] subunit beta, mitochondrial	1.06	1
COF1_HUMAN	7 (1)	337.17	0.23	Cofilin-1	3.62	1
MACF1_HUMAN	45 (6)	337.11	0.47	Microtubule-actin cross-linking factor 1, isoforms 1/2/3/5	1	1.39
RS17_HUMAN	6 (5)	336.62	0.54	40S ribosomal protein S17	1.4	1
NOP58_HUMAN	12 (2)	335.85	0.42	Nucleolar protein 58	1	1.68
GTR1_HUMAN	6 (3)	334.89	0.75	Solute carrier family 2, facilitated glucose transporter member 1	1.37	1
CPSF5_HUMAN	7 (5)	332.58	0.03	Cleavage and polyadenylation specificity factor subunit 5	1	1.2
DYN2_HUMAN	12 (1)	331.07	0.02	Dynamin-2	1	9.4
1433G_HUMAN	8 (1)	328.4	0.44	14-3-3 protein gamma	1	1.28
ABCF1_HUMAN	12 (5)	325.31	0.02	ATP-binding cassette sub-family F member 1	1.97	1
FUBP1_HUMAN	7 (3)	325.28	6.94E-03	Far upstream element-binding protein 1	1.8	1
AT2B2_HUMAN	9 (1)	325.17	0.09	Plasma membrane calcium-transporting ATPase 2	1	2.74
NOMO2_HUMAN	7 (2)	324.73	0.73	Nodal modulator 2	1	1.03
TOM70_HUMAN	12 (4)	324.1	0.23	Mitochondrial import receptor subunit TOM70	1.44	1
ESYT1_HUMAN	12 (4)	322.23	0.06	Extended synaptotagmin-1	1	5.55
NDKA_HUMAN	7 (1)	319.4	0.48	Nucleoside diphosphate kinase A	41.12	1
RL11_HUMAN	8 (1)	318.76	3.36E-03	60S ribosomal protein L11	3.32	1
RL3_HUMAN	15 (4)	317.7	0.06	60S ribosomal protein L3	2.01	1
RAB5A_HUMAN	7 (2)	316.3	0.01	Ras-related protein Rab-5A	1.66	1
RS5_HUMAN	9 (3)	315.38	0.84	40S ribosomal protein S5	1.57	1
STIP1_HUMAN	15 (6)	314.39	0.6	Stress-induced-phosphoprotein 1	1.51	1
SYAC_HUMAN	15 (5)	314.39	0.04	Alanine--tRNA ligase, cytoplasmic	4.53	1

MYH11_HUMAN	22 (1)	314.04	0.01	Myosin-11	1	1.8
MBB1A_HUMAN	15 (5)	310.12	0.33	Myb-binding protein 1A	1	1.32
G6PI_HUMAN	3 (3)	309.91	0.09	Glucose-6-phosphate isomerase	1.69	1
AT1B3_HUMAN	5 (2)	308.01	3.93E-05	Sodium/potassium-transporting ATPase subunit beta-3	2.15	1
TMED9_HUMAN	4 (1)	307.83	0.73	Transmembrane emp24 domain-containing protein 9	1	1.08
MCM3_HUMAN	8 (3)	307.73	0.43	DNA replication licensing factor MCM3	1.14	1
HSDL2_HUMAN	7 (1)	304.73	0.4	Hydroxysteroid dehydrogenase-like protein 2	1.41	1
SRSF3_HUMAN	7 (2)	303.89	0.55	Serine/arginine-rich splicing factor 3	1	1.13
RL13A_HUMAN	10 (4)	302.19	0.42	60S ribosomal protein L13a	1.17	1
IDHP_HUMAN	12 (6)	301.2	0.03	Isocitrate dehydrogenase [NADP], mitochondrial	1	1.76
SRP14_HUMAN	4 (4)	300	0.31	Signal recognition particle 14 kDa protein	2.22	1
PABP3_HUMAN	14 (1)	299.61	8.99E-03	Polyadenylate-binding protein 3	1	4.14
UCRIL_HUMAN	6 (1)	298.22	0.24	Putative cytochrome b-c1 complex subunit Rieske-like protein 1	1	1.51
SF3B3_HUMAN	13 (5)	296.32	0.02	Splicing factor 3B subunit 3	3.37	1
RS13_HUMAN	8 (2)	295.02	0.03	40S ribosomal protein S13	3.32	1
PCBP2_HUMAN	5 (1)	294.52	0.14	Poly(rC)-binding protein 2	4.58	1
VDAC3_HUMAN	5 (3)	291.29	0.47	Voltage-dependent anion-selective channel protein 3	1.18	1
LETM1_HUMAN	13 (2)	291.02	0.03	Mitochondrial proton/calcium exchanger protein	2.59	1
NDUV2_HUMAN	5 (3)	290.61	0.7	NADH dehydrogenase [ubiquinone] flavoprotein 2, mitochondrial	1.06	1
TOP2B_HUMAN	11 (3)	289.67	0.07	DNA topoisomerase 2-beta	1.14	1
RL29_HUMAN	6 (2)	289.43	0.01	60S ribosomal protein L29	1	2.62
H2A1B_HUMAN	5 (1)	286.86	0.2	Histone H2A type 1-B/E	1.89	1
NUMA1_HUMAN	35 (10)	286.85	0.72	Nuclear mitotic apparatus protein 1	1	1.07
ADT4_HUMAN	12 (1)	286.73	0.83	ADP/ATP translocase 4	1	1.02
MPCP_HUMAN	10 (3)	286.05	0.62	Phosphate carrier protein, mitochondrial	1.29	1
FKBP3_HUMAN	12 (7)	286.04	0.36	Peptidyl-prolyl cis-trans isomerase FKBP3	1	1.25
COPE_HUMAN	8 (5)	285.98	0.46	Coatomer subunit epsilon	1.3	1
SRRT_HUMAN	12 (3)	285.86	0.27	Serrate RNA effector molecule homolog	1	1.74
ODO1_HUMAN	11 (3)	285.77	0.08	2-oxoglutarate dehydrogenase, mitochondrial	1	3.2
H2AV_HUMAN	4 (1)	285.57	0.05	Histone H2A.V	7.91	1
IF6_HUMAN	5 (4)	283.42	0.79	Eukaryotic translation initiation factor 6	1.03	1
HNRH3_HUMAN	6 (2)	283.06	0.94	Heterogeneous nuclear ribonucleoprotein H3	1.26	1
PGAM1_HUMAN	7 (2)	279.48	0.13	Phosphoglycerate mutase 1	1	3.03
PPIA_HUMAN	5 (2)	279.29	0.59	Peptidyl-prolyl cis-trans isomerase A	1.34	1
AIMP1_HUMAN	5 (1)	279.24	0.35	Aminoacyl tRNA synthase complex-interacting multifunctional protein 1	1.58	1
DECR_HUMAN	7 (5)	278.65	0.01	2,4-dienoyl-CoA reductase, mitochondrial	3	1
SF3B2_HUMAN	17 (10)	278.13	8.71E-03	Splicing factor 3B subunit 2	2.38	1
MSH2_HUMAN	6 (2)	275.1	0.82	DNA mismatch repair protein Msh2	1	1.02
BUB3_HUMAN	8 (5)	273.74	0.33	Mitotic checkpoint protein BUB3	1.31	1
TPM3_HUMAN	15 (4)	273.37	0.01	Tropomyosin alpha-3 chain	2.69	1
RAB5B_HUMAN	5 (1)	272.24	0.4	Ras-related protein Rab-5B	1	1.27
RAD50_HUMAN	19 (2)	272.24	0.23	DNA repair protein RAD50	16.9	1
ACLY_HUMAN	11 (4)	269.43	0.04	ATP-citrate synthase	5.05	1
TIM44_HUMAN	6 (4)	267.77	0.15	Mitochondrial import inner membrane translocase subunit TIM44	1.16	1
RS16_HUMAN	7 (3)	266.54	0.55	40S ribosomal protein S16	2.64	1
RL27_HUMAN	7 (4)	266.2	0.02	60S ribosomal protein L27	1.96	1
DPM1_HUMAN	10 (3)	265.96	0.04	Dolichol-phosphate mannosyltransferase subunit 1	2.55	1
SSBP_HUMAN	4 (4)	264.89	0.9	Single-stranded DNA-binding protein, mitochondrial	1.1	1
RALY_HUMAN	9 (4)	264.51	0.05	RNA-binding protein Raly	1.5	1
HNRDL_HUMAN	6 (3)	263.18	0.89	Heterogeneous nuclear ribonucleoprotein D-like 3	1	1.06
RL12_HUMAN	3 (2)	262.18	0.3	60S ribosomal protein L12	1.88	1
TBAL3_HUMAN	8 (1)	261.79	0.74	Tubulin alpha chain-like 3	1	92.62
TM14C_HUMAN	4 (2)	260.07	0.34	Transmembrane protein 14C	1	1.34
OBSCN_HUMAN	45 (15)	259.19	0.07	Obscurin	1	10.76
SDHB_HUMAN	9 (4)	258.81	0.45	Succinate dehydrogenase [ubiquinone] iron-sulfur subunit, mitochondrial	1.29	1
DSRAD_HUMAN	13 (2)	258.71	0.07	Double-stranded RNA-specific adenosine deaminase	1	8.34
GTF2I_HUMAN	15 (5)	258.33	0.02	General transcription factor II-I	1.71	1
PSA2_HUMAN	7 (4)	258.28	0.05	Proteasome subunit alpha type-2	1	1.49

NIPS1_HUMAN	7 (4)	258.06	0.04	Protein NipSnap homolog 1	1	2.01
PARK7_HUMAN	5 (3)	257.4	0.87	Protein DJ-1	1.04	1
CPNE1_HUMAN	6 (3)	254.73	0.35	Copine-1	1.81	1
NOG1_HUMAN	9 (3)	251.53	0.25	Nucleolar GTP-binding protein 1	1.59	1
IPYR2_HUMAN	5 (5)	248.15	0.38	Inorganic pyrophosphatase 2, mitochondrial	1	1.68
PODXL_HUMAN	6 (3)	247.45	0.15	Podocalyxin	5.99	1
TPD54_HUMAN	7 (3)	246.74	0.35	Tumor protein D54	1	1.07
RS24_HUMAN	4 (3)	246.49	0.06	40S ribosomal protein S24	2.73	1
PGK2_HUMAN	14 (1)	245.2	0.04	Phosphoglycerate kinase 2	2.38	1
PGRC2_HUMAN	5 (2)	244.37	0.58	Membrane-associated progesterone receptor component 2	1.2	1
3HIDH_HUMAN	6 (4)	244.01	0.53	3-hydroxyisobutyrate dehydrogenase, mitochondrial	2.02	1
LMAN2_HUMAN	5 (4)	243.86	0.16	Vesicular integral-membrane protein VIP36	1.74	1
SURF4_HUMAN	4 (2)	243.65	0.49	Surfeit locus protein 4	3.3	1
MAP2_HUMAN	3 (3)	243.04	0.4	Methionine aminopeptidase 2	3.03	1
EIFCL_HUMAN	14 (3)	242.23	0.09	Eukaryotic translation initiation factor 3 subunit C-like protein	2.71	1
MCM4_HUMAN	11 (3)	242.1	0.56	DNA replication licensing factor MCM4	1	1.07
RAB10_HUMAN	7 (1)	240.86	0.12	Ras-related protein Rab-10	1	2.02
RL19_HUMAN	5 (3)	238.22	0.9	60S ribosomal protein L19	1.1	1
RBBP7_HUMAN	5 (2)	238.14	0.51	Histone-binding protein RBBP7	1.19	1
ATD3B_HUMAN	16 (4)	237.26	0.14	ATPase family AAA domain-containing protein 3B	1	2.53
PLOD3_HUMAN	8 (1)	237.17	0.07	Procollagen-lysine,2-oxoglutarate 5-dioxygenase 3	1	236.32
NDK8_HUMAN	7 (1)	236.88	0.45	Putative nucleoside diphosphate kinase	1	1.34
CDC42_HUMAN	4 (3)	236.15	0.02	Cell division control protein 42 homolog	1	5.87
EIF3M_HUMAN	6 (3)	235.49	0.2	Eukaryotic translation initiation factor 3 subunit M	2.81	1
ROA0_HUMAN	3 (2)	235.02	0.37	Heterogeneous nuclear ribonucleoprotein A0	1.46	1
ARF3_HUMAN	5 (3)	234.31	0.41	ADP-ribosylation factor 3	1.89	1
1433T_HUMAN	4 (1)	233.97	0.8	14-3-3 protein theta	1.16	1
ODP2_HUMAN	14 (4)	233.89	0.89	Dihydrolipoyllysine-residue acetyltransferase component of pyruvate dehydrogenase complex, mitochondrial3	1	1.8
RHOC_HUMAN	3 (1)	233.16	0.36	Rho-related GTP-binding protein RhoC	10.55	1
RAB8A_HUMAN	5 (1)	232.83	0.36	Ras-related protein Rab-8A	1	1.51
OST48_HUMAN	5 (3)	232.19	0.28	Dolichyl-diphosphooligosaccharide--protein glycosyltransferase 48 kDa subunit	1.41	1
RL14_HUMAN	7 (1)	231.7	0.06	60S ribosomal protein L14	1	2.03
1433S_HUMAN	4 (2)	231.25	0.23	14-3-3 protein sigma	1	1.65
RCC2_HUMAN	6 (3)	230.84	0.02	Protein RCC2	3.52	1
1433B_HUMAN	11 (2)	229.95	0.67	14-3-3 protein beta/alpha	1	1.16
CC124_HUMAN	4 (3)	228.18	0.06	Coiled-coil domain-containing protein 124	1	4.02
RAN_HUMAN	6 (3)	226.41	0.04	GTP-binding nuclear protein Ran	1.96	1
TECR_HUMAN	8 (4)	226.31	0.24	Very-long-chain enoyl-CoA reductase	43.97	1
SYFA_HUMAN	6 (2)	225.8	0.77	Phenylalanine--tRNA ligase alpha subunit	1	1.2
NICA_HUMAN	10 (2)	224.4	0.59	Nicastrin	1.86	1
SRSF2_HUMAN	2 (1)	223.82	0.75	Serine/arginine-rich splicing factor 2	1.09	1
DNJA1_HUMAN	8 (4)	222.15	0.02	DnaJ homolog subfamily A member 1	7.74	1
PSA5_HUMAN	3 (3)	222.02	0.88	Proteasome subunit alpha type-5	1.25	1
SPB6_HUMAN	5 (3)	221.91	0.78	Serpin B6	1.01	1
IPO5_HUMAN	11 (2)	221.38	0.83	Importin-5	1.1	1
GYS1_HUMAN	9 (2)	220.92	2.61E-05	Glycogen [starch] synthase, muscle	1	2
FSCN1_HUMAN	2 (2)	220.67	0.98	Fascin	1	1.23
CN166_HUMAN	6 (4)	220.36	0.68	UPF0568 protein C14orf166	1.82	1
TOP1_HUMAN	11 (4)	220.18	0.01	DNA topoisomerase 1	1.51	1
DHTK1_HUMAN	7 (1)	219.55	0.67	Probable 2-oxoglutarate dehydrogenase E1 component DHKTD1, mitochondrial	11.99	1
ABCA4_HUMAN	36 (7)	219.45	0.1	Retinal-specific ATP-binding cassette transporter	1	2.27
GSTM3_HUMAN	6 (2)	219.36	0.04	Glutathione S-transferase Mu 3	2.6	1
TCTP_HUMAN	4 (1)	219.26	0.03	Translationally-controlled tumor protein	1.65	1
SAHH_HUMAN	11 (5)	218.5	0.33	Adenosylhomocysteinase	1.73	1
RCN1_HUMAN	7 (4)	218.33	0.04	Reticulocalbin-1	2.27	1
TCRG1_HUMAN	16 (5)	218.08	0.55	Transcription elongation regulator 1	1.15	1
LDH6B_HUMAN	4 (1)	216.94	0.05	L-lactate dehydrogenase A-like 6B	1	5.59
PSA1_HUMAN	4 (3)	216.44	0.92	Proteasome subunit alpha type-1	1.09	1

CPNS1_HUMAN	2 (2)	216.08	0.05	Calpain small subunit 1	1	2.57
EWS_HUMAN	13 (1)	215.29	0.16	RNA-binding protein EWS	1	4.58
KCRB_HUMAN	4 (2)	215.24	6.48E-03	Creatine kinase B-type	1	1.99
TBA4B_HUMAN	5 (1)	213.93	0.63	Putative tubulin-like protein alpha-4B	2.33	1
MUC18_HUMAN	7 (3)	213.39	0.12	Cell surface glycoprotein MUC18	6.03	1
PCYOX_HUMAN	4 (2)	213.01	0.09	Prenylcysteine oxidase 1	2.76	1
SEPT9_HUMAN	13 (5)	212.52	0.35	Septin-9	1	6.73
M2OM_HUMAN	8 (5)	211.73	0.21	Mitochondrial 2-oxoglutarate/malate carrier protein	2.82	1
RFC4_HUMAN	5 (3)	210.85	0.11	Replication factor C subunit 4	1.51	1
IF4G1_HUMAN	20 (7)	210.33	0.11	Eukaryotic translation initiation factor 4 gamma 1	3.3	1
NU155_HUMAN	4 (2)	208.14	0.92	Nuclear pore complex protein Nup155	1	1.03
PCBP3_HUMAN	5 (1)	207.32	0.28	Poly(rC)-binding protein 3	1	1.24
RL35_HUMAN	4 (3)	206.72	0.29	60S ribosomal protein L35	3.72	1
SMHD1_HUMAN	13 (3)	205.28	0.06	Structural maintenance of chromosomes flexible hinge domain-containing protein 1	1	1.98
MRRP1_HUMAN	7 (6)	202.26	0.02	Mitochondrial ribonuclease P protein 1	1	1.88
BAG2_HUMAN	4 (3)	202.05	0.73	BAG family molecular chaperone regulator 2	1	1.08
RB11A_HUMAN	4 (3)	201.98	0.22	Ras-related protein Rab-11A	1.11	1
PDIP2_HUMAN	5 (2)	201.55	0.04	Polymerase delta-interacting protein 2	1	1.22
VTNC_HUMAN	3 (2)	200.93	3.94E-03	Vitronectin	3.03	1
DDX50_HUMAN	13 (1)	200.31	0.07	ATP-dependent RNA helicase DDX50	1	2.13
RS11_HUMAN	5 (2)	199.8	0.21	40S ribosomal protein S11	1	1.82
CATA_HUMAN	6 (3)	198.25	0.4	Catalase	1.46	1
RBCC1_HUMAN	32 (6)	197.87	0.05	RB1-inducible coiled-coil protein 1	1	4.9
GTR14_HUMAN	5 (2)	197.67	7.38E-03	Solute carrier family 2, facilitated glucose transporter member 14	12.43	1
MCM7_HUMAN	8 (3)	196.38	0.02	DNA replication licensing factor MCM7	1	3.11
DEK_HUMAN	8 (4)	196.08	0.6	Protein DEK	1	1.74
RAB6A_HUMAN	7 (2)	193.96	0.83	Ras-related protein Rab-6A	1.03	1
RPAC1_HUMAN	5 (3)	193.3	0.25	DNA-directed RNA polymerases I and III subunit RPAC1	1	1.61
TCEA1_HUMAN	5 (2)	193.23	9.29E-03	Transcription elongation factor A protein 1	1	1.95
ODB2_HUMAN	4 (3)	192.07	0.45	Lipoamide acyltransferase component of branched-chain alpha-keto acid dehydrogenase complex, mitochondrial	1	1.26
CNPY2_HUMAN	2 (1)	192.01	0.15	Protein canopy homolog 2	3.12	1
SNAA_HUMAN	5 (4)	191.66	0.4	Alpha-soluble NSF attachment protein	1.44	1
NP1L1_HUMAN	4 (2)	191.6	2.72E-04	Nucleosome assembly protein 1-like 1	4.09	1
NDUAA_HUMAN	7 (4)	191.45	0.06	NADH dehydrogenase [ubiquinone] 1 alpha subcomplex subunit 10, mitochondrial	1.37	1
THOC6_HUMAN	6 (2)	190.2	0.87	THO complex subunit 6 homolog	1.07	1
NNTM_HUMAN	6 (2)	189.83	0.69	NAD(P) transhydrogenase, mitochondrial	1	1.07
KHDR1_HUMAN	14 (1)	189.01	0.34	KH domain-containing, RNA-binding, signal transduction-associated protein 1	1	1.82
NIPS2_HUMAN	6 (2)	188.26	0.19	Protein NipSnap homolog 2	1	1.81
CLPP_HUMAN	8 (2)	188.12	0.56	ATP-dependent Clp protease proteolytic subunit, mitochondrial	1	1.1
RBP56_HUMAN	4 (1)	187.84	0.36	TATA-binding protein-associated factor 2N	1	1.38
SMD1_HUMAN	3 (1)	186.74	0.96	Small nuclear ribonucleoprotein Sm D1	8.97	1
TIF1B_HUMAN	8 (2)	186.48	0.09	Transcription intermediary factor 1-beta	1	3.31
IF2G_HUMAN	10 (3)	185.78	0.02	Eukaryotic translation initiation factor 2 subunit 3	1.69	1
FKB10_HUMAN	8 (2)	185.38	0.57	Peptidyl-prolyl cis-trans isomerase FKBP10	1	3.15
UBP2L_HUMAN	5 (3)	184.96	0.04	Ubiquitin-associated protein 2-like	1	7.39
LAP2B_HUMAN	9 (5)	183.7	0.12	Lamina-associated polypeptide 2, isoforms beta/gamma	2.16	1
HDHD5_HUMAN	8 (3)	183.05	0.46	Haloacid dehalogenase-like hydrolase domain-containing 5	1	1.29
HPPD_HUMAN	10 (6)	182.81	0.99	4-hydroxyphenylpyruvate dioxygenase	1.21	1
NDUA9_HUMAN	4 (2)	182.63	0.06	NADH dehydrogenase [ubiquinone] 1 alpha subcomplex subunit 9, mitochondrial	1	2.74
MK67I_HUMAN	3 (2)	182.28	0.84	MKI67 FHA domain-interacting nucleolar phosphoprotein	1.1	1
GNAI3_HUMAN	7 (1)	181.69	7.85E-05	Guanine nucleotide-binding protein G(k) subunit alpha	0	∞
SODM_HUMAN	4 (2)	181.46	0.49	Superoxide dismutase [Mn], mitochondrial	1.31	1
EFGM_HUMAN	11 (4)	181.03	0.05	Elongation factor G, mitochondrial	1.52	1
RENT1_HUMAN	7 (1)	181.01	0.48	Regulator of nonsense transcripts 1	104.75	1
QOR_HUMAN	6 (2)	180.97	0.05	Quinone oxidoreductase	5.28	1
SMC4_HUMAN	14 (1)	180.08	0.2	Structural maintenance of chromosomes protein 4	1	1.69
RHG01_HUMAN	5 (3)	179.94	0.15	Rho GTPase-activating protein 1	3.99	1
PRP8_HUMAN	16 (4)	178.86	0.05	Pre-mRNA-processing-splicing factor 8	2.64	1

RS18_HUMAN	6 (2)	178.78	6.00E-05	40S ribosomal protein S18	2.09	1
KTNB1_HUMAN	13 (3)	178.62	0.06	Katanin p80 WD40 repeat-containing subunit B1	3.01	1
ASPM_HUMAN	24 (1)	178.61	0.37	Abnormal spindle-like microcephaly-associated protein	2.32	1
NAT10_HUMAN	7 (4)	178.51	0.28	RNA cytidine acetyltransferase	1	1.46
EMD_HUMAN	4 (4)	178.29	0.46	Emerin	1	1.26
ACAD9_HUMAN	10 (3)	177	0.65	Acyl-CoA dehydrogenase family member 9, mitochondrial	5.96	1
PUR2_HUMAN	8 (3)	176.04	0.01	Trifunctional purine biosynthetic protein adenosine-3	3.54	1
SORCN_HUMAN	5 (1)	175.62	0.45	Sorcin	1.47	1
ACOX1_HUMAN	9 (2)	174.89	0.03	Peroxisomal acyl-coenzyme A oxidase 1	2.71	1
DNJC9_HUMAN	6 (2)	174.56	0.14	DnaJ homolog subfamily C member 9	1	1.86
DNMT1_HUMAN	12 (1)	174.13	0.14	DNA (cytosine-5)-methyltransferase 1	∞	0
VAPA_HUMAN	7 (3)	173.89	0.72	Vesicle-associated membrane protein-associated protein A	1	1.05
HBA_HUMAN	3 (1)	173.3	0.38	Hemoglobin subunit alpha 2	2.07	1
RBM14_HUMAN	7 (3)	173.21	0.05	RNA-binding protein 14	1.81	1
RU17_HUMAN	6 (3)	171.76	0.42	U1 small nuclear ribonucleoprotein 70 kDa	1	1.2
RAP2C_HUMAN	3 (1)	171.42	0.36	Ras-related protein Rap-2c Ras-related protein Rap-2c	1	1.26
CHD3_HUMAN	17 (3)	170.18	0.03	Chromodomain-helicase-DNA-binding protein 3	1	4.6
RM11_HUMAN	6 (1)	170.04	0.1	39S ribosomal protein L11, mitochondrial	1	5.38
RAB13_HUMAN	4 (2)	169.74	0.14	Ras-related protein Rab-13	1.41	1
PRDX5_HUMAN	3 (2)	169.32	0.23	Peroxiredoxin-5, mitochondrial	5.66	1
RU1C_HUMAN	2 (2)	169.31	0.16	U1 small nuclear ribonucleoprotein C	1	2.66
COPG1_HUMAN	11 (3)	169.28	0.36	Coatomer subunit gamma-1	3.98	1
NDUV1_HUMAN	8 (1)	168.33	0.33	NADH dehydrogenase [ubiquinone] flavoprotein 1, mitochondrial	2.35	1
BTF3_HUMAN	5 (4)	167.42	0.36	Transcription factor BTF3	1.58	1
SSRG_HUMAN	3 (3)	167.2	0.65	Translocon-associated protein subunit gamma	1	1.4
PSMD2_HUMAN	7 (3)	167.15	0.28	26S proteasome non-ATPase regulatory subunit 2	1.34	1
CPT2_HUMAN	11 (3)	166.85	0.14	Carnitine O-palmitoyltransferase 2, mitochondrial	3.04	1
SCAM3_HUMAN	3 (1)	166.64	0.9	Secretory carrier-associated membrane protein 3	1.07	1
PO210_HUMAN	6 (2)	166.55	5.41E-04	Nuclear pore membrane glycoprotein 210	2.06	1
NDUS7_HUMAN	3 (1)	165.9	0.93	NADH dehydrogenase [ubiquinone] iron-sulfur protein 7, mitochondrial	1.07	1
MUC19_HUMAN	33 (4)	165.08	0.26	Mucin-19	1.49	1
TMED4_HUMAN	3 (1)	165.07	0.86	Transmembrane emp24 domain-containing protein 4	1	1.08
TADBP_HUMAN	5 (2)	164	0.8	TAR DNA-binding protein 43	1.25	1
TCP4_HUMAN	2 (1)	163.82	0.23	Activated RNA polymerase II transcriptional coactivator p15	4.43	1
LARP4_HUMAN	2 (1)	163.6	0.01	La-related protein 4	1	12.65
CCD47_HUMAN	7 (3)	163.33	0.34	Coiled-coil domain-containing protein 47	1.76	1
NOLC1_HUMAN	6 (3)	163.26	0.06	Nucleolar and coiled-body phosphoprotein 1	1	4.6
ANX11_HUMAN	12 (4)	162.49	0.86	Annexin A11	1	1.02
DDX6_HUMAN	6 (4)	162.26	0.16	Probable ATP-dependent RNA helicase DDX6	1.52	1
HEXB_HUMAN	4 (2)	161.92	0.69	Beta-hexosaminidase subunit beta	1	1.04
CAZA1_HUMAN	4 (3)	161.52	0.16	F-actin-capping protein subunit alpha-1	1.26	1
NOP16_HUMAN	3 (3)	161.05	0.39	Nucleolar protein 16	1.26	1
DJB11_HUMAN	4 (4)	161	0.91	DnaJ homolog subfamily B member 11	1.11	1
IF2B1_HUMAN	6 (2)	160.87	0.24	Insulin-like growth factor 2 mRNA-binding protein 1	4.23	1
CYB5B_HUMAN	3 (2)	160.85	2.83E-03	Cytochrome b5 type B	1.59	1
RUVB2_HUMAN	6 (1)	160.78	0.04	RuvB-like 2	6.45	1
CPNE3_HUMAN	6 (3)	160.44	0.1	Copine-3	1	2.82
MPRI_HUMAN	13 (1)	159.71	0.94	Cation-independent mannose-6-phosphate receptor	28.8	1
CLIC1_HUMAN	3 (2)	159.67	0.4	Chloride intracellular channel protein 1	1.6	1
HP1B3_HUMAN	6 (1)	159.11	0.67	Heterochromatin protein 1-binding protein 3	1	1.05
AT2A1_HUMAN	9 (1)	158.51	1.19E-03	Sarcoplasmic/endoplasmic reticulum calcium ATPase 1	3.86	1
NP1L4_HUMAN	6 (2)	157.72	0.51	Nucleosome assembly protein 1-like 4	1.84	1
ATPK_HUMAN	4 (1)	156.97	0.61	ATP synthase subunit f, mitochondrial	1	1.15
DYH5_HUMAN	29 (4)	156.82	0.09	Dynein heavy chain 5, axonemal	4.73	1
EMC2_HUMAN	5 (2)	156.64	0.04	ER membrane protein complex subunit 2	4.94	1
PRPS1_HUMAN	6 (1)	156.29	0.74	Ribose-phosphate pyrophosphokinase 1	1.12	1
SSRP1_HUMAN	9 (4)	155.75	0.28	FACT complex subunit SSRP1	2.79	1
PCH2_HUMAN	6 (1)	153.87	0.03	Pachytene checkpoint protein 2 homolog	42.91	1

TMCO1_HUMAN	4 (1)	153.65	0.59	Calcium load-activated calcium channel	5.91	1
GBB1_HUMAN	4 (2)	152.66	0.82	Guanine nucleotide-binding protein G(I)/G(S)/G(T) subunit beta-1	1.37	1
SARNP_HUMAN	4 (2)	151.81	0.04	SAP domain-containing ribonucleoprotein	1.44	1
SC24C_HUMAN	8 (1)	151.81	0.57	Protein transport protein Sec24C	26.75	1
COPB_HUMAN	17 (2)	150.61	0.11	Coatomer subunit beta	1	6.46
S10AB_HUMAN	1 (1)	150.56	0.09	Protein S100-A11	4.28	1
H2B3B_HUMAN	3 (2)	150.41	2.05E-03	Histone H2B type 3-B	1	4.07
MSH6_HUMAN	8 (3)	150.22	0.03	DNA mismatch repair protein Msh6	1	2.61
SRS11_HUMAN	11 (2)	149.2	3.85E-03	Serine/arginine-rich splicing factor 11	18.09	1
PRS6A_HUMAN	10 (4)	149.02	0.06	26S proteasome regulatory subunit 6A	2.2	1
PSDE_HUMAN	3 (2)	148.93	0.17	26S proteasome non-ATPase regulatory subunit 14	2.74	1
RS10_HUMAN	3 (2)	148.79	0.2	40S ribosomal protein S10	2.99	1
KCY_HUMAN	3 (2)	147.95	0.36	UMP-CMP kinase	1.53	1
PRS56_HUMAN	8 (5)	147.75	0.2	Serine protease 56	1.83	1
CD63_HUMAN	4 (2)	147.4	0.02	CD63 antigen	5.84	1
DX39A_HUMAN	5 (2)	146.98	0.44	ATP-dependent RNA helicase DDX39A	1	1.33
SYCM_HUMAN	2 (2)	146.48	0.1	Probable cysteine--tRNA ligase, mitochondrial	27.13	1
RRP5_HUMAN	14 (2)	146.33	0.38	Protein RRP5 homolog	1	1.55
H1X_HUMAN	5 (1)	146.1	0.02	Histone H1x	1.75	1
COASY_HUMAN	6 (2)	145.82	0.61	Bifunctional coenzyme A synthase	1	1.31
SCRB2_HUMAN	5 (3)	145.81	0.67	Lysosome membrane protein 2	1	1.04
RBP2_HUMAN	15 (2)	145.17	0.67	E3 SUMO-protein ligase RanBP2	1	1.04
VAPB_HUMAN	3 (1)	144.55	0.46	Vesicle-associated membrane protein-associated protein B/C	1	1.18
OLA1_HUMAN	1 (1)	144.46	7.63E-03	Obg-like ATPase 1	1	4.56
ARPC3_HUMAN	4 (1)	144.39	0.14	Actin-related protein 2/3 complex subunit 3	2.14	1
ANXA3_HUMAN	5 (2)	143.83	0.07	Annexin A3	1	4.73
MMAB_HUMAN	7 (2)	143.75	0.41	Cob(I)yrinic acid a,c-diamide adenosyltransferase, mitochondrial	1.29	1
MDN1_HUMAN	29 (3)	143.46	2.12E-03	Midasin	3.56	1
CMC2_HUMAN	11 (2)	142.77	0.08	Calcium-binding mitochondrial carrier protein Aralar2	1	5.21
REV3L_HUMAN	21 (3)	141.97	0.13	DNA polymerase zeta catalytic subunit	1	4.05
HNRL1_HUMAN	8 (4)	141.76	0.02	Heterogeneous nuclear ribonucleoprotein U-like protein 1	1	1.88
EGFR_HUMAN	8 (1)	140.9	0.68	Epidermal growth factor receptor	1	1.05
RL31_HUMAN	5 (2)	140.89	0.4	60S ribosomal protein L31	5.8	1
PRP19_HUMAN	4 (2)	140.69	0.57	Pre-mRNA-processing factor 19	1.12	1
EIF3E_HUMAN	6 (2)	140.45	0.78	Eukaryotic translation initiation factor 3 subunit E	1	1.99
MCA3_HUMAN	3 (3)	140.21	0.08	Eukaryotic translation elongation factor 1 epsilon-1	2.72	1
FLNC_HUMAN	16 (1)	139.75	0.45	Filamin-C	4.88	1
PGAM5_HUMAN	3 (1)	138.55	0.13	Serine/threonine-protein phosphatase PGAM5, mitochondrial	2.35	1
RMXL2_HUMAN	11 (1)	138.04	0.7	RNA-binding motif protein, X-linked-like-2	1	1.07
HECD4_HUMAN	22 (7)	138.01	0.02	Probable E3 ubiquitin-protein ligase HECTD4	1	2.82
PCNA_HUMAN	4 (1)	137.97	0.14	Proliferating cell nuclear antigen	2.59	1
BAZ1B_HUMAN	12 (5)	137.59	0.08	Tyrosine-protein kinase BAZ1B	1	3.22
RL27A_HUMAN	4 (1)	137.51	0.08	60S ribosomal protein L27a	2.08	1
ERLN2_HUMAN	5 (3)	137.37	0.78	Erlin-2 OS=Homo sapiens	1	1
IF5A1_HUMAN	4 (2)	137.35	0.07	Eukaryotic translation initiation factor 5A-1	3.46	1
DYH1_HUMAN	20 (3)	137.26	0.1	Dynein heavy chain 1, axonemal	1.96	1
PP1B_HUMAN	4 (3)	137.16	2.84E-03	Serine/threonine-protein phosphatase PP1-beta catalytic subunit	1	5.34
IF2B2_HUMAN	6 (1)	137.01	1	Insulin-like growth factor 2 mRNA-binding protein 2	1	1.55
MCM6_HUMAN	7 (2)	136.38	0.04	DNA replication licensing factor MCM6	4.09	1
RBM25_HUMAN	10 (2)	136.34	0.4	RNA-binding protein 25	1	1.31
DNLI3_HUMAN	13 (1)	136.28	0.05	DNA ligase 3	1	4.73
ABCG2_HUMAN	7 (2)	135.85	0.68	ATP-binding cassette sub-family G member 2	1.29	1
DDX18_HUMAN	11 (3)	135.46	0.08	ATP-dependent RNA helicase DDX18	2.28	1
ZC3HD_HUMAN	20 (3)	135.44	0.18	Zinc finger CCCH domain-containing protein 13	1	1.71
EIF3I_HUMAN	2 (2)	134.91	0.25	Eukaryotic translation initiation factor 3 subunit I	1.38	1
NSDHL_HUMAN	2 (1)	134.65	0.14	Sterol-4-alpha-carboxylate 3-dehydrogenase, decarboxylating	1.59	1
SRPRB_HUMAN	4 (2)	134.57	0.22	Signal recognition particle receptor subunit beta	1	2
RTN4_HUMAN	13 (2)	134.19	0.85	Reticulon-4	1	1.33

TBRG4_HUMAN	9 (3)	134.02	4.18E-03	Protein TBRG4	6.86	1
GSLG1_HUMAN	12 (3)	133.56	0.08	Golgi apparatus protein 1	2.74	1
SYK_HUMAN	10 (3)	132.21	0.13	Lysine--tRNA ligase	1	2.76
SMCA5_HUMAN	12 (1)	131.1	0.19	SWI/SNF-related matrix-associated actin-dependent regulator of chromatin subfamily A member 5	∞	0
RL7L_HUMAN	6 (1)	130.81	0.14	60S ribosomal protein L7-like 1	1	5.67
IPO9_HUMAN	2 (1)	130.12	0.32	Importin-9	71.77	1
PRC2C_HUMAN	11 (3)	129.77	0.25	Protein PRRC2C	1	1.57
TPT1L_HUMAN	3 (1)	129.76	0.02	TPT1-like protein	1	3.66
LIMA1_HUMAN	6 (4)	128.12	5.74E-03	LIM domain and actin-binding protein 1	1	4.41
VA0D1_HUMAN	4 (3)	127.75	0.02	V-type proton ATPase subunit d 1	2.15	1
RCC1_HUMAN	3 (1)	127.38	0.94	Regulator of chromosome condensation	1	6.24
DYN1_HUMAN	10 (1)	127.09	0.68	Dynamin-1	1.05	1
PSME3_HUMAN	4 (2)	125.9	0.14	Proteasome activator complex subunit 3	1	1.54
RS23_HUMAN	2 (1)	124.51	0.51	40S ribosomal protein S23	1.41	1
RS20_HUMAN	4 (1)	124.23	0.69	40S ribosomal protein S20	1.59	1
SRSF4_HUMAN	13 (1)	124.2	0.26	Serine/arginine-rich splicing factor 4	2.34	1
COX5A_HUMAN	4 (2)	123.75	0.02	Cytochrome c oxidase subunit 5A, mitochondrial	2.8	1
GOGA2_HUMAN	6 (1)	123.52	0.07	Golgin subfamily A member 2	2.78	1
PEBP1_HUMAN	2 (1)	123.27	0.32	Phosphatidylethanolamine-binding protein 1	1.55	1
FAHD1_HUMAN	3 (3)	122.87	0.12	Acylpyruvase FAHD1, mitochondrial	1	3.24
CPSF6_HUMAN	4 (1)	121.79	1	Cleavage and polyadenylation specificity factor subunit 6	8.77	1
UTRO_HUMAN	18 (1)	121.25	0.29	Utrophin	2.33	1
RFC1_HUMAN	15 (3)	121.04	0.73	Replication factor C subunit 1	1	1.06
CDK1_HUMAN	2 (1)	120.95	0.19	Cyclin-dependent kinase 1	4	1
PLCA_HUMAN	9 (4)	120.92	0.56	1-acyl-sn-glycerol-3-phosphate acyltransferase alpha	1.17	1
MCM5_HUMAN	13 (2)	120.9	0.12	DNA replication licensing factor MCM5	1	1.29
NOP2_HUMAN	6 (1)	120.52	0.19	Probable 28S rRNA (cytosine(4447)-C(5))-methyltransferase	1	2.53
VPP1_HUMAN	6 (2)	120.38	0.14	V-type proton ATPase 116 kDa subunit a isoform 1	1	5.12
KAD4_HUMAN	6 (3)	120.01	0.25	Adenylate kinase 4, mitochondrial	1	1.2
PSB1_HUMAN	2 (2)	119.86	0.52	Proteasome subunit beta type-1	1.76	1
ERF1_HUMAN	4 (2)	119.78	0.05	Eukaryotic peptide chain release factor subunit 1	1.55	1
AP1B1_HUMAN	11 (1)	119.58	0.83	AP-1 complex subunit beta-1	3.66	1
MTFP1_HUMAN	3 (1)	119.54	0.05	Mitochondrial fission process protein 1	4.04	1
PSA7_HUMAN	3 (1)	119.27	0.03	Proteasome subunit alpha type-7	5.74	1
HEAT1_HUMAN	10 (1)	119.23	0.09	HEAT repeat-containing protein 1	39.75	1
MINT_HUMAN	18 (3)	117.99	0.99	Msx2-interacting protein	1.56	1
GRSF1_HUMAN	6 (2)	117.39	0.04	G-rich sequence factor 1	1	39.69
SLTM_HUMAN	7 (1)	117.28	0.93	SAFB-like transcription modulator	1.17	1
LEG3_HUMAN	4 (4)	117.22	0.38	Galectin-3	1	1.47
COQ9_HUMAN	4 (2)	116.6	0.64	Ubiquinone biosynthesis protein COQ9, mitochondrial	1.89	1
S38A2_HUMAN	3 (1)	115.89	0.1	Sodium-coupled neutral amino acid transporter 2	5.31	1
SAR1A_HUMAN	2 (1)	115.44	0.83	GTP-binding protein SAR1a	1.6	1
PR40A_HUMAN	8 (1)	115.25	0.35	Pre-mRNA-processing factor 40 homolog A	1	1.37
STAR9_HUMAN	25 (5)	115.19	0.55	StAR-related lipid transfer protein 9	1	1.28
H2B1L_HUMAN	3 (1)	114.28	0.8	Histone H2B type 1-L	1	1.32
CTNA1_HUMAN	10 (2)	113.94	0.79	Catenin alpha-1	1.41	1
SYQ_HUMAN	10 (2)	113.81	0.3	Glutamine--tRNA ligase	1.48	1
FRIL_HUMAN	2 (1)	113.72	4.60E-04	Ferritin light chain	2.26	1
MTCH2_HUMAN	4 (1)	113.48	0.11	Mitochondrial carrier homolog 2	2.55	1
MCTS1_HUMAN	6 (1)	113.33	0.98	Malignant T-cell-amplified sequence 1	1.4	1
ALDOC_HUMAN	2 (2)	113.29	0.98	Fructose-bisphosphate aldolase C	1.11	1
SDCB1_HUMAN	2 (2)	113.26	0.47	Syntenin-1	1.39	1
CHTOP_HUMAN	4 (1)	112.94	0.1	Chromatin target of PRMT1 protein	1	2.33
CAC1I_HUMAN	17 (2)	111.47	0.71	Voltage-dependent T-type calcium channel subunit alpha-1I	1.09	1
DDX23_HUMAN	9 (2)	111.37	0.69	Probable ATP-dependent RNA helicase DDX23	1	1.13
PRS8_HUMAN	9 (3)	110.96	0.63	26S proteasome regulatory subunit 8	1	1.36
FXR2_HUMAN	4 (1)	110.95	0.99	Fragile X mental retardation syndrome-related protein 2	1.93	1
MYCB2_HUMAN	28 (3)	110.62	0.23	E3 ubiquitin-protein ligase MYCBP2	1	2.22

DAF_HUMAN	4 (1)	109.59	0.2	Complement decay-accelerating factor	2.62	1
NAKD2_HUMAN	6 (2)	109.46	0.29	NAD kinase 2, mitochondrial	1.47	1
SC23A_HUMAN	5 (1)	109.31	0.87	Protein transport protein Sec23A	7.36	1
ECM29_HUMAN	9 (2)	109.21	0.66	Proteasome-associated protein ECM29 homolog	1.15	1
NMD3A_HUMAN	19 (2)	109.05	0.62	Glutamate receptor ionotropic, NMDA 3A	1	1.07
THOC2_HUMAN	8 (1)	109.04	0.71	THO complex subunit 2	1.27	1
PSIP1_HUMAN	7 (1)	108.95	0.79	PC4 and SFRS1-interacting protein	1	1
SYFB_HUMAN	12 (2)	108.56	0.7	Phenylalanine--tRNA ligase beta subunit	1	1.48
DNJB1_HUMAN	2 (2)	108.42	0.21	DnaJ homolog subfamily B member 1	1	1.84
CATD_HUMAN	5 (2)	108.31	0.2	Cathepsin D	1	1.57
NDUS8_HUMAN	7 (4)	108.2	0.22	NADH dehydrogenase [ubiquinone] iron-sulfur protein 8, mitochondrial	2.54	1
CCD51_HUMAN	3 (1)	107.98	0.55	Coiled-coil domain-containing protein 51	1	1.09
KAP2_HUMAN	5 (2)	107.8	0.06	cAMP-dependent protein kinase type II-alpha regulatory subunit	1	7.2
COPG2_HUMAN	10 (2)	107.76	0.32	Coatomer subunit gamma-2	1	1.23
RASK_HUMAN	5 (1)	107.75	0.62	GTPase KRas	1.74	1
SAFB1_HUMAN	13 (3)	107.42	0.24	Scaffold attachment factor B1	1	1.51
RT22_HUMAN	5 (2)	106.26	0.67	28S ribosomal protein S22, mitochondrial	1	1.07
NAV1_HUMAN	17 (1)	106.22	0.5	Neuron navigator 1	1	132.44
MARCS_HUMAN	3 (1)	105.95	1.02E-03	Myristoylated alanine-rich C-kinase substrate	11.76	1
GNA11_HUMAN	3 (2)	105.84	0.2	Guanine nucleotide-binding protein subunit alpha-11	1	1.98
STX4_HUMAN	3 (1)	105.8	0.35	Syntaxin-4	1.48	1
RL18A_HUMAN	8 (3)	105.45	0.25	60S ribosomal protein L18a	3.1	1
RANG_HUMAN	7 (2)	105.12	0.02	Ran-specific GTPase-activating protein	2.43	1
MRP1_HUMAN	9 (1)	105.09	0.01	Multidrug resistance-associated protein 1	1	1.40E+04
IF2B_HUMAN	4 (3)	105.08	0.13	Eukaryotic translation initiation factor 2 subunit 2	1	5.07
SCOT2_HUMAN	6 (1)	104.94	0.42	Succinyl-CoA:3-ketoacid coenzyme A transferase 2, mitochondrial	1	6.73
TP4A1_HUMAN	4 (2)	104.85	0.1	Protein tyrosine phosphatase type IVA 1	2.06	1
BLK_HUMAN	8 (2)	103.46	0.03	Tyrosine-protein kinase Blk	1	3.91
PLOD1_HUMAN	4 (1)	103.22	0.37	Procollagen-lysine,2-oxoglutarate 5-dioxygenase 1	1	1.35
PSD13_HUMAN	5 (1)	102.75	0.12	26S proteasome non-ATPase regulatory subunit 13	1	1.99
RPN2_HUMAN	4 (2)	102.46	0.04	Dolichyl-diphosphooligosaccharide--protein glycosyltransferase subunit 2	5.38	1
AT11B_HUMAN	6 (1)	102.05	0.24	Probable phospholipid-transporting ATPase IF	1.62	1
ODO2_HUMAN	4 (2)	101.79	0.14	Dihydrolipoyllysine-residue succinyltransferase component of 2-oxoglutarate dehydrogenase complex, mitochondrial	1	3.21
BRX1_HUMAN	4 (3)	101.62	0.06	Ribosome biogenesis protein BRX1 homolog	1	3.79
RM40_HUMAN	1 (1)	101.43	0.58	39S ribosomal protein L40, mitochondrial	1	1.28
TI23B_HUMAN	3 (1)	100.7	0.04	Putative mitochondrial import inner membrane translocase subunit Tim23B	3.88	1
ATD3C_HUMAN	6 (1)	100.68	0.25	ATPase family AAA domain-containing protein 3C	1	2.01
GDIB_HUMAN	3 (2)	100.61	0.6	Rab GDP dissociation inhibitor beta	1.77	1
P5CR2_HUMAN	4 (1)	100.41	0.75	Pyrroline-5-carboxylate reductase 2	1	1.07
GNA12_HUMAN	6 (2)	99.38	0.01	Guanine nucleotide-binding protein subunit alpha-12	1.72	1
RS26_HUMAN	4 (1)	99.32	0.35	40S ribosomal protein S26	2.63	1
AP2B1_HUMAN	10 (2)	98.5	0.99	AP-2 complex subunit beta	1.24	1
RT26_HUMAN	5 (1)	98.26	0.04	28S ribosomal protein S26, mitochondrial	1.96	1
MDHC_HUMAN	5 (1)	98.16	0.34	Malate dehydrogenase, cytoplasmic	0	∞
CAPG_HUMAN	3 (1)	97.98	0.73	Macrophage-capping protein	1.3	1
RRS1_HUMAN	8 (2)	97.91	0.62	Ribosome biogenesis regulatory protein homolog	1.1	1
ACACA_HUMAN	14 (3)	97.32	0.82	Acetyl-CoA carboxylase 1	1.05	1
PP1RA_HUMAN	7 (2)	96.7	0.85	Serine/threonine-protein phosphatase 1 regulatory subunit 10	1.31	1
CIP4_HUMAN	7 (2)	96.58	0.65	Cdc42-interacting protein 4	1.06	1
EIF3H_HUMAN	6 (5)	95.82	0.17	Eukaryotic translation initiation factor 3 subunit H	1	7.1
CHIP_HUMAN	6 (1)	95.72	0.15	E3 ubiquitin-protein ligase CHIP	1	3.84
DYR_HUMAN	3 (2)	95.43	0.03	Dihydrofolate reductase	2.57	1
CPNE7_HUMAN	6 (2)	95.15	0.5	Copine-7	1.97	1
C1TM_HUMAN	10 (3)	94.64	0.11	Monofunctional C1-tetrahydrofolate synthase, mitochondrial	1	3.6
PSB2_HUMAN	4 (2)	94.59	0.34	Proteasome subunit beta type-2	2.04	1
S61A2_HUMAN	5 (1)	94.59	0.17	Protein transport protein Sec61 subunit alpha isoform 2	∞	0
PERI_HUMAN	8 (2)	94.56	0.43	Peripherin	1	1.42
MIC25_HUMAN	6 (2)	94.14	0.36	MICOS complex subunit MIC25	1.52	1

RT27_HUMAN	5 (1)	93.97	0.9	28S ribosomal protein S27, mitochondrial	4.83	1
CSPG4_HUMAN	12 (1)	93.86	0.25	Chondroitin sulfate proteoglycan 4	1	2.97
RECQ1_HUMAN	6 (1)	93.7	0.01	ATP-dependent DNA helicase Q1	1	7.05
ES1_HUMAN	3 (1)	93.43	0.03	ES1 protein homolog, mitochondrial	3.16	1
SQSTM_HUMAN	2 (1)	93.42	0.09	Sequestosome-1	4.35	1
NDUBA_HUMAN	2 (1)	92.99	0.2	NADH dehydrogenase [ubiquinone] 1 beta subcomplex subunit 10	1	1.51
PON2_HUMAN	1 (1)	92.73	0.1	Serum paraoxonase/arylesterase 2	1.89	1
CHD5_HUMAN	10 (1)	92.51	0.01	Chromodomain-helicase-DNA-binding protein 5	1	3.85
RM13_HUMAN	3 (2)	92.48	0.63	39S ribosomal protein L13, mitochondrial	1	1.08
STML1_HUMAN	11 (3)	92.47	0.65	Stomatin-like protein 1	1.41	1
T126A_HUMAN	2 (1)	92.18	0.52	Transmembrane protein 126A	2.81	1
RFC2_HUMAN	5 (2)	92.15	0.49	Replication factor C subunit 2	1	1.18
NOMO1_HUMAN	5 (2)	92.1	0.54	Nodal modulator 1	2.59	1
NIBL1_HUMAN	5 (2)	92.03	0.24	Niban-like protein 1	1	1.64
EIF2A_HUMAN	3 (1)	91.97	0.97	Eukaryotic translation initiation factor 2A	1	9.82
VAT1_HUMAN	2 (1)	91.88	0.8	Synaptic vesicle membrane protein VAT-1 homolog	1.01	1
PRAF3_HUMAN	4 (1)	91.84	0.22	PRA1 family protein 3	1	1.7
PP2AA_HUMAN	2 (1)	91.75	0.03	Serine/threonine-protein phosphatase 2A catalytic subunit alpha isoform	1.83	1
EI2BB_HUMAN	7 (1)	91.69	4.33E-03	Translation initiation factor eIF-2B subunit beta	2.26	1
DYSF_HUMAN	8 (1)	91.53	0.02	Dysferlin	1	3.26
DJC10_HUMAN	8 (2)	91.45	0.01	DnaJ homolog subfamily C member 10	2.52	1
LCAP_HUMAN	5 (1)	91.09	0.47	Leucyl-cystinyl aminopeptidase	2.38	1
KRR1_HUMAN	3 (1)	91.05	0.49	KRR1 small subunit processome component homolog	1	1.42
ATP9B_HUMAN	8 (1)	90.62	0.59	Probable phospholipid-transporting ATPase IIB V=4	3.16	1
SMRC1_HUMAN	4 (1)	90.21	0.75	SWI/SNF complex subunit SMARCC1	2.28	1
SFI1_HUMAN	10 (3)	90.12	0.89	Protein SFI1 homolog	1	1.23
AFG32_HUMAN	5 (1)	90.11	0.41	AFG3-like protein 2	1	1.24
SULF1_HUMAN	10 (1)	89.66	0.07	Extracellular sulfatase Sulf-1	1	6.03
AKAP1_HUMAN	4 (2)	89.61	0.22	A-kinase anchor protein 1, mitochondrial	2.89	1
KPYR_HUMAN	9 (2)	89.52	0.17	Pyruvate kinase PKLR	1	12.91
DIC_HUMAN	5 (1)	89.2	0.8	Mitochondrial dicarboxylate carrier	1.54	1
COX41_HUMAN	7 (3)	88.85	0.03	Cytochrome c oxidase subunit 4 isoform 1, mitochondrial	1	11.63
2AAA_HUMAN	8 (2)	88.36	0.1	Serine/threonine-protein phosphatase 2A 65 kDa regulatory subunit A alpha isoform	3.37	1
API5_HUMAN	4 (1)	88.21	0.07	Apoptosis inhibitor 5	79.26	1
RAB18_HUMAN	2 (1)	88.07	0.01	Ras-related protein Rab-18	1.84	1
HMGB3_HUMAN	2 (1)	88.05	0.36	High mobility group protein B3	1.21	1
THIK_HUMAN	5 (2)	87.9	0.04	3-ketoacyl-CoA thiolase, peroxisomal	7.63	1
PIWL4_HUMAN	8 (3)	87.68	0.18	Piwi-like protein 4	1	2.93
APT_HUMAN	3 (1)	87.29	0.02	Adenine phosphoribosyltransferase	1.65	1
SLK_HUMAN	8 (2)	87.16	0.75	STE20-like serine/threonine-protein kinase	1	1.14
MRP4_HUMAN	7 (2)	87.08	0.16	Multidrug resistance-associated protein 4	1.57	1
AHSA1_HUMAN	5 (2)	87.07	0.14	Activator of 90 kDa heat shock protein ATPase homolog 1	1	5.59
RT09_HUMAN	3 (2)	87.05	0.66	28S ribosomal protein S9, mitochondrial	1.17	1
PDXK_HUMAN	4 (1)	86.96	0.05	Pyridoxal kinase	1	7.68
AT1B1_HUMAN	4 (3)	86.53	0.6	Sodium/potassium-transporting ATPase subunit beta-1	1	1.11
IQGA2_HUMAN	7 (1)	86.46	0.03	Ras GTPase-activating-like protein IQGAP2	10.9	1
NDUS2_HUMAN	4 (1)	86.43	0.24	NADH dehydrogenase [ubiquinone] iron-sulfur protein 2, mitochondrial	1	2.1
BCAT2_HUMAN	3 (1)	86.3	0.79	Branched-chain-amino-acid aminotransferase, mitochondrial	1.18	1
SPTN2_HUMAN	12 (1)	85.94	0.07	Spectrin beta chain, non-erythrocytic 2	3.12	1
FMR1_HUMAN	6 (1)	85.76	0.25	Synaptic functional regulator FMR1	1	2.76
CPSF7_HUMAN	2 (1)	85.72	0.24	Cleavage and polyadenylation specificity factor subunit 7	2.13	1
H2AW_HUMAN	6 (2)	85.71	0.16	Core histone macro-H2A.2	1	1.65
ACTZ_HUMAN	1 (1)	85.69	0.9	Alpha-centractin	1	1.07
F10A5_HUMAN	6 (1)	85.63	0.27	Putative protein FAM10A5	1	4.58
ERP44_HUMAN	6 (1)	85.54	0.35	Endoplasmic reticulum resident protein 44	1	1.53
TRI47_HUMAN	4 (1)	85.49	0.06	Tripartite motif-containing protein 47	5.43	1
WDR61_HUMAN	2 (1)	85.14	5.28E-03	WD repeat-containing protein 61	7.94	1
ZN326_HUMAN	3 (1)	84.92	0.98	DBIRD complex subunit ZNF326	1.06	1

KBTB3_HUMAN	8 (1)	84.36	7.06E-03	Kelch repeat and BTB domain-containing protein 3	4.33	1
SPTB1_HUMAN	11 (3)	84.35	0.13	Spectrin beta chain, erythrocytic	1	2.53
LEG12_HUMAN	4 (1)	83.5	0.27	Galectin-12	1.37	1
AP3D1_HUMAN	11 (1)	83.42	0.31	AP-3 complex subunit delta-1	1.8	1
SURF1_HUMAN	6 (1)	83.41	0.55	Surfeit locus protein 1	1	1.12
DEN5B_HUMAN	14 (3)	83.36	0.4	DENN domain-containing protein 5B	1	1.3
H2BFS_HUMAN	6 (1)	83.35	0.07	Histone H2B type F-S	3.32	1
MARC1_HUMAN	3 (1)	83.32	0.48	Mitochondrial amidoxime-reducing component 1	1.47	1
RM44_HUMAN	3 (1)	83.04	0.11	39S ribosomal protein L44, mitochondrial	1	1.89
RL32_HUMAN	2 (1)	83.03	0.22	60S ribosomal protein L32	2.53	1
KAD1_HUMAN	3 (1)	83.03	0.18	Adenylate kinase isoenzyme 1	4.16	1
CHMP5_HUMAN	3 (1)	82.88	0.78	Charged multivesicular body protein 5	9.06	1
MIMIT_HUMAN	4 (2)	81.49	0.41	Mimitin, mitochondrial	2.19	1
PUR6_HUMAN	3 (1)	81.2	0.14	Multifunctional protein ADE2	1	4.89
RRFM_HUMAN	2 (1)	81.11	0.76	Ribosome-recycling factor, mitochondrial	1.09	1
NOP56_HUMAN	5 (2)	81.05	0.52	Nucleolar protein 56	1	1.18
MTDC_HUMAN	2 (1)	80.87	0.64	Bifunctional methylenetetrahydrofolate dehydrogenase/cyclohydrolase, mitochondrial	1.74	1
UTP20_HUMAN	14 (5)	80.71	0.17	Small subunit processome component 20 homolog	1	1.54
SYDC_HUMAN	5 (2)	80.63	0.2	Aspartate--tRNA ligase, cytoplasmic	1.7	1
ASNA_HUMAN	2 (1)	80.26	0.69	ATPase ASNA1	1.28	1
SPCS3_HUMAN	2 (1)	80.21	1.76E-03	Signal peptidase complex subunit 3	4.09	1
PDS5A_HUMAN	11 (5)	80.02	0.06	Sister chromatid cohesion protein PDS5 homolog A	3.43	1
PSB7_HUMAN	5 (2)	80	0.55	Proteasome subunit beta type-7	1.24	1
CLIP1_HUMAN	15 (6)	79.79	0.72	CAP-Gly domain-containing linker protein 1	1	2.7
AINX_HUMAN	5 (1)	79.62	0.04	Alpha-internexin	3.23	1
GDIR1_HUMAN	1 (1)	79.5	0.15	Rho GDP-dissociation inhibitor 1	2.33	1
DHX30_HUMAN	9 (1)	79.13	0.02	Putative ATP-dependent RNA helicase DHX30	1	3.31
STIM1_HUMAN	4 (1)	79.12	0.01	Stromal interaction molecule 1	1	3.87
SAP18_HUMAN	2 (1)	78.89	0.14	Histone deacetylase complex subunit SAP18	∞	0
CAPS2_HUMAN	8 (1)	78.24	0.07	Calcium-dependent secretion activator 2	1	115.54
TSNAX_HUMAN	4 (2)	78.04	0.77	Translin-associated protein X	2.31	1
D39U1_HUMAN	3 (1)	77.91	0.23	Epimerase family protein SDR39U1	1	46.93
TERT_HUMAN	8 (3)	77.71	0.27	Telomerase reverse transcriptase	1	1.9
BAX_HUMAN	1 (1)	77.11	0.11	Apoptosis regulator BAX	1	4.57
SEC13_HUMAN	1 (1)	77.06	0.55	Protein SEC13 homolog	1.15	1
SRPRA_HUMAN	12 (4)	76.91	0.25	Signal recognition particle receptor subunit alpha	1.9	1
MRM3_HUMAN	4 (1)	76.56	0.35	rRNA methyltransferase 3, mitochondrial	23.27	1
CX057_HUMAN	7 (2)	76.39	0.75	Uncharacterized protein CXorf57	1	1.41
SRSF8_HUMAN	5 (1)	76.28	0.07	Serine/arginine-rich splicing factor 8	2.92	1
CIRBP_HUMAN	2 (1)	76.13	0.21	Cold-inducible RNA-binding protein	7.28	1
U2AF1_HUMAN	5 (1)	76.01	0.13	Splicing factor U2AF 35 kDa subunit	1	1.23
SCO1_HUMAN	6 (1)	75.77	0.43	Protein SCO1 homolog, mitochondrial	1	1.31
ABCCB_HUMAN	11 (2)	75.73	0.26	ATP-binding cassette sub-family C member 11	1.61	1
ITPA_HUMAN	2 (1)	75.57	0.08	Inosine triphosphate pyrophosphatase	1	4.8
TTC37_HUMAN	11 (2)	74.79	0.3	Tetratricopeptide repeat protein 37	1.56	1
GRWD1_HUMAN	4 (1)	74.67	0.45	Glutamate-rich WD repeat-containing protein 1	1.23	1
NUBP2_HUMAN	3 (2)	74.41	0.58	Cytosolic Fe-S cluster assembly factor NUBP2	2.84	1
ATP6_HUMAN	1 (1)	74.31	0.09	ATP synthase subunit a	2.19	1
ETHE1_HUMAN	1 (1)	74.04	0.39	Persulfide dioxygenase ETHE1, mitochondrial	1	1.28
CATZ_HUMAN	2 (1)	73.88	0.79	Cathepsin Z 1	1	1.02
FLOT1_HUMAN	5 (1)	73.77	0.55	Flotillin-1	1.53	1
NHP2_HUMAN	2 (1)	73.49	0.03	H/ACA ribonucleoprotein complex subunit 2	1.8	1
ACSL3_HUMAN	2 (1)	73.1	0.14	Long-chain-fatty-acid--CoA ligase 3	5.04	1
RS25_HUMAN	2 (1)	73	7.25E-03	40S ribosomal protein S25	2.54	1
RT07_HUMAN	4 (1)	72.88	3.23E-03	28S ribosomal protein S7, mitochondrial	3.24	1
RTF2_HUMAN	4 (1)	72.46	0.22	Protein RTF2 homolog	2.38	1
1C01_HUMAN	3 (2)	72.43	0.08	HLA class I histocompatibility antigen, Cw-1 alpha chain	4.25	1
CALM1_HUMAN	3 (1)	71.99	0.26	Calmodulin-1	2865.33	1

RM01_HUMAN	5 (3)	71.98	0.14	39S ribosomal protein L1, mitochondrial	2.13	1
TM109_HUMAN	2 (1)	71.71	0.13	Transmembrane protein 109	2.03	1
RAE1L_HUMAN	2 (1)	71.58	0.6	mRNA export factor	1	1.11
ITAV_HUMAN	6 (1)	71.41	0.33	Integrin alpha-V	1	1.45
RBM8A_HUMAN	2 (1)	70.87	0.09	RNA-binding protein 8A	1	3.54
ASPH_HUMAN	7 (1)	70.42	0.7	Aspartyl/asparaginyl beta-hydroxylase	1.73	1
PSA4_HUMAN	4 (1)	70.24	0.37	Proteasome subunit alpha type-41	14.73	1
RAB21_HUMAN	2 (1)	70.13	0.21	Ras-related protein Rab-21	1.28	1
NUDC_HUMAN	5 (2)	70.09	0.2	Nuclear migration protein nudC	1	1.62
SMD3_HUMAN	3 (1)	69.62	0.56	Small nuclear ribonucleoprotein Sm D3	2.99	1
NDUA8_HUMAN	2 (1)	69.49	0.37	NADH dehydrogenase [ubiquinone] 1 alpha subcomplex subunit 8 3	1.73	1
ELP1_HUMAN	7 (1)	69.47	0.1	Elongator complex protein 1	1.52	1
KSR2_HUMAN	9 (1)	69.44	0.11	Kinase suppressor of Ras 2	1	2.87
RS27L_HUMAN	2 (1)	69.32	0.17	40S ribosomal protein S27-like	2.82	1
CAV1_HUMAN	3 (1)	69.06	0.09	Caveolin-1	4.68	1
UBP7_HUMAN	9 (4)	69	0.22	Ubiquitin carboxyl-terminal hydrolase 7	1	2.51
PSB4_HUMAN	2 (2)	68.86	0.05	Proteasome subunit beta type-4	1.27	1
G3PT_HUMAN	6 (1)	68.78	0.66	Glyceraldehyde-3-phosphate dehydrogenase, testis-specific	1	1.11
NNRE_HUMAN	2 (1)	68.68	8.23E-03	NAD(P)H-hydrate epimerase	1.6	1
SREC2_HUMAN	8 (1)	68.58	0.87	Scavenger receptor class F member 2	1.23	1
TRA2B_HUMAN	4 (2)	68.44	0.29	Transformer-2 protein homolog beta	43.86	1
SUCA_HUMAN	4 (1)	68.16	0.94	Succinate--CoA ligase [ADP/GDP-forming] subunit alpha, mitochondrial	1	6.02
RFA1_HUMAN	3 (1)	68.04	0.15	Replication protein A 70 kDa DNA-binding subunit	5.49	1
DECR2_HUMAN	5 (2)	67.94	0.02	Peroxisomal 2,4-dienoyl-CoA reductase	1	3.23
APMAP_HUMAN	2 (1)	67.6	0.04	Adipocyte plasma membrane-associated protein	8.26	1
F120C_HUMAN	4 (4)	67.49	0.27	Constitutive coactivator of PPAR-gamma-like protein 2	1.72	1
ICAL_HUMAN	3 (1)	67.46	0.11	Calpastatin	1	2.8
DDRGK_HUMAN	3 (1)	66.85	0.37	DDRGK domain-containing protein 1	1	1.55
TULP1_HUMAN	7 (3)	66.84	0.31	Tubby-related protein 1	1	1.69
1C04_HUMAN	3 (2)	66.72	0.14	HLA class I histocompatibility antigen, Cw-4 alpha chain	50.35	1
SYDM_HUMAN	5 (1)	66.6	0.71	Aspartate--tRNA ligase, mitochondrial	1.31	1
PTPM1_HUMAN	3 (2)	66.56	0.09	Phosphatidylglycerophosphatase and protein-tyrosine phosphatase 1	1	1.94
ABHDA_HUMAN	6 (3)	66.53	0.74	Mycophenolic acid acyl-glucuronide esterase, mitochondrial	1.23	1
PLP2_HUMAN	2 (1)	66.11	0.14	Proteolipid protein 2	2.8	1
SEP11_HUMAN	6 (2)	66.05	0.52	Septin-11	1	1.01
TRPM7_HUMAN	15 (3)	65.8	0.65	Transient receptor potential cation channel subfamily M member 7	1	1.07
LMAN1_HUMAN	2 (1)	65.56	0.39	Protein ERGIC-53	1.47	1
TNNI3_HUMAN	3 (1)	64.71	0.03	Troponin I, cardiac muscle	1.37	1
CSN4_HUMAN	4 (1)	64.69	0.04	COP9 signalosome complex subunit 4	1	157.52
ZCH18_HUMAN	6 (2)	64.68	0.31	Zinc finger CCCH domain-containing protein 18	2.02	1
RFIP4_HUMAN	7 (1)	64.66	0.56	Rab11 family-interacting protein 4	1	1.13
BYST_HUMAN	5 (3)	64.51	0.93	Bystin	1	9.36
CAP1_HUMAN	2 (2)	64.51	0.8	Adenylyl cyclase-associated protein 1	1	1.39
ISY1_HUMAN	9 (3)	64.42	0.33	Pre-mRNA-splicing factor ISY1 homolog	1.32	1
ESRP1_HUMAN	6 (1)	64.34	0.61	Epithelial splicing regulatory protein 1	1	1.01
WDR12_HUMAN	4 (1)	64.2	0.44	Ribosome biogenesis protein WDR12	20.89	1
RM18_HUMAN	2 (1)	63.89	0.01	39S ribosomal protein L18, mitochondrial	1	4.31
DCXR_HUMAN	3 (1)	63.68	0.28	L-xylulose reductase	4.89	1
GFAP_HUMAN	1 (1)	63.54	0.25	Glial fibrillary acidic protein	1	6.9
RT05_HUMAN	3 (1)	62.59	5.43E-03	28S ribosomal protein S5, mitochondrial	1	17.92
OCAD1_HUMAN	3 (1)	62.21	0.29	OCIA domain-containing protein 1	1	1.48
RSU1_HUMAN	4 (1)	62.08	0.92	Ras suppressor protein 1	1.58	1
SNR40_HUMAN	3 (1)	62	0.86	U5 small nuclear ribonucleoprotein 40 kDa protein	1.01	1
MLEC_HUMAN	1 (1)	61.83	0.44	Malectin	3.17	1
CBPC4_HUMAN	5 (1)	61.75	0.3	Cytosolic carboxypeptidase 4	1	1.45
LAMP2_HUMAN	1 (1)	61.47	0.36	Lysosome-associated membrane glycoprotein 2	12.03	1
PADI1_HUMAN	4 (2)	61.24	0.11	Protein-arginine deiminase type-	1	2.78
WNT7A_HUMAN	10 (3)	61.15	0.14	Protein Wnt-7a	1	2.78

YETS2_HUMAN	6 (1)	61.02	0.47	YEATS domain-containing protein 2	7.53	1
RM24_HUMAN	3 (1)	61.01	0.1	39S ribosomal protein L24, mitochondrial	1	2.99
AN32E_HUMAN	1 (1)	60.85	0.29	Acidic leucine-rich nuclear phosphoprotein 32 family member E	1.7	1
GRPE1_HUMAN	3 (1)	60.34	1.78E-03	GrpE protein homolog 1, mitochondrial	29	1
NDRG1_HUMAN	5 (1)	59.73	0.21	Protein NDRG1	1	2.47
IMDH2_HUMAN	2 (1)	59.54	0.89	Inosine-5'-monophosphate dehydrogenase 2	12.59	1
DNJA2_HUMAN	3 (1)	59.3	1.70E-03	DnaJ homolog subfamily A member 2	1.89	1
RRP15_HUMAN	5 (1)	59.08	0.11	RRP15-like protein	1	1.55
PITM2_HUMAN	8 (2)	59.06	0.13	Membrane-associated phosphatidylinositol transfer protein 2	1.64	1
ISOC2_HUMAN	3 (1)	58.68	0.94	Isochorismatase domain-containing protein 2	1.43	1
STB5L_HUMAN	5 (1)	58.62	0.01	Syntaxin-binding protein 5-like	1	31.55
RS30_HUMAN	1 (1)	58.59	0.14	40S ribosomal protein S30	1	1.29
NAA15_HUMAN	5 (1)	58.58	7.33E-04	N-alpha-acetyltransferase 15, NatA auxiliary subunit	1	15.13
AIMP2_HUMAN	2 (2)	58.41	0.88	Aminoacyl tRNA synthase complex-interacting multifunctional protein 2	1.08	1
MAP7_HUMAN	4 (1)	58.13	0.34	Ensconsin	1	1.46
PININ_HUMAN	7 (4)	58.05	0.63	Pinin	1.13	1
EIF3K_HUMAN	3 (1)	57.57	0.91	Eukaryotic translation initiation factor 3 subunit K	1.01	1
SGMR1_HUMAN	2 (2)	57.55	0.01	Sigma non-opioid intracellular receptor 1	2.04	1
TFEB_HUMAN	2 (1)	57.44	0.12	Transcription factor EB	1.93	1
ADAP2_HUMAN	7 (3)	57.33	0.91	Arf-GAP with dual PH domain-containing protein 2	1.45	1
FA98B_HUMAN	6 (2)	57.06	0.34	Protein FAM98B	2.58	1
PEF1_HUMAN	1 (1)	56.93	0.07	Peflin	5.69	1
AP2A2_HUMAN	7 (2)	56.88	0.1	AP-2 complex subunit alpha-2	3.62	1
FXR1_HUMAN	4 (1)	56.82	0.02	Fragile X mental retardation syndrome-related protein 1	55.28	1
CLUS_HUMAN	2 (1)	56.69	0.14	Clusterin	5.13	1
COPB2_HUMAN	4 (1)	56.59	0.02	Coatomer subunit beta'	14.02	1
RBM39_HUMAN	4 (1)	56.44	0.05	RNA-binding protein 39	2.68	1
THEM4_HUMAN	2 (2)	56.32	0.42	Acyl-coenzyme A thioesterase THEM4	1.41	1
HPRT_HUMAN	4 (2)	56.03	0.19	Hypoxanthine-guanine phosphoribosyltransferase	1	1.54
PPIF_HUMAN	2 (2)	55.88	0.24	Peptidyl-prolyl cis-trans isomerase F, mitochondrial	1.55	1
CCHCR_HUMAN	7 (2)	55.86	0.31	Coiled-coil alpha-helical rod protein 1	1	2.09
RUVB1_HUMAN	4 (1)	55.84	0.62	RuvB-like 1	1.09	1
ARC1B_HUMAN	3 (1)	55.79	0.08	Actin-related protein 2/3 complex subunit 1B	31.83	1
SET_HUMAN	4 (2)	55.7	0.03	Protein SETV=3	2.19	1
EMC7_HUMAN	1 (1)	55.68	0.83	ER membrane protein complex subunit 7	1.13	1
MLX_HUMAN	7 (2)	55.47	0.67	Max-like protein X	1	1.05
MBLC2_HUMAN	2 (1)	55.4	7.50E-03	Metallo-beta-lactamase domain-containing protein 2	1	230.42
UFD1_HUMAN	2 (1)	55.1	0.65	Ubiquitin recognition factor in ER-associated degradation protein 1	1.18	1
IPYR_HUMAN	2 (1)	54.79	0.21	Inorganic pyrophosphatase	1.79	1
ZFP91_HUMAN	7 (4)	54.72	0.03	E3 ubiquitin-protein ligase ZFP91	1	3.46
DIAP1_HUMAN	7 (2)	54.59	0.37	Protein diaphanous homolog 1	3	1
DDX46_HUMAN	7 (1)	54.54	0.24	Probable ATP-dependent RNA helicase DDX46	1	2.13
PNMA2_HUMAN	5 (2)	54.48	0.18	Paraneoplastic antigen Ma2	1	1.81
BPHL_HUMAN	2 (1)	54.48	0.55	Valacyclovir hydrolase	1	1.1
TRA2A_HUMAN	4 (2)	54.37	0.06	Transformer-2 protein homolog alpha	1.73	1
RAC1_HUMAN	2 (1)	54.34	0.43	Ras-related C3 botulinum toxin substrate 1	1.46	1
UTS2_HUMAN	2 (1)	54.25	0.88	Urotensin-2	1.03	1
DSG2_HUMAN	3 (2)	54.12	0.54	Desmoglein-2	1	1.57
HACD3_HUMAN	2 (1)	54.12	0.2	Very-long-chain (3R)-3-hydroxyacyl-CoA dehydratase 3	2.01	1
RFC5_HUMAN	2 (1)	53.3	0.97	Replication factor C subunit 5	1	1.11
FAF2_HUMAN	2 (1)	53.01	0.53	FAS-associated factor 2	1	1.1
PSB3_HUMAN	1 (1)	52.78	0.13	Proteasome subunit beta type-3	1.66	1
PROF1_HUMAN	1 (1)	52.75	3.29E-03	Profilin-1	4.18	1
SERC_HUMAN	3 (1)	52.26	0.35	Phosphoserine aminotransferase	1	1.27
DCLK3_HUMAN	8 (1)	52.07	0.03	Serine/threonine-protein kinase DCLK3	17.85	1
RNPS1_HUMAN	5 (2)	51.94	0.37	RNA-binding protein with serine-rich domain 1	1	1.56
ARMC9_HUMAN	6 (1)	51.93	0.13	LisH domain-containing protein ARMC9	5.67	1
COMT_HUMAN	3 (2)	51.76	0.36	Catechol O-methyltransferase	1	1.49

SYLM_HUMAN	4 (3)	51.76	0.99	Probable leucine--tRNA ligase, mitochondrial	1.15	1
DTD1_HUMAN	2 (2)	51.75	0.19	D-tyrosyl-tRNA(Tyr) deacylase 1	20.32	1
MCM2_HUMAN	4 (1)	51.45	0.1	DNA replication licensing factor MCM2	1	8.82
PMA6E_HUMAN	4 (1)	51.28	0.1	Paraneoplastic antigen Ma6E	2.64	1
MALD2_HUMAN	7 (1)	51.26	0.16	MARVEL domain-containing protein 2	76.53	1
NFS1_HUMAN	1 (1)	50.93	0.75	Cysteine desulfurase, mitochondrial	1	1.11
CRTAP_HUMAN	1 (1)	50.76	0.83	Cartilage-associated protein	3.28	1
SYTM_HUMAN	4 (1)	50.57	0.06	Threonine--tRNA ligase, mitochondrial	1	5.4
TTC33_HUMAN	2 (1)	50.37	0.16	Tetratricopeptide repeat protein 33	1	5.9
IDH3G_HUMAN	3 (1)	50.13	0.2	Isocitrate dehydrogenase [NAD] subunit gamma, mitochondrial	1	2.41
PWP2_HUMAN	7 (1)	50.07	0.55	Periodic tryptophan protein 2 homolog2	1.12	1
IF4B_HUMAN	5 (2)	49.26	0.25	Eukaryotic translation initiation factor 4B	2.23	1
RM28_HUMAN	2 (1)	49.19	0.61	39S ribosomal protein L28, mitochondrial	1	1.29
FOXO6_HUMAN	3 (1)	49.17	0.54	Forkhead box protein O6	1	3.1
PCDA7_HUMAN	4 (3)	49.04	0.04	Protocadherin alpha-7	2.96	1
RMD3_HUMAN	5 (1)	49.04	0.29	Regulator of microtubule dynamics protein 3	988.89	1
ULK3_HUMAN	7 (1)	48.97	1	Serine/threonine-protein kinase ULK3	2.08	1
NRL_HUMAN	4 (2)	48.92	0.21	Neural retina-specific leucine zipper protein	1.65	1
SNP23_HUMAN	2 (1)	48.13	0.33	Synaptosomal-associated protein 23	9.61	1
ULK2_HUMAN	4 (1)	47.88	0.37	Serine/threonine-protein kinase ULK2	2.48	1
SUMF2_HUMAN	1 (1)	47.78	0.19	Sulfatase-modifying factor 2	1	1.97
OTU1_HUMAN	4 (1)	47.78	0.71	Ubiquitin thioesterase OTU1	17.35	1
L2HDH_HUMAN	3 (2)	47.74	0.92	L-2-hydroxyglutarate dehydrogenase, mitochondrial 3	1.2	1
SNF5_HUMAN	3 (1)	47.73	0.12	SWI/SNF-related matrix-associated actin-dependent regulator of chromatin subfamily B member 1	1.79	1
ERF3B_HUMAN	4 (1)	47.72	0.37	Eukaryotic peptide chain release factor GTP-binding subunit ERF3B	0	∞
RAB9A_HUMAN	2 (2)	47.58	0.57	Ras-related protein Rab-9A	1	1.08
HCFC1_HUMAN	6 (2)	47.54	0.19	Host cell factor 1	1	1.67
EMAL4_HUMAN	4 (1)	47.33	0.08	Echinoderm microtubule-associated protein-like 4	1	5.8
WDR36_HUMAN	9 (2)	47.21	0.05	WD repeat-containing protein 36	1	1.77
ASNS_HUMAN	4 (1)	47.17	0.59	Asparagine synthetase [glutamine-hydrolyzing]	1.37	1
GG6L3_HUMAN	5 (1)	46.8	0.36	Putative golgin subfamily A member 6-like protein 3	1	1.57
SDF2L_HUMAN	2 (2)	46.79	0.36	Stromal cell-derived factor 2-like protein 1	1	1.57
EMAL1_HUMAN	4 (2)	46.69	0.71	Echinoderm microtubule-associated protein-like 1	1.78	1
LC7L3_HUMAN	4 (2)	46.33	5.26E-04	Luc7-like protein 3	2.5	1
RS19_HUMAN	5 (2)	46.31	0.48	40S ribosomal protein S19 2	2.32	1
MKKS_HUMAN	2 (1)	46.31	0.37	McKusick-Kaufman/Bardet-Biedl syndromes putative chaperonin	∞	0
GUAA_HUMAN	2 (1)	46.28	0.34	GMP synthase [glutamine-hydrolyzing]	4.19	1
AASD1_HUMAN	4 (1)	45.42	0.11	Alanyl-tRNA editing protein Aarsd1	1	225.39
RPF2_HUMAN	3 (1)	45.17	0.49	Ribosome production factor 2 homolog	1.35	1
TMED7_HUMAN	1 (1)	45.07	0.94	Transmembrane emp24 domain-containing protein 7	24.87	1
SRSF9_HUMAN	1 (1)	44.94	0.01	Serine/arginine-rich splicing factor 9	1.36	1
FA49B_HUMAN	3 (1)	44.91	0.91	Protein FAM49B	1	1.25
PGRC1_HUMAN	1 (1)	44.84	0.13	Membrane-associated progesterone receptor component 1	1.47	1
RL28_HUMAN	3 (2)	44.65	0.82	60S ribosomal protein L28	1	1.07
TBG1_HUMAN	3 (1)	44.28	0.34	Tubulin gamma-1 chain	2.39	1
FUBP3_HUMAN	3 (1)	44.2	0.55	Far upstream element-binding protein 3	1.54	1
FBX5_HUMAN	3 (1)	44.11	0.14	F-box only protein 5	1	4.29
RT33_HUMAN	2 (1)	44.05	0.43	28S ribosomal protein S33, mitochondrial	1.66	1
6PGL_HUMAN	2 (1)	43.87	0.87	6-phosphogluconolactonase	1	1.26
LRP6_HUMAN	6 (3)	43.39	0.75	Low-density lipoprotein receptor-related protein 6	1	1.04
PRP16_HUMAN	6 (1)	43.38	0.09	Pre-mRNA-splicing factor ATP-dependent RNA helicase PRP16 V=2	1	6.8
CLC4F_HUMAN	5 (1)	42.68	0.02	C-type lectin domain family 4 member F	7.61	1
LONP2_HUMAN	6 (2)	42.66	0.35	Lon protease homolog 2, peroxisomal	1	2.35
CO5A3_HUMAN	6 (1)	42.57	0.45	Collagen alpha-3(V) chain	1	1.3
MORC2_HUMAN	6 (3)	42.51	0.76	MORC family CW-type zinc finger protein 2	1	1.32
FA50A_HUMAN	2 (2)	42.23	0.14	Protein FAM50A	15.38	1
CK040_HUMAN	3 (1)	41.98	0.11	Putative uncharacterized protein C11orf40	2.09	1
HYEP_HUMAN	3 (2)	41.59	0.81	Epoxide hydrolase 1	1	2.4

TRI31_HUMAN	4 (1)	41.57	0.26	E3 ubiquitin-protein ligase TRIM31	3.96	1
HMGA1_HUMAN	1 (1)	41.33	0.04	High mobility group protein HMG-I/HMG-Y	3.58	1
IST1_HUMAN	1 (1)	41.12	0.98	IST1 homolog	1.18	1
SEPT8_HUMAN	2 (1)	41	6.01E-03	Septin-8	34.78	1
UT14A_HUMAN	4 (1)	40.99	0.33	U3 small nucleolar RNA-associated protein 14 homolog A	1	1.25
BGAL_HUMAN	1 (1)	40.77	0.75	Beta-galactosidase	1	1.54
F210A_HUMAN	2 (1)	40.73	0.15	Protein FAM210A	17.1	1
SKP1_HUMAN	2 (1)	40.51	0.53	S-phase kinase-associated protein 1	1	1.47
SMYD4_HUMAN	7 (1)	40.15	0.28	SET and MYND domain-containing protein 4	1.87	1
SYSM_HUMAN	5 (2)	39.96	0.44	Serine--tRNA ligase, mitochondrial	1	4.33
ZN516_HUMAN	9 (4)	39.82	0.5	Zinc finger protein 516	1.17	1
BZW1_HUMAN	3 (3)	39.42	0.34	Basic leucine zipper and W2 domain-containing protein 1	1	1.36
NPS3A_HUMAN	3 (2)	39.37	0.25	Protein NipSnap homolog 3A	1	1.55
MYO5B_HUMAN	6 (2)	39.22	1	Unconventional myosin-Vb	2.18	1
SQOR_HUMAN	2 (1)	39.15	0.03	Sulfide:quinone oxidoreductase, mitochondrial	3.65	1
EYA2_HUMAN	3 (1)	39.08	0.37	Eyes absent homolog 2	1	1.36
CD81_HUMAN	1 (1)	38.74	0.04	CD81 antigen	44.06	1
LGUL_HUMAN	3 (1)	38.69	0.9	Lactoylglutathione lyase	1.64	1
TXLNB_HUMAN	4 (1)	38.52	0.24	Beta-taxilin	1	1.63
KCRS_HUMAN	4 (1)	38.24	0.1	Creatine kinase S-type, mitochondrial	1	3.96
GLRX3_HUMAN	6 (2)	38.22	0.05	Glutaredoxin-3	1	1.68
MRT4_HUMAN	3 (1)	38.2	0.09	mRNA turnover protein 4 homolog	19.99	1
AATC_HUMAN	1 (1)	38.12	0.21	Aspartate aminotransferase, cytoplasmic 3	1	1.97
AGRF4_HUMAN	6 (2)	37.81	0.05	Adhesion G protein-coupled receptor F4	1	4.94
CH033_HUMAN	2 (1)	37.67	0.25	UPF0488 protein C8orf33	1	5.39
RL30_HUMAN	2 (1)	37.37	0.14	60S ribosomal protein L30	1.87	1
TEX9_HUMAN	2 (1)	37.21	6.92E-05	Testis-expressed protein 9	3.22	1
DYDC2_HUMAN	2 (1)	36.96	0.72	DPY30 domain-containing protein 2	1	158.41
NQO1_HUMAN	1 (1)	36.75	0.31	NAD(P)H dehydrogenase [quinone] 1	2.84	1
RBM10_HUMAN	3 (1)	36.69	0.44	RNA-binding protein 10	1	4.75
SRS10_HUMAN	2 (1)	36.52	0.03	Serine/arginine-rich splicing factor 10	1	12.32
BAKOR_HUMAN	4 (2)	36.4	0.11	Beclin 1-associated autophagy-related key regulator	7.14	1
UBP28_HUMAN	6 (1)	36.22	0.09	Ubiquitin carboxyl-terminal hydrolase 28	1	5.79
HDAC2_HUMAN	4 (1)	36.17	0.04	Histone deacetylase 2	13.9	1
EPHB4_HUMAN	6 (1)	36.08	0.25	Ephrin type-B receptor 4	4.89	1
MTA2_HUMAN	7 (3)	36.05	0.57	Metastasis-associated protein MTA2	1	1.36
RS27_HUMAN	1 (1)	35.92	0.47	40S ribosomal protein S27	15.71	1
SF3A2_HUMAN	1 (1)	35.34	0.16	Splicing factor 3A subunit 2	7.92	1
ABCBA_HUMAN	5 (2)	34.83	0.29	ATP-binding cassette sub-family B member 10, mitochondrial	1.48	1
NDUB8_HUMAN	2 (1)	34.67	0.05	NADH dehydrogenase [ubiquinone] 1 beta subcomplex subunit 8, mitochondrial	5.78	1
BAP31_HUMAN	2 (1)	34.65	0.21	B-cell receptor-associated protein 31	30.87	1
SYWC_HUMAN	2 (1)	34.4	0.05	Tryptophan--tRNA ligase, cytoplasmic	1	3.42
TPC_HUMAN	2 (2)	34.19	0.06	Mitochondrial thiamine pyrophosphate carrier	1	15.66
HTRA2_HUMAN	3 (1)	33.38	0.22	Serine protease HTRA2, mitochondrial	1	18.67
AL3A2_HUMAN	1 (1)	33.21	0.19	Fatty aldehyde dehydrogenase	1.12	1
NTPCR_HUMAN	3 (2)	32.54	0.02	Cancer-related nucleoside-triphosphatase	1	4.9
ATAD1_HUMAN	2 (1)	32.53	0.1	ATPase family AAA domain-containing protein 1	2.51	1
PSMG2_HUMAN	2 (1)	32.2	0.82	Proteasome assembly chaperone 2	1	1.15
PSME1_HUMAN	1 (1)	31.98	0.23	Proteasome activator complex subunit 1	1	5.64
RALB_HUMAN	3 (1)	31.8	0.08	Ras-related protein Ral-B	2.87	1
RPP30_HUMAN	1 (1)	31.59	0.16	Ribonuclease P protein subunit p30	1	2.14
MARE1_HUMAN	1 (1)	31.19	0.07	Microtubule-associated protein RP/EB family member 1	139.74	1
SGO2_HUMAN	5 (4)	31.05	0.25	Shugoshin 2	1	1.54
EGF_HUMAN	5 (1)	30.82	0.83	Pro-epidermal growth factor	3.19	1
RM38_HUMAN	4 (1)	30.76	0.01	39S ribosomal protein L38, mitochondrial	1	44.79
HPHL1_HUMAN	4 (1)	30.38	0.12	Hephaestin-like protein 1	13.1	1
IPO7_HUMAN	5 (1)	30.31	0.03	Importin-7	1	61.17
MOONR_HUMAN	5 (1)	30.1	0.31	Protein moonraker	17.46	1

ADAM2_HUMAN	4 (1)	29.86	0.05	Disintegrin and metalloproteinase domain-containing protein 2	1	10.75
RAI3_HUMAN	1 (1)	29.51	0.06	Retinoic acid-induced protein 3	24.07	1
CCD22_HUMAN	3 (1)	29.13	0.02	Coiled-coil domain-containing protein 22	3.5	1
CTG1B_HUMAN	2 (1)	28.79	0.16	Cancer/testis antigen 1	1.89	1
MYDGF_HUMAN	1 (1)	28.16	0.48	Myeloid-derived growth factor	1.95	1
CEP83_HUMAN	3 (1)	28.09	0.01	Centrosomal protein of 83 kDa	1	17.79
NDUB9_HUMAN	1 (1)	27.36	0.89	NADH dehydrogenase [ubiquinone] 1 beta subcomplex subunit 9	1.02	1
LOXL2_HUMAN	3 (1)	25.83	0.49	Lysyl oxidase homolog 2	1.59	1
MOGS_HUMAN	3 (1)	25.65	1.16E-03	Mannosyl-oligosaccharide glucosidase	13.42	1
SLIK4_HUMAN	4 (2)	24.94	7.03E-04	SLIT and NTRK-like protein 4	1	14.11
RGPA1_HUMAN	6 (2)	24.74	6.48E-03	Ral GTPase-activating protein subunit alpha-1	1	14.05
CWC27_HUMAN	2 (1)	24.69	0.02	Peptidyl-prolyl cis-trans isomerase CWC27 homolog	1	2.01
PGES2_HUMAN	6 (1)	24.53	0.04	Prostaglandin E synthase 2	3.29	1
MYPC2_HUMAN	4 (1)	23.85	0.1	Myosin-binding protein C, fast-type	13.45	1
RFA2_HUMAN	1 (1)	22.49	0.27	Replication protein A 32 kDa subunit	79.57	1
TNR16_HUMAN	1 (1)	20.69	0.03	Tumor necrosis factor receptor superfamily member 16	1	2.63
TMED5_HUMAN	2 (1)	20.49	0.52	Transmembrane emp24 domain-containing protein 5	1.33	1
CXE1_HUMAN	2 (2)	20.04	0.71	Gap junction epsilon-1 protein	2.05	1
WDR31_HUMAN	2 (1)	20.02	0.52	WD repeat-containing protein 31	1.46	1
F25DE_HUMAN	2 (1)	20	0.23	Protein FAM25D/E	1	1.55
GNMT_HUMAN	1 (1)	19.81	0.19	Glycine N-methyltransferase	1	2.77
YS049_HUMAN	1 (1)	18.92	0.46	Zinc finger protein ENSP00000375192	1	5.75
BAIP3_HUMAN	6 (1)	17.54	1.67E-04	BAI1-associated protein 3	28.04	1
PRR30_HUMAN	4 (1)	17.13	0.37	Proline-rich protein 30	∞	0
CAC1D_HUMAN	5 (1)	17.06	0.12	Voltage-dependent L-type calcium channel subunit alpha-1D	0	∞
IL1R2_HUMAN	1 (1)	17.04	0.3	Interleukin-1 receptor type 2	1	2.27
SCIMP_HUMAN	1 (1)	16.96	0.02	SLP adapter and CSK-interacting membrane protein	1	3.02
NR4A3_HUMAN	2 (1)	15.37	0.19	Nuclear receptor subfamily 4 group A member 3	4.77	1
GCR_HUMAN	4 (1)	10.63	0.71	Glucocorticoid receptor	1	3.85
CAH12_HUMAN	3 (1)	8.4	0.11	Carbonic anhydrase 12	1	1.75

Table S4. Proteins (1119 in total) identified by bottom-up proteomics approach in membrane preparations of viable Hela-ICAM-3 and apoptotic Hela-ICAM-3 cells. Proteins were considered identified if at least one unique peptide was confidently identified by searching against SwissProt data base. Relative quantification was performed using Progenesis QI for proteomics software. Three most intense peptides per protein were used for quantification. Data in the table are normalised to the lower protein content (1.00). Values higher that 1.00 are 'fold increase' compared to the value 1.00. Measurements of three biological replicates allowed for Anova test to be performed on quantified results.

Uniprot ID	Identified peptides (unique)	Score	Anova, *p*	Protein name	Viable	Apoptotic
SP16H_HUMAN	10 (7)	230.41	0.94	FACT complex subunit SPT16	1	1
CAND1_HUMAN	13 (2)	229.25	0.12	Cullin-associated NEDD8-dissociated protein 1	1	1.54
SYMC_HUMAN	8 (5)	229.19	0.71	Methionine--tRNA ligase, cytoplasmic	1	1.23
SMC2_HUMAN	24 (2)	229.19	0.43	Structural maintenance of chromosomes protein 2	1.23	1
TIF1B_HUMAN	8 (3)	227.71	0.96	Transcription intermediary factor 1-beta	1.05	1
TOP2B_HUMAN	11 (1)	226.97	0.13	DNA topoisomerase 2-beta	1	1.27
RLA2_HUMAN	3 (1)	226.49	0.2	60S acidic ribosomal protein P2	1	1.54
IPO5_HUMAN	10 (2)	226.47	0.03	Importin-5	1	1.69
MBB1A_HUMAN	6 (2)	226.31	0.62	Myb-binding protein 1A	1	1.08
1433F_HUMAN	5 (1)	226.23	0.91	14-3-3 protein eta	1	1.08
BUB3_HUMAN	6 (4)	226.2	0.68	Mitotic checkpoint protein BUB3	1.17	1
COPE_HUMAN	5 (2)	225.41	0.91	Coatomer subunit epsilon	1	1.26
ANXA7_HUMAN	7 (5)	222.94	0.08	Annexin A7	1	2.42
CCD47_HUMAN	3 (3)	221.37	0.2	Coiled-coil domain-containing protein 47	1.22	1
DDB1_HUMAN	8 (4)	221.25	0.46	DNA damage-binding protein 1	1.31	1
DYHC1_HUMAN	17 (4)	220.81	0.45	Cytoplasmic dynein 1 heavy chain 1	1	1.12
EFGM_HUMAN	7 (3)	218.52	0.2	Elongation factor G, mitochondrial	1	1.74
2AAA_HUMAN	7 (1)	218.15	2.14E-03	Serine/threonine-protein phosphatase 2A 65 kDa regulatory subunit A alpha isoform	1	1.26
NOG1_HUMAN	6 (3)	217.96	0.36	Nucleolar GTP-binding protein 1	1	2.54
MCM4_HUMAN	8 (3)	217.95	0.19	DNA replication licensing factor MCM4	4.41	1
RAN_HUMAN	4 (1)	217.56	0.02	GTP-binding nuclear protein Ran	1.78	1
RL19_HUMAN	2 (2)	217.07	0.35	60S ribosomal protein L19	1	1.34
SNRPA_HUMAN	3 (2)	215.47	0.12	U1 small nuclear ribonucleoprotein A	1	1.49
MSH6_HUMAN	10 (3)	214.45	0.55	DNA mismatch repair protein Msh6	1	1.14
PSIP1_HUMAN	6 (4)	213.81	0.22	PC4 and SFRS1-interacting protein	1.75	1
TXND5_HUMAN	5 (2)	210.05	0.42	Thioredoxin domain-containing protein 5	1	1.03
TPM4_HUMAN	6 (3)	207.64	0.02	Tropomyosin alpha-4 chain	1	1.69
DECR_HUMAN	4 (4)	207.24	0.56	2,4-dienoyl-CoA reductase, mitochondrial	1	1.32
SEPT7_HUMAN	6 (1)	206.8	2.24E-04	Septin-7	2.3	1
IDHP_HUMAN	5 (4)	206.17	0.13	Isocitrate dehydrogenase [NADP], mitochondrial	1	1.71
RS13_HUMAN	6 (2)	206.01	0.13	40S ribosomal protein S13	1	1.63
TCOF_HUMAN	12 (4)	204.76	4.82E-03	Treacle protein	5.17	1
HNRDL_HUMAN	5 (3)	204.5	0.27	Heterogeneous nuclear ribonucleoprotein D-like	1.64	1
IF2G_HUMAN	9 (4)	204.19	0.28	Eukaryotic translation initiation factor 2 subunit 3	1.41	1
HNRL1_HUMAN	5 (2)	204.03	0.21	Heterogeneous nuclear ribonucleoprotein U-like protein 1	1	1.34
TPM3_HUMAN	7 (4)	203.15	0.32	Tropomyosin alpha-3 chain	1	1.59
MOT4_HUMAN	5 (2)	202.22	0.05	Monocarboxylate transporter 4	1.31	1
EIF3H_HUMAN	9 (5)	201.04	0.05	Eukaryotic translation initiation factor 3 subunit H	1	1.47
NOP2_HUMAN	7 (4)	200.88	0.37	Probable 28S rRNA (cytosine(4447)-C(5))-methyltransferase	1.18	1
ACINU_HUMAN	10 (2)	199.4	0.64	Apoptotic chromatin condensation inducer in the nucleus	1	1.06
PSA6_HUMAN	4 (1)	198.28	0.32	Proteasome subunit alpha type-6	1	1.32
GNAI3_HUMAN	4 (3)	197.07	0.86	Guanine nucleotide-binding protein G(k) subunit alpha	1.24	1
SAFB1_HUMAN	16 (5)	195.78	0.39	Scaffold attachment factor B1	1	1.1

ANX11_HUMAN	9 (5)	194.6	0.05	Annexin A11	1	1.19
HAP28_HUMAN	4 (3)	194.59	0.07	28 kDa heat- and acid-stable phosphoprotein	2.28	1
RAB8A_HUMAN	3 (1)	193.07	0.76	Ras-related protein Rab-8A	1	1.08
SSRP1_HUMAN	7 (4)	192.88	0.35	FACT complex subunit SSRP1	1.67	1
GDIB_HUMAN	7 (3)	192.63	0.03	Rab GDP dissociation inhibitor beta	2.96	1
ROA0_HUMAN	2 (1)	192.01	0.43	Heterogeneous nuclear ribonucleoprotein A0	1.24	1
PSA2_HUMAN	4 (3)	191.44	0.22	Proteasome subunit alpha type-2	1	1.24
HEXB_HUMAN	4 (2)	191.35	0.47	Beta-hexosaminidase subunit beta	1	1.28
PDCD4_HUMAN	8 (4)	191.13	5.37E-03	Programmed cell death protein 4	1.49	1
PRC2C_HUMAN	16 (2)	190.84	0.17	Protein PRRC2C	1	1.41
TCEA1_HUMAN	4 (1)	189.88	0.71	Transcription elongation factor A protein 1	1	1.52
G3BP2_HUMAN	4 (1)	189.06	0.27	Ras GTPase-activating protein-binding protein 2	1	1.03
FSCN1_HUMAN	2 (1)	188.59	0.59	Fascin	1	1.01
CAZA1_HUMAN	3 (3)	188.54	0.56	F-actin-capping protein subunit alpha-1	1.14	1
MIC19_HUMAN	4 (3)	188.03	0.02	MICOS complex subunit MIC19	1	2.95
CDC42_HUMAN	5 (3)	187.77	0.18	Cell division control protein 42 homolog	1	1.87
U2AF2_HUMAN	3 (2)	187.2	9.99E-05	Splicing factor U2AF 65 kDa subunit	28.36	1
SPB6_HUMAN	3 (3)	185.94	0.33	Serpin B6	1	1.32
SC24C_HUMAN	12 (3)	185.76	0.28	Protein transport protein Sec24C	1	1.38
SNAA_HUMAN	3 (3)	185.26	0.28	Alpha-soluble NSF attachment protein	1.25	1
SYQ_HUMAN	10 (5)	185.19	0.39	Glutamine--tRNA ligase	1	1.18
PSA1_HUMAN	5 (4)	184.83	3.49E-04	Proteasome subunit alpha type-1	1	1.33
MK67I_HUMAN	4 (3)	184.25	0.32	MKI67 FHA domain-interacting nucleolar phosphoprotein	1	1.61
EBP2_HUMAN	5 (1)	184.24	0.73	Probable rRNA-processing protein EBP2	1	1.05
RBCC1_HUMAN	20 (3)	184.08	0.26	RB1-inducible coiled-coil protein 1	1.44	1
TOM70_HUMAN	7 (3)	183.3	2.34E-03	Mitochondrial import receptor subunit TOM70	1	2.34
SRP14_HUMAN	3 (2)	182.83	0.75	Signal recognition particle 14 kDa protein	1.31	1
PSDE_HUMAN	3 (2)	181.95	0.79	26S proteasome non-ATPase regulatory subunit 14	1	1.19
H2AW_HUMAN	7 (1)	181.22	0.82	Core histone macro-H2A.2	1.46	1
SRRM1_HUMAN	10 (3)	180.34	0.55	Serine/arginine repetitive matrix protein 1	1	1.16
GPDM_HUMAN	9 (2)	179.52	0.03	Glycerol-3-phosphate dehydrogenase, mitochondrial	1	2.09
GYS1_HUMAN	9 (5)	179.03	0.27	Glycogen [starch] synthase, muscle	1.54	1
RENT1_HUMAN	4 (2)	178.92	4.78E-03	Regulator of nonsense transcripts 1	1.71	1
TIM50_HUMAN	3 (2)	177.6	0.06	Mitochondrial import inner membrane translocase subunit TIM50	1	2.15
ARF1_HUMAN	5 (1)	177.56	0.16	ADP-ribosylation factor 1	1	2.59
DDX50_HUMAN	11 (3)	177.23	0.43	ATP-dependent RNA helicase DDX50	1	1.35
EMD_HUMAN	3 (3)	176.87	0.18	Emerin	1	1.62
KCRB_HUMAN	3 (2)	176.18	0.49	Creatine kinase B-type	1.07	1
LEG3_HUMAN	4 (2)	175.81	0.7	Galectin-3	1.05	1
WBP11_HUMAN	9 (4)	175.66	0.03	WW domain-binding protein 11	1.37	1
EWS_HUMAN	3 (2)	174.83	0.33	RNA-binding protein EWS	1	1.31
SCMC1_HUMAN	8 (2)	174.5	0.62	Calcium-binding mitochondrial carrier protein SCaMC-1	1	1.28
ADT4_HUMAN	5 (1)	174.25	0.94	ADP/ATP translocase 4	1	1.15
SORCN_HUMAN	4 (2)	173.55	0.4	Sorcin	1.22	1
PSME2_HUMAN	2 (2)	171.89	0.09	Proteasome activator complex subunit 2	1	1.46
RL40_HUMAN	6 (4)	171.78	0.93	Ubiquitin-60S ribosomal protein L40	1.07	1
CROCC_HUMAN	20 (1)	171.53	0.45	Rootletin	1	1.58
PDS5A_HUMAN	6 (4)	170.46	0.67	Sister chromatid cohesion protein PDS5 homolog A	1.27	1
EIF2A_HUMAN	4 (2)	170.35	0.11	Eukaryotic translation initiation factor 2A	1.81	1
H2B3B_HUMAN	4 (2)	169.27	0.58	Histone H2B type 3-B	1.28	1
NDUV2_HUMAN	3 (2)	168.63	0.75	NADH dehydrogenase [ubiquinone] flavoprotein 2, mitochondrial	1	1.17
HDHD5_HUMAN	5 (2)	168.55	0.58	Haloacid dehalogenase-like hydrolase domain-containing 5	1	1.18
TMED4_HUMAN	3 (1)	167.98	0.22	Transmembrane emp24 domain-containing protein 4	1.33	1
OBSCN_HUMAN	28 (3)	167.75	0.57	Obscurin	1	1.5
TCRG1_HUMAN	10 (3)	166.92	0.4	Transcription elongation regulator 1	1.12	1
EIF3I_HUMAN	3 (2)	166.32	0.41	Eukaryotic translation initiation factor 3 subunit I	1.32	1
LAT1_HUMAN	3 (1)	165.82	0.78	Large neutral amino acids transporter small subunit 1	1.82	1
ABCA4_HUMAN	26 (6)	165.1	0.05	Retinal-specific ATP-binding cassette transporter	1.44	1

SCAM3_HUMAN	2 (1)	164.91	0.34	Secretory carrier-associated membrane protein 3	1.63	1
SMCA5_HUMAN	12 (2)	164.81	0.3	SWI/SNF-related matrix-associated actin-dependent regulator of chromatin subfamily A member 5	1	1.45
RAP2C_HUMAN	3 (1)	164.52	0.07	Ras-related protein Rap-2c	1	1.99
COPG1_HUMAN	6 (1)	163.65	0.16	Coatomer subunit gamma-1	1	2.06
NDUAA_HUMAN	4 (1)	163.03	0.45	NADH dehydrogenase [ubiquinone] 1 alpha subcomplex subunit 10, mitochondrial	1	1.49
TOM34_HUMAN	4 (3)	162.89	0.16	Mitochondrial import receptor subunit TOM34	1.9	1
CTNA1_HUMAN	12 (3)	162.82	0.01	Catenin alpha-1	1.35	1
H1X_HUMAN	5 (1)	162.29	0.2	Histone H1x	1.59	1
GTR14_HUMAN	5 (2)	162.02	0.02	Solute carrier family 2, facilitated glucose transporter member 14	2.42	1
PRPS2_HUMAN	4 (1)	161.46	0.99	Ribose-phosphate pyrophosphokinase 2	1	1.01
RS24_HUMAN	3 (2)	161.24	0.5	40S ribosomal protein S24	1	1.19
NP1L1_HUMAN	3 (2)	160.89	0.85	Nucleosome assembly protein 1-like 1	1.79	1
LRRK2_HUMAN	17 (3)	160.59	0.49	Leucine-rich repeat serine/threonine-protein kinase 2	1.21	1
HMOX2_HUMAN	5 (4)	159.29	0.04	Heme oxygenase 2	4.03	1
SSRG_HUMAN	2 (2)	159.22	0.78	Translocon-associated protein subunit gamma	1.07	1
TM14C_HUMAN	4 (2)	159.21	0.17	Transmembrane protein 14C	1	1.51
LIMA1_HUMAN	4 (4)	158.54	0.34	LIM domain and actin-binding protein 1	3.38	1
DUT_HUMAN	5 (1)	158.51	0.47	Deoxyuridine 5'-triphosphate nucleotidohydrolase, mitochondrial	1	1.38
CIP4_HUMAN	8 (2)	158.39	0.27	Cdc42-interacting protein 4	1.82	1
DNMT1_HUMAN	9 (3)	158.35	0.02	DNA (cytosine-5)-methyltransferase 1	1.22	1
NSF_HUMAN	9 (4)	157.75	0.35	Vesicle-fusing ATPase	1	1.3
PSA5_HUMAN	2 (2)	157.5	8.41E-03	Proteasome subunit alpha type-5	1	1.1
STRAP_HUMAN	6 (1)	157.4	0.03	Serine-threonine kinase receptor-associated protein	6.84	1
CYB5B_HUMAN	4 (4)	157.05	0.46	Cytochrome b5 type B	1	1.15
MRRP1_HUMAN	6 (4)	155.81	0.22	Mitochondrial ribonuclease P protein 1	1	1.38
RS16_HUMAN	5 (3)	155.56	0.4	40S ribosomal protein S16	1	1.19
ALBU_HUMAN	13 (4)	155.23	0.24	Serum albumin	1	1.15
AP2B1_HUMAN	5 (2)	155.12	0.2	AP-2 complex subunit beta	1.46	1
HP1B3_HUMAN	4 (1)	155.11	0.18	Heterochromatin protein 1-binding protein 3	1	1.45
ODP2_HUMAN	10 (4)	154.96	5.24E-04	Dihydrolipoyllysine-residue acetyltransferase component of pyruvate dehydrogenase complex, mitochondrial	2.08	1
LAP2A_HUMAN	5 (2)	154.61	0.05	Lamina-associated polypeptide 2, isoform alpha	2	1
SRPRB_HUMAN	5 (2)	154.39	0.27	Signal recognition particle receptor subunit beta	1	1.32
DX39B_HUMAN	4 (2)	154.04	0.51	Spliceosome RNA helicase DDX39B	9.67	1
NOP58_HUMAN	3 (2)	154.02	0.17	Nucleolar protein 58	1	1.58
RU17_HUMAN	6 (4)	153.97	0.07	U1 small nuclear ribonucleoprotein 70 kDa	1	2.07
PYM1_HUMAN	3 (2)	153.69	0.35	Partner of Y14 and mago	2.05	1
SSRD_HUMAN	4 (2)	153.65	0.01	Translocon-associated protein subunit delta	1	1.51
PGM1_HUMAN	4 (2)	153.22	0.05	Phosphoglucomutase-1	1	1.88
PGAM4_HUMAN	3 (1)	153.03	0.06	Probable phosphoglycerate mutase 4	1.78	1
QOR_HUMAN	5 (2)	152.87	0.88	Quinone oxidoreductase	1	1.38
PURA_HUMAN	3 (3)	152.3	0.91	Transcriptional activator protein Pur-alpha	1.16	1
RS17_HUMAN	4 (3)	151.88	0.04	40S ribosomal protein S17	1	2.44
NUMA1_HUMAN	15 (1)	150.64	0.33	Nuclear mitotic apparatus protein 1	1.24	1
RAB13_HUMAN	2 (1)	150.33	0.23	Ras-related protein Rab-13	1	1.5
SURF4_HUMAN	2 (2)	150.18	0.35	Surfeit locus protein 4	1.34	1
AP2A1_HUMAN	4 (1)	150.18	0.22	AP-2 complex subunit alpha-1	27.19	1
RBBP7_HUMAN	3 (3)	150.08	2.10E-06	Histone-binding protein RBBP7	1.36	1
ARPC3_HUMAN	3 (2)	149.22	0.96	Actin-related protein 2/3 complex subunit 3	1.08	1
SYK_HUMAN	7 (2)	148.98	0.04	Lysine--tRNA ligase	1.75	1
UTRO_HUMAN	18 (2)	148.8	5.02E-05	Utrophin	1	1.4
NU155_HUMAN	2 (1)	148.28	0.31	Nuclear pore complex protein Nup155	1.41	1
IPO9_HUMAN	2 (1)	147.96	0.56	Importin-9	1	1.03
RS4Y2_HUMAN	6 (1)	147.88	0.11	40S ribosomal protein S4, Y isoform 2	34.65	1
KAD4_HUMAN	5 (2)	147.68	0.09	Adenylate kinase 4, mitochondrial	1	1.19
MCM7_HUMAN	7 (2)	146.97	0.6	DNA replication licensing factor MCM7	1	1.99
RS11_HUMAN	2 (1)	146.68	0.1	40S ribosomal protein S11	1	3.61
RM11_HUMAN	6 (2)	146.64	0.03	39S ribosomal protein L11, mitochondrial	2.64	1
TCTP_HUMAN	4 (2)	146.07	0.39	Translationally-controlled tumor protein	1.48	1

RAB31_HUMAN	1 (1)	145.04	0.16	Ras-related protein Rab-31	1	1.41
PININ_HUMAN	6 (3)	145.03	0.55	Pinin	1	1.2
HSP74_HUMAN	12 (4)	144.77	0.55	Heat shock 70 kDa protein 4	1	1.07
OLA1_HUMAN	1 (1)	144.46	0.04	Obg-like ATPase 1	1	3.31
FKB10_HUMAN	4 (1)	144.03	0.2	Peptidyl-prolyl cis-trans isomerase FKBP10	1	4.8
ACTN2_HUMAN	5 (1)	143.5	0.67	Alpha-actinin-2	1.93	1
CHIP_HUMAN	3 (1)	143.1	0.23	E3 ubiquitin-protein ligase CHIP	1	1.18
ROCK1_HUMAN	16 (2)	142.97	0.86	Rho-associated protein kinase 1	1.19	1
PNPT1_HUMAN	9 (2)	142.39	0.12	Polyribonucleotide nucleotidyltransferase 1, mitochondrial	1	2.33
PRP19_HUMAN	4 (2)	142.33	0.23	Pre-mRNA-processing factor 19	1.01	1
MDHC_HUMAN	7 (4)	141.91	0.2	Malate dehydrogenase, cytoplasmic	2.3	1
TADBP_HUMAN	8 (4)	141.83	0.47	TAR DNA-binding protein 43	1.2	1
ICAM3_HUMAN	3 (1)	141.36	0.74	Intercellular adhesion molecule 3	1.04	1
CPSF6_HUMAN	5 (1)	141.09	0.52	Cleavage and polyadenylation specificity factor subunit 6	1.51	1
RL15_HUMAN	5 (1)	140.65	2.48E-03	60S ribosomal protein L15	1.53	1
NIPS1_HUMAN	4 (1)	140.56	0.65	Protein NipSnap homolog 1	1	1.09
ATPK_HUMAN	3 (2)	139.8	0.15	ATP synthase subunit f, mitochondrial	1	1.44
IPYR2_HUMAN	2 (2)	139.67	0.24	Inorganic pyrophosphatase 2, mitochondrial	1	2.19
RS18_HUMAN	4 (1)	139.45	0.37	40S ribosomal protein S18	1	1.72
PUF60_HUMAN	5 (2)	139.19	0.03	Poly(U)-binding-splicing factor PUF60	1	2.92
DDX27_HUMAN	7 (1)	139.12	0.38	Probable ATP-dependent RNA helicase DDX27	1	1.2
PP1B_HUMAN	3 (2)	139.01	0.2	Serine/threonine-protein phosphatase PP1-beta catalytic subunit	1	2
ACOX1_HUMAN	6 (1)	138.82	0.76	Peroxisomal acyl-coenzyme A oxidase 1	1	1.08
AP1B1_HUMAN	6 (1)	138.12	0.88	AP-1 complex subunit beta-1	1.01	1
TFAM_HUMAN	4 (1)	137.48	6.39E-04	Transcription factor A, mitochondrial	1	1.46
NNTM_HUMAN	7 (3)	137.18	0.85	NAD(P) transhydrogenase, mitochondrial	1.14	1
CPSF7_HUMAN	3 (2)	136.39	0.06	Cleavage and polyadenylation specificity factor subunit 7	2.11	1
DDX18_HUMAN	11 (3)	136.04	0.28	ATP-dependent RNA helicase DDX18	1	1.63
PGRC2_HUMAN	3 (1)	135.59	0.96	Membrane-associated progesterone receptor component 2	1.03	1
NDUA9_HUMAN	4 (3)	135.48	0.89	NADH dehydrogenase [ubiquinone] 1 alpha subcomplex subunit 9, mitochondrial	1	1.05
SYDC_HUMAN	2 (2)	135.25	0.75	Aspartate--tRNA ligase, cytoplasmic	1.55	1
MAP7_HUMAN	4 (1)	134.1	0.24	Ensconsin	1	1.42
RBM8A_HUMAN	2 (2)	134.01	0.18	RNA-binding protein 8A	1	1.52
ITAV_HUMAN	5 (3)	133.96	0.22	Integrin alpha-V	1.32	1
FXR2_HUMAN	5 (2)	132.78	0.05	Fragile X mental retardation syndrome-related protein 2	4.3	1
DYN1_HUMAN	7 (1)	132.52	0.79	Dynamin-1	1.56	1
NIBL1_HUMAN	5 (2)	132.2	0.07	Niban-like protein 1	1	1.94
CATD_HUMAN	5 (2)	131.67	0.49	Cathepsin D	1	1.31
KTNB1_HUMAN	11 (1)	131.64	1.73E-03	Katanin p80 WD40 repeat-containing subunit B1	4	1
CLIC1_HUMAN	2 (2)	131.57	0.02	Chloride intracellular channel protein 1	2.32	1
DNJC9_HUMAN	8 (4)	131.04	0.13	DnaJ homolog subfamily C member 9	4.36	1
RT07_HUMAN	4 (1)	130.77	0.1	28S ribosomal protein S7, mitochondrial	1.32	1
IF2B_HUMAN	6 (3)	130.51	4.28E-03	Eukaryotic translation initiation factor 2 subunit 2	1	1.33
MRT4_HUMAN	4 (3)	130.43	0.53	mRNA turnover protein 4 homolog	1	1.44
PLOD1_HUMAN	3 (2)	130.16	0.96	Procollagen-lysine,2-oxoglutarate 5-dioxygenase 1	1	1.01
ANXA3_HUMAN	3 (1)	129.79	1	Annexin A3	1	1.08
CHD3_HUMAN	16 (8)	129.51	0.67	Chromodomain-helicase-DNA-binding protein 3	1.17	1
NP1L4_HUMAN	4 (3)	129.17	0.09	Nucleosome assembly protein 1-like 4	1	1.89
RM04_HUMAN	3 (1)	127.7	0.66	39S ribosomal protein L4, mitochondrial	1	1.26
RALY_HUMAN	6 (2)	127.67	0.12	RNA-binding protein Raly	8.18	1
RBP2_HUMAN	12 (2)	127.64	0.4	E3 SUMO-protein ligase RanBP2	1.66	1
SRSF5_HUMAN	3 (3)	127.18	0.09	Serine/arginine-rich splicing factor 5	2.21	1
PGES2_HUMAN	5 (2)	127.14	0.09	Prostaglandin E synthase 2	1.37	1
RL7L_HUMAN	5 (1)	126.2	6.97E-04	60S ribosomal protein L7-like 1	1	530.11
CDK2_HUMAN	4 (1)	125.98	0.48	Cyclin-dependent kinase 2	1	1.03
TOP1_HUMAN	4 (1)	125.62	0.06	DNA topoisomerase 1	1	1.48
SRSF2_HUMAN	2 (2)	124.92	0.68	Serine/arginine-rich splicing factor 2	1.09	1
AKAP1_HUMAN	6 (3)	124.84	0.37	A-kinase anchor protein 1, mitochondrial	1	1.98

RFC2_HUMAN	3 (2)	124.7	0.19	Replication factor C subunit 2	1	1.21
HMGB3_HUMAN	3 (1)	124.51	0.03	High mobility group protein B3	1.75	1
RUVB1_HUMAN	4 (2)	124.51	7.28E-03	RuvB-like 1	1.88	1
DC1I2_HUMAN	3 (1)	124.42	0.01	Cytoplasmic dynein 1 intermediate chain 2	3.39	1
UBP10_HUMAN	4 (1)	124.12	0.03	Ubiquitin carboxyl-terminal hydrolase 10	1.92	1
RT22_HUMAN	4 (2)	123.72	0.05	28S ribosomal protein S22, mitochondrial	1	2.7
RYR3_HUMAN	21 (3)	123.67	0.34	Ryanodine receptor 3	1	1.42
GBB1_HUMAN	4 (1)	123.53	4.28E-03	Guanine nucleotide-binding protein G(I)/G(S)/G(T) subunit beta-1	4.5	1
ACTN3_HUMAN	5 (1)	122.89	0.85	Alpha-actinin-3	1.1	1
C1TM_HUMAN	9 (2)	122.27	0.15	Monofunctional C1-tetrahydrofolate synthase, mitochondrial	1	2.08
SYSC_HUMAN	5 (1)	121.88	0.45	Serine--tRNA ligase, cytoplasmic	1.5	1
EIF3K_HUMAN	4 (2)	121.87	0.01	Eukaryotic translation initiation factor 3 subunit K	1.19	1
DIAP1_HUMAN	8 (2)	121.84	6.57E-03	Protein diaphanous homolog 1	1	2
SMC4_HUMAN	11 (2)	121.5	0.11	Structural maintenance of chromosomes protein 4	1	1.25
ICAL_HUMAN	5 (2)	121.27	0.95	Calpastatin	1	1
MCM6_HUMAN	5 (2)	119.91	0.67	DNA replication licensing factor MCM6	1.04	1
NMT1_HUMAN	4 (1)	119.68	0.03	Glycylpeptide N-tetradecanoyltransferase 1	1.57	1
GNL3_HUMAN	3 (1)	119.51	1	Guanine nucleotide-binding protein-like 3	1.13	1
SUCA_HUMAN	2 (2)	117.16	0.04	Succinate--CoA ligase [ADP/GDP-forming] subunit alpha, mitochondrial	1	3.05
GRSF1_HUMAN	4 (3)	116.72	8.94E-03	G-rich sequence factor 1	1	1.36
PCNA_HUMAN	5 (1)	116.25	0.49	Proliferating cell nuclear antigen	1	1.17
KPYR_HUMAN	5 (2)	116.1	2.59E-04	Pyruvate kinase PKLR	2.24	1
AAAT_HUMAN	3 (1)	115.87	0.34	Neutral amino acid transporter B(0)	2.87	1
AFG32_HUMAN	6 (2)	114.72	0.02	AFG3-like protein 2	1.45	1
NUCB2_HUMAN	2 (2)	114.43	0.09	Nucleobindin-2	1.74	1
CAPZB_HUMAN	3 (2)	114.2	0.53	F-actin-capping protein subunit beta	1.56	1
RBM25_HUMAN	3 (2)	113.86	0.97	RNA-binding protein 25	1	1.06
GNA13_HUMAN	3 (2)	113.77	0.57	Guanine nucleotide-binding protein subunit alpha-13	2.39	1
SYFB_HUMAN	10 (4)	113.5	2.63E-03	Phenylalanine--tRNA ligase beta subunit	3.26	1
HPDL_HUMAN	2 (2)	113.25	0.04	4-hydroxyphenylpyruvate dioxygenase-like protein	1	1.45
CAPG_HUMAN	3 (1)	112.72	0.94	Macrophage-capping protein	1.4	1
ERLN2_HUMAN	5 (3)	112.61	1.23E-04	Erlin-2 O	1	1.29
RS10_HUMAN	4 (3)	112.53	0.08	40S ribosomal protein S10	1	2.21
GOGA2_HUMAN	5 (2)	112.36	5.84E-03	Golgin subfamily A member 2	1.36	1
SDCB1_HUMAN	3 (2)	112.26	0.83	Syntenin-1	1	1.1
PAP1L_HUMAN	6 (1)	112.09	0.12	Polyadenylate-binding protein 1-like	1	1.6
AP180_HUMAN	5 (2)	111.99	0.97	Clathrin coat assembly protein AP180	1	1.02
F10A1_HUMAN	4 (2)	111.99	2.37E-03	Hsc70-interacting protein	1.79	1
COQ9_HUMAN	2 (1)	111.85	0.68	Ubiquinone biosynthesis protein COQ9, mitochondrial	1	1.38
UBB_HUMAN	3 (1)	111.69	9.06E-03	Polyubiquitin-B	1	2.01
RAGP1_HUMAN	5 (1)	111.66	0.58	Ran GTPase-activating protein 1	1	1.2
CHTOP_HUMAN	4 (2)	111.31	0.32	Chromatin target of PRMT1 protein	1.66	1
PUR2_HUMAN	7 (2)	111.26	0.05	Trifunctional purine biosynthetic protein adenosine-3	1.05	1
CCD51_HUMAN	1 (1)	111.18	0.31	Coiled-coil domain-containing protein 51	1	1.43
DJB11_HUMAN	4 (3)	110.55	0.65	DnaJ homolog subfamily B member 11	1.03	1
PGRC1_HUMAN	2 (2)	110.23	0.3	Membrane-associated progesterone receptor component 1	1.18	1
IDHC_HUMAN	2 (1)	110	0.55	Isocitrate dehydrogenase [NADP] cytoplasmic	1	1.48
ACTL8_HUMAN	3 (1)	109.95	1.28E-04	Actin-like protein 8	1	1.5
PLCA_HUMAN	11 (5)	109.54	0.28	1-acyl-sn-glycerol-3-phosphate acyltransferase alpha	1.54	1
PON2_HUMAN	2 (2)	109.48	0.16	Serum paraoxonase/arylesterase 2	2.02	1
VTNC_HUMAN	3 (1)	108.9	0.59	Vitronectin	1.53	1
DEK_HUMAN	4 (3)	108.86	3.76E-03	Protein DEK	1.66	1
IF5_HUMAN	3 (1)	108.69	0.4	Eukaryotic translation initiation factor 5	6.64	1
RBP56_HUMAN	2 (1)	108.58	0.09	TATA-binding protein-associated factor 2N	1.36	1
DNJB1_HUMAN	2 (2)	108.42	0.41	DnaJ homolog subfamily B member 1	1	1.43
IMP3_HUMAN	3 (2)	107.83	5.04E-04	U3 small nucleolar ribonucleoprotein protein IMP3	1	3.85
GSLG1_HUMAN	7 (2)	107.75	0.33	Golgi apparatus protein 1	1.3	1
HBA_HUMAN	3 (2)	107.66	0.41	Hemoglobin subunit alpha	1	1.44

FRIL_HUMAN	2 (1)	107.52	0.86	Ferritin light chain	1.04	1
GNA11_HUMAN	2 (1)	107.41	0.97	Guanine nucleotide-binding protein subunit alpha-11	1	1.21
KCRU_HUMAN	3 (1)	107.35	0.47	Creatine kinase U-type, mitochondrial	1	3.03
AMOT_HUMAN	14 (3)	107.26	0.36	Angiomotin	1.21	1
FXR1_HUMAN	10 (2)	107.24	0.61	Fragile X mental retardation syndrome-related protein 1	1	1.07
NDK8_HUMAN	6 (2)	107.11	0.05	Putative nucleoside diphosphate kinase	1	6.74
IMDH2_HUMAN	3 (1)	106.83	2.02E-05	Inosine-5'-monophosphate dehydrogenase 2	1.69	1
IF2B3_HUMAN	5 (1)	106.61	0.79	Insulin-like growth factor 2 mRNA-binding protein 3	1.39	1
TIAR_HUMAN	3 (1)	106.49	0.24	Nucleolysin TIAR	1	1.59
RM40_HUMAN	1 (1)	106.31	0.32	39S ribosomal protein L40, mitochondrial	1	1.4
DDX46_HUMAN	10 (3)	105.51	0.31	Probable ATP-dependent RNA helicase DDX46	1.29	1
RTCA_HUMAN	3 (2)	105.3	0.61	RNA 3'-terminal phosphate cyclase	1	1.11
PSA7L_HUMAN	3 (1)	104.74	0.25	Proteasome subunit alpha type-7-like	1	1.06
STX4_HUMAN	2 (1)	104.65	0.31	Syntaxin-4	1	1.12
TRPM7_HUMAN	18 (2)	104.41	0.97	Transient receptor potential cation channel subfamily M member 7	1.46	1
RAB6B_HUMAN	4 (1)	104.38	0.72	Ras-related protein Rab-6B	1	1.19
PSB1_HUMAN	2 (2)	104.37	0.07	Proteasome subunit beta type-1	24.05	1
THOC3_HUMAN	6 (1)	103.94	0.2	THO complex subunit 3	6.15	1
ODO2_HUMAN	2 (2)	103.91	0.14	Dihydrolipoyllysine-residue succinyltransferase component of 2-oxoglutarate dehydrogenase complex, mitochondrial	1.43	1
RRP12_HUMAN	8 (4)	103.64	5.38E-03	RRP12-like protein	1	1.36
RS20_HUMAN	4 (2)	103.5	0.24	40S ribosomal protein S20	1.44	1
KAP2_HUMAN	2 (2)	102.61	0.03	cAMP-dependent protein kinase type II-alpha regulatory subunit	1	2.04
DJC10_HUMAN	6 (1)	102.15	0.94	DnaJ homolog subfamily C member 10	1	1.03
STIM1_HUMAN	6 (1)	102.09	0.15	Stromal interaction molecule 1	1	1.91
SLTM_HUMAN	5 (1)	102.04	0.09	SAFB-like transcription modulator	1	1.26
EIF3E_HUMAN	4 (2)	101.6	3.95E-04	Eukaryotic translation initiation factor 3 subunit E	1	5.1
ZCH18_HUMAN	11 (4)	101.58	0.11	Zinc finger CCCH domain-containing protein 18	1	1.49
PAXX_HUMAN	3 (1)	101.1	0.05	Protein PAXX	2.08	1
K1C12_HUMAN	4 (2)	101.04	0.72	Keratin, type I cytoskeletal 12	1	1.34
P5CR2_HUMAN	5 (1)	100.64	0.49	Pyrroline-5-carboxylate reductase 2	1	1.31
PERI_HUMAN	9 (2)	100.25	0.8	Peripherin	1.01	1
ODB2_HUMAN	2 (2)	100.14	3.71E-05	Lipoamide acyltransferase component of branched-chain alpha-keto acid dehydrogenase complex, mitochondrial	1	2.21
PRPF3_HUMAN	6 (2)	100.14	0.58	U4/U6 small nuclear ribonucleoprotein Prp3	1	1.11
FAHD1_HUMAN	3 (2)	99.32	0.05	Acylpyruvase FAHD1, mitochondrial	1	3.46
PSMD7_HUMAN	3 (1)	98.89	0.09	26S proteasome non-ATPase regulatory subunit 7	1	1.07
NAT10_HUMAN	5 (1)	98.34	0.63	RNA cytidine acetyltransferase	1.04	1
MCTS1_HUMAN	7 (1)	98.13	0.03	Malignant T-cell-amplified sequence 1	1	27.16
NICA_HUMAN	6 (1)	97.69	0.48	Nicastrin	1	1.71
RS23_HUMAN	2 (1)	97.67	0.21	40S ribosomal protein S23	1	1.53
PSME3_HUMAN	3 (2)	97.43	0.21	Proteasome activator complex subunit 3	1	1.81
DNLI3_HUMAN	8 (1)	96.56	0.37	DNA ligase 3	1	1.62
RT26_HUMAN	3 (1)	95.08	0.02	28S ribosomal protein S26, mitochondrial	1	3.47
GFAP_HUMAN	4 (2)	94.96	0.41	Glial fibrillary acidic protein	1.18	1
RM28_HUMAN	3 (1)	94.64	0.6	39S ribosomal protein L28, mitochondrial	1	1.26
CATZ_HUMAN	2 (1)	94.54	0.8	Cathepsin Z	1.03	1
AT12A_HUMAN	8 (1)	94.18	0.77	Potassium-transporting ATPase alpha chain 23	1	1.09
UTP20_HUMAN	18 (5)	94.07	0.13	Small subunit processome component 20 homolog	1	2
GSTM3_HUMAN	3 (1)	94.02	0.9	Glutathione S-transferase Mu 3	1	1.55
GOGB1_HUMAN	13 (2)	93.97	0.21	Golgin subfamily B member 1	1	1.19
NDUS2_HUMAN	3 (2)	93.63	0.31	NADH dehydrogenase [ubiquinone] iron-sulfur protein 2, mitochondrial	1	1.99
NDRG1_HUMAN	4 (1)	93.47	0.26	Protein NDRG1	1.56	1
SCO1_HUMAN	6 (2)	93.38	0.93	Protein SCO1 homolog, mitochondrial	1	1.04
RSU1_HUMAN	3 (3)	92.63	0.02	Ras suppressor protein 1	1.28	1
RU1C_HUMAN	1 (1)	92.26	0.58	U1 small nuclear ribonucleoprotein C	1	1.35
LMAN1_HUMAN	2 (2)	92.07	0.34	Protein ERGIC-53	1	1.3
GLRX3_HUMAN	6 (1)	91.55	0.46	Glutaredoxin-3	1.27	1
SEC13_HUMAN	1 (1)	90.62	0.54	Protein SEC13 homolog	1	1.07
IF2P_HUMAN	9 (2)	90.5	0.28	Eukaryotic translation initiation factor 5B	1.64	1

EIF3M_HUMAN	2 (1)	90.03	0.96	Eukaryotic translation initiation factor 3 subunit M	1	1.32
PDXK_HUMAN	5 (3)	89.75	0.76	Pyridoxal kinase	1.18	1
TXTP_HUMAN	5 (2)	89.73	0.77	Tricarboxylate transport protein, mitochondrial	1.11	1
RM13_HUMAN	3 (2)	89.59	0.84	39S ribosomal protein L13, mitochondrial	1.1	1
SAR1A_HUMAN	2 (1)	89.58	0.06	GTP-binding protein SAR1a	1	3.33
RT09_HUMAN	4 (2)	88.98	4.98E-03	28S ribosomal protein S9, mitochondrial	1	1.34
NDUBA_HUMAN	2 (1)	88.81	0.08	NADH dehydrogenase [ubiquinone] 1 beta subcomplex subunit 10	1	1.56
SRPRA_HUMAN	6 (1)	88.77	0.32	Signal recognition particle receptor subunit alpha	1	1.36
LRP1_HUMAN	9 (1)	88.76	0.12	Prolow-density lipoprotein receptor-related protein 1	1	2.67
PUR6_HUMAN	4 (2)	88.11	0.04	Multifunctional protein ADE2	1.28	1
THTR_HUMAN	4 (2)	87.68	0.89	Thiosulfate sulfurtransferase	1.08	1
ACSL4_HUMAN	8 (1)	87.65	0.42	Long-chain-fatty-acid--CoA ligase 4	1.24	1
RM44_HUMAN	2 (2)	87.24	0.79	39S ribosomal protein L44, mitochondrial	1.15	1
LEG12_HUMAN	6 (1)	87.16	0.02	Galectin-12	1	5.79
GNA12_HUMAN	4 (2)	87.16	0.66	Guanine nucleotide-binding protein subunit alpha-12	1.35	1
RCC2_HUMAN	2 (1)	87.05	1.65E-04	Protein RCC2	1.69	1
MYO7A_HUMAN	14 (2)	87.03	3.12E-03	Unconventional myosin-VIIa	1.61	1
KRR1_HUMAN	4 (2)	86.66	0.6	KRR1 small subunit processome component homolog	1.07	1
LAP2B_HUMAN	6 (2)	86.62	0.03	Lamina-associated polypeptide 2, isoforms beta/gamma	1.23	1
S10AB_HUMAN	1 (1)	86.47	0.89	Protein S100-A11	1.33	1
CTNA2_HUMAN	10 (1)	86.27	0.54	Catenin alpha-2	1.31	1
TAGL3_HUMAN	2 (1)	86.12	0.53	Transgelin-3	1	1.23
RFC5_HUMAN	2 (2)	85.93	0.04	Replication factor C subunit 5	1.8	1
ACTZ_HUMAN	1 (1)	85.69	1	Alpha-centractin	1	2.19
DDX23_HUMAN	7 (1)	85.65	0.57	Probable ATP-dependent RNA helicase DDX23	1.01	1
LARP1_HUMAN	5 (1)	85.53	7.17E-04	La-related protein 1	3.17	1
BAX_HUMAN	2 (2)	85.5	0.43	Apoptosis regulator BAX	1	1.24
AK1A1_HUMAN	4 (1)	85.21	0.54	Alcohol dehydrogenase [NADP(+)]	1.1	1
CPT2_HUMAN	2 (1)	85.05	5.22E-08	Carnitine O-palmitoyltransferase 2, mitochondrial	1	4.23
AT11B_HUMAN	5 (1)	84.73	0.59	Probable phospholipid-transporting ATPase IF	1.09	1
DHX30_HUMAN	8 (2)	84.53	0.81	Putative ATP-dependent RNA helicase DHX30	1.17	1
RPN2_HUMAN	3 (2)	84.27	0.37	Dolichyl-diphosphooligosaccharide--protein glycosyltransferase subunit 2	1	1.15
D39U1_HUMAN	4 (1)	84.05	0.23	Epimerase family protein SDR39U1	1	71.04
SDF2L_HUMAN	2 (2)	83.84	0.29	Stromal cell-derived factor 2-like protein 1	1	1.55
AIMP2_HUMAN	3 (2)	83.69	0.19	Aminoacyl tRNA synthase complex-interacting multifunctional protein 2	2.65	1
GGYF2_HUMAN	4 (1)	83.65	0.36	GRB10-interacting GYF protein 2	2.77	1
FMR1_HUMAN	5 (2)	83.52	0.03	Synaptic functional regulator FMR1	1.44	1
PO210_HUMAN	3 (2)	83.42	0.2	Nuclear pore membrane glycoprotein 210	1.28	1
ARPC2_HUMAN	4 (1)	82.91	0.69	Actin-related protein 2/3 complex subunit 2	22.88	1
IMA1_HUMAN	2 (1)	82.39	0.77	Importin subunit alpha-1	1	1.02
CG050_HUMAN	3 (1)	82.3	0.77	Uncharacterized protein C7orf50	1.04	1
UFD1_HUMAN	1 (1)	81.83	0.31	Ubiquitin recognition factor in ER-associated degradation protein 1	1	1.36
PSD13_HUMAN	4 (1)	81.66	0.09	26S proteasome non-ATPase regulatory subunit 13	1	1.54
ZN326_HUMAN	4 (1)	81.47	0.2	DBIRD complex subunit ZNF326	1	8.94
IF5A1_HUMAN	2 (1)	80.99	0.27	Eukaryotic translation initiation factor 5A-1	1	2.77
GRWD1_HUMAN	2 (2)	80.66	0.08	Glutamate-rich WD repeat-containing protein 1	1	2.43
PR40A_HUMAN	6 (1)	80.6	0.87	Pre-mRNA-processing factor 40 homolog A	1	1.1
RD23B_HUMAN	2 (1)	80.5	2.30E-05	UV excision repair protein RAD23 homolog B	5.38	1
PSA3_HUMAN	4 (1)	80.18	0.29	Proteasome subunit alpha type-3	1.22	1
DJC17_HUMAN	4 (1)	80.01	0.25	DnaJ homolog subfamily C member 17	36.42	1
MIMIT_HUMAN	3 (1)	79.66	0.05	Mimitin, mitochondrial	1	1.41
ENAH_HUMAN	2 (1)	79.62	0.59	Protein enabled homolog	1	1.06
SF3A3_HUMAN	2 (1)	79.49	0.02	Splicing factor 3A subunit 3	1.68	1
DRG1_HUMAN	1 (1)	79.43	3.07E-04	Developmentally-regulated GTP-binding protein 1	1.8	1
BCAT2_HUMAN	3 (1)	79.18	0.02	Branched-chain-amino-acid aminotransferase, mitochondrial	1	1.23
DHRS4_HUMAN	3 (1)	79.06	0.39	Dehydrogenase/reductase SDR family member 4	1.2	1
VAT1_HUMAN	3 (1)	79.03	0.83	Synaptic vesicle membrane protein VAT-1 homolog	4.74	1
NOP56_HUMAN	4 (3)	78.93	0.22	Nucleolar protein 56	1.26	1

CSK21_HUMAN	3 (1)	78.72	0.37	Casein kinase II subunit alpha	1.19	1
RALB_HUMAN	3 (2)	78.7	0.11	Ras-related protein Ral-B	1	2.52
NFH_HUMAN	7 (1)	78.47	0.63	Neurofilament heavy polypeptide	1	1.08
NNRE_HUMAN	3 (2)	78.35	0.52	NAD(P)H-hydrate epimerase	1	1.3
CH033_HUMAN	4 (2)	78.24	0.83	UPF0488 protein C8orf33	1.16	1
RRS1_HUMAN	5 (2)	78.16	0.6	Ribosome biogenesis regulatory protein homolog	1.08	1
SETLP_HUMAN	1 (1)	78.03	0.52	Protein SETSIP	1	2.62
SNUT1_HUMAN	6 (1)	77.95	0.53	U4/U6.U5 tri-snRNP-associated protein 1	1	1.15
ES1_HUMAN	2 (1)	77.89	0.06	ES1 protein homolog, mitochondrial	1	4.04
TOM22_HUMAN	1 (1)	77.87	0.04	Mitochondrial import receptor subunit TOM22 homolog	1	2.59
PCKGM_HUMAN	5 (2)	77.87	0.08	Phosphoenolpyruvate carboxykinase [GTP], mitochondrial	1	1.52
IDH3G_HUMAN	3 (2)	77.74	0.44	Isocitrate dehydrogenase [NAD] subunit gamma, mitochondrial	1	1.66
PIWL4_HUMAN	5 (1)	77.34	2.38E-06	Piwi-like protein 4	1	5.14
SAHH_HUMAN	4 (1)	77.2	0.65	Adenosylhomocysteinase	1.13	1
RMXL3_HUMAN	2 (1)	77.01	0.14	RNA-binding motif protein, X-linked-like-3	5.3	1
CTND1_HUMAN	7 (2)	76.9	0.22	Catenin delta-1	1	1.77
EGLN1_HUMAN	1 (1)	76.69	0.34	Egl nine homolog 1	1.63	1
SODM_HUMAN	1 (1)	76.53	0.16	Superoxide dismutase [Mn], mitochondrial	1	1.25
PRS10_HUMAN	3 (1)	76.19	0.18	26S proteasome regulatory subunit 10B	1	4.56
RBM14_HUMAN	6 (2)	76.17	0.44	RNA-binding protein 14	1	1.06
AHSA1_HUMAN	3 (2)	76.06	0.5	Activator of 90 kDa heat shock protein ATPase homolog 1	1	1.5
SERC_HUMAN	3 (2)	75.76	0.08	Phosphoserine aminotransferase	1	25.74
GDIA_HUMAN	3 (1)	75.68	0.29	Rab GDP dissociation inhibitor alpha	6.28	1
VATA_HUMAN	3 (2)	75.65	0.07	V-type proton ATPase catalytic subunit A	1.58	1
PSB2_HUMAN	2 (1)	75.24	0.93	Proteasome subunit beta type-2	1	1.19
RL27A_HUMAN	1 (1)	75.23	0.11	60S ribosomal protein L27a	1	1.55
MIC25_HUMAN	4 (1)	74.62	0.43	MICOS complex subunit MIC25	1	1.15
RAB12_HUMAN	3 (1)	74.36	0.14	Ras-related protein Rab-12	1.69	1
SYWC_HUMAN	2 (2)	74.26	0.03	Tryptophan--tRNA ligase, cytoplasmic	1.62	1
MTA2_HUMAN	11 (5)	74.23	0.02	Metastasis-associated protein MTA2	1	2.25
RTN4_HUMAN	4 (1)	73.99	0.32	Reticulon-4	1	1.72
THOC6_HUMAN	4 (2)	73.81	0.37	THO complex subunit 6 homolog	1	1.19
THOC2_HUMAN	6 (1)	73.74	6.80E-03	THO complex subunit 2	1	74.08
IF4E_HUMAN	2 (2)	73.68	1.99E-03	Eukaryotic translation initiation factor 4E	1.54	1
ABCG2_HUMAN	2 (1)	73.67	0.58	ATP-binding cassette sub-family G member 2	1.12	1
PMVK_HUMAN	2 (1)	73.34	0.28	Phosphomevalonate kinase	3.39	1
SHLB1_HUMAN	3 (2)	73.26	0.13	Endophilin-B1	1	2.61
MTCH2_HUMAN	3 (1)	73	0.11	Mitochondrial carrier homolog 2	1	2.18
KHDR1_HUMAN	3 (2)	72.98	1.30E-03	KH domain-containing, RNA-binding, signal transduction-associated protein 1	1.15	1
HPPD_HUMAN	2 (2)	72.96	0.86	4-hydroxyphenylpyruvate dioxygenase	1	1.04
BZW2_HUMAN	3 (1)	72.47	0.87	Basic leucine zipper and W2 domain-containing protein 2	1	1
GDIR1_HUMAN	1 (1)	72.31	0.51	Rho GDP-dissociation inhibitor 1	1.06	1
STAR9_HUMAN	12 (1)	72.22	0.55	StAR-related lipid transfer protein 9	1.17	1
PABP2_HUMAN	2 (1)	72.03	4.25E-03	Polyadenylate-binding protein 2	2.5	1
ADAS_HUMAN	4 (1)	71.89	0.29	Alkyldihydroxyacetonephosphate synthase, peroxisomal 1	1.6	1
CAP1_HUMAN	2 (2)	71.78	5.06E-04	Adenylyl cyclase-associated protein 1	1	2.43
IF2B1_HUMAN	2 (2)	71.64	0.47	Insulin-like growth factor 2 mRNA-binding protein 1	2.81	1
NAA15_HUMAN	3 (1)	71.44	0.93	N-alpha-acetyltransferase 15, NatA auxiliary subunit	6.19	1
PTPM1_HUMAN	2 (1)	71.43	0.47	Phosphatidylglycerophosphatase and protein-tyrosine phosphatase 1	1	1.49
RL32_HUMAN	1 (1)	71.25	0.32	60S ribosomal protein L32	1	1.36
SMD3_HUMAN	3 (2)	70.82	0.13	Small nuclear ribonucleoprotein Sm D3	1	2.62
RUVB2_HUMAN	4 (1)	70.8	0.01	RuvB-like 2	815.82	1
HECD4_HUMAN	16 (3)	70.57	0.36	Probable E3 ubiquitin-protein ligase HECTD4	1.27	1
SYRC_HUMAN	4 (3)	70.48	0.21	Arginine--tRNA ligase, cytoplasmic	1.61	1
CSN4_HUMAN	4 (1)	70.44	0.12	COP9 signalosome complex subunit 4	1	1.68
DPM1_HUMAN	2 (2)	70.4	0.03	Dolichol-phosphate mannosyltransferase subunit 1	1	1.81
CMC2_HUMAN	3 (1)	70.32	0.27	Calcium-binding mitochondrial carrier protein Aralar2	1	2.69
RL18A_HUMAN	5 (3)	70.3	3.70E-03	60S ribosomal protein L18a	3.72	1

BLK_HUMAN	3 (1)	69.85	0.31	Tyrosine-protein kinase Blk	1.44	1
SCRB2_HUMAN	3 (2)	69.79	0.65	Lysosome membrane protein 2	1.1	1
RTN3_HUMAN	4 (1)	69.77	0.25	Reticulon-3	1	1.24
SF01_HUMAN	5 (2)	69.77	0.1	Splicing factor 1	3.85	1
DHX29_HUMAN	4 (1)	69.56	0.99	ATP-dependent RNA helicase DHX29	1	1.51
SAM50_HUMAN	3 (1)	69.37	0.03	Sorting and assembly machinery component 50 homolog	2.37	1
SYNC_HUMAN	2 (1)	69.33	0.1	Asparagine--tRNA ligase, cytoplasmic	1.85	1
RS27L_HUMAN	2 (1)	69.32	0.95	40S ribosomal protein S27-like	1.05	1
THTM_HUMAN	2 (1)	69.31	0.94	3-mercaptopyruvate sulfurtransferase	1.06	1
RTF2_HUMAN	2 (1)	69.18	0.27	Protein RTF2 homolog	18.1	1
PSB5_HUMAN	2 (1)	68.99	0.45	Proteasome subunit beta type-5	1.02	1
AN32A_HUMAN	2 (1)	68.98	0.71	Acidic leucine-rich nuclear phosphoprotein 32 family member A	1.01	1
ECHB_HUMAN	1 (1)	68.79	0.02	Trifunctional enzyme subunit beta, mitochondrial	1	2.47
NETR_HUMAN	6 (2)	68.67	0.37	Neurotrypsin	1.63	1
TPT1L_HUMAN	2 (1)	68.66	0.51	TPT1-like protein	1	1.33
AT1B1_HUMAN	2 (2)	68.56	0.94	Sodium/potassium-transporting ATPase subunit beta-1	1	1.07
SYCM_HUMAN	1 (1)	68.47	1.01E-03	Probable cysteine--tRNA ligase, mitochondrial	1	5.07
E2AK2_HUMAN	2 (1)	68.43	0.09	Interferon-induced, double-stranded RNA-activated protein kinase	2.26	1
TMOD3_HUMAN	2 (1)	68.3	0.14	Tropomodulin-3	2.63	1
OCAD1_HUMAN	2 (1)	68.28	0.1	OCIA domain-containing protein 1	1	4.7
VPS35_HUMAN	3 (1)	68.28	0.44	Vacuolar protein sorting-associated protein 35	1	1.21
NDUA8_HUMAN	2 (2)	68.13	0.06	NADH dehydrogenase [ubiquinone] 1 alpha subcomplex subunit 8	1	3.12
TECR_HUMAN	5 (2)	68.07	0.02	Very-long-chain enoyl-CoA reductase	1.77	1
FLII_HUMAN	5 (2)	67.8	0.93	Protein flightless-1 homolog	1	1.01
RAPH1_HUMAN	3 (1)	67.64	0.96	Ras-associated and pleckstrin homology domains-containing protein 1	1	1.25
CSPG4_HUMAN	6 (1)	66.98	0.02	Chondroitin sulfate proteoglycan 4	1	67.23
TMED7_HUMAN	1 (1)	66.37	0.54	Transmembrane emp24 domain-containing protein 7	1	1.1
CAPS2_HUMAN	5 (2)	66.28	0.32	Calcium-dependent secretion activator 2	1	1.92
MCA3_HUMAN	2 (1)	66.27	0.4	Eukaryotic translation elongation factor 1 epsilon-1	1.34	1
DIC_HUMAN	3 (1)	65.76	0.04	Mitochondrial dicarboxylate carrier	1	1.67
ITPA_HUMAN	1 (1)	65.74	0.93	Inosine triphosphate pyrophosphatase	1.03	1
RAVR1_HUMAN	2 (1)	65.28	0.01	Ribonucleoprotein PTB-binding 1	1	3.94
EXOS6_HUMAN	2 (1)	65.24	0.48	Exosome complex component MTR3	1.13	1
HCFC1_HUMAN	3 (1)	65.17	0.79	Host cell factor 1	1.04	1
NEP1_HUMAN	5 (2)	64.89	0.52	Ribosomal RNA small subunit methyltransferase NEP1	1.56	1
SMD1_HUMAN	3 (1)	64.82	0.39	Small nuclear ribonucleoprotein Sm D1	1	2.32
TPP1_HUMAN	2 (1)	64.77	0.69	Tripeptidyl-peptidase 1	1	1.97
UBP7_HUMAN	3 (1)	64.04	0.26	Ubiquitin carboxyl-terminal hydrolase 7	1.26	1
FAT2_HUMAN	12 (1)	63.89	0.01	Protocadherin Fat 2	1	1.54
RT27_HUMAN	3 (1)	63.68	0.12	28S ribosomal protein S27, mitochondrial	∞	1
NIP7_HUMAN	3 (1)	63.53	0.51	60S ribosome subunit biogenesis protein NIP7 homolog	1.2	1
LRP6_HUMAN	7 (3)	63.42	6.78E-03	Low-density lipoprotein receptor-related protein 6	1.6	1
RBM4_HUMAN	2 (1)	63.08	0.56	RNA-binding protein 4	1	1.48
APT_HUMAN	3 (3)	62.8	0.02	Adenine phosphoribosyltransferase	1	1.48
ZC3H4_HUMAN	7 (3)	62.37	0.72	Zinc finger CCCH domain-containing protein 4	1	1.03
RCC1_HUMAN	2 (2)	62.18	0.04	Regulator of chromosome condensation	8.32	1
PACN3_HUMAN	2 (1)	61.61	0.36	Protein kinase C and casein kinase substrate in neurons protein 3	1.24	1
SRP68_HUMAN	3 (1)	61.54	0.66	Signal recognition particle subunit SRP68	1	1.06
RASK_HUMAN	3 (1)	61.51	0.91	GTPase Kras	1	1.04
NHP2_HUMAN	1 (1)	61.49	0.7	H/ACA ribonucleoprotein complex subunit 2	1.64	1
WNT7A_HUMAN	8 (3)	61.48	0.01	Protein Wnt-7a	2.31	1
NMD3A_HUMAN	8 (3)	60.88	0.54	Glutamate receptor ionotropic, NMDA 3A	1	1.89
TM109_HUMAN	2 (1)	60.69	0.1	Transmembrane protein 109	1	1.43
1A34_HUMAN	3 (1)	60.67	0.14	HLA class I histocompatibility antigen, A-34 alpha chain	10.4	1
ILVBL_HUMAN	4 (1)	60.55	0.75	Acetolactate synthase-like protein	1.29	1
XPO1_HUMAN	6 (3)	59.71	0.8	Exportin-1	1.02	1
EAA1_HUMAN	2 (1)	59.52	0.96	Excitatory amino acid transporter 1	1.46	1
LG3BP_HUMAN	4 (3)	59.41	0.07	Galectin-3-binding protein	2.25	1

SRS10_HUMAN	3 (1)	59.3	0.75	Serine/arginine-rich splicing factor 10	3.37	1
ARP3B_HUMAN	2 (1)	59.05	0.46	Actin-related protein 3B	1.56	1
RS30_HUMAN	1 (1)	58.59	0.08	40S ribosomal protein S30	1.02	1
PLK1_HUMAN	6 (1)	58.29	0.03	Serine/threonine-protein kinase PLK1	2.32	1
RT05_HUMAN	3 (1)	57.98	0.3	28S ribosomal protein S5, mitochondrial	1	1.54
SNP29_HUMAN	2 (1)	57.81	0.01	Synaptosomal-associated protein 29	17.81	1
UTS2_HUMAN	3 (2)	57.79	0.63	Urotensin-2	1.14	1
EFHD2_HUMAN	5 (1)	57.44	0.02	EF-hand domain-containing protein D2	30.26	1
IPYR_HUMAN	1 (1)	57.34	0.45	Inorganic pyrophosphatase	1	1.16
LAMP2_HUMAN	1 (1)	57.31	0.84	Lysosome-associated membrane glycoprotein 2	1	1
PSB7_HUMAN	2 (2)	57.21	0.06	Proteasome subunit beta type-7	1	4.37
PSB6_HUMAN	1 (1)	56.97	0.01	Proteasome subunit beta type-6	1.31	1
Z705G_HUMAN	5 (1)	56.71	0.39	Putative zinc finger protein 705G	1	2.67
SUMF2_HUMAN	1 (1)	56.39	0.11	Sulfatase-modifying factor 2	1	3.28
LAMB1_HUMAN	2 (1)	56.2	0.16	Laminin subunit beta-1	1	2.31
PDZD2_HUMAN	12 (2)	56.17	0.36	PDZ domain-containing protein 2	1	1.56
BGAL_HUMAN	3 (2)	56.03	0.22	Beta-galactosidase	1	1.64
VA0D1_HUMAN	2 (2)	55.72	0.43	V-type proton ATPase subunit d 1	1.08	1
EMC7_HUMAN	1 (1)	55.68	0.27	ER membrane protein complex subunit 7	1.16	1
RT35_HUMAN	2 (1)	55.45	0.65	28S ribosomal protein S35, mitochondrial	1	1.67
LRMP_HUMAN	5 (1)	55.36	0.22	Lymphoid-restricted membrane protein	1.23	1
ATD3C_HUMAN	3 (2)	55.03	0.16	ATPase family AAA domain-containing protein 3C	1	1.97
PCYOX_HUMAN	2 (1)	54.53	0.51	Prenylcysteine oxidase 1	1.2	1
BPHL_HUMAN	2 (1)	54.47	0.25	Valacyclovir hydrolase	3.68	1
PDC10_HUMAN	1 (1)	54.45	0.35	Programmed cell death protein 10	1	1.17
NVL_HUMAN	7 (1)	54.35	0.5	Nuclear valosin-containing protein-like	1.35	1
SRS11_HUMAN	1 (1)	53.77	0.41	Serine/arginine-rich splicing factor 11	1.55	1
EGFR_HUMAN	5 (2)	53.66	0.6	Epidermal growth factor receptor	1	1.2
API5_HUMAN	3 (1)	53.38	0.22	Apoptosis inhibitor 5	1.2	1
PTH2_HUMAN	2 (1)	52.87	0.05	Peptidyl-tRNA hydrolase 2, mitochondrial	1	3.87
TRA2A_HUMAN	3 (1)	52.82	0.99	Transformer-2 protein homolog alpha	1.02	1
NDUS8_HUMAN	2 (2)	52.79	0.06	NADH dehydrogenase [ubiquinone] iron-sulfur protein 8, mitochondrial	1	2.35
ISY1_HUMAN	4 (1)	52.7	0.09	Pre-mRNA-splicing factor ISY1 homolog	1.47	1
NEP_HUMAN	5 (3)	52.67	0.32	Neprilysin	1.53	1
T126A_HUMAN	2 (2)	52.22	0.03	Transmembrane protein 126A	1.68	1
NFS1_HUMAN	3 (2)	52.02	0.66	Cysteine desulfurase, mitochondrial	1.39	1
TTC33_HUMAN	2 (1)	51.81	0.44	Tetratricopeptide repeat protein 33	1.3	1
ANK2_HUMAN	10 (3)	51.49	0.87	Ankyrin-2	1	1.16
RAC1_HUMAN	2 (1)	51.48	0.52	Ras-related C3 botulinum toxin substrate 1	1.3	1
STB5L_HUMAN	6 (2)	51.26	0.46	Syntaxin-binding protein 5-like	1	2.17
ISOC2_HUMAN	1 (1)	51.14	0.03	Isochorismatase domain-containing protein 2	1	3.14
KINH_HUMAN	3 (1)	50.73	0.91	Kinesin-1 heavy chain	1	1.79
RM01_HUMAN	5 (1)	50.7	7.12E-03	39S ribosomal protein L1, mitochondrial	1	1.89
PCCA_HUMAN	5 (2)	50.47	0.93	Propionyl-CoA carboxylase alpha chain, mitochondrial	1.03	1
SRSF9_HUMAN	1 (1)	50.32	0.06	Serine/arginine-rich splicing factor 9	1	2.99
BRX1_HUMAN	2 (1)	50.29	0.05	Ribosome biogenesis protein BRX1 homolog	1	2.6
RFIP4_HUMAN	5 (1)	50.28	7.37E-04	Rab11 family-interacting protein 4	1	12.64
MUC19_HUMAN	5 (1)	49.75	0.24	Mucin-19	1.64	1
AATC_HUMAN	1 (1)	49.72	0.67	Aspartate aminotransferase, cytoplasmic	1.1	1
PRP8_HUMAN	6 (2)	49.71	0.81	Pre-mRNA-processing-splicing factor 8	1	1.03
FAF2_HUMAN	2 (1)	49.67	1.48E-06	FAS-associated factor 2	1	1.62
NAKD2_HUMAN	4 (1)	49.55	0.26	NAD kinase 2, mitochondrial	1	1.42
TMED1_HUMAN	1 (1)	49.5	0.56	Transmembrane emp24 domain-containing protein 1	1	1.19
RS26_HUMAN	3 (1)	49.45	0.89	40S ribosomal protein S26	1.8	1
NTPCR_HUMAN	3 (2)	49.25	0.57	Cancer-related nucleoside-triphosphatase	1.19	1
RM38_HUMAN	1 (1)	49.18	0.09	39S ribosomal protein L38, mitochondrial	1	4.81
DDX6_HUMAN	3 (1)	49.07	0.34	Probable ATP-dependent RNA helicase DDX6	1.07	1
AP3D1_HUMAN	4 (1)	49.03	0.65	AP-3 complex subunit delta-1 1	1.35	1

SGCD_HUMAN	3 (1)	48.92	0.69	Delta-sarcoglycan	1	1.14
PRS6A_HUMAN	2 (1)	48.91	0.81	26S proteasome regulatory subunit 6A	1.07	1
RAE1L_HUMAN	1 (1)	48.46	0.13	mRNA export factor	1.39	1
DDRGK_HUMAN	2 (1)	48.45	0.83	DDRGK domain-containing protein 1	1.03	1
MYL6_HUMAN	3 (1)	48.4	0.12	Myosin light polypeptide 6	1	2.35
RAB9A_HUMAN	2 (1)	48.15	0.04	Ras-related protein Rab-9A	1.96	1
NOP16_HUMAN	1 (1)	48.11	0.77	Nucleolar protein 16	1	1.35
RPP30_HUMAN	2 (1)	47.79	0.19	Ribonuclease P protein subunit p30	1	2.11
DECR2_HUMAN	3 (2)	47.64	4.75E-03	Peroxisomal 2,4-dienoyl-CoA reductase	1	3.42
MUC18_HUMAN	3 (2)	46.99	0.02	Cell surface glycoprotein MUC18	1	3.44
CN166_HUMAN	2 (2)	46.94	0.34	UPF0568 protein C14orf166	1.53	1
CD97_HUMAN	2 (1)	46.78	0.62	CD97 antigen	1	2.74
AHRR_HUMAN	2 (1)	46.77	0.94	Aryl hydrocarbon receptor repressor	1.04	1
PWP2_HUMAN	7 (1)	46.45	0.07	Periodic tryptophan protein 2 homolog	1	4.02
VASP_HUMAN	2 (1)	46.28	0.35	Vasodilator-stimulated phosphoprotein	1	1.29
PRP16_HUMAN	7 (1)	46.1	0.32	Pre-mRNA-splicing factor ATP-dependent RNA helicase PRP16	1	1.72
AP2S1_HUMAN	2 (1)	45.89	0.25	AP-2 complex subunit sigma	1.61	1
DPH5_HUMAN	1 (1)	45.8	0.7	Diphthine methyl ester synthase	1	2.03
ZN500_HUMAN	2 (1)	45.46	0.19	Zinc finger protein 500	1.8	1
RPF2_HUMAN	4 (3)	45.42	0.37	Ribosome production factor 2 homolog	1	1.64
SCO2_HUMAN	2 (1)	45.29	0.9	Protein SCO2 homolog, mitochondrial	1.01	1
EYA2_HUMAN	4 (1)	45.08	2.60E-03	Eyes absent homolog 2	1	2.76
CAVN1_HUMAN	1 (1)	44.98	6.16E-04	Caveolae-associated protein 1	3.48	1
IKIP_HUMAN	4 (1)	44.7	0.27	Inhibitor of nuclear factor kappa-B kinase-interacting protein	4.86	1
ESRP1_HUMAN	5 (1)	44.59	0.69	Epithelial splicing regulatory protein 1	1	1.08
SNF5_HUMAN	3 (2)	44.55	0.09	SWI/SNF-related matrix-associated actin-dependent regulator of chromatin subfamily B member 1	13.99	1
HM20A_HUMAN	3 (2)	44.44	0.06	High mobility group protein 20A	14.57	1
KBP_HUMAN	3 (2)	44.15	0.57	KIF1-binding protein	1	2.55
NAA10_HUMAN	2 (2)	44.11	0.33	N-alpha-acetyltransferase 10	3.49	1
TPP2_HUMAN	5 (2)	43.95	0.2	Tripeptidyl-peptidase 2	1.45	1
DAF_HUMAN	1 (1)	43.94	3.84E-08	Complement decay-accelerating factor	1.34	1
SFXN3_HUMAN	2 (1)	43.82	0.15	Sideroflexin-3	5.23	1
RRP15_HUMAN	2 (2)	43.68	0.53	RRP15-like protein	1.92	1
KCY_HUMAN	2 (1)	43.61	0.98	UMP-CMP kinase	1	1
DENR_HUMAN	3 (1)	42.55	0.94	Density-regulated protein	1.68	1
ZCCHL_HUMAN	3 (3)	42.5	0.9	Zinc finger CCCH-type antiviral protein 1-like	1	1.34
NXF1_HUMAN	2 (1)	42.26	0.37	Nuclear RNA export factor 1	8.45	1
ITAE_HUMAN	3 (1)	41.43	0.96	Integrin alpha-E	1	1.04
PI3R5_HUMAN	3 (3)	41.21	0.21	Phosphoinositide 3-kinase regulatory subunit 5	1	1.42
DDX47_HUMAN	1 (1)	41.15	0.56	Probable ATP-dependent RNA helicase DDX47	1	1.11
SC23B_HUMAN	4 (2)	41.14	0.03	Protein transport protein Sec23B	1	1.19
PSB3_HUMAN	1 (1)	40.94	0.43	Proteasome subunit beta type-3	1.2	1
DNJA1_HUMAN	2 (1)	40.9	0.68	DnaJ homolog subfamily A member 1	1.4	1
PCNP_HUMAN	1 (1)	40.84	0.57	PEST proteolytic signal-containing nuclear protein	1.3	1
KAD1_HUMAN	2 (1)	40.48	0.03	Adenylate kinase isoenzyme 1	1	284.55
RSMN_HUMAN	3 (3)	40.44	0.94	Small nuclear ribonucleoprotein-associated protein N	1.05	1
ZN622_HUMAN	2 (1)	40.32	0.04	Zinc finger protein 622	1.78	1
IMA6_HUMAN	2 (1)	40.23	6.33E-03	Importin subunit alpha-6	3.01	1
CCHL_HUMAN	1 (1)	40.11	0.45	Cytochrome c-type heme lyase	1.37	1
G6PD_HUMAN	4 (2)	40	0.03	Glucose-6-phosphate 1-dehydrogenase	9.97	1
SKP1_HUMAN	1 (1)	39.87	0.37	S-phase kinase-associated protein 1	1	1.55
6PGL_HUMAN	1 (1)	39.3	0.88	6-phosphogluconolactonase	1	1.18
MARE1_HUMAN	2 (2)	38.77	0.61	Microtubule-associated protein RP/EB family member 1	1.48	1
LASP1_HUMAN	1 (1)	38.43	0.41	LIM and SH3 domain protein 1	1.88	1
EXOS8_HUMAN	3 (2)	38.35	0.3	Exosome complex component RRP43	1	1.29
DNJC7_HUMAN	4 (1)	38.18	0.72	DnaJ homolog subfamily C member 7	1.15	1
PSME1_HUMAN	2 (1)	37.86	0.45	Proteasome activator complex subunit 1	1	4.32
GG6L3_HUMAN	3 (2)	37.65	0.03	Putative golgin subfamily A member 6-like protein 3	1	1.82

PGAM5_HUMAN	1 (1)	37.34	0.29	Serine/threonine-protein phosphatase PGAM5, mitochondrial	2.13	1
AASS_HUMAN	4 (1)	37.01	0.81	Alpha-aminoadipic semialdehyde synthase, mitochondrial	1	1.16
STAG2_HUMAN	4 (1)	36.68	0.04	Cohesin subunit SA-2	5.64	1
RISC_HUMAN	1 (1)	36.28	0.14	Retinoid-inducible serine carboxypeptidase	1.58	1
ZN207_HUMAN	1 (1)	36.08	0.07	BUB3-interacting and GLEBS motif-containing protein ZNF207	1.23	1
CPNE3_HUMAN	2 (1)	35.78	0.09	Copine-3	1	4.82
RL31_HUMAN	2 (1)	35.62	0.55	60S ribosomal protein L31	1.16	1
TULP1_HUMAN	2 (1)	35.26	0.67	Tubby-related protein 1	1	1.31
LANC1_HUMAN	1 (1)	35.08	0.95	LanC-like protein 1	1	1.35
MRGBP_HUMAN	2 (2)	34.99	0.87	MRG/MORF4L-binding protein	1.59	1
MTDC_HUMAN	2 (1)	34.81	0.26	Bifunctional methylenetetrahydrofolate dehydrogenase/cyclohydrolase, mitochondrial	1.28	1
ELAV3_HUMAN	1 (1)	34.72	6.56E-03	ELAV-like protein 3	1.11	1
NUDC_HUMAN	2 (1)	34.39	0.1	Nuclear migration protein nudC	1	5.53
FBLN2_HUMAN	2 (2)	33.86	1.64E-04	Fibulin-2	4.65	1
RM45_HUMAN	3 (2)	33.79	0.24	39S ribosomal protein L45, mitochondrial	1.38	1
ATX10_HUMAN	2 (1)	33.56	0.7	Ataxin-10	1.17	1
OSTF1_HUMAN	1 (1)	33.51	0.67	Osteoclast-stimulating factor 1	1.23	1
P3H1_HUMAN	2 (1)	33.09	0.02	Prolyl 3-hydroxylase 1	1	2.62
STXB3_HUMAN	2 (1)	32.57	0.04	Syntaxin-binding protein 3	1	2.41
TET2_HUMAN	3 (1)	31.97	1.86E-03	Methylcytosine dioxygenase TET2	1	14.81
TSR1_HUMAN	3 (1)	31.94	0.16	Pre-rRNA-processing protein TSR1 homolog	2.77	1
LGUL_HUMAN	1 (1)	31.48	0.98	Lactoylglutathione lyase	1	1.01
CO5A2_HUMAN	8 (1)	31.17	0.06	Collagen alpha-2(V) chain	1	5.57
ABCD3_HUMAN	3 (3)	30.88	0.42	ATP-binding cassette sub-family D member 3	2.41	1
RL35A_HUMAN	3 (1)	30.02	0.35	60S ribosomal protein L35a	1	1.28
SPRY7_HUMAN	1 (1)	29.62	0.56	SPRY domain-containing protein 7	1.14	1
PPIC_HUMAN	1 (1)	29.45	0.08	Peptidyl-prolyl cis-trans isomerase C	1	3.29
ZFP91_HUMAN	2 (2)	28.99	0.03	E3 ubiquitin-protein ligase ZFP91	1	4.04
ANXA8_HUMAN	2 (1)	28.52	0.13	Annexin A8	∞	1
GNAL_HUMAN	3 (1)	27.86	0.39	Guanine nucleotide-binding protein G(olf) subunit alpha	1.76	1
RT23_HUMAN	2 (1)	27.69	0.49	28S ribosomal protein S23, mitochondrial	1	1.18
GPC5_HUMAN	3 (1)	27.41	0.66	Glypican-5	1.84	1
NDUB9_HUMAN	1 (1)	27.36	0.48	NADH dehydrogenase [ubiquinone] 1 beta subcomplex subunit 9	1.14	1
GEMI8_HUMAN	1 (1)	27.34	0.36	Gem-associated protein 8	1	1.23
PSMD2_HUMAN	2 (1)	27.31	0.32	26S proteasome non-ATPase regulatory subunit 2	1	3
CFA99_HUMAN	4 (1)	26.58	0.07	Cilia- and flagella-associated protein 99	1	18.79
RL30_HUMAN	1 (1)	26.16	0.5	60S ribosomal protein L30	1.36	1
LST2_HUMAN	2 (2)	25.86	0.18	Lateral signaling target protein 2 homolog	1.04	1
CALU_HUMAN	1 (1)	25.79	6.70E-04	Calumenin	1	1.3
TF3C5_HUMAN	3 (1)	25.68	0.86	General transcription factor 3C polypeptide 5	1.05	1
NUP88_HUMAN	3 (1)	25.43	3.17E-04	Nuclear pore complex protein Nup88	1.38	1
REEP6_HUMAN	1 (1)	24.8	0.7	Receptor expression-enhancing protein 6	3.15	1
ERGI1_HUMAN	1 (1)	24.24	0.14	Endoplasmic reticulum-Golgi intermediate compartment protein 1	1	2.27
CS043_HUMAN	2 (1)	23.48	0.42	Uncharacterized protein C19orf43 =1	1	1.85
COX41_HUMAN	1 (1)	23.19	0.69	Cytochrome c oxidase subunit 4 isoform 1, mitochondrial	1	1.54
VSXL2_HUMAN	2 (1)	21.54	0.95	V-set and immunoglobulin domain-containing protein 10-like 2	1	1.03
MORC3_HUMAN	2 (2)	21.35	0.01	MORC family CW-type zinc finger protein 3	1	2.77
HDGF_HUMAN	1 (1)	20.68	0.36	Hepatoma-derived growth factor	1	1.26
PSB4_HUMAN	1 (1)	20.44	0.42	Proteasome subunit beta type-4	1	1.82
EDC4_HUMAN	7 (2)	20.3	0.63	Enhancer of mRNA-decapping protein 4	1.39	1
HBS1L_HUMAN	1 (1)	20.13	0.89	HBS1-like protein	1	1.08
FST_HUMAN	3 (2)	19.53	0.16	Follistatin	5	1
SRPK2_HUMAN	1 (1)	19.47	0.79	SRSF protein kinase 2	1	1.04
MKLN1_HUMAN	3 (1)	18.02	5.97E-05	Muskelin	1	4.64
SPN1_HUMAN	2 (1)	17.96	3.26E-05	Snurportin-1	1	10.46
GEMI2_HUMAN	2 (1)	17.77	0.13	Gem-associated protein 2	1	2.65
MARC1_HUMAN	2 (1)	16.83	0.19	Mitochondrial amidoxime-reducing component 1	1	2.15
BRNP1_HUMAN	4 (1)	15.86	0.02	BMP/retinoic acid-inducible neural-specific protein 1	19.12	1

MSH3_HUMAN	4 (1)	15.02	0.8	DNA mismatch repair protein Msh3	1	1.47
BAG1_HUMAN	1 (1)	13.73	8.96E-03	BAG family molecular chaperone regulator 1	1.21	1
CAH12_HUMAN	2 (1)	12.5	0.03	Carbonic anhydrase 12	1.42	1
UBE2K_HUMAN	2 (1)	11.8	0.16	Ubiquitin-conjugating enzyme E2 K	1.95	1
KCNT1_HUMAN	2 (1)	6.91	0.37	Potassium channel subfamily T member 1	1	3.41
SIN3B_HUMAN	4 (1)	6.37	0.16	Paired amphipathic helix protein Sin3b	1	2.36
DCXR_HUMAN	3 (1)	6	0.4	L-xylulose reductase	1	1.24
RL23_HUMAN	1 (1)	3.98	0.54	60S ribosomal protein L23	1	1.02
GPR75_HUMAN	1 (1)	1.91	0.07	Probable G-protein coupled receptor 75	1	2.09
KCNK3_HUMAN	1 (1)	0.86	0.12	Potassium channel subfamily K member 3	1	1.35

Table S5. Proteins (632 in total) identified by bottom-up proteomics approach in membrane preparations of ACdEVs from Hela WT (WT) and Hela-ICAM-3 (ICAM-3). Proteins were considered identified if at least one unique peptide was confidently identified by searching against SwissProt data base. Relative quantification was performed using Progenesis QI for proteomics software. Three most intense peptides per protein were used for quantification. Data in the table are normalised to the lower protein content (1.00). Values higher that 1.00 are 'fold increase' compared to the value 1.00. Measurements of three biological replicates allowed for Anova test to be performed on quantified results.

Uniprot ID	Identified peptides (unique)	Score	Protein name	Hela WT	Hela-ICAM-3
ACTG_HUMAN	44 (5)	3651.08	Actin, cytoplasmic 2	1.18	1.00
ACTB_HUMAN	42 (3)	3605.35	Actin, cytoplasmic 1	1.14	1.00
CPSM_HUMAN	61 (47)	3402.6	Carbamoyl-phosphate synthase [ammonia], mitochondrial	1.00	1.06
GRP78_HUMAN	40 (34)	3115.11	78 kDa glucose-regulated protein	1.00	1.05
4F2_HUMAN	34 (22)	3017.28	4F2 cell-surface antigen heavy chain	1.37	1.00
TBB5_HUMAN	31 (3)	2675.21	Tubulin beta chain	1.00	1.2
CLH1_HUMAN	38 (17)	2595.17	Clathrin heavy chain 1	1.00	1.00
FLNA_HUMAN	45 (28)	2494.18	Filamin-A	1.00	1.9
ANXA2_HUMAN	37 (7)	2492.74	Annexin A2	1.38	1.00
TFR1_HUMAN	31 (21)	2443.82	Transferrin receptor protein 1	1.01	1.00
IQGA1_HUMAN	41 (20)	2321.2	Ras GTPase-activating-like protein IQGAP1	1.35	1.00
TBB4B_HUMAN	29 (1)	2258.12	Tubulin beta-4B chain	1.12	1.00
HS90B_HUMAN	34 (11)	2244.07	Heat shock protein HSP 90-beta	1.24	1.00
CH60_HUMAN	30 (19)	2102.17	60 kDa heat shock protein, mitochondrial	1.00	1.24
HSP7C_HUMAN	28 (11)	2043.09	Heat shock cognate 71 kDa protein	1.00	1.03
ENPL_HUMAN	34 (15)	2041.32	Endoplasmin	1.00	1.13
ENOA_HUMAN	27 (14)	1962.27	Alpha-enolase	1.27	1.00
G3P_HUMAN	32 (23)	1919.93	Glyceraldehyde-3-phosphate dehydrogenase	1.04	1.00
TBB2A_HUMAN	26 (1)	1913.12	Tubulin beta-2A chain	1.00	1.24
RLA0_HUMAN	27 (5)	1884.98	60S acidic ribosomal protein P0	1.24	1.00
ANXA5_HUMAN	21 (18)	1811.61	Annexin A5	1.07	1.00
EF2_HUMAN	33 (20)	1762.86	Elongation factor 2	1.08	1.00
AT1A1_HUMAN	25 (8)	1721.93	Sodium/potassium-transporting ATPase subunit alpha-1	1.42	1.00
HS90A_HUMAN	27 (6)	1677.1	Heat shock protein HSP 90-alpha	1.27	1.00
DYHC1_HUMAN	43 (22)	1638.89	Cytoplasmic dynein 1 heavy chain 1	1.2	1.00
SYEP_HUMAN	36 (25)	1616.44	Bifunctional glutamate/proline--tRNA ligase	1.00	1.53
PRKDC_HUMAN	43 (23)	1615.36	DNA-dependent protein kinase catalytic subunit	1.00	1.21
HNRPU_HUMAN	20 (10)	1599.77	Heterogeneous nuclear ribonucleoprotein U	1.00	1.02
NUCL_HUMAN	27 (16)	1591.12	Nucleolin	1.00	1.14
RL6_HUMAN	23 (12)	1576.78	60S ribosomal protein L6	1.14	1.00
RL4_HUMAN	30 (25)	1552.81	60S ribosomal protein L4	1.00	1.55
FAS_HUMAN	24 (19)	1529.22	Fatty acid synthase	1.00	1.99

ILF3_HUMAN	25 (15)	1512.05	Interleukin enhancer-binding factor 3	1.02	1.00
KPYM_HUMAN	23 (13)	1482.45	Pyruvate kinase PKM	1.00	1.18
ACTN4_HUMAN	23 (6)	1452.28	Alpha-actinin-4	1.48	1.00
TCPB_HUMAN	18 (14)	1431.83	T-complex protein 1 subunit beta	1.00	1.00
ATPB_HUMAN	21 (7)	1429.28	ATP synthase subunit beta, mitochondrial	1.00	1.46
TBA1B_HUMAN	17 (3)	1425.35	Tubulin alpha-1B chain	1.00	1.53
PDIA3_HUMAN	18 (10)	1318.45	Protein disulfide-isomerase A3	1.00	1.24
PDIA1_HUMAN	22 (15)	1317.93	Protein disulfide-isomerase	1.00	1.11
RS3_HUMAN	20 (16)	1316.25	40S ribosomal protein S3	1.03	1.00
SYIC_HUMAN	30 (25)	1284.59	Isoleucine--tRNA ligase, cytoplasmic	1.02	1.00
TCPE_HUMAN	23 (10)	1284.31	T-complex protein 1 subunit epsilon	1.29	1.00
RL5_HUMAN	26 (18)	1265.29	60S ribosomal protein L5	1.00	1.06
TCPQ_HUMAN	20 (13)	1251.52	T-complex protein 1 subunit theta	1.00	1.46
RL7_HUMAN	23 (12)	1248.05	60S ribosomal protein L7	1.09	1.00
RLA0L_HUMAN	17 (1)	1233.53	60S acidic ribosomal protein P0-like	1.02	1.00
RSSA_HUMAN	16 (11)	1233.41	40S ribosomal protein SA	1.2	1.00
ACTBL_HUMAN	22 (2)	1215.85	Beta-actin-like protein 2	1.00	1.39
HNRPC_HUMAN	20 (5)	1201.77	Heterogeneous nuclear ribonucleoproteins C1/C2	1.15	1.00
SPTN1_HUMAN	30 (14)	1200.88	Spectrin alpha chain, non-erythrocytic 1	1.00	1.02
TCPH_HUMAN	20 (13)	1171.81	T-complex protein 1 subunit eta	1.00	1.05
FLNB_HUMAN	26 (13)	1165.48	Filamin-B	1.32	1.00
CALX_HUMAN	16 (11)	1152.25	Calnexin	1.03	1.00
RS4X_HUMAN	17 (10)	1149.99	40S ribosomal protein S4, X isoform	1.01	1.00
SPTB2_HUMAN	30 (15)	1123.1	Spectrin beta chain, non-erythrocytic 1	1.32	1.00
BASP1_HUMAN	15 (10)	1121.22	Brain acid soluble protein 1	1.2	1.00
RL3_HUMAN	21 (15)	1115.05	60S ribosomal protein L3	1.00	1.41
GRP75_HUMAN	18 (10)	1109.59	Stress-70 protein, mitochondrial	1.00	1.24
ANXA1_HUMAN	16 (13)	1108.4	Annexin A1	1.17	1.00
GANAB_HUMAN	20 (12)	1105.63	Neutral alpha-glucosidase AB	1.00	1.12
MYH9_HUMAN	30 (13)	1092.1	Myosin-9	1.00	1.12
TCPA_HUMAN	20 (11)	1089.56	T-complex protein 1 subunit alpha	1.06	1.00
MYO1C_HUMAN	22 (11)	1086.64	Unconventional myosin-Ic	1.21	1.00
TBA4A_HUMAN	15 (1)	1044.3	Tubulin alpha-4A chain	1.29	1.00
TERA_HUMAN	17 (12)	1034.88	Transitional endoplasmic reticulum ATPase	1.07	1.00
SERA_HUMAN	18 (9)	1020.95	D-3-phosphoglycerate dehydrogenase	1.14	1.00
ILF2_HUMAN	12 (10)	1002.71	Interleukin enhancer-binding factor 2	1.01	1.00
RL7A_HUMAN	14 (7)	987.66	60S ribosomal protein L7a OS=Homo sapiens	1.00	1.04
EF1A1_HUMAN	19 (11)	985.1	Elongation factor 1-alpha 1 OS=Homo sapiens	4.56	1.00
HS71A_HUMAN	16 (4)	957.19	Heat shock 70 kDa protein 1A	2.02	1.00
RS6_HUMAN	11 (6)	955.63	40S ribosomal protein S6	1.07	1.00
DDX21_HUMAN	21 (12)	952.81	Nucleolar RNA helicase 2	1.16	1.00
RACK1_HUMAN	13 (13)	928.2	Receptor of activated protein C kinase 1	1.04	1.00
SYTC_HUMAN	16 (7)	919.51	Threonine--tRNA ligase, cytoplasmic	1.15	1.00
TCPG_HUMAN	22 (15)	913.96	T-complex protein 1 subunit gamma	1.18	1.00
LAT1_HUMAN	13 (10)	901.88	Large neutral amino acids transporter small subunit 1	1.00	1.22
PDIA6_HUMAN	12 (8)	898.19	Protein disulfide-isomerase A6	1.00	1.16
RL12_HUMAN	9 (7)	895.75	60S ribosomal protein L12	1.00	1.07

CALR_HUMAN	12 (8)	889.1	Calreticulin	1.00	1.17
MOES_HUMAN	17 (5)	875.21	Moesin	1.13	1.00
PGK1_HUMAN	15 (9)	868.3	Phosphoglycerate kinase 1	1.27	1.00
TCPZ_HUMAN	18 (10)	867.45	T-complex protein 1 subunit zeta	1.00	1.00
RS3A_HUMAN	16 (12)	860.5	40S ribosomal protein S3a	1.00	1.19
NPM_HUMAN	9 (7)	849.66	Nucleophosmin OS=Homo sapiens	1.46	1.00
NAT10_HUMAN	14 (9)	840.65	RNA cytidine acetyltransferase	1.24	1.00
HYOU1_HUMAN	16 (8)	831.74	Hypoxia up-regulated protein 1	1.00	1.65
RL13_HUMAN	10 (8)	824.18	60S ribosomal protein L13	1.11	1.00
MYOF_HUMAN	20 (12)	823.58	Myoferlin	1.02	1.00
H2B1D_HUMAN	8 (4)	812.01	Histone H2B type 1-D	1.62	1.00
H14_HUMAN	13 (2)	800.32	Histone H1.4	1.00	1.12
LDHB_HUMAN	13 (9)	777.67	L-lactate dehydrogenase B chain	1.11	1.00
H12_HUMAN	12 (1)	776.57	Histone H1.2	1.00	1.12
RS15_HUMAN	10 (9)	776.55	40S ribosomal protein S15	1.00	1.07
SYLC_HUMAN	16 (11)	770.74	Leucine--tRNA ligase, cytoplasmic	1.16	1.00
RS7_HUMAN	11 (8)	759.27	40S ribosomal protein S7	1.00	1.05
LG3BP_HUMAN	9 (6)	756.95	Galectin-3-binding protein	1.00	1.02
ATPA_HUMAN	16 (10)	749.65	ATP synthase subunit alpha, mitochondrial	1.00	1.65
SYMC_HUMAN	14 (11)	738.54	Methionine--tRNA ligase, cytoplasmic	1.06	1.00
DHX9_HUMAN	14 (7)	735.02	ATP-dependent RNA helicase A	1.09	1.00
ACTN1_HUMAN	13 (2)	724.01	Alpha-actinin-1	1.28	1.00
RL1D1_HUMAN	11 (6)	714.58	Ribosomal L1 domain-containing protein 1	1.12	1.00
TKT_HUMAN	11 (9)	712.04	Transketolase	1.35	1.00
TCPD_HUMAN	9 (5)	700.66	T-complex protein 1 subunit delta	1.00	1.03
MDHM_HUMAN	9 (7)	699.28	Malate dehydrogenase, mitochondrial	1.00	1.12
TLN1_HUMAN	19 (9)	694.34	Talin-1	1.00	2.48
LDHA_HUMAN	9 (5)	690.77	L-lactate dehydrogenase A chain	1.3	1.00
ANXA6_HUMAN	14 (7)	686.32	Annexin A6	1.00	1.08
AAAT_HUMAN	8 (5)	684.3	Neutral amino acid transporter B(0)	1.00	1.12
BASI_HUMAN	9 (7)	676.27	Basigin	1.09	1.00
GCN1_HUMAN	17 (14)	670.06	eIF-2-alpha kinase activator GCN1	1.00	1.08
PPIB_HUMAN	11 (6)	666.66	Peptidyl-prolyl cis-trans isomerase B	1.00	1.14
RS8_HUMAN	11 (7)	661.19	40S ribosomal protein S8	1.06	1.00
SYAC_HUMAN	17 (12)	657.14	Alanine--tRNA ligase, cytoplasmic	1.07	1.00
RL10_HUMAN	12 (11)	646.22	60S ribosomal protein L10	1.03	1.00
AT2B1_HUMAN	14 (2)	645.49	Plasma membrane calcium-transporting ATPase 1	1.00	1.2
L1CAM_HUMAN	11 (7)	637.81	Neural cell adhesion molecule L1 OS	1.39	1.00
RL18_HUMAN	6 (1)	633.19	60S ribosomal protein L18	1.00	1.05
U5S1_HUMAN	13 (5)	632.38	116 kDa U5 small nuclear ribonucleoprotein component	1.00	1.13
GNAS1_HUMAN	11 (8)	630.45	Guanine nucleotide-binding protein G(s) subunit alpha isoforms Xlas	1.00	1.05
HS71L_HUMAN	16 (1)	628.73	Heat shock 70 kDa protein 1-like	1.62	1.00
A2MG_HUMAN	14 (3)	621.21	Alpha-2-macroglobulin	1.00	1.72
EZRI_HUMAN	17 (9)	610.07	Ezrin	1.00	1.36
H13_HUMAN	10 (2)	600.28	Histone H1.3	1.00	1.12
FRIH_HUMAN	10 (8)	599.41	Ferritin heavy chain	1.12	1.00
1433Z_HUMAN	8 (5)	593.53	14-3-3 protein zeta/delta	1.08	1.00

YBOX1_HUMAN	9 (6)	585.24	Nuclease-sensitive element-binding protein 1	1.00	2.94
RL23A_HUMAN	10 (6)	580.06	60S ribosomal protein L23a	1.00	1.15
ACLY_HUMAN	13 (6)	572.32	ATP-citrate synthase	1.04	1.00
PRDX1_HUMAN	10 (4)	564.66	Peroxiredoxin-1	1.00	1.05
ASSY_HUMAN	13 (8)	561.77	Argininosuccinate synthase	1.44	1.00
RS9_HUMAN	11 (9)	561.56	40S ribosomal protein S9	1.11	1.00
IF4A1_HUMAN	12 (5)	538.07	Eukaryotic initiation factor 4A-I	1.00	1.05
PLEC_HUMAN	30 (10)	537.94	Plectin	1.03	1.00
RL10A_HUMAN	11 (8)	536.44	60S ribosomal protein L10a	1.15	1.00
ITAV_HUMAN	13 (8)	521.46	Integrin alpha-V	1.00	1.00
SERPH_HUMAN	11 (7)	520.75	Serpin H1	1.00	1.1
IMB1_HUMAN	11 (7)	516.26	Importin subunit beta-1	1.36	1.00
PDCD6_HUMAN	8 (7)	512.18	Programmed cell death protein 6	1.00	1.00
RL9_HUMAN	6 (5)	508.96	60S ribosomal protein L9	1.00	1.11
RLA1_HUMAN	4 (1)	505.36	60S acidic ribosomal protein P1	1.07	1.00
C1TC_HUMAN	12 (6)	503.21	C-1-tetrahydrofolate synthase, cytoplasmic	1.00	1.1
RL14_HUMAN	9 (5)	502.34	60S ribosomal protein L14	1.04	1.00
RLA2_HUMAN	4 (2)	501.02	60S acidic ribosomal protein P2	1.32	1.00
AT1B3_HUMAN	8 (7)	496.03	Sodium/potassium-transporting ATPase subunit beta-3	1.17	1.00
RL13A_HUMAN	11 (10)	495.86	60S ribosomal protein L13a	1.00	1.01
ACTBM_HUMAN	6 (1)	490.12	Putative beta-actin-like protein 3	1.00	8.15
HNRPM_HUMAN	15 (8)	484.95	Heterogeneous nuclear ribonucleoprotein M	1.1	1.00
PSMD2_HUMAN	7 (4)	479.81	26S proteasome non-ATPase regulatory subunit 2	1.49	1.00
H15_HUMAN	8 (7)	479.47	Histone H1.5	1.06	1.00
NACAM_HUMAN	12 (8)	477.17	Nascent polypeptide-associated complex subunit alpha, muscle-specific form	1.23	1.00
RS17_HUMAN	7 (6)	477.06	40S ribosomal protein S17	1.00	1.42
MOT4_HUMAN	8 (7)	474.22	Monocarboxylate transporter 4	1.04	1.00
RL26_HUMAN	9 (7)	467.87	60S ribosomal protein L26	1.03	1.00
RL15_HUMAN	7 (5)	466.57	60S ribosomal protein L15	1.12	1.00
PDC6I_HUMAN	6 (1)	463.91	Programmed cell death 6-interacting protein	1.00	1.26
RL24_HUMAN	6 (5)	459.34	60S ribosomal protein L24	1.00	1.02
TPP2_HUMAN	9 (7)	458.84	Tripeptidyl-peptidase 2	1.00	1.14
G6PI_HUMAN	6 (5)	453.39	Glucose-6-phosphate isomerase	1.16	1.00
RS5_HUMAN	7 (4)	453.17	40S ribosomal protein S5	1.00	1.00
EF1G_HUMAN	10 (8)	444.75	Elongation factor 1-gamma	3.07	1.00
TAGL2_HUMAN	7 (5)	444.28	Transgelin-2	1.00	1.09
MARCS_HUMAN	6 (4)	442.13	Myristoylated alanine-rich C-kinase substrate	1.7	1.00
EBP2_HUMAN	10 (5)	441.59	Probable rRNA-processing protein EBP2	1.24	1.00
GDIB_HUMAN	7 (3)	438.61	Rab GDP dissociation inhibitor beta	1.00	1.01
RL17_HUMAN	11 (8)	433.88	60S ribosomal protein L17	1.12	1.00
PYR1_HUMAN	24 (7)	427.47	CAD protein	1.00	3.55
TPIS_HUMAN	6 (4)	421.91	Triosephosphate isomerase	1.47	1.00
PRP8_HUMAN	11 (9)	421.87	Pre-mRNA-processing-splicing factor 8	1.03	1.00
RS2_HUMAN	7 (6)	418.8	40S ribosomal protein S2	1.04	1.00
UBA1_HUMAN	11 (5)	416.87	Ubiquitin-like modifier-activating enzyme 1	1.23	1.00
SYDC_HUMAN	6 (6)	413.97	Aspartate--tRNA ligase, cytoplasmic	1.00	1.01
ALDOA_HUMAN	9 (5)	412.67	Fructose-bisphosphate aldolase A	1.00	1.02

EF1D_HUMAN	6 (5)	407.41	Elongation factor 1-delta	1.09	1.00
U520_HUMAN	8 (6)	406.57	U5 small nuclear ribonucleoprotein 200 kDa helicase	1.00	1.00
S38A2_HUMAN	6 (4)	395.34	Sodium-coupled neutral amino acid transporter 2	1.00	1.07
NOP58_HUMAN	6 (4)	394.51	Nucleolar protein 58	1.00	1.37
RAB1B_HUMAN	6 (2)	394.36	Ras-related protein Rab-1B	1.03	1.00
1433E_HUMAN	7 (4)	393.35	14-3-3 protein epsilon	1.13	1.00
AT2B4_HUMAN	12 (1)	393.18	Plasma membrane calcium-transporting ATPase 4	1.00	2.81
HNRPF_HUMAN	8 (3)	391.69	Heterogeneous nuclear ribonucleoprotein F	11.1	1.00
ITB1_HUMAN	8 (5)	386.22	Integrin beta-1	1.00	1.00
RS27A_HUMAN	6 (4)	385.13	Ubiquitin-40S ribosomal protein S27a	1.05	1.00
RL8_HUMAN	7 (6)	382.96	60S ribosomal protein L8	1.08	1.00
AT2B2_HUMAN	11 (1)	382.73	Plasma membrane calcium-transporting ATPase 2	1.00	1.24
ADT2_HUMAN	13 (1)	378.7	ADP/ATP translocase 2	1.00	1.24
RL21_HUMAN	8 (7)	377.72	60S ribosomal protein L21	1.00	1.05
GLU2B_HUMAN	5 (3)	373.81	Glucosidase 2 subunit beta	1.00	1.06
RS13_HUMAN	8 (5)	372.86	40S ribosomal protein S13	1.00	1.21
VIME_HUMAN	8 (8)	371.27	Vimentin	1.07	1.00
TBB1_HUMAN	9 (1)	367.59	Tubulin beta-1 chain	1.37	1.00
LAMP1_HUMAN	5 (2)	364.43	Lysosome-associated membrane glycoprotein 1	1.04	1.00
RS10_HUMAN	8 (8)	364.18	40S ribosomal protein S10	1.00	1.03
SAHH_HUMAN	6 (6)	363.18	Adenosylhomocysteinase	1.06	1.00
VDAC1_HUMAN	6 (4)	362.41	Voltage-dependent anion-selective channel protein 1	1.01	1.00
RAB7A_HUMAN	5 (4)	360.53	Ras-related protein Rab-7a	1.05	1.00
MUC18_HUMAN	9 (5)	351.24	Cell surface glycoprotein MUC18	1.1	1.00
COF1_HUMAN	5 (2)	348.27	Cofilin-1	1.00	1.19
PHB2_HUMAN	6 (5)	346.49	Prohibitin-2	1.14	1.00
MOT1_HUMAN	7 (6)	346.35	Monocarboxylate transporter 1	1.63	1.00
AHNK_HUMAN	50 (8)	345.13	Neuroblast differentiation-associated protein AHNAK	2.02	1.00
VDAC2_HUMAN	5 (3)	345.07	Voltage-dependent anion-selective channel protein 2	1.00	1.3
ADT3_HUMAN	9 (1)	344.84	ADP/ATP translocase 3	1.00	1.32
LPPRC_HUMAN	11 (6)	344.65	Leucine-rich PPR motif-containing protein, mitochondrial	1.07	1.00
CPNE1_HUMAN	4 (4)	344.53	Copine-1	1.11	1.00
FBRL_HUMAN	9 (6)	341.55	rRNA 2'-O-methyltransferase fibrillarin	1.01	1.00
RL19_HUMAN	5 (4)	341.37	60S ribosomal protein L19	1.14	1.00
PRDX6_HUMAN	5 (2)	335.09	Peroxiredoxin-6	1.31	1.00
PDIA4_HUMAN	7 (4)	335.07	Protein disulfide-isomerase A4	1.00	2.12
BRX1_HUMAN	7 (5)	333.59	Ribosome biogenesis protein BRX1 homolog	1.27	1.00
RS18_HUMAN	8 (3)	332.73	40S ribosomal protein S18	1.00	1.02
2AAA_HUMAN	6 (3)	320.29	Serine/threonine-protein phosphatase 2A 65 kDa regulatory subunit A alpha isoform	1.07	1.00
AT2B3_HUMAN	11 (1)	318.82	Plasma membrane calcium-transporting ATPase 3	1.00	1.47
SYYC_HUMAN	7 (3)	318.09	Tyrosine--tRNA ligase, cytoplasmic	1.47	1.00
GARS_HUMAN	9 (4)	316.46	Glycine--tRNA ligase	2.15	1.00
RL11_HUMAN	4 (3)	314.16	60S ribosomal protein L11	1.00	1.03
NIBAN_HUMAN	6 (5)	312.7	Protein Niban	1.56	1.00
AIMP1_HUMAN	5 (4)	310	Aminoacyl tRNA synthase complex-interacting multifunctional protein 1	1.05	1.00
ENOG_HUMAN	6 (1)	305.87	Gamma-enolase	1.00	1.45
IPO5_HUMAN	8 (4)	305.77	Importin-5	1.23	1.00

H11_HUMAN	9 (2)	301.48	Histone H1.1	1.08	1.00
1433T_HUMAN	4 (2)	294.64	14-3-3 protein theta	1.12	1.00
CPNE3_HUMAN	7 (4)	292.37	Copine-3	1.12	1.00
GNAI3_HUMAN	5 (3)	288.6	Guanine nucleotide-binding protein G(k) subunit alpha	1.29	1.00
RAB1A_HUMAN	5 (1)	287.43	Ras-related protein Rab-1A	1.03	1.00
HPPD_HUMAN	7 (5)	284.91	4-hydroxyphenylpyruvate dioxygenase	1.1	1.00
RUVB2_HUMAN	6 (4)	283.42	RuvB-like 2	1.21	1.00
PLSL_HUMAN	6 (3)	277.94	Plastin-2	1.00	1.61
SF3B1_HUMAN	14 (7)	277.78	Splicing factor 3B subunit	1.00	2.53
RL27A_HUMAN	4 (3)	276.23	60S ribosomal protein L27a	1.00	1.25
HP1B3_HUMAN	11 (5)	275.81	Heterochromatin protein 1-binding protein 3	1.18	1.00
EIF3A_HUMAN	10 (2)	274.49	Eukaryotic translation initiation factor 3 subunit A	1.55	1.00
RALY_HUMAN	7 (4)	272.37	RNA-binding protein Raly	1.00	1.08
ALBU_HUMAN	9 (5)	269.26	Serum albumin	1.00	1.03
RL29_HUMAN	7 (2)	267.48	60S ribosomal protein L29	1.00	1.00
MBB1A_HUMAN	10 (7)	267.07	Myb-binding protein 1A	1.00	1.21
CKAP4_HUMAN	6 (2)	266.26	Cytoskeleton-associated protein 4	1.00	1.43
HSPB1_HUMAN	4 (4)	264.5	Heat shock protein beta-1	1.1	1.00
ANXA4_HUMAN	6 (3)	264.45	Annexin A4	1.08	1.00
SF3B3_HUMAN	9 (4)	264.11	Splicing factor 3B subunit 3	1.00	1.15
PRDX2_HUMAN	5 (4)	264.04	Peroxiredoxin-2	1.00	1.02
RAB2A_HUMAN	3 (3)	263.42	Ras-related protein Rab-2A	1.13	1.00
SYWC_HUMAN	3 (3)	260.52	Tryptophan--tRNA ligase, cytoplasmic	1.94	1.00
COR1A_HUMAN	6 (3)	260.4	Coronin-1A	1.00	2.02
HNRPQ_HUMAN	7 (3)	255.99	Heterogeneous nuclear ribonucleoprotein Q	1.00	2.61
NSUN2_HUMAN	13 (4)	255.62	tRNA (cytosine(34)-C(5))-methyltransferase	1.00	1.04
SYRC_HUMAN	5 (4)	254.94	Arginine--tRNA ligase, cytoplasmic	1.00	1.06
RS24_HUMAN	4 (3)	254.83	40S ribosomal protein S24	1.00	1.29
NDKA_HUMAN	5 (1)	251.55	Nucleoside diphosphate kinase A	1.39	1.00
DKC1_HUMAN	10 (4)	250.65	H/ACA ribonucleoprotein complex subunit 4	1.28	1.00
GNAI2_HUMAN	3 (2)	243.86	Guanine nucleotide-binding protein G(i) subunit alpha-2	1.00	1.19
ARF1_HUMAN	4 (1)	243.48	ADP-ribosylation factor 1	1.17	1.00
MATR3_HUMAN	5 (1)	241.45	Matrin-3	1.61	1.00
PUR6_HUMAN	3 (3)	241.06	Multifunctional protein ADE2	1.12	1.00
PLST_HUMAN	5 (1)	240.2	Plastin-3	1.63	1.00
CLIC1_HUMAN	5 (3)	236.65	Chloride intracellular channel protein 1	1.00	1.19
NP1L1_HUMAN	4 (3)	236.49	Nucleosome assembly protein 1-like 1	1.54	1.00
YBOX3_HUMAN	6 (1)	235.82	Y-box-binding protein 3	1.00	3.95
RUVB1_HUMAN	6 (4)	231.77	RuvB-like 1	1.00	1.04
LONM_HUMAN	9 (6)	231.2	Lon protease homolog, mitochondrial	1.00	2.03
GTR1_HUMAN	4 (2)	230.12	Solute carrier family 2, facilitated glucose transporter member 1	1.00	1.31
PUR2_HUMAN	5 (2)	230	Trifunctional purine biosynthetic protein adenosine-3	1.31	1.00
PRS56_HUMAN	5 (3)	228.68	Serine protease 56	1.00	1.37
EFTU_HUMAN	6 (2)	227.12	Elongation factor Tu, mitochondrial	1.12	1.00
GNAQ_HUMAN	5 (2)	223.34	Guanine nucleotide-binding protein G(q) subunit alpha	1.00	1.11
COPA_HUMAN	11 (5)	220.28	Coatomer subunit alpha	1.47	1.00
H2A1B_HUMAN	2 (2)	218.71	Histone H2A type 1-B/E	1.62	1.00

PA2G4_HUMAN	6 (4)	218.03	Proliferation-associated protein 2G4	10.75	1.00
PGM1_HUMAN	6 (4)	215.47	Phosphoglucomutase-1	1.00	3.03
PSA1_HUMAN	5 (5)	215.15	Proteasome subunit alpha type-1	1.08	1.00
THOC2_HUMAN	4 (2)	213.79	THO complex subunit 2	1.00	1.00
RAP2B_HUMAN	3 (1)	212.67	Ras-related protein Rap-2b	1.00	1.07
HS904_HUMAN	5 (2)	208.93	Putative heat shock protein HSP 90-alpha A4	1.00	1.15
H4_HUMAN	6 (3)	208.86	Histone H4	1.07	1.00
FLNC_HUMAN	5 (1)	208.43	Filamin-C	1.00	2.26
VTNC_HUMAN	3 (1)	208	Vitronectin	1.39	1.00
SYVC_HUMAN	9 (3)	207.76	Valine--tRNA ligase	1.00	1.05
RAB10_HUMAN	4 (1)	206.33	Ras-related protein Rab-10	1.00	1.04
GTR14_HUMAN	5 (2)	206.16	Solute carrier family 2, facilitated glucose transporter member 14	1.00	1.4
ABCG2_HUMAN	3 (3)	205.44	ATP-binding cassette sub-family G member 2	1.00	1.68
PRS6A_HUMAN	6 (3)	205.04	26S proteasome regulatory subunit 6A	1.00	1.39
MYO1E_HUMAN	6 (3)	203.85	Unconventional myosin-Ie	1.00	1.04
ERP29_HUMAN	4 (4)	202.17	Endoplasmic reticulum resident protein 29	1.00	1.07
PLSI_HUMAN	9 (2)	201.8	Plastin-1	1.00	3.09
PHB_HUMAN	5 (4)	201.66	Prohibitin	1.08	1.00
CAP1_HUMAN	2 (1)	199.97	Adenylyl cyclase-associated protein 1	2.11	1.00
IDHC_HUMAN	5 (4)	198.88	Isocitrate dehydrogenase [NADP] cytoplasmic	1.3	1.00
PRS6B_HUMAN	6 (3)	193.91	26S proteasome regulatory subunit 6B	2.13	1.00
RAP2C_HUMAN	3 (1)	188.94	Ras-related protein Rap-2c1	1.02	1.00
HNRL2_HUMAN	4 (2)	188.78	Heterogeneous nuclear ribonucleoprotein U-like protein 2	1.03	1.00
CD109_HUMAN	4 (3)	188.37	CD109 antigen	1.08	1.00
GBB2_HUMAN	7 (3)	188.1	Guanine nucleotide-binding protein G(I)/G(S)/G(T) subunit beta-2	1.00	1.05
PRS4_HUMAN	6 (1)	186.91	26S proteasome regulatory subunit 4	1.00	1.22
CAZA1_HUMAN	3 (3)	186.66	F-actin-capping protein subunit alpha-1	1.31	1.00
HNRPR_HUMAN	5 (2)	184.73	Heterogeneous nuclear ribonucleoprotein R	1.31	1.00
EIF3F_HUMAN	1 (1)	184.04	Eukaryotic translation initiation factor 3 subunit F	8	1.00
RL27_HUMAN	3 (3)	183.28	60S ribosomal protein L27	1.04	1.00
RAB5C_HUMAN	3 (2)	181.43	Ras-related protein Rab-5C	1.03	1.00
PSA6_HUMAN	2 (1)	180.52	Proteasome subunit alpha type-6	1.39	1.00
DYH9_HUMAN	24 (7)	179.58	Dynein heavy chain 9, axonemal	1.36	1.00
AP2B1_HUMAN	7 (1)	179.2	AP-2 complex subunit beta	1.00	1.09
NOP56_HUMAN	8 (3)	178.1	Nucleolar protein 56	1.00	1.1
VAT1_HUMAN	5 (3)	178.06	Synaptic vesicle membrane protein VAT-1 homolog	1.26	1.00
RS16_HUMAN	5 (1)	177.48	40S ribosomal protein S16	1.58	1.00
RRS1_HUMAN	5 (2)	173.9	Ribosome biogenesis regulatory protein homolog	1.22	1.00
PODXL_HUMAN	2 (1)	172.69	Podocalyxin	1.94	1.00
ANXA7_HUMAN	5 (4)	171.4	Annexin A7	1.00	1.75
SQSTM_HUMAN	4 (2)	171.36	Sequestosome-1	1.23	1.00
NCPR_HUMAN	6 (3)	171.34	NADPH--cytochrome P450 reductase	1.00	1.08
H2AY_HUMAN	5 (1)	169.07	Core histone macro-H2A.1	1.82	1.00
VINC_HUMAN	18 (1)	168.82	Vinculin	1.00	1.48
HCD2_HUMAN	3 (2)	168.42	3-hydroxyacyl-CoA dehydrogenase type-2	1.00	1.03
AT1B1_HUMAN	5 (4)	167.75	Sodium/potassium-transporting ATPase subunit beta-1	1.09	1.00
HSP74_HUMAN	9 (2)	166.84	Heat shock 70 kDa protein 4	1.00	2.76

SSRA_HUMAN	3 (2)	166.23	Translocon-associated protein subunit alpha	1.03	1.00
AP1B1_HUMAN	5 (1)	165.66	AP-1 complex subunit beta-1	1.21	1.00
STX4_HUMAN	3 (2)	165	Syntaxin-4	1.27	1.00
RAP1A_HUMAN	2 (2)	160.41	Ras-related protein Rap-1A	1.11	1.00
GLYM_HUMAN	5 (2)	159.12	Serine hydroxymethyltransferase, mitochondrial	1.00	1.19
RAB8A_HUMAN	3 (1)	158.96	Ras-related protein Rab-8A	1.00	1.02
PSA5_HUMAN	2 (1)	158.93	Proteasome subunit alpha type-5	1.17	1.00
PRDX4_HUMAN	3 (2)	158.46	Peroxiredoxin-4	1.06	1.00
SSRD_HUMAN	3 (3)	157.66	Translocon-associated protein subunit delta	1.01	1.00
HBA_HUMAN	4 (1)	155.71	Hemoglobin subunit alpha	1.00	2.37
RL18A_HUMAN	5 (4)	155.42	60S ribosomal protein L18a	1.08	1.00
BRCA2_HUMAN	18 (4)	154.83	Breast cancer type 2 susceptibility protein	1.00	1.69
DHX15_HUMAN	3 (1)	154.69	Pre-mRNA-splicing factor ATP-dependent RNA helicase DHX15	1.95	1.00
RHOA_HUMAN	3 (3)	154.47	Transforming protein RhoA	1.02	1.00
ICAM1_HUMAN	5 (4)	154.41	Intercellular adhesion molecule 1	1.27	1.00
NDK8_HUMAN	5 (1)	153.86	Putative nucleoside diphosphate kinase	1.00	1.62
ASNS_HUMAN	4 (3)	153.12	Asparagine synthetase [glutamine-hydrolyzing]	1.07	1.00
AATM_HUMAN	3 (1)	152.27	Aspartate aminotransferase, mitochondrial	1.00	1.3
FRIL_HUMAN	2 (2)	148.46	Ferritin light chain	1.3	1.00
THOC6_HUMAN	3 (2)	148	THO complex subunit 6 homolog	1.09	1.00
PGK2_HUMAN	6 (1)	147.96	Phosphoglycerate kinase 2	1.00	1.28
H2AW_HUMAN	5 (1)	147.48	Core histone macro-H2A.2	1.00	1.09
PSDE_HUMAN	2 (1)	147.08	26S proteasome non-ATPase regulatory subunit 14	1.3	1.00
RS25_HUMAN	3 (2)	146.69	40S ribosomal protein S25	1.01	1.00
RRBP1_HUMAN	8 (4)	146.61	Ribosome-binding protein 1	1.00	1.33
CISY_HUMAN	3 (2)	145.48	Citrate synthase, mitochondrial	1.15	1.00
RRP12_HUMAN	6 (3)	145.2	RRP12-like protein	1.00	1.28
CGL_HUMAN	2 (2)	145.05	Cystathionine gamma-lyase	1.14	1.00
RS11_HUMAN	5 (4)	144.38	40S ribosomal protein S11	1.00	1.11
PGAM1_HUMAN	3 (2)	144.23	Phosphoglycerate mutase 1	1.02	1.00
FSCN1_HUMAN	3 (2)	144.12	Fascin	1.03	1.00
HNRPK_HUMAN	4 (1)	142.95	Heterogeneous nuclear ribonucleoprotein K	2.08	1.00
HNRL1_HUMAN	4 (2)	142.73	Heterogeneous nuclear ribonucleoprotein U-like protein 1	1.2	1.00
RAN_HUMAN	4 (2)	141.12	GTP-binding nuclear protein Ran	1.14	1.00
IPYR_HUMAN	3 (2)	139.58	Inorganic pyrophosphatase	1.11	1.00
SRSF3_HUMAN	4 (2)	139.53	Serine/arginine-rich splicing factor 3	1.16	1.00
SERC_HUMAN	4 (1)	138.74	Phosphoserine aminotransferase	1.42	1.00
ZNT1_HUMAN	5 (2)	137.7	Zinc transporter 1	1.52	1.00
SYQ_HUMAN	7 (3)	137.15	Glutamine--tRNA ligase	1.17	1.00
RASN_HUMAN	2 (2)	136.84	GTPase Nras	1.04	1.00
PSA7_HUMAN	4 (4)	136.5	Proteasome subunit alpha type-7	1.15	1.00
MYH11_HUMAN	5 (1)	136.48	Myosin-11	1.00	2.35
S43A3_HUMAN	3 (1)	135.81	Solute carrier family 43 member 3	1.02	1.00
RB11A_HUMAN	2 (2)	135.76	Ras-related protein Rab-11A	1.00	1.00
FUMH_HUMAN	4 (3)	135.24	Fumarate hydratase, mitochondrial	1.00	3.31
SATT_HUMAN	3 (1)	134.85	Neutral amino acid transporter A	1.00	1.16
SF3A1_HUMAN	4 (3)	134.5	Splicing factor 3A subunit 1	1.35	1.00

ROA2_HUMAN	5 (3)	134.48	Heterogeneous nuclear ribonucleoproteins A2/B1	1.35	1.00
H1X_HUMAN	4 (2)	134.34	Histone H1x	1.01	1.00
HNRPD_HUMAN	3 (1)	133.96	Heterogeneous nuclear ribonucleoprotein D0	1.66	1.00
MUC19_HUMAN	22 (3)	133.07	Mucin-19	1.00	1.00
GNA13_HUMAN	2 (1)	132.49	Guanine nucleotide-binding protein subunit alpha-13	1.14	1.00
RL3L_HUMAN	3 (1)	129.02	60S ribosomal protein L3-like	1.00	1.74
XRCC6_HUMAN	5 (2)	128.66	X-ray repair cross-complementing protein 6	1.00	1.73
PTPRC_HUMAN	4 (1)	128.34	Receptor-type tyrosine-protein phosphatase C	1.00	1.35
CO3_HUMAN	6 (2)	127.93	Complement C3	1.41	1.00
MPCP_HUMAN	3 (1)	126.67	Phosphate carrier protein, mitochondrial	1.00	1.41
TP4A1_HUMAN	3 (2)	125.96	Protein tyrosine phosphatase type IVA 1	1.08	1.00
NOP2_HUMAN	6 (3)	125.68	Probable 28S rRNA (cytosine(4447)-C(5))-methyltransferase	1.22	1.00
PARP1_HUMAN	2 (2)	125.34	Poly [ADP-ribose] polymerase 1	1.14	1.00
EIF3B_HUMAN	3 (2)	125.26	Eukaryotic translation initiation factor 3 subunit B	1.07	1.00
PUM3_HUMAN	4 (2)	125.17	Pumilio homolog 3	1.34	1.00
NOP16_HUMAN	4 (3)	124.54	Nucleolar protein 16	1.04	1.00
COPE_HUMAN	3 (2)	124.2	Coatomer subunit epsilon	1.00	1.17
FYN_HUMAN	5 (1)	123.56	Tyrosine-protein kinase Fyn	1.00	1.09
STRBP_HUMAN	4 (1)	123.41	Spermatid perinuclear RNA-binding protein	1.03	1.00
RAB14_HUMAN	2 (1)	122.05	Ras-related protein Rab-14	1.00	1.02
STIP1_HUMAN	10 (5)	119.94	Stress-induced-phosphoprotein 1	1.00	1.32
FLVC1_HUMAN	2 (2)	119.76	Feline leukemia virus subgroup C receptor-related protein 1	1.75	1.00
PRS8_HUMAN	3 (1)	118.99	26S proteasome regulatory subunit 8	1.00	1.42
SMHD1_HUMAN	12 (3)	118.78	Structural maintenance of chromosomes flexible hinge domain-containing protein 1	1.01	1.00
ABCAD_HUMAN	16 (3)	117.73	ATP-binding cassette sub-family A member 13	1.00	1.1
S39AE_HUMAN	2 (2)	117.15	Zinc transporter ZIP14	1.00	1.62
MYH10_HUMAN	11 (2)	116.4	Myosin-10	1.00	1.01
TECR_HUMAN	2 (2)	116.02	Very-long-chain enoyl-CoA reductase	1.00	3.16
PSA2_HUMAN	4 (4)	116.02	Proteasome subunit alpha type-2	1.08	1.00
SYFA_HUMAN	8 (5)	115.66	Phenylalanine--tRNA ligase alpha subunit	1.1	1.00
IF6_HUMAN	2 (1)	114.88	Eukaryotic translation initiation factor 6	1.00	1.05
FRY_HUMAN	13 (3)	114.73	Protein furry homolog	1.00	2.55
AT12A_HUMAN	11 (2)	114.71	Potassium-transporting ATPase alpha chain 2	1.00	1.71
PLXB2_HUMAN	7 (1)	114.68	Plexin-B2	1.58	1.00
S29A1_HUMAN	3 (3)	114.09	Equilibrative nucleoside transporter 1	1.00	2.22
RL35_HUMAN	3 (3)	113.83	60S ribosomal protein L35	1.08	1.00
RL28_HUMAN	2 (2)	112.47	60S ribosomal protein L28	1.00	1.16
CD44_HUMAN	3 (1)	111.86	CD44 antigen	1.41	1.00
ARPC3_HUMAN	3 (2)	111.78	Actin-related protein 2/3 complex subunit 3	1.00	1.14
LCK_HUMAN	3 (1)	111.6	Tyrosine-protein kinase Lck	1.00	1.11
SDCB1_HUMAN	2 (1)	108.85	Syntenin-1	1.00	1.32
TOP2A_HUMAN	8 (1)	108.46	DNA topoisomerase 2-alpha	1.00	1.67
GFPT1_HUMAN	6 (1)	106.87	Glutamine--fructose-6-phosphate aminotransferase [isomerizing] 1	1.53	1.00
DC1L1_HUMAN	3 (1)	106.61	Cytoplasmic dynein 1 light intermediate chain 1	1.72	1.00
ACADM_HUMAN	2 (1)	106.14	Medium-chain specific acyl-CoA dehydrogenase, mitochondrial	1.00	1.98
MCA3_HUMAN	2 (2)	106.09	Eukaryotic translation elongation factor 1 epsilon-1	1.00	1.01
STML2_HUMAN	2 (2)	105.82	Stomatin-like protein 2, mitochondrial	1.00	1.07

NP1L4_HUMAN	3 (1)	105.28	Nucleosome assembly protein 1-like 4	2.2	1.00
RBCC1_HUMAN	11 (1)	104.94	RB1-inducible coiled-coil protein 1	1.00	1.46
RBM28_HUMAN	4 (2)	102.29	RNA-binding protein 28	1.00	1.2
IF2B1_HUMAN	3 (1)	102.12	Insulin-like growth factor 2 mRNA-binding protein 1	1.00	2.5
PPIA_HUMAN	2 (1)	101.01	Peptidyl-prolyl cis-trans isomerase A	1.34	1.00
PSB1_HUMAN	2 (1)	100.74	Proteasome subunit beta type-1	1.00	1.02
RCN1_HUMAN	3 (3)	99.93	Reticulocalbin-1	1.00	1.08
MYO1B_HUMAN	5 (1)	99.87	Unconventional myosin-Ib	1.00	1.16
DDX50_HUMAN	7 (2)	99.18	ATP-dependent RNA helicase DDX50	1.00	1.28
GTF2I_HUMAN	5 (2)	98.57	General transcription factor II-I	1.21	1.00
IF2A_HUMAN	1 (1)	98.08	Eukaryotic translation initiation factor 2 subunit 1	1.21	1.00
ROA1_HUMAN	1 (1)	97.93	Heterogeneous nuclear ribonucleoprotein A1	1.41	1.00
NICA_HUMAN	5 (2)	97.55	Nicastrin	1.00	1.14
SP16H_HUMAN	4 (2)	97.32	FACT complex subunit SPT16	1.09	1.00
SR140_HUMAN	10 (3)	97.04	U2 snRNP-associated SURP motif-containing protein	1.00	1.44
MOV10_HUMAN	4 (3)	96.73	Putative helicase MOV-10	1.01	1.00
PGRC2_HUMAN	3 (1)	96.46	Membrane-associated progesterone receptor component 2	1.00	1.15
RPN1_HUMAN	4 (1)	96.4	Dolichyl-diphosphooligosaccharide--protein glycosyltransferase subunit 1	1.00	1.14
RL40_HUMAN	5 (2)	95.8	Ubiquitin-60S ribosomal protein L40	1.00	1.08
GSTP1_HUMAN	2 (2)	94.85	Glutathione S-transferase P	1.00	1.8
BAZ1B_HUMAN	8 (1)	94.29	Tyrosine-protein kinase BAZ1B	1.28	1.00
TXND5_HUMAN	3 (2)	93.93	Thioredoxin domain-containing protein 5	1.00	1.1
PDXK_HUMAN	3 (1)	93.9	Pyridoxal kinase	1.56	1.00
DDX18_HUMAN	3 (2)	93.81	ATP-dependent RNA helicase DDX18	1.00	1.11
PABP1_HUMAN	5 (2)	93.67	Polyadenylate-binding protein 1	1.07	1.00
TRRAP_HUMAN	12 (1)	93.23	Transformation/transcription domain-associated protein	1.00	1.07
OST48_HUMAN	2 (1)	92.91	Dolichyl-diphosphooligosaccharide--protein glycosyltransferase 48 kDa subunit	1.00	1.38
PLCB3_HUMAN	7 (2)	92.53	1-phosphatidylinositol 4,5-bisphosphate phosphodiesterase beta-3	1.03	1.00
ITB5_HUMAN	1 (1)	92.28	Integrin beta-5	1.00	1.03
PABP4_HUMAN	5 (1)	91.7	Polyadenylate-binding protein 4	1.06	1.00
PAIRB_HUMAN	3 (2)	91.34	Plasminogen activator inhibitor 1 RNA-binding protein	1.17	1.00
EAA1_HUMAN	2 (1)	91.32	Excitatory amino acid transporter 1	1.00	2.2
SSRG_HUMAN	2 (1)	91.04	Translocon-associated protein subunit gamma	1.00	1.57
APEX1_HUMAN	1 (1)	91.03	DNA-(apurinic or apyrimidinic site) lyase	1.68	1.00
SMC2_HUMAN	9 (2)	91.02	Structural maintenance of chromosomes protein 2	1.06	1.00
SCOT1_HUMAN	2 (1)	90.86	Succinyl-CoA:3-ketoacid coenzyme A transferase 1, mitochondrial	1.00	1.03
SF3B2_HUMAN	3 (3)	90.79	Splicing factor 3B subunit 2	1.00	1.3
ABCA4_HUMAN	10 (4)	89.96	Retinal-specific ATP-binding cassette transporter	1.00	1.47
TCOF_HUMAN	6 (1)	89.04	Treacle protein	1.36	1.00
GSLG1_HUMAN	8 (1)	88.97	Golgi apparatus protein 1	1.00	2.37
PRS7_HUMAN	4 (1)	88.59	26S proteasome regulatory subunit 7	17.39	1.00
RS23_HUMAN	1 (1)	88.34	40S ribosomal protein S23	1.31	1.00
BAG2_HUMAN	2 (1)	87.88	BAG family molecular chaperone regulator 2	1.17	1.00
ATP5H_HUMAN	3 (2)	87.84	ATP synthase subunit d, mitochondrial	1.00	1.28
ACTZ_HUMAN	1 (1)	87.8	Alpha-centractin	1.00	1.32
RANG_HUMAN	4 (2)	87.66	Ran-specific GTPase-activating protein	1.00	1.34
PRPS3_HUMAN	4 (1)	87.34	Ribose-phosphate pyrophosphokinase 3	1.19	1.00

SLTM_HUMAN	5 (2)	86.34	SAFB-like transcription modulator	1.00	1.27
DDX24_HUMAN	3 (1)	85.8	ATP-dependent RNA helicase DDX24	1.47	1.00
SMC1B_HUMAN	6 (1)	85.76	Structural maintenance of chromosomes protein 1B	1.00	1.65
ROA0_HUMAN	1 (1)	85.23	Heterogeneous nuclear ribonucleoprotein A0	1.00	1.04
RS26_HUMAN	3 (1)	85.23	40S ribosomal protein S26	1.96	1.00
LRC59_HUMAN	3 (1)	85.21	Leucine-rich repeat-containing protein 59	1.00	1.08
MDHC_HUMAN	3 (2)	83.39	Malate dehydrogenase, cytoplasmic	1.07	1.00
PSMD7_HUMAN	3 (3)	83.14	26S proteasome non-ATPase regulatory subunit 7	1.00	2.65
PPBI_HUMAN	4 (1)	82.75	Intestinal-type alkaline phosphatase	1.00	1.17
OLA1_HUMAN	1 (1)	82.53	Obg-like ATPase 1	1.3	1.00
DAF_HUMAN	2 (1)	82.05	Complement decay-accelerating factor	1.17	1.00
DX39B_HUMAN	4 (1)	81.94	Spliceosome RNA helicase DDX39B	1.09	1.00
PSB7_HUMAN	3 (3)	81.17	Proteasome subunit beta type-7	1.00	1.00
CIP4_HUMAN	4 (1)	80.66	Cdc42-interacting protein 4	4.16	1.00
GNAT2_HUMAN	2 (1)	79.97	Guanine nucleotide-binding protein G(t) subunit alpha-2	1.11	1.00
GBF1_HUMAN	7 (1)	79.81	Golgi-specific brefeldin A-resistance guanine nucleotide exchange factor 1	1.00	1.05
RMXL1_HUMAN	3 (1)	78.85	RNA binding motif protein, X-linked-like-1	1.4	1.00
SFPQ_HUMAN	2 (2)	78.08	Splicing factor, proline- and glutamine-rich	1.00	2.69
PP2AA_HUMAN	1 (1)	77.49	Serine/threonine-protein phosphatase 2A catalytic subunit alpha isoform	1.18	1.00
FA5_HUMAN	6 (2)	76.67	Coagulation factor V	1.00	3.84
RL32_HUMAN	1 (1)	76.31	60S ribosomal protein L32	1.00	1.17
COX2_HUMAN	2 (2)	76.24	Cytochrome c oxidase subunit 2	1.00	1.53
THIL_HUMAN	2 (2)	76.04	Acetyl-CoA acetyltransferase, mitochondrial	1.23	1.00
DSRAD_HUMAN	3 (1)	75.92	Double-stranded RNA-specific adenosine deaminase	1.00	1.27
TSP1_HUMAN	2 (1)	75.74	Thrombospondin-1	1.00	1.74
KAD2_HUMAN	3 (2)	75.12	Adenylate kinase 2, mitochondrial	1.00	1.41
PCBP2_HUMAN	3 (2)	75.01	Poly(rC)-binding protein 2	1.32	1.00
POP1_HUMAN	3 (1)	74.89	Ribonucleases P/MRP protein subunit POP1	1.11	1.00
HS105_HUMAN	5 (2)	74.84	Heat shock protein 105 kDa	1.08	1.00
SERB_HUMAN	1 (1)	74.6	Phosphoserine phosphatase	1.24	1.00
AASS_HUMAN	9 (3)	73.81	Alpha-aminoadipic semialdehyde synthase, mitochondrial	1.00	1.24
KMO_HUMAN	8 (1)	73.72	Kynurenine 3-monooxygenase	1.6	1.00
RS30_HUMAN	3 (1)	73.67	40S ribosomal protein S30	1.00	1.13
G6PD_HUMAN	4 (1)	73.47	Glucose-6-phosphate 1-dehydrogenase	1.28	1.00
PSB2_HUMAN	2 (1)	72.77	Proteasome subunit beta type-2	1.00	1.26
HNRH3_HUMAN	1 (1)	72.04	Heterogeneous nuclear ribonucleoprotein H3	1.02	1.00
LIMA1_HUMAN	4 (2)	71.71	LIM domain and actin-binding protein 1	1.05	1.00
PLP2_HUMAN	1 (1)	71.15	Proteolipid protein 2	1.13	1.00
PSMD6_HUMAN	3 (1)	70.72	26S proteasome non-ATPase regulatory subunit 6	1.29	1.00
GDIR1_HUMAN	1 (1)	70.54	Rho GDP-dissociation inhibitor 1	1.34	1.00
CDC42_HUMAN	1 (1)	70.48	Cell division control protein 42 homolog	1.14	1.00
HBD_HUMAN	2 (1)	69.69	Hemoglobin subunit delta	1.00	1.67
AP3D1_HUMAN	3 (2)	68.55	AP-3 complex subunit delta-1	1.04	1.00
KATL2_HUMAN	5 (2)	67.79	Katanin p60 ATPase-containing subunit A-like 2	1.00	1.71
CO9_HUMAN	4 (1)	67.42	Complement component C9	3.08	1.00
PCBP1_HUMAN	1 (1)	67.24	Poly(rC)-binding protein 1	1.19	1.00
PUF60_HUMAN	3 (1)	65.87	Poly(U)-binding-splicing factor PUF60	1.03	1.00

PSA4_HUMAN	2 (1)	65.66	Proteasome subunit alpha type-4	1.11	1.00
AIMP2_HUMAN	1 (1)	65.54	Aminoacyl tRNA synthase complex-interacting multifunctional protein 2	1.05	1.00
SPB6_HUMAN	3 (1)	65.32	Serpin B6	1.65	1.00
EPIPL_HUMAN	3 (1)	65.26	Epiplakin	1.08	1.00
MPRI_HUMAN	7 (3)	64.56	Cation-independent mannose-6-phosphate receptor	1.00	1.21
S10AB_HUMAN	1 (1)	64.49	Protein S100-A11	1.55	1.00
SND1_HUMAN	3 (2)	64.26	Staphylococcal nuclease domain-containing protein 1	1.00	1.1
RPN2_HUMAN	2 (1)	63.94	Dolichyl-diphosphooligosaccharide--protein glycosyltransferase subunit 2	1.00	1.3
DSG2_HUMAN	2 (2)	62.77	Desmoglein-2	1.27	1.00
EMC2_HUMAN	2 (1)	62.2	ER membrane protein complex subunit 2	1.14	1.00
GYS1_HUMAN	6 (2)	62.02	Glycogen [starch] synthase, muscle	1.00	3.47
BYST_HUMAN	3 (1)	61.44	Bystin	1.00	1.16
PSB3_HUMAN	1 (1)	61.2	Proteasome subunit beta type-3	1.05	1.00
PARD3_HUMAN	5 (1)	61	Partitioning defective 3 homolog	1.00	1.68
HTR5B_HUMAN	5 (2)	60.66	HEAT repeat-containing protein 5B	1.00	1.00
PRS10_HUMAN	3 (2)	60.37	26S proteasome regulatory subunit 10B	1.35	1.00
ODPB_HUMAN	3 (1)	60.31	Pyruvate dehydrogenase E1 component subunit beta, mitochondrial	1.00	1.27
PSME2_HUMAN	3 (2)	59.85	Proteasome activator complex subunit 2	1.00	1.05
PRC2C_HUMAN	3 (1)	59.77	Protein PRRC2C	1.31	1.00
LRRK2_HUMAN	4 (1)	59.36	Leucine-rich repeat serine/threonine-protein kinase 2	1.00	2.8
2ABB_HUMAN	2 (1)	59.2	Serine/threonine-protein phosphatase 2A 55 kDa regulatory subunit B beta isoform	1.19	1.00
ARC1B_HUMAN	2 (1)	58.77	Actin-related protein 2/3 complex subunit 1B	1.00	1.2
RRP15_HUMAN	2 (1)	58.62	RRP15-like protein	1.39	1.00
ARHGA_HUMAN	7 (2)	58.58	Rho guanine nucleotide exchange factor 10	1.00	2.01
DYSF_HUMAN	3 (1)	58.37	Dysferlin	1.00	3.96
KIF23_HUMAN	5 (1)	58.13	Kinesin-like protein KIF23	1.00	1.35
XRP2_HUMAN	3 (1)	57.99	Protein XRP2	1.00	1.08
H2B1A_HUMAN	2 (1)	57.73	Histone H2B type 1-A	1.08	1.00
CD63_HUMAN	2 (1)	57.54	CD63 antigen	1.00	1.51
PSB6_HUMAN	1 (1)	57.16	Proteasome subunit beta type-6	1.02	1.00
RAC1_HUMAN	2 (1)	56.81	Ras-related C3 botulinum toxin substrate 1	1.09	1.00
ANX11_HUMAN	3 (1)	56.51	Annexin A11	1.14	1.00
ATP6_HUMAN	1 (1)	56.2	ATP synthase subunit a	1.00	1.42
TOM40_HUMAN	3 (1)	56.03	Mitochondrial import receptor subunit TOM40 homolog	1.15	1.00
TRXR1_HUMAN	2 (1)	55.93	Thioredoxin reductase 1, cytoplasmic	2.14	1.00
IQGA3_HUMAN	4 (1)	55.04	Ras GTPase-activating-like protein IQGAP3	1.00	1.07
CHIP_HUMAN	2 (1)	54.65	E3 ubiquitin-protein ligase CHIP	1.16	1.00
CD81_HUMAN	1 (1)	54.12	CD81 antigen	1.00	1.24
PEF1_HUMAN	1 (1)	53.65	Peflin	1.24	1.00
RBBP4_HUMAN	1 (1)	53	Histone-binding protein RBBP4	1.1	1.00
LAMP2_HUMAN	2 (2)	52.85	Lysosome-associated membrane glycoprotein 2	1.00	1.02
VPS35_HUMAN	3 (3)	52.83	Vacuolar protein sorting-associated protein 35	1.00	3.05
PELP1_HUMAN	3 (1)	52.29	Proline-, glutamic acid- and leucine-rich protein 1	1.00	1.37
MED14_HUMAN	4 (2)	51.96	Mediator of RNA polymerase II transcription subunit 14	1.00	1.23
ITA4_HUMAN	3 (1)	51.6	Integrin alpha-4	1.00	1.14
COPG2_HUMAN	5 (1)	51.14	Coatomer subunit gamma-2	1.00	1.09
PRP19_HUMAN	2 (1)	50.7	Pre-mRNA-processing factor 19	1.26	1.00

RPF2_HUMAN	2 (1)	50.55	Ribosome production factor 2 homolog	1.07	1.00
CO5_HUMAN	2 (1)	50.26	Complement C5	2.2	1.00
BSN_HUMAN	7 (3)	49.97	Protein bassoon	1.00	1.36
ATPO_HUMAN	3 (1)	49.83	ATP synthase subunit O, mitochondrial	1.00	1.8
PRP6_HUMAN	6 (2)	49.73	Pre-mRNA-processing factor 6	1.79	1.00
PSD12_HUMAN	1 (1)	48.54	26S proteasome non-ATPase regulatory subunit 12	1.58	1.00
UCRIL_HUMAN	1 (1)	48.13	Putative cytochrome b-c1 complex subunit Rieske-like protein 1	1.00	1.4
PSMD1_HUMAN	4 (2)	47.45	26S proteasome non-ATPase regulatory subunit 1	1.6	1.00
ROAA_HUMAN	2 (1)	46.79	Heterogeneous nuclear ribonucleoprotein A/B	2.66	1.00
RU17_HUMAN	3 (2)	46.72	U1 small nuclear ribonucleoprotein 70 kDa	1.42	1.00
NUDC_HUMAN	3 (1)	46.68	Nuclear migration protein nudC	1.00	1.9
NOG1_HUMAN	1 (1)	46.43	Nucleolar GTP-binding protein 1	1.57	1.00
ALDR_HUMAN	1 (1)	45.44	Aldose reductase	1.18	1.00
DDX51_HUMAN	4 (3)	45.21	ATP-dependent RNA helicase DDX51	1.00	1.02
KAP2_HUMAN	2 (1)	45.15	cAMP-dependent protein kinase type II-alpha regulatory subunit	1.23	1.00
TADBP_HUMAN	1 (1)	44.84	TAR DNA-binding protein 43	1.23	1.00
PSA3_HUMAN	2 (1)	44.43	Proteasome subunit alpha type-3	1.00	1.23
ARPC4_HUMAN	1 (1)	44.09	Actin-related protein 2/3 complex subunit 4	1.00	1.35
TRIB1_HUMAN	2 (1)	44.01	Tribbles homolog 1	1.00	1.05
PRDX3_HUMAN	2 (2)	43.85	Thioredoxin-dependent peroxide reductase, mitochondrial	1.00	1.04
IFRD2_HUMAN	1 (1)	43.49	Interferon-related developmental regulator 2	1.35	1.00
APT_HUMAN	2 (2)	43.36	Adenine phosphoribosyltransferase	1.06	1.00
DREB_HUMAN	1 (1)	43.18	Drebrin	1.16	1.00
JKIP2_HUMAN	1 (1)	42.84	Janus kinase and microtubule-interacting protein 2	1.00	1.16
M3K12_HUMAN	7 (2)	42.54	Mitogen-activated protein kinase kinase kinase 12	2.97	1.00
SRPK1_HUMAN	2 (1)	42.26	SRSF protein kinase 1	1.34	1.00
TMPSD_HUMAN	2 (1)	41.8	Transmembrane protease serine 13	1.4	1.00
IF4G1_HUMAN	2 (1)	41.44	Eukaryotic translation initiation factor 4 gamma 1	5.97	1.00
STML1_HUMAN	4 (3)	41.17	Stomatin-like protein 1	1.01	1.00
SUMF2_HUMAN	1 (1)	41.1	Sulfatase-modifying factor 2	1.00	1.11
AP2M1_HUMAN	1 (1)	40.44	AP-2 complex subunit mu	1.00	1.29
Z518A_HUMAN	4 (1)	39.52	Zinc finger protein 518A	1.22	1.00
PSD13_HUMAN	3 (1)	39.49	26S proteasome non-ATPase regulatory subunit 13	1.56	1.00
AATC_HUMAN	2 (2)	39.38	Aspartate aminotransferase, cytoplasmic	1.68	1.00
ECI1_HUMAN	2 (1)	38.75	Enoyl-CoA delta isomerase 1, mitochondrial	2.73	1.00
RS15A_HUMAN	3 (1)	38.31	40S ribosomal protein S15a	1.84	1.00
UBP7_HUMAN	1 (1)	38.18	Ubiquitin carboxyl-terminal hydrolase 7	1.00	1.1
CN37_HUMAN	2 (1)	37.96	2',3'-cyclic-nucleotide 3'-phosphodiesterase	1.00	1.29
HPRT_HUMAN	2 (2)	37.89	Hypoxanthine-guanine phosphoribosyltransferase	1.00	2.17
DFNA5_HUMAN	1 (1)	37.32	Non-syndromic hearing impairment protein 5	1.34	1.00
UCHL3_HUMAN	2 (1)	36.87	Ubiquitin carboxyl-terminal hydrolase isozyme L3	1.86	1.00
FCG2A_HUMAN	2 (1)	36.4	Low affinity immunoglobulin gamma Fc region receptor II-a	1.00	2.21
ANR31_HUMAN	5 (1)	35.99	Putative ankyrin repeat domain-containing protein 31	1.29	1.00
MRP_HUMAN	1 (1)	35.88	MARCKS-related protein	2.47	1.00
SYT6_HUMAN	3 (1)	34.92	Synaptotagmin-6	1.00	1.04
SPEE_HUMAN	1 (1)	34.7	Spermidine synthase	1.00	1.24
ETFA_HUMAN	3 (1)	33.56	Electron transfer flavoprotein subunit alpha, mitochondrial	1.00	1.14

SULF1_HUMAN	3 (1)	32.77	Extracellular sulfatase Sulf-1	6.33	1.00
MTA2_HUMAN	2 (1)	32.49	Metastasis-associated protein MTA2	1.04	1.00
CHTOP_HUMAN	2 (1)	31.69	Chromatin target of PRMT1 protein	1.24	1.00
XRCC5_HUMAN	2 (2)	31.08	X-ray repair cross-complementing protein 5	1.00	1.08
PSB4_HUMAN	3 (3)	30.99	Proteasome subunit beta type-4	1.00	1.04
LCAP_HUMAN	2 (1)	30.87	Leucyl-cystinyl aminopeptidase	1.00	1.7
CG050_HUMAN	2 (2)	30.71	Uncharacterized protein C7orf50	1.00	1.2
NINL_HUMAN	3 (1)	30.55	Ninein-like protein	1.56	1.00
SBP1_HUMAN	3 (1)	30.42	Selenium-binding protein 1	1.00	1.19
KCY_HUMAN	1 (1)	30.04	UMP-CMP kinase	1.00	1.09
VN1R5_HUMAN	1 (1)	29.77	Vomeronasal type-1 receptor 5	1.16	1.00
LGUL_HUMAN	1 (1)	29.48	Lactoylglutathione lyase	1.2	1.00
ELP1_HUMAN	2 (1)	28.64	Elongator complex protein 1	1.00	1.49
FAK2_HUMAN	5 (1)	27.57	Protein-tyrosine kinase 2-beta	1.00	3.12
NUBP2_HUMAN	2 (1)	27.29	Cytosolic Fe-S cluster assembly factor NUBP2	1.01	1.00
K1614_HUMAN	3 (1)	27.26	Uncharacterized protein KIAA1614	1.09	1.00
EPHB6_HUMAN	2 (1)	27.05	Ephrin type-B receptor 6	1.00	1.08
FZD8_HUMAN	2 (2)	25.31	Frizzled-8	1.07	1.00
PLCA_HUMAN	1 (1)	24.76	1-acyl-sn-glycerol-3-phosphate acyltransferase alpha	1.00	3.03
SRSF5_HUMAN	1 (1)	24.7	Serine/arginine-rich splicing factor 5	1.46	1.00
H2B2C_HUMAN	1 (1)	24.19	Putative histone H2B type 2-C	1.00	21.06
PPAP_HUMAN	1 (1)	24.07	Prostatic acid phosphatase	1.13	1.00
TCPQL_HUMAN	1 (1)	22.55	Putative T-complex protein 1 subunit theta-like 1	1.08	1.00
EMP3_HUMAN	1 (1)	22.03	Epithelial membrane protein 3	1.00	1.37
GG6L3_HUMAN	2 (2)	21.18	Putative golgin subfamily A member 6-like protein 3	1.00	1.25
UGPA_HUMAN	1 (1)	20.29	UTP--glucose-1-phosphate uridylyltransferase	1.00	1.18
ITPA_HUMAN	1 (1)	20.07	Inosine triphosphate pyrophosphatase	1.00	1.08
MRC1_HUMAN	4 (2)	19.63	Macrophage mannose receptor 1	1.00	2.17
MIC60_HUMAN	3 (1)	19.44	MICOS complex subunit MIC60	1.00	1.97
HSFX3_HUMAN	2 (1)	17.6	Heat shock transcription factor, X-linked member 3	1.00	1.01
FOG2_HUMAN	2 (1)	17.43	Zinc finger protein ZFPM2	1.00	1.33
ACON_HUMAN	1 (1)	16.55	Aconitate hydratase, mitochondrial	1.00	1.06
EXOC2_HUMAN	3 (1)	16.35	Exocyst complex component 2	1.58	1.00
CAC1I_HUMAN	3 (2)	10.45	Voltage-dependent T-type calcium channel subunit alpha-1I	1.01	1.00
TXLNA_HUMAN	2 (1)	7.3	Alpha-taxilin	1.01	1.00